UNIVERSITY OF CALIFORNIA, SAN DIEGO
SAN DIEGO STATE UNIVERSITY

Studies on Bis Protic N-Heterocylic Carbene Pincer Complexes and on Water Oxidation Catalysts

A dissertation submitted in partial satisfaction of the
requirements for the degree Doctor of Philosophy in

Chemistry

by

David Charles Marelius

Committee in charge:

University of California, San Diego

Professor Joseph M. O'Connor
Professor Michael J. Tauber

San Diego State University

Professor Douglas B. Grotjahn, Chair
Professor B. Mikael Bergdahl
Professor Asfaw Beyene

2015

The dissertation of David Charles Marelius is approved, and it is acceptable in quality and form for publication on microfilm:

_____

_____

_____

_____

_____

Chair

University of California, San Diego

San Diego State University

2015

TABLE OF CONTENTS

LIST OF FIGURES

LIST OF TABLES

ACKNOWLEDGEMENTS

First and foremost I would like to thank Dr. Douglas Grotjahn for the years of mentoring. I would not be the chemist I am today without all of his guidance. The trait I admire the most and feel that I have learned from by his example is his work ethic. Next, I thank my wife for everything she did to help me finish my PhD, and making every day much more enjoyable. Casey Larsen was the TA in my first chemistry class at SDSU, she got me involved in research, and without a doubt I would not be here without her help over the years. Jayneil Kamdar, I don't think I could have gotten this far without you always being there, since the first day in the master's program. We went through the PhD program together, worked on the same water oxidation project, and spent many crazy hours together and gained a number of stories that we will never forget. Erik Paulson, you were always willing to talk, be it about science, life, or sports and just talking to you had a way of making my day just a little bit better. I would like to thank all of the undergrads that I have worked with over the years for all of their hard work; Evan Darrow, Kristine Schroeder, Khoi Le Ryan Shirey, Jake Gooing, and Robert Vasquez. I am sure they will accomplish great things. I have to thank my best friends John Repking, Ricky Knowles, and Phil Dement for being there for me when I just needed to relax and not think about chemistry. I must also thank, Jim and Gerry Repking for always being there when I needed them. Lastly I would like to thank my family, I would not have been able to get where I am without their years of support.

Part of the material and discussion covered in chapter 1 is from published work. I would like to thank Evan Darrow, Dr. James Golen, Dr. Curtis Moore, and Dr. Arnold Rheingold, for their contribution to "Hydrogen-bonding pincer complexes with two protic N-heterocyclic carbenes from direct metalation of a 1,8-bis(imidazol-1-yl)carbazole by platinum, palladium, and nickel" which appeared in *Chem. Eur. J.* **2015**, *21*, 10988. I must thank Dr. Curtis Moore, Dr. Arnold Rheingold, and Dr. Douglas Grotjahn for their work on "Reactivity Studies of Bis Protic N-Heterocylic Carbene Complexes1,8-Bis(imidazol-1-ylidene)carbazole Platinum and Palladium under Basic Conditions" which was submitted to *Inorg. Chem.*

Part of the material and discussion covered in chapter 2 is from published work "Evolution of iridium-based molecular catalysts during water oxidation with ceric ammonium nitrate", which appeared in *J. Am. Chem. Soc.* **2011**, *133*, 19024. I would like to thank; Dr. Douglas Grotjahn, Derek Brown, Jessica Martin, Dr. Caline Abadjian, Hai Tran, Dr. Gregory Kalyuzhny, Dr. Kenneth Vecchio, Dr. Zephen Specht, Dr. Sara Cortes-Llamas, Dr. Valentin Miranda-Soto, Christoffel van Niekerk, Dr. Curtis Moore, and Dr. Arnold Rheingold for their contributions.

Part of the material and discussion covered in chapter 3 is from published work "How Do Proximal Hydroxy or Methoxy Groups on the Bidentate Ligand Affect (terpy)Ru(N,N)X Water Oxidation Catalysts? Synthesis, Characterization, and Reactivity at Acidic and Near-neutral pH" which was published in *Eur. J. Inorg. Chem.* **2014**, *2014*, 676. This work was a result of collaboration between four different universities. I would like to thank Dr. Salome Bhagan, David Charboneau, Kristine Schroeder, Jayneil Kamdar, Amanda McGettigan, Benjamin Freeman, Dr. Curtis Moore, Dr. Arnold Rheingold, Dr. Andrew Cookey, Dr. Diane Smith, Dr. Jared Paul, Dr. Elizabeth Papish, and Dr. Douglas Grotjahn for their contributions. I must also thank Ryan J. Shirey, Farhana Barmare, and Dr. Douglas B. Grotjahn for their work on another section covered in the chapter, which is part of a manuscript that is in preparation titled "Synthesis and Water Oxidation Activity of Sterically Hindered [Ru(Cl)(terpy)pyridylnaphthyridine] Cl Analogs; an Attempt at Fluorinated Oxidatively Resilient Ligands"

VITA

Education

2009	B.S., Chemistry San Diego State University
2015	Ph.D., Chemistry University of California, San Diego

Major Fields of Study

Major Field: Chemistry (Organic and Inorganic)

Studies in Synthesis and Organometallic Catalysis.
Professor Douglas B. Grotjahn

Publications

"Reacitivity Studies of Bis Protic N-Heterocylic Carbene Complexes1,8-Bis(imidazol-1-ylidene)carbazole Platinum and Palladium under Basic Conditions," **D. C. Marelius**, Curtis E. Moore, Arnold L. Rheingold, Douglas B. Grotjahn, *Submitted to Inorg. Chem.* November 2015.

"Hydrogen-bonding Pincer Complexes with Two Protic N-Heterocyclic Carbenes from Direct Metalation of a 1,8-Bis(imidazol-1-yl)carbazole by Platinum, Palladium, as well as Nickel," **D. C. Marelius**, E. H. Darrow, C. E. Moore, J. A. Golen, A. L. Rheingold, D. B. Grotjahn, *Chem. Eur. J.* **2015**, *21*, 10988-10992.

"How Do Proximal Hydroxy or Methoxy Groups on the Bidentate Ligand Affect (terpy)Ru(N,N)X Water Oxidation Catalysts? Synthesis, Characterization, and Reactivity at Acidic and Near-neutral pH," **D. C. Marelius**, S. Bhagan, D. J. Charboneau, K. M. Schroeder, J. M. Kamdar, A. R. McGettigan, B. J. Freeman, C. E. Moore, A. L. Rheingold, A. L. Cooksy, D. K. Smith, J. J. Paul, E. T. Papish, D. B. Grotjahn, *Eur. J. Inorg. Chem.* **2014**, 676–689 (invited for special issue on water oxidation).

"Evolution of Iridium-Based Molecular Catalysts during Water Oxidation with Ceric Ammonium Nitrate" D. B. Grotjahn, D. B. Brown, J. K. Martin, **D. C. Marelius**, M. C. Abadjian, H. N. Tran, G. Kalyuzhny, K. S. Vecchio, Z. G. Specht, S. A. Cortes-Llamas, V. Miranda-Soto, C. van Niekerk, C. E. Moore, A. L. Rheingold, *J. Am. Chem. Soc.* **2011**, *133*, 19024-19027.

Manuscripts in Preparation

"Synthesis and Water Oxidation Activity of Sterically Hindered [Ru(Cl)(terpy)(pyridylnaphthyridine)] Cl Analogs: an Attempt at Fluorinated Oxidatively Resilient Ligands" **D. C. Marelius**, R. J. Shirey, F. Barmare, D. B. Grotjahn, Planned submission date, December 2015

Presentations

"How do proximal groups on the bidentate ligand affect (terpy)Ru(N,N)X water oxidation catalysts? Synthesis, characterization, and reactivity" **D. C. Marelius**, J. M. Kamdar, Q. Cao, S. Bhagan, C. E. Moore, A. L. Rheingold, J. J. Paul, E. T. Papish, D. B. Grotjahn, poster presentation (INOR-321) at the American Chemical Society meeting, in San Francisco CA, August 10-14, 2014. *Selected for Sci-Mix*.

"Hydrogen-bonding pincer complexes with two protic N-heterocyclic carbenes from direct metalation of a 1,8-bis(imidazol-1-yl)carbazole by platinum, palladium, as well as nickel" **D. C. Marelius**, E. H. Darrow, C. E. Moore, J. A. Golen, A. L. Rheingold, D. B.

Grotjahn, poster presentation (ORGN-692) at the American Chemical Society meeting, in San Francisco CA, August 10-14, 2014.

"Limitless carbon-free storage of solar energy" **D. C. Marelius**, invited speaker at the 38th International Precious Metal Institute, in Orlando FL, June 7-10, 2014.

"Hydrogen-bonding Pincer Complexes with Two Protic N-Heterocyclic Carbenes from Direct Metalation of a 1,8-Bis(imidazol-1-yl)carbazole by Platinum, Palladium, as well as Nickel," **D. C. Marelius**, E. H. Darrow, C. E. Moore, J. A. Golen, A. L. Rheingold, D. B. Grotjahn, poster at the 25th Biennial Organic Reaction Catalysis Society Conference, in Tucson, AZ, March 2-6, 2014.

"How Do Proximal Hydroxy or Methoxy Groups on the Bidentate Ligand Affect (terpy)Ru(N,N)X Water Oxidation Catalysts? Synthesis, Characterization, and Reactivity," **D. C. Marelius**, S. Bhagan, D. J. Charboneau, K. M. Schroeder, J. M. Kamdar, A. R. McGettigan, B. J. Freeman, C. E. Moore, A. L. Rheingold, A. L. Cooksy, D. K. Smith, J. J. Paul, E. T. Papish, D. B. Grotjahn, poster presentation at the IX International Symposium, Chemical Research in the Border Region, Tijuana, Nov. 2013.

"NMR and MS studies of iridium based molecular catalysts during water oxidation with ceric ammonium nitrate" **D. C. Marelius**, D. B. Grotjahn, D. B. Brown, J. K. Martin, H. N. Tran, G. Kalyuzhny, K. S. Vecchio, S. A. Cortes-Llamas, V. Miranda-Soto, Z. G. Specht, C. van Niekerk, C. E. Moore, A. L. Rheingold, poster at the American Chemical Society meeting, San Diego, March 2012.

"Reactivity studies of pincer protic N-heterocyclic carbene complexes of nickel, palladium, and platinum" **D. C. Marelius**, E. H. Darrow, C. E. Moore, A. L. Rheingold, D. B. Grotjahn, poster presentation (INOR-714) at the American Chemical Society meeting, Anaheim, March 2011.

Presentations to which I have contributed but presented by colleagues

"New Ligands and Complexes for Water Oxidation Catalysis," D. B. Grotjahn, **D. C. Marelius**, J. M. Kamdar, F. Saeedifard, C. E. Moore, A. L. Rheingold, oral presentation, X Simposio Internacional: Investigación Química en la Frontera, Tijuana, BC, Mexico. Nov. 2015

"Ruthenium Complexes of 2,2'-bipyridine-6,6'-diphosphonate Ligands for Water Oxidation," J. M. Kamdar, **D. C. Marelius**, C. E. Moore, A. L. Rheingold, D. K. Smith, D. B. Grotjahn, oral presentation, X Simposio Internacional: Investigación Química en la Frontera, Tijuana, BC, Mexico. Nov. 2015

"Bifunctional Catalysis for Selective Oxidation of Water and Organic Substrate," R. M. Vasquez, J. M. Kamdar, **D. C. Marelius**, D. B. Grotjahn, poster, X Simposio Internacional: Investigación Química en la Frontera, Tijuana, BC, Mexico. Nov. 2015

"Bifunctional Catalysis for Selective Oxidation of Water and Organic Substrate," Robert M. Vasquez, J. M. Kamdar, **D. C. Marelius**, D. B. Grotjahn, poster, Southern California Undergraduate Research Conference, University of California-San Diego, CA. April 2015.

"Protecting Extended Naphthyridine π Systems for Pendant Base Assisted Water Oxidation Catalysts" R. J. Shirey, **D. C. Marelius**, and D. B. Grotjahn. The ACS Southern California Undergraduate Research Conference in Chemistry and Biochemistry in San Diego, CA. April 2015.

"Protecting Extended Naphthyridine π Systems for Pendant Base Assisted Water Oxidation Catalysts" R. J. Shirey, **D. C. Marelius**, and D. B. Grotjahn. San Diego State Student Research Symposium in San Diego, CA. March, 2015.

"Protecting Extended Naphthyridine π Systems for Pendant Base Assisted Water Oxidation Catalysts" R. J. Shirey, **D. C. Marelius**, and D. Grotjahn. San Diego State Student Research Symposium in San Diego, CA. March, 2015.

"Bifunctional Catalysis for Selective Oxidation of Water and Organic Substrates," Robert M. Vasquez, J. M. Kamdar, **D. C. Marelius**, D. B. Grotjahn, poster, Student Research Symposium, San Diego State University, CA. 2014

"Bifunctional Catalysis for Selective Oxidation of Water and Organic Substrates," Robert M. Vasquez, J. M. Kamdar, **D. C. Marelius**, D. B. Grotjahn, poster, Annual Biomedical Research Conference for Minority Students, San Antonio, TX. 2014

"Exploring the effect of varying the 6,6' substituents on 2,2'-bipyridyl ruthenium complexes for water oxidation," J. M. Kamdar, **D. C. Marelius**, D. B. Grotjahn, C. E. Moore, A. L. Rheingold, poster, ACS, San Francisco CA, Aug. 10-14, 2014.

"Catalytic water oxidation by 2,2'-bipyridyl ruthenium complexes: The effect of varying the basicity of 6,6' Substituents," J. M. Kamdar, **D. C. Marelius**, D. B. Grotjahn, C. E. Moore, A. L. Rheingold, poster at the IX International Symposium, Chemical Research in the Border Region, Tijuana, November 2013.

"Dihydroxybiypyridine Complexes of Ruthenium and Iridium show that Ligand Deprotonation Can Dramatically Enhance Rates of Catalytic Water Oxidation and Hydrogenation in Some Cases," E. T. Papish, J. DePasquale, S. Bhagan, **D. C Marelius**, D. J. Charboneau, J. M. Kamdar, A. R. McGettigan, B. J. Freeman, C. E. Moore, A. L. Rheingold, J. J. Paul, D. B. Grotjahn, I. Nieto, oral presentation at Southeastern Regional Meeting American Chemical Society, Atlanta, GA, November 2013.

"PNHC (Protic N-Heterocyclic Carbene) Complexes after 98 Years: the First Pincer PNHC Complexes, and Synthetic, Structural and Reactivity Studies of PNHC

Bifunctionality," D. B. Grotjahn, **D. C. Marelius**, E. H. Darrow, V. Miranda-Soto, C. E. Moore, A. L. Rheingold, poster presented at Organometallic Chemistry Gordon Research Conference, Newport, RI, July, 2013.

"Behavior of molecular organometallic and inorganic catalysts during water oxidation**,"** D. B. Grotjahn, **D. C. Marelius**, J. M. Kamdar, D. B. Brown, J. K. Martin, M. C. Abadjian, H. N. Tran, G. Kalyuzhny, K. S. Vecchio, Z. G. Specht, M. M. Uteuliyev, Q. Cao, invited speaker at symposium on Hydrogen Production, Storage, and Utilization at 245th National Meeting, American Chemical Society, New Orleans, April 2013.

"Reactivity studies of pincer protic N-heterocyclic carbene complexes of nickel, palladium, and platinum," **D. C. Marelius**, E. H. Darrow, C. E. Moore, A. L. Rheingold, D. B. Grotjahn, poster presented at Inorganic Reaction Mechanisms Gordon Research Conference, Galveston, TX, March, 2013.

"Design and synthesis of ligands for improved water-oxidation catalysis," K. J. Schroeder, **D. C. Marelius**, D. B. Grotjahn. Poster at Ivy Plus STEM Symposium for Diverse Scholars, Phila., Oct. 2012.

"Behavior of iridium-based molecular catalysts during water oxidation with cerium(IV)," D. B. Grotjahn, **D. C. Marelius**, D. B. Brown, J. K. Martin, M. C. Abadjian, H. N. Tran, G. Kalyuzhny, K. S. Vecchio, Z. G. Specht, oral presentation at 40th Int. Coordination Chemistry Conf., Valencia, Spain, 9-13 Sept. 2012.

"Evolution of iridium-based molecular catalysts during water oxidation with ceric ammonium nitrate" D. B. Grotjahn, D. B. Brown, J. K. Martin, **D. C. Marelius**, M. C. Abadjian, H. N. Tran, G. Kalyuzhny, K. S. Vecchio, Z. G. Specht, S. A. Cortes-Llamas, V. Miranda-Soto, C. van Niekerk, C. E. Moore, A. L. Rheingold, oral presentation at the American Chemical Society meeting in San Diego, March 2012.

"Pincer ligand synthesis and formation of the first protic pincer N-heterocyclic carbene complexes" E. H. Darrow, **D. C. Marelius**, C. E. Moore, A. L. Rheingold, D. B. Grotjahn, poster presentation (INOR-709) at the American Chemical Society meeting in Anaheim, March 2011.

Awards

International Precious Metals Institute (IPMI) Richard Rubin memorial scholarship, which recognizes achievement in precious metals research, June 2014.

Student Travel Award for Organic Reactions Catalysis Society (ORCS) Conference Participation, March 2014.

ABSTRACT OF THE DISSERTATION

Studies on Bis Protic N-Heterocylic Carbene Pincer Complexes and on Water Oxidation Catalysts

by

David Charles Marelius

Doctor of Philosophy in Chemistry

University of California, San Diego, 2015

San Diego State University, 2015

Professor Douglas B. Grotjahn, Chair

It is imperative that we improve clean and renewable energy technology in the face of growing energy demand. Solar energy is potentially abundant, but we need to capture, convert and store solar energy in usable forms. Hydrogen could be ideal for energy storage, if made using sunlight energy to split water by oxidizing water to dioxygen and protons and using the released electrons to reduce protons to hydrogen in a net transfer of electrons. In Chapter 2, we explored water oxidation which is believed to be the more challenging of the two steps. We found evidence for catalyst degradation

while using iridium complexes with ceric ammonium nitrate (CAN) as a sacrificial oxidant, possibly forming iridium oxide nanoparticles. Chapter 3 describes studies of analogs of well-known ruthenium water oxidation catalysts with bipyridine ligands that were designed to be bifunctional, by adding potential pendant bases such as hydroxy, alkoxy, amino, and heterocyclic amines, and some combinations of these groups. One successful catalyst was the methoxy complex which proved to be more robust than the parent unsubstituted complex while using CAN. Extended π systems, e.g. naphthyridine were found to lead to less active catalysts; therefore, we attempted to slow degradation and increase duration of catalysis by protecting the complex with sterically hindered groups, but we suspect that ligand loss interfered. Chapter 4 focused on ligands that would support formation of binuclear complexes which could improve catalysis, taking into account one of the proposed mechanisms for water oxidation involving two metal complexes

Work presented in Chapter 1 involves synthesis (by direct metalation of C-H bonds) and characterization of bis protic N-heterocylic carbene (PNHC) pincer complexes of platinum, palladium, and even nickel, in addition to their reactivity with alkynes and under basic conditions. Alkynes were converted to aldehydes as the major *anti*-Markovnikov addition products. The complexes were treated with different bases to form proposed trifunctional complexes containing one PNHC and one basic imidazolyl ligand. Addition of sodium alkoxide yielded dimeric species and lithium bases gave LiCl-imidazolyl adducts, which proved to be moisture sensitive but did not lose LiCl and undergo ligand exchange with substrates.

CHAPTER 1

Studies on bis Protic N-Heterocylic Carbene Complexes of Platinum, Palladium, and Nickel

A. Introduction to Bifunctional Catalysis

Nature has had a long time to optimize very challenging chemical transformations, such as converting solar energy into chemical energy, i.e. photosynthesis[1], or perfoming complex organic synthesis[2], both of which feats we humans attempt to copy. The way nature is able to do a number of these chemical transformations is by the use of enzymes, which in some cases contain a metal or metals. In attempts to mimic enzymes, organometallic chemists try to increase the rates of reactions using much simpler organic scaffolds called ligands that typically use sterics or electronics to enable catalysis. One interesting feature that has been seen in enzymes is the use of basic or acidic groups in specific positions around the metal that can assist in proton transfers[3,4]. Incorporating basic groups in organometallic ligands in a way that they do not coordinate and are

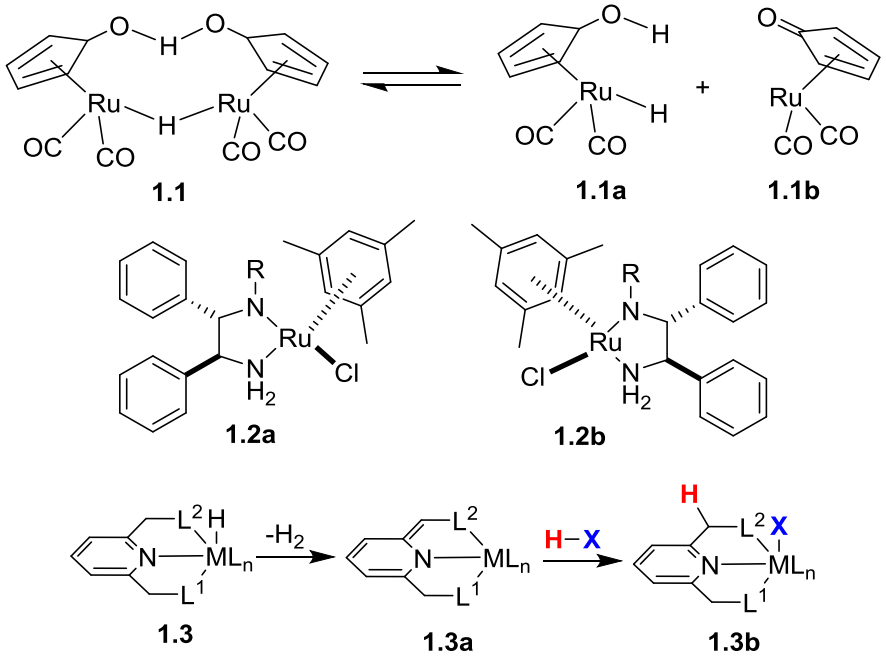

Figure 1.1. Structures of Shvo catalyst **1.1**, Noyori catalyst **1.2,** and generic structure of Milstein catalyst analogs **1.3**

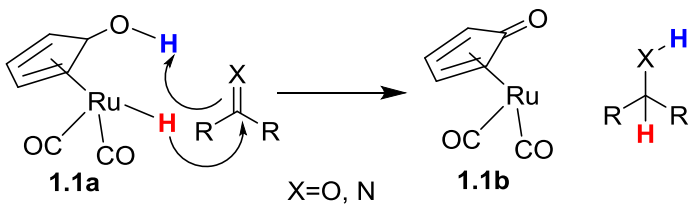

Figure 1.2. Proposed mechanism for hydrogen transfer from the active intermediate derived from the Shvo catalyst, showing the bifunctional interaction.

pendant bases, available to assist the metal in proton transfers, could accelerate the overall reaction, depending on the rate limiting step. It is important to emphasize that we are targeting cases where the metal still does chemistry but is assisted by a pendant base, as examples of bifunctional catalysis.

Well known catalyst systems that are believed to be bifunctional include the Shvo catalyst, **1.1**, which breaks up into **1.1a** and **1.1b** (Figure 1.1**),** where **1.1a** is the active species that transfers both a proton and hydride in a concerted fashion to a ketone or imine, giving the corresponding alcohol[5] or amine[6] (Figure 1.2). Another bifunctional catalyst by Noyori does the same transfer hydrogenation reaction of ketones to alcohols[7] and imines to amines[8], but it also contains a chiral ligand so the obtained products are enantiomerically enriched. Either enantiomer of the alcohol or the amine can be obtained

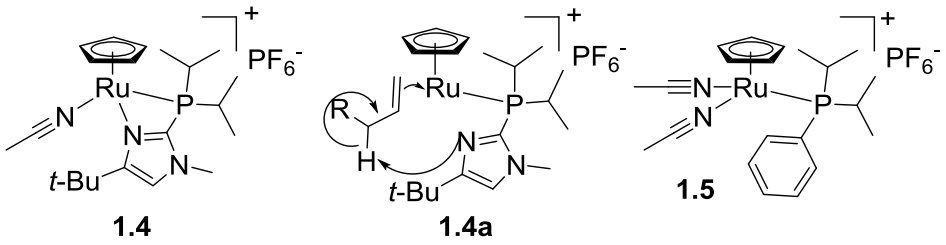

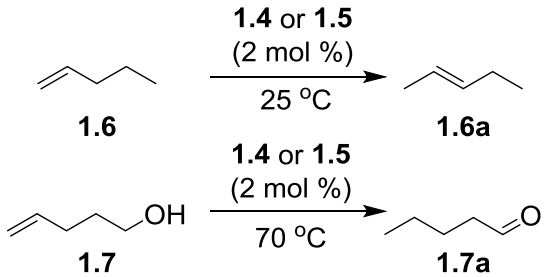

Figure 1.3. Alkene isomerization, work previously done in the Grotjahn lab utilizing bifunctional catalysts.

Table 1.1. Reaction rate comparison of catalysts **1.4** and **1.5** acting on substrates **1.6** and **1.7**.

Substrate	**1.4**	**1.5**	Rate Difference
1.6	190[a]	0.56[a]	340
1.7	45[a]	0.0042[a]	10800

[a]TOF= Turnover frequency (h^{-1})

depending on which enantiomer of the catalyst is used: complex **1.2a** yields the S enantiomer whereas **1.2b** yields the R enantiomer (Figure 1.1). A third example of a bifunctional catalyst system has been explored by Milstein, in that complexes of type **1.3** convert alcohols to esters[9], reduce an ester to an alcohol[10], synthesize an amide from an alcohol and an amine[11], or form an imine from an alcohol and an amine[12]. The bifunctional aspect of catalysts of form **1.3** is that the side arm CH_2 can act as an H donor, or the side-arm unsaturation of structure **1.3a** can accept an H to form **1.3b**[13].

Previous work by our group has looked at alkene isomerization: **1.4** is a very active catalyst that is believed to operate by a bifunctional mechanism, with a proposed key step shown in **1.4b**, during which the imidazole accepts a proton from the alkene forming an allyl complex (Figure 1.3). The proposed mechanism highlights the importance of the imidazole acting as a base. An analog without a pendant base, structure **1.5,** where the imidazole is replaced with a phenyl, was used under the same reaction

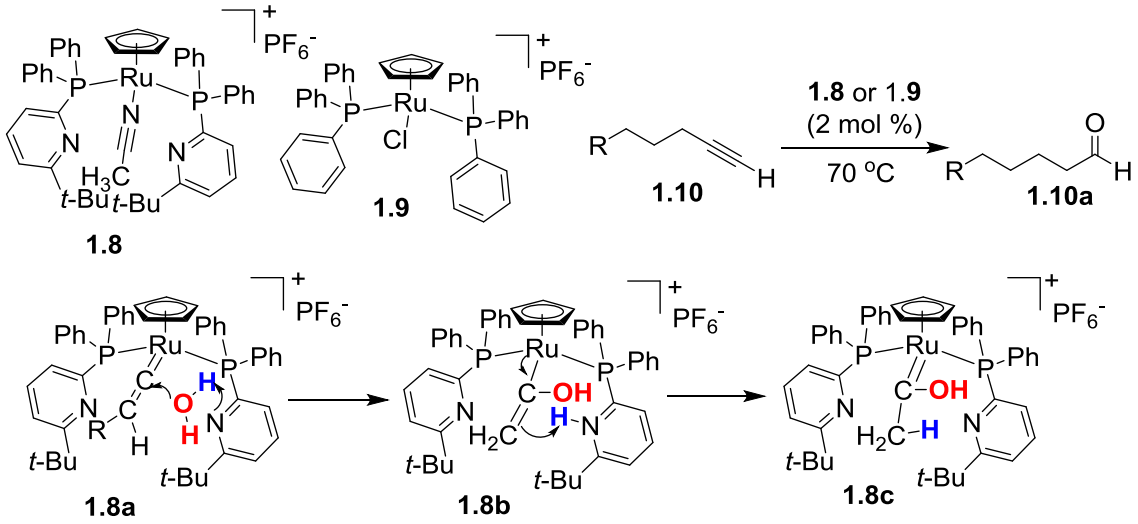

Figure 1.4. *Anti*-Markovnikov alkyne hydration catalyst **1.8**, and the proposed bifunctional key mechanistic steps (**1.8a**-**1.8c**).

conditions as **1.4**, showing that substantial rate differences. **1.4** is 340 times faster than **1.5** in converting **1.6** to **1.6a** or about 10800 times faster converting **1.7** to **1.7a**, as determined by comparing turnover frequencies (TOF), the moles of product formed per mole of catalyst over a certain time period, in this case per hour (Table 1.1)[14-16].

Another example of a Grotjahn lab bifunctional catalyst is **1.8**, which is capable of *anti*-Markovnikov hydration of an alkyne (Figure 1.4)[17]. The proposed mechanism shows the importance of the basic pyridyl group accepting a proton from the water that attacks the vinylidene, **1.8a**. The proton is then transferred to the substrate, **1.8b**. Evidence of the importance of the pendant base is that base-free analog **1.9** is 1,000 times slower (Table 1.2)[18] than catalyst **1.8** in the conversion of **1.10** to **1.10a**.

Table 1.2. Reaction rate comparison of catalysts **1.8** and **1.9** acting on substrate **1.10**.

Substrate	**1.8**	**1.9**	Rate Difference
1.10	23.8[a]	0.0238[a]	1000

[a]TOF= Turnover frequency (h^{-1})

B. Introduction to Protic N-Heterocylic Carbene Complexes, and Design of the Study

The ligands described so far contain phosphine ligands, but there are other ligand types such as N-heterocyclic carbene (NHC) complexes which have become an exceptionally fruitful area of research in organometallic chemistry as demonstrated by numerous reviews[19-29]. The first carbene complex is typically thought to be a tungsten carbene published by Fisher in 1964[30], but in fact this was just the first correctly-reported carbene. In 1915 Chugaev reported the synthesis of complex **1.11** by addition of

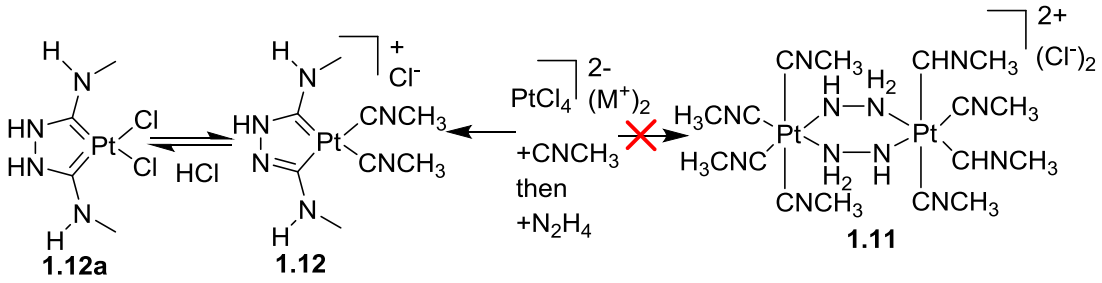

Figure 1.5. Chugaev first reported in 1915 a product mischaracterized as **1.11**; crystal structures done in 1970 showed correct carbene-containing structures **1.12** and **1.12a**.

methylisocyanide to tetrachloroplatinate(II) to give tetrakis(methylisocyanide)platinum(II)[31,32], to which hydrazine was added giving what was thought to be **1.11**. In 1970 the work was repeated and X-ray diffraction crystal structures were obtained, showing that structure **1.11** had been incorrectly assigned; instead, **1.12** was what was formed, making the product the first synthesized NHC complex[33] (Figure 1.5).

Complexes **1.12** and **1.12a** do not contain typical NHC ligands, which are usually altered by changing the alkyl or aryl groups on each nitrogen, for either steric or electronic reasons. Instead, **1.12** and **1.12a** contain a proton on one of the nitrogens making them protic NHC (PNHC) complexes. Even with the overwhelming amount of research being done with typical NHCs there is relatively little work on PNHCs. One of the barriers to studying PNHC complexes has been their synthesis, which typically has followed one of four different paths: (1) intentional applications of Chugaev's method, namely coordination of isocyanide to metal, followed by addition of an amine, forming

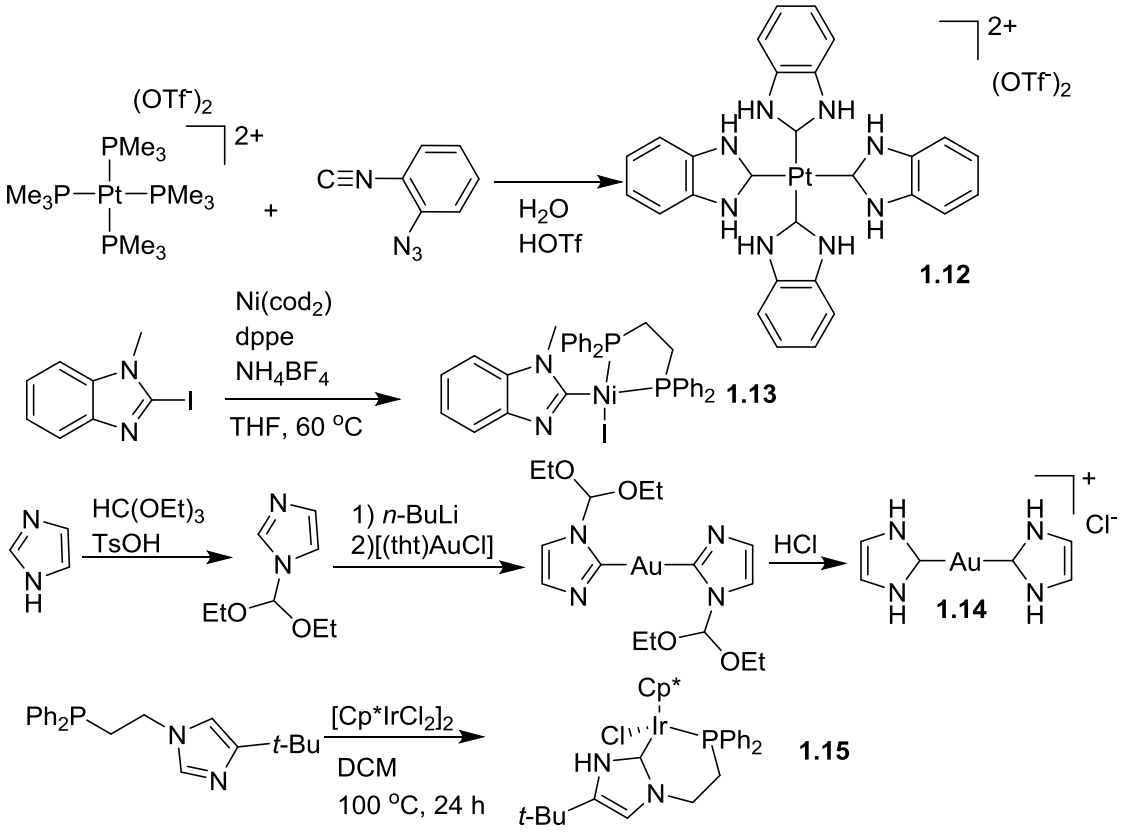

Figure 1.6. Examples of the synthetic methods for PNHC complexes.

the PNHC complex[34-41] (Figure 1.6, example **1.12**[34]); (2) starting with a 2-halogenated heterocycle, performing metal oxidative addition, giving the conjugate base form of a PNHC complex, followed by N-protonation[42,43] (example **1.13**[42]); (3) starting with an imidazole without a substituent at the C-2 position, protecting one of the imidazole nitrogens, deprotonating at C-2, forming a metal-C bond by salt metathesis, and then removal of the protecting group generating the PNHC[44-47] complex (example **1.14**[44]); and (4) using a unfunctionalized heterocycle without a substituent at C-2, but then just adding a metal which can generate a PNHC complex in a single synthetic step[48-54] (example **1.15**). Example **1.15** also shows the most common application of method 4, where there is a substituent containing a coordinating ligand attached to the future carbene such as a phosphine[48-51], ethylenediamine[52], pyridine[53], or an olefin[54].

As for reactivity of PNHC complexes, Meier *et al*. studied a Rh-PNHC complex and monitored the hydrogenation of 1-dodecene and an alkene containing an ester functionality, showing that the ester alkene reacted three times faster. The proposed rate difference comes from the hydrogen bond donation of the PNHC to the ester[55]. As for studies in our lab, PNHC complex **1.15** shows interesting reactivity that typical NHC complexes do not, the ability to deprotonate the PNHC proton giving **1.15a**. **1.15a** is capable of activating bonds such as the H-H bond of dihydrogen giving **1.15b** or the C-H bond of acetylene giving **1.15c**[49], where the pendant nitrogen accepts a proton and after ionization the metal forms a bond to the substrate (hydride or acetylide) (Figure 1.7). Another catalyst, **1.16**, has the same PNHC ligand but with CpRu instead of Cp*Ir. This complex was shown to form the imidazolyl complex **1.16a** after ionization with KPF_6 and the presence of an amine followed by the addition of a base, where now a neutral amine is coordinated to the metal. Interestingly using a lithium base such as LDA or *n*-BuLi led to structure **1.16b** where the lithium shows a strong interaction with the anionic nitrogen. A crystal structure of **1.16b** showed that the lithium is interacting with the nitrogen, chloride, and is solvated by two THF molecules[56]. Both **1.16a** and **1.16b** were capable of activating dihydrogen, with **1.16b** being the fastest. **1.16** was found to be a rather active catalyst for the transfer hydrogenation of acetophenone to 1-phenyl-1-ethanol with a

catalyst loading of 0.05 % and 0.2 mol % KOH, giving 97% yield after 3 h or quantitative yield after 24 h (Figure 1.8).

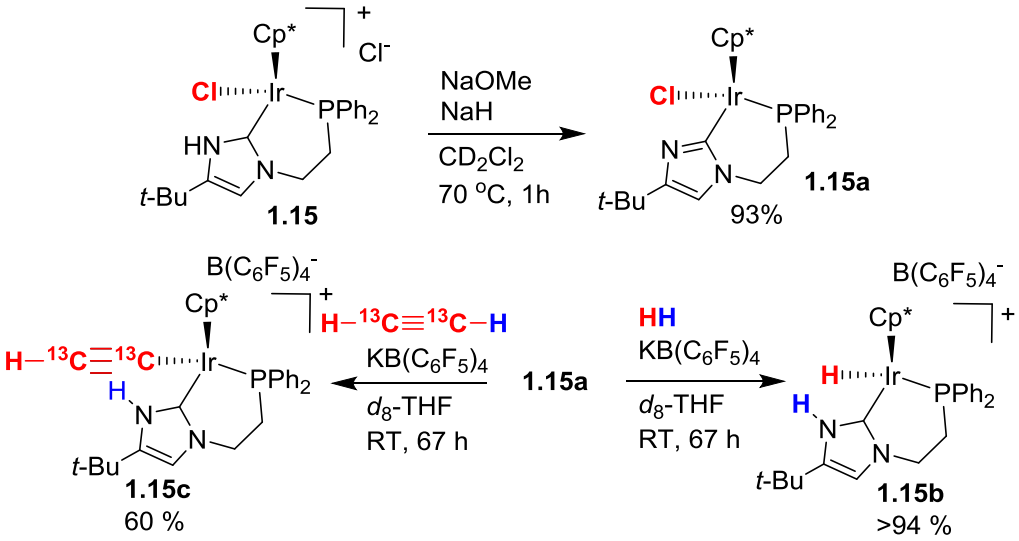

Figure 1.7. Work previously done in the Grotjahn lab showing bond activation of hydrogen gas and acetylene by conjugate bases of PNHC complexes.

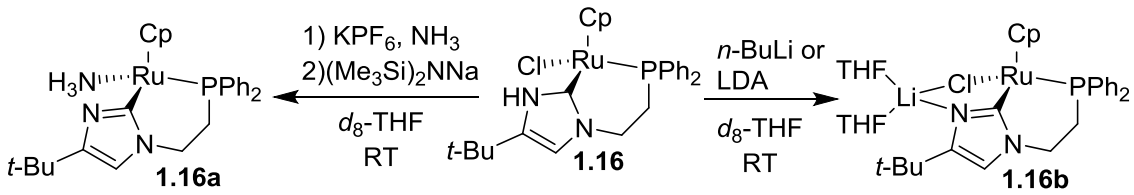

Figure 1.8. Work previously done in the Grotjahn lab showing formation of an imidazole-2-yl complex **1.16a** or LiCl adduct **1.16b** depending on the base used.

Hahn and co-workers made tetrakis-PNHC complexes of type **1.12**, and related Fe species,[34,57] that are coordinatively saturated which may prevent further chemistry at the metal, although alkylation of the nitrogens was demonstrated. Cossairt et al. were capable of forming a bis PNHC complex using phosphine-facilitated direct metalation,[48] however their product was coordinatively saturated. Kunz et al. reported **1.14**, made as discussed earlier using a three-step protecting group strategy, but without an indication of its chemistry, other than aqueous acid stability.[44]

We wanted to study complexes like **1.12** and **1.14** that have more than one PNHC ligand on the metal, but make complexes that would maintain an open site. To do this, we

wanted to utilize the well-known stability of pincer complexes[13,22,58-62], and the ability to form a rigid pre-arranged structure. One target design would be **1.17** (Figure 1.9), containing two NH moieties in close proximity to the open site of the metal, bridged together by a linker. **1.17** could then be deprotonated, giving an intriguing structure **1.17a**, where now the complex would contain a proton donor as well as a proton accepting ligand. Looking for analogs of **1.17** gave ligand design ideas; Kunz published complexes **1.18a**[63] and later **1.18b**-**1.18g**[64], which are typical NHC complexes but whose X-ray crystal structures showed favorable accommodation of a metal in the binding pocket (Figure 1.9). However, the challenge now becomes synthesizing a PNHC complexes because different synthetic routes than for normal NHC analogs are required. The carbazole NH moiety could assist in metalation, for example by losing the NH

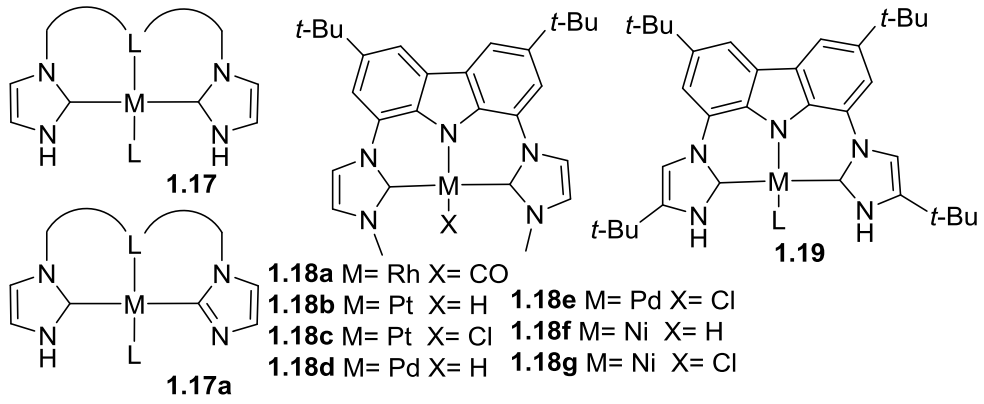

Figure 1.9. Structures of complexes leading to identification of the target molecule **1.19**.

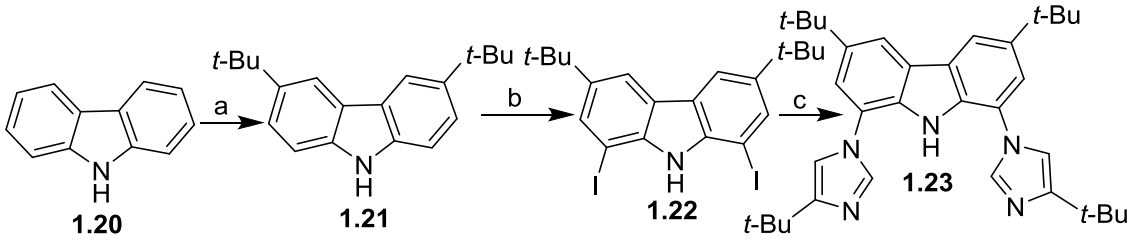

Figure 1.10. Synthesis of ligand **1.23**.
(a) **1.20** (1.0 equiv), $ZnCl_2$ (3.0 equiv), 2-chloro-2-methyl-propane (2.5 equiv), nitromethane, RT, 15 h, 75% yield. (b) **1.21** (1.0 equiv), $PhCH_2NEt_3^+$ ICl_2^- (2.5 equiv), acetic acid, sulfuric acid, 7 h, 75 ^oC, 53% yield. (c) **1.22** (1.0 equiv), 4-*tert*-butyl imidazole (5.0 equiv), $Cs(CO_3)_2$ (2.2 equiv), $(CuOTf)_2$ benzene complex (20 mol %), 1,10-phenanthroline (2.0 equiv), dibenzylideneacetone (20 mol %), dry toluene, 14 d, 120 ^oC, 62 % yield.

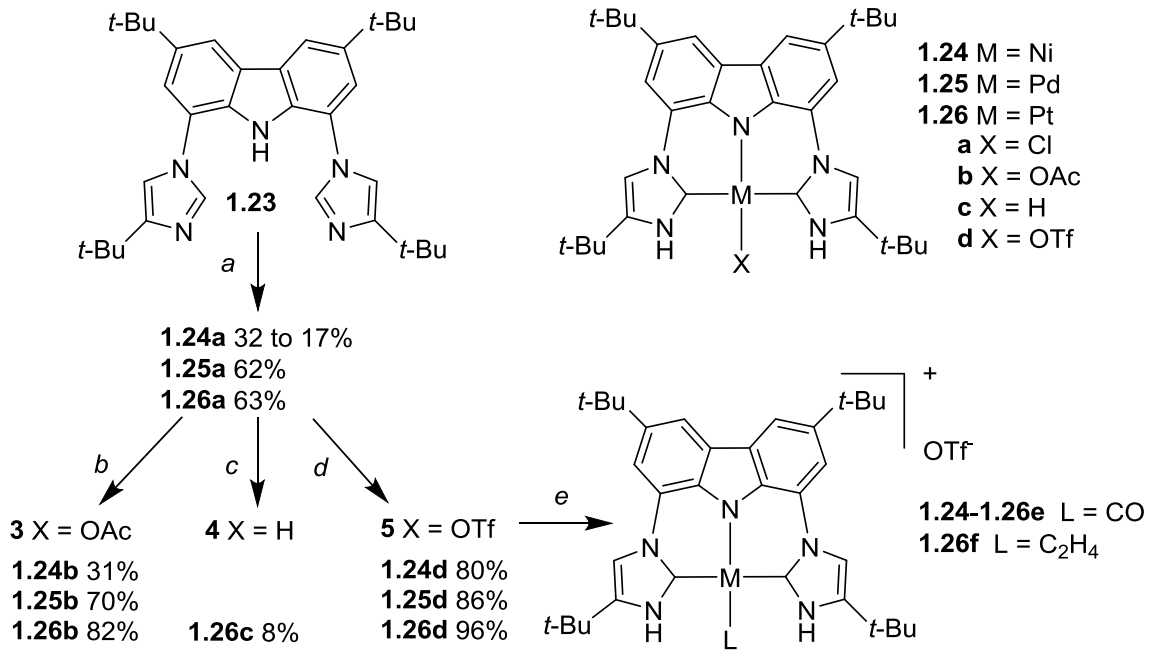

Figure 1.11. Synthesis of complexes **1.24-1.26**.
(a) for **1.24a**: **1.23** (1.0 equiv), $Ni(OAc)_2$ (2.0 equiv), AcOH (2.4 equiv), benzene, 10 d, 150 ^oC, 32 to 17 % yield; NaCl, for **1.25a**: **1.23** (1.0 equiv), $Pd(OAc)_2$ (1.1 equiv), AcOH (1.9 equiv), benzene, 7 d, 70 ^oC, 62 % yield; NaCl, for **1.26a**: **1.23** (1.0 equiv), $PtCl_2(COD)$ (1.05 equiv), benzene, 6 d, 100 ^oC, 63 % yield. (b) for **1.24b**: AgOAc (1.15 equiv), acetone, 13.5 h, RT, 31 % yield, for **1.25b**: AgOAc (1.07 equiv), acetone, 15 h, RT, 70 % yield, for **1.26b**: AgOAc (1.09 equiv), acetone, 12 h, RT, 82 % yield. (c) for **1.26c**: $NaBH_4$ (4.3 equiv), THF, 20 h, 70 ^oC, 8 % yield. (d) for **1.24d**: AgOTf (1.05 equiv), THF, 40 min, RT, 80 % yield, for **1.25d**: AgOTf (1.07 equiv), acetone, 1 h, RT, 86 % yield, for **1.26d**: AgOTf (1.2 equiv), THF, 7.5 h, RT, 96 % yield. (e) for **1.24e-1.26e**: CO (1 atm), d_6-benzene, characterized in situ. (f) for **1.26f**: ethylene (1 atm), d_6-benzene, characterized in situ.

proton and forming a N-metal bond, but to avoid potentially problematic coordination at the pendant imidazole nitrogen or on the back of the imidazole ring, not the target C-2 position, *tert*-butyl groups on the imidazoles were used to disfavour undesired metalation at those positions, to enhance chances of forming structure **1.19**.

C. Ligand and PNHC Complex Synthesis

Synthesis of **1.23** was done on multigram scale giving a 37% overall yield in three steps from carbazole, **1.20**. The *tert*-butylation method of Hou[65] using $ZnCl_2$ as a Lewis acid gave 3,6-di-tert-butyl-carbazole, **1.21**, in a good yield (75 %), which was subjected to electrophilic iodination, described by Nakada[66] on a like compound, utilizing $PhCH_2NEt_3^+$ ICl_2^-,[67] yielding 1,8-di-iodo-3,6-di-tert-butyl-carbazole, **1.22**, in moderate

53 % yield. Then copper-catalyzed coupling described by Kunz[63] but using 4-*tert*-butylimidazole[68] in a much longer reaction time of 14 d gave **1.23** in 62 % yield. The difference in reaction times may be ascribed to the more hindered *tert*-butyl imidazole coupling partner (Figure 1.10).

In the first attempts to form metal complexes using **1.23**, metals of square planar geometry were targeted so that the fourth coordination site would be proximal to the NH of the PNHCs. Even though to our knowledge there is no report of a Group 10 metal making PNHC complexes by direct metalation, Pd(II) and Pt(II) were explored first, because of their extensive C-H metalation literature.[59,69] Ligand **1.23** was metalated using $Cl_2Pt(COD)$ at 100 ^oC for 6 d (Figure 1.11), which was then purified by silica column chromatography giving Pt analog **1.26a** in 63 % yield. After experimentation, it was found that the best way to make **1.25a** was to use $Pd(OAc)_2$ to enable metalation, but attempts at purification of **1.25b** by silica column chromatography were unsuccessful. The reaction mixture was then treated with aqueous NaCl, converting crude acetate product to the chloride analog, **1.25a**, which was then purified by silica column chromatography in reasonable yield (62 %). Most remarkably, the Ni chloride analog **1.24a** could be made in a similar manner as the Pd chloride analog, except at a much higher temperature, 150 ^oC, albeit in lower yield after silica column chromatography, 17 %. The acetate in the $Pd(OAc)_2$ and $Ni(OAc)_2$ precursors are believed to help in the metalation process. Carboxylate-assisted C-H bond activation is widespread, where various proton-shuttling roles have been suggested.[70-72]

The chlorides **1.24a**-**1.26a** were converted to the acetates, **1.24b**-**1.26b** or triflates, **1.24b**-**1.26d,** using the respective silver salts (Figure 1.11). The CO complexes, **1.24e**-**1.26e,** were formed by bubbling CO through a solution of the triflate complexes **1.24d**-**1.26d**. Removal of solvent from solutions of **1.24e** and **1.25e** led to loss of CO and recovery of **1.24d** and **1.25d**, which suggests that the M-CO bond is weaker in the Ni and Pd cases, than for Pt, which should have the slowest ligand exchange rate out of the three complexes. Bubbling ethene through solutions of **1.24d**-**1.26d** in benzene yielded only the Pt analog **1.25f** as observed by NMR spectroscopy, with no reaction in the Ni and Pd cases. The Pt hydride species **1.25c** was purified by silica gel chromatography and proved

to be air sensitive, whereas attempts at isolating the Pd and Ni hydrides were unsuccessful, as they appear to decompose in solution.

D. X-Ray Crystal Structures

To explore the bonding of the complexes, crystal structures of a number of the analogs were obtained which also showed the tendency of hydrogen bonding. Table 1.3 compares the bond lengths and angles of the PNHC analogs to the NHC analogs synthesized by Kunz. With the exception of **1.26e**, the structures of the new PNHC pincers are close to ideal square planar geometry, with C-M-C and N-M-X angles near 180°. As would be expect in comparing second and third row metals, the bond lengths in comparing second and third row metals, the bond lengths in the Pd and Pt species are

Table 1.3. Key bond lengths (Å) and angle (°) from the crystal structures of PNHC complexes and aprotic complexes.

complex	C-M (Å)	N-M (Å)	X-M (Å)	C-M-C (°)	N-M-X (°)
1.18a[63]	2.060(6), 2.047(5)	2.028(4)	1.814 (6)	166.68(19)	161.0(2)
1.25a	2.006(4), 1.998(4)	1.961(3)	2.3424(12)	175.43(17)	178.09(10)
1.18c[64]	2.037(4), 2.037(5)	1.991(3)	2.3477(13)	164.8(2)	160.80(12)
1.26a	2.007(2), 2.014(2)	1.9627(19)	2.3451(6)	176.29(9)	179.85(6)
1.24b[a]	1.8902(16), 1.8920(16)	1.8259(13)	1.9067(11)	175.95(7)	174.84(5)
1.25b[b]	2.003(4)[c]	1.957(5)	2.035(5)	177.7(2)	180.0[c]
	2.014(5)	1.947(5)	2.052(6)	177.1(3)	180.0[c]
1.26c	2.007(3), 2.012(3)	2.027(2)	1.46(3)	177.07(10)	178.9(12)
1.18b[64]	2.032(3)	2.019(2)	1.590	179.13(15)	180.0
1.25d[b]	2.017(6), 2.006(6)	1.952(7)	2.111(7), 2.11(3)	178.2(3)	172.8(2), 166.0(8)
	2.007(6)[d]	1.954(10)	2.097(10)[d]	179.1(4)	170.0(3)[d]
1.26e	2.017(3), 2.020(3)	1.973(3)	1.864(4)	164.41(13)	167.63(13)

[a] HOAc solvate molecule donates a hydrogen bond to the bound OAc; no intramolecular NH---OAc interaction (Fig. 1.12). [b] Two independent molecules in unit cell, values for each given on separate rows. [c] Crystal structure refinement determined N-M-X angle to be 180° with no uncertainty and C-M distances equal; –OAc atoms refined at 50% occupancy. [d] OTf refined at 50% occupancy.

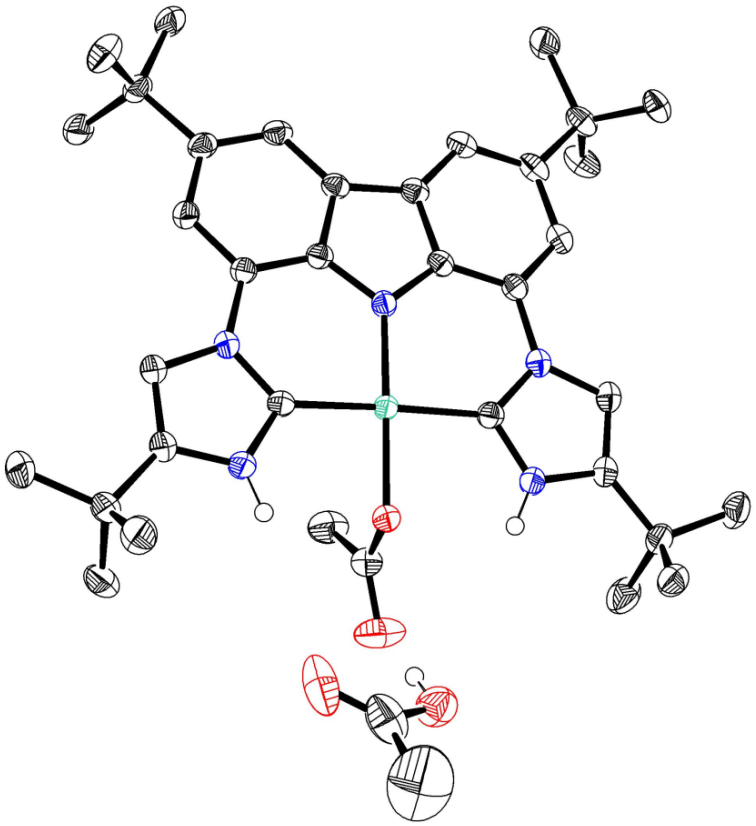

Figure 1.12. Crystal structure of **1.24b** (Ni-OAc), C = black, N = blue, O = red, H = white sphere, and Ni = green. Hydrogens attached to carbons were excluded for clarity.

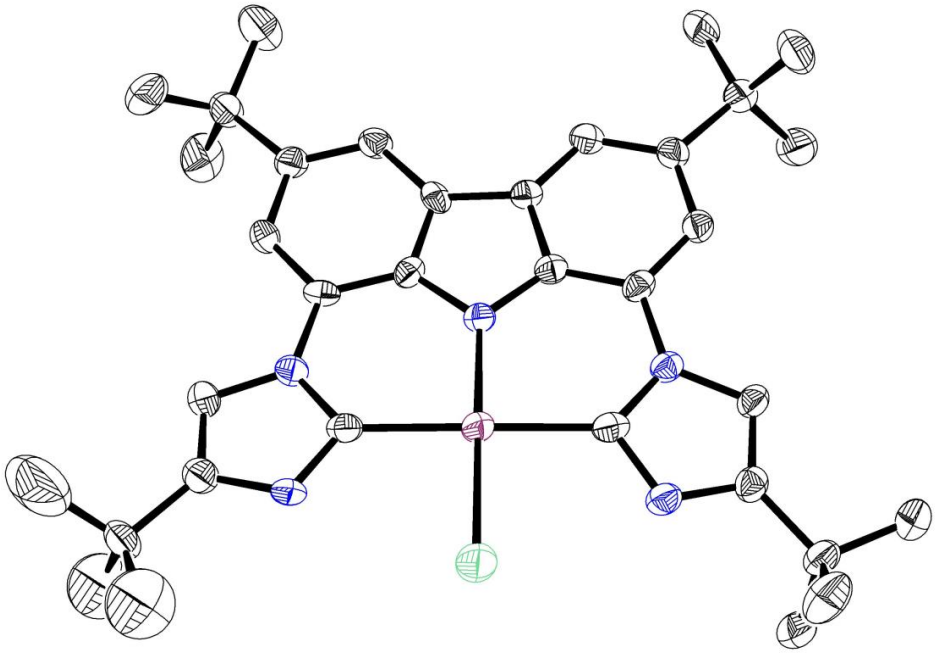

Figure 1.13. Crystal structure of **1.25a** (Pd-Cl), C = black, N = blue, and Pd = maroon. All hydrogens and solvent molecules were excluded for clarity.

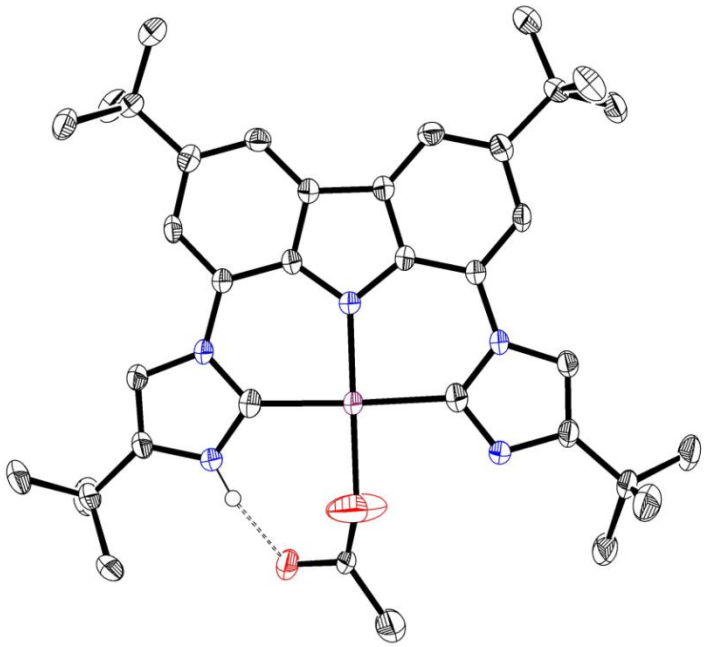

Figure 1.14. Crystal structure of **1.25b** (Pd-OAc), C = black, N = blue, O = red, H = white sphere and Pd = maroon. All hydrogens not involved in hydrogen bonding were excluded for clarity. Structure shows hydrogen bonding between the acetato ligand and one NH wingtip.

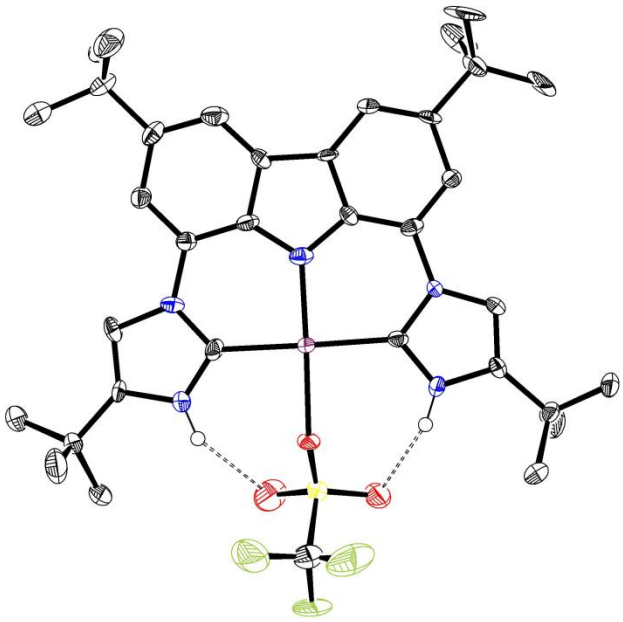

Figure 1.15. Crystal structure of **1.25d** (Pd-OTf), C = black, N = blue, O = red, S = yellow, F = green, H = white sphere and Pd = maroon. All hydrogens not involved in hydrogen bonding were excluded for clarity. Structure shows concurrent interaction of the triflato ligand and two NH wingtips. For the two independent molecules in the unit cell, H-bond networks exhibited d(H---O) = 2.087 to 2.676 Å.

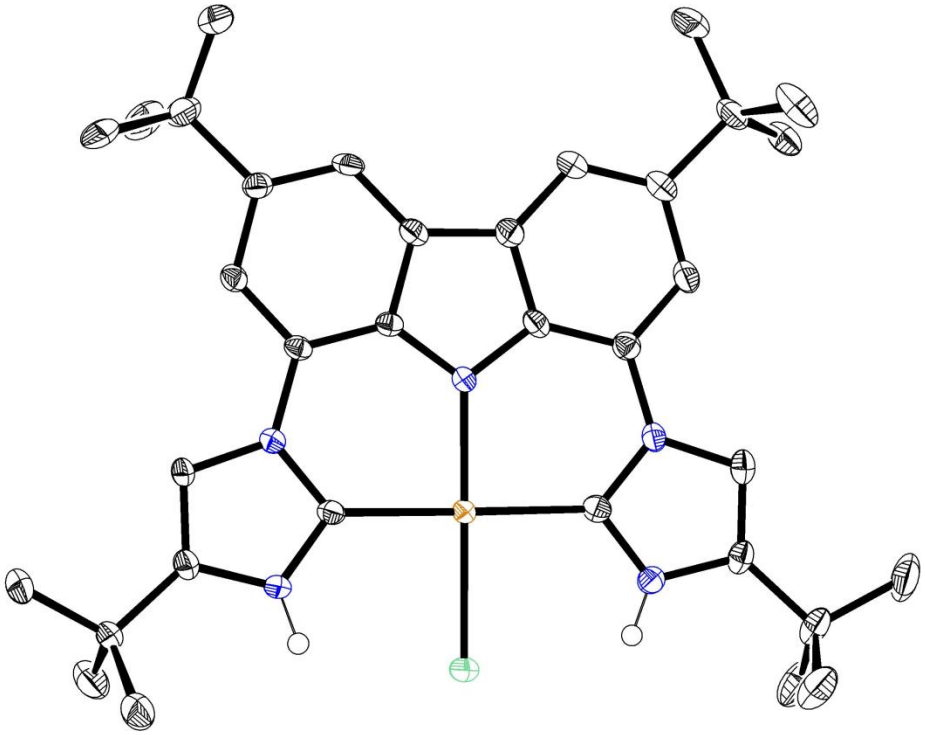

Figure 1.16. Crystal structure of **1.26a** (Pt-Cl), C = black, N = blue, Cl = green, H = white sphere and Pt = copper color. Hydrogens attached to carbons were excluded for clarity.

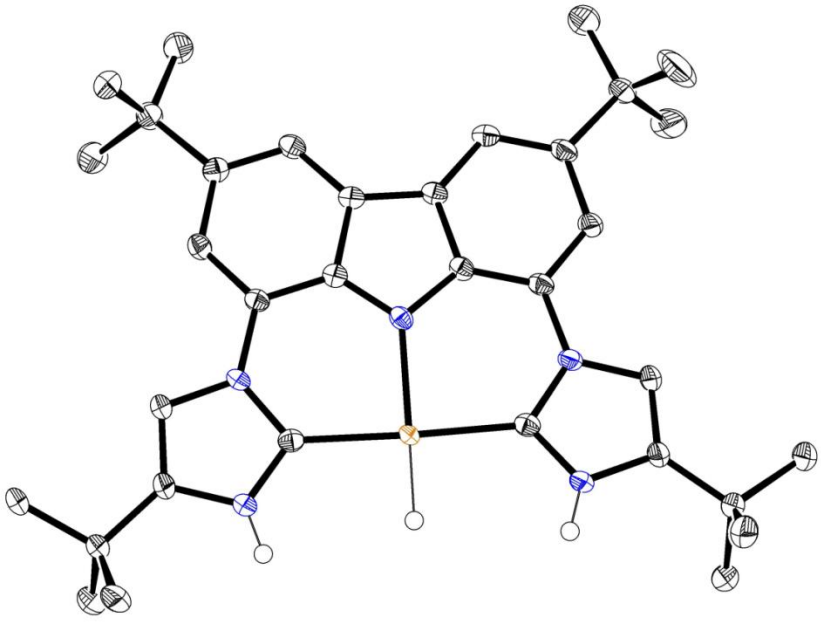

Figure 1.17. Crystal structure of **1.26c** (Pt-Cl), C = black, N = blue, H = white sphere and Pt = copper color. Hydrogens attached to carbons were excluded for clarity.

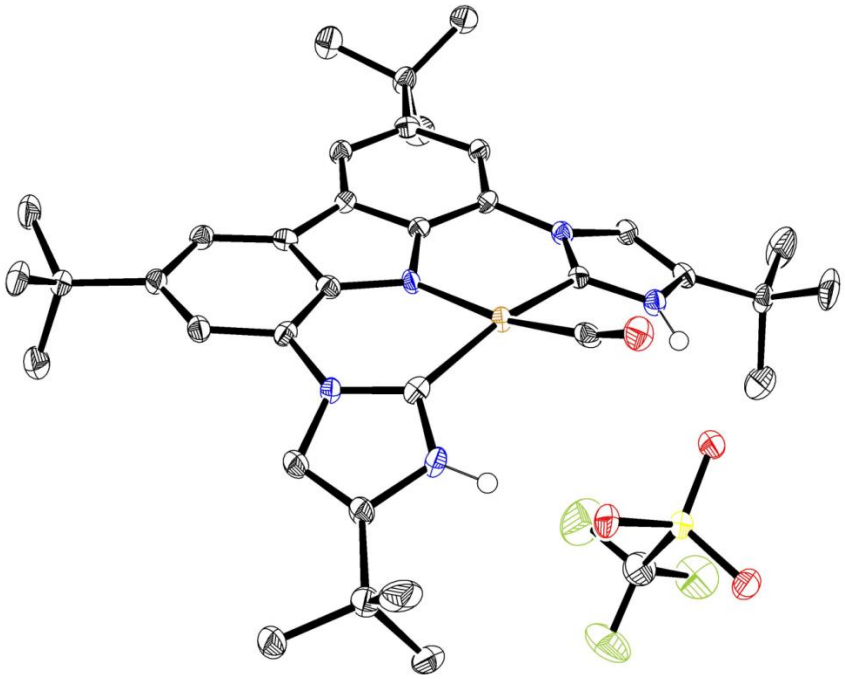

Figure 1.18. Crystal structure of **1.26e** (Pt-CO)OTf, C = black, N = blue, O = red, S = yellow, F = green, H = white sphere and Pt = copper color. All hydrogens not involved in hydrogen bonding were excluded for clarity. Structure shows bonding between the free triflate and both NH wingtips. For the two H-bonds, d(H---O) = 1.993(13), d(N---O) = 2.849(4) Å, <(N-H---O) = 167(3)^{o} , and d(H---O) = 2.055(16), d(N---O) = 2.873(4) Å, <(N-H----O) = 159(3)^{o}.

similar, whereas the first-row Ni complex, **1.24b**, shows shorter bonds than Pd analog **1.25b**.

According to structures from X-ray crystallography, complexes with acetato and triflato ligands (**1.25b** and **1.25d**) exhibit intramolecular hydrogen bonding, whereas intermolecular hydrogen bonding was seen in **1.26e**. The structure of **1.25b** (Figure 1.14) shows that the acetato ligand interacts with one NH, whereas **1.25d** (Figure 1.15) shows that the triflato ligand interacts with both NH moieties concurrently. For both **1.25 b** and **d**, the pincer ligand is essentially planar, but is able to accommodate the asymmetry introduced by the tetrahedral sulfur of the triflate in **1.25d**. The planarity of the pincer ligand can be examined by looking at the dihedral angle between the bond between PNHC carbene C and protic N atoms, and the bond between metal and coordinated atom of X or L, which in the case of **1.25b** is 3.2 and 4.7^{o} for the two independent molecules in the unit cell, and for **1.24d** is slightly larger (9.5, 11.1^{o}). Complex **1.25e** shows greater

distortion with the CO ligand between the two PNHC pincer arms, and now the triflate shows stronger hydrogen bonding, as evidenced by shorter distances between the PNHC NH and triflate oxygen. The relative orientation of the CO ligand and the two PNHC ligands can be defined by the torsion angles (H)N-C-Pt-C(O) = 34.7 and 35.4°; and for **1.18a**, (CH_3)N-C-Rh-C(O) = 29.6 and 41.6°). The interligand angles across the metal for **1.26e** (164.4, 167.6°) also reflect distortions, which show the ability of the pincer backbone to alter the typical square planner geometry which might be important for catalysis.

E. NMR and IR Data

IR and NMR spectroscopy were explored to examine if the hydrogen bonding persisted in solution and not just the solid state. A combination of COSY, HSQC, and HMBC data were used to establish connectivity and assign all ^{1}H, ^{13}C, and ^{15}N signals. All of the complexes were characterized in d_6-benzene. The greatest change was seen in the NH ^{1}H chemical shift (Table 1.5); the chloride analogs (**1.24-1.26a**), with no hydrogen bonding, compared to the acetate compounds (**1.24-1.26b**) show that the NH

Table 1.4. ^{15}N NMR chemical shifts (ppm).

metal	atom	N1= NH of PNHC	N2 = aprotic N of PNHC	N3 = carbazolyl N
Ni	**1.24a** (Cl)	-201.8	-192.8	-293.5
	1.24b (OAc)	-199.1 (**2.7**)	-192.8 (0.0)	-310.7 (-17.2)
	1.24d (OTf)	-204.4 (-2.6)	-191.8 (1.0)	-321.6 (-28.1)
	1.24e	-195.5 (**6.3**)	-191.6 (1.2)	nd
Pd	**1.25a** (Cl)	-205.9	-194.5	-277.1
	1.25b (OAc)	-198.3 (**7.6**)	-195.1 (-0.6)	-295.6 (-18.5)
	1.25d (OTf)	-205.5 (0.4)	-193.8 (0.7)	-300.3 (-23.2)
	1.25e	-196.8 (**9.1**)	-192.9 (1.6)	-259.4 (17.7)
Pt	**1.26a** (Cl)	-210.6	-197.9	-298.4
	1.26b (OAc)	-200.3 (**10.3**)	-197.6 (0.3)	-324.6 (-26.2)
	1.26c (H)	-191.9 (18.7)	-196.2 (1.7)	nd
	1.26d (OTf)	-207.1 (3.5)	-196.4 (1.5)	-330.5 (-32.1)
	1.26e	-196.1 (**14.5**)	-195.8 (2.1)	-266.8 (31.6)

[a] Natural abundance material in d_6-benzene, using ^{1}H-^{15}N gHMBC. Differences between X = Cl in parentheses. "nd" = not detected.

Table 1.5. ^{1}H NMR data[a].

complex	HN [^{15}N satellites][b]	H2b	H3	H5	H6b	H7	X
1.24a	11.32 (br s) [dd, $^{1}J_{H^{15}N}$ = 99.3, $^{3}J_{HH}$ = 2.2]	0.94 (s)	7.24 (dd, 2.2, 0.5)	7.58 (dd, 1.6, 0.5)	1.52 (s)	8.38 (d, 1.6)	-
1.24b	12.88 (s)	1.13 (s)	7.26 (d, 2.1)	7.59 (d, 1.9)	1.51 (s)	8.32 (d, 1.8)	2.24 (s)
1.24d	11.01 (s)	1.14 (s)	7.14 (d, 2.3)	7.53 (d, 1.9)	1.49 (s)	8.30 (d, 1.9)	-
1.24e	12.75 (s)	1.24 (s)	7.15 (d, 1.6)	7.63 (d, 1.8)	1.51 (s)	8.38 (d, 1.7)	-
1.25a	11.20 (br s) [dd, $^{1}J_{H^{15}N}$ = 100.3, $^{3}J_{HH}$ = 2.3]	0.92 (s)	7.30 (dd, 2.3, 0.6)	7.68 (dd, 1.6, 0.6)	1.54 (s)	8.48 (d, 1.6)	-
1.25b	13.91 (br s) [dd, $^{1}J_{H^{15}N}$ = 96.5, $^{3}J_{HH}$ = 2.1]	1.16 (s)	7.33 (dd, 2.2, 0.7)	7.67 (dd, 1.6, 0.7)	1.53 (s)	8.43 (d, 1.6)	2.32 (s)
1.25d	11.16 (br s) [dd, $^{1}J_{H^{15}N}$ = 99.9, $^{3}J_{HH}$ = 2.1]	1.10 (s)	7.20 (dd, 2.1, 0.6)	7.61 (dd, 1.6, 0.6)	1.51 (s)	8.41 (d, 1.6)	-
1.25e	12.36 (s)	1.20 (s)	7.11 (d, 1.9)	7.64 (d, 1.6)	1.50 (s)	8.43 (d, 1.6)	-
1.26a	11.29 (br s) [dd, $^{1}J_{H^{15}N}$ = 100.1, $^{3}J_{HH}$ = 2.3]	0.92 (s)	7.34 (dd, 2.3, 0.6)	7.67 (dd, 1.6, 0.6)	1.53 (s)	8.48 (d, 1.6)	-
1.26b	13.81 (br s) [dd, $^{1}J_{H^{15}N}$ 96.5, $^{3}J_{HH}$ = 2.2]	1.16 (s)	7.38 (dd, 2.2, 0.6)	7.67 (dd, 1.6, 0.6)	1.52 (s)	8.42 (d, 1.6)	2.29 (s)
1.26c	12.75 (s)	0.81 (s)	7.43 (d, 2.2)	7.92 (d, 1.6)	1.56 (s)	8.60 (d, 1.6)	-7.77 ($^{1}J_{H^{195}Pt}$ = 1160)
1.26d	11.11 (br s) [dd, $^{1}J_{H^{15}N}$ = 99.6, $^{3}J_{HH}$ = 2.2]	1.10 (s)	7.23 (dd, 2.1, 0.6)	7.62 (dd, 1.6, 0.6)	1.50 (s)	8.40 (d, 1.5)	-
1.26e	12.40 (br s) [dd, $^{1}J_{H^{15}N}$ = 99.6, $^{3}J_{HH}$ = 2.0]	1.24 (s)	7.15 (d, 1.9)	7.66 (1.5)	1.49 (s)	8.39 (d, 1.5)	-

[a] Chemical shifts in ppm, referenced from the resonance for C_6HD_5 = 7.16 ppm. Coupling constants *J* (Hz) are listed after multiplicity, observed at 600 MHz, 30 °C. The *J* values were determined by using a shifted sine bell weighting function. Instead of using the difference of the top of the peaks, the difference of the center of the peak at its widest point were used, followed by the averaging of like coupling constants for a given proton. [b] Small satellite peaks seen on either side of main large broad NH resonance.

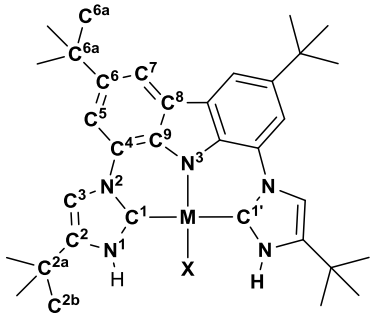

Table 1.6. Solution phase IR data (cm^{-1}).[a]

complex	M	X or L	ν (NH)	Δ from chloride[b]	ν(CO)
1.24a	Ni	Cl	3363.3 (s)	-	
1.24b[c]		OAc	3403.9 (s) 2650 (vb)	40.6 -713	
1.24d		OTf	3331.2 (b)	-32.1	
1.24e		CO^+ $^-$OTf	3190.6 (vb)	-172.2	2092.8 (s)
1.25a[c]	Pd	Cl	3373.7 (s)	-	
1.25b[c]		OAc	3359.3 (s) 2668 (vb)	-14.4 -706	
1.25d		OTf	3320.5 (b)	-53.2	
1.25e		CO^+ $^-$OTf	3249.8 (b)	-123.9	2120.6 (s)
1.26a	Pt	Cl	3383.5 (s)	-	
1.26b[c]		OAc	3384.7 (s) 2690 (vb)	1.2 -695	
1.26d		OTf	3338.6 (b)	-44.9	
1.26e		CO^+ $^-$OTf	3206.8 (b)	-176.7	2092.1 (s)

[a] C_6H_6 solutions in a CaF_2 cell. "s" = sharp, "b" = broad, "vb" = very broad. See Figures 1.27 -1.39 for spectra. [b] Change in absorbance from that of corresponding chloride complex. [c] d_6-benzene solution.

peak was shifted downfield by 1.56 to 2.71 ppm, which is evidence that the intramolecular hydrogen bonding persists in solution. To study bonding further, ^{15}N chemical shifts were examined (Table 1.4).[56,73] For the PNHC nitrogen incapable of hydrogen bonding (N2), δ_N hardly changes between the complexes. In contrast, δ_N for the NH nitrogen (N1) is sensitive to X, as would be expected, there is a downfield shift going from the chloro analog to acetato which is 2.7 for nickel, 7.6 for palladium, and 10.3 for platinum (green boldface entries for **1.24-1.26b**). A similar trend of downfield shifts comparing the chloro analogs to the CO complexes with a shift of 6.3 for Ni, 9.1 for Pd, 14.5 for Pt (blue entries for **1.23-1.25e**). Another notable change is the sensitivity of δ_N for the carbazolyl nitrogen (N3) to the change of X, being 17 to 32 ppm upfield for X = OAc and OTf compared with X = Cl, and 17.7 to 31.6 ppm *downfield* for X = CO. Keeping X constant but comparing the different metals show that, δ_N for the carbene nitrogens shifts upfield in the order Ni, Pd, Pt, but for N3 the order is Pd, Ni, Pt.

Another solution phase characterization method used IR spectra in benzene, the same (though for IR, usually undeuterated) solvent as for the NMR spectra. The NH peaks for the chloride analogs **1.24-1.26a** were relatively sharp between 3360-3380 cm^{-1} (Table 1.6). In contrast, for the acetate complexes **1.24-1.26b**, there was still one sharp peak at a similar frequency as the chloride NH, but also one very broad peak was

centered around 2650 cm^{-1}. We explain these observations by noting that on the time scale of the IR experiment, both distinct NH environments are seen: one NH is donating a hydrogen bond to the acetate, as evidenced by the very broad peak that is shifted to a lower wave number, and the other NH is not, as seen from the sharp peak in the same location as the NH absorbance of the Cl complexes. In contrast, in the case of the ^{1}H NMR spectrum, a single average chemical shift is seen because of rapid (on the NMR time scale) movement of the acetate between accepting a hydrogen bond from one NH group or the other. As for the bound triflate cases **1.24-1.26d** a single slightly broadened NH peak is observed, which is shifted only ~30-50 cm^{-1} lower in frequency than their chloride counterparts, showing that hydrogen bonding to both of the NHs is occurring. When the complexes are ionized to the CO complex **1.24-1.26e** the NH stretch is ~125-175 cm^{-1} lower, showing that the triflate outer sphere ion with greater negative charge is more strongly bonding to both NHs, as seen in the **1.26e** crystal structure. The values for ν(CO) observed from complexes **1.24-1.26e** are similar and not that shifted from the value for free CO, which is consistent with minimal backbonding and observed reversible CO binding.

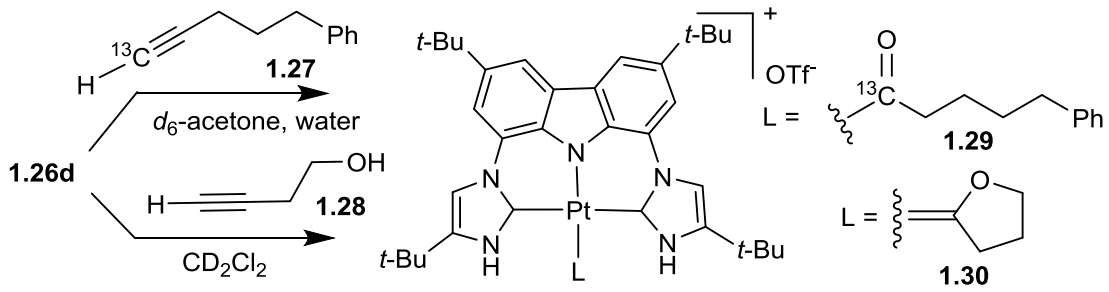

Figure 1.19. Alkyne-derived complexes from complex **1.26d**.

F. Reactivity

Complex **1.26d** has been shown to bind CO or ethylene, so we looked more closely at the reactivity of this Pt complex. Since the triflato ligand was displaced in favour of making a pi complex such as that of ethylene, we decided to look at other pi systems such as alkynes. Hence, **1.26d** was dissolved in a mixture of acetone/water, then 1-hexyne (20 x **1.26d**) was added. The reaction was heated at 70 ^{o}C and a mixture of hexanal and 2-hexanone in ~4 to 1 ratio appeared in increasing amounts throughout the

reaction. In contrast, the proton-catalyzed reaction done without any metal yields 33 times more ketone than aldehyde.[17] The reaction with **1.26d** was monitored by ^{1}H NMR and after 1 h, 14 h, and 24h the yield of hexanal was 7, 63, and 79 % respectively, after which the starting hexyne was completely consumed. Another alkyne, phenylacetylene, was hydrated to the aldehyde, without formation of the isomeric ketone. Reaction of **1.26d** with alkynol **1.28** (Figure 1.19) in CD_2Cl_2 was stoichiometric, giving cyclic carbene complex **1.30**. When **1.26d** was dissolved in d_6-acetone and water, it gave a mixture of two complexes, with a ratio of 2.5 to 1, where the major complex shows a broad 2H singlet consistent with it being an aquo complex. To look in more detail at the formation of aldehyde products, we decided to monitor the reaction while using a ^{13}C-labeled alkyne, **1.27**[74], which led to observing a new species which was identified by 2D NMR as acyl complex **1.29**, based on a broadened resonance with Pt satellites at δ 251.5 ppm. The formation of complexes **1.29** and **1.30** and formation of the aldehyde product are all consistent with alkyne-to-vinylidene transformation at the pincer active site.[75,76]

G. PNHC Complex Reactivity with Bases and Product Characterization

Exploration of another reactivity mode was inspired by the reactivity described earlier for **1.15a** and **1.16a**, the imidazolyl complexes. The target structure would be **1.31** (Figure 1.20), containing one PNHC proton donor ligand and one basic imidazolyl. The first attempt at synthesis of an analog of **1.31** was done by dissolving **1.25a**, the Pd-Cl complex, in CD_2Cl_2, followed by bubbling ethylene through the solution. The initial ^{1}H NMR spectrum showed unreacted **1.25a** and dissolved ethylene, so the chloride was not labile. Sodium *tert*-butoxide was then added to the reaction mixture and after 2 h the ^{1}H NMR spectrum showed that there was a new unsymmetrical species that exhibited seven aromatic peaks, all integrating to one proton, with one of the seven presumably being the NH proton, which would fit for a complex like **1.31** where L = ethylene and M = Pd. To confirm the structure, crystals were grown by vapor diffusion of pentanes into benzene and analysed, but showed the structure was not what was expected, instead that dimer **1.32** had formed, where the open site did not contain ethylene but rather was occupied by an imidazolyl nitrogen from a second half of the complex (Figure 1.23). The Pd and Pt

dimer complexes were synthesized intentionally from the chloro analogs in CD_2Cl_2 with tert-butoxide giving **1.32-Pd** and **1.32-Pt** respectively (Figure 1.21).

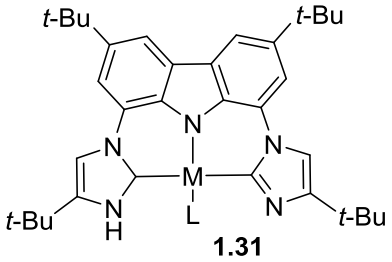

Figure 1.20. Target imidazolyl complex, **1.31**.

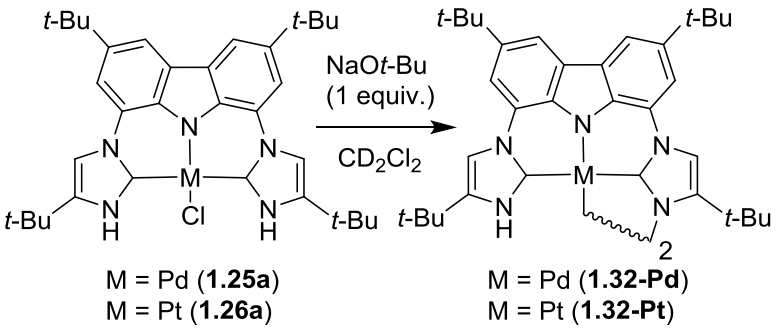

Figure 1.21. Synthesis of dimer structures **1.32-Pd** and **1.32-Pt**.

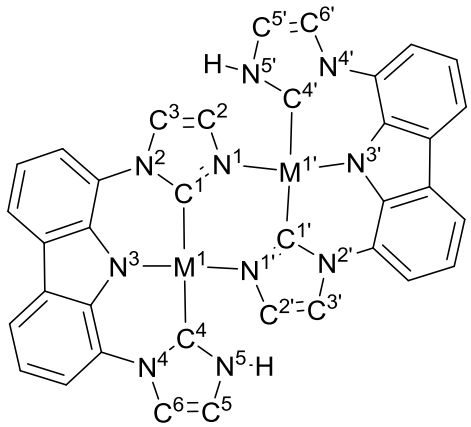

Figure 1.22. Structure showing number used in discussion of dimer complexes.

Looking at the bonding in the crystal structures of the dimer shows that there is strain in the Pd1-N1' (and Pd1'-N1) bond, where the metal is still in the plane defined by the three coordinating atoms of the tridentate ligand (C1, N3, and C4) however the metal relative to the fourth donor atom, the imidazole on the other complex, must bend out of the plane with the N1' imidazole ring because of the adjacent sterics of the *tert*-butyl

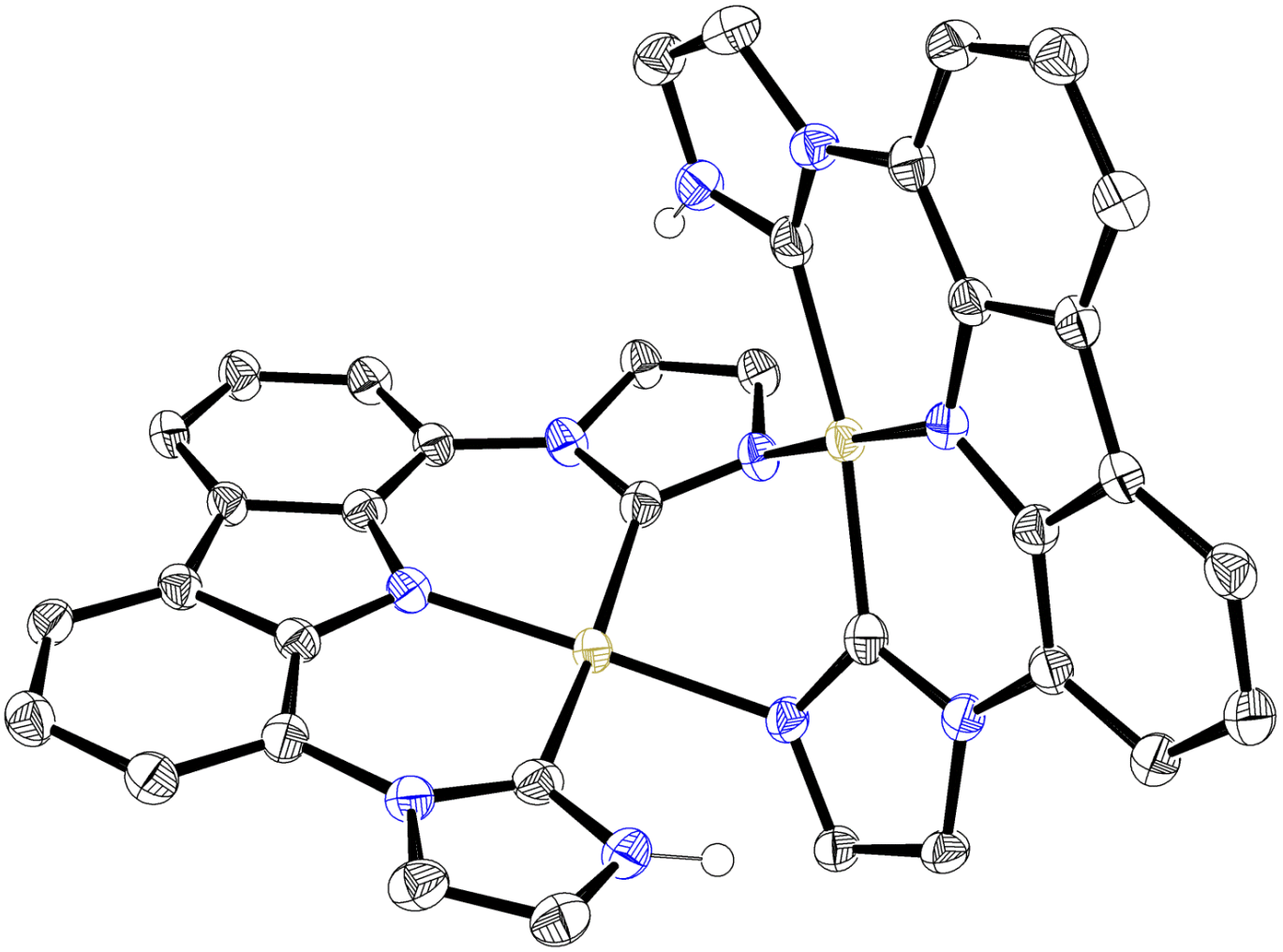

Figure 1.23. Crystal structure of **1.32-Pd**, where atoms of *tert*-butyls, C-H bonds, and solvent have been omitted for clarity.

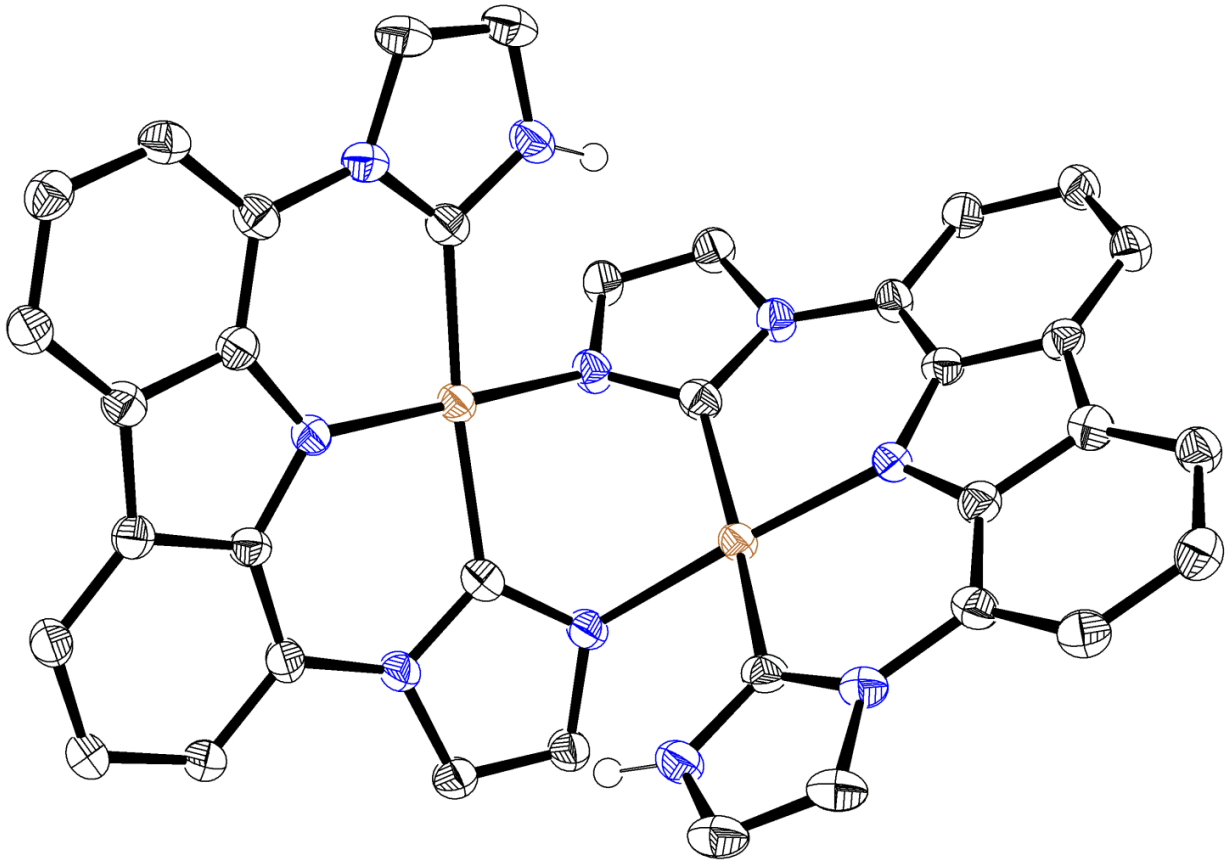

Figure 1.24. Crystal structure of **1.32-Pt**, where atoms of *tert*-butyls, C-H bonds, and solvent have been omitted for clarity.

groups on the imidazole (Figure 1.23 and Figure 1.24, for numbering of atoms see Figure 1.22). The strain can been seen in the distance the metal (Pd1/Pt1 or Pd1'/Pt1') is from the N1' (or N1)-bound imidazole plane (C1'-C2'-C3'-N1'-N2' or C1-C2-C3-N1-N2): for **1.32-Pd** the distance is 1.241 Å and for **1.32-Pt** it is 1.094 Å (Table 1.7). Another piece of evidence to illustrate the strain are the dihedral angles M1-C1-N1-M1' = -40.4(4) ^{o} and 36.5(3) ^{o} for **1.32-Pd** and **1.32-Pt**, respectively, C1-M1-N1'-C1' = 72.4(3) ^{o} and 67.3(2) ^{o} for **1.32-Pd** and **1.32-Pt**, respectively; without strain these values would be approximately zero.

Table 1.7. Key bond lengths (Å) and angle (^{o}) from the dimer crystal structures complexes compared to the monomeric PNHC complexes.

	1.25a	**1.32-Pd**	**1.26a**	**1.32-Pt**
M-N1	-	2.092(3)	-	2.079(3)
M-N3	1.961(3)	1.962(3)	1.9627(19)	1.969(3)
M-C4	2.006(4), 1.998(4)	2.034(4)	2.007(2), 2.014(2)	2.014(3)
M-C1	-	1.984(4)	-	1.996(3)
N3-M-N1	178.09(10)	176.3(1)	179.85(6)	175.6(1)
C1-M-C4	175.43(17)	167.9(2)	176.29(9)	168.3(1)
M out plane[a]	-	1.241	-	1.094

[a]The distance of the metal to the plane defined by the five atoms of the imidazole to which it is N-coordinated; value would be near-zero in absence of strain.

NMR data are consistent with dimers persisting in solution. For the monomeric species such as **1.25a** and **1.26a**, the NH proton resonance is at 11.20 ppm and 11.29 ppm in d_6-benzene, respectively; in contrast, for the dimer complexes the NH signal is strongly shifted upfield to 8.03 for **1.32-Pd** or 8.19 ppm for **1.32-Pt**, which is a 3.17 ppm or 3.20 ppm shift, respectively. Looking at the crystal structures for insight to explain the shift of the NH resonance, it is apparent that both NH moieties in the **1.32-Pd** and **1.32-Pt** complexes are located above the π system of the imidazole ring of the other half of the dimer, which would be expected to shield the NH and cause a significant upfield chemical shift (See Figure 1.23 and Figure 1.24 for the crystal structures). To probe the location of the NH in more detail a ROESY experiment was done for both complexes, where for **1.33** (Figure 1.62) shows that there is a through-space correlation between the NH (N5', Figure 1.22) and the proton on the imidazole ring that is believed to be

shielding the proton (C3, Figure 1.22), which would be impossible for a monomeric structure.

H. Synthesis, Characterization, and Reactivity of Lithium Chloride Adducts

Attempts at synthesis of **1.31** using sodium alkoxide bases led to the formation of dimer structures **1.32-Pd** and **1.32-Pt** with the presumed loss of NaCl. Another route for the synthesis would be using lithium bases which could give lithium chloride adducts **1.33**, a promising route because LiCl adduct **1.16b** was isolable yet highly reactive. For the synthesis of **1.33-Pt**, **1.26a** was dissolved in a mixture of dry THF (0.7 mL) and d_6-benzene (0.1 mL), after an initial ^{1}H NMR spectrum, one equivalent of LDA was added which deprotonated one of the PNHC as seen by NMR spectroscopy giving **1.33-Pt**, without evidence of dimer formation. **1.34-Pt** was then formed by the addition of a second equivalent of LDA, which deprotonated the second PNHC. A combination of COSY, HSQC, and HMBC data were used to establish connectivity and assign all ^{1}H, ^{13}C, and ^{15}N signals for **1.26a**, **1.33-Pt**, and **1.34-Pt** in THF (0.7 mL) and d_6-benzene (0.1 mL) (See Figures 1.59-1.61). The ^{1}H NMR spectrum for compound **1.33-Pt** shows the asymmetry in the structure which consists of a single NH peak at 10.90 ppm and six aromatic peaks, which all integrate to one proton. The dimer structure has a similar ^{1}H NMR, however the difference being that the NH proton has large upfield shift in the dimer case, that is not seen here, which appears to be diagnostic. The asymmetry is also observed in the ^{13}C NMR spectrum which contains 18 peaks between 100 and 170 ppm, the peaks for all of the unique aromatic carbons. As for **1.34-Pt** the ^{1}H NMR spectrum has no peak where the NH proton is typically is located, from 10 to 12 ppm, but in the

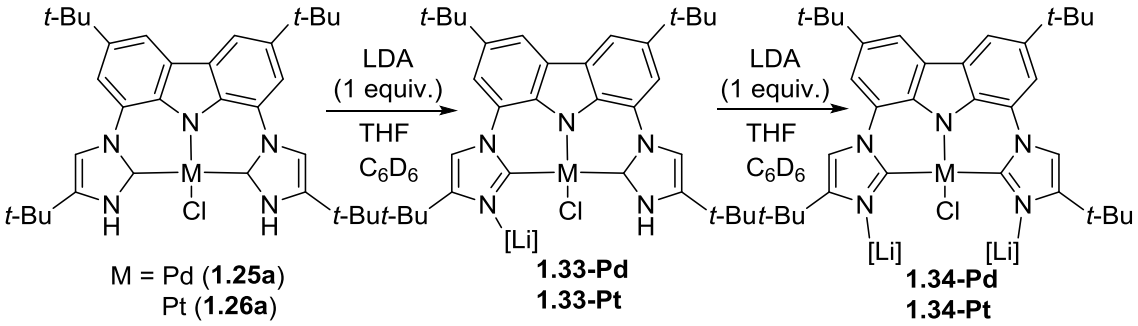

Figure 1.25. Formation of **1.33** and **1.34** by addition of LDA (1 or 2 equiv) in THF (0.7 mL) and d_6-benzene (0.1 mL). .

Table 1.8. ^{15}N chemical shift values (ppm) of the dimer and lithium chloride adduct complexes.

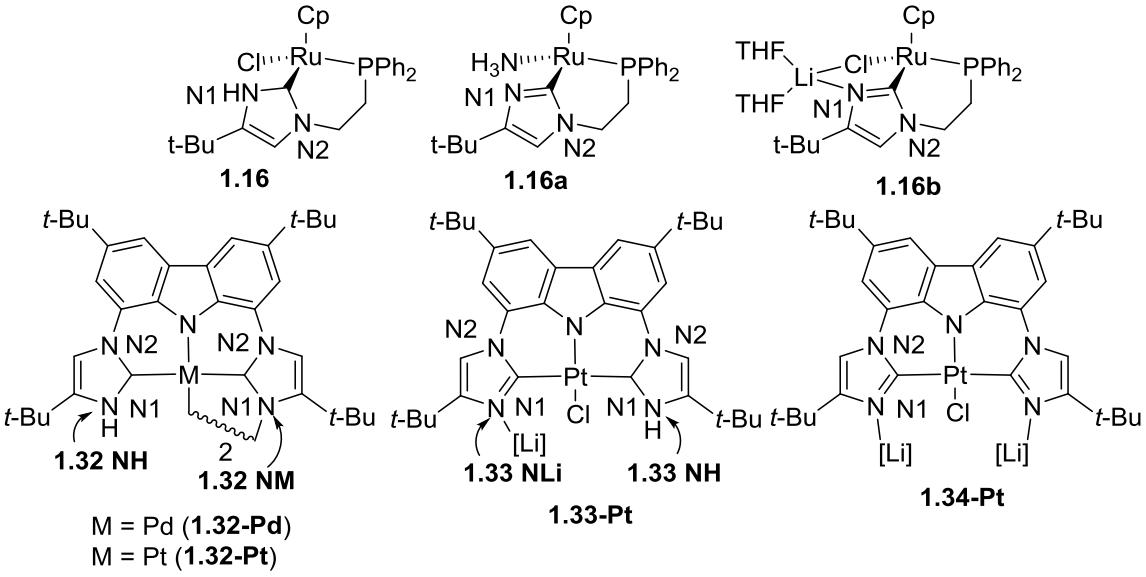

Complex	N1[b]	N2[c]	Δ_x[d]	$\Delta\Delta$[e]
1.16	-197.1	-198.6	1.5	0 (defined)
1.16a	-110.4	-199.9	89.5	88.0
1.16b	-122.1	-196.8	74.7	73.2
1.25a	-210.9	-197.8	-13.1	0 (defined)
1.33-Pt NH	-212.7	-198.4	-14.4	-1.3
1.33-Pt Li	-129.9	-197.3	67.4	80.5
1.34-Pt	-127.4	-192.0	64.7	77.8
1.32-Pd NH	-209.9	-197.0	-12.9	0.3
1.32-Pd NPd	-215.3	-197.8	-17.5	-4.4
1.32-Pt NH	-208.3	-192.6	-15.7	2.6
1.32-Pt NPt	-193.5	-195.8	2.3	17.4

[a] Determined using ^{1}H-^{15}N gHMBC on natural abundance material in THF (0.7 mL) and d_6-benzene (0.1 mL) (**1.25a**, **1.33**, **1.34**), or CD_2Cl_2 (**1.32**). [b] N1 = either NH or derivative of PNHC. [c] N2 = aprotic nitrogen incapable of acid base chemistry. [d] Δ**x** = N1-N2. e$\Delta\Delta$ = Δ**x** - Δref where Δref = -13.1 for **1.25a**-type compounds and 1.5 for **1.16**-type compounds

aromatic region there are only three peaks, showing that symmetry was restored. The ^{13}C NMR spectrum confirms the symmetry which now only consists of 9 peaks between 100 and 170, all of the aromatic carbons.

Previously in this chapter we used ^{15}N chemical shift data to give insight into hydrogen bonding to the NH proton, now we will use it to gain structural insight (Table 1.8), as exemplified by **1.16**, **1.16a**, and **1.16b**. The N1 nitrogen is the nitrogen that shifts depending on the environment surrounding it, whereas N2 the aprotic nitrogen, is incapable of acid base chemistry only shifts very slightly. The Δx value is the difference in the N1 and N2 ^{15}N chemical shifts for the given compound, which is near-zero for a PNHC (**1.16**), showing the similar bonding and charge on the nitrogens. The Δx is greatest for the imidazolyl conjugate base (**1.16a**), where the bonding between the nitrogens is now significantly different. As for the imidazolyl lithium chloride adduct (**1.16b**), Δx is slightly less than for **1.16a** showing that structure **1.16b** is more similar to **1.16a** than to **1.16**. In the following discussion, **1.16** and **1.25a** are considered the reference starting material complexes because they are each neutral PNHC species with M-Cl moieties, and their Δx values are called Δref. For **1.16**, Δref = 1.5, whereas for **1.25a**, Δref = -13.1, a difference that is likely due to a variety of factors having to do with electronics of the non-protic substituent of the PNHC and / or the ring size of the chelates. For a given metal center and mono- or bis-NHC framework, we want to diagnose the effects of chemical changes at N1, hence we introduce the quantity ΔΔ = Δx - Δref to account for the change in Δx that accompanies a chemical change in going from the reference compound to a new species x. Looking at complex **1.32-Pd**, ΔΔ for the NH nitrogen is only 0.3 ppm and that of the NM nitrogen only -4.4 ppm; the ΔΔ values for both nitrogens are relatively unchanged as the carbene character of the ligand is still intact. Interestingly **1.32-Pt** shows a similar small ΔΔ value for the NH (2.6) but a greater ΔΔ for the NM of 17.4 ppm, possibly a result of different ring strain in the Pt case (M out of plane 1.094 Å for **1.32-Pt** vs. 1.241 for **1.32-Pd**) and / or smaller M-N distance [2.079(3) Å vs. 2.092(3) Å for **1.32-Pd**, Table 1.7].

Looking now at **1.33-Pt** and **1.34-Pt**, we note that the deprotonated nitrogens of **1.33-Pt** and **1.34-Pt** show large values of ΔΔ = 80.5 ppm and 77.8 ppm, respectively, thus resembling data for CpRu species **1.16a** and **1.16b** (ΔΔ = 88.0 ppm and 73.2 ppm, respectively). The values of ΔΔ for the deprotonated nitrogens (that bear a Pt or Pd) in crystallographically characterized dimers **1.32-Pt** and **1.32- Pd** are much smaller (17.4, -

4.4). The large ΔΔ values for the deprotonated nitrogens of **1.33-Pt** and **1.34-Pt** could be consistent with either structural formulation as a LiCl adduct or free imidazolyl species, but the dependence of the stability of **1.33** and **1.34** on the presence of chloride (see later) argues strongly for a chloride ligand on the central metal, leading us to assign structures **1.33-Pt** and **1.34-Pt** as LiCl-imidazolyl adducts. All attempts at characterization by crystallography have been unsuccessful due to the very water-sensitive nature of **1.33** and **1.34**, so the environment of the lithium and chloride is unknown but is assumed to be similar to that of **1.16b**, being formed under very similar conditions.

As for reactivity of the imidazolyl complexes, we wanted to explore their bond activation chemistry as was done for **1.16b**. To a freshly prepared solution of **1.33-Pt** in THF and d_6-benzene, an initial ^{1}H NMR spectrum was obtained to check for purity followed by bubbling hydrogen through the solution. After 16 h there was mostly **1.33-Pt** with only a small amount of **1.26a** being regenerated, likely from adventitious water. Addition of AgOTf to the solution did not facilitate H_2 heterolysis, instead it formed dimer complex, **1.32-Pt** (Figure 1.63). To explore if the chloride could be displaced, ethylene was bubbled through a solution of freshly prepared **1.33-Pt** which again gave no reaction with only minor regeneration of **1.26a**, likely from adventitious water (Figure 1.64). Since it appears that water is a problem with the substrates, a rigorously dried substrate, 1-heptene (20 equiv), was added to **1.34-Pt**, which gave no reaction even after heating at 70 ^{o}C for 4 h (Figure 1.65). Unlike imidazolyl complex **1.16b**, it appears that **1.33-Pt** and **1.34-Pt** showed no tendency to lose LiCl. One possible solution is to form a

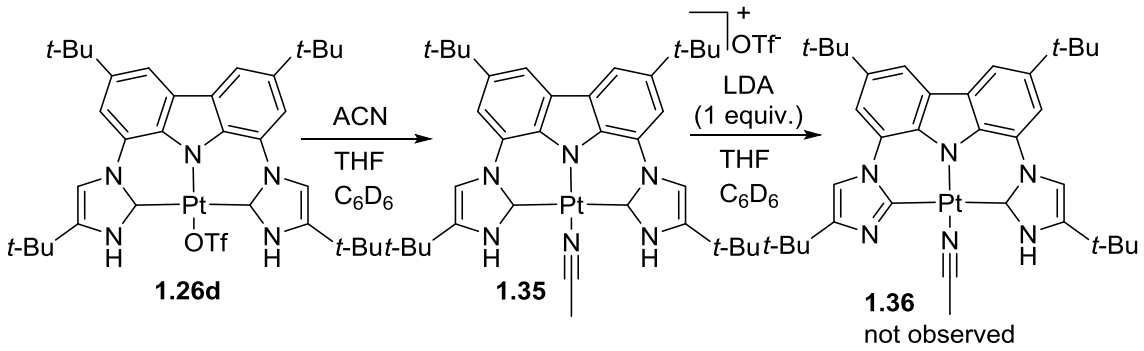

Figure 1.26. Attempted synthesis of complex **1.36** by addition of ACN to **1.26d** giving **1.35**. Addition of LDA to **1.35** did not yield **1.36**, instead it yielded a number of species.

more labile LiOTf adduct by deprotonating **1.26d**, the Pt-OTf complex, but in practice addition of LDA yielded mostly dimer **1.32-Pt** (Figure 1.66). Another thought was to deprotonate the PNHC ligand where the cationic complex contained an L type ligand, such as **1.35**, which was synthesized by addition of acetonitrile (ACN) to **1.26d** in a mixture of THF and d_6-benzene. However addition of LDA (1 equiv) to a solution of **1.35** yielded a number of species (Figure 1.26; for NMR spectra see Figure 1.67).

It appears that LiCl-imidazolyl adduct complexes **1.33-Pt** and **1.34-Pt** have a much slower ligand exchange rate compared to complex **1.16b**, which is not surprising when comparing ruthenium to platinum complexes.[77] Looking for a faster ligand exchange rate than on platinum we explored the palladium complex **1.33-Pd** which was synthesized by the same procedure as **1.33-Pt**. To explore the lability, we went straight to the dry substrate, 1-heptene which was added to a freshly prepared solution of **1.33-Pd** in a mixture of THF and d_6-benzene, but did not react even after heating at 70 ^{o}C for 16 h. One equivalent of LDA was then added to the reaction mixture, generating **1.34-Pd**. After no change was observed, AgOTf was added to **1.34-Pd** which appears to have formed the deprotonated dimer complex by the ^{1}H NMR spectrum (Figure 1.68). So even in the case of the palladium analog, loss of presumedly coordinated LiCl seems too slow to lead to a viable catalyst.

I. Conclusions

In conclusion, we successfully synthesized palladium, platinum, and even nickel bis PNHC pincer complexes, all by direct metalation. Even though the yield in the nickel case was lower, direct metalation forming a PNHC complex with a first-row metal appears to be unprecedented. The structure of the complexes were explored by obtaining X-ray crystal structures which showed a tendency for intermolecular hydrogen bonding, or intramolecular if there is an outer sphere anion, as is the case for **1.26e**. The hydrogen bonding was further explored by NMR and IR spectroscopy which confirmed the observations in the crystal structures. The reactivity of the complexes was tested, and **1.26d** gave mostly the *anti*-Markovnikov hydration productd of alkynes. As for the reactivity of these PNHC complexes with base in an attempt to form a possibly trifunctional complex, **1.31**, we showed that addition of sodium alkoxide bases gave the

dimer complexes **1.32-Pt** and **1.32-Pd**. If LDA was used then we were able to obtain the lithium chloride adducts **1.33-Pt** /**1.33-Pd** or **1.34-Pt**/**1.34-Pd** depending on the amount of LDA that was added. However the ligand exchange rate of the lithium chloride adduct was not great enough for binding of substrates. The addition of an ionizing agent, such as AgOTf, was added to abstract the chloride, but dimer complexes **1.32Pt** or **1.32Pd** formed again. A solution to the above problems of not being able to form a stable complex like **1.31** is that the *tert*-butyl groups are not large enough to stop formation of a metal-nitrogen bond of the basic imidazole, so to stop undesired metalation a larger group than *tert*-butyl would have to be installed on the imidazole.

Part of the material and discussion covered in this chapter is from published work. I would like to thank Evan Darrow, Dr. James Golen, Dr. Curtis Moore, and Dr. Arnold Rheingold, for their contribution to "Hydrogen-bonding pincer complexes with two protic N-heterocyclic carbenes from direct metalation of a 1,8-bis(imidazol-1-yl)carbazole by platinum, palladium, and nickel" which appeared in *Chem. Eur. J.* **2015**, *21*, 10988. I must thank Dr. Curtis Moore, Dr. Arnold Rheingold, and Dr. Douglas Grotjahn for their work on "Reactivity Studies of Bis Protic N-Heterocylic Carbene Complexes1,8-Bis(imidazol-1-ylidene)carbazole Platinum and Palladium under Basic Conditions" which was submitted to *Inorg. Chem.*

J. Experimental Section

Manipulations were carried out in a nitrogen-filled glovebox or using Schlenk techniques unless otherwise specified. THF and diethyl ether were distilled from sodium and benzophenone, whereas dichloromethane and hexane were distilled from calcium hydride under nitrogen, was used as received from Aldrich. d_6-benzene and $CDCl_3$ were purchased from Cambridge Isotope Labs, dried over calcium hydride, and vacuum transferred prior to use. d_6-acetone and CD_2Cl_2 were purchased from Cambridge Isotope Labs, and further deoxygenated by bubbling nitrogen gas through the liquid before being transferred to a glovebox. ^{1}H NMR spectra were obtained on Varian spectrometers, usually at 500 or 600 MHz. ^{13}C NMR and 2D NMR spectra were obtained on the same instruments. Both ^{1}H NMR and ^{13}C NMR chemical shifts were reported in parts per million downfield from tetramethylsilane and referenced to the solvent resonances (^{1}H NMR: 7.16 ppm for C_6HD_5 7.27 ppm for $CHCl_3$, 5.32 ppm for $CHDCl_2$ and 2.05 ppm for d_5-acetone . ^{13}C NMR: 128.39 ppm for d_6-benzene, 77.23 ppm for $CDCl_3$, 54.00 ppm for CD_2Cl_2, and 29.92 ppm for d_6-acetone), where ^{1}H NMR chemical shifts are followed by multiplicity, coupling constants J in hertz, and integration in parentheses.

^{15}N chemical shifts on unlabeled materials were determined from gradient HSQC or HMBC experiments run on a Varian INOVA 600 MHz spectrometer. Sweep widths and the number of increments in the ^{15}N dimension were chosen so as to give digital resolutions in the ^{15}N dimension of less than 1.5 ppm. The ^{15}N chemical shift of a standard reference sample of formamide solution in d_6-dimethylsulfoxide (90%) was determined and set to be −267.8 ppm. Then, using the same sweep width and offsets, samples of nitromethane (1.0 M in $CDCl_3$) and quinine (0.5 M in $CDCl_3$) gave ^{15}N chemical shifts of −4.2 for CH_3NO_2 and −72.4 and −349.2 ppm for the sp^2 and sp^3 hybridized nitrogens of quinine, respectively. Elemental analyses were performed at NuMega Resonance Labs, San Diego, CA.

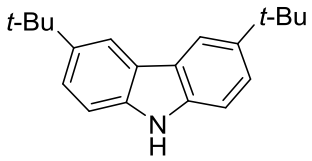

Synthesis of 3,6-di-*tert*-butyl-carbazole (1.21)

To a three neck round bottom flask (500 mL) in the glovebox equipped with a magnetic stir bar was added carbazole (**1.20**, 10.046 g, 59.8 mmol) and $ZnCl_2$ (24.5450 g, 180.1 mmol). The reaction flask was stoppered with septa and transferred to a hood under nitrogen where deoxygenated nitromethane (275 mL) was added, followed by the dropwise addition of 2-chloro-2-methyl-propane (13.881 g, 150.0 mmol) by syringe pump over 20 min. The reaction was allowed to stir for 15 h before water (275 mL) was added in one portion and the resulting mixture was extracted with DCM (400 mL, 2 x 200 mL). The combined organic layers were washed with water (3 x 400 mL) and brine (100 mL), then dried with sodium sulfate. After filtration, solvent was removed by rotary evaporation. The residue was ground to a fine powder in a mortar and pestle. The light brown solid was transferred to a medium frit and washed with pentane (3 x 30 mL), then dried under oil pump vacuum, yielding 3,6-di-*tert*-butyl-carbazole (**1.21**, 12.4644 g, 44.6 mmol, 75% yield) as an off white solid. NMR spectral data matched those reported by Liu *et al.*[65].

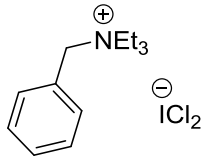

Synthesis of benzyltriethylammonium dichloroiodate (BTEA ICl_2)[67]

To an Erlenmeyer flask (1 L) was added sodium iodide (52.50 g, 350 mmol) and water (340 mL); once dissolved, concentrated HCl (120 mL) was added. The yellow solution was transferred to a three neck round bottom flask equipped with a stir bar and addition funnel. The reaction flask was placed in an ice bath and Essential Everyday bleach (316 mL, sodium hypochlorite 8.25%, 350 mmol) was added dropwise over 1 h maintaining a solution temperature below 10 ^{o}C. The orange/brown solution with a minimal amount of grey solid was allowed to warm to room temperature and stir for 20 min until the mixture became homogeneous and bright orange. A solution of sodium

iodide (0.80 g in 8 mL) was added dropwise until the solution maintained a very slight brown color, yielding a solution of sodium dichloroiodate. To a three neck round bottom flask (3 L) equipped with an addition funnel was added benzyltriethylammonium chloride (159.68 g, 701 mmol) and water (220 mL). The sodium dichloroiodate solution was added dropwise over 30 min with swirling (a mechanical stirrer would be recommended) to obtain a bright yellow heterogeneous mixture. The mixture was filtered through a course frit, washing the solid with water (3 x 100 mL) and diethyl ether (4 x 500 mL). The bright yellow solid was dried under oil pump vacuum, yielding benzyltriethylammonium dichloroiodate (123.69 g, 317 mmol, 91% yield), which was used without further purification.

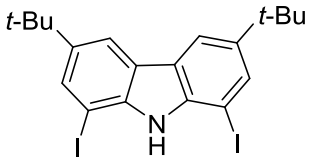

Synthesis of 1,8-diiodo-3,6-di-*tert*-butyl-carbazole (1.22)

To a three neck round bottom flask (1 L) equipped with a magnetic stir bar and reflux condenser was added 3,6-di-*tert*-butyl-carbazole (**1.21**, 10.00 g, 35.8 mmol), BTEA ICl_2 (34.91 g, 89.5 mmol), acetic acid (500 mL), and sulfuric acid (45 mL). The reaction was heated in a 75^{o}C oil bath for 7 h, then allowed to cool to room temperature and poured into water (1 L). The mixture was filtered through a medium frit, washing the solid with water (3 x 100 mL). The solid was dissolved in diethyl ether (250 mL) and the resulting solution washed with saturated sodium thiosulfate (3 x 50 mL), and water (50 mL), then dried with sodium sulfate. After filtration, solvent was removed by rotary evaporation. The crude solid was purified on silica gel (50 g), eluting with petroleum ether (R_f~0.65) (It should be noted that product is only slightly soluble in petroleum ether and dry loading the column would be preferred). Pure fractions containing only the TLC spot of R_f~0.65 were combined; once an impurity (R_f~0.3) began to elute, those fractions were discarded. The combined pure fractions were washed with saturated sodium thiosulfate (50 mL) and water (3 x 50 mL), then dried with sodium sulfate. After filtration, solvent was removed by rotary evaporation followed by storage of the residue under oil pump vacuum to obtain 1,8-diiodo-3,6-di-*tert*-butyl-carbazole (**1.22**, 10.0005 g,

18.8 mmol, 53% yield) as a white solid. Anal. calcd. for $C_{20}H_{23}I_2N_1$ (mol. wt. 531.22): C, 45.22; H, 4.36; N, 2.64. Found: C, 44.99; H, 4.58; N, 2.81. ^{1}H NMR ($CDCl_3$, 600 MHz): δ 8.00 (dd, *J* = 1.2, 0.6, 2H), 7.93 (bs, 1H), 7.83 (d, *J*= 1.2, 2H), 1.44 ppm (s, 18H). It should be noted that the typical yield for this reaction was 80 %, and that the NMR spectra matched that of the sample successfully analyzed by combustion.

Synthesis of $(CuOTf)_2$ benzene complex[78]

To a three neck round bottom flask in a glovebox added Cu_2O (4.0246 g, 28.1 mmol), anhydrous benzene (140 mL), and triflic anhydride (11.1251 g, 39.4 mmol). After necks were stoppered with septa, the reaction flask was transferred to a hood, a nitrogen inlet was attached to a reflux condenser which was then attached to the flask, and magnetic stir bar. The reaction was refluxed for 1.5 h, then allowed to cool to room temperature and transferred to a glovebox. The mixture was filter through a medium frit, washing the solid with benzene (10 mL, 2 x 5 mL) and pentane (3 x 10 mL). The light brown solid was transferred to a vial and dried under oil pump vacuum to obtain $(CuOTf)_2$ benzene complex (9.6978 g, 19.3 mmol, 69% yield). The reagent was used without further purification.

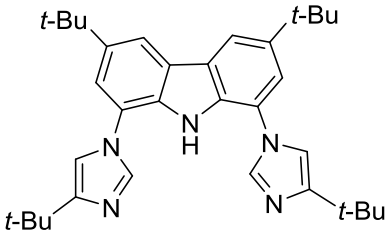

Synthesis of 3,6-di-tert-butyl-1,8-bis(4-*tert*-butyl-imidazol-1-yl)-carbazole (1.23)

To a thick wall glass pressure vessel (150 mL) in a glovebox, equipped with a magnetic stir bar added 1,8-diiodo-3,6-di-*tert*-butyl-carbazole (**1.22**, 6.6500 g, 12.5 mmol), 4-*tert*-butyl-imidazole[68] (7.7815g, 62.7 mmol), cesium carbonate (9.0251 g, 27.7 mmol), $(CuOTf)_2$ benzene complex (1.2629 g, 2.5 mmol), 1,10-phenanthroline (4.5230 g, 25.1 mmol), dibenzylideneacetone (0.5874 g, 2.5 mmol), and dry toluene (50 mL). The tube was sealed and placed in a 120 ^{o}C oil bath for 14 d, as the contents were stirred vigorously. After cooling to room temperature, the reaction was filtered through a medium frit, washing the solid with toluene (4 x 50 mL). Discarding the solid, the brown

filtrate was washed with 10% ammonium hydroxide (3 x 100 mL), water (3 x 100 mL), and brine (50 mL), then dried with sodium sulfate. After filtration, solvent was removed by rotary evaporation followed by oil pump vacuum. The crude product was transferred to a medium frit as a powder and washed with cold acetone (4 x 10 mL), then transferred to a round bottom flask with acetone (20 mL). The mixture was heated to reflux for 15 min and then allowed to cool to room temperature and filtered through a medium frit washing the white solid with acetone (10 mL). The white product was transferred to a vial and dried under oil pump vacuum to obtain (**1.23** dihydrate, 4.4204 g, 7.90 mmol, 62 % yield). Anal. calcd. for $C_{34}H_{45}N_5$ (mol. wt. 523.77): C, 77.97; H, 8.66; N, 13.37. Found: C, 72.50; H, 8.99; N, 12.76. Anal. calcd. for $C_{34}H_{45}N_5(2\ H_2O)$ (mol. wt. 559.80): C, 72.95; H, 8.82; N, 12.51.

Synthesis of 1.24a (Ni-Cl)

To a thick wall glass pressure vessel (150 mL) in a glovebox, equipped with a magnetic stir bar added **1.23** (250.3 mg, 0.479 mmol), $Ni(OAc)_2$ tetrahydrate (239.0 mg, 0.98 mmol), acetic acid (70.0 mg, 1.17 mmol), and dry benzene (25 mL). The sealed vessel was heated in a 150 ^oC oil bath for 10 d as the contents were stirred, after which the cooled solution was transferred to a round bottom flask and solvent was removed by rotary evaporation. Acetone (40 mL) was added to the crude solid **1.24b**, and filtered through a fine frit. An aqueous solution of sodium chloride (0.51 M, 10.0 mL) was added dropwise and the mixture stirred for 30 min generating the crude chloride compound (2a). The acetone was removed by rotary evaporation, leaving a heterogeneous mixture that was extracted with DCM (15 mL). The organic layer was washed with water (10 mL), and dried with sodium sulfate. After filtration, the volume was reduced by rotary evaporation to approximately 5 mL, and the solution transferred to a vial containing silica (1.0 g). Solvent was removed by oil pump vacuum, which was then loaded on top of a silica (15 g) column which was previously loaded with hexanes and diethyl ether (12:1). Chromatography was done under air. The same solvent system was maintained to elute product with R_f = 0.1. All fractions containing product were combined and solvent was removed by rotary evaporation and the residue dried under oil pump vacuum to obtain

1.24a (52.1 mg, 0.084 mmol, 17% yield) as a red solid. Anal. calcd. for $C_{34}H_{44}N_5Cl_1Ni_1$ (mol. wt. 616.90): C, 66.20; H, 7.19; N, 11.35. Found: C, 66.65; H, 7.60; N, 10.92.

Synthesis of 1.25a (Pd-Cl)

To a vial in a glovebox equipped with a magnetic stir bar was added **1.23** (250.4 mg, 0.478 mmol), $Pd(OAc)_2$ (115.7 mg, 0.515 mmol), acetic acid (58.4 mg, 0.976 mmol), and dry benzene (15 mL). The sealed vial was heated in a 70 ^oC oil bath for 7 d, after which the solution was filtered through a fine frit in air. Solvent was removed by a gentle flow of nitrogen gas over the filtrate, then dissolving the residual solid in acetone (15 mL) and filtering through a fine frit. A solution of sodium chloride (0.60 M, 10.0 mL) in water was added dropwise and the mixture was stirred for 30 min generating the crude chloride compound, **1.25b**. Acetone was removed by rotary evaporation, leaving a heterogeneous mixture that was extracted with diethyl ether (40 mL). The organic layer was washed with water (20 mL), and dried with sodium sulfate. After filtration, solvent was removed by rotary evaporation, and the residue was dissolved in DCM then transferred to a vial containing silica (1.5 g). Solvent was removed by oil pump vacuum; then the crude mixture on silica was loaded on top of a silica (15 g) column which was previously loaded with hexanes and diethyl ether (12:1). Chromatography was done under air. The same solvent system was maintained to elute product with $R_f = 0.1$. All fractions containing product were combined and solvent was removed by rotary evaporation and the residual yellow solid dried under oil pump vacuum to obtain **1.25a** (195.6 mg, 0.294 mmol, 62% yield). Anal. calcd. for $C_{34}H_{44}N_5Cl_1Pd_1$(mol. wt. 664.63) C, 61.44; H, 6.67; N, 10.54. Found: C, 62.56; H, 7.33; N, 9.77. Anal. calcd. for $C_{34}H_{44}N_5Cl_1Pd_1–0.5(C_6H_{14})$(mol. wt. 707.72): C, 62.79; H, 7.26; N, 9.90.

Synthesis of 1.26a (Pt-Cl)

To a vial in a glovebox equipped with a magnetic stir bar was added **1.23** (250.2 mg, 0.478 mmol), $PtCl_2$(COD) (187.9 mg, 0.502 mmol), and dry benzene (15 mL). The sealed vial was heated in a 100 ^oC oil bath for 6 d, after which solvent was removed by a gentle flow of nitrogen gas over the solution. DCM (20 mL) was added to the residual

solid and the mixture filtered through a fine frit. The volume of the filtrate was reduced to approximately 5 mL and the solution transferred to a vial containing silica (3.0 g). Solvent was removed by oil pump vacuum, and the crude product on silica was loaded on top of a silica (15 g) column which was previously loaded with hexanes and ethyl acetate (12:1). Chromatography was done under air. The same solvent system was maintained to elute product with R_f=0.15. All fractions containing product were combined and solvent was removed by rotary evaporation and the residue dried under oil pump vacuum to obtain **1.26a** (225.9 mg, 0.300 mmol, 63% yield) as a bright yellow solid. Anal. calcd. for $C_{34}H_{44}N_5Cl_1Pt_1$ (mol. wt. 753.29): C, 54.21; H, 5.89; N, 9.30. Found: C, 54.55; H, 6.20; N, 8.93.

Synthesis of 1.24b (Ni-OAc)

To a vial in a glovebox equipped with a magnetic stir bar was added **1.24a** (52.7 mg, 0.085 mmol), silver acetate (16.4 mg, 0.098 mmol), and acetone (5.0 mL). The reaction was stirred for 13.5 h then filtered through a fine frit under air. From the filtrate, solvent was removed by a flow of nitrogen gas over the solution. The residual solid was dissolved in pentane (12 mL) and the resulting solution washed with water (3 x 3 mL) and dried with sodium sulfate. After filtration, the filtrate was placed in a -20 ^oC freezer until crystals formed. The cold solvent was decanted (which did contain more product but goal was to get pure compound) and the crystals were washed with cold pentane (3 x 1 mL) and then dried under oil pump vacuum to obtain **1.24b**-(0.7 H_2O) (17.2 mg, 0.026 mmol, 31% yield) as a red solid. Anal. calcd. for $C_{36}H_{47}N_5O_2Ni_1$ (mol. wt. 640.50): C, 67.51; H, 7.40; N, 10.93. Found: C, 66.62; H, 7.96; N, 10.83. Anal. calcd. for $C_{36}H_{47}N_5O_2Ni_1$-(0.7 H_2O)(mol. wt. 653.11): C, 66.21; H, 7.47; N, 10.72.

Synthesis of 1.25b (Pd-OAc)

To a vial in a glovebox equipped with a magnetic stir bar was added **1.25a** (50.5 mg, 0.076 mmol), silver acetate (13.6 mg, 0.081 mmol), and acetone (5 mL). The reaction was allowed to stir for 15 h, after which the solvent was removed by a flow of nitrogen. Benzene (12 mL) was added to dissolve most of the solid, and the mixture was

filtered through a fine frit. From the filtrate, solvent was removed by a flow of nitrogen, and the residue was dried under oil pump vacuum to obtain **1.25b** (36.5 mg, 0.53 mmol, 70% yield) as a yellow solid. Anal. calcd. for $C_{36}H_{47}N_5O_2Pd_1$(mol. wt. 688.22): C, 62.83; H, 6.88; N, 10.18. Found: C, 63.20; H, 6.87; N, 10.34.

Synthesis of 1.26b (Pt-OAc)

To a vial in a glovebox equipped with a magnetic stir bar was added **1.26a** (50.1 mg, 0.067 mmol), silver acetate (12.2 mg, 0.073 mmol), and acetone (5.0 mL). The reaction was stirred for 12 h, filtered through a fine frit, and from the filtrate solvent was removed by a flow of nitrogen gas. The solid thus obtained was dissolved in pentane (15 mL) and the resulting solution washed with water (3 x 2 mL), dried with sodium sulfate, and filtered through a fine frit. From the filtrate solvent was removed by a flow of nitrogen, and the residue dried under oil pump vacuum to obtain **1.26b**-(0.5 C_5H_{12}) (44.1 mg, 0.054 mmol, 82% yield) as a yellow solid. Anal. calcd. for $C_{36}H_{47}N_5O_2Pt_1$ (mol. wt. 776.89): C, 55.66; H, 6.10; N, 9.01. Found: C, 56.62; H, 6.95; N, 8.68. Anal. calcd. for $C_{36}H_{47}N_5O_2Pt_1$-(0.5 C_5H_{12})(mol. wt. 812.96): C, 56.88; H, 6.57; N, 8.61.

Synthesis of 1.26c (Pt-H)

To a vial in a glovebox equipped with a magnetic stir bar was added **1.26a** (100.7 mg, 0.134 mmol), sodium borohydride (21.6 mg, 0.571 mmol), and dry THF (6.0 mL). The vial was sealed and the reaction was heated in a 70 ^oC oil bath for 20 h, after which the reaction was transferred to a glovebox and water (10 mL) was added. The mixture was extracted with a mixture of diethyl ether and pentane (2:4) (6 mL x 3). The organic fractions were combined and washed with water (4 mL x 3) and then dried with sodium sulfate. After filtration, solvent was removed by a diaphragm vacuum pump. The crude product was purified on a silica (5.0 g) column under nitrogen, loading the column with benzene, and maintaining pure benzene until an orange fraction eluted from the column. Afterwards MeOH (1%) was added to the benzene eluant and the product was next to elute as a bright yellow band. Care was taken to only collect the bright yellow fraction and not a trailing brown fraction. The fraction containing only the yellow band was

concentrated and dried under oil pump vacuum to obtain **1.26c** as a bright yellow solid (7.9 mg, 0.011 mmol, 8% yield). Anal. calcd for $C_{34}H_{45}N_5Pt_1$ (mol. wt. 718.85): C, 56.81; H, 6.31; N, 9.74. Found: C, 56.91; H, 6.80; N, 9.30.

Synthesis of 1.24d (Ni-OTf)

To a vial in a glovebox equipped with a magnetic stir bar was added **1.24a** (50.0 mg, 0.081 mmol), silver trifluoromethanesulfonate (21.9 mg, 0.085 mmol), and THF (4 mL). The color changed from that of red/orange solid to a dark purple/red solution right after addition of solvent. The reaction was allowed to stir for 40 min, followed by removal of solvent by a flow of nitrogen. The solid was mostly dissolved in pentane (12 mL) and acetone (1 mL), and the mixture filtered through a fine frit with a pad of celite (0.50 g). From the filtrate, solvent was removed by a flow of nitrogen and the residue dried under oil pump vacuum to obtain **1.24d** (0.5 C_5H_{12}) (49.5 mg, 0.065 mmol, 80% yield) as a red/purple solid. Anal. calcd. for $C_{35}H_{44}F_3N_5Ni_1O_3S_1$ (mol. wt. 730.52): C, 57.55; H, 6.07; N, 9.59. Found: C, 58.40; H, 7.03; N, 9.37. Anal. calcd. for $C_{35}H_{44}F_3N_5Ni_1O_3S_1$(0.5 C_5H_{12}) (mol. wt. 766.59): C, 58.76; H, 6.57; N, 9.14.

Synthesis of 1.25d (Pd-OTf)

To a vial in a glovebox equipped with a magnetic stir bar was added **1.25a** (50.4 mg, 0.076 mmol), silver trifluoromethanesulfonate (20.9 mg, 0.081 mmol), and acetone (4 mL). The reaction was allowed to stir for 1 h, after which the volume was reduced to approximately 2 mL by a flow of nitrogen. Pentane (12 mL) was added to dissolve most of the solid, and the mixture was filtered through a fine frit. From the filtrate, solvent was removed by a flow of nitrogen, and the residue dissolved in benzene (10 mL). The cloudy solution was then filtered through a fine frit with a pad of Celite (0.5 g). From the filtrate, solvent was removed by a flow of nitrogen and the residue dried under oil pump vacuum to obtain **1.25d** (0.5 C_5H_{12}) (53.3 mg, 0.065 mmol, 86% yield) as a light yellow solid. Anal. calcd for $C_{35}H_{44}F_3N_5O_3S_1Pd_1$ (mol. wt. 777.22): C, 54.02; H, 5.70; N, 9.00. Found: C, 55.11; H, 6.32; N, 8.62. Anal. calcd. for $C_{35}H_{44}F_3N_5O_3S_1Pd_1$-(0.5 C_5H_{12}) (mol. wt. 814.32): C, 55.31; H, 6.19; N, 8.60.

Synthesis of 1.26d (Pt-OTf)

To a vial in a glovebox equipped with a magnetic stir bar was added **1.26a** (46.8 mg, 0.062 mmol), silver trifluoromethanesulfonate (18.8 mg, 0.073 mmol), and dry THF (4 mL). The reaction was allowed to stir for 7.5 h, after which the solvent was removed on a diaphragm vacuum pump. Benzene (10 mL) was added to dissolve most of the solid, and the mixture was filtered through a fine frit. From the filtrate solvent was removed by a flow of nitrogen, and the residue was dried on oil pump vacuum to obtain **1.26d** as a yellow solid (51.8 mg, 0.060 mmol, 96% yield). Anal. calcd. for $C_{35}H_{44}F_3N_5O_3S_1Pt_1$ (mol. wt. 866.91): C, 48.49; H, 5.12; N, 8.08. Found: C, 47.99; H, 4.90; N, 8.00.

General synthesis of 1.24-1.26e

To a J. Young tube in a glovebox was added the requisite triflate complex **e** (5-15 mg) which was dissolved in d_6-benzene (0.7 mL). Outside the glovebox, carbon monoxide was bubbled through solution for 10 min to give CO complexes **1.24-1.26e**.

Synthesis of 1.26f

In a glovebox to a J. Young NMR tube was added **1.26d** (15.2 mg, 0.018 mmol) and d_6-benzene (1.0 mL). In air, ethylene was bubbled through solution for 10 min and then the tube was close and let to sit for 24 h, giving **1.26f** which was characterized in solution.

Catalyzed hydration of 1-hexyne

To a J. Young NMR tube in a glovebox was added 1-hexyne (19.0 mg, 0.231 mmol), acetone (0.7 mL), water (21.8 mg, 1.21 mmol), d_6-benzene (0.1 mL, for NMR lock and shim), and $C(SiMe_3)_4$ as an internal standard. Non-deuterated acetone was used to avoid H/D exchange with added water. An initial NMR spectrum was acquired to obtain the initial integral values for substrate and $C(SiMe_3)_4$. The NMR tube was returned to the glovebox and **1.26d** (10.0 mg, 0.012 mmol) was added. The tube was

sealed and the reaction was heated at 70 ^{o}C in an oil bath for 1 h to obtain 7% of aldehyde, 14 h to obtain 62% aldehyde, 24 h to obtain 79% which maintained at 79% upon further heating. The hexanal aldehyde triplet at 9.42 ppm was integrated to give the above yields compared to the initial hexyne peaks. The remaining 21% formed was 2-hexanone.

Reaction with labeled alkyne 1.27, $PhCH_2CH_2CH_2C^{13}CH$ to make 1.29

To a J. Young NMR tube in the glovebox was added **1.26d** (16.7 mg, 0.019 mmol), d_6-acetone (0.7 mL), and water (6.9 mg, 0.383 mmol). An initial NMR spectrum showed a mixture of **1.26d** and the aquo complex in a ratio of 1 to 2.5. In glovebox was added labeled alkyne **1.27** (5.4 mg, 0.037 mmol). Another NMR spectrum revealed a mixture of three complexes, two of which were present before and a new complex that was characterized by 1D and 2D NMR.

Reaction with but-3-yn-1-ol (1.28) to make 1.30

To a J. Young NMR tube in the glovebox was added **1.26d** (10.4 mg, 0.012 mmol), followed by but-3-yn-1-ol (2.6 mg, 0.037 mmol) onto the walls of the NMR tube, all of which was rinsed down with CD_2Cl_2 (0.7 mL). After 21 h the reaction had completely formed the carbene complex.

Synthesis of 1.32-Pd

To a J. Young NMR tube in a glove box was added **1.25a** (20.1 mg, 0.030 mmol), sodium tert-butoxide (3.6 mg, 0.037 mmol), and CD_2Cl_2 (1.0 mL). After 10 minutes the reaction was checked by NMR which showed product has formed. In a glovebox the solution was filtered through a pipet loaded with cotton, then solvent was removed by diaphragm pump yielding **1.32-Pd** $(H_2O)_4$ $(acetone)_2$ (18.7 mg, 0.015 mmol, 98 % yield). Anal. calcd. for $C_{68}H_{86}N_{10}Pd_2$ $(H_2O)_4(C_3H_6O)_2$ (mol. wt. 1444.57): C, 61.53; H, 7.40; N, 9.70. Found C, 61.34; H, 6.97; N, 9.34

Synthesis of 1.32-Pt

To a J. Young NMR tube in a glove box was added **1.26a** (15.7 mg, 0.021 mmol), sodium tert-butoxide (2.2 mg, 0.023 mmol), and CD_2Cl_2 (1.0 mL). The solution was heated in a 50 ^oC oil bath for 67.5 h, checking the reaction periodically it appears the reaction progresses had stopped, so more sodium tert-butoxide (2.5 mg, 0.026 mmol) was added in a glovebox. After heating in a 50 ^oC oil bath for another 24 h, the reaction was complete. The organic layer was washed with water (3 x 2 mL), dried with sodium sulfate and filtered through a pipet loaded with cotton. Solvent was removed under oil pump vacuum, purified by vapor diffusion of pentanes into chloroform yielding **1.32-Pt**.

K. IR Spectra

IR spectra

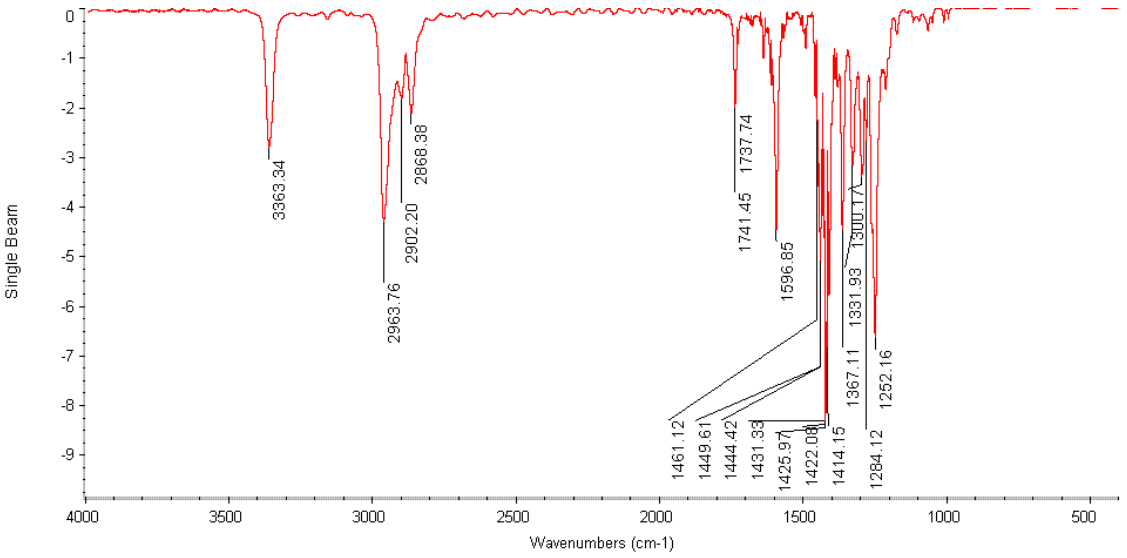

Figure 1.27. IR spectrum of **1.24a** (NiCl) (C_6H_6, CaF_2 cell).

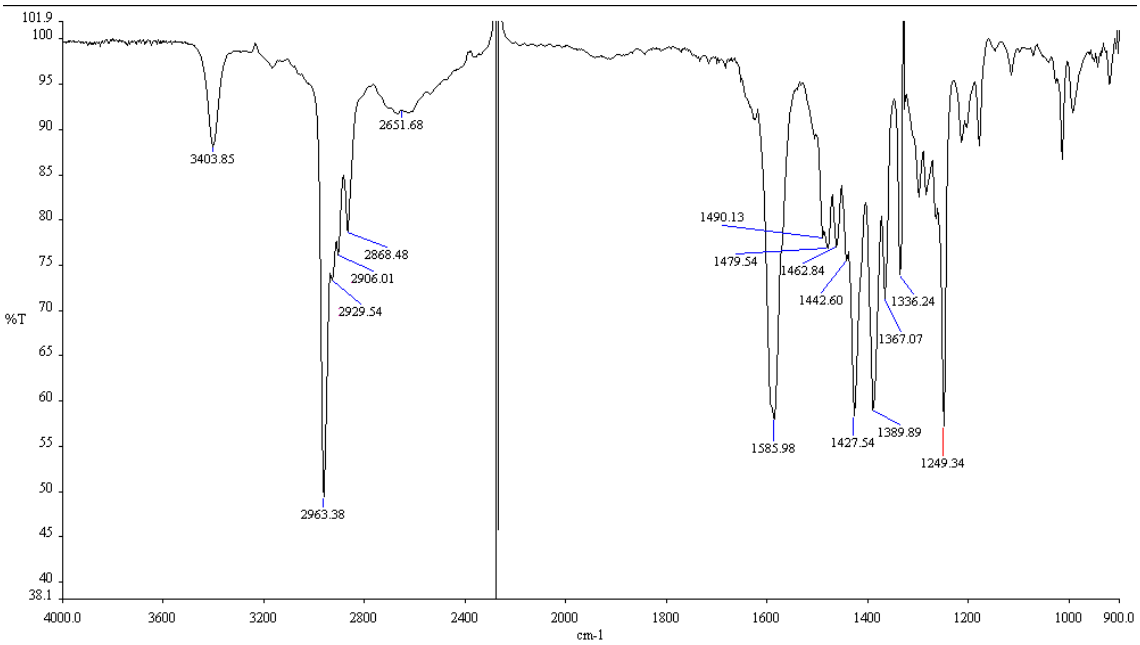

Figure 1.28. IR spectrum of **1.24b** (NiOAc) (d_6-benzene, CaF_2 cell).

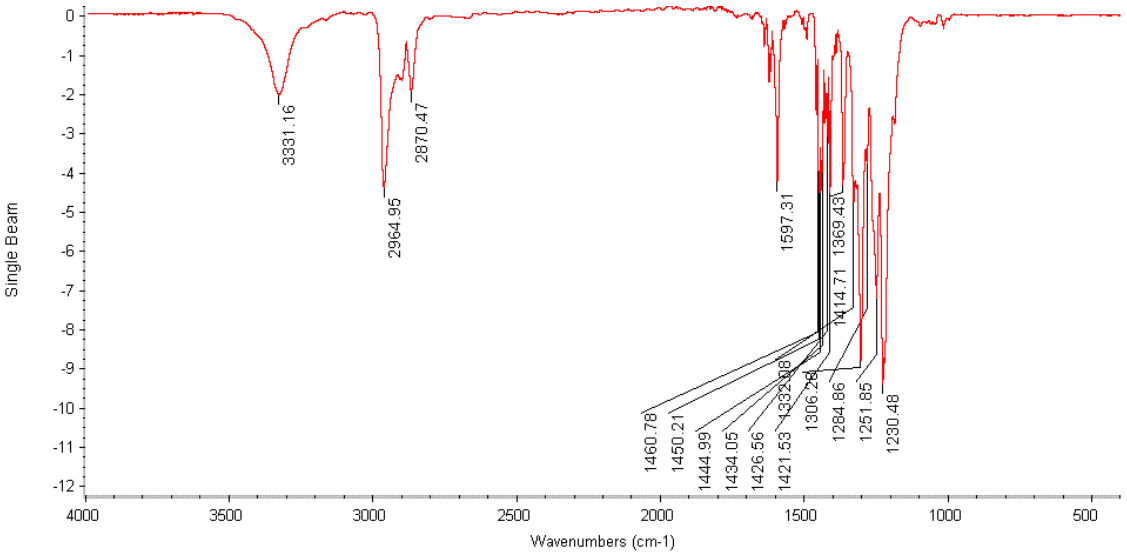

Figure 1.29. IR spectrum of **1.24d** (Ni-OTf) (C_6H_6, CaF_2 cell).

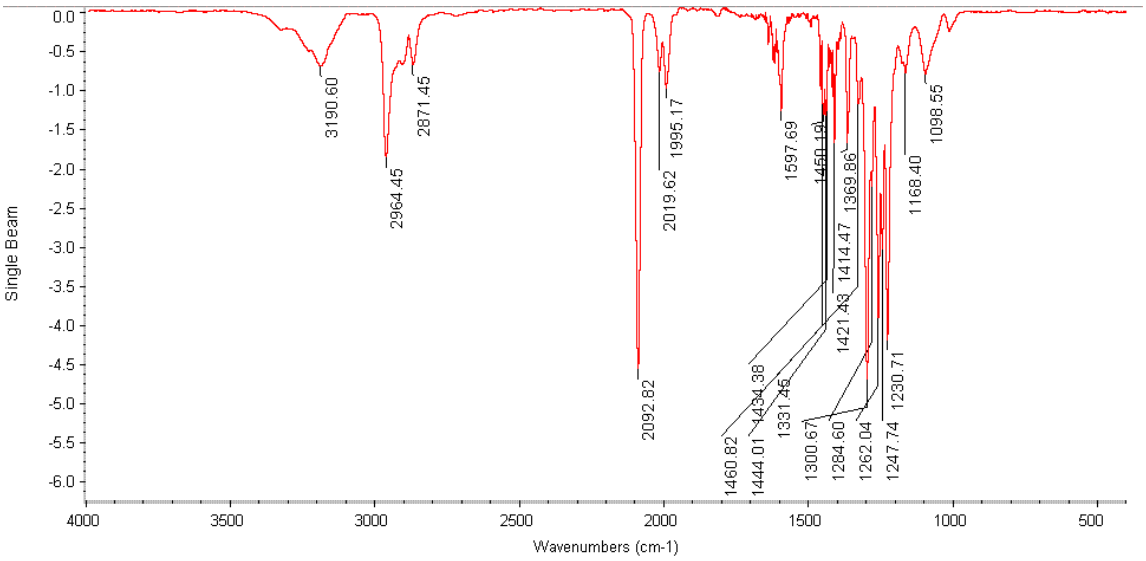

Figure 1.30. IR spectrum of **1.24e** ([Ni(CO)]OTf) (C_6H_6, CaF_2 cell).

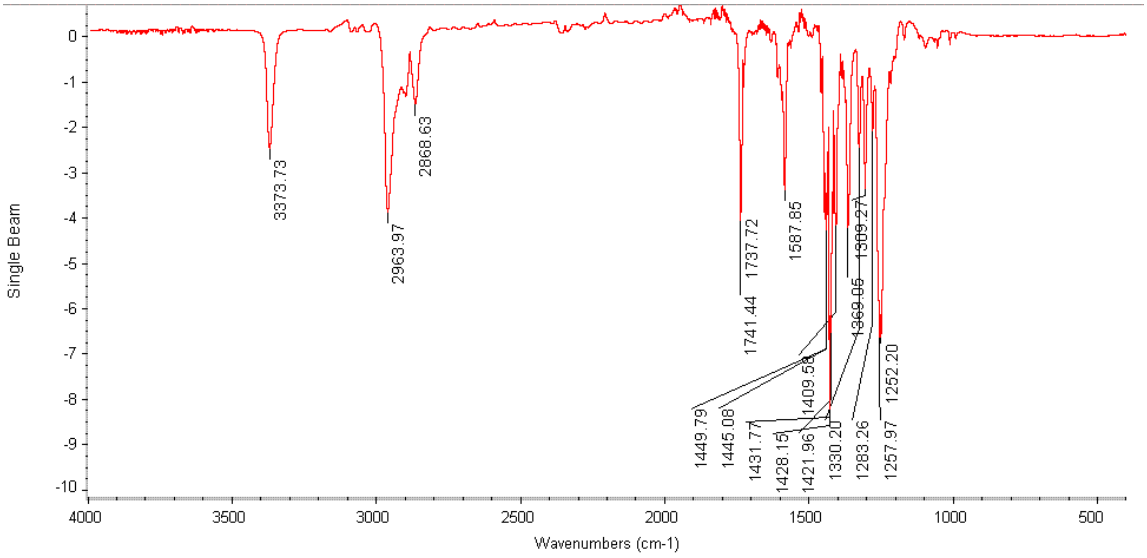

Figure 1.31. IR spectrum of **1.25a** (Pd-Cl) (C_6H_6, CaF_2 cell).

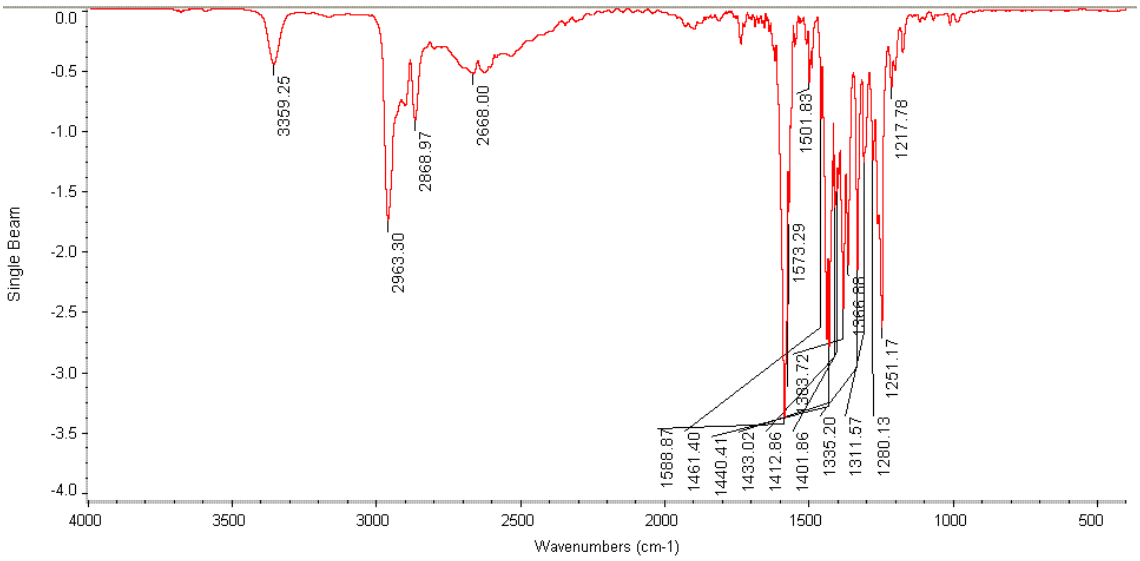

Figure 1.32. IR spectrum of **1.25b** (Pd-OAc) (C_6H_6, CaF_2 cell).

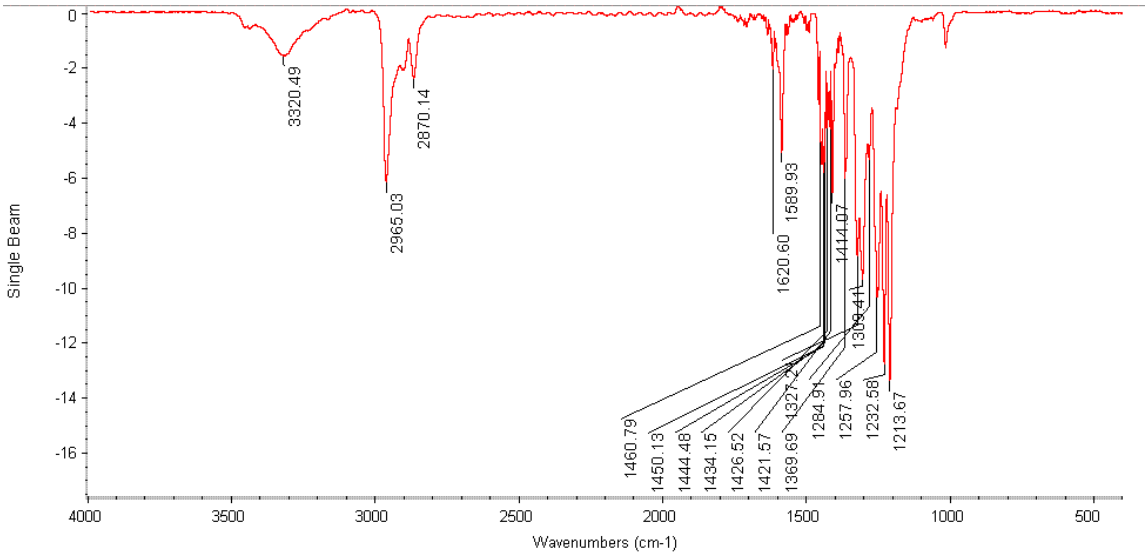

Figure 1.33. IR spectrum of **1.25d** (Pd-OTf)(C_6H_6, CaF_2 cell).

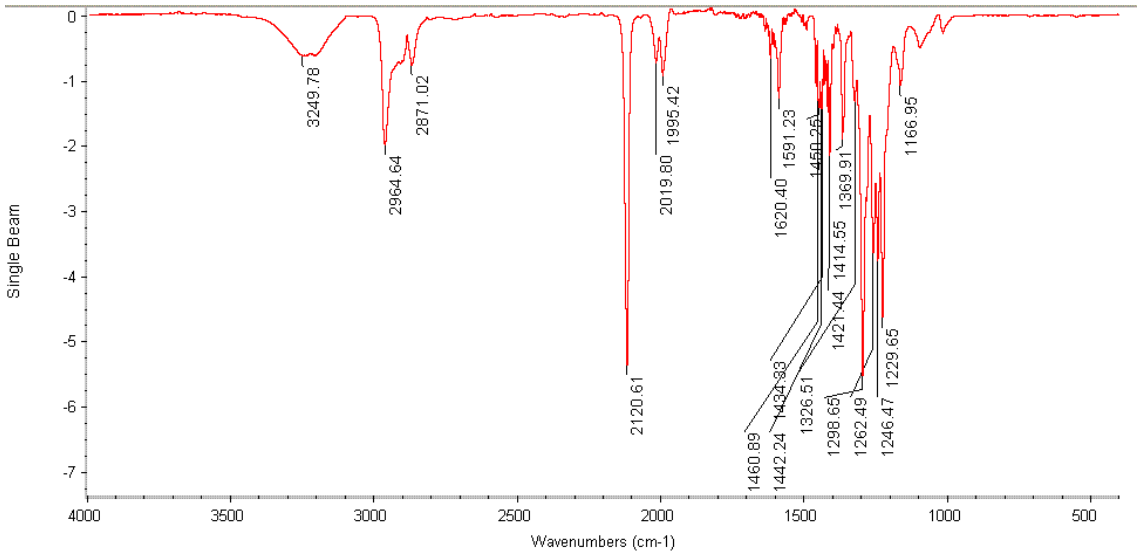

Figure 1.34. IR spectrum of **1.25e** ([Pd(CO)]OTf) (C_6H_6, CaF_2 cell).

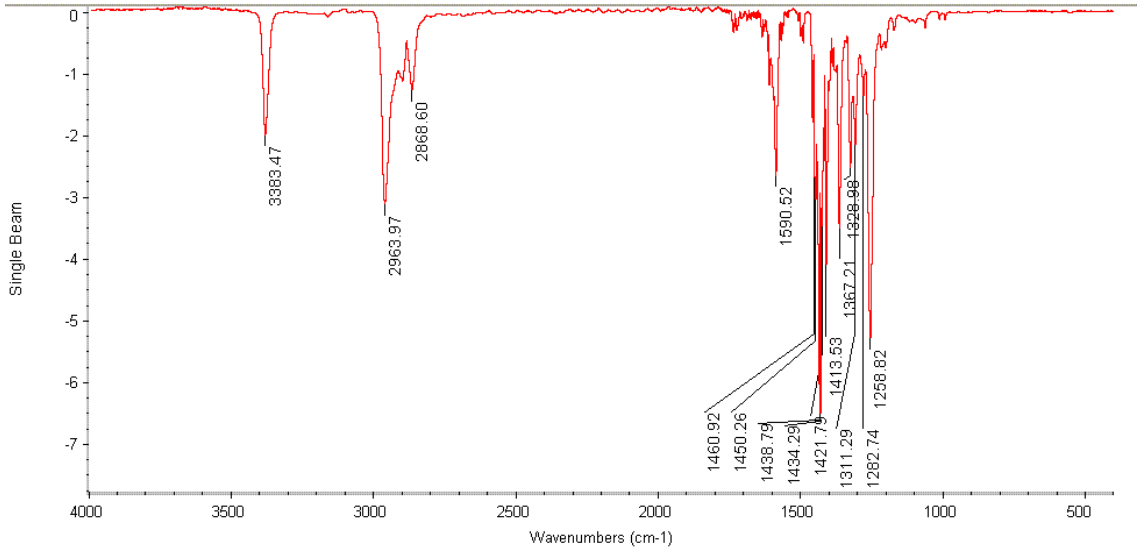

Figure 1.35. IR spectrum of **1.26a** (Pt-Cl) (C_6H_6, CaF_2 cell).

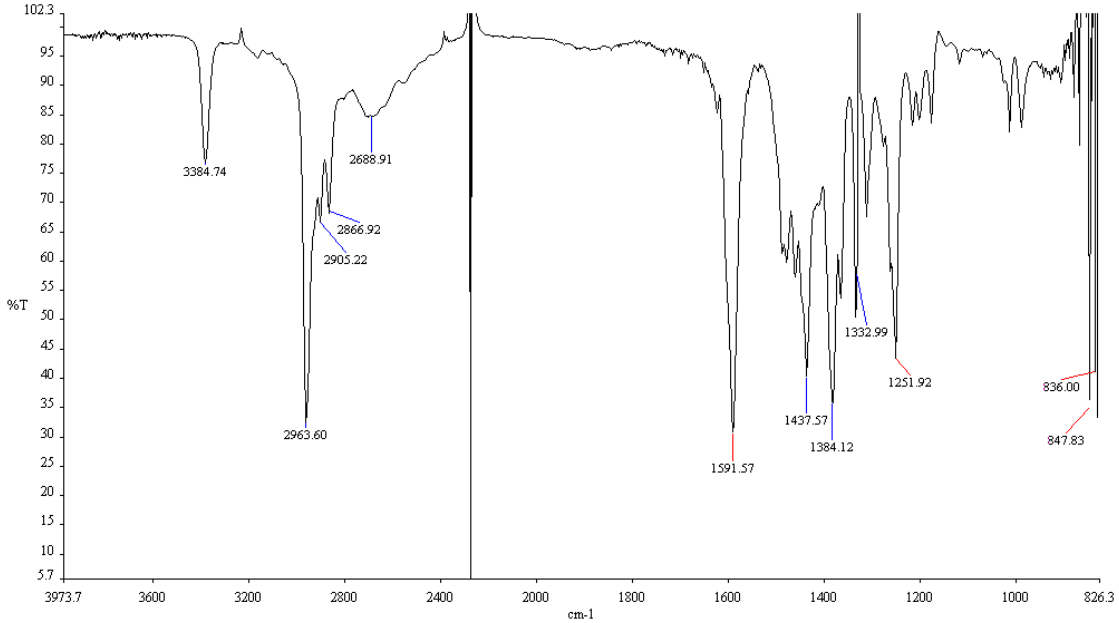

Figure 1.36. IR spectrum of **1.26b** (Pt-OAc) (d_6-benzene, CaF_2 cell).

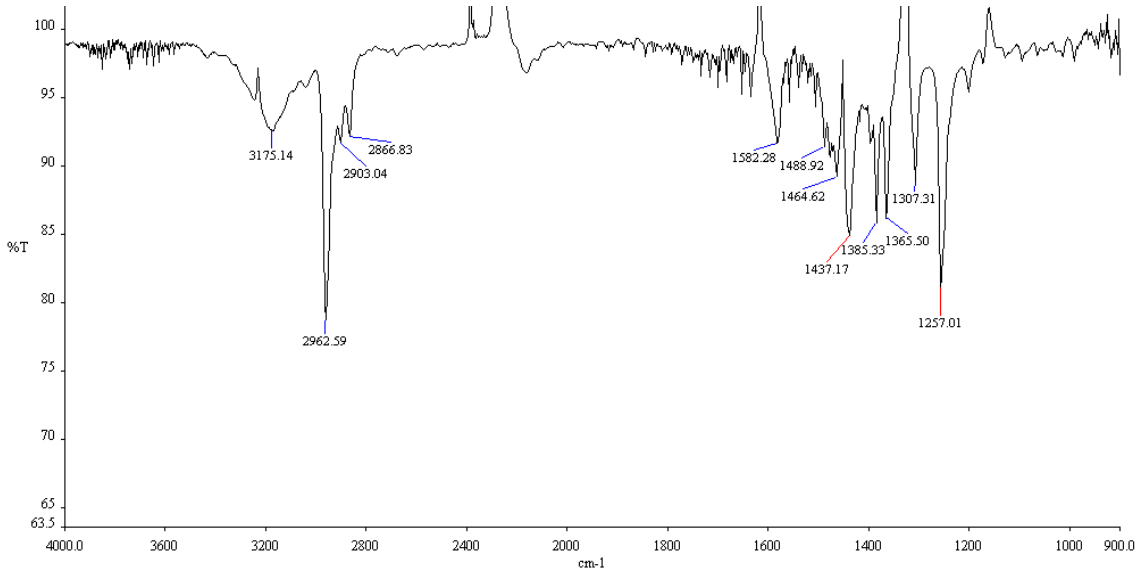

Figure 1.37. IR spectrum of **1.26c** (Pt-H) (d_6-benzene, CaF_2 cell).

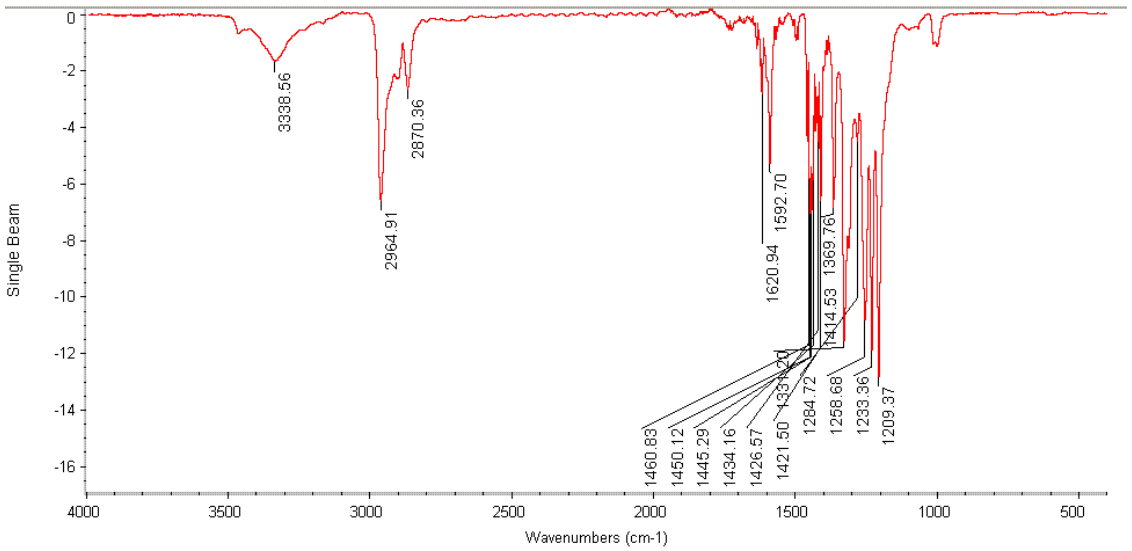

Figure 1.38. IR spectrum of **1.26d** (Pt-OTf) (C_6H_6, CaF_2 cell).

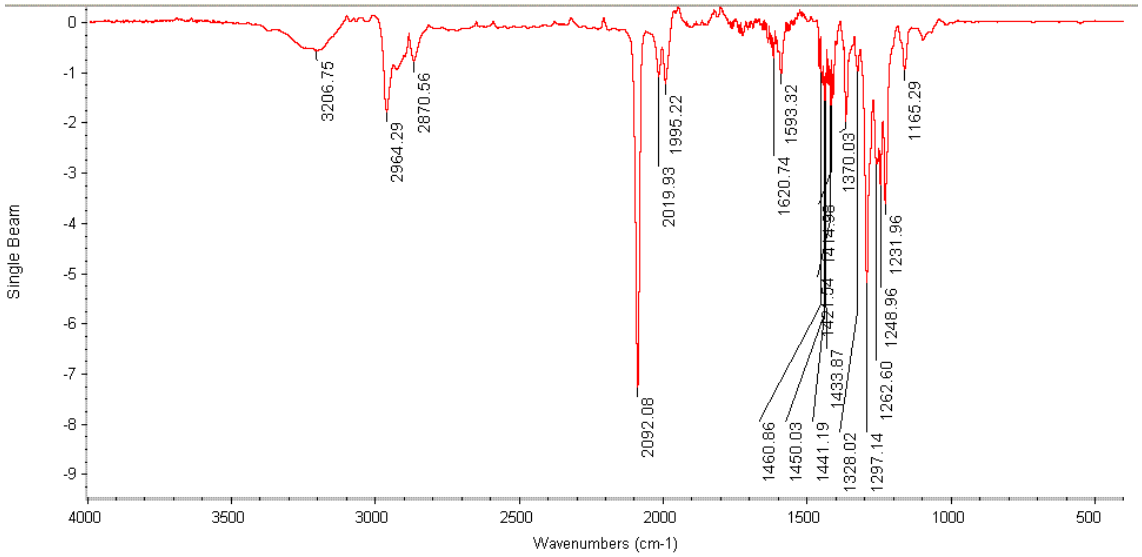

Figure 1.39. IR spectrum of **1.26e** ([Pt(CO)]OTf) (C_6H_6, CaF_2 cell).

L. NMR Figures

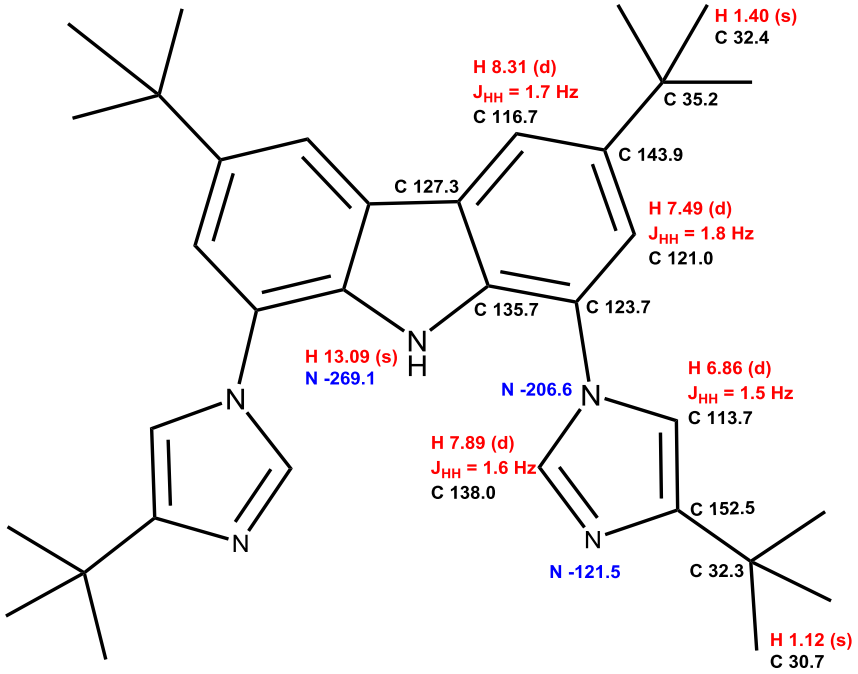

^{1}H -^{13}C gHMBCAD[b] continued		
H	bonds	C
7.49	3	35.2
7.49	3	116.7
7.49	2	123.7
7.49	4	127.3
7.49	3	135.7
7.49	2	143.9(w)
7.89	3	113.7
7.89	3	123.7
7.89	3	152.5
8.31	3	35.2
8.31	3	121.0
8.31	4	123.7
8.31	2	127.3
8.31	3	135.7
[b]J_{nxh} = 8.0 Hz J_{1xh} = 146.0 Hz		

^{1}H -^{15}N gHMBC[a]		
H	bonds	N
6.86	3	-121.5
6.86	2	-206.6
7.49	3	-206.6
7.49	4	-269.1
7.89	2	-121.5
7.89	2	-206.6
[a]J_{nxh}= 8 Hz J_{1xh}= 86 Hz		

^{1}H -^{15}N gHSQC	
H	N
13.09	-269.1

gCOSY
8.31↔7.49
7.89↔6.86

^{1}H -^{13}C gHMBCAD[b]		
H	bonds	C
1.12	1,3	30.7
1.12	2	32.3
1.12	3	152.5
1.40	1,3	32.4
1.40	2	35.2
1.40	3	143.9
6.86	3	123.7
6.86	3	138.0
6.86	2	152.5

^{1}H-^{13}C gHSQC	
H	C
1.12	30.7
1.40	32.4
6.86	113.7
7.49	121.0
7.89	138.0
8.31	116.7

Figure 1.40. NMR data for **1.23** in d_6-benzene.

Proton shifts were found to shift depending on concentration, possibly due to intermolecular hydrogen bonding

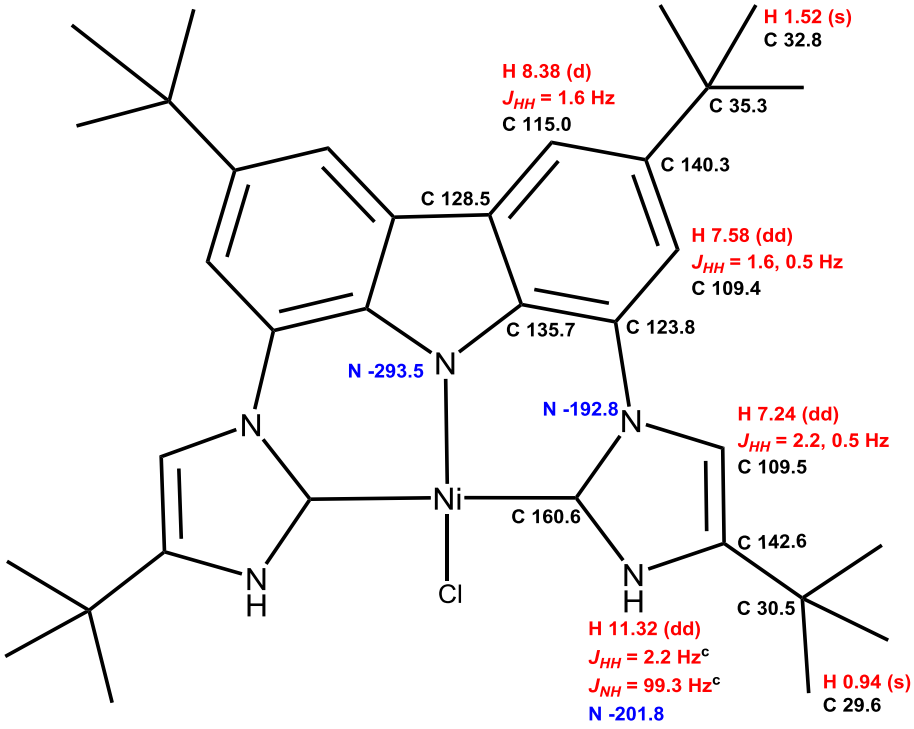

^{1}H -^{13}C gHMBCAD[b]		
H	bonds	C
0.94	1,3	29.6
0.94	2	30.5
0.94	3	142.6
1.52	1,3	32.8
1.52	2	35.3
1.52	3	140.3
7.24	3	123.8(w)
7.24	2	142.6
7.24	3	160.6
7.58	3	35.3
7.58	3	115.0
7.58	2	123.8
7.58	4	128.5(w)
7.58	3	135.7
7.58	2	140.3
8.38	3	35.3
8.38	3	109.4
8.38	4	123.8
8.38	2	128.5
8.38	3	135.7
[b] J_{nxh} = 8.0 Hz J_{1xh} = 146.0 Hz		

^{1}H -^{15}N gHMBC[a]		
H	bonds	N
7.24	2	-192.8
7.24	3	-201.8
7.58	3	-192.8
7.58	4	-293.5
[a] J_{nxh}= 5 Hz J_{1xh}= 86 Hz		

^{1}H -^{15}N gHSQC	
H	N
11.32	-201.8

gCOSY
11.32↔7.24
8.38↔7.58

^{1}H-^{13}C HSQCAD	
H	C
0.94	29.6
1.52	32.8
7.24	109.5
7.58	109.4
8.38	115.0

Figure 1.41. NMR data for **1.24a** in d_6-benzene.

[c] Couplings observed on the N^{14}-H^{1} satellites, the N^{15} –H^{1} main peak is a broad singlet.

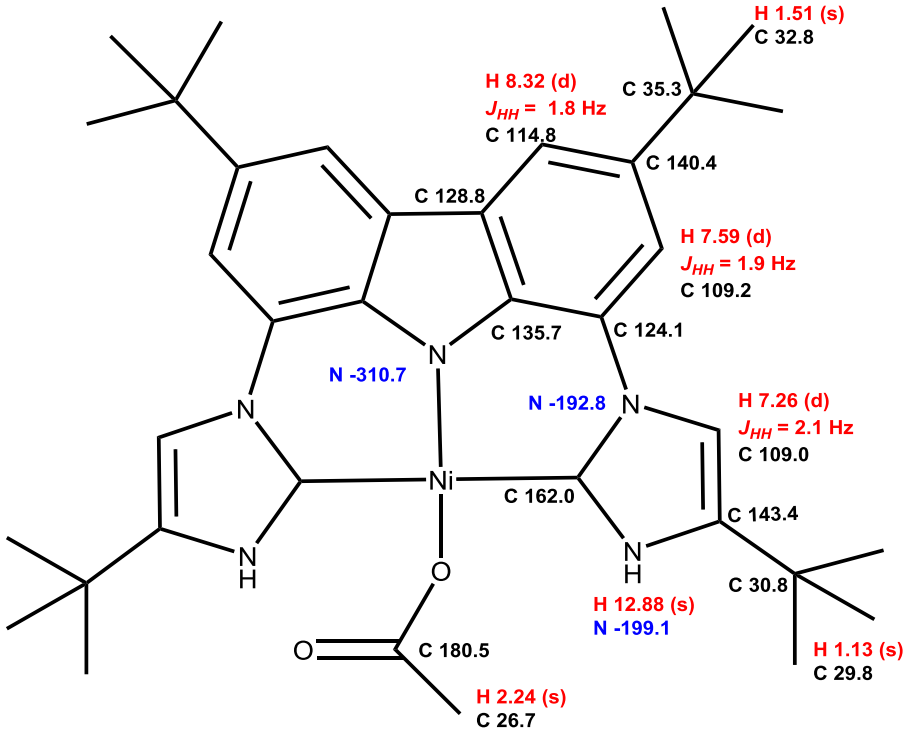

^{1}H -^{13}C gHMBCAD[b]		
H	bonds	C
1.13	1,3	29.8
1.13	2	30.8
1.13	3	143.4
1.51	1,3	32.8
1.51	2	35.3
1.51	3	140.4
2.24	2	180.5
7.26	3	124.1(w)
7.26	2	143.4
7.26	3	162.0
7.59	3	35.3
7.59	3	114.8
7.59	2	124.1
7.59	4	128.8(w)
7.59	3	135.7
7.59	2	140.4
8.32	3	35.3
8.32	3	109.2
8.32	4	124.1
8.32	2	128.8
8.32	3	135.7
[b]J_{nxh} = 8.0 Hz J_{1xh} = 146.0 Hz		

^{1}H-^{13}C HSQCAD	
H	C
1.13	29.8
1.51	32.8
2.24	26.7
7.26	109.0
7.59	109.2
8.32	114.8

^{1}H -^{15}N gHMBCAD[a]		
H	bonds	N
7.26	2	-192.8
7.26	3	-199.1
7.59	3	-192.8
7.59	4	-310.7
[a]J_{nxh}= 5 Hz J_{1xh}= 90 Hz		

^{1}H -^{15}N gHSQCAD	
H	N
12.88	-199.1

gCOSY
12.88↔7.26
8.32↔7.59
7.59↔7.26(w)

Figure 1.42. NMR data for **1.24b** in d_6-benzene.

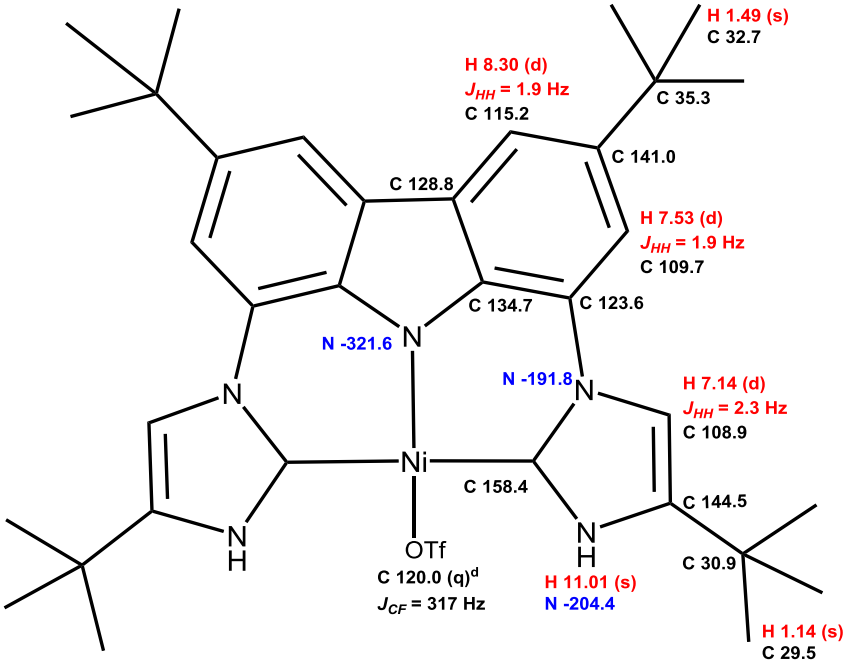

^{1}H -^{13}C gHMBCAD[b]		
1.14	1,3	29.5
1.14	2	30.9
1.14	3	144.5
1.49	1,3	32.7
1.49	2	35.3
1.49	3	141.0
7.14	3	123.6(w)
7.14	2	144.5
7.14	2	144.5
7.14	3	158.4
7.53	3	35.3
7.53	3	115.2
7.53	2	123.6
7.53	4	128.8(w)
7.53	3	134.7
7.53	2	141.0
8.30	3	35.3
8.30	3	109.7
8.30	4	123.6
8.30	2	128.8
8.30	3	134.7
[b]J_{nxh} = 8.0 Hz J_{1xh} = 146.0 Hz		

^{1}H -^{15}N gHMBCAD[a]		
H	bonds	N
7.14	2	-191.8
7.14	3	-204.4
7.53	3	-191.8
7.53	4	-321.6
[a]J_{nxh}= 5 Hz J_{1xh}= 90 Hz		

^{1}H -^{15}N gHSQCAD	
H	N
11.01	-204.4

^{1}H-^{13}C HSQCAD	
H	C
1.14	29.5
1.49	32.7
7.14	108.9
7.53	109.7
8.30	115.2

gCOSY
11.01↔7.14
8.30↔7.53
7.53↔7.14(w)

Figure 1.43. NMR data for **1.24d** in d_6-benzene.

[d] Only the two most intense peaks of the quartet are observed, which were broad.

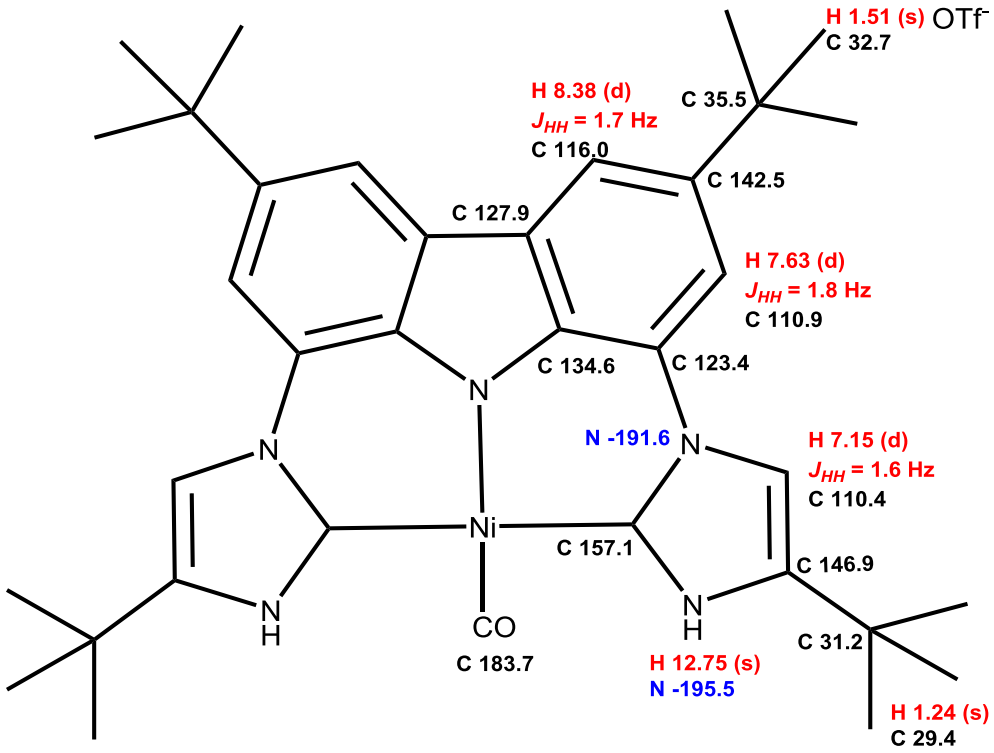

^{1}H -^{13}C gHMBCAD[b]		
H	bonds	C
1.24	1,3	29.4
1.24	2	31.2
1.24	3	146.9
1.51	1,3	32.7
1.51	2	35.5
1.51	3	142.5
7.15	3	123.4(w)
7.15	2	146.9
7.15	3	157.1
7.66	3	35.5
7.66	3	116.0
7.66	2	123.4
7.66	4	127.9(w)
7.66	3	133.4
7.66	2	143.1
8.39	3	35.5
8.39	3	112.5
8.39	4	124.7
8.39	2	127.9
8.39	3	133.4
[b] J_{nxh} = 8.0 Hz J_{1xh} = 146.0 Hz		

^{1}H -^{15}N gHMBCAD[a]		
H	bonds	N
7.15	2	-191.6
7.15	3	-195.5
7.63	3	-191.6
[a] J_{nxh}= 5 Hz J_{1xh}= 90 Hz		

^{1}H-^{13}C HSQCAD	
H	C
1.24	29.4
1.51	32.7
7.15	110.4
7.63	110.9
8.38	116.0

gCOSY
8.38↔7.63
7.63↔7.15

Figure 1.44. NMR data for **1.24e** in d_6-benzene.

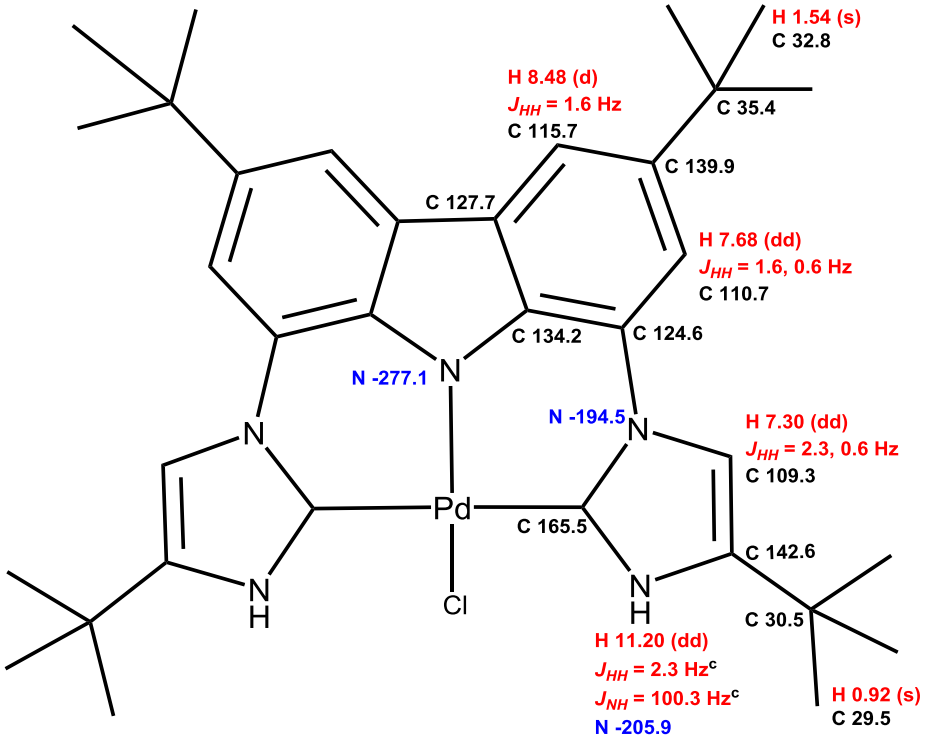

^{1}H -^{13}C gHMBCAD[b]		
H	bonds	C
0.92	1,3	29.5
0.92	2	30.5
0.92	3	142.6
1.54	1,3	32.8
1.54	2	35.4
1.54	3	139.9
7.30	3	124.6(w)
7.30	2	142.6
7.30	3	165.5
7.68	3	35.4
7.68	3	115.7
7.68	2	124.6
7.68	4	127.7(w)
7.68	3	134.2
7.68	2	139.9
7.68	4	165.5(w)
8.48	3	35.4
8.48	3	110.7
8.48	4	124.6

^{1}H -^{13}C gHMBCAD[b] continued		
H	bonds	C
8.48	2	127.7
8.48	3	134.2
11.20	3	109.3(w)
11.20	2	142.6(w)
11.20	2	165.5(w)
[b]J_{nxh} = 8.0 Hz J_{1xh} = 146.0 Hz		

^{1}H -^{15}N gHMBCAD[a]		
H	bonds	N
7.30	2	-194.5
7.30	3	-205.9
7.68	3	-194.5
7.68	4	-277.1
[a]J_{nxh}= 5 Hz J_{1xh}= 90 Hz		

^{1}H -^{15}N HSQCAD	
H	N
11.20	-205.9

^{1}H-^{13}C HSQCAD	
H	C
0.92	29.5
1.54	32.8
7.30	109.3
7.68	110.7
8.48	115.7

gCOSY
11.20↔7.30
8.48↔7.68
7.68↔7.30

Figure 1.45. NMR data for **1.25a** in d_6-benzene.

[c] Couplings observed on the N^{14}-H^{1} satellites, the N^{15} –H^{1} main peak is a broad singlet.

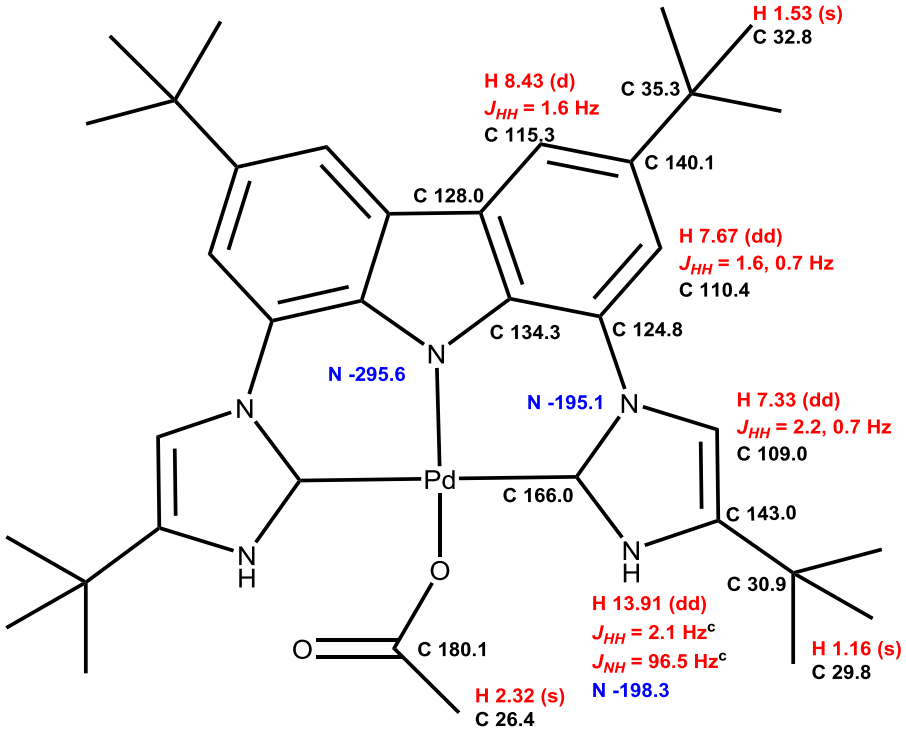

^{1}H -^{13}C gHMBCAD[b]		
H	bonds	C
1.16	1,3	29.8
1.16	2	30.9
1.16	3	143.0
1.53	1,3	32.8
1.53	2	35.3
1.53	3	140.1
2.32	2	180.1
7.33	3	124.8(w)
7.33	2	143.0
7.33	3	166.0
7.67	3	35.3
7.67	3	115.3
7.67	2	124.8
7.67	4	128.0(w)
7.67	3	134.3
7.67	2	140.1
7.67	4	166.0(w)
8.43	3	35.3

^{1}H -^{13}C gHMBCAD[b] continued		
H	bonds	C
8.43	3	110.4
8.43	4	124.8
8.43	2	128.0
8.43	3	134.3
11.20	3	109.0(w)
11.20	2	143.0(w)
11.20	2	166.0(w)
[b]J_{nxh} = 8.0 Hz J_{1xh} = 146.0 Hz		

^{1}H -^{15}N gHMBCAD[a]		
H	bonds	N
7.33	2	-195.1
7.33	3	-198.3
7.67	3	-195.1
7.67	4	-295.6
[a]J_{nxh}= 5 Hz J_{1xh}= 90 Hz		

^{1}H -^{15}N gHSQCAD	
H	N
13.91	-198.3

^{1}H-^{13}C HSQCAD	
H	C
1.16	29.8
1.53	32.8
2.32	26.4
7.33	109.0
7.67	110.4
8.43	115.3

gCOSY
13.91↔7.33
8.43↔7.67
7.67↔7.33(w)

Figure 1.46. NMR data for **1.25b** in d_6-benzene.

[c] Couplings observed on the N^{14}-H^{1} satellites, the N^{15} –H^{1} main peak is a broad singlet.

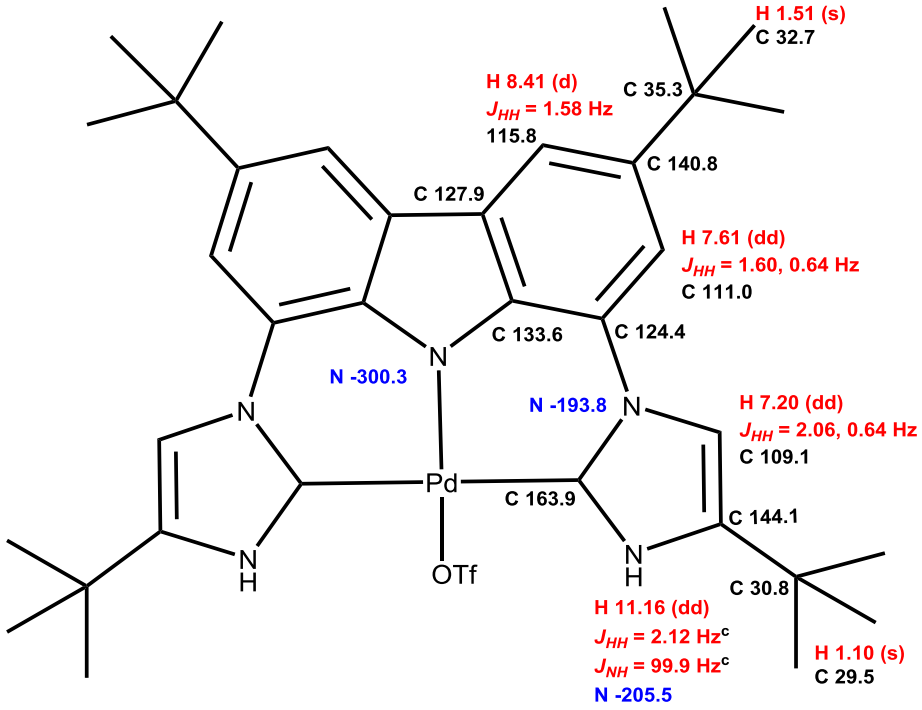

^{1}H -^{13}C gHMBCAD[b]		
H	bonds	C
1.10	1,3	29.5
1.10	2	30.8
1.10	3	144.1
1.51	1,3	32.7
1.51	2	35.3
1.51	3	140.8
7.20	3	124.4(w)
7.20	2	144.1
7.20	3	163.9
7.61	3	35.3
7.61	3	115.8
7.61	2	124.4
7.61	4	127.9(w)
7.61	3	133.6
7.61	2	140.8
7.61	4	163.9(w)
8.41	3	35.3
8.41	3	111.0
8.41	4	124.4

^{1}H -^{13}C gHMBCAD[b] continued		
H	bonds	C
8.41	2	127.9
8.41	3	133.6
11.20	3	109.1(w)
11.20	2	144.1(w)
11.20	2	163.9(w)
[b]J_{nxh} = 8.0 Hz J_{1xh} = 146.0 Hz		

^{1}H -^{15}N gHMBCAD[a]		
H	bonds	N
7.20	2	-193.8
7.20	3	-205.5
7.61	3	-193.8
7.61	4	-300.3
[a]J_{nxh}= 5 Hz J_{1xh}= 90 Hz		

^{1}H-^{13}C HSQCAD	
H	C
1.10	29.5
1.51	32.7
7.20	109.1
7.61	111.0
8.41	115.8

^{1}H -^{15}N gHSQCAD	
H	N
11.16	-205.5

gCOSY
11.16↔7.20
8.41↔7.61
7.61↔7.20(w)

Figure 1.47. NMR data for **1.25d** in d_6-benzene.

[c] Couplings observed on the N^{14}-H^{1} satellites, the N^{15} –H^{1} main peak is a broad singlet.

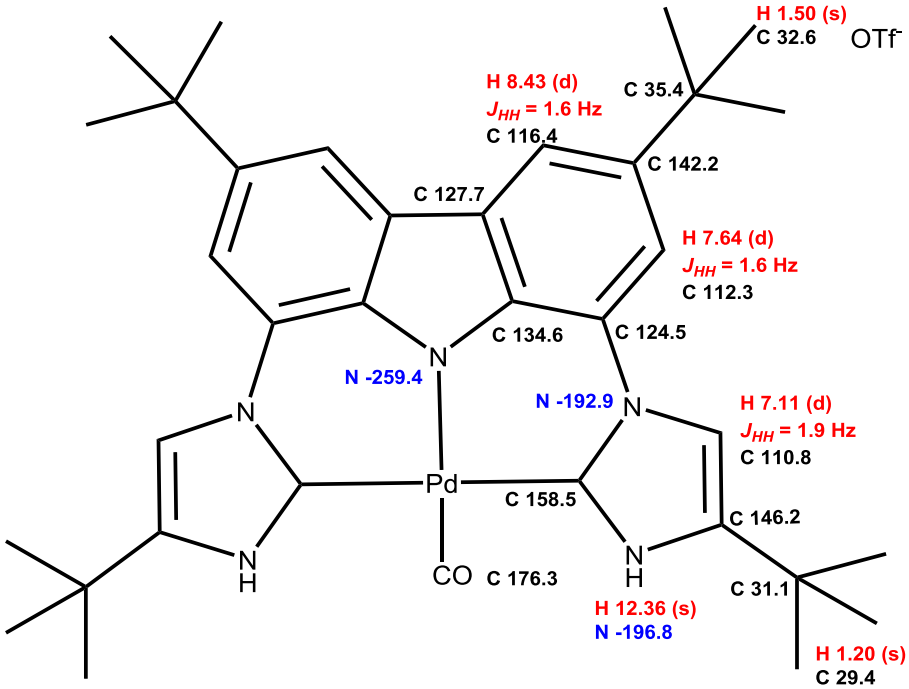

^{1}H -^{13}C gHMBCAD[b]		
H	bonds	C
1.20	1,3	29.4
1.20	2	31.1
1.20	3	146.2
1.50	1,3	32.6
1.50	2	35.4
1.50	3	142.2
7.20	3	124.5(w)
7.20	2	146.2
7.20	3	158.5
7.64	3	35.4
7.64	3	116.4
7.64	2	124.5
7.64	4	127.7(w)
7.64	3	134.6
7.64	2	142.2
8.43	3	35.4
8.43	3	112.3
8.43	4	124.5
8.43	2	127.7
8.43	3	134.6
[b]J_{nxh} = 8.0 Hz J_{1xh} = 146.0 Hz		

^{1}H-^{13}C HSQCAD	
H	C
1.20	29.4
1.50	32.6
7.11	110.8
7.64	112.3
8.43	116.4

gCOSY
12.36↔7.11
8.43↔7.64
7.64↔7.11(w)

^{1}H -^{15}N gHMBCAD[a]		
H	bonds	N
7.11	2	-192.9
7.11	3	-196.8
7.64	3	-192.9
7.64	4	-259.4
[a]J_{nxh}= 5 Hz J_{1xh}= 90 Hz		

^{1}H -^{15}N gHSQCAD	
H	N
12.36	-196.8

Figure 1.48. NMR data for **1.25e** in d_6-benzene.

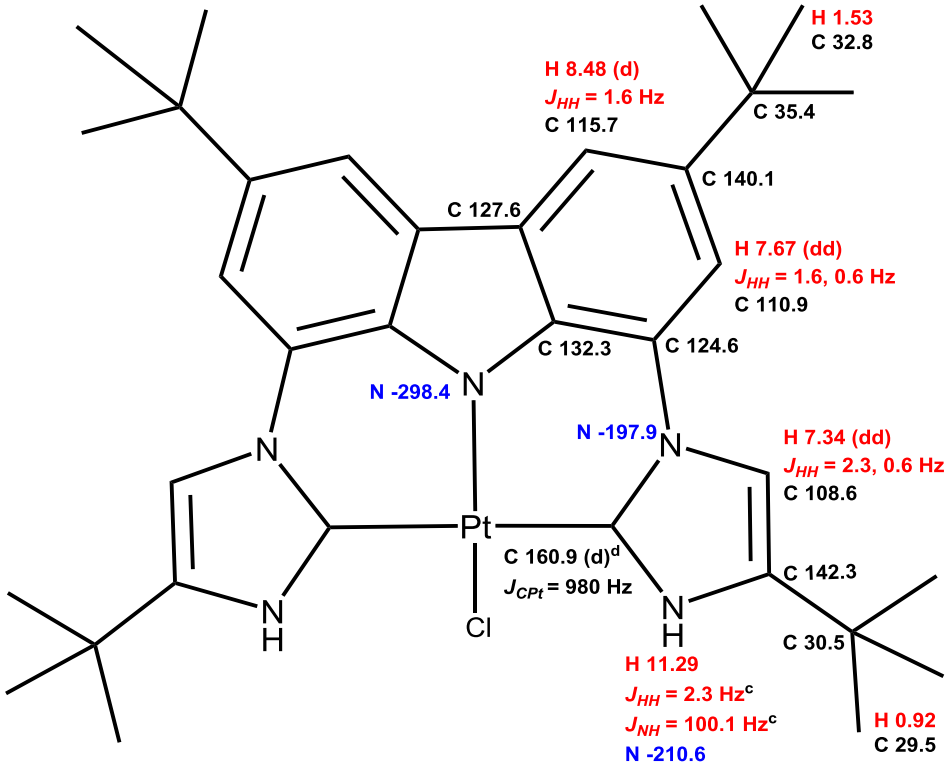

^{1}H -^{13}C gHMBCAD[b]		
H	bonds	C
0.92	1,3	29.5
0.92	2	30.5
0.92	3	142.3
1.53	1,3	32.8
1.53	2	35.4
1.53	3	140.1
7.34	3	124.6(w)
7.34	2	142.3
7.34	3	160.9
7.67	3	35.4
7.67	3	115.7
7.67	2	124.6
7.67	4	127.6(w)
7.67	3	132.3
7.67	2	140.1
7.67	4	160.9(w)

^{1}H -^{13}C gHMBCAD[b] cont		
8.48	3	35.4
8.48	3	110.9
8.48	4	124.6
8.48	2	127.6
8.48	3	132.3
11.29	3	108.6(w)
11.29	2	142.3(w)
11.29	2	160.9(w)
[b]J_{nxh} = 8.0 Hz J_{1xh} = 146.0 Hz		

^{1}H -^{15}N gHMBCAD[a]		
H	bonds	N
7.34	2	-197.9
7.34	3	-210.6
7.67	3	-197.9
7.67	4	-298.4
[a]J_{nxh}= 5 Hz J_{1xh}= 90 Hz		

^{1}H -^{15}N gHSQCAD	
H	N
11.29	-210.6

^{1}H-^{13}C HSQCAD	
H	C
0.92	29.5
1.53	32.8
7.34	108.6
7.67	110.9
8.48	115.7

gCOSY
11.29↔7.34
8.48↔7.67
7.67↔7.34

Figure 1.49. NMR data for **1.26a** in d_6-benzene.

[c] Couplings observed on the N^{14}-H^{1} satellites, the N^{15} –H^{1} main peak is a broad singlet.
[d] The Pt satellite peaks around the singlet carbon peak at 160.9 is a broad doublet.

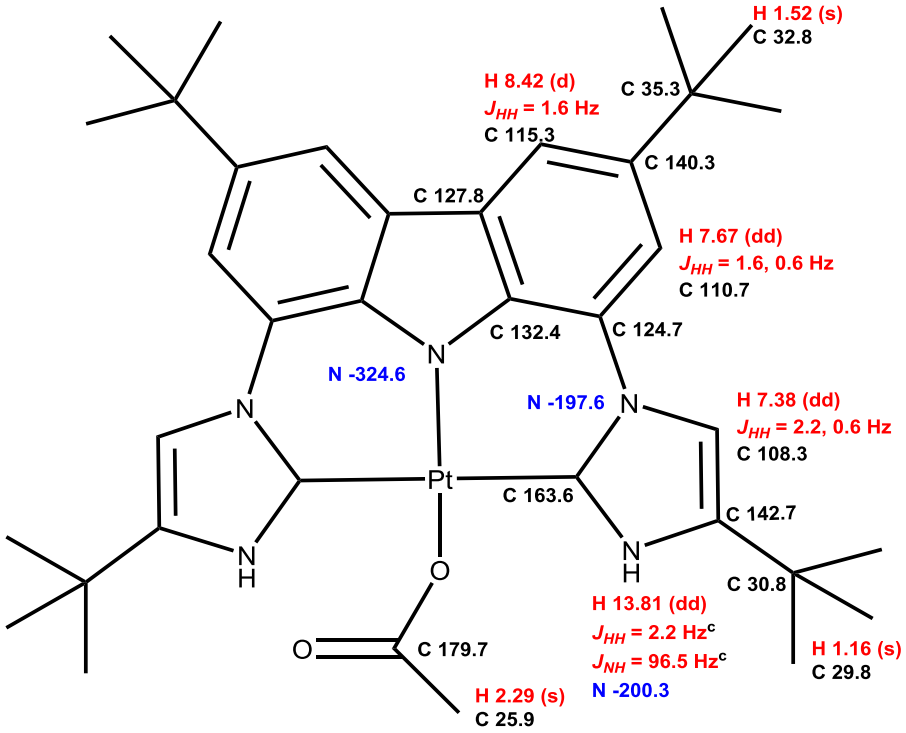

^{1}H -^{13}C gHMBCAD[b]		
H	bonds	C
1.16	1,3	29.8
1.16	2	30.8
1.16	3	142.7
1.52	1,3	32.8
1.52	2	35.3
1.52	3	140.3
2.29	2	179.7
7.38	3	124.7(w)
7.38	2	142.7
7.38	3	163.6
7.67	3	35.3
7.67	3	115.3

^{1}H-^{13}C HSQCAD	
H	C
1.16	29.8
1.52	32.8
2.29	25.9
7.38	108.3
7.67	110.7
8.42	115.3

^{1}H -^{13}C gHMBCAD[b] continued		
H	bonds	C
7.67	2	124.7
7.67	4	127.8(w)
7.67	3	132.4
7.67	2	140.3
8.42	3	35.3
8.42	3	110.7
8.42	4	124.7
8.42	2	127.8
8.42	3	132.4
13.81	3	108.3(w)
13.81	2	142.7(w)
13.81	2	163.6(w)
[b] J_{nxh} = 8.0 Hz J_{1xh} = 146.0 Hz		

^{1}H -^{15}N gHMBCAD[a]		
H	bonds	N
7.38	2	-197.6
7.38	3	-200.3
7.67	3	-197.6
7.67	4	-324.6
[a] J_{nxh}= 5 Hz J_{1xh}= 90 Hz		

^{1}H -^{15}N gHSQCAD	
H	N
13.81	-200.3

gCOSY
13.81↔7.38
8.42↔7.67
7.67↔7.38(w)

Figure 1.50. NMR data for **1.26b** in d_6-benzene.

[c] Couplings observed on the N^{14}-H^{1} satellites, the N^{15} –H^{1} main peak is a broad singlet.

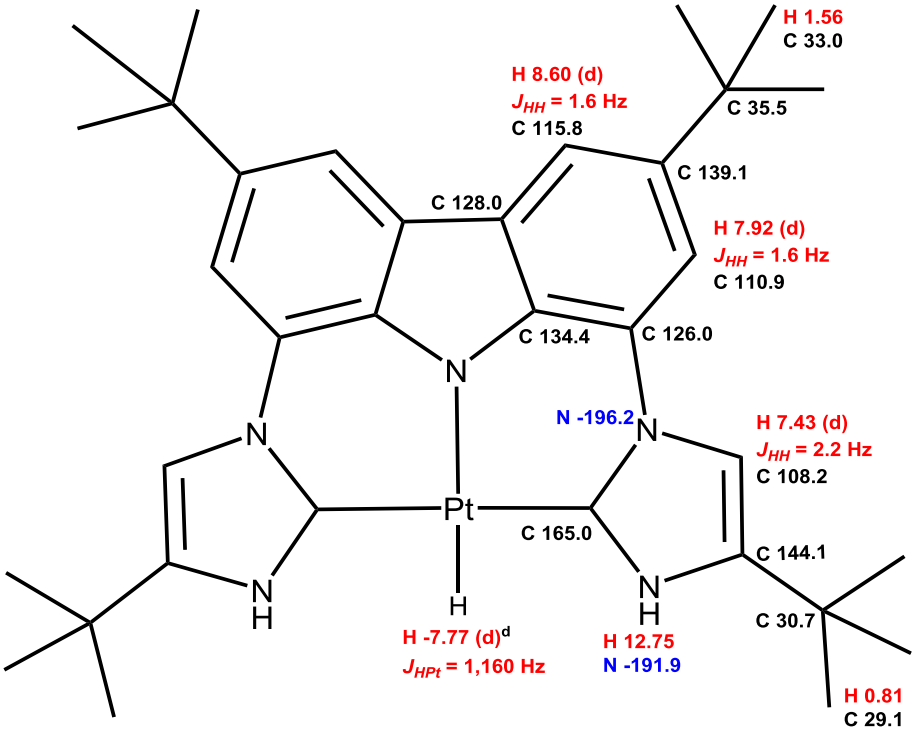

^{1}H -^{13}C gHMBCAD[b]		
H	bonds	C
0.81	1,3	29.1
0.81	2	30.7
0.81	3	144.1
1.56	1,3	33.0
1.56	2	35.5
1.56	3	139.1
7.43	3	126.0(w)
7.43	2	144.1
7.43	3	165.0
7.92	3	35.5
7.92	3	115.8
7.92	2	126.0
7.92	3	134.4
7.92	2	139.1
8.60	3	35.5
8.60	3	110.9
8.60	4	126.0
8.60	2	128.0
[b]J_{nxh} = 8.0 Hz J_{1xh} = 146.0 Hz		

^{1}H-^{13}C HSQCAD	
H	C
0.81	29.1
1.56	33.0
7.43	108.2
7.92	110.9
8.60	115.8

gCOSY
12.75↔7.43
8.60↔7.92
7.92↔7.43

^{1}H -^{15}N gHMBCAD[a]		
H	bonds	N
7.43	3	-191.9
7.43	2	-196.2
7.92	3	-196.2
[a]J_{nxh}= 5 Hz J_{1xh}= 90 Hz		

^{1}H -^{15}N gHSQCAD	
H	N
12.75	-191.9

Figure 1.51. NMR data for **1.26c** in d_6-benzene.

[d] The Pt satellite peaks around the singlet proton peak at -7.77 is a broad doublet.

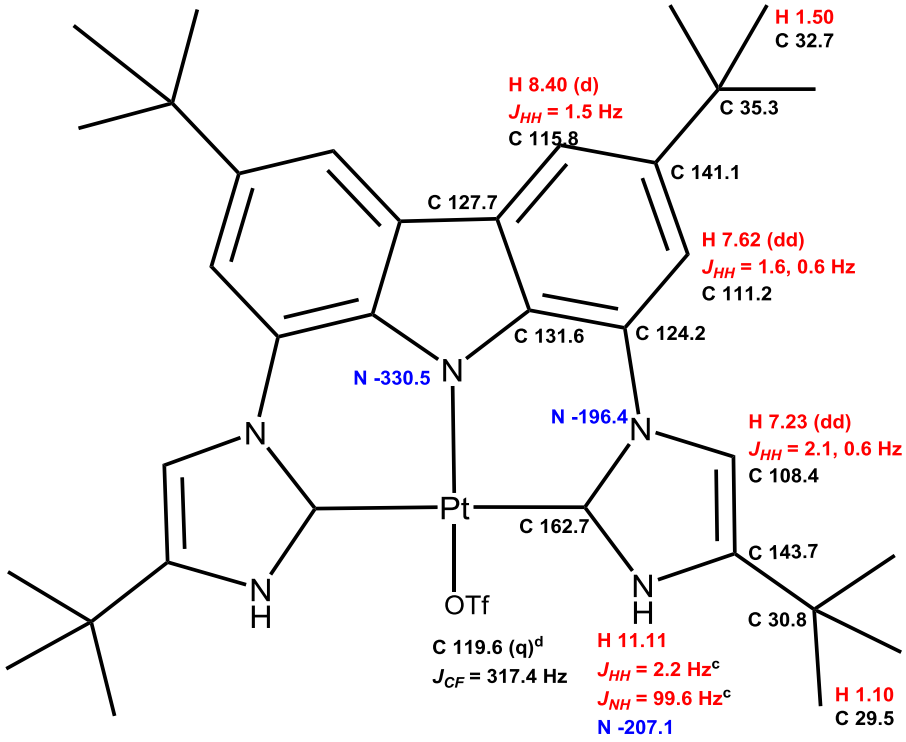

^{1}H -^{13}C gHMBCAD[b]		
H	bonds	C
1.10	1,3	29.5
1.10	2	30.8
1.10	3	143.7
1.50	1,3	32.7
1.50	2	35.3
1.50	3	141.1
7.23	3	124.2(w)
7.23	2	143.7
7.23	3	162.7
7.62	3	35.3
7.62	3	115.8

^{1}H-^{13}C **HSQCAD**	
H	C
1.10	29.5
1.50	32.7
7.23	108.4
7.62	111.2
8.40	115.8

^{1}H -^{13}C gHMBCAD[b]		
H	bonds	C
7.62	2	124.2
7.62	4	127.7(w)
7.62	3	131.6
7.62	2	141.1
8.40	3	35.3
8.40	3	111.2
8.40	4	124.2
8.40	2	127.7
8.40	3	131.6
11.11	3	108.4(w)
11.11	2	143.7(w)
11.11	2	162.7(w)
[b]J_{nxh} = 8.0 Hz J_{1xh} = 146.0 Hz		

^{1}H -^{15}N gHMBCAD[a]		
H	bonds	N
7.23	2	-196.4
7.23	3	-207.1
7.62	3	-196.4
7.62	4	-330.5
[a]J_{nxh}= 5 Hz J_{1xh}= 90 Hz		

^{1}H -^{15}N **gHSQCAD**	
H	N
11.11	-207.1

gCOSY
11.11↔7.23
8.40↔7.62
7.62↔7.23

Figure 1.52. NMR data for **1.26d** in d_6-benzene.

[c] Couplings observed on the N^{14}-H^{1} satellites, the N^{15} –H^{1} main peak is a broad singlet.
[d] Only the two most intense peaks of the quartet are observed.

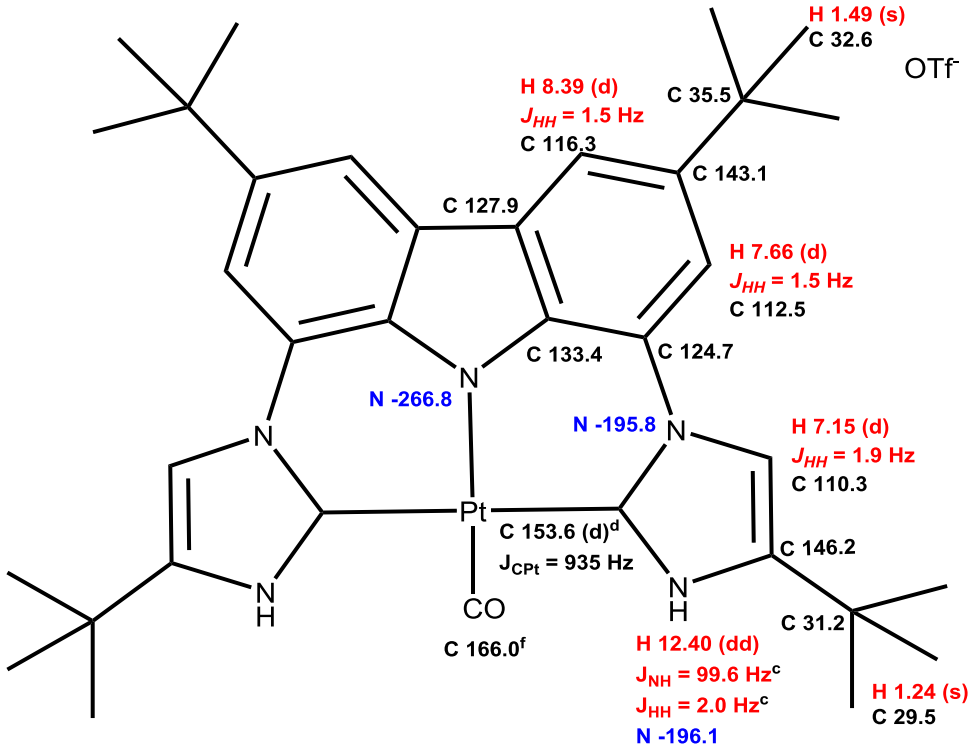

^{1}H -^{13}C gHMBCAD[b]		
H	bonds	C
1.24	1,3	29.5
1.24	2	31.2
1.24	3	146.2
1.49	1,3	32.6
1.49	2	35.5
1.49	3	143.1
7.15	3	124.7(w)
7.15	2	146.2
7.15	3	153.6
7.66	3	35.5
7.66	3	116.3
7.66	2	124.7

^{1}H -^{13}C gHMBCAD[b] continued		
H	bonds	C
7.66	4	127.9(w)
7.66	3	133.4
7.66	2	143.1
8.39	3	35.5
8.39	3	112.5
8.39	4	124.7
8.39	2	127.9
8.39	3	133.4
[b] J_{nxh} = 8.0 Hz J_{1xh} = 146.0 Hz		

gCOSY
12.40↔7.15
8.39↔7.66
7.66↔7.15(w)

^{1}H -^{15}N gHMBCAD[a]		
H	bonds	N
7.15	2 or 3[e]	-196.0[e]
7.66	3	-195.8
7.66	4	-266.8
[a] J_{nxh}= 5 Hz J_{1xh}= 90 Hz		

^{1}H -^{15}N gHSQCAD	
H	N
12.40	-196.1

^{1}H-^{13}C HSQCAD	
H	C
1.24	29.5
1.49	32.6
7.15	110.3
7.66	112.5
8.39	116.3

Figure 1.53. NMR data for **1.26e** in d_6-benzene.

[c] Couplings observed on the N^{14}-H^{1} satellites, the N^{15} –H^{1} main peak is a broad singlet.
[d] The Pt satellite peaks around the singlet carbon peak at 153.6 is a broad doublet
[e] The two imidazole nitrogen chemical shifts were too close to differentiate by the cross peak with 7.15, an averaged larger peak centered at -196.0 was observed.
[f] Not observed in 2D experiments, but is one of two unassigned carbons peaks. The remaining carbon peak at 184.8 ppm is most likely due to free carbon monoxide.

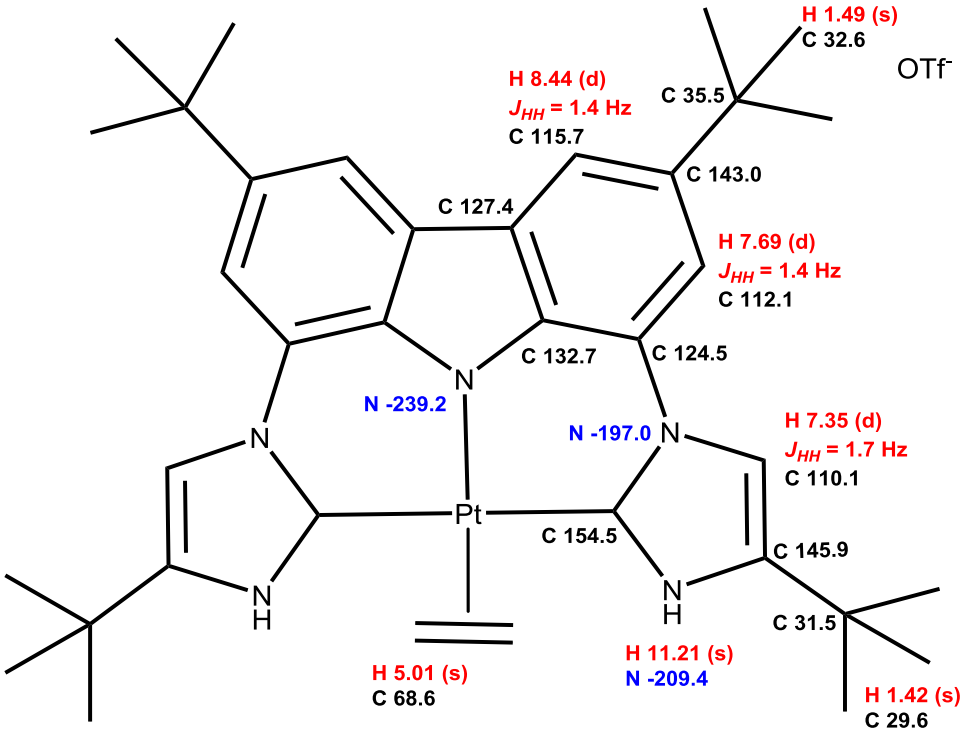

^{1}H -^{13}C gHMBCAD[b]		
H	bonds	C
1.42	1,3	29.6
1.42	2	31.5
1.42	3	145.9
1.49	1,3	32.6
1.49	2	35.5
1.49	3	143.0
5.01	3	154.5
7.35	3	124.5(w)
7.35	2	145.9
7.35	3	154.5
7.69	3	35.5
7.69	3	115.7
7.69	4	124.5
7.69	2	127.4(w)

^{1}H -^{13}C gHMBCAD[b] continued		
H	bonds	C
7.69	3	132.7
7.69	2	143.0
8.44	3	35.5
8.44	3	112.1
8.44	4	124.5
8.44	2	127.4
8.44	3	132.7
11.21	3	110.1(w)
11.21	2	145.9(w)
11.21	2	154.(w)5
[b]J_{nxh} = 8.0 Hz J_{1xh} = 146.0 Hz		

^{1}H -^{15}N gHMBCAD[a]		
H	bonds	N
7.35	2	-197.0
7.35	3	-209.4
7.69	3	-197.0
7.69	4	-239.2
11.21	3	-197.0
[a]J_{nxh}= 5 Hz J_{1xh}= 90 Hz		

^{1}H -^{15}N gHSQCAD	
H	N
11.21	-209.4

gCOSY
11.21↔7.35
8.44↔7.69
7.69↔7.35(w)

^{1}H-^{13}C HSQCAD	
H	C
1.42	29.6
1.49	32.6
5.01	68.6
7.35	110.1
7.69	112.1
8.44	115.7

Figure 1.54. NMR data for **1.26f** in d_6-benzene.

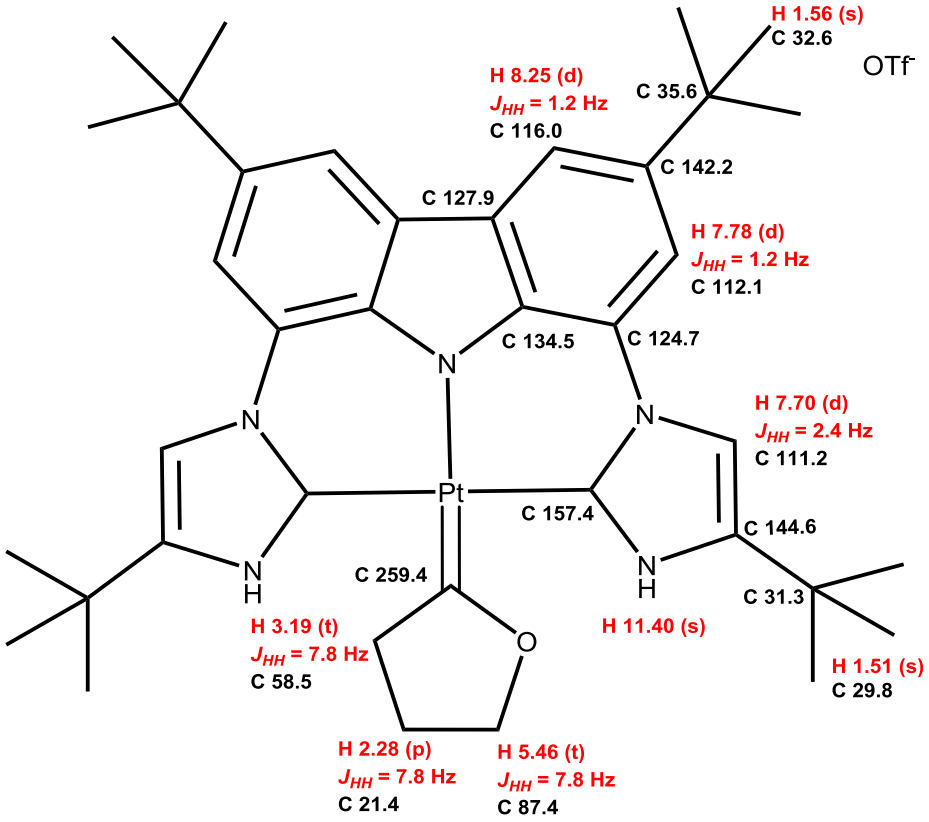

^{1}H -^{13}C gHMBCAD[b]		
H	bonds	C
1.51	1,3	29.8
1.51	2	31.3
1.51	3	144.6
1.56	1,3	32.6
1.56	2	35.6
1.56	3	142.2
2.28	2	58.5
2.28	2	87.4
2.28	3	259.4
3.19	2	21.4
3.19	3	87.4
3.19	2	259.4
5.46	2	21.4
5.46	3	58.5
5.46	3	259.4

^{1}H -^{13}C gHMBCAD[b]		
H	bonds	C
7.70	3	124.7
7.70	2	144.6
7.70	3	157.4
7.78	3	35.6
7.78	3	116.0
7.78	2	124.7
7.78	4	127.9(w)
7.78	3	134.5
7.78	2	142.2
8.25	3	35.6
8.25	3	112.1
8.25	4	124.7
8.25	2	127.9
8.25	3	134.5
[b]J_{nxh} = 8.0 Hz J_{1xh} = 146.0 Hz		

^{1}H-^{13}C HSQCAD	
H	C
1.51	29.8
1.56	32.6
2.28	21.4
3.19	58.5
5.76	87.4
7.70	111.2
7.78	112.1
8.25	116.0

gCOSY
11.40↔7.70
8.25↔7.78
5.46↔2.28
3.19↔2.28

Figure 1.55. NMR data for **1.30** in CD_2Cl_2.

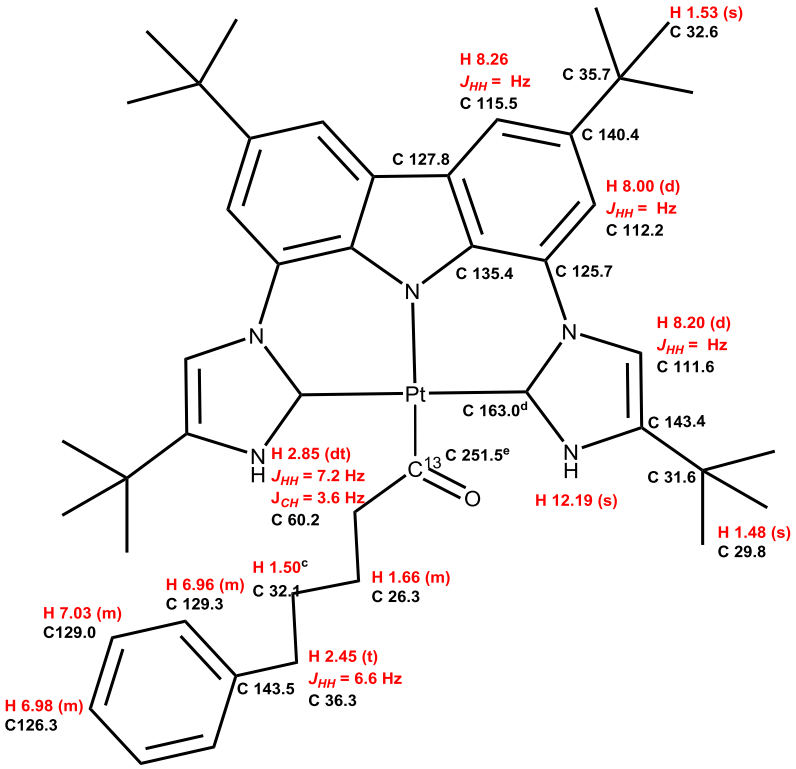

^{1}H -^{13}C gHMBCAD[b]		
H	bonds	C
1.48	1,3	29.8
1.48	2	31.6
1.48	3	143.4
1.53	1,3	32.6
1.53	2	35.7
1.53	3	140.4
1.66	3	36.3
1.66	2	60.2
1.66	3	251.5
2.45	3	26.3
2.45	2	32.1
2.45	3	129.3
2.45	2	143.5
2.85	2	26.3
2.85	3	32.1
2.85	2	251.5
6.96	3	126.3
6.96	2	129.0

^{1}H -^{13}C gHMBCAD[b] continued		
H	bonds	C
6.98	2	129.0
7.03	1,3	129.0
7.03	3	143.5
8.00	3	35.7
8.00	3	115.5
8.00	2	125.7
8.00	4	127.8
8.00	2	140.4
8.20	3	125.7
8.20	2	143.4
8.20	3	163.0
8.26	3	35.7
8.26	3	112.2
8.26	4	125.7
8.26	2	127.8
8.26	3	135.4
[b] J_{nxh} = 8.0 Hz J_{1xh} = 146.0 Hz		

gCOSY
12.19↔8.20
8.26↔8.00
2.85↔1.66
2.45↔1.50

^{1}H-^{13}C HSQCAD	
H	C
1.48	29.8
1.53	32.6
1.50	-
1.66	26.3
2.45	36.3
2.85	60.2
6.96	129.3
6.98	126.3
7.03	129.0
8.00	112.2
8.20	111.6
8.26	115.5

Figure 1.56. NMR data for **1.29** in d_6-acetone.

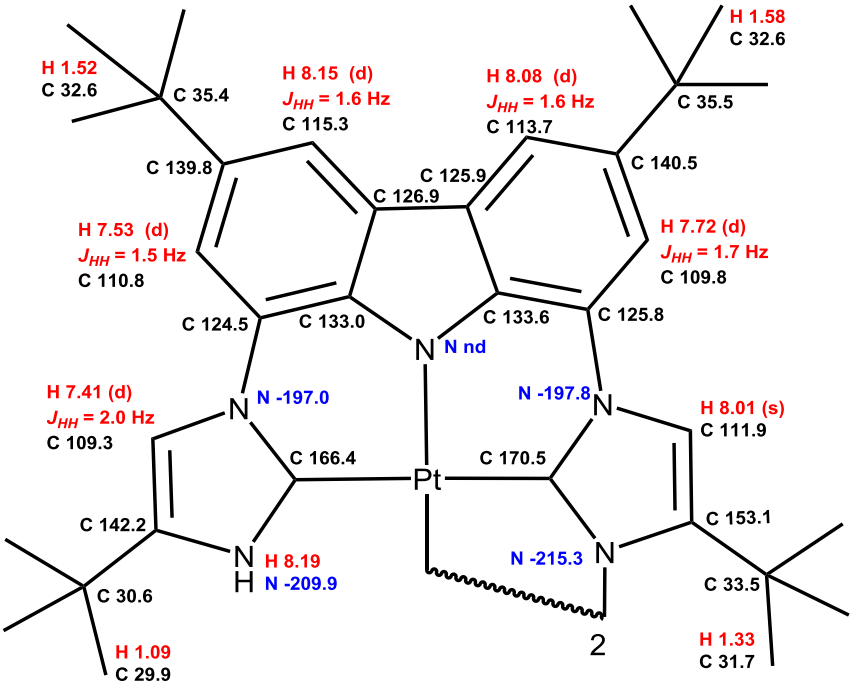

^{1}H -^{13}C gHMBC[b]		
H	bonds	C
8.19	2	166.4
8.19	2	142.2
8.19	3	109.3
8.15	3	133.1
8.15	2	126.9(w)
8.15	3	125.9
8.15	4	124.5(w)
8.15	3	110.8
8.15	3	35.4
8.08	3	133.6
8.08	3	126.9
8.08	2	125.9(w)
8.08	3	109.8
8.08	3	35.5
8.01	3	170.5
8.01	2	153.1
8.01	3	125.8(w)
7.72	2	140.5(w)
7.72	3	133.6
7.72	4	125.9
7.72	3	113.7
7.72	3	35.5
7.53	2	139.8(w)

^{1}H -^{13}C gHMBCAD Continued[b]		
H	bonds	C
7.53	3	133.0
7.53	4	126.9(w)
7.53	2	124.5
7.53	3	115.3
7.53	3	35.4
7.41	3	166.4
7.41	2	142.2
7.41	3	124.5(w)
1.58	3	140.5
1.58	2	35.5
1.58	1,3	32.6
1.52	3	139.8
1.52	2	35.4
1.52	1,3	32.6
1.33	3	153.1
1.33	2	33.5
1.33	1,3	31.7
1.09	3	142.2
1.09	2	30.6
1.09	1,3	29.9
[b]J_{nxh} = 8.0 Hz J_{1xh} = 140.0 Hz		

^{1}H -^{15}N gHMBCAD[a]		
H	bonds	N
8.01	3	-215.3
8.01	2	-197.8
7.72	3	-197.8
7.53	3	-197.0
7.41	3	-209.9
7.41	2	-197.0
[a]J_{nxh}= 5 Hz J_{1xh}= 90 Hz		

^{1}H-^{13}C HSQCAD	
H	C
8.15	115.3
8.08	113.7
8.01	111.9
7.72	109.8
7.53	110.8
7.41	109.3
1.58	32.6
1.52	32.6
1.33	31.7
1.09	29.9

gCOSY
8.19↔7.41
8.15↔7.53
8.08↔7.72

Figure 1.57. NMR data for **1.32-Pt** in CD_2Cl_2.

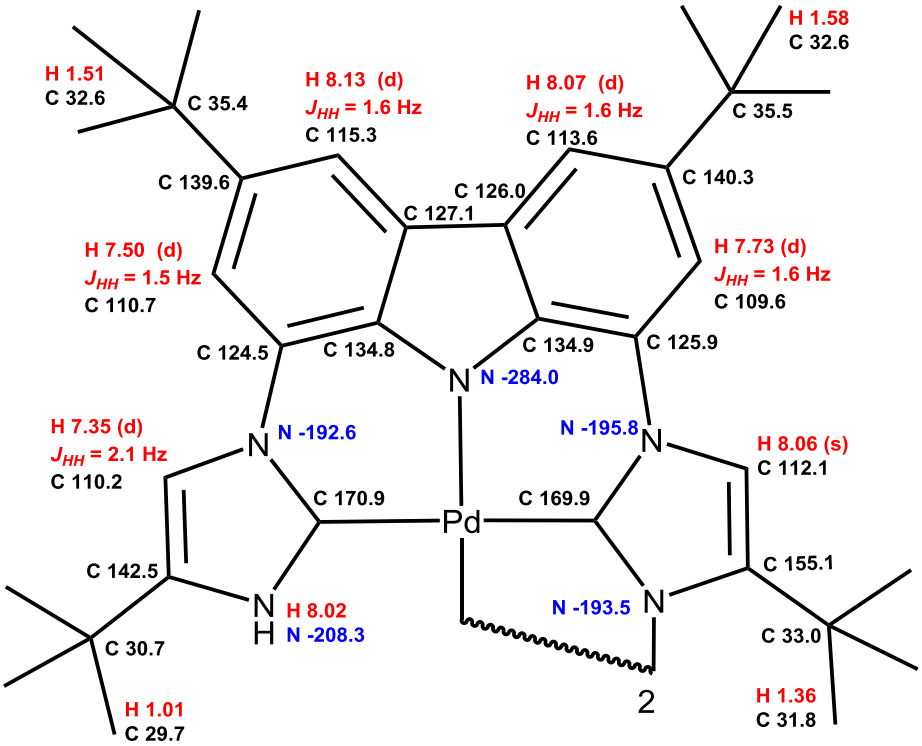

^{1}H -^{13}C gHMBC[b]		
H	bonds	C
8.13	3	134.8
8.13	3	126.0
8.13	3	110.7
8.13	3	35.4
8.07	3	134.9
8.07	3	127.1
8.07	2	126.0(w)
8.07	3	109.6
8.07	3	35.5
8.06	3	169.9
8.06	2	155.1
8.02	2	170.9(w)
8.02	2	142.5(w)
8.02	3	110.2(w)
7.73	3	134.9
7.73	2	125.9(w)
7.73	3	113.6
7.73	3	35.5
7.50	3	134.8
7.50	2	124.5(w)
7.50	3	115.3
7.50	3	35.4

^{1}H -^{13}C gHMBCAD Continued[b]		
H	bonds	C
7.35	3	170.9
7.35	2	142.5
1.58	3	140.3
1.58	2	35.5
1.58	1,3	326
1.51	3	139.6
1.51	2	35.4
1.51	1,3	32.6
1.36	3	155.1
1.36	2	33.0
1.36	1,3	31.8
1.01	3	142.5
1.01	2	30.7
1.01	1,3	29.7
$^{b}J_{nxh}$ = 8.0 Hz J_{1xh} = 146.0 Hz		

gCOSY
8.13↔7.50
8.07↔7.73
8.02↔7.35

^{1}H -^{15}N gHMBCAD[a]		
H	bonds	N
8.06	2	-195.8
8.06	3	-193.5
7.73	4	-284.0
7.73	3	-195.8
7.50	4	-284.0
7.50	3	-192.6
7.35	3	-208.3
7.35	2	-192.6
$^{a}J_{nxh}$= 5 Hz J_{1xh}= 90 Hz		

^{1}H-^{13}C HSQCAD	
H	C
8.13	115.3
8.07	113.6
8.06	112.1
7.73	109.6
7.50	110.7
7.35	110.2
1.58	32.6
1.51	32.6
1.36	31.8
1.01	29.7

Figure 1.58. NMR data for **1.32-Pd** in CD_2Cl_2.

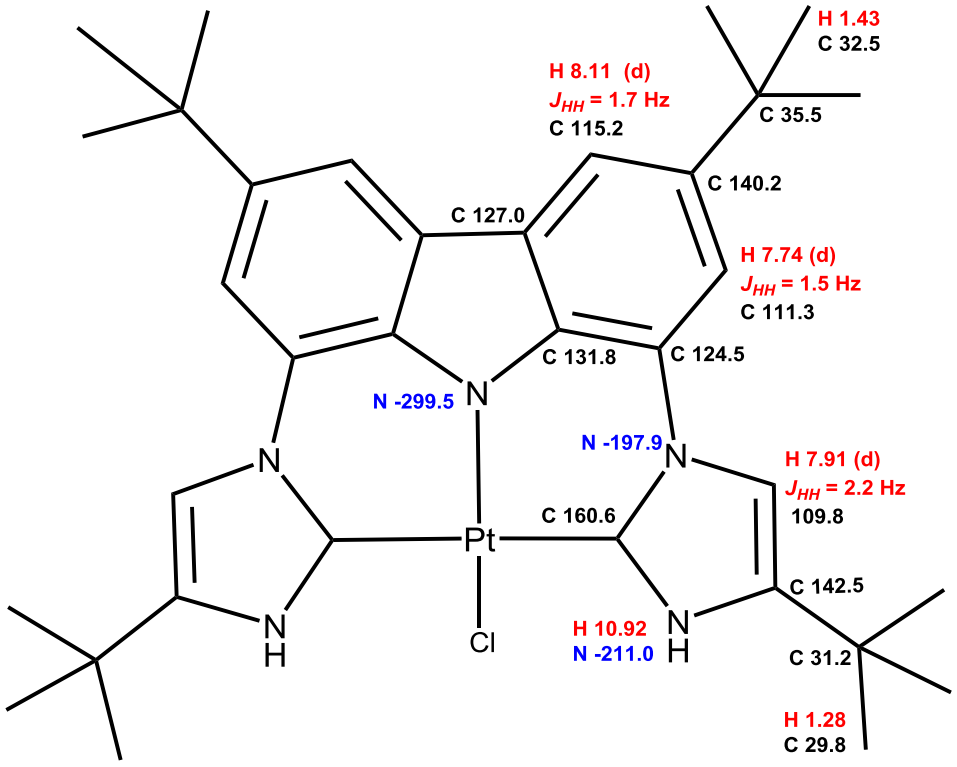

^{1}H -^{13}C gHMBCAD[b]		
H	bonds	C
8.11	3	35.5
8.11	3	111.3
8.11	2	127.0(w)
8.11	3	131.8
7.91	2	142.5
7.91	3	160.6(w)
7.74	3	35.5
7.74	3	115.2
7.74	2	124.5(w)
7.74	3	131.8
1.43	1,3	32.5
1.43	2	35.5
1.43	3	140.2
1.28	1,3	29.8
1.28	2	31.2
1.28	3	142.5
[b]J_{nxh} = 8.0 Hz J_{1xh} = 146.0 Hz		

^{1}H-^{13}C HSQCAD	
H	C
8.11	115.2
7.91	109.8
7.74	111.3
1.43	32.5
1.28	29.8

gCOSY
10.92↔7.92
8.11↔7.74

^{1}H -^{15}N gHMBCAD[a]		
H	bonds	N
7.91	2	-197.9
7.91	3	-211.0
7.74	3	-197.9
7.74	4	-299.5
[a]J_{nxh}= 5 Hz J_{1xh}= 90 Hz		

Figure 1.59. NMR data for **1.26a** in THF (0.6 mL) and d_6-benzene (0.1 mL).

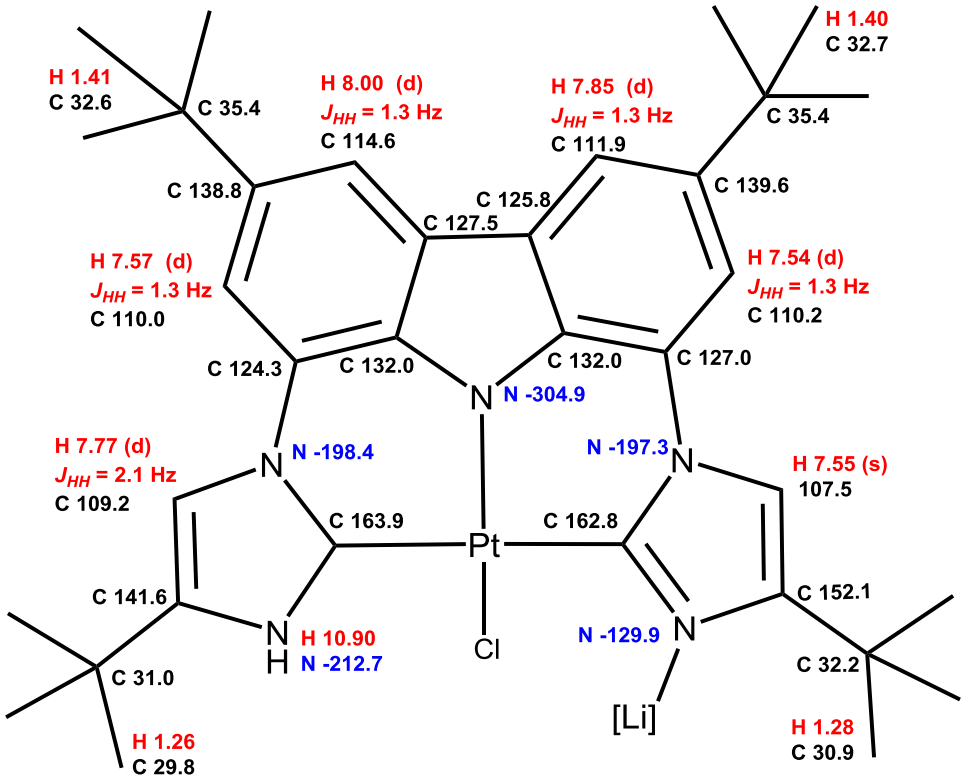

^{1}H -^{13}C gHMBCAD[b]		
H	bonds	C
8.00	3	110.0
8.00	4	124.3(w)
8.00	3	125.8
8.00	2	127.5(w)
8.00	3	132.0
8.00	3	35.4
7.85	3	110.2
7.85	2	125.8(w)
7.85	3	127.5
7.85	3	132.0
7.85	3	35.4
7.77	2	141.6
7.77	3	163.9
7.57	3	114.6
7.57	2	124.3(w)
7.57	4	127.5(w)
7.57	3	132.0
7.57	2	138.8(w)
7.57	3	35.4
7.55	2	152.1
7.55	3	162.8

^{1}H -^{13}C gHMBCAD Continued		
H	bonds	C
7.54	3	111.9
7.54	4	125.8(w)
7.54	2	127.0
7.54	3	132.0
7.54	2	139.6(w)
7.54	3	35.4
1.41	1,3	32.6
1.41	2	35.4
1.41	3	138.8
1.40	1,3	32.7
1.40	2	35.4
1.40	3	139.6
1.28	1,3	30.9
1.28	2	32.2
1.28	3	152.1
1.26	1,3	29.8
1.26	2	31.0
1.26	3	141.6

[b] J_{nxh} = 8.0 Hz
J_{1xh} = 146.0 Hz

^{1}H -^{15}N gHMBCAD[a]		
H	bonds	N
7.77	3	-212.7
7.77	2	-198.4
7.57	4	-304.9
7.57	3	-198.4
7.55	2	-197.3
7.55	3	-129.9
7.54	4	-304.9
7.54	3	-197.3

[a] J_{nxh}= 5 Hz
J_{1xh}= 90 Hz

^{1}H-^{13}C HSQCAD	
H	C
8.00	114.6
7.85	111.9
7.77	109.2
7.57	110.0
7.55	107.5
7.54	110.2
1.41	32.6
1.40	32.7
1.28	30.9
1.26	29.8

gCOSY
10.90↔7.77
8.00↔7.57
7.85↔7.54

^{1}H -^{15}N gHSQC	
H	N
10.90	-212.7

Figure 1.60. NMR data for **1.33-Pt** in THF (0.6 mL) and d_6-benzene (0.1 mL).

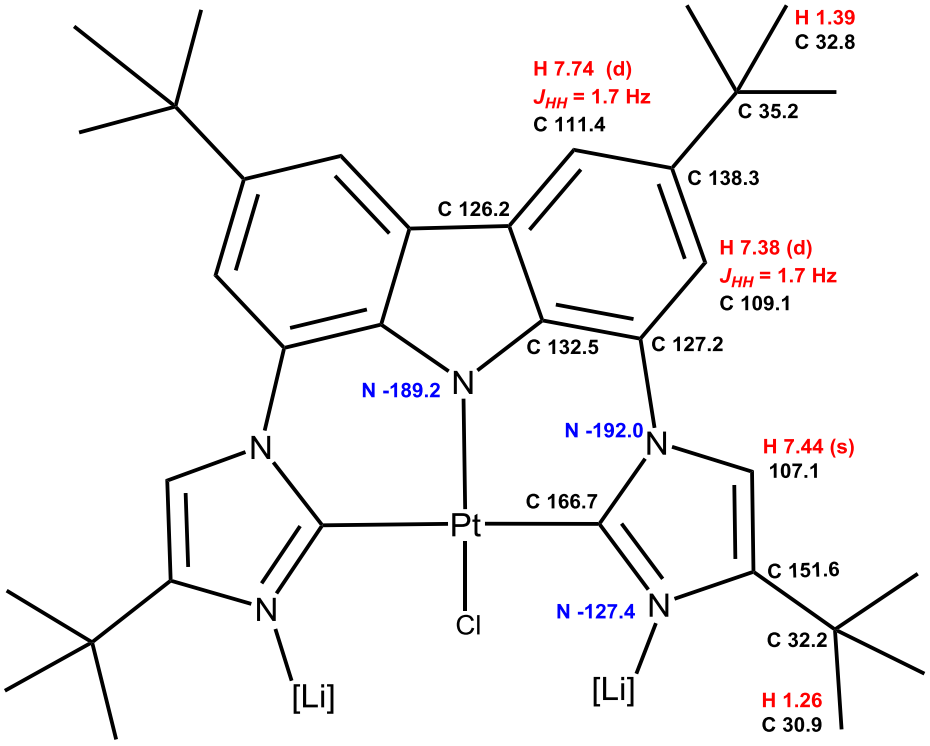

^{1}H -^{13}C gHMBCAD[b]		
H	bonds	C
7.74	3	109.1
7.74	2	126.2
7.74	4	127.2(w
7.74	3	132.5
7.44	2	151.6
7.44	3	166.7
7.38	3	111.4
7.38	2	127.2
7.38	3	132.5
1.39	1,3	32.8
1.39	2	35.2
1.39	3	138.3
1.26	1,3	30.9
1.26	2	32.2
1.26	3	151.6
[b]J_{nxh} = 8.0 Hz J_{1xh} = 146.0 Hz		

^{1}H-^{13}C HSQCAD	
H	C
7.74	111.4
7.44	107.1
7.38	109.1
1.39	32.8
1.26	30.9

gCOSY
7.74↔7.38

^{1}H -^{15}N gHMBCAD[a]		
H	bonds	N
7.74	4	-189.2
7.44	2	-192.0
7.44	3	-127.4
7.38	3	-192.0
[a]J_{nxh}= 5 Hz J_{1xh}= 90 Hz		

Figure 1.61. NMR data for **1.34-Pt** in THF (0.6 mL) and d_6-benzene (0.1 mL).

M. NMR Spectra

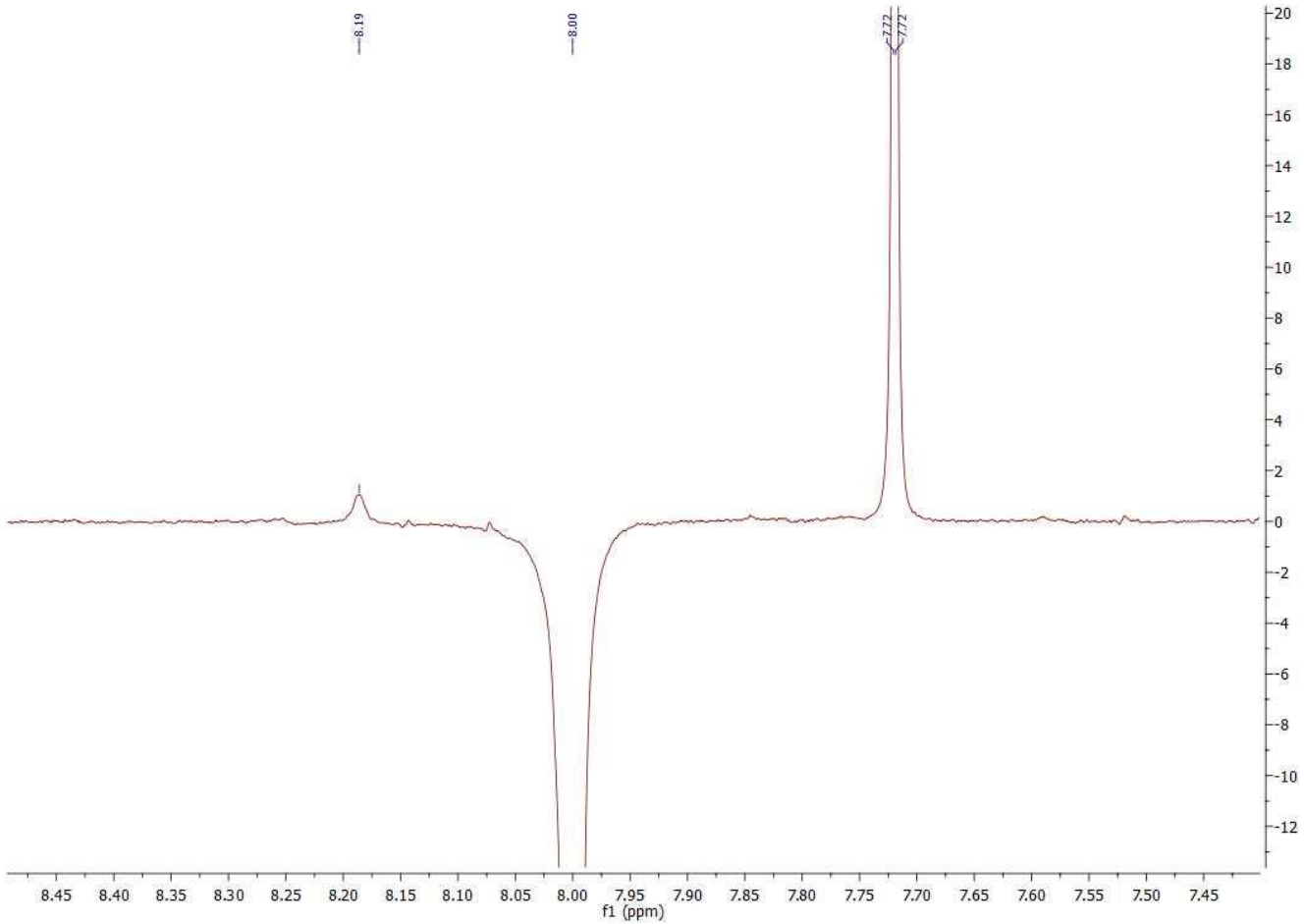

Figure 1.62. ROESY 1D spectrum of **1.32-Pt**, irradiating peak at 8.01, C4 on MNHC imidazole and seeing the correlating peaks at 7.72 ppm from the carbazole, and 8.19 ppm from the NH on the PNHC.

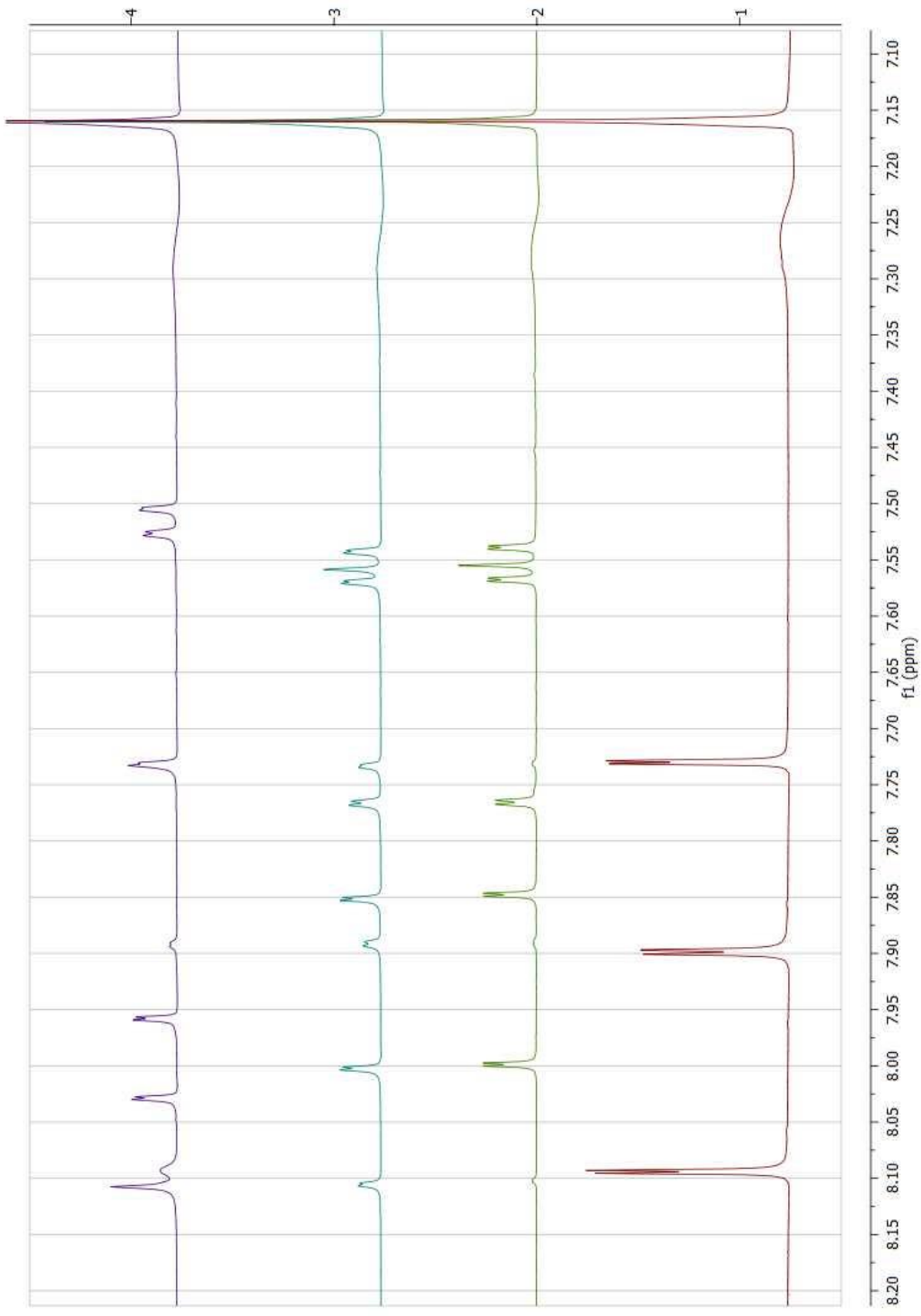

Figure 1.63. ^{1}H NMR spectra of **1.26a** (red, 1), **1.33-Pt** (green, 2), 19 h after bubbling H_2 in solution (blue, 3) mostly still **1.33-Pt** with some **1.26a**, NMR after addition of AgOTf (1.25 equiv) (purple, 4), formation of dimer **1.32-Pt**.

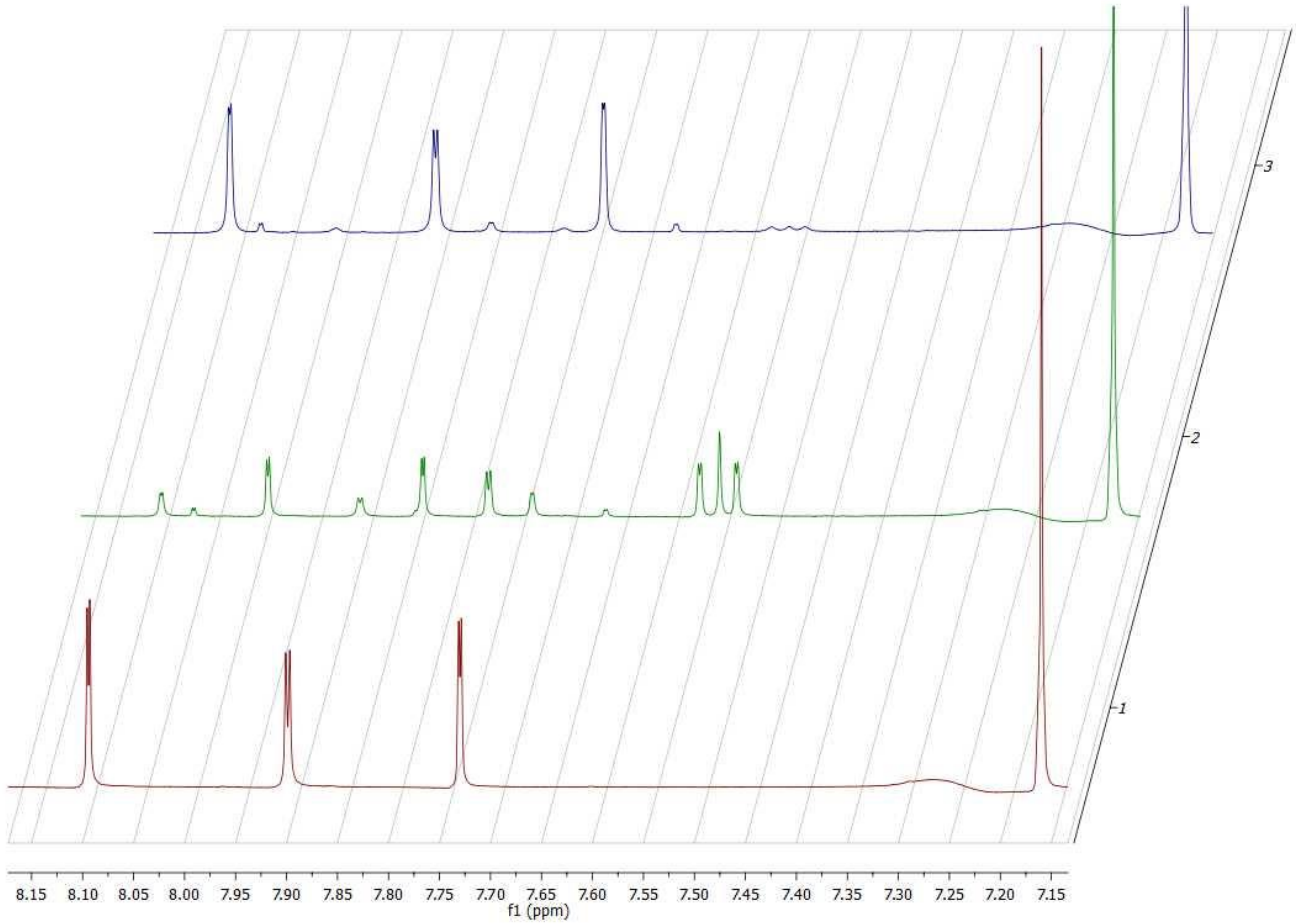

Figure 1.64. ^{1}H NMR spectra of **1.26a** (red) in THF (0.6 mL) and d_6-benzene(0.1 mL), ^{1}H NMR of **1.33-Pt** (green), formed from **1.26a** and n-BuLi (2.5 M, 1 equiv), ^{1}H NMR after bubbling ethylene gas through solution for 4 min (blue), showing mostly **1.26a**.

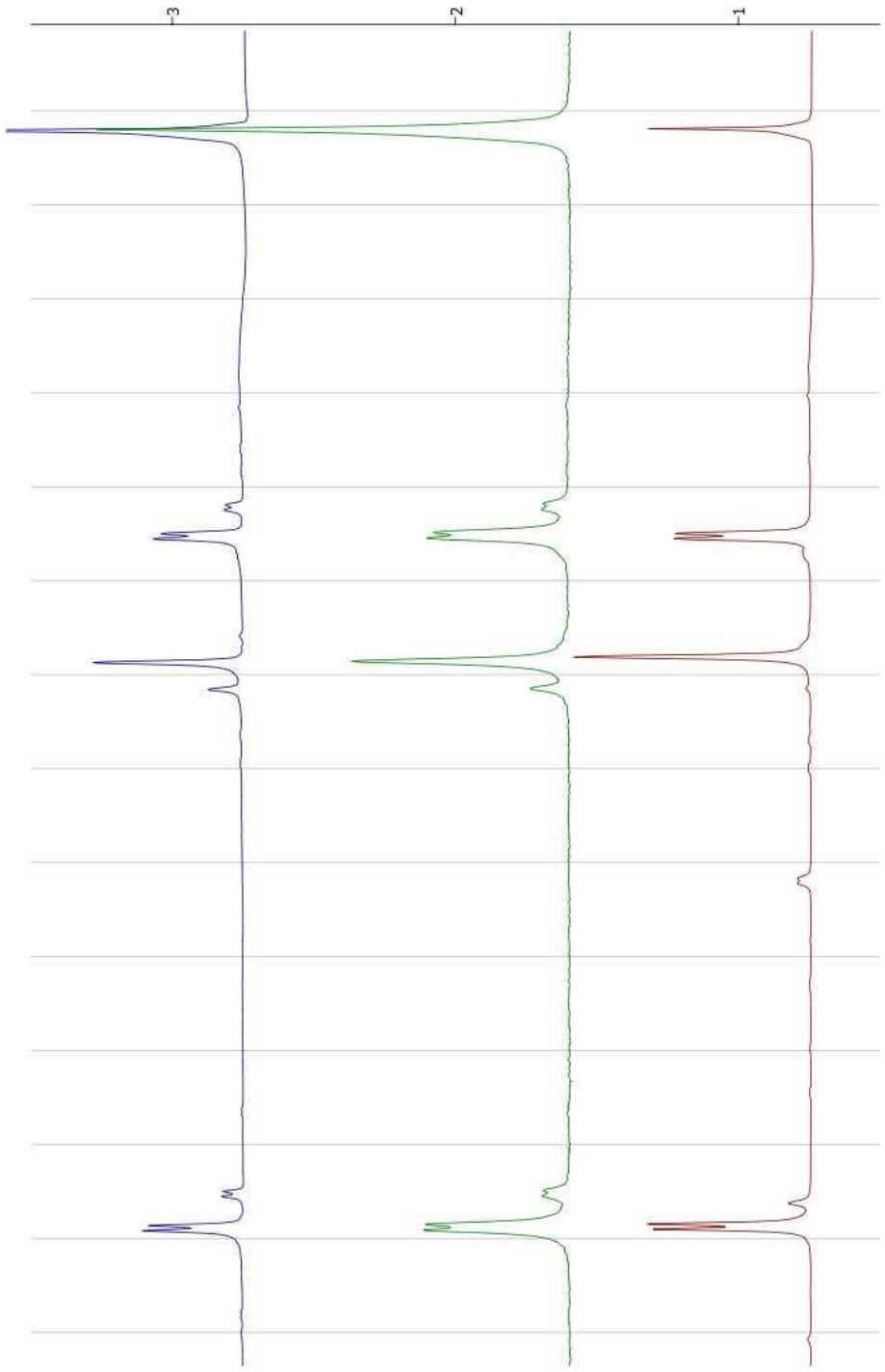

Figure 1.65. ^{1}H NMR spectra of **1.34-Pt** (red, 1) in THF (0.6 mL) and d_6-benzene (0.1 mL), after addition of 1-heptene (20 equiv) (green, 2), after heating for 4 h at 70 ^{o}C (purple, 3).

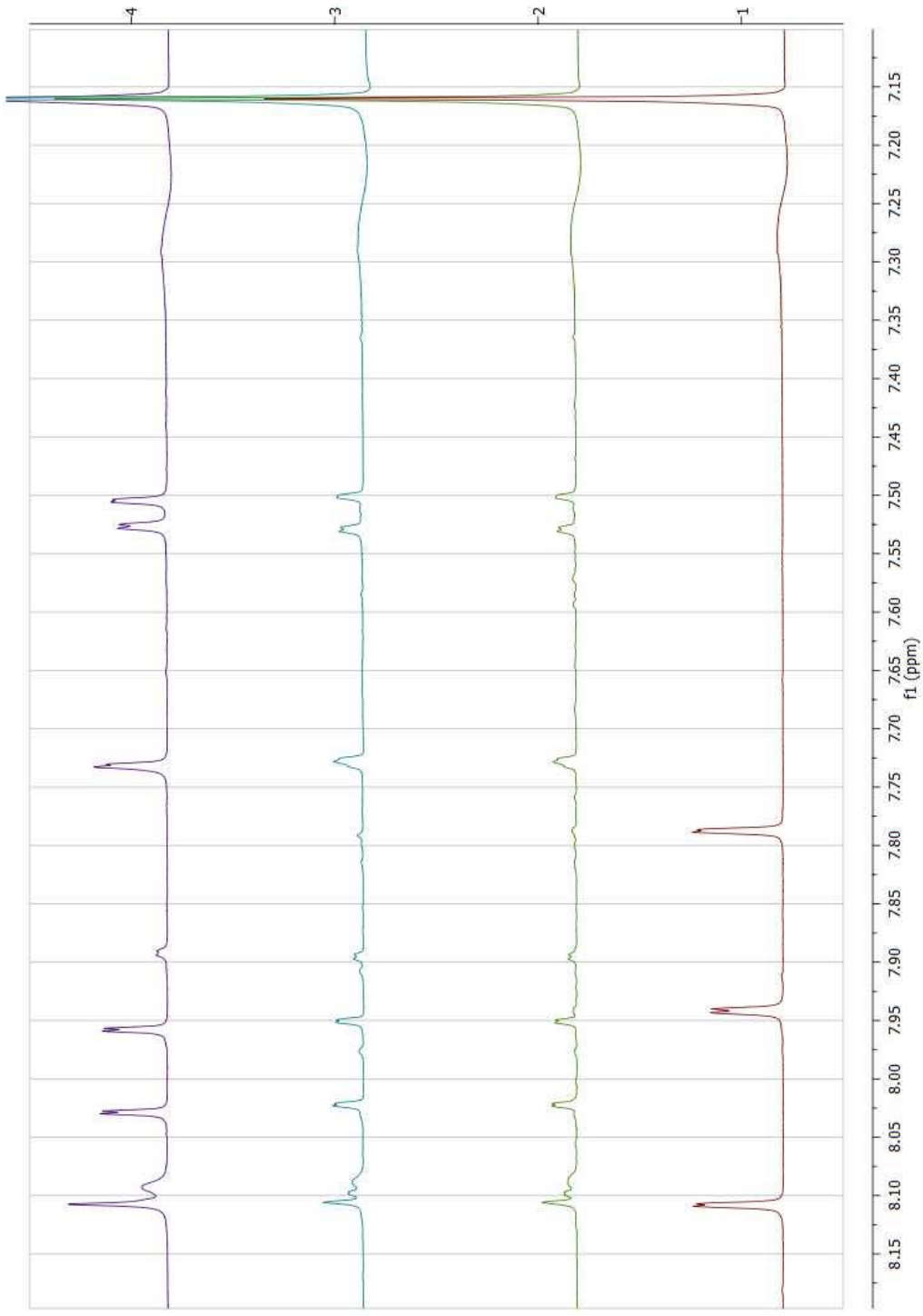

Figure 1.66. ^{1}H NMR spectra of **1.26d** (red, 1) in THF (0.6 mL) and d_6-benzene (0.1 mL), after addition of LDA (1 equiv) (green, 2), after sitting at room temperature for 27 h (blue, 3), **1.32-Pt** (purple, 4) from Figure 1.63 for comparison.

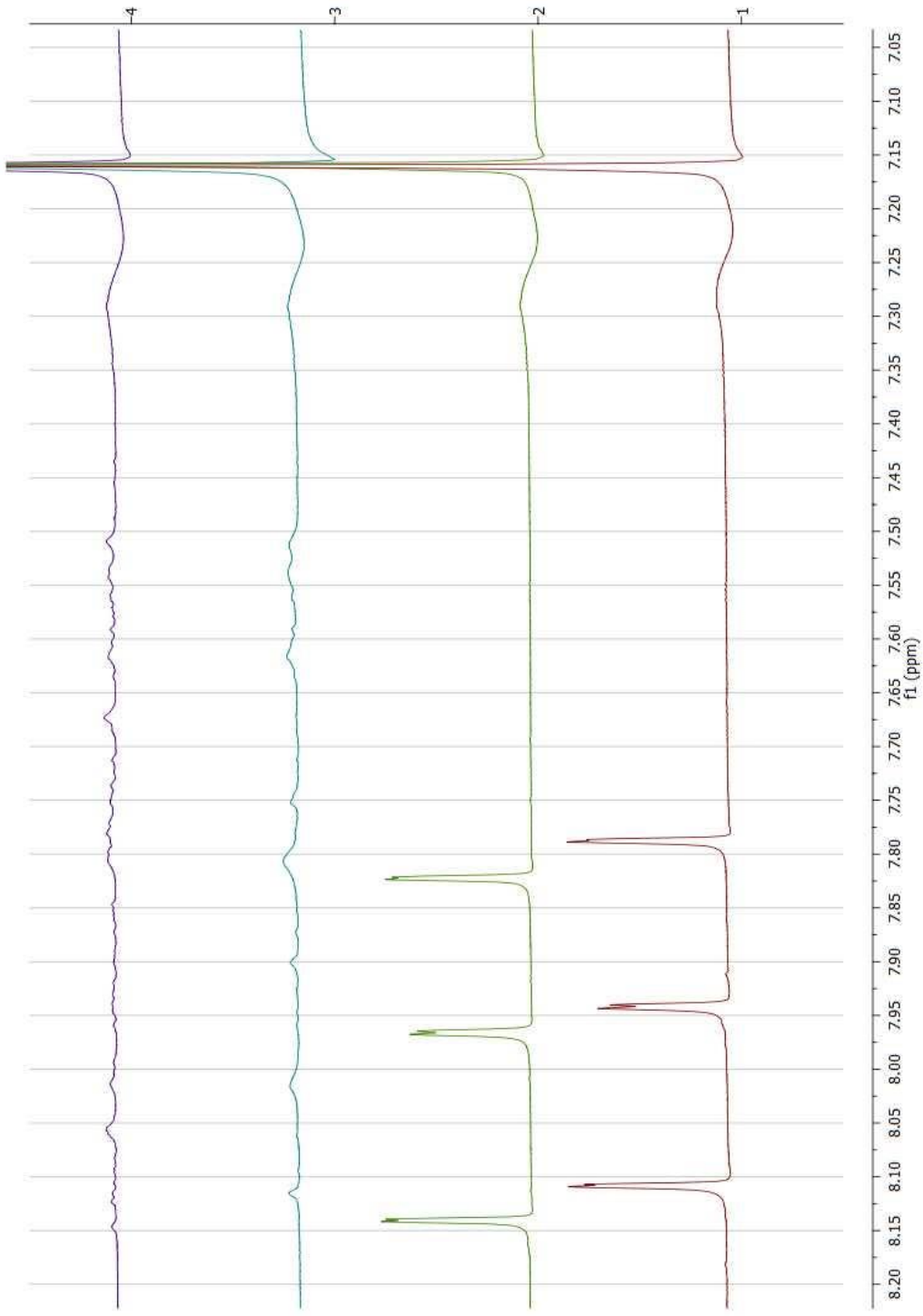

Figure 1.67. ^{1}H NMR spectra of **1.26d** (red, 1) in THF (0.6 mL) d_6-benzene (0.1 mL); **1.35** (green, 2), after addition of ACN (10 equiv.); 5 minutes after addition of LDA (1 equiv) (blue, 3); 24 hours after addition of LDA (1 equiv) (purple, 4).

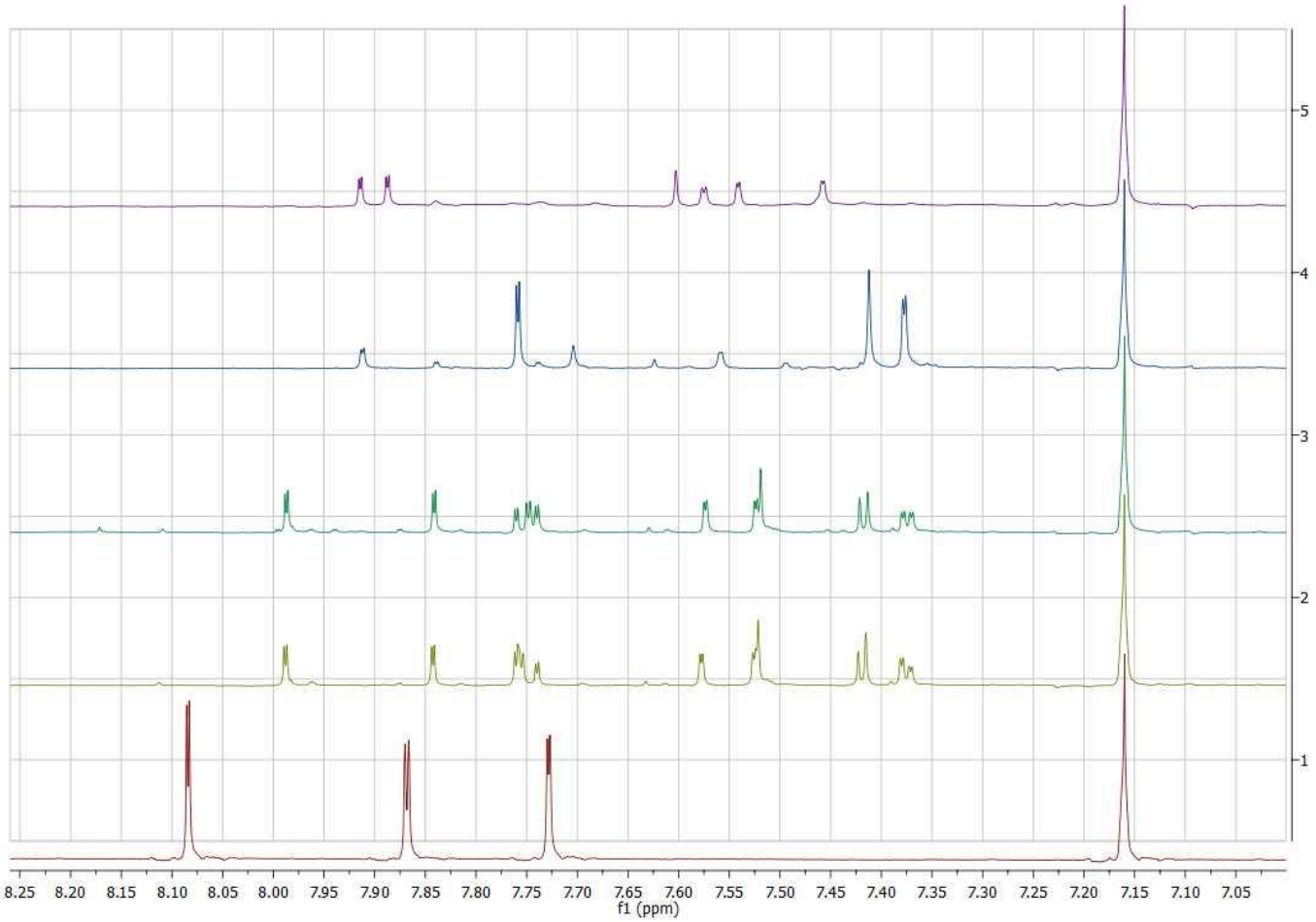

Figure 1.68. Starting **1.25a** complex in THF (0.6 mL) and d_6-benzene (0.1 mL) (red, 1); after addition of LDA (~1 equiv), giving a mixture of **1.33-Pd** and **1.34-Pd** (light green, 2); after addition of 1-heptene and heating at 70 ^{o}C for 16 h (green, 3) giving the same mixture of **1.33-Pd** and **1.34-Pd**; after addition of more LDA (1 equiv.), giving **1.34-Pd** with impurities; after addition of AgOTf (1.5 equiv), giving what appears to be deprotonated dimer **1.32-Pd**.

N. References

(1) Balzani, V.; Credi, A.; Venturi, M. *ChemSusChem* **2008**, *1*, 26.

(2) Mercer, J. A. M.; Burns, N. Z. *Nat. Chem.* **2015**, *7*, 860.

(3) Que, L.; Tolman, W. B. *Nature* **2008**, *455*, 333.

(4) Whittaker, J. W. *Arch. Biochem. Biophys.* **2005**, *433*, 227.

(5) Conley, B. L.; Pennington-Boggio, M. K.; Boz, E.; Williams, T. J. *Chem. Rev.* **2010**, *110*, 2294.

(6) Samec, J. S. M.; Bäckvall, J.-E. *Chem. – Eur. J.* **2002**, *8*, 2955.

(7) Fujii, A.; Hashiguchi, S.; Uematsu, N.; Ikariya, T.; Noyori, R. *J. Am. Chem. Soc.* **1996**, *118*, 2521.

(8) Uematsu, N.; Fujii, A.; Hashiguchi, S.; Ikariya, T.; Noyori, R. *J. Am. Chem. Soc.* **1996**, *118*, 4916.

(9) Zhang, J.; Leitus, G.; Ben-David, Y.; Milstein, D. *J. Am. Chem. Soc.* **2005**, *127*, 10840.

(10) Zhang, J.; Leitus, G.; Ben-David, Y.; Milstein, D. *Angew. Chem. Int. Ed.* **2006**, *45*, 1113.

(11) Gunanathan, C.; Ben-David, Y.; Milstein, D. *Science* **2007**, *317*, 790.

(12) Gnanaprakasam, B.; Zhang, J.; Milstein, D. *Angew. Chem. Int. Ed.* **2010**, *49*, 1468.

(13) Gunanathan, C.; Milstein, D. *Acc. Chem. Res.* **2011**, *44*, 588.

(14) Grotjahn, D. B.; Larsen, C. R.; Gustafson, J. L.; Nair, R.; Sharma, A. *J. Am. Chem. Soc.* **2007**, *129*, 9592.

(15) Larsen, C. R.; Grotjahn, D. B. *J. Am. Chem. Soc.* **2012**, *134*, 10357.

(16) Larsen, C. R.; Erdogan, G.; Grotjahn, D. B. *J. Am. Chem. Soc.* **2014**, *136*, 1226.

(17) Grotjahn, D. B.; Lev, D. A. *J. Am. Chem. Soc.* **2004**, *126*, 12232.

(18) Arita, A. J.; Cantada, J.; Grotjahn, D. B.; Cooksy, A. L. *Organometallics* **2013**, *32*, 6867.

(19) Herrmann, W. A. *Angew. Chem. Int. Ed.* **2002**, *41*, 1290.

(20) Hahn, F. E.; Jahnke, M. C. *Angew. Chem. Int. Ed.* **2008**, *47*, 3122.

(21) Díez-González, S.; Marion, N.; Nolan, S. P. *Chem. Rev.* **2009**, *109*, 3612.

(22) Peris, E.; Crabtree, R. H. *Coord. Chem. Rev.* **2004**, *248*, 2239.

(23) Crudden, C. M.; Allen, D. P. *Coord. Chem. Rev.* **2004**, *248*, 2247.

(24) Garrison, J. C.; Youngs, W. J. *Chem. Rev.* **2005**, *105*, 3978.

(25) Díez-González, S.; Nolan, S. P. *Coord. Chem. Rev.* **2007**, *251*, 874.

(26) Scott, N. M.; Nolan, S. P. *Eur. J. Inorg. Chem.* **2005**, *2005*, 1815.

(27) Perry, M. C.; Burgess, K. *Tetrahedron: Asymmetry* **2003**, *14*, 951.

(28) Poyatos, M.; Mata, J. A.; Peris, E. *Chem. Rev.* **2009**, *109*, 3677.

(29) Glorius, F.; Springer Berlin Heidelberg: 2006.

(30) Fischer, E. O.; Maasböl, A. *Angew. Chem. Int. Ed.* **1964**, *3*, 580.

(31) Tschugajeff, L. S.-G., M. *J. Russ. Phys. -Chem. Ges.* **1915**, *47*, 776.

(32) Tschugajeff, L.; Skanawy-Grigorjewa, M.; Posnjak, A.; Skanawy-Grigorjewa, M. *Z. Anorg. Allg. Chem.* **1925**, *148*, 37.

(33) Rouschias, G.; Shaw, B. L. *J. Chem. Soc. D* **1970**, 183.

(34) Hahn, F. E.; Langenhahn, V.; Lügger, T.; Pape, T.; Le Van, D. *Angew. Chem. Int. Ed.* **2005**, *44*, 3759.

(35) Flores-Figueroa, A.; Pape, T.; Feldmann, K.-O.; Hahn, F. E. *Chem. Commun.* **2010**, *46*, 324.

(36) Liu, C.-Y.; Chen, D.-Y.; Lee, G.-H.; Peng, S.-M.; Liu, S.-T. *Organometallics* **1996**, *15*, 1055.

(37) Hahn, F. E.; Langenhahn, V.; Pape, T. *Chem. Commun.* **2005**, 5390.

(38) Hahn, F. E.; Langenhahn, V.; Meier, N.; Lügger, T.; Fehlhammer, W. P. *Chem. – Eur. J.* **2003**, *9*, 704.

(39) Ito, Y.; Hirao, T.; Tsubata, K.; Saegusa, T. *Tetrahedron Lett.* **1978**, *19*, 1535.

(40) Ruiz, J.; García, G.; Mosquera, M. E. G.; Perandones, B. F.; Gonzalo, M. P.; Vivanco, M. *J. Am. Chem. Soc.* **2005**, *127*, 8584.

(41) Ruiz, J.; Perandones, B. F.; García, G.; Mosquera, M. E. G. *Organometallics* **2007**, *26*, 5687.

(42) Kosterke, T.; Pape, T.; Hahn, F. E. *Chem. Commun.* **2011**, *47*, 10773.

(43) Kösterke, T.; Pape, T.; Hahn, F. E. *J. Am. Chem. Soc.* **2011**, *133*, 2112.

(44) Kunz, P. C.; Wetzel, C.; Kogel, S.; Kassack, M. U.; Spingler, B. *Dalton Trans.* **2011**, *40*, 35.

(45) Wang, X.; Chen, H.; Li, X. *Organometallics* **2007**, *26*, 4684.

(46) Brendler, E.; Hill, A. F.; Wagler, J. *Chem. – Eur. J.* **2008**, *14*, 11300.

(47) Dobereiner, G. E.; Chamberlin, C. A.; Schley, N. D.; Crabtree, R. H. *Organometallics* **2010**, *29*, 5728.

(48) Flowers, S. E.; Cossairt, B. M. *Organometallics* **2014**, *33*, 4341.

(49) Miranda-Soto, V.; Grotjahn, D. B.; DiPasquale, A. G.; Rheingold, A. L. *J. Am. Chem. Soc.* **2008**, *130*, 13200.

(50) Hahn, F. E.; Naziruddin, A. R.; Hepp, A.; Pape, T. *Organometallics* **2010**, *29*, 5283.

(51) Naziruddin, A. R.; Hepp, A.; Pape, T.; Hahn, F. E. *Organometallics* **2011**, *30*, 5859.

(52) Price, C.; Elsegood, M. R. J.; Clegg, M.; Rees, N. H.; Houlton, A. *Angew. Chem. Int. Ed.* **1997**, *36*, 1762.

(53) Araki, K.; Kuwata, S.; Ikariya, T. *Organometallics* **2008**, *27*, 2176.

(54) Tan, K. L.; Bergman, R. G.; Ellman, J. A. *J. Am. Chem. Soc.* **2002**, *124*, 3202.

(55) Meier, N.; Hahn, F. E.; Pape, T.; Siering, C.; Waldvogel, S. R. *Eur. J. Inorg. Chem.* **2007**, *2007*, 1210.

(56) Miranda-Soto, V.; Grotjahn, D. B.; Cooksy, A. L.; Golen, J. A.; Moore, C. E.; Rheingold, A. L. *Angew. Chem. Int. Ed.* **2011**, *50*, 631.

(57) Hahn, F. E. *ChemCatChem* **2013**, *5*, 419.

(58) van der Boom, M. E.; Milstein, D. *Chem. Rev.* **2003**, *103*, 1759.

(59) Albrecht, M.; van Koten, G. *Angew. Chem. Int. Ed.* **2001**, *40*, 3750.

(60) Pugh, D.; Danopoulos, A. A. *Coord. Chem. Rev.* **2007**, *251*, 610.

(61) Benito-Garagorri, D.; Kirchner, K. *Acc. Chem. Res.* **2008**, *41*, 201.

(62) Choi, J.; MacArthur, A. H. R.; Brookhart, M.; Goldman, A. S. *Chem. Rev.* **2011**, *111*, 1761.

(63) Moser, M.; Wucher, B.; Kunz, D.; Rominger, F. *Organometallics* **2007**, *26*, 1024.

(64) Seyboldt, A.; Wucher, B.; Hohnstein, S.; Eichele, K.; Rominger, F.; Törnroos, K. W.; Kunz, D. *Organometallics* **2015**.

(65) Liu, Y.; Nishiura, M.; Wang, Y.; Hou, Z. *J. Am. Chem. Soc.* **2006**, *128*, 5592.

(66) Inoue, M.; Nakada, M. *Heterocycles* **2007**, *72*, 133.

(67) Kosynkin, D. V.; Tour, J. M. *Org. Lett.* **2001**, *3*, 991.

(68) Lipshutz, B. H.; Morey, M. C. *J. Org. Chem.* **1983**, *48*, 3745.

(69) Engle, K. M.; Mei, T.-S.; Wasa, M.; Yu, J.-Q. *Acc. Chem. Res.* **2012**, *45*, 788.

(70) Maleckis, A.; Kampf, J. W.; Sanford, M. S. *J. Am. Chem. Soc.* **2013**, *135*, 6618.

(71) Cross, W. B.; Hope, E. G.; Lin, Y.-H.; Macgregor, S. A.; Singh, K.; Solan, G. A.; Yahya, N. *Chem. Commun.* **2013**, *49*, 1918.

(72) Davies, D. L.; Donald, S. M. A.; Macgregor, S. A. *J. Am. Chem. Soc.* **2005**, *127*, 13754.

(73) Arduengo, A. J.; Harlow, R. L.; Marshall, W. J.; Prakasha, T. K. *Heteroat. Chem.* **1996**, *7*, 421.

(74) Grotjahn, D. B.; Kragulj, E. J.; Zeinalipour-Yazdi, C. D.; Miranda-Soto, V.; Lev, D. A.; Cooksy, A. L. *J. Am. Chem. Soc.* **2008**, *130*, 10860.

(75) Belluco, U.; Bertani, R.; Meneghetti, F.; Michelin, R. A.; Mozzon, M. *J Organomet. Chem.* **1999**, *583*, 131.

(76) Carlisle, S.; Matta, A.; Valles, H.; Bracken, J. B.; Miranda, M.; Yoo, J.; Hahn, C. *Organometallics* **2011**, *30*, 6446.

(77) Helm, L.; Merbach, A. E. *Chem. Rev.* **2005**, *105*, 1923.

(78) Salomon, R. G.; Kochi, J. K. *J. Am. Chem. Soc.* **1973**, *95*, 3300.

CHAPTER 2

Fate of Iridium Water Oxidation Catalysts While Testing With Ceric Ammonium Nitrate

A. Introduction to Water Oxidation and Iridium-based Water Oxidation Catalysts (WOC)

With global energy needs ever increasing and our increasing dependence on using finite resources, it is imperative that we develop more clean and renewable energy sources such as solar, wind, geothermal, hydroelectric, and biomass. Solar energy is believed to be one of the sources that has the most potential for the future[1,2]. There are two steps in the process of utilizing solar energy: (1) the capture and conversion of solar energy into usable energy, and (2) the storage of that energy. One of the down sides of the use of solar energy is that at a given location, energy output will fluctuate due to the movement of the sun and changes in cloudiness. To counteract the fluctuation we need to be able to store energy and be able use it when it is needed[3]. The ideal way to store energy would be in chemical bonds, such as by splitting water into its elements, where the electrons derived from water are stored in hydrogen with oxygen as the byproduct[2]. Splitting water into its elements can be thought of as the sum of two half reactions (Figure 2.1): water oxidation that takes two water molecules and converts them to molecular oxygen, four protons, and four electrons, and proton reduction, that combines the generated protons and electrons to make molecular hydrogen. Thus, the electrons can be stored in the H-H bond until energy is needed, in which case the reverse reaction is conducted in a fuel cell, or by combustion. Of the two half reactions water oxidation is considered to be the more challenging due to both the kinetics and thermodynamics,

$$2\ H_2O \rightleftharpoons 2\ H_2 + O_2 \qquad \text{overall reaction}$$

$$2\ H_2O \rightleftharpoons O_2 + 4\ H^+ + 4e^- \qquad \text{water oxidation}$$

$$4\ H^+ + 4e^- \rightleftharpoons 2\ H_2 \qquad \text{proton reduction}$$

Figure 2.1. Overall water splitting reaction.

where a catalyst can lower the kinetic "overpotential"[4] to as close to the thermodynamic lower limit as possible. The majority of the research I report in this thesis is focused on studying catalysis of the water oxidation half reaction.

There are two proposed mechanisms for water oxidation, water nucleophilic attack (WNA) and the radical coupling mechanism, I2M (Figure 2.2). Both mechanisms go through a metal oxo intermediate where in the WNA case the oxo is attacked by water forming the O-O bond (mononuclear) or in the I2M case where two oxo complexes come together to form the O-O bond (binuclear). The rate limiting step in the mechanism requires determination for each case[5] and in some cases has been documented to vary depending on catalyst and operating conditions[6,7], but for each type of mechanism, there are a number of proton transfers, a subject that the Grotjahn lab has studied in detail in other contexts with great success (see Chapter 1)[8-12].

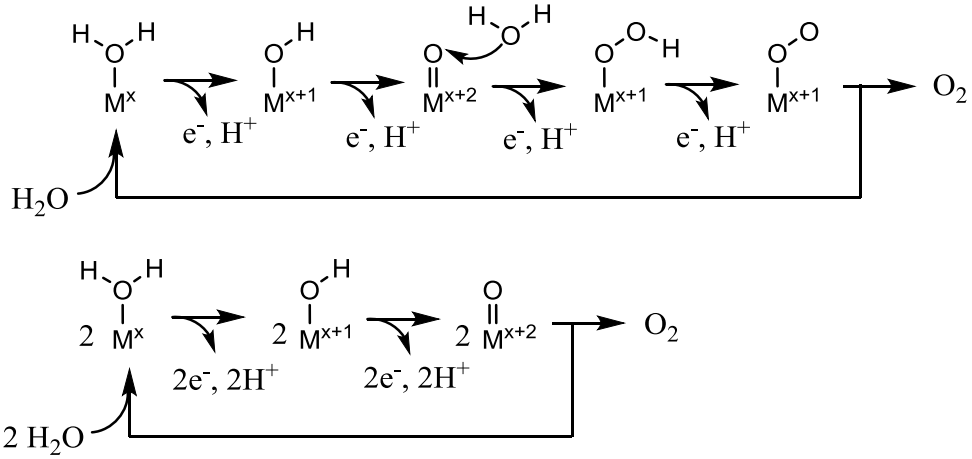

Figure 2.2. Purposed water oxidation mechanisms, water nucleophilic attack (WNA, top) and radical coupling (I2M, bottom).

One advance in water oxidation studies was the 2008 report from Bernhard's group, who showed that a mononuclear iridium catalyst, bis(phenylpyridine) complex **2.1**[13] (Figure 2.3), was capable of oxidizing water to oxygen. A number of analogs of **2.1** with differing electronics were studied, where either a chemical oxidant, ceric(IV) ammonium nitrate (CAN) (Figure 2.4) or electrode potential was used to drive the oxidation reaction. Using CAN, **2.1** gave 2490 turnovers after 7 d with 0.5 µmol of **2.1**

and 15000 µmol of CAN (vol = 10 mL, cat = 0.05 mM, CAN = 1500 mM, ratio of cat:CAN 1:30000) gave 1240 µmol of O_2.

The benefit of using electrochemistry is that it can be done under a variety of pH conditions and the electrochemical potential at which the catalyst oxidizes water can be found which also gives the overpotential. The challenging part of using electrochemistry is to quantitate how much oxygen is produced, and for catalyst development it is important to be able to calculate turnover numbers (TON) and frequencies (TOF). To calculate TON and TOF it is much simpler to use a chemical oxidant such as ceric(IV) ammonium nitrate (CAN), and detect the generated oxygen by pressure, Clark electrode, or fluorescence. The down side of using CAN is that four moles are needed per mole of generated oxygen. The large excess of CAN to obtain high turnover numbers is significant, because such an aqueous solution exhibits a pH of approximately 1 which could affect the chemistry. One way to change the acidity of CAN would be to buffer the solution, but unfortunately if the pH of a CAN solution becomes high enough the cerium precipitates from the solution.

In 2009 Crabtree et al.[14] published a paper exploring **2.2a** and **2.2b**, Cp*Ir

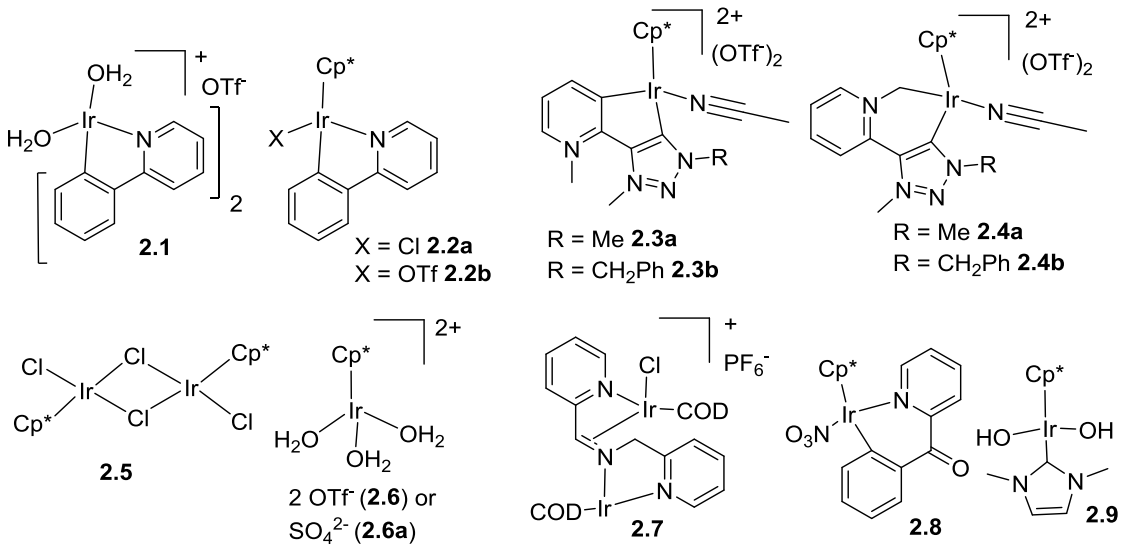

Figure 2.3. Selected iridium water oxidation catalysts published from 2008 to 2011.

$$2\ H_2O + 4\ Ce^{4+} \rightleftharpoons O_2 + 4\ H^+ + 4\ Ce^{3+}$$

Figure 2.4. Balanced reaction for chemically driven water oxidation reaction using cerium.

phenylpyridine complexes derived from the same heterocyclic ligand as **2.1**. They looked at the first minutes of catalysis using CAN to obtain the initial rates; **2.2a** gave an initial rate of 54 turnovers/min compared to 2.6 turnovers/min for **2.1**. The longer-term CAN studies over hours showed that **2.2a** generated approximately 1500 turnovers but in a much shorter time period of 5.5 h. The Crabtree group complexes were the first iridium water oxidation catalysts that contained a Cp* ligand, which became a reoccurring motif in later complexes, such as **2.3b**, **2.4b**, **2.6**, **2.8**, and **2.9.**

In 2010 Bernhard et al[15] published another paper looking at a Cp*Ir complex with a substituted triazolylmethylpyridine ligand that is metalated via one aromatic carbon and the pyridine giving **2.3b** or via the methyl giving **2.4b**. Short-term CAN studies with 900 equiv of CAN gave approximately quantitative O_2 formation after 80 min with **2.3b** and about 100 min for **2.4b**. Longer-term CAN studies showed that **2.3b** and **2.4b** were capable of reacting for about 10000 and 8350 turnovers, respectively.

$[IrCp^*Cl_2]_2$,**2.5** is a common iridium precursor that Crabtree tested that ended up being a decent WOX catalyst[16]. The initial rate using CAN was about 10 turnovers over the first minute. In the same paper $[IrCp^*(H_2O)_3]$ SO_4, **2.6a**, which is made by ionization of **2.5** in water, gave 5.5 turnovers over the first minute.

The dinuclear iridium(I) COD complex **2.7** published in 2011 by de Bruin's group had a turnover number of at least 1000 with an initial rate of of 56.7 turnovers per min[17].

In 2010, Macchioni's group published complex **2.8** which is similar to **2.1**, with the insertion of a -C(O)- bridging electron withdrawing group between the aryl groups and instead of chloride the counter ion is NO_3^-. The initial rate was found to be 8.46 ± 0.06 turnovers per min, which is almost two times faster than **2.1**[18]. They also showed

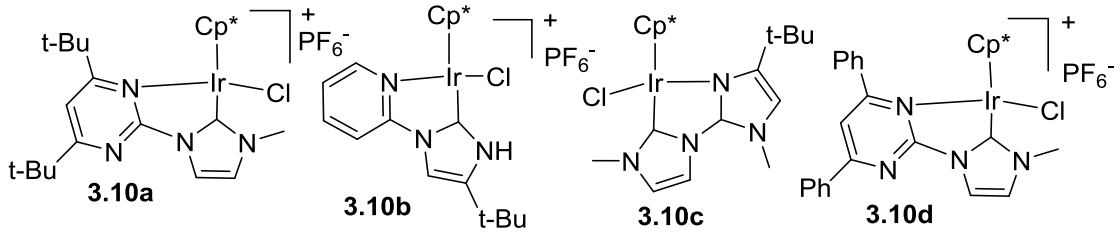

Figure 2.5. Ir Cp* complexes that had been synthesized in the Grotjahn lab.

that **2.6-NO_3** was faster than both complexes with an initial rate of 15.72 ± 1.08 turnovers per min.

In 2011, Hetterscheid et al published a novel iridium carbene complex **2.9**, which had a TOF of 1.5 per second (90 per min), with at least 2000 turnovers[19]. This was the fastest catalyst at the time to reach 500 turnovers.

B. Evolution of Iridium-Based WOC Driven by Ceric Ammonium Nitrate

The Grotjahn lab became interested in water oxidation after Bernhard showed that simple organometallic complexes were capable of water oxidation via a mononuclear mechanism. As discussed in Chapter 1 the Grotjahn lab has accelerated reactions by having pendant bases which can help proton transfers, and with both WOX reaction mechanisms having a number of proton transfers we thought we could make faster catalysts by adding pendant bases. The project began by testing a number of complexes that had been made for previous projects[20,21], but were thought to be viable WOX catalysts. Complexes **3.10a-d** (Figure 2.5) were synthesized by Douglas Grotjahn, Hai Tran, Sara Cortes-Llamas, and Zephen Specht with the testing of the catalysts using CAN being done by Derek Brown and Hai Tran. We were surprised to see that a number of these were active catalysts, but over the course of the reaction the solutions changes to a blue/purple color. Because cerium(IV) aquo species are yellow or orange, cerium(III) species are colorless, and the iridium(III) initial complexes are typically orange or yellow, the blue/purple color was striking; one hypothesis is that the blue/purple must be coming from the iridium after oxidation.

To explore if the color was observed when using other iridium complexes, we synthesized **2.1**-**2.9**, which are some of the well-known WOC of the time, as discussed earlier. There were problems in isolation of the known complexes **2.3b** and **2.4b** so the methyl analogs **2.3a** and **2.4a** were synthesized. To look at the color of the iridium throughout the water oxidation reactions, one of the co-authors on the paper (Dr. Gregory Kalyuzhny) monitored the color change over the course of the reactions by UV-vis absorption (Figure 2.6). The reaction conditions for the UV-vis were a solution of CAN ($[CAN]_0$ = 75.8-78.9 mM) was added to a cuvette, an initial spectrum was observed, then catalyst ($[cat]_0 \approx 0.05$ mM) was injected, defining time = 0 min. The figures depict

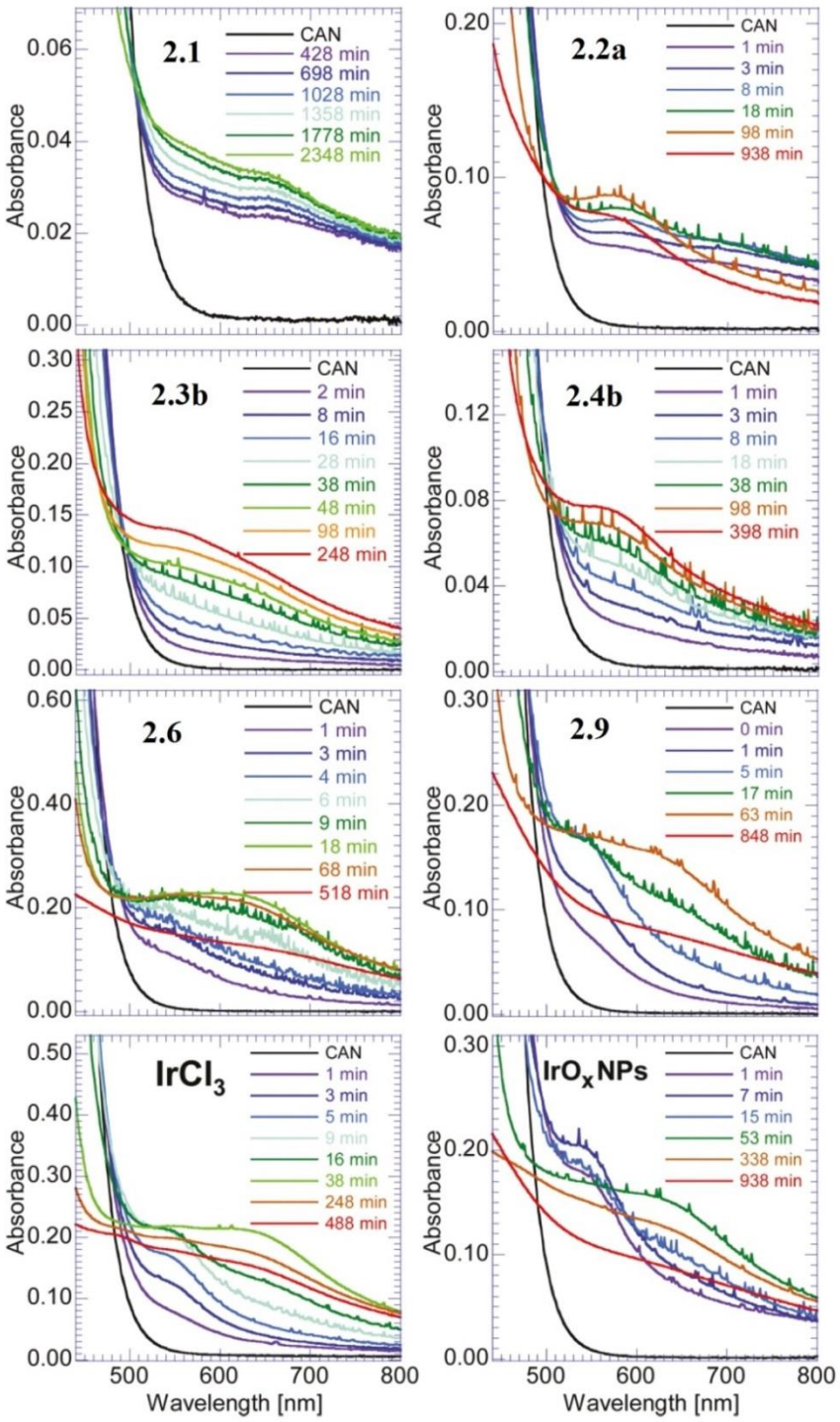

Figure 2.6. UV-vis absorption spectra of indicated catalysts ($[cat]_0 \approx 0.05$ mM) at different time points after addition to a solution of CAN ($[CAN]_0 = 75.8$-78.9 mM). The small spikes are attributed to gas bubbles. We assigned the absorbances between 550 and 650 nm to IrO_x NPs, but later studies show that molecular Ir(IV) species may be responsible.

changes in the UV-vis spectra over time, and different time points were used for each catalyst depending on the rate of change observed in the UV-vis spectra. Examining the spectra of reactions using catalysts **2.1**, **2.2a**, **2.3b**, and **2.4b**, all spectra have absorbances that appear between 550 and 650 nm typically over the first 1.5 h, except for the spectrum using **2.1**, which required much longer times and gave smaller absorbance values. Reactions involving **2.6** and **2.9** feature an initial absorbance that appears around 550 nm followed by a second absorbance around 630 nm. When no organic ligands are present, such as when using $IrCl_3$ and IrO_x nanoparticles, there is a similar trend as for the latter compounds, with early appearance of an absorbance around 550 nm followed by a second around 630-650 nm. The IrO_x nanoparticles themselves absorb at 550 nm, and hence it is not surprising that in their reaction the absorbance is already intense at 1 min, but then within an hour transforms into the absorbance in the 630-650 nm, possibly because the NP are forming larger aggregates with iridium or even cerium (see below for discussion of STEM data). Reexamining the UV-vis data for molecular catalyst reactions in light of the results when starting with authentic IrO_x NP, the slow appearance of an absorbance at 550 nm could be the formation of similar IrO_x nanoparticles which then either stay the same or form larger aggregates, as the authentic nanoparticles did. Using the data shown

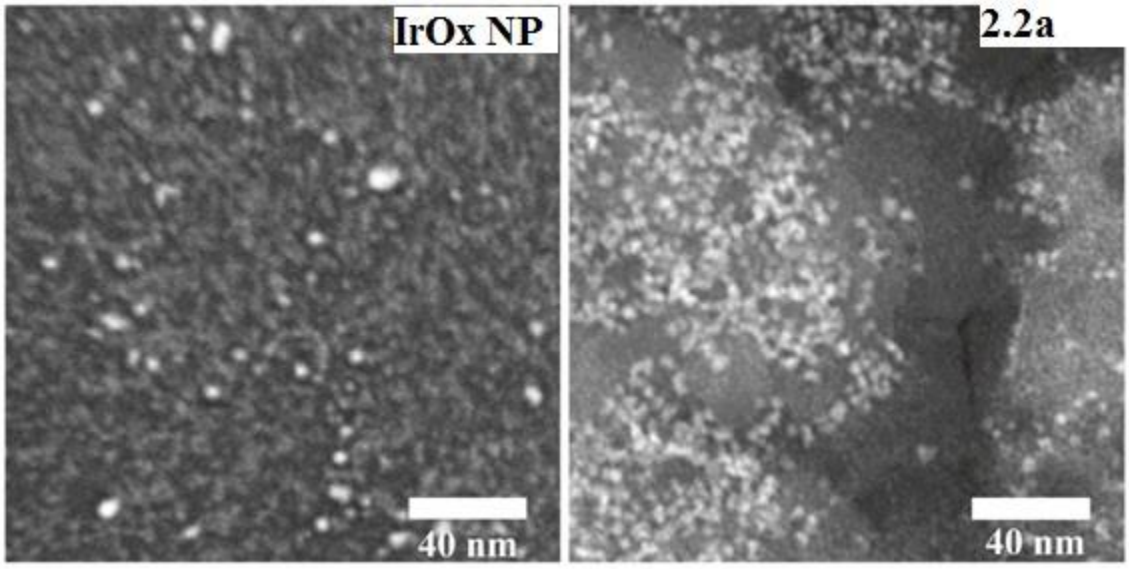

Figure 2.7. STEM images of authentic iridium oxide nanoparticles (left), and sample of WOX reaction using CAN of **2.2a** after 15 min, where $[\mathbf{2.2a}]_0$ = 1.35 mM, $[CAN]_0$ = 78 mM. The bright dots ~ 2 nm wide are iridium rich nanoparticles on a cerium rich matrix (grey background).

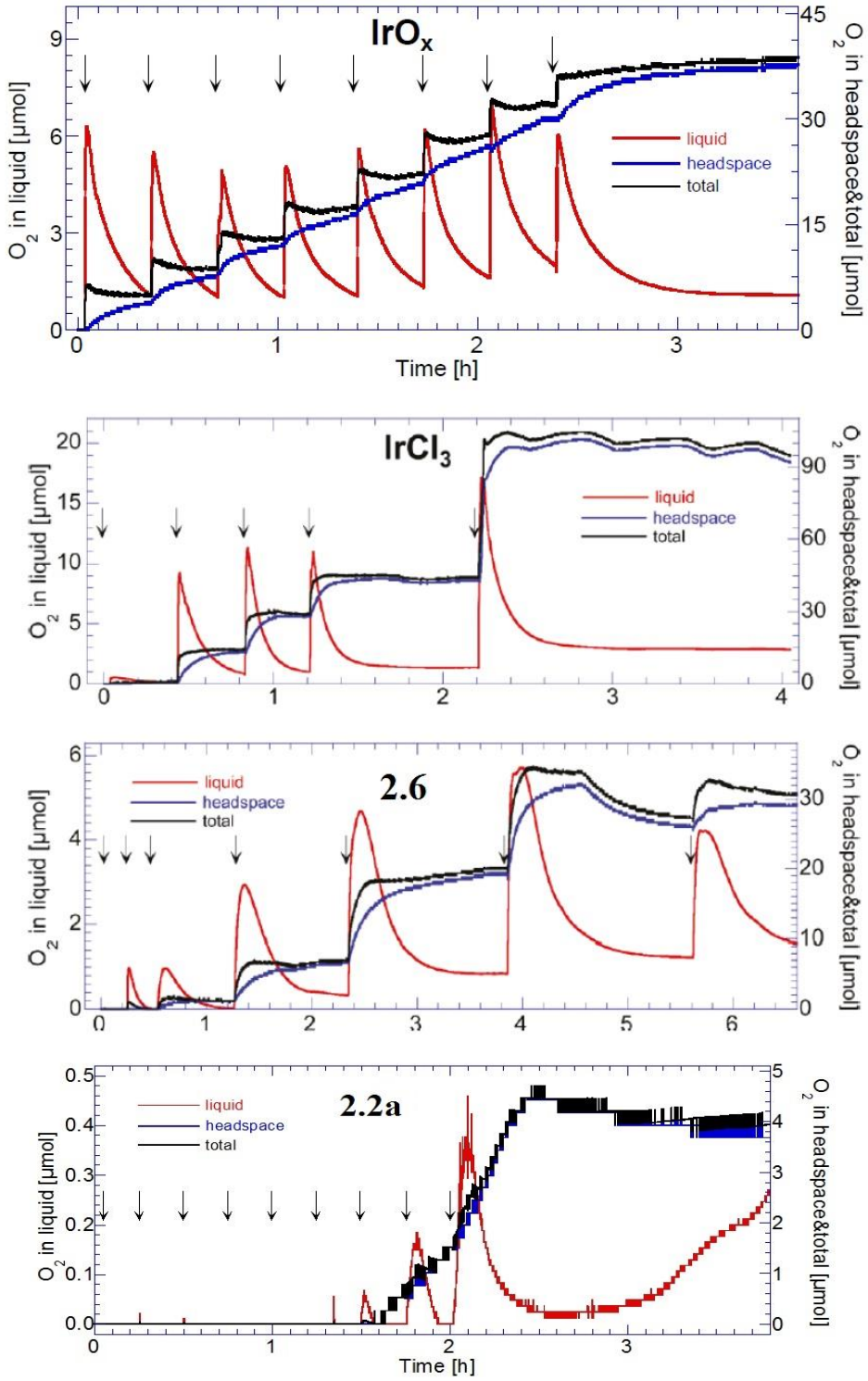

Figure 2.8. Stepwise addition of CAN (5 equiv/arrow) to catalyst solution, where the generated oxygen is monitored by two clark electrodes one in the liquid (red) and the other in the headspace (blue) with the total (black). The last addition of CAN to $IrCl_3$ was of 15 equiv of CAN.

in Figure 2.6 as well as other data obtained by adding portions of CAN to molecular species such as **2.3a** (see Figures S25 and S26 of reference[22]), we assigned the absorbances between 550 and 650 nm to IrO_x NPs. However, later studies by others, especially using periodate oxidant and other Ir catalysts show that molecular Ir(IV) species can be responsible for absorbances in this region[23-26].

To further identify the presence of iridium nanoparticles, the reactions were checked by scanning tunneling electron microscopy (STEM). This part of the project was done by Dr. Kenneth Vecchio, Jessica Martin, and Dr. Caline Abadjian, who tried a variety of conditions and experiments; I assisted towards the end of the project in obtaining the published images. The typical sample preparation procedure was as follows: to a CAN solution (78 mM), catalyst (1.35 mM to 1.57 mM final concentration in the mixture) was injected, then after 15 min a portion of the mixture was removed and placed on a grid which was then coated with carbon. We were able to observe authentic iridium oxide nanoparticles (Figure 2.7 left), where the nanoparticles are 2-10 nm in diameter with the composition being iridium which was shown by EDX. Compounds **2.1** (after 6.3 h), **2.2a**, **2.3a**, **2.6**, **2.9**, and IrO_x NP were tested as described but did not show free iridium-rich nanoparticles; instead, the nanoparticles were associated with cerium (see Figure 2.7 right for an example of iridium on cerium matrix).

So far we have looked at what happens with 1500 equivalents of CAN by UV-vis and about 60 equiv in the STEM experiments, but we wanted to look at what happens to the catalyst initially. To do so, Derek Brown added small amounts of CAN, typically 5 equiv, by injection into a solution of catalyst, and the oxygen evolution was monitored by a Clark electrode. After oxygen evolution stopped, more CAN was added, and the observation continued. The first catalyst to be discussed are IrO_x nanoparticles (2.54 mM in the reaction mixture) where each addition of CAN was 5 equiv, and all additions give approximately the same amount of oxygen (Figure 2.8). From the very beginning IrO_x nanoparticles are an active catalyst. In comparison, using $IrCl_3$ (2.14 mM in the reaction), the first addition of CAN (5 equiv) generates very minimal O_2 but the other additions generate near theoretical amounts of O_2. This observation can be explained because $IrCl_3$, as an Ir(III) species, needs to be oxidized to at least Ir(V) to begin water oxidation

catalysis, therefore the first two equiv are consumed without oxygen formation and we do not see the theoretical amount of oxygen after the first addition. For the Cp* iridium(III) tris(aquo) complex **2.6**, it was of interest to see if the same amount of CAN would start generating oxygen as when using $IrCl_3$, 2-5 equiv. Remarkably, the first 3 additions of CAN (15 equiv) generate only minimal amounts of O_2. The need for extra oxidizing equivalents must be to oxidize the only new part of the compound, the organic ligand Cp*. In confirmation, a complex such as **2.2a** with more organic ligands requires 30 equiv of CAN for significant oxygen evolution to occur. The results above suggest that there are transformations of these organic ligands occurring even with a few equiv of CAN. What are these transformations and can we observe them?

After the suggestion of a manuscript reviewer we decided to monitor the reactions and changes of organic ligands by ^{1}H NMR and mass spectroscopies. Co-worker Dr. Zephen Specht was the first to try this, but by using >100 equiv of CAN could not observe any recognizable peaks in the ^{1}H NMR spectra. My contribution was to observe the state of the catalyst after addition of a small amount of CAN (total of 1, 5, and 15 equiv) to get an idea of what was happening to the ligands before significant O_2 evolution began. The catalysts were dissolved in D_2O, along with an internal standard, $Me_3SiCH_2CH_2CH_2SO_3Na$. These stock solutions were added to a J. Young NMR tube and diluted with D_2O to give solutions 1.35 mM in catalyst as well as the internal standard. An initial ^{1}H NMR spectrum was acquired and after the additions of CAN (1, then 4, then 10 equiv). Because of the low analyte concentrations, 128 scans were needed to increase the signal-to-noise ratio. Since the integral values were important we used a 20 sec delay between scans, which meant that each observation of a ^{1}H NMR spectrum required about 1 h.

The results of the NMR experiments will be discussed for compound **2.4a** (for the other compounds see the supporting information for the 2011 *JACS* paper). The initial NMR spectrum of **2.4** shows that there are two species that are closely related, **2.4a** and the complex that has lost the coordinated acetonitrile and is assumed to now contain a D_2O, **2.4a-D_2O** (Figure 2.9). The ratio of **2.4a** to **2.4a-D_2O** is 69 to 31. After addition of 5 equiv of CAN, it is apparent that there is a loss of symmetry because there are 4 equal

methyl signals, data that would be consistent with the formation of a new species where one of the methyls on the Cp* ring has been oxidized to a primary alcohol, **2.4-ox** (Figure 2.9). The structure was assigned by the four equal singlets (3H) between 1.58 and 1.81 ppm (Figure 2.12, blue), and a pair of mutually coupled doublets (1H, 13.2 Hz) at 4.02 and 3.85 ppm (Figure 2.13, green). The state of the heterocyclic ligand is unknown so was not drawn.

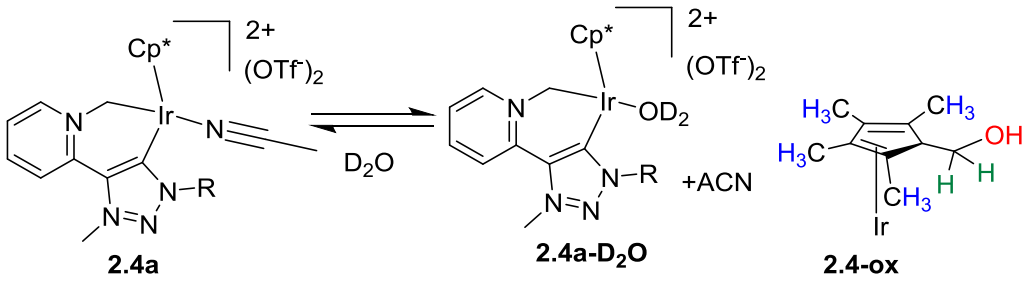

Figure 2.9. Dissolving complex **2.4a** in D_2O gives a mixture of **2.4a** and **2.4a-D_2O** (left). Oxidation of the Cp* giving **2.4-ox** (right).

Another oxidized product was observed as a singlet at 2.087 ppm, which was found to be acetic acid (Figure 2.12, red). Another interesting product was seen after the addition of 15 equiv of CAN, formic acid, was assigned by the appearance of a singlet at 8.24 ppm. As for the state of the catalyst after 15 equiv of CAN, there are no peaks for initial catalyst or the oxidized **2.4-ox**, however there were 0.37 equiv of acetic acid and 0.25 equiv of formic acid (Table 2.1, see Table 2.2 and Table 2.3 for details of calculations of equiv values). The presence of acetic acid was confirmed by a gHMBC experiment showing a crosspeak with a ^{13}C NMR resonance at 179.4 ppm. Also, addition of authentic acetic acid to a water oxidation mixture caused the peak at 2.087 ppm to grow larger. As for formic acid, addition of authentic formic acid to a water oxidation mixture caused the peak at 8.24 ppm to grow larger.

The amounts of oxidized complex, acetic acid and formic acid can be found in Table 2.4. In summary of the ^{1}H NMR experiments all five complexes tested formed formic acid, but complex **2.1** was the only one which did not produce acetic acid (Table 2.4); our hypothesis is that the Cp* ligand is the source of acetic acid but can also lead to formic acid.

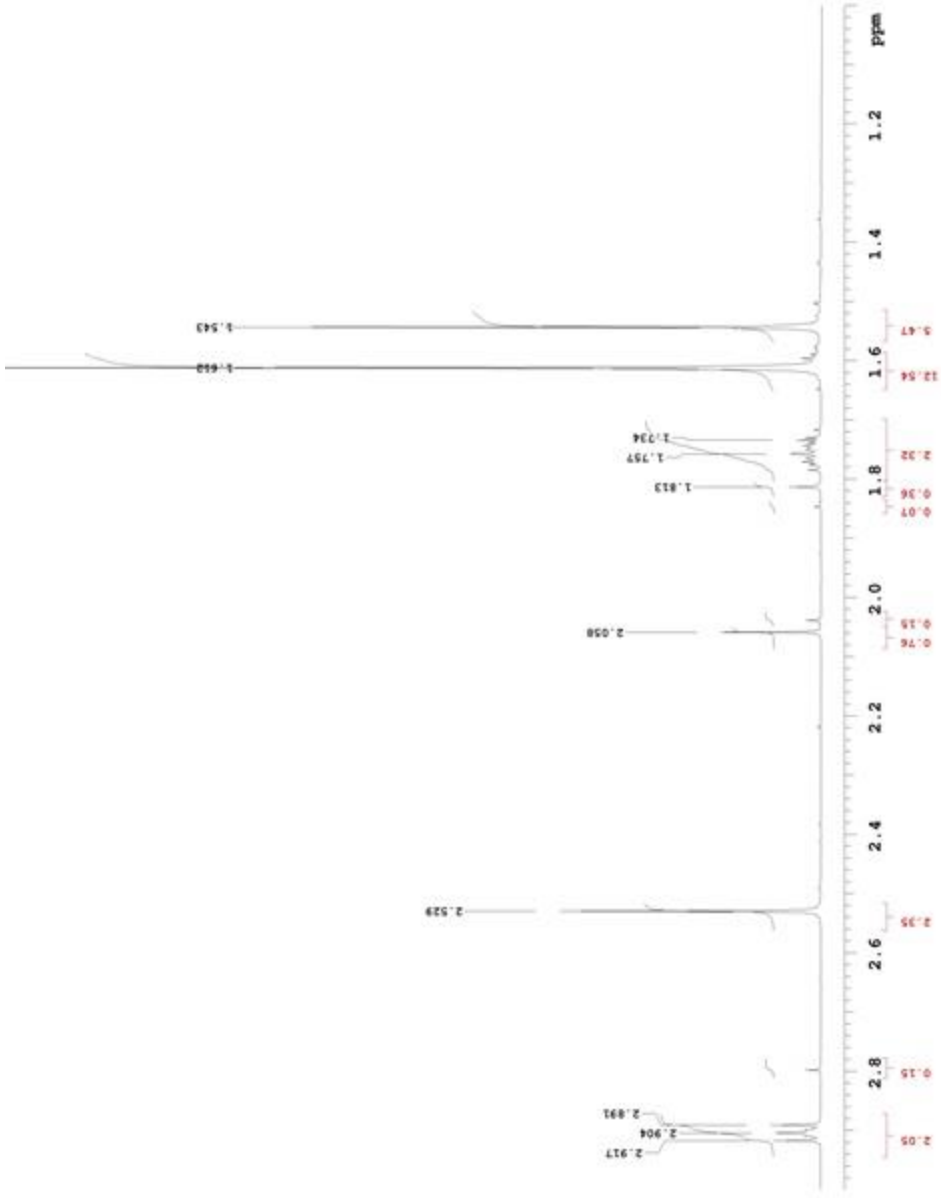

Figure 2.10. Enlarged view, initial mixture of **2.4a** (1.0 to 3.0 ppm). Multiplets 1.72-1.78 and 2.88-2.92 ppm are for $(CH_3)_3SiCH_2CH_2CH_2SO_3Na$. Major singlets at 1.61 and 2.53 are for $C_5(CH_3)_5$ and coordinated CH_3CN of **2.4a**, whereas minor singlet at 1.54 is for $C_5(CH_3)_5$ of **2.4a-D$_2$O** and singlet at 2.06 is for free CH_3CN. See Table 2.2 and 2.3 for all assignments and integral values.

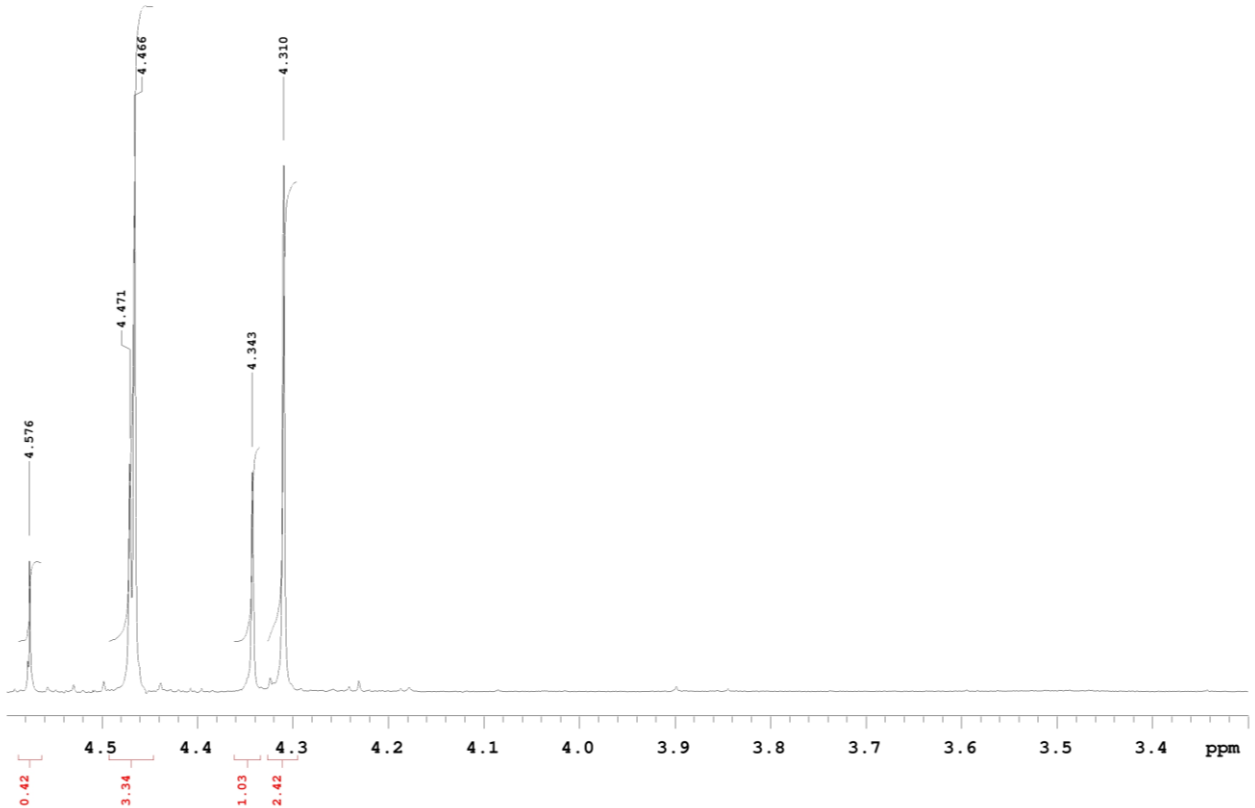

Figure 2.11. Enlarged view, initial mixture of **2.4a** (3.3 to 4.6 ppm). Major singlets at 4.470 and 4.31 are for *N*-methyl groups on **2.4a**, minor singlets at 4.466 and 4.34 ppm are for *N*-methyl protons on **2.4a-D_2O**. The signal at 4.57 ppm is an unknown peak present in the D_2O. See Table 2.2 and 2.3 for assignments and integral values.

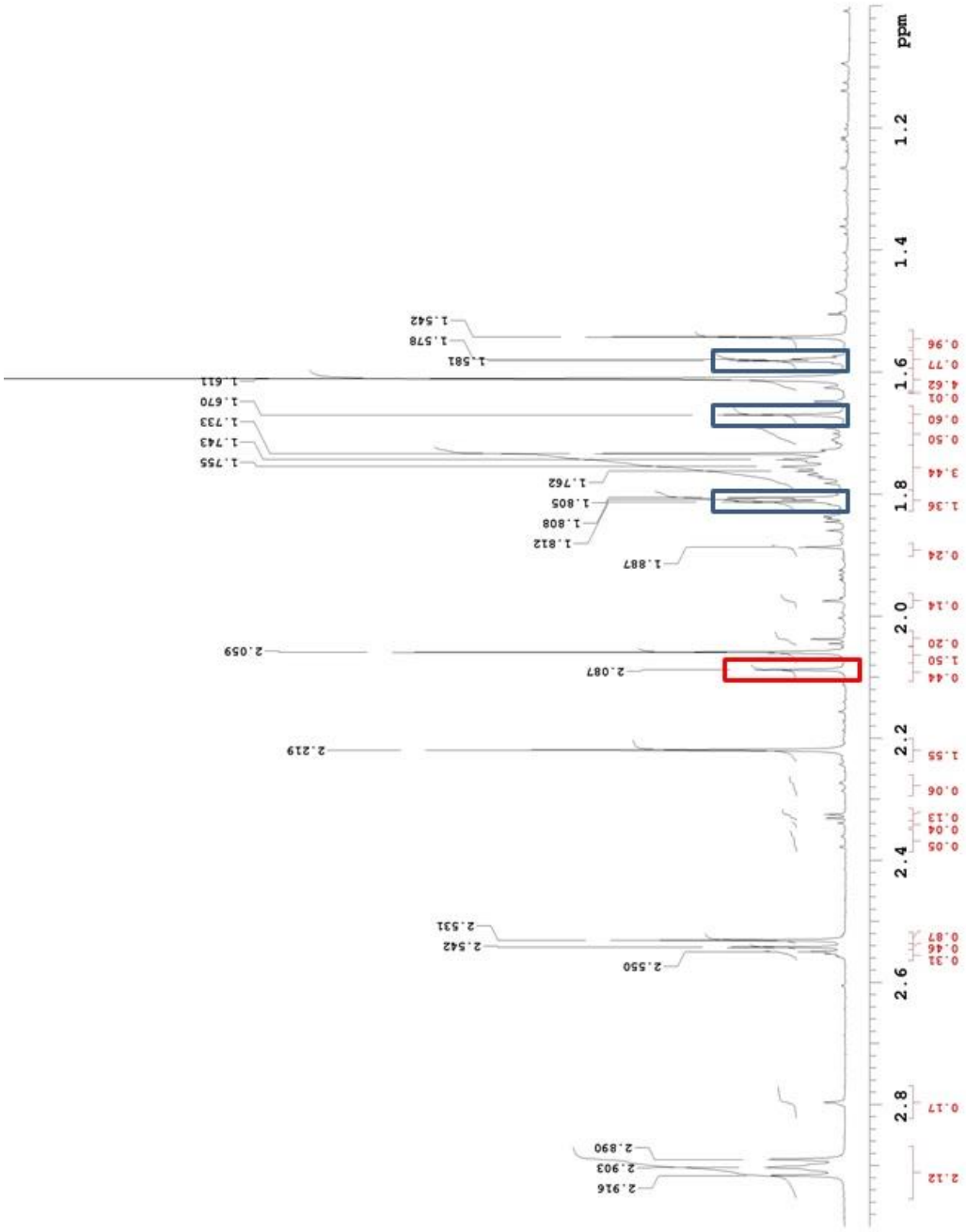

Figure 2.12. **2.4a** after CAN (5 equiv) (1.0 to 3.0 ppm). New peaks include acetic acid (red box) and four methyl protons of the oxidized Cp* in structure **2.4-ox** (blue boxes) See Table 2.2 and 2.3 for assignments and integral values.

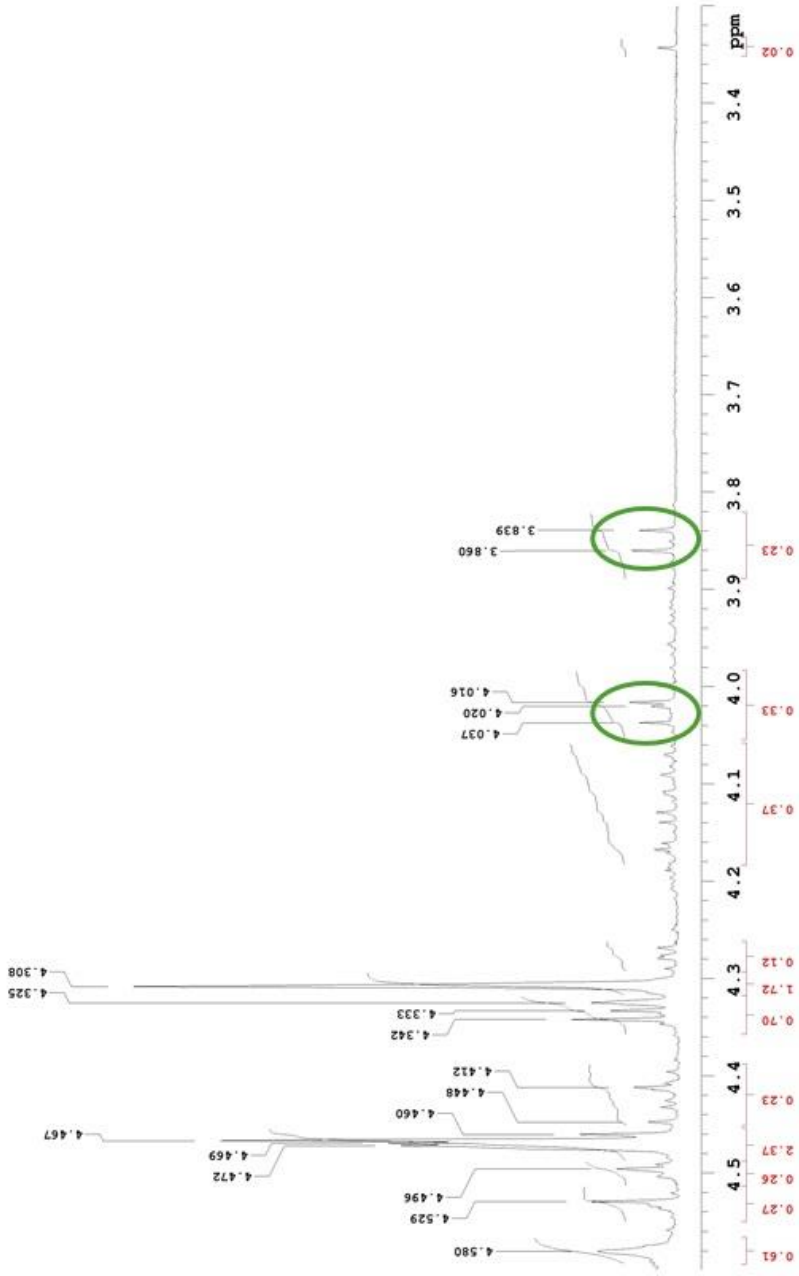

Figure 2.13. Enlarged view, mixture of **2.4a** after CAN (5 equiv) (3.3 to 4.6 ppm). Note the appearance of at least 20 new minor peaks in addition to the identifiable more major ones, including the diastereotopic protons form the oxidized methyl in structure **2.4-ox** (green ovals). See Table 2.2 and 2.3 for assignments and integral values.

Table 2.1. Calculations of amounts of intact catalyst **2.4a**, **2.4a-D_2O**, and oxidized species **2.4-ox**.

CAN (total equiv)	% yields			moles formed per mole **2.4a** used	
	2.4a[a]	**2.4a-D_2O**[a]	**2.4-ox**	Acetic acid	Formic acid
0	12.54 (Cp*-Me) + 2.35 (coord CH_3CN) + 0.79 (H-6) = 15.68 units; 15.68 / 19H = 0.825 units per H; **69%**	5.47 (Cp*-Me) + 0.36 (H-6) = 4.50 units; 5.83 / 16H = 0.364 units per H; **31%**	0	0	0
	Combined units per H for **2.4a** + **2.4a-D_2O** = 1.189 = **100%**				
1	10.85 (Cp*-Me) + 2.03 (coord CH_3CN) = 12.88 units; 12.88 / 18H = 0.716 units per H; **60%**	4.34 (Cp*-Me); 4.34 / 15H = 0.289 units per H; **24%**	0.66 / 8H = 0.083 units per H = **7%**	nd	nd
5	4.62 (Cp*-Me); 4.62 / 15H = 0.308 units per H; **26%**	0.96 (Cp*-Me); 0.96 / 15H = 0.064 units per H; **5%**	2.96 / 13H = 0.228 units per H = **19%**	0.44 / 3H = 0.147 units per H = **0.12**	[b]
15	No identifiable peaks remain; **0%**	No identifiable peaks remain; **0%**	No identifiable peaks remain; **0%**	1.31 / 3H = 0.437 units per H = **0.37**	0.30 / 1H = 0.30 units per H = **0.25**

[a] When **2.4a** is dissolved in water, equilibrium is set up between **2.4a** and its substitution product **2.4a-D_2O**. [b] Overlap of peaks precludes determination.

Table 2.2. ^{1}H NMR data showing the effects of increasing amounts of CAN on [**2.4a**]$_0$ = 1.35 mM in D_2O. Chemical shifts for observed peaks are given, with integrals (units) in parentheses. The singlet for $(CH_3)_3SiCH_2CH_2CH_2SO_3Na$ was set to 9.00 units.

	Aromatic H					
CAN (total equiv)	H-6 (d)	H-5 (t)	H-4 (t)	H-3 (d)	Formic acid HCO_2H	$(NH_4)^+$
0	**2.4a**: 9.12 (0.79) **2.4a-D_2O**: 9.16 (0.36)	**2.4a**: 7.93[a] **2.4a-D_2O**: 7.91[a]	**2.4a**: 8.45[a] **2.4a-D_2O**: 8.50[a]	**2.4a**: 8.23[a] **2.4a-D_2O**: 8.21[a]	nd	nd
integral total	**1.15**	**1.11**	**1.12**	**1.12**	**0**	**0**
1	At least 4 d: 9.192 (minor) and 9.163 (0.33), 9.115 (0.72), 9.08 (0.04)	Four t: 7.96, 7.93 and 7.91 (1.04), 7.70 (0.06)	Three t: 8.50, 8.45 (major) and 8.44	Four d: 8.23, 8.21 (major), 8.19 , 8.16	nd	7.14 (1:1:1 triplet, 0.06)
integral total	**1.09**	**1.10**	**1.07**	**1.13**	**0**	**0.06**
5	At least six d between 9.06-9.24 (0.84)	At least four t: several between 7.90-8.00 (0.76), and at 7.70 (0.10)	Two readily identifiable t and at least four others: 8.50 and 8.45 (major) and others	At least four d between 8.14-8.30	8.245 (cannot be integrated because of overlap with signals for H-3)	7.14 (1:1:1 triplet, 0.28)
integral total	**0.84**	**0.86**	**0.96**	**1.23** (includes 8.245 ppm singlet)	Cannot be determined	**0.28**
15	Many doublets and triplets between 7.6 and 9.5 ppm				8.242	7.14 (1:1:1 triplet, 1.04)
integral total	Total of all aromatic H = **ca. 4** units				**0.30**	**1.04**

[a] Peaks overlapping, preventing individual integration.

Table 2.3. Continuation of Table 2.2.

CAN (total equiv)	CH_2 (two d each species)	*N*-CH_3 (two s each species)	Coord. CH_3CN	Free CH_3CN	Acetic acid	$C_5(CH_3)_5$ or $C_5(CH_3)_4(CH_2X)$
0	**2.4a**: 5.59 (0.79), 5.06 (0.81) **2.4a-D_2O**: 5.52 (br, 0.28), 5.18 (br, 0.30)	**2.4a**: 4.466 (total with 4.471 = 3.34),[a] 4.31 (2.42) **2.4a-D_2O**: 4.471,[a] 4.34 (1.03)	**2.4a**: 2.53 (2.35)	2.06 (0.76)	**nd**	**2.4a**: 1.61 (12.54) **2.4a-D_2O**: 1.54 (5.47)
int total	**2.18**	**6.79**	**2.35**	**0.76**	**0**	**18.01**
1	**2.4a**: 5.59 (0.71), 5.06 (0.74) **2.4a-D_2O**: 5.52 (br, 0.22), 5.18 (br, 0.21, overlapping with 5.14) Others: 5.14, 5.57	4.529 (0.07), 4.471 and 4.466 (3.15), 4.342 and 4.323 (0.92), 4.309 (2.29)	2.541 (0.14), 2.529 (2.03)	2.06 (0.81)	**nd**	**2.4a**: 1.61 (10.85) **2.4a-D_2O**: 1.54 (4.34) **2.4a-ox**: 1.812 and 1.805 (0.37), 1.67 (0.16), 1.58[a] and others (0.31), and two d at 4.02 (0.07), 3.85 (0.06)
integral total	**1.88**	**6.43**	**2.17**	**0.83**	**0**	**2.4a and 2.4a-D_2O (15H): 15.19 2.4a-ox (8H): 0.66**
5	At least 10 identifiable d, and many smaller peaks: 5.59, 5.57, and 5.55 (3 d, total 0.58, ~2:2:1), 5.27, 5.25 and 5.23 (3 d, total 0.08), 5.14 (0.13), 5.05 (0.28) 5.28-5.53 (~20 peaks, 0.39)	Four major s and many minor ones: 4.472, 4.469 and 4.467 (2.37), 4.31 (1.72), many minor peaks 4.26-4.30 (0.12), 4.31-4.36 (0.70), 4.38-4.45 (0.23)	Five singlets: two minor and 2.550 (total 0.31), 2.542 (0.46), 2.531 (0.87)	2.06 (1.50)	2.087 (0.44)	**2.4a**: 1.61 (4.62) **2.4a-D_2O**: 1.54 (0.96) **2.4a-ox**: 1.812 and 1.805 (equal, total 1.36), 1.67 (0.60), 1.58 (0.77), 4.03 (d, *J* = 13.2) overlapping with 4.01 (d) (total 0.33), 3.85 (0.23) Others: 1.89 (0.24), 1.73,[a] 3.86-4.00 (~10 peaks), 4.16-4.20 (~15 peaks, 0.37)
integral total	**1.46**	**5.42**	**1.64**	**1.50**	**0.44**	**2.4a and 2.4a-D_2O (15H): 5.58 2.4a-ox (13H): 2.96 Others: ~1**
15	Ten identifiable 5.2-6.1 ppm (total 0.43)	Three major s (4.304, 4.306, and 4.474); perhaps 30 other minor peaks between 4.26-4.60 ppm (total for 4.26-4.49[b] = 3.18)	Four singlets between 2.55 and 2.56 ppm (total 0.49)	2.06 (2.41)	2.088 (1.31)	Many minor peaks between 1.0 and 2.06 ppm: ~2.04 (2 peaks, 0.36), ~1.98 (2 peaks, 0.32), 1.83-1.86 (5 peaks, 0.49), 1.78-1.83 (4 peaks, 0.82), 1.71-1.78 (1.36[c]), ~1.67 (2 peaks, 0.27), ~1.58 (2 peaks, 0.42) as many as 10 d (20 peaks) 3.8-4.2 ppm (total 0.53)
int total	**0.43**	**3.18**	**0.49**	**2.41**	**1.31**	**4.04** (between 1.58-2.04 ppm)

[a] Peaks overlapping, preventing individual integration. [b] Overlap with base of peak for water prevented accurate integration above 4.49 ppm. [c] Measured integral value in this region = 3.36 units. Subtracting the 2.00 units expected from the multiplet for $Me_3SiCH_2CH_2CH_2SO_3Na$ in this region leaves 1.36 units.

Table 2.4. Percentage yields or moles per mole catalyst of identifiable species from **2.4a**, **2.3a**, **2.6**[a], **2.9**, and **2.1**.

Total CAN added (equiv)	Total **2.4a** + **2.4a-D_2O**	**2.4a-ox**	A	F	Total **2.3a** + **2.3a-D_2O**	**2.3a-ox**	A	F	**2.6**	**2.6-ox**	A	F	**2.9**	**2.9-ox**	A	F	**2.1**	Ar H[c]	A	F
0	100 (69+31)	0	0	0	100 (69+31)	0	0	0	100	0	0	0	100	0	0	0	100	100	0	0
1	84 (60+24)	7	0	0	58 (43+15)	23	0	0	90	5	0.03	0.02	87	tr[d]	tr[d]	0	59	73	0	0
5	31 (26+5)	19	0.12	[b]	4 (4+0)	14	0.14	0.12	68	12	0.13	0.05	58	7	0.31	0	6	57	0	0.12
15	0	0	0.37	0.25	0	0	0.49	0.43	39	12	0.38	0.15	10	4	0.72	0.05	0	14	0	0.43

[a] For intact catalyst and oxidized species **2.4a-ox**, **2.3a-ox**, **2.6-ox**, and **2.9-ox**, % based on starting complex; for acetic and formic acids (A and F, respectively) moles of degradation product per mole of starting complex. [b] Detected but overlap of integrals precluded quantitation.[c] Aromatic H remaining. [d] Perhaps a trace.

The possible role of formic acid as an intermediate in formation of CO_2 during water oxidation catalysis was probed. The ^{1}H and ^{13}C NMR spectra of $H^{13}CO_2H$ (5 mM), HNO_3 (15 mM), and standard $(CH_3)_3SiCH_2CH_2CH_2SO_3Na$ in D_2O revealed a doublet (J = 219 Hz) for the formyl proton $H^{13}CO_2H$, and a singlet for the carbon at 168.4 ppm. The chemical shift of the carbon changed by about 2 ppm on addition of nitric acid, which was added to model the acidic conditions produced by CAN during water oxidation reactions. Once CAN (5 equiv) was added to the mixture, 95% of the formic acid was consumed, and the ^{13}C NMR spectrum showed a new major peak at 127.4 ppm, which shows the formation of CO_2. We propose that one route to formation of CO_2 from molecular water oxidation catalysts is via formic acid.

CAN was shown to degrade water oxidation catalysts by NMR where we identify simple organic products such as acetic acid and formic acid with formic acid being shown to degrade into carbon dioxide. The quantity of acetic and formic acids varied (Table 2.4), but taken together added up to between 0.43 to 0.92 moles per mole of initial complex, which coupled with degradation of catalysts **2.1**, **2.3a**, or **2.4a** and 90% (**2.9**) or 61% (**2.6**) consumption could mean many oxidation events on a small fraction of catalyst molecules, or less-pervasive oxidation of a greater fraction of catalyst molecules, but either way, either none or little intact catalyst remains after only 15 equiv of CAN.

After concluding that the Cp* was being oxidized in all cases, we looked to study the fate of the heterocyclic ligand. Is the ligand being degraded to formic acid as seen with complex **2.1**? To explore this we decided to synthesize **2.3a** and **2.4a** with ^{13}C labels in different parts of the ligand, **2.13** and **2.15**. The two ligands, **2.13** and **2.15**, were thought to be ideal because when complexed to ruthenium, both ligands would form complexes that contained different M-^{13}C bonds, such as **2.4-methyl** and **2.3-ring**. With the labeled carbons in different positions we can then monitor the reaction by ^{13}C NMR and easily detect ^{13}C-labeled carbon monoxide, formic acid, or acetic acid and know which part of the ligand is degrading and to what.

2.11 was synthesized by Dr. Grotjahn, I then formed the triazole **2.12** by a copper-catalyzed azide-alkyne cycloaddition using a microwave at 100 ^{o}C for 10 min[27]. **2.12** was methylated using methyl triflate in DCM, and the product was recrystallized to obtain

pure compound. **2.13** was then metalated under the normal conditions of forming the silver carbene with silver oxide followed by transmetallation using $(IrCp^*Cl_2)_2$, forming **2.3-ring**. **2.4-ring** was not synthesized because the newly formed bond would not be ^{13}C labeled. **2.14** was synthesized using the known procedure[27] followed by methylation using $^{13}CH_3OH$ and triflic anhydride generating ^{13}C-methyl triflate in situ giving **2.15**[27]. **2.15** was then metalated in the same manner as above giving **2.3-methyl**, which was then converted to **2.4-methyl** under oil pump vacuum at 170 ^oC[15,22].

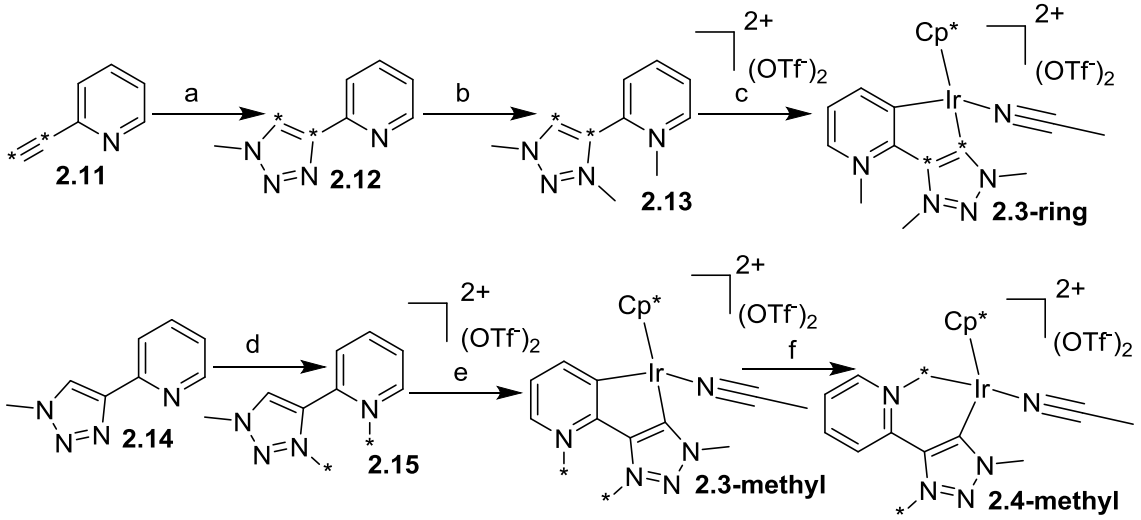

Figure 2.14. Synthesis of ^{13}C labeled metal complexes **2.3-ring**, **2.3-methyl**, and **2.4-methyl**.
(a) **2.11** (1.0 equiv), NaN_3 (1.0 equiv), CuI (0.5 equiv), methyl iodide (1.2 equiv), t-BuOH, and water, microwave 100 ^oC, 10 min, 45 % yield. (b) **2.12** (1.0 equiv), methyl triflate (5.8 equiv), DCM, 50 ^oC, 22 h, 36 % yield. (c) **2.13** (1 equiv), Ag_2O (1.3 equiv), ACN, 80 ^oC, 5 h, $(IrCp^*Cl_2)_2$ (0.51 equiv), 92 ^oC, 12 h, 9 % yield. (d) **2.14** (1.0 equiv), 2,4,6-tri-tert-butyl-pyridine (3.0 equi.), $^{13}CH_3OH$ (3.0 equiv), triflate anhydride (3.0 equiv), 50 ^oC, 14.5 h, 66 % yield. (e) **2.15** (1.0 equiv), Ag_2O (1.3 equiv), ACN, 80 ^oC, 29.5 h, $(IrCp^*Cl_2)_2$ (0.54 equiv), 92 ^oC, 3.5 h, 22 % yield. (f) **2.3-methyl** (1.0 equiv), 170 ^oC, oil pump vacuum, 100 % yield.

NMR testing for the ^{13}C labeled compounds was done at higher concentration than that used for the unlabeled analogs (Fig. 2.10-2.13) to obtain ^{13}C NMR spectra with adequate signal to noise. The initial NMR solution was prepared containing catalyst, at 6.75 mM, with the same internal standard as previously at 6.75 mM in D_2O. Initial ^1H and ^{13}C NMR spectra were acquired. Then 1 equiv of CAN was added, followed by observation of ^1H and ^{13}C NMR spectra. The same procedure was repeated after addition

of 4 and 10 equiv more CAN. Examining the obtained spectra for **2.3-methyl** and **2.3-ring** there was no detectable ^{13}C labeled small-molecule degradation products such as formic acid or carbon dioxide after addition of 15 equiv of CAN (See Figure 2.17-2.20 for **2.3-methyl** and Figure 2.21-2.24 for **2.3-ring**). In the case of **2.4-methyl**, after only 5 equiv of CAN there is formation of ^{13}C-formic acid detected in the ^{1}H NMR (Figure 2.26) and ^{13}C NMR spectra (Figure 2.28) (^{1}H NMR = 8.23 ppm, *d*, *J* = 219.1 Hz; ^{13}C NMR = 165.6 ppm) as well as formation of carbon dioxide which was detected in the ^{13}C NMR spectrum (124.6 ppm) (see Figure 2.25-2.30 for all **2.4-methyl** spectra). The quantity of ^{13}C-formic acid in solution can be determined by ^{1}H NMR, but since the formic acid is oxidized to carbon dioxide, we cannot determine the total amount of ^{13}C-oxidation product. The initial ^{1}H NMR spectrum showed that the average integral value for aromatic protons was 0.93 units (Figure 2.31). After addition of 15 equiv of CAN the integral of the $H^{12}COOH$ singelt was 0.27 units and of the $H^{13}COOH$ doublet was 0.07 (Figure 2.32), showing that about 4 % of both or 8 % of one of the initial ^{13}C carbons have been oxidized to formic acid and only 20 % of the formic acid was coming from one or both of the methyl positions after 15 equiv of CAN. Comparing the $H^{13}COOH$ to the initial amount of catalyst is not reliable since, as was previously shown, the formic acid is oxidized to carbon dioxide. What it can determine is that at the very least, 4 % or 8 % of the initial catalyst has lost a key atom that was bonding the metal to the ligand.

C. Conclusions

In conclusion, we wanted to make better water oxidation catalysts based on promising literature results in the 2008-2009 time range, but became concerned with the fate of the iridium-based catalysts after a color change of the reaction mixture. With the help of many colleagues thanked above, we showed that iridium catalysts while being tested using CAN are transforming to new molecular species, and then possibly into iridium oxide nanoparticles. The stepwise addition of CAN to solutions of iridium-based molecular catalysts showed that more cerium was needed to form the active catalyst when there were more carbon-containing ligands, hinting that the ligands were being oxidized. The Cp* ligand of several Cp*Ir-based catalysts was then showed to be oxidized in the stepwise addition studies that were monitored by ^{1}H NMR. Further

studies using specifically ^{13}C-labeled catalysts showed that parts of the non-Cp* ligands were being oxidized to formic acid and carbon dioxide. Lastly the UV-vis and STEM images show that the fate of the iridium could be the formation of iridium rich nanoparticles. These results bring into question if CAN should be used as a sacrificial oxidant to screen for iridium water oxidation catalysts.

The water oxidation field is a booming area of research, as evidenced by citation of the 2011 *JACS* paper 91 times over four years. Some of the following research came from Macchioni et al. which was published in 2011 showed the oxidation of the Cp* ring by NMR. Using higher catalyst concentrations than what we described earlier (30 mM) and adding CAN (6 equiv) they were able to monitor the reaction by 2D NMR which enabled them to conclude that not only was the methyl Cp* being oxidized but also the Cp* ring was oxidized. They observed two different oxidation products **2.8a**, where the methyl is oxidized to the alcohol, and **2.8b**, where the alcohol is further oxidized to the aldehyde (Figure 2.15)[28]. Macchioni in 2014 looked at the same issue in more detail, and "intercepted and characterized" three different oxidation products[29]. Crabtree et al. looked at the same problem of oxidation, but they changed the sacrificial oxidant to sodium periodate, a milder reagent that can be used under neutral conditions. They concluded that Cp* in complex **2.16** was oxidized and would eventually be displaced,

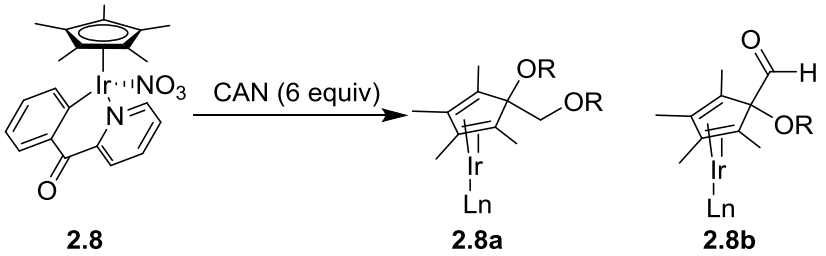

Figure 2.15. Cp* oxidation shown by Macchioni.

forming an Ir(IV) dimer **2.16a** stripped of its Cp* ligands, which is the active water oxidation catalyst (Figure 2.16)[24]. Hetterscheid in 2014 looked at the role of sodium periodate in the mechanism of water oxidation. DFT calculations showed that periodate may act as an oxygen atom transfer and that water may not even be involved[30]. In summary, the half reactions depicted in Figure 2.1 are simple, but the catalysis involved

is extremely complex, as will be made even more clear in the next two Chapters of this thesis.

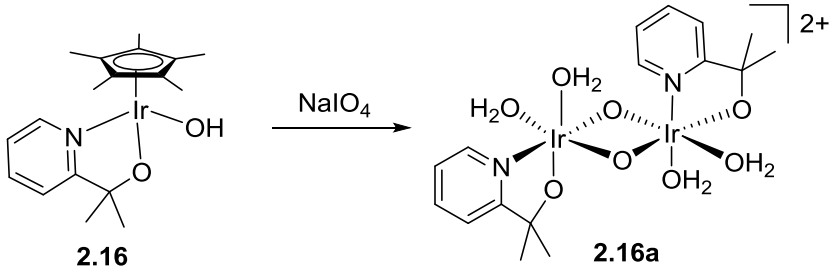

2.16 **2.16a**

Figure 2.16. Compelx degradation of **2.16** to active catalyst **2.16a** shown by Crabtree.

Part of the material and discussion covered in Chapter 2 is from published work "Evolution of iridium-based molecular catalysts during water oxidation with ceric ammonium nitrate", which appeared in *J. Am. Chem. Soc.* **2011**, *133*, 19024. I would like to thank; Dr. Douglas Grotjahn, Derek Brown, Jessica Martin, Dr. Caline Abadjian, Hai Tran, Dr. Gregory Kalyuzhny, Dr. Kenneth Vecchio, Dr. Zephen Specht, Dr. Sara Cortes-Llamas, Dr. Valentin Miranda-Soto, Christoffel van Niekerk, Dr. Curtis Moore, and Dr. Arnold Rheingold for their contributions.

D. NMR Spectra

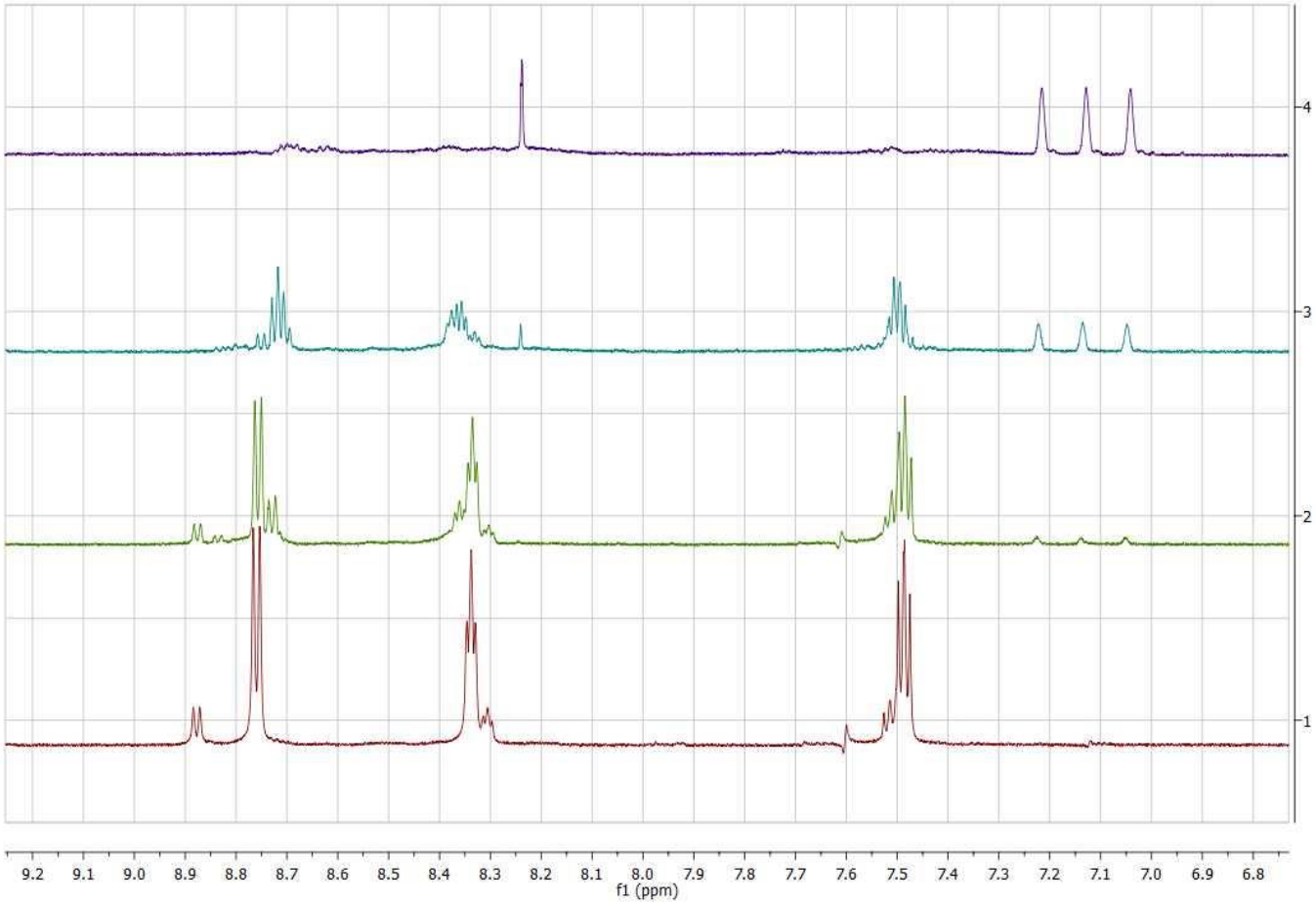

Figure 2.17. Enlarged ^{1}H NMR spectra of **2.3-methyl** (initially 6.75 mM, red, 1) from 6.7 to 9.3 ppm, after addition of CAN (1 equiv) (green,2), after addition of CAN (4 equiv, 5 total, blue, 3), and after addition of CAN (10 equiv, 15 total, purple, 4).

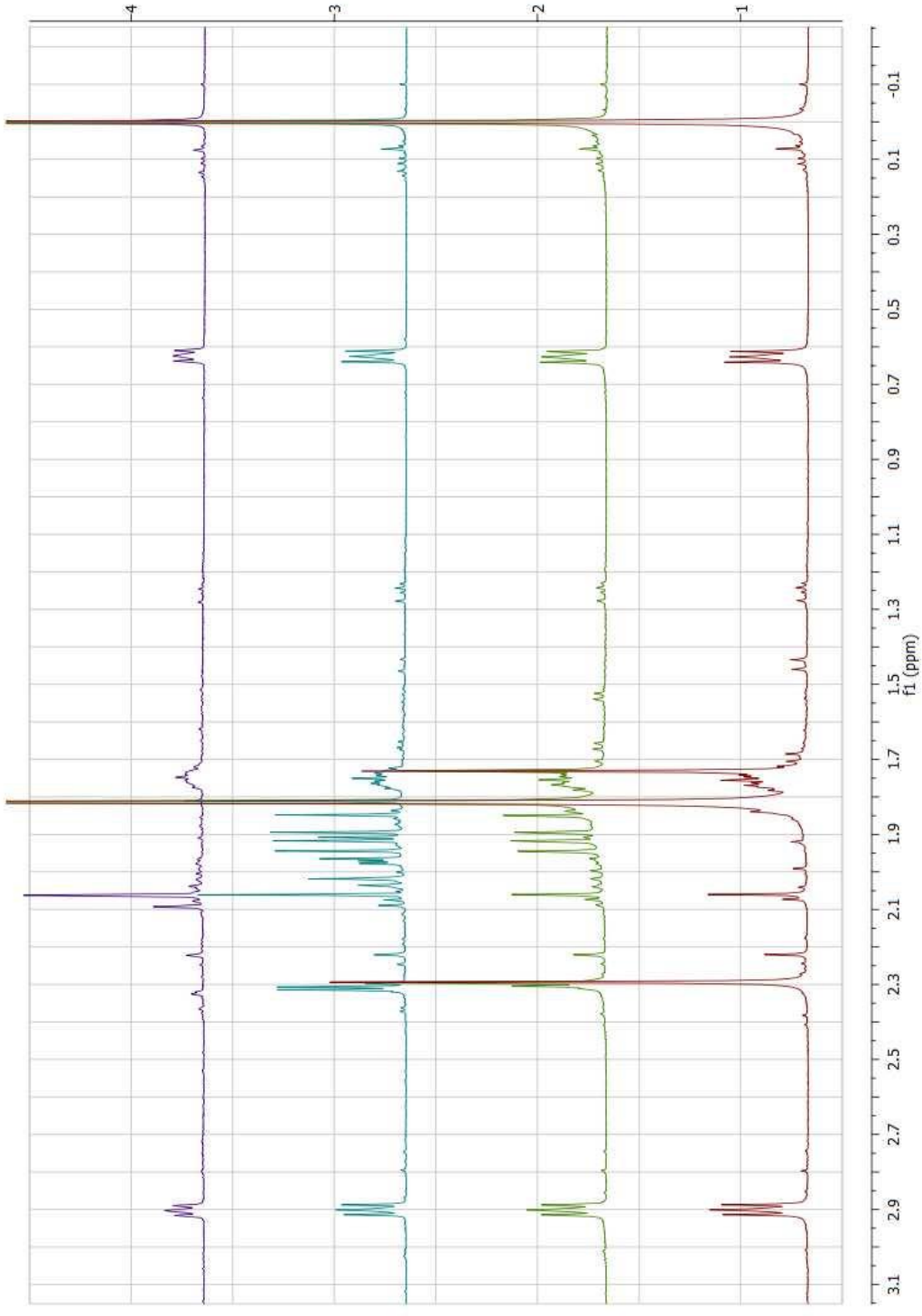

Figure 2.18. Enlarged ^{1}H NMR spectra of **2.3-methyl** (initially 6.75 mM, red, 1) from -0.2 to 3.1 ppm, after addition of CAN (1 equiv) (green, 2), after addition of CAN (4 equiv, 5 total, blue, 3), and after addition of CAN (10 equiv, 15 total, purple, 4).

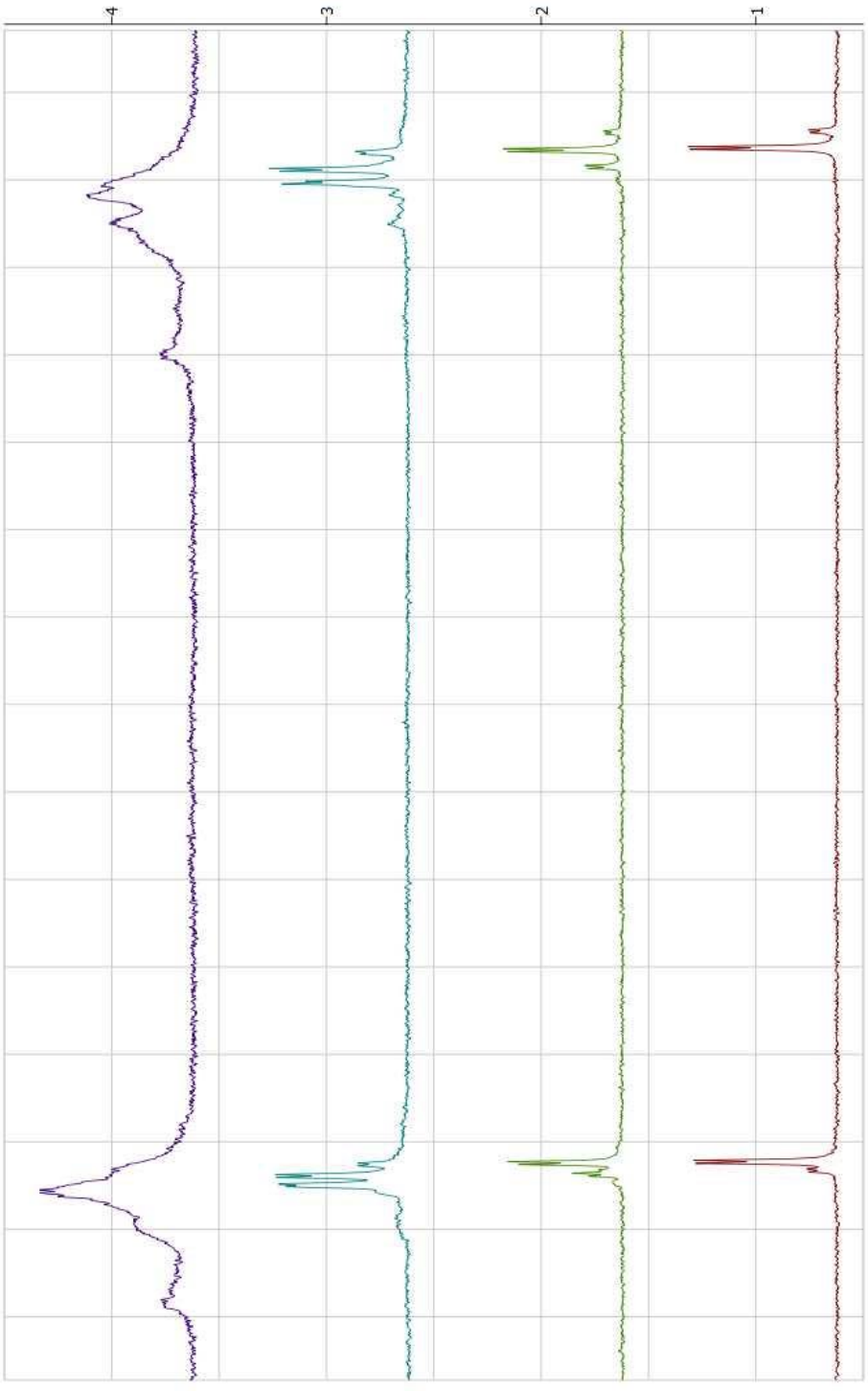

Figure 2.19. Enlarged ^{13}C NMR spectra of **2.3-methyl** (initially 6.75 mM, red (1)) from 42 to 51 ppm, after addition of CAN (1 equiv) (green, 2), after addition of CAN (4 equiv, 5 total, blue, 3), and after addition of CAN (10 equiv, 15 total, purple, 4).

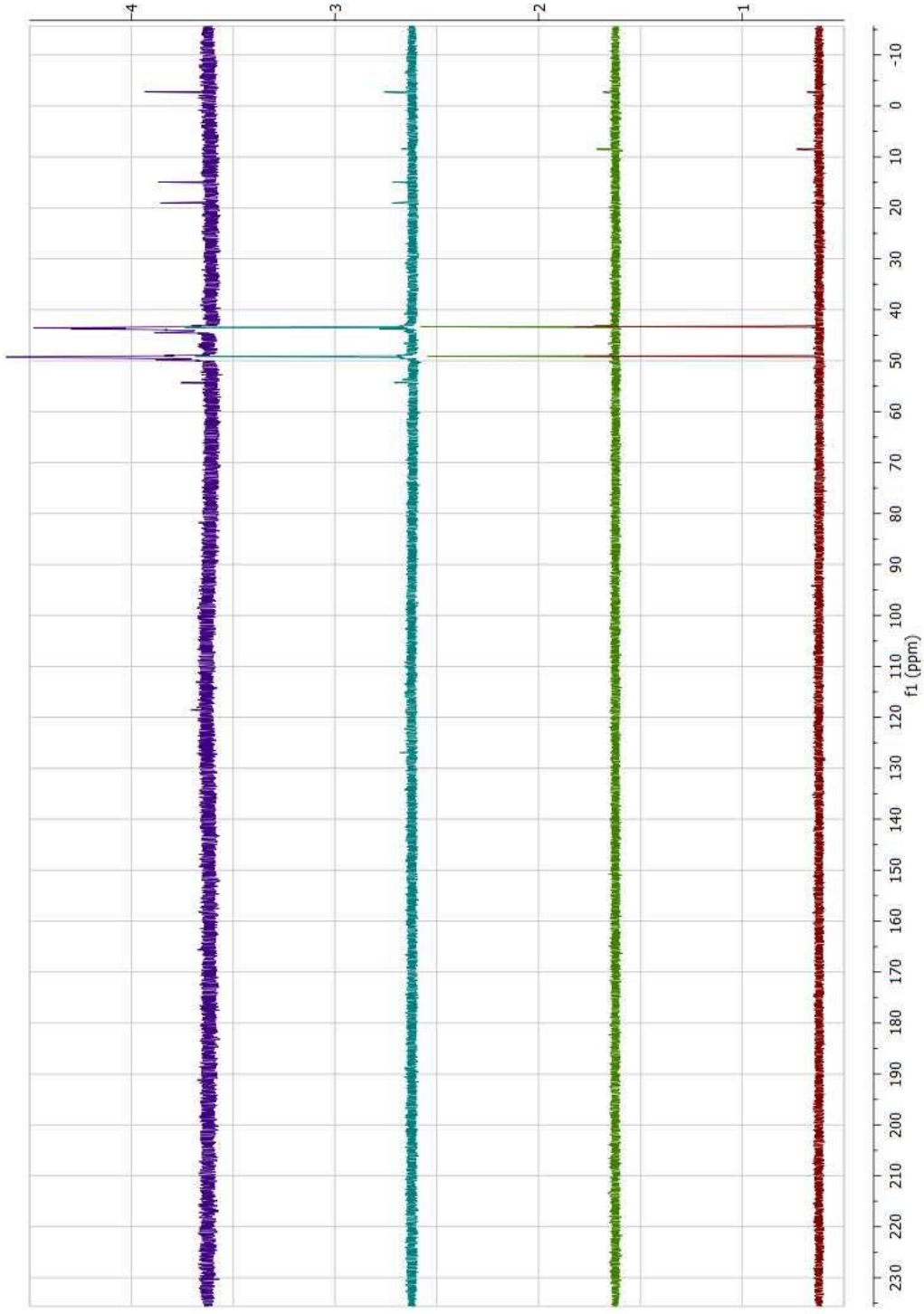

Figure 2.20. Full ^{13}C NMR spectra of **2.3-methyl** (initially 6.75 mM, red (1)), after addition of CAN (1 equiv) (green, 2), after addition of CAN (4 equiv, 5 total, blue, 3), and after addition of CAN (10 equiv, 15 total, purple, 4).

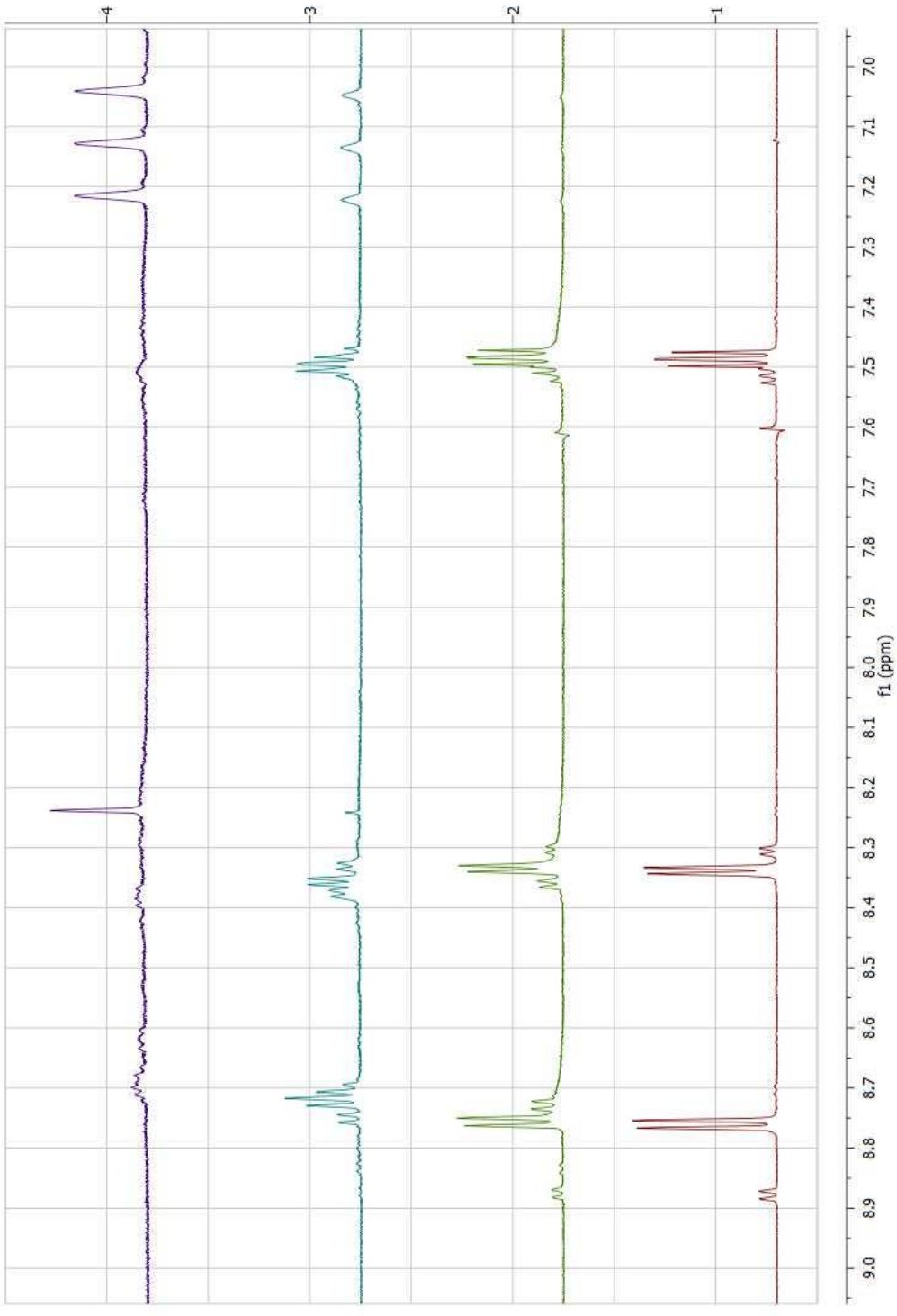

Figure 2.21. Enlarged ^{1}H NMR spectra of **2.3-ring** (initially 6.75 mM, red, 1) from 6.9 to 9.1 ppm, after addition of CAN (1 equiv) (green, 2), after addition of CAN (4 equiv, 5 total, blue, 3), and after addition of CAN (10 equiv, 15 total, purple, 4).

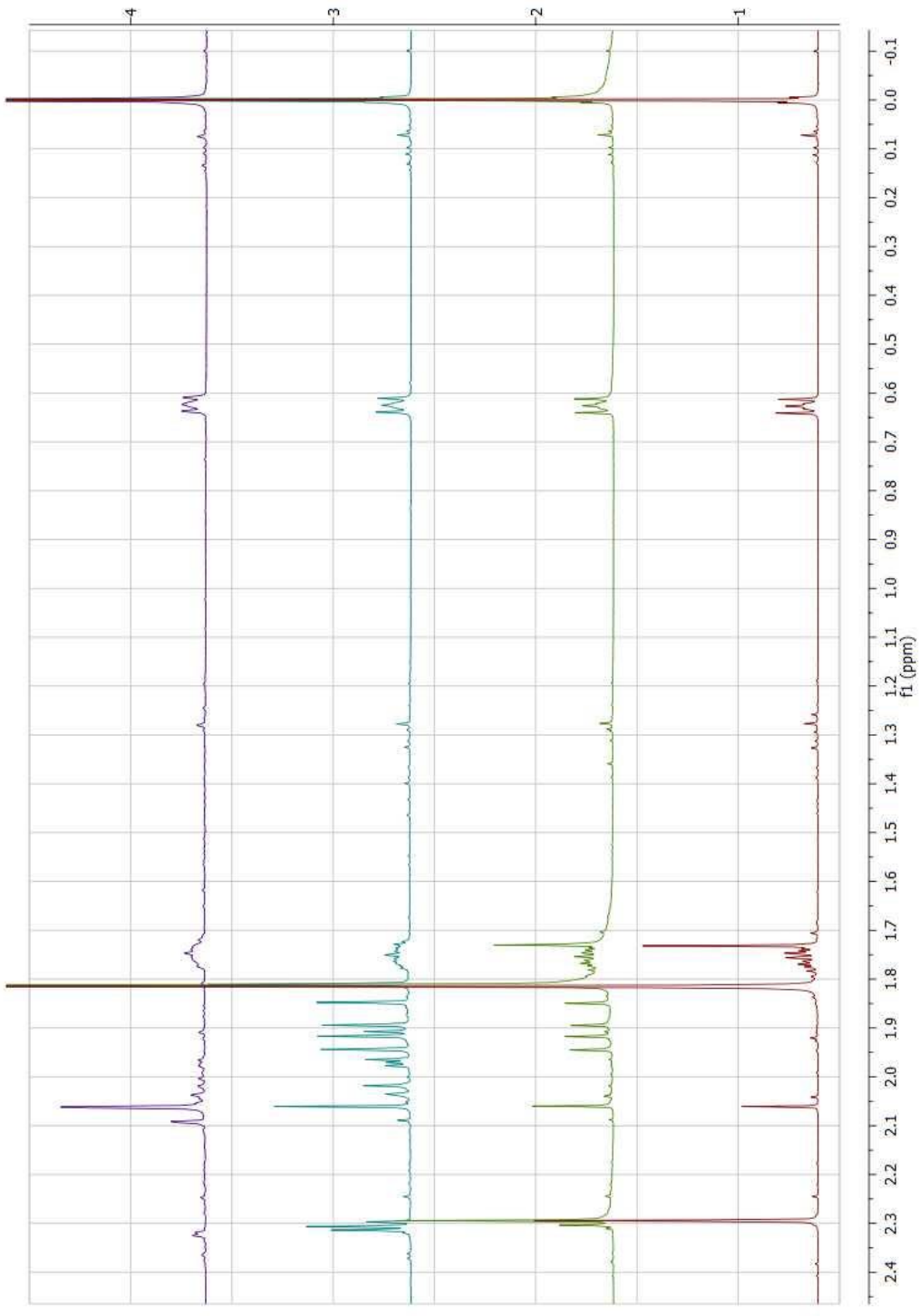

Figure 2.22. Enlarged ^{1}H NMR spectra of **2.3-ring** (initially 6.75 mM, red, 1) from -0.2 to 2.5 ppm, after addition of CAN (1 equiv) (green, 2), after addition of CAN (4 equiv, 5 total, blue, 3), and after addition of CAN (10 equiv, 15 total, purple, 4).

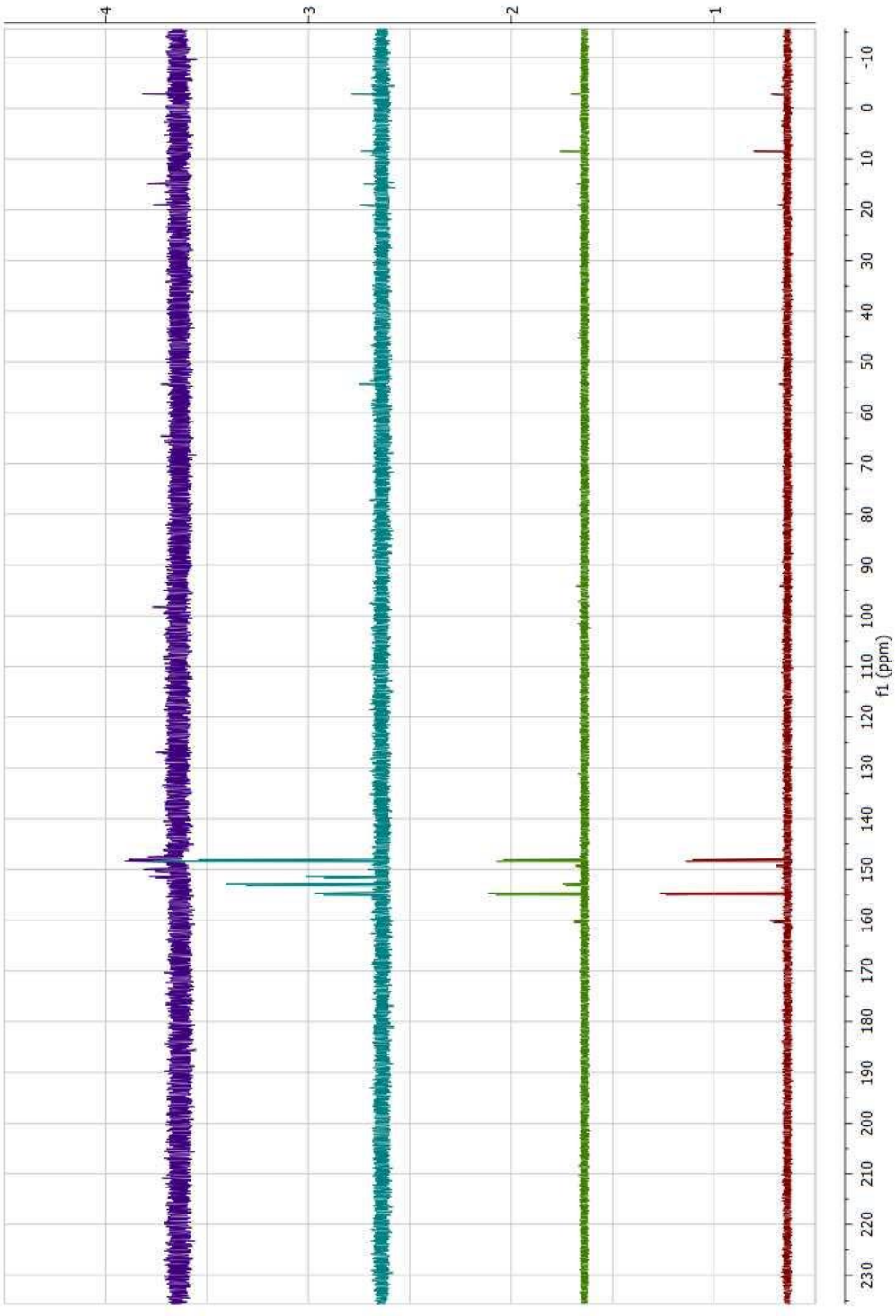

Figure 2.23. Full ^{13}C NMR spectra of **2.3-ring** (initially 6.75 mM, red (1)), after addition of CAN (1 equiv.) (green, 2), after addition of CAN (4 equiv, 5 total, blue, 3), and after addition of CAN (10 equiv, 15 total, purple, 4).

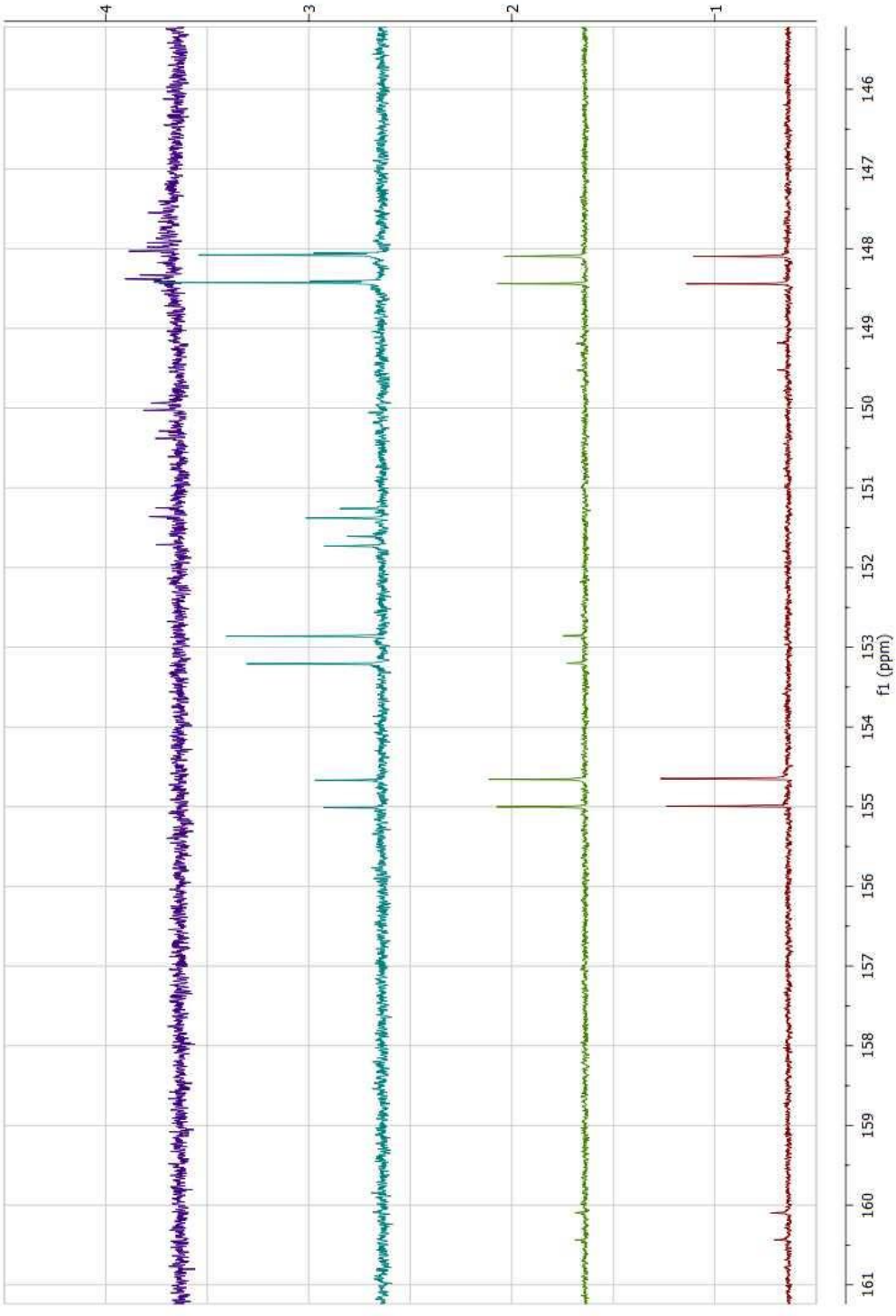

Figure 2.24. Enlarged ^{13}C NMR spectra of **2.3-ring** (initially 6.75 mM, red (1)) from 145 to 161 ppm, after addition of CAN (1 equiv) (green, 2), after addition of CAN (4 equiv, 5 total, blue, 3), and after addition of CAN (10 equiv, 15 total, purple, 4).

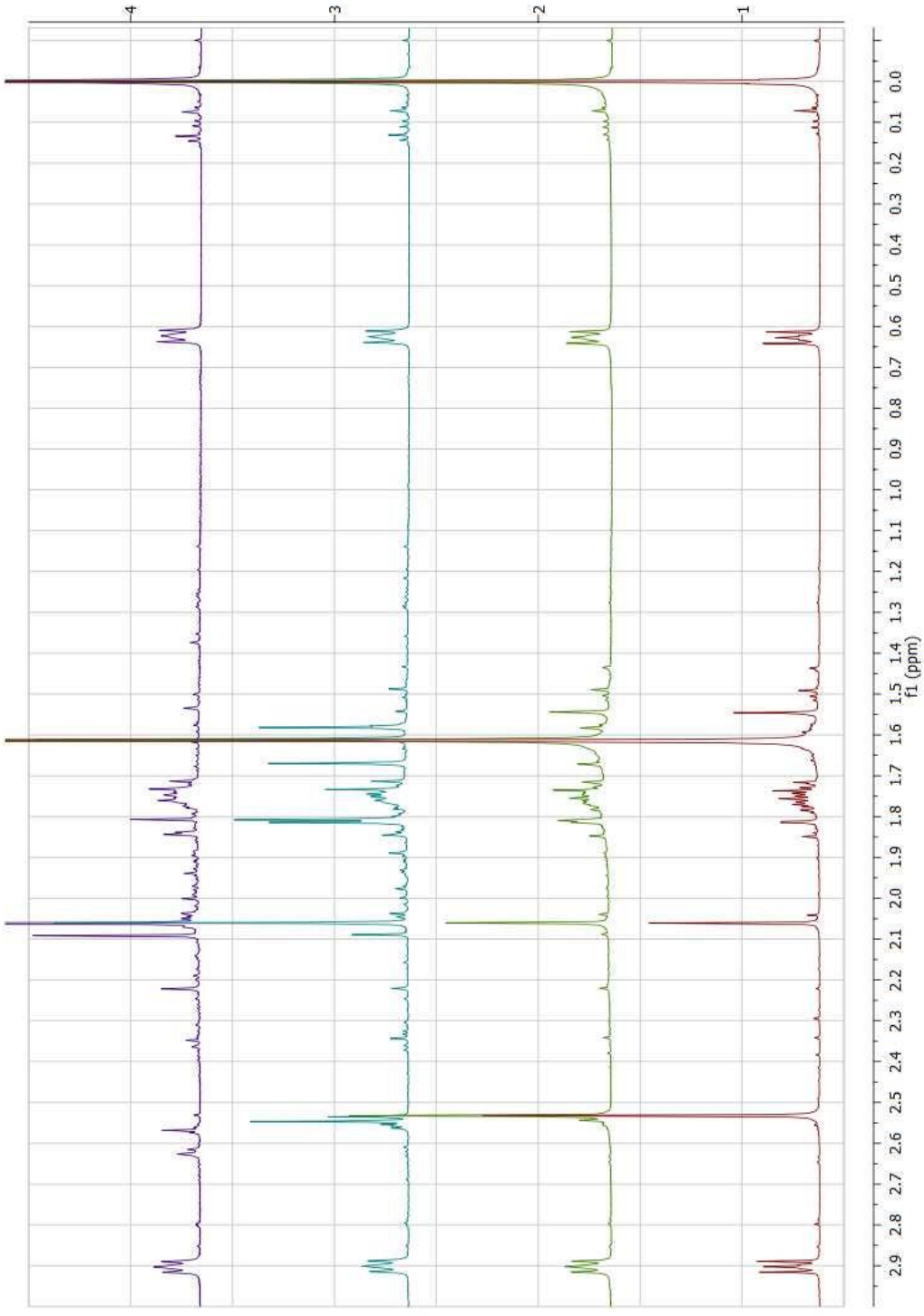

Figure 2.25. Enlarged ^{1}H NMR spectra of **2.4-methyl** (initially 6.75 mM, red, 1) from -0.1 to 3.0 ppm, after addition of CAN (1 equiv) (green, 2), after addition of CAN (4 equiv, 5 total, blue, 3), and after addition of CAN (10 equiv, 15 total, purple, 4).

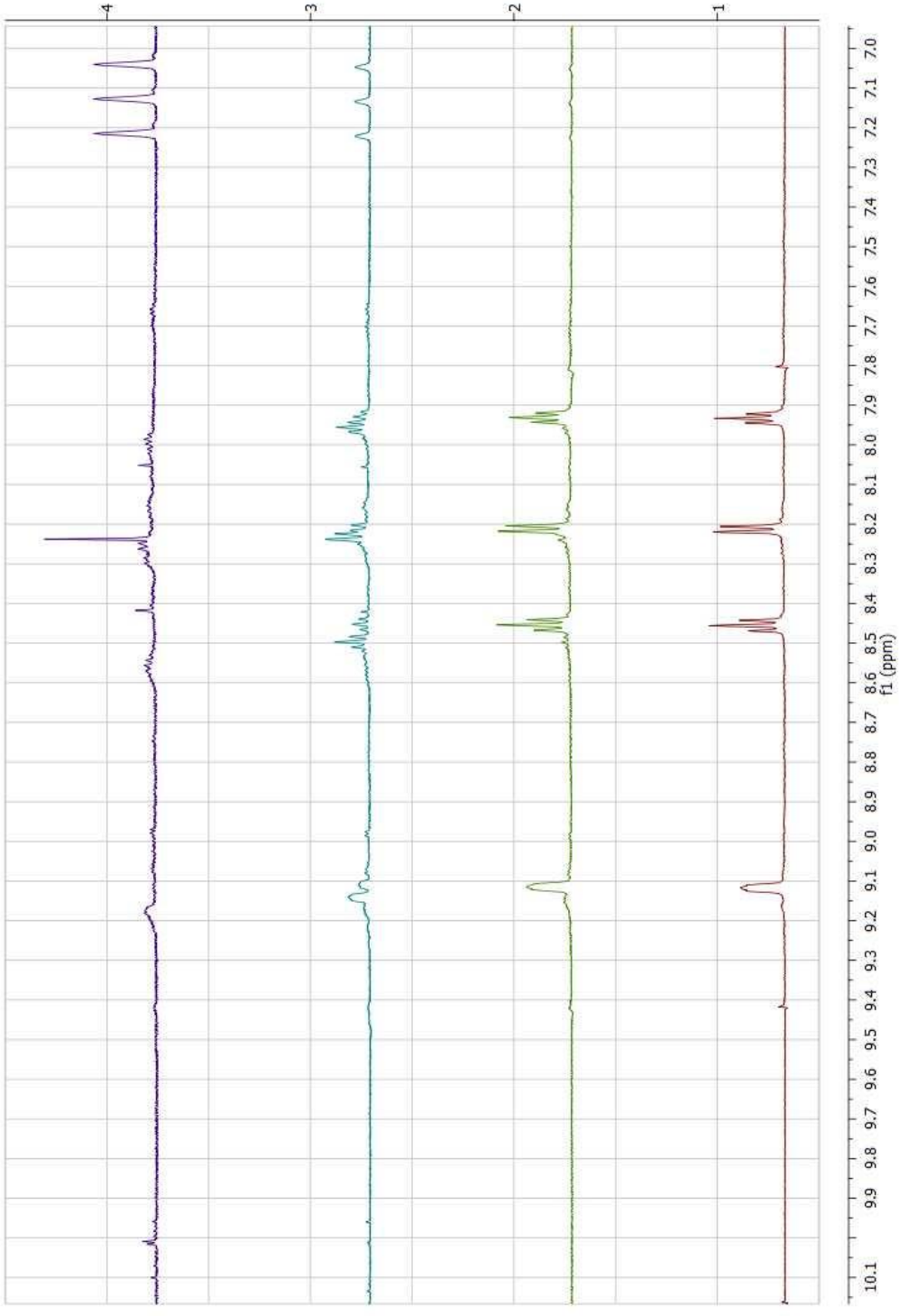

Figure 2.26. Enlarged ^{1}H NMR spectra of **2.4-methyl** (initially 6.75 mM, red, 1) from 6.9 to 10.1 ppm, after addition of CAN (1 equiv) (green, 2), after addition of CAN (4 equiv., 5 total, blue, 3), and after addition of CAN (10 equiv, 15 total, purple, 4).

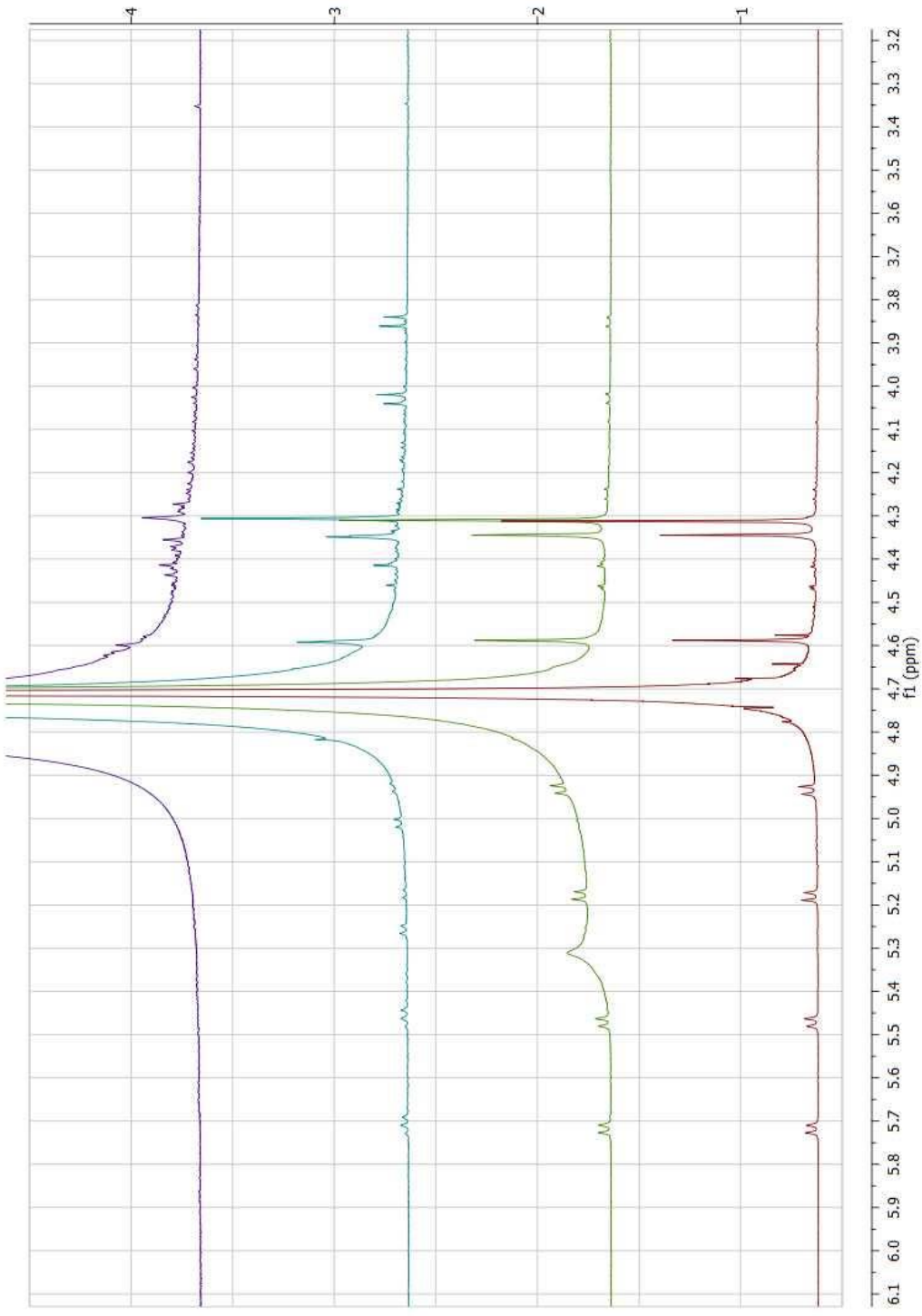

Figure 2.27. Enlarged ^{1}H NMR spectra of **2.4-methyl** (initially 6.75 mM, red, 1) from 3.2 to 6.1 ppm, after addition of CAN (1 equiv) (green,2), after addition of CAN (4 equiv, 5 total, blue, 3), and after addition of CAN (10 equiv, 15 total, purple, 4).

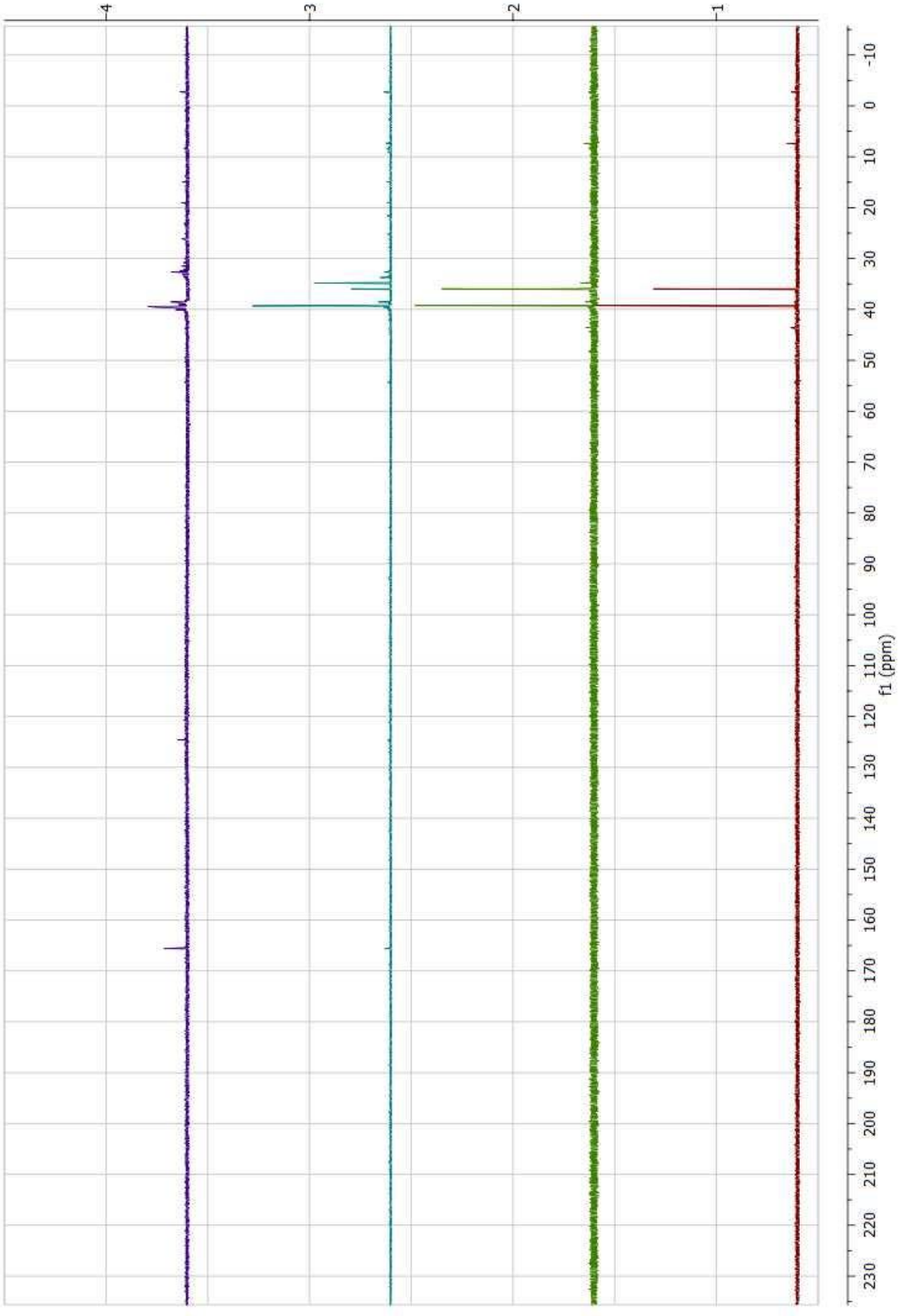

Figure 2.28. Full ^{13}C NMR spectra of **2.4-methyl** (initially 6.75 mM, red (1)), after addition of CAN (1 equiv) (green,2), after addition of CAN (4 equiv, 5 total, blue, 3), and after addition of CAN (10 equiv, 15 total, purple, 4).

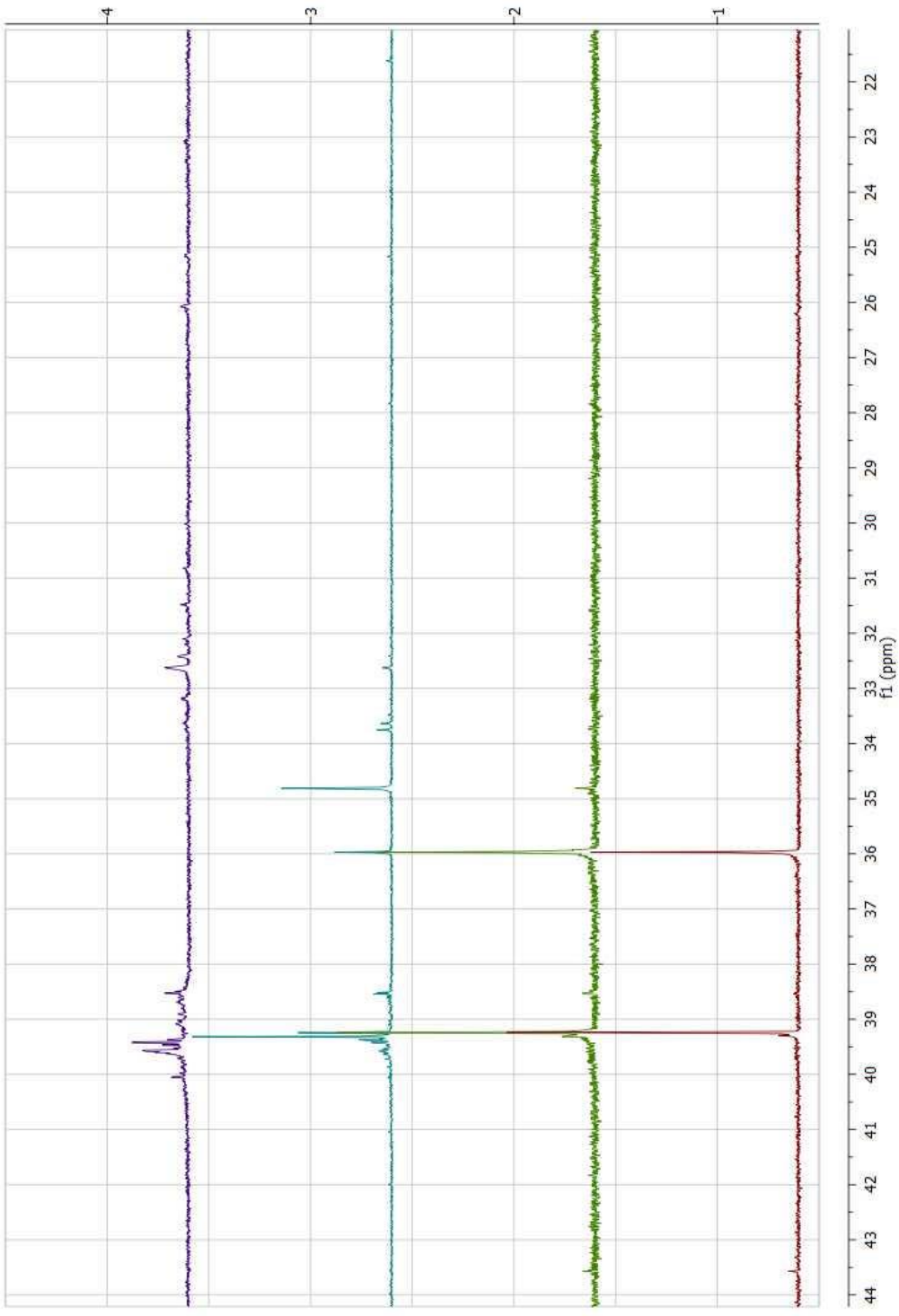

Figure 2.29. Enlarged ^{13}C NMR spectra of **2.4-methyl** (initially 6.75 mM, red, 1) from 21 to 44 ppm, after addition of CAN (1 equiv) (green,2), after addition of CAN (4 equiv, 5 total, blue, 3), and after addition of CAN (10 equiv, 15 total, purple, 4).

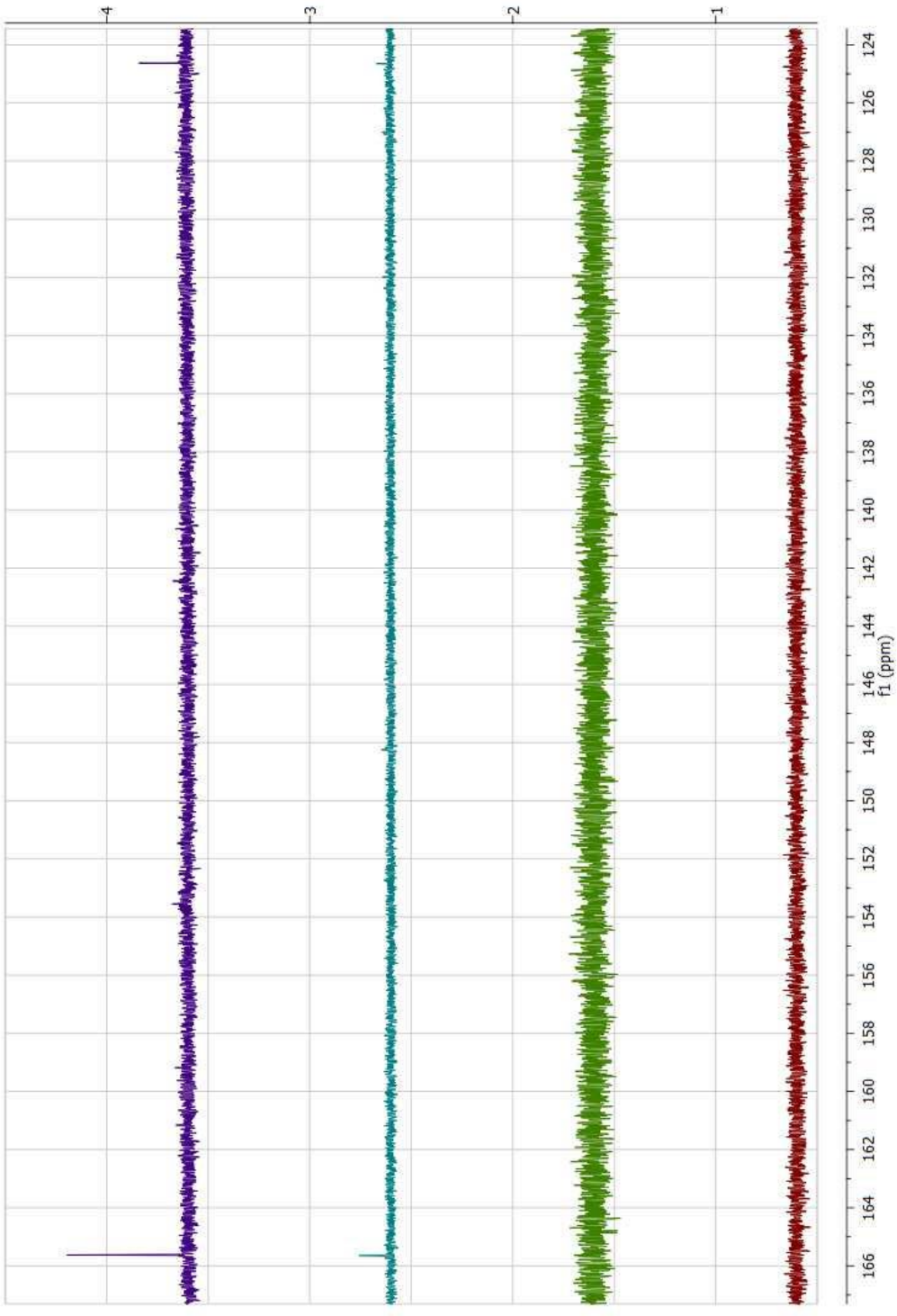

Figure 2.30. Enlarged ^{13}C NMR spectra of **2.4-methyl** (initially 6.75 mM, red, 1) from 124 to 167 ppm, after addition of CAN (1 equiv) (green, 2), after addition of CAN (4 equiv, 5 total, blue, 3), and after addition of CAN (10 equiv, 15 total, purple, 4).

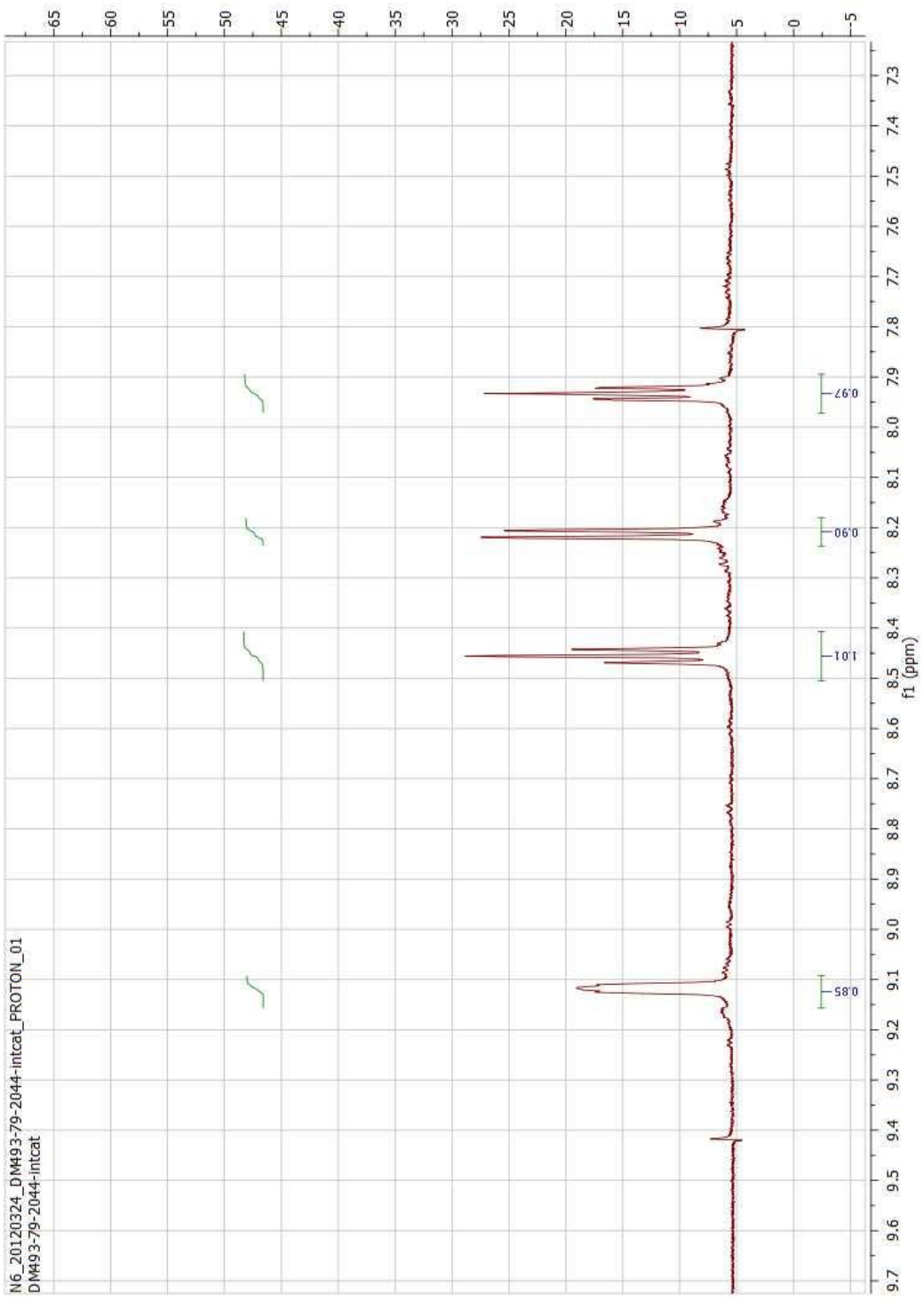

Figure 2.31. ^{1}H NMR spectrum of **2.4-methyl** (6.75 mM) in D_2O enlarged view from 7.3 to 9.7 ppm, where the internal standard trimethyl silyl peaks was set to 9. The average aromatic peak integration is 0.93 H.

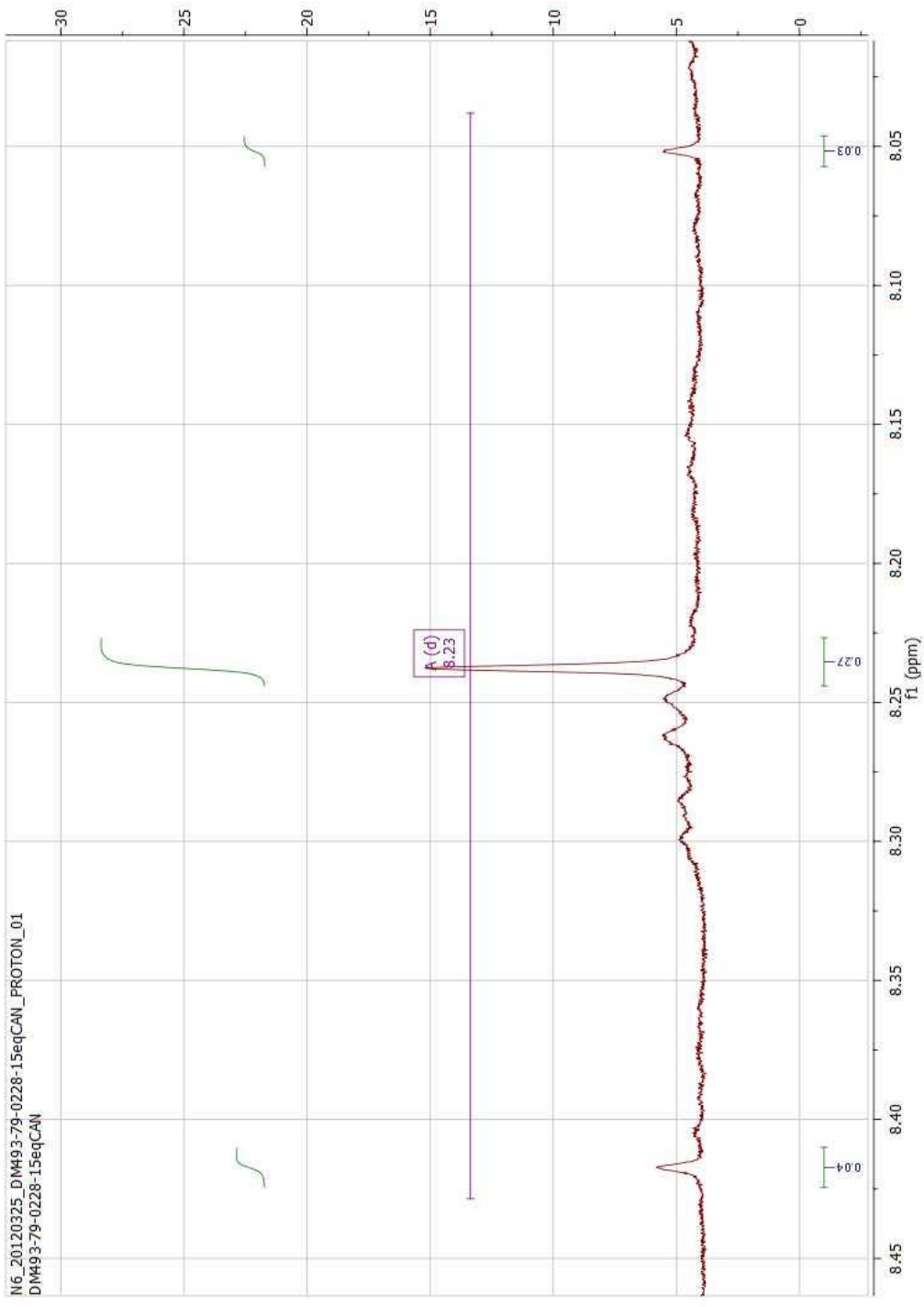

Figure 2.32. ^{1}H NMR spectrum of **2.4-methyl** after addition of CAN (15 equiv), showing the integral values of $^{12}CO_2H_2$ (0.27 H) and $^{13}CO_2H_2$ (0.07 H), the internal standard trimethylsilyl peak was set to 9. About 20 % of the formic acid is ^{13}C labeled.

E. Synthesis

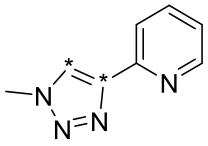

Synthesis of 2.12

Sodium azide (72.7 mg, 1.12 mmol), CuI (100.3 mg, 0.53 mmol), *t*-BuOH (1 mL), water (1 mL), **2.11** (115.5 mg, 1.10 mmol), methyl iodide (141.7 mg, 1.23 mmol) were added to a microwave vial (2-5 mL capacity). Another three vials were prepared in the same manner, than each vial was heated at 100 ^{o}C for 10 min in a microwave. The reaction mixtures were combined and diluted with DCM (100 mL) and washed with EDTA solution (7.5 g in 100 mL water), NH_4Cl (10 %, 100 mL), and water (2 x 100 mL). The aqueous layers were combined and back extracted with DCM (200 mL), the organic layers were then dried with Na_2SO_4, filtered through a course frit and solvent removed by rotary evaporation. The crude product was purified on by silica column chromatography (40 g), maintaining a solvent system of EtOAc :Hexanes (20:1). Pure fractions were combined and solvent was removed by rotary evaporation and dried under oil pump vacuum yielding a white solid, **2.12** (321.1 mg, 1.98 mmol, 45 % yield). ^{1}H NMR (499.9 MHz, $CDCl_3$) δ 8.55 (d, *J* = 4.6 Hz, 1H), 8.13 (d, *J* = 7.9 Hz, 1H), 8.09 (dd, *J* = 195.5, 8.8 Hz, 1H), 7.74 (t, *J* = 7.7 Hz, 1H), 7.19 (dd, *J* = 7.2, 5.1 Hz, 1H), 4.13 ppm (d, *J* = 2.4 Hz, 3H). ^{13}C NMR (125.7 MHz, $CDCl_3$) δ 150.3 (dd, *J* = 79.7, 8.5 Hz), 149.3 (d, *J* = 7.1 Hz), 148.6 (d, *J* = 70.3 Hz, ^{13}C labeled), 136.8 (d, *J* = 3.3 Hz), 122.9 (d, *J* = 70.3 Hz, ^{13}C labeled), 120.1 (dd, *J* = 5.1, 2.7 Hz), 36.7 ppm (dd, *J* = 3.6, 2.2 Hz). One of the aromatic peaks is not observed, it is possibly under the larger ^{13}C labeled peak at 122.9 ppm.

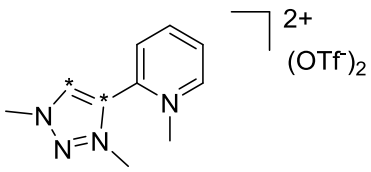

Synthesis of 2.13

2.12 (154.0 mg, 0.950 mmol), DCM (3.3 mL), methyl triflate (900 mg, 5.48 mmol), and a stir bar were added to a vial in a glovebox. The vial was heated in a 50 ^{o}C

oil bath for 22 h, after which the reaction was filtered through a fine frit and washed with cold DCM (2 x 3 mL). The solid was then transferred to a vial and dissolved in acetone, solvent was then removed by rotary evaporation and under oil pump vacuum giving an oil. EtOAc was added to the oil, forming a powder which was filtered through a fine frit. The solid was then dissolved in acetone and purified by vapor diffusion of pentane into the acetone solution, giving nice crystals, which were washed with cold acetone (3 x 2 mL) and dried under oil pump vacuum yielding a white solid, **2.13** (169.6 mg, 0.346 mmol, 36 %). ^{1}H NMR (599.3 MHz, CD_3CN) δ 9.02 (d, *J* = 6.1 Hz, 1H), 8.82 (dd, *J* = 207.1, 18.1 Hz, 1H), 8.74 (t, *J* = 7.6 Hz, 1H), 8.31 (ddd, *J* = 7.8, 6.2, 1.4 Hz, 1H), 8.28-8.21 (m, 1H), 4.41 (d, *J* = 2.7 Hz, 3H), 4.21 (s, 3H), 4.20 ppm (d, *J* = 2.4 Hz, 3H). Partial ^{13}C NMR showing only the two labeled carbons (150.7 MHz, CD_3CN) δ 134.99 (d, *J* = 73.6 Hz, ^{13}C), 133.49 ppm (d, *J* = 73.7 Hz, ^{13}C).

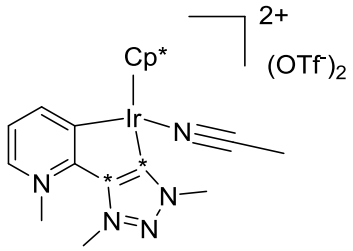

Synthesis of 2.3-ring

2.13 (70.8 mg, 144 µmol), Ag_2O (44.8 mg, 193 µmol), ACN (1.5 mL), and a stir bar were added to a vial in a glovebox. The vial was heated for 5 h in a 82 ^{o}C oil bath. $(IrCp^*Cl_2)_2$ (57.8 mg, 72.6 µmol) was added to the vial in a glovebox. The vial was then heated in a 92 ^{o}C oil bath for 12 h. After cooling to room temperature the reaction was filtered through Celite, and from the filtrate solvent was removed by rotary evaporation. Product was purified by vapor diffusion of pentane into acetone, which gave a dark oil and red solution. The red solution was then purified by another vapor diffusion of pentane into acetone giving crystals which were dried under oil pump vacuum yielding an orange solid, **2.3-ring** (11.3 mg, 13.2 µmol, 9 % yield). ^{1}H NMR (599.3 MHz, d_6-acetone) δ 8.89 (d, *J* = 7.6 Hz, 1H), 8.63 (d, *J* = 6.1 Hz, 1H), 7.64 (dd, *J* = 7.5, 6.2 Hz, 1H), 4.92 (s, *J* = 6.3 Hz, 3H), 4.87 (d, *J* = 2.0 Hz, 3H), 4.49 (d, *J* = 3.1 Hz, 3H), 2.47 (s, 3H), 1.94 ppm (d, *J* = 0.6 Hz, 15H). ^{13}C NMR (125.7 MHz, d_6-acetone) δ 155.16 (d, *J* =

52.4 Hz), 154.31 (d, *J* = 52.7 Hz), 153.33 (dd, *J* = 4.3, 1.0 Hz), 150.0 (d, *J* = 55.2 Hz) 149.84 (d, *J* = 52.4 Hz), 141.05 (s), 126.11 (s), 120.91 (d, *J* = 39.2 Hz), 95.11 (s), 50.56 (s), 44.76 (s), 40.62 (s), 9.64 (s), 3.84 ppm (s).

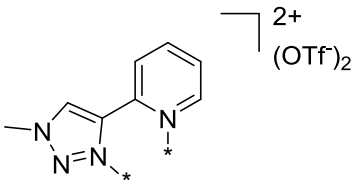

Synthesis of 2.15

2-(1-methyl-1H-1,2,3-triazol-4-yl)pyridine (50.2 mg, 313.4 µmol), 2,4,6-tri-*tert*-butyl-pyridine (232.7 mg, 940.5 µmol), $^{13}CH_3OH$ (31.1 mg, 941.6 µmol), CH_2Cl_2 (0.9 mL), and CD_2Cl_2 (0.2 mL) were added to a vial in a glovebox. Triflic anhydride (261.6 mg, 927.2 µmol) was then added in a glovebox after cooling the reaction to -30 ^oC. The reaction mixture was transferred to a J. Young NMR tube and placed in a 50 ^oC oil bath for 14.5 h. Crystals had formed; the solution was decanted, and the crystals were washed with DCM (2 x 1 mL). The solid was transferred to a vial and dried under oil pump vacuum yielding a white solid, **2.15** (102.1 mg, 208.2 µmol, 66 % yield). ^1H NMR (599.3 MHz, d_6-acetone) δ 9.47–9.42 (m, 1H), 9.38 (s, 1H), 8.97 (td, *J* = 7.9, 1.4 Hz, 1H), 8.69 (dd, *J* = 7.9, 1.3 Hz, 1H), 8.51 (ddd, *J* = 7.8, 6.1, 1.5 Hz, 1H), 4.68 (s, 3H), 4.56 (d, *J* = 146.6 Hz, 3H), 4.48 (d, *J* = 147.1 Hz, 3H).^{13}C NMR (150.7 MHz, d_6-acetone) δ 150.9, 147.9, 135.3, 133.5, 131.9 (d, *J* = 2.0 Hz), 49.0, 43.0, 40.2 (two peaks missing).

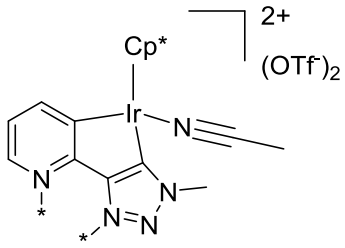

Synthesis of 2.3-methyl

2.15 (102.1 mg, 208.2 µmol), Ag_2O (62.9 mg, 271.4 µmol), stir bar, and acetonitrile (2 mL) were added to a vial in a glovebox. The vial was then heated in an 82 ^oC oil bath for 29.5 h. $(IrCp^*Cl_2)_2$ (90.0 mg, 113.0 µmol) and more Ag_2O (60 mg, 258.9 µmol) were then added in a glovebox. The vial was then heated in a 92 ^oC oil bath for 3.5

h, which after cooling to room temperature was filtered through Celite (1 g). From the filtrate, solvent was removed by rotary evaporation, then EtOAc was added giving a red flowing solution with a dark oil, the red solution was decanted and solvent was removed by rotary evaporation. The solid was then subjected to vapor diffusion of pentanes into acetone, which gave a brown oil and a red solution. The vapor diffusion was then repeated giving the same result, with a third crystallization giving nice crystals instead of an oil which were washed with acetone (3 x 1 mL) and dried under oil pump vacuum yielding an orange solid, **2.3-methyl** (38.7 mg, 45.1 µmol, 22 % yield). ^{1}H NMR (499.9 MHz, d_6-acetone) δ 8.86 (d, *J* = 7.3 Hz, 1H), 8.60 (t, *J* = 5.1 Hz, 1H), 7.61 (dd, *J* = 7.6, 6.1 Hz, 1H), 5.01 (d, *J* = 22.7 Hz, 3H), 4.72 (d, *J* = 24.1 Hz, 3H), 4.47 (s, 3H), 2.44 (s, 3H), 1.92 ppm (s, 15H). ^{13}C NMR (125.7 MHz, d_6-acetone) δ 155.1 (s), 154.4 (s), 154.2 (s), 153.3 (s), 149.9 (s), 141.0 (s), 126.1 (d, *J* = 2.1 Hz), 120.9 (d, *J* = 38.7 Hz), 95.1 (s), 50.5 (d, *J* = 2.5 Hz), 44.8 (d, *J* = 2.5 Hz), 40.6 (s, *J* = 7.4 Hz), 9.6 (s), 3.8 ppm (s).

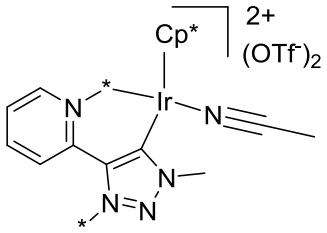

Synthesis of 2.4-methyl

2.3-methyl (10.6 mg, 12.4 µmol) was added to a J. Young NMR tube, which was backfilled with nitrogen. The reaction was then put under oil pump vacuum and heated in a 170 ^{o}C oil bath for 40 min yielding an orange solid, **2.4-methyl** (10.6 mg, 12.4 µmol, 100 % yield). Acetonitrile was used to dissolve the solid to make sure ACN was coordinated to iridium.

^{1}H NMR (599.3 MHz, d_6-acetone) δ 9.46–9.40 (m, 1H), 8.62 (t, *J* = 7.9 Hz, 1H), 8.55 (d, *J* = 7.2 Hz, 1H), 8.12 (ddd, *J* = 7.6, 6.2, 1.4 Hz, 1H), 5.92 (dd, *J* = 148.7, 10.3 Hz, 1H), 5.25 (dd, *J* = 146.7, 10.3 Hz, 1H), 4.61 (d, *J* = 145.8 Hz, 3H), 4.44 (s, *J* = 6.1 Hz, 3H), 2.71 (s, 3H), 1.73 ppm (s, 15H).

F. Refrences

(1) Kärkäs, M. D.; Verho, O.; Johnston, E. V.; Åkermark, B. *Chem. Rev.* **2014**, *114*, 11863.

(2) Lewis, N. S.; Nocera, D. G. *Proc. Natl. Acad. Sci. U.S.A.* **2006**, *103*, 15729.

(3) Cho, A. *Science* **2010**, *329*, 786.

(4) Blakemore, J. D.; Crabtree, R. H.; Brudvig, G. W. *Chem. Rev.* **2015**.

(5) Kang, R.; Chen, K.; Yao, J.; Shaik, S.; Chen, H. *Inorg. Chem.* **2014**, *53*, 7130.

(6) Duan, L. L.; Bozoglian, F.; Mandal, S.; Stewart, B.; Privalov, T.; Llobet, A.; Sun, L. C. *Nat. Chem.* **2012**, *4*, 418.

(7) Song, N.; Concepcion, J. J.; Binstead, R. A.; Rudd, J. A.; Vannucci, A. K.; Dares, C. J.; Coggins, M. K.; Meyer, T. J. *Proc. Natl. Acad. Sci.* **2015**, *112*, 4935.

(8) Grotjahn, D. B. *Pure Appl. Chem.* **2010**, *82*, 635.

(9) Grotjahn, D. B. *Dalton Trans.* **2008**, 6497.

(10) Grotjahn, D. B.; Larsen, C. R.; Gustafson, J. L.; Nair, R.; Sharma, A. *J. Am. Chem. Soc.* **2007**, *129*, 9592.

(11) Grotjahn, D. B.; Lev, D. A. *J. Am. Chem. Soc.* **2004**, *126*, 12232.

(12) Grotjahn, D. B. *Chem. – Eur. J.* **2005**, *11*, 7146.

(13) McDaniel, N. D.; Coughlin, F. J.; Tinker, L. L.; Bernhard, S. *J. Am. Chem. Soc.* **2008**, *130*, 210.

(14) Hull, J. F.; Balcells, D.; Blakemore, J. D.; Incarvito, C. D.; Eisenstein, O.; Brudvig, G. W.; Crabtree, R. H. *J. Am. Chem. Soc.* **2009**, *131*, 8730.

(15) Lalrempuia, R.; McDaniel, N. D.; Muller-Bunz, H.; Bernhard, S.; Albrecht, M. *Angew. Chem. Int. Ed.* **2010**, *49*, 9765.

(16) Blakemore, J. D.; Schley, N. D.; Balcells, D.; Hull, J. F.; Olack, G. W.; Incarvito, C. D.; Eisenstein, O.; Brudvig, G. W.; Crabtree, R. H. *J. Am. Chem. Soc.* **2010**, *132*, 16017.

(17) Dzik, W. I.; Calvo, S. E.; Reek, J. N. H.; Lutz, M.; Ciriano, M. A.; Tejel, C.; Hetterscheid, D. G. H.; de Bruin, B. *Organometallics* **2011**, *30*, 372.

(18) Savini, A.; Bellachioma, G.; Ciancaleoni, G.; Zuccaccia, C.; Zuccaccia, D.; Macchioni, A. *Chem. Commun.* **2010**, *46*, 9218.

(19) Hetterscheid, D. G. H.; Reek, J. N. H. *Chem. Commun.* **2011**, *47*, 2712.

(20) Specht, Z. G.; Grotjahn, D. B.; Moore, C. E.; Rheingold, A. L. *Organometallics* **2013**, *32*, 6400.

(21) Specht, Z. G.; Cortes-Llamas, S. A.; Tran, H. N.; van Niekerk, C. J.; Rancudo, K. T.; Golen, J. A.; Moore, C. E.; Rheingold, A. L.; Dwyer, T. J.; Grotjahn, D. B. *Chem. – Eur. J.* **2011**, *17*, 6606.

(22) Grotjahn, D. B.; Brown, D. B.; Martin, J. K.; Marelius, D. C.; Abadjian, M.-C.; Tran, H. N.; Kalyuzhny, G.; Vecchio, K. S.; Specht, Z. G.; Cortes-Llamas, S. A.; Miranda-Soto, V.; van Niekerk, C.; Moore, C. E.; Rheingold, A. L. *J. Am. Chem. Soc.* **2011**, *133*, 19024.

(23) Hintermair, U.; Hashmi, S. M.; Elimelech, M.; Crabtree, R. H. *J. Am. Chem. Soc.* **2012**, *134*, 9785.

(24) Hintermair, U.; Sheehan, S. W.; Parent, A. R.; Ess, D. H.; Richens, D. T.; Vaccaro, P. H.; Brudvig, G. W.; Crabtree, R. H. *J. Am. Chem. Soc.* **2013**, *135*, 10837.

(25) Woods, J. A.; Lalrempuia, R.; Petronilho, A.; McDaniel, N. D.; Muller-Bunz, H.; Albrecht, M.; Bernhard, S. *Energy Environ. Sci.* **2014**, *7*, 2316.

(26) Savini, A.; Bellachioma, G.; Bolaño, S.; Rocchigiani, L.; Zuccaccia, C.; Zuccaccia, D.; Macchioni, A. *ChemSusChem* **2012**, *5*, 1415.

(27) Fleischel, O.; Wu, N.; Petitjean, A. *Chem. Commun.* **2010**, *46*, 8454.

(28) Savini, A.; Belanzoni, P.; Bellachioma, G.; Zuccaccia, C.; Zuccaccia, D.; Macchioni, A. *Green Chem.* **2011**, *13*, 3360.

(29) Zuccaccia, C.; Bellachioma, G.; Bortolini, O.; Bucci, A.; Savini, A.; Macchioni, A. *Chem. – Eur. J.* **2014**, *20*, 3446.

(30) Hetterscheid, D. G. H.; Reek, J. N. H. *Eur. J. Inorg. Chem.* **2014**, *2014*, 742.

CHAPTER 3

Addition of a Pendant Base to the Well-Known [Ru(OH_2)(2,2'-bipyridine)(2,2';6',2"-terpyridine)]X_2 System

A. Introduction

After the issues described in chapter 2 with iridium water oxidation catalysts, we decided that complexes of other metals should be targeted. Instead of trying to develop effective catalysts with entirely new structures, we wanted to take a well-known water oxidation catalyst and incorporate a pendant base to see if that would increase the rate of catalysis. Looking at the proposed WOX mechanisms, it was thought that altering a catalyst that operates by the water nucleophilic attack (WNA) mechanism would benefit the most from having a pendant base. One of the most well-known catalysts that is believed to operate by the WNA mechanism, came from the group of T. J. Meyer in 2008, in work that was published shortly after the report of Bernhard's iridium catalyst. Catalysts **3.1a-3.1c** are ruthenium (II) complexes consisting of two heterocyclic ligands, 2,2';6',2"-terpyridine (terpy), a tridentate ligand, and either 2,2'-bipyridine (**3.1a**), 2,2'-bipyrimidine (**3.1b**), or 2,2′-bipyrazine (**3.1c**), all bidentate ligands, together occupying 5 of 6 coordination sites; the last site is occupied by water in each case (Figure 3.1). The T. J. Meyer group paper tested **3.1a-3.1c** using electrochemistry and CAN, coming to the conclusion that "one site is enough" for water oxidation and that these catalysts operate by

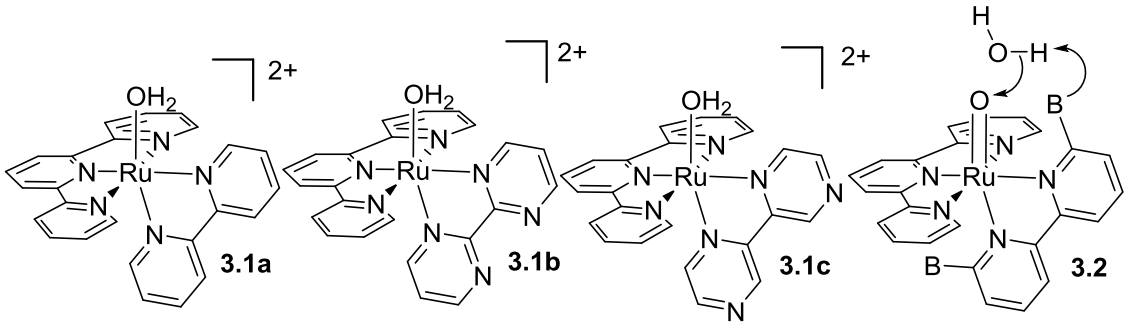

Figure 3.1. T.J. Meyer catalysts, **3.1a-c** (left); illustration of possible bifunctional interaction (right).

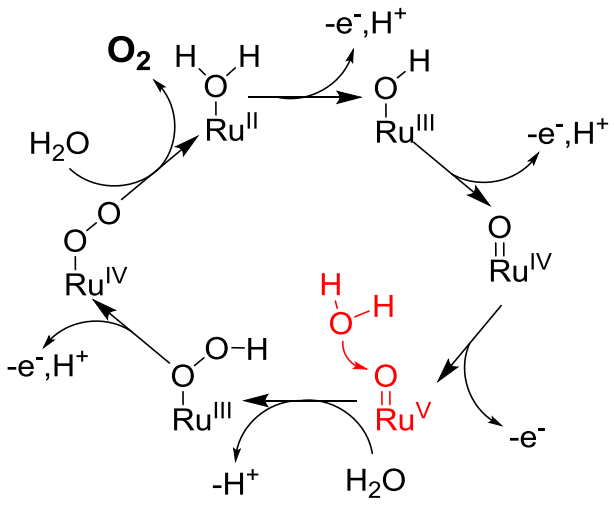

Figure 3.2. Proposed mechanism for catalyst **3.1** using CAN.

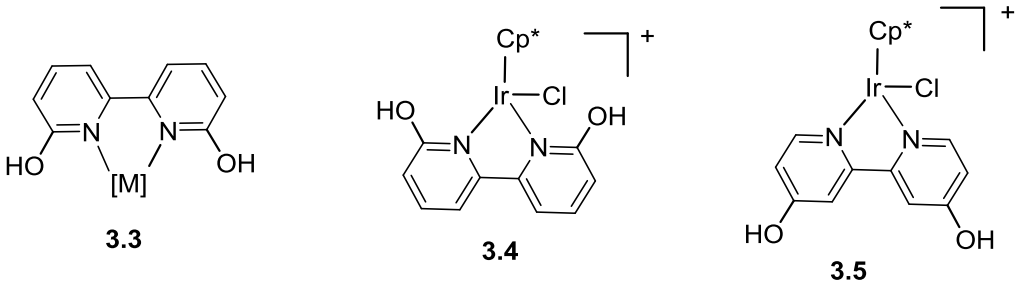

Figure 3.3. Hydroxylated bipyridine complexes.

WNA mechanism (Figure 3.2)[1]. The possible benefit of adding a pendant base (B) to **3.1** would be the ability for the base to accept a proton (or a hydrogen bond) from a reacting water molecule (illustrated in **3.2** in Figure 3.1 right), making the water oxygen more nucleophilic. We wanted to make a number of different analogs with different bases to see if there was a change in reactivity. The first targeted ligands were analogs where the pendant base was methoxy or hydroxy.

There have been multiple papers that have used dihydroxy-bipyridine (**3.6**) as a ligand in catalysis for transfer hydrogenation[2], transfer dehydrogenation[3], hydrogenation of carbon dioxide[4], and for water oxidation[5,6]. Our group began a collaboration with the groups of Papish and Paul when we learned they were interested in studying analogs of

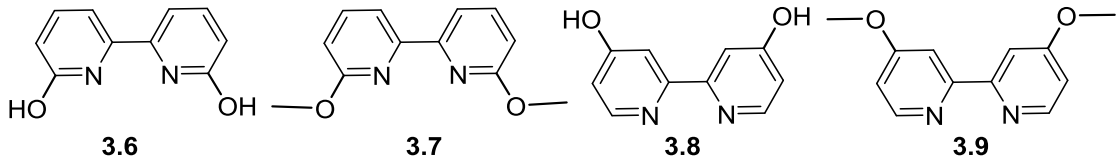

Figure 3.4. Bipyridine analogs of interest.

compound **3.3**. Papish et al previously showed that complex **3.4** was five times more active than the bipyridine anolog and that **3.5** was about a 100 times more active (Figure 3.3). The rate enhancements were found to be pH dependant, where the catalyst performed best when the hydroxy group(s) was(were) deprotonated[5].

B. Synthesis and Characterization of Complexes with Oxygenated Substituent Directly Attached to Ligand Ring

The target ligands for the project were **3.6** for its bifunctional possibilities and **3.8** because it is electronically similar to **3.6** but incapable of bifunctional interactions, and the aprotic analogs **3.7** and **3.9** (Figure 3.4). Ligand **3.6** was synthesized from 6-chloro-2-hydroxypyridine, in an interesting procedure reported by Gross[7] using palladium on carbon in basic water and methanol to do the reductive coupling. Ligand **3.7** was synthesized from 6-chloro-2-methoxypyridine by a reductive coupling with nickel and zinc, according to a procedure by Oda[8]. The 4,4' ligands, **3.8** and **3.9,** were synthesized by the Paul group.

The classic route for synthesizing analogs of **3.12** starts by complexation of terpy to $RuCl_3$, forming precursor **3.10** (Figure 3.5), which is followed by addition of the desired bidentate ligand, such as **3.11**, in the presence of alcohol and tertiary amine, which reduces the metal from Ru(III) to Ru(II). Lithium chloride is often added in this

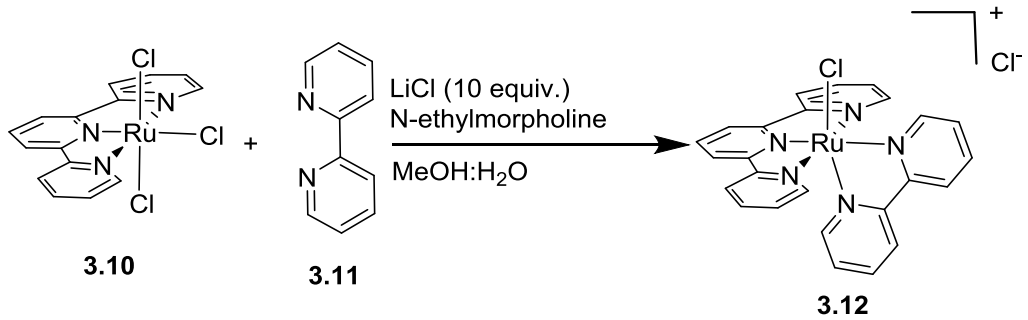

Figure 3.5. Known synthetic pathway to form [Ru(Cl)(terpy)(bipy)]Cl complexes.[10]

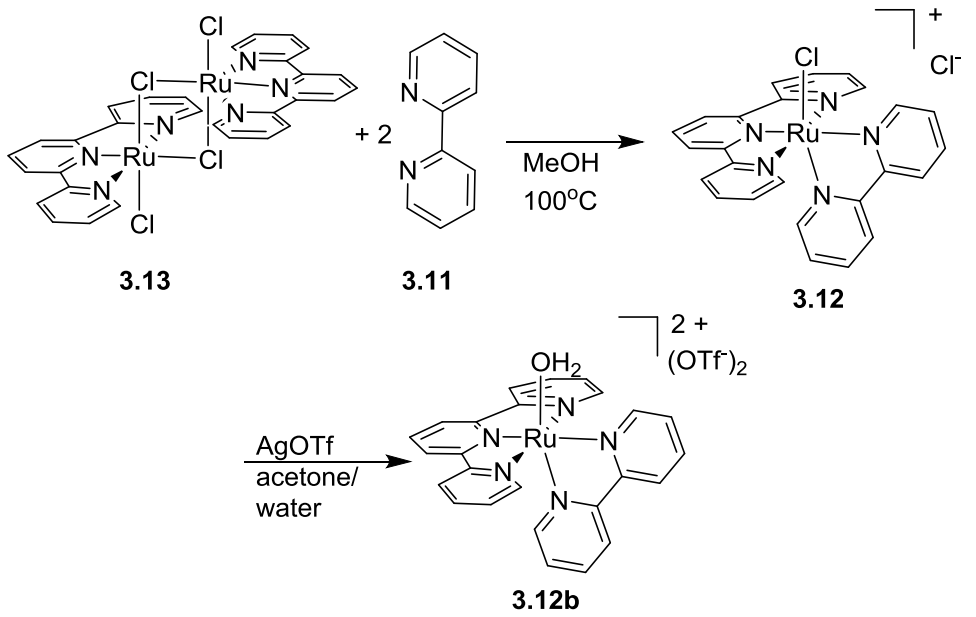

Figure 3.6. Optimal synthetic pathway to form [Ru(Cl)(trpy)(bipy)]Cl complexes, with minimal byproducts.

step to ensure that chloride stays coordinated to the metal. The resulting products are isolated by a number of different methods, such as a change in pH, precipitation and / or chromatography[9,10]. When similar procedures were used for protic ligands **3.6** or **3.8**, the resulting complexes were difficult to purify, possibly due to solubilities changed unfavorably depending on pH.

To simplify purification we sought a general synthetic solution in which the immediate precursor to **3.12** would release either no byproducts, or byproducts that could be easily removed. The Ru(II) species (terpy)Ru(Cl)$_2$(L) where L = CH_3CN[11] or DMSO[12] have been used to make additional complexes with loss of L, but the Ru(II) dimer

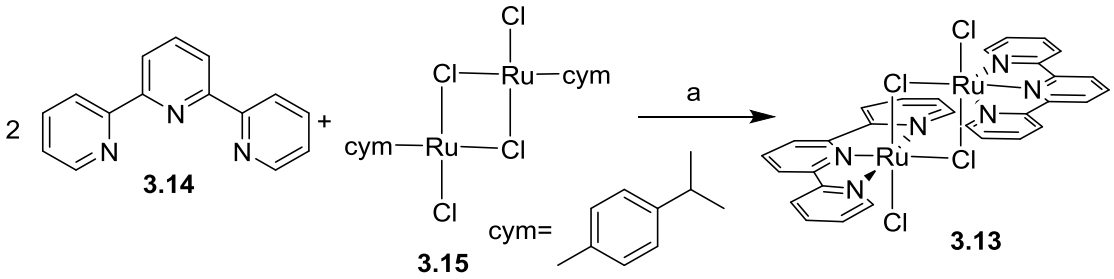

Figure 3.7. Synthesis of [$RuCl_2$(terpy)]$_2$, **3.13**.
(a) [$RuCl_2$(cymene)]$_2$ (0.5 equiv), DCM, terpy (1.0 equiv), addition over 1 h, RT, 83 % yield.

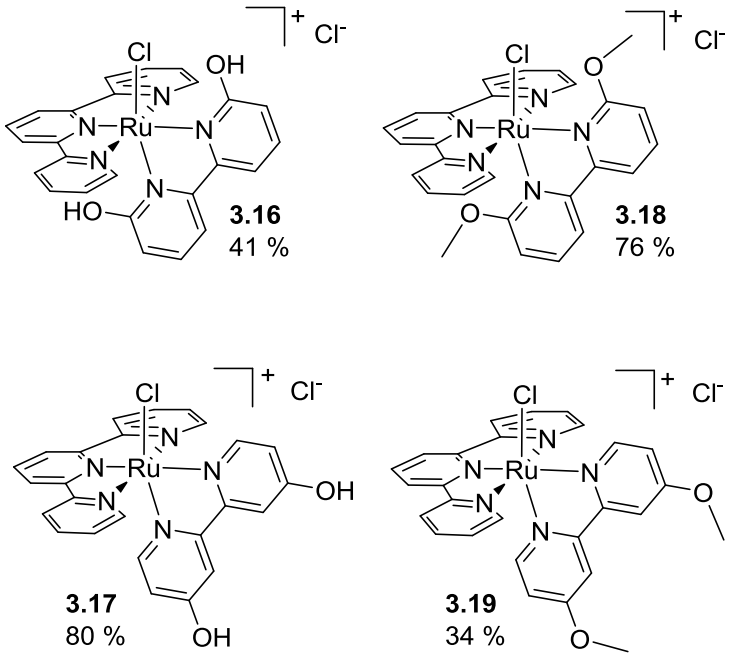

Figure 3.8. [Ru(Cl)(terpy)(hydroxy/methoxy bipy]Cl complexes.

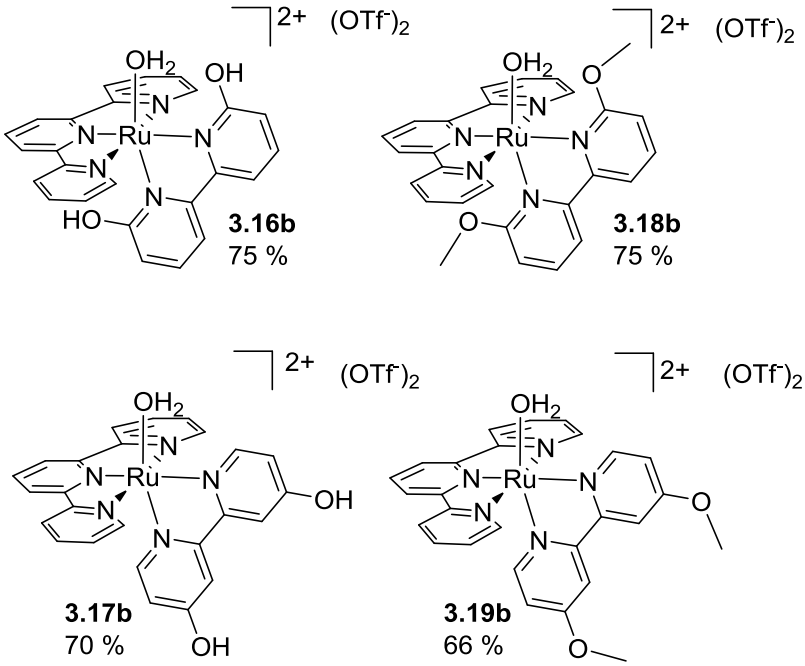

Figure 3.9. [Ru(OH_2)(terpy)(hydroxy/methoxy bipy)] $(OTf)_2$ complexes.

[(terpy)Ru$(Cl)_2$]$_2$ (**3.13**) could potentially be simpler to use. Concepcion et al. reported synthesis of a similar dimer from another tridentate ligand.[13] The synthesis of **3.13** proved to be simple; in CH_2Cl_2, terpy (**3.14**) displaced cymene from [(cymene)Ru$(Cl)_2$]$_2$

(**3.15**) under very mild conditions, within 1 h at room temperature, forming a highly insoluble dark purple solid that was purified by filtration and washes with different solvents. Combustion analysis for C, H, and N was consistent with the purple solid being **3.13**+H_2O, isolated pure in 83%yield.

Compound **3.13**+H_2O was poorly soluble in anything but DMSO, where the DMSO complex was likely formed. Even though **3.13** was insoluble it could be used very effectively in methanol, where heating **3.13** with bipy derivatives **3.6** through **3.9** for hours at 80-100 ^oC cleanly gave **3.16** to **3.19**, as evidenced by analysis by ^1H NMR spectroscopy of reaction mixture aliquots or crude products obtained in high yields after evaporation of solvent; however to obtain pure material, samples were recrystallized to give homogeneous materials, with lower final yields (34–80%) (Figure 3.8). Compounds **3.17** and **3.19** were synthesized by David Charboneau from the Paul lab. The corresponding triflate salts were made by ionizing with AgOTf (2 equiv) in a mixture of acetone and water. The compounds were then purified by crystallization allowing ether to diffuse into mixtures of acetone, methanol, and water giving best results (Figure 3.9).

To characterize the complexes, we looked for an NMR solvent that would not only dissolve the complexes at sufficient concentrations for 2D NMR work, but also not bind to the metal. Thus acetonitrile or DMSO were not used. Instead, methanol, acetone, and mixtures of water with the two organic solvents were tried. H_2O or CH_3OH were used in conjunction with either d_6-acetone or CD_3OD, respectively, in order to see any OH or NH peaks should they be present. A favorable combination of solubility, sharpest peaks, and ability to see bound water was obtained when using d_6-acetone and water in 85:15 volumetric ratio, so unless otherwise specified this mixture was used to characterize the complexes in this Chapter and Chapter 4. Some ^1H NMR peaks for the OH-containing species **3.16b** showed some broadening, that was sharpened completely on addition of triflic acid (5 equiv).

A combination of COSY, HSQC, and HMBC data were used to establish connectivity and assign all ^1H, ^{13}C, and ^{15}N signals (for graphical representations of all complexes and their NMR data, see NMR section at the end of the Chapter). In proton NMR data (Table 3.3, see Figure 3.10 for the numbering scheme for the NMR tables),

Table 3.1. ^{15}N chemical-shift comparison for chloro and aquo complexes, in which Δ is the difference upon going from chloro to aquo.[a]

		parent			6,6‘-substituted								4,4‘-substituted			
ligand	atom	**3.12**	Δ	**3.12b**	**3.16**	Δ	**3.16b**	**3.18-PF$_6$**[b]	Δ	**3.18b**	**3.18-Cl**[c]	**3.17**	Δ	**3.17b**	**3.19**	Δ	**3.19b**
bipy	N1	-119.8	-1.9	-121.7	-161.4	+0.1	-161.3	-149.8	-4.6	-154.4	-154.6	-147.9	-2.2	-150.1	-143.6	-2.2	-145.8
bipy	N1’	-130.7	-7.2	-137.9	-178.3	-3.0	-181.3	-160.9	-12.6	-173.5	-173.4	-163.8	-8.7	-172.5	-158.4	-8.3	-166.7
terpy	Nc1	-132.5	-6.6	-139.1	-133.4	-4.1	-137.5	-128.7	-9.6	-138.3	-138.3	-129.7	-7.1	-136.8	-131	-6.6	-137.6
terpy	Nt1	-94.9	-6.2	-101.1	-89.0	-4.2	-93.2	-83.2	-11.7	-94.9	-95	-89.5	-7.1	-96.6	-91.8	-6.2	-98.0

[a] Data (ppm) obtained on natural abundance material using ^{1}H-^{15}N gHMBC experiments. In d_6-acetone / H_2O (85 : 15 v/v) unless otherwise specified. [b] In d_6-acetone without water, to avoid ionization of bound chloride; because **3.18** did not dissolve well in acetone alone, KPF_6 (1 equiv) was added to dissolve the complex by making *in situ* the PF_6 salt of **3.18**, [Ru(Cl)(terpy)(6,6’-methoxy-2,2’-bipyridine)]PF_6 (**3.18-PF$_6$**). [c] Values in this column are for the species seen when **3.18** was dissolved in d_6-acetone-d_6 / H_2O (70 : 30 v/v), which according to the ^{15}N shift data forms the same cation as in **3.18b**.

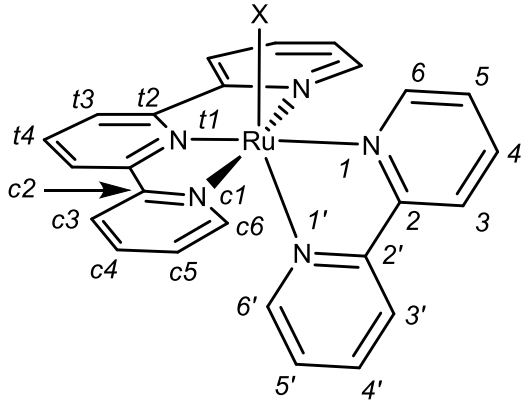

Figure 3.10. Numbering scheme for identifying atoms in NMR and crystal structures.

Table 3.2. ^{13}C {^{1}H} NMR spectral data for complexes.[a]

	parent		6,6‘-disubstituted				4.4‘-disubstituted			
	3.12	**3.12b**	**3.16**	**3.16b**	**3.18**[b]	**3.18b**	**3.17**	**3.17b**	**3.19**	**3.19b**
C6	153.0	151.2	170.2	171.4	171.5/57.6	170.4/58.0	153.8	152.0	153.9	152.1
C5	127.7	128.2	113.9	114.5	109.7	109.5	115.7	116.2	114.1	114.7
C4	137.6	138.2	140.8	140.3	141.4	141.6	166.4	166.6	167.5/57.1	167.8/57.2
C3	124.3	124.7	116.7	115.3	117.4	117.9	111.7	112.2	110.7	111.1
C2	156.8	156.6	156.0	155.7	157.3	156.3	157.9	157.7	157.8	157.6
C2’	159.5	160.0	158.7	159.2	159.4	159.1	160.1	160.4	160.2	160.5
C3’	124.1	124.2	116.0	115.7	118.0	117.6	111.9	112.1	110.7	111.0
C4’	136.4	136.8	139.7	139.6	139.8	140.4	165.5	165.5	166.5/56.9	166.7/56.9
C5’	126.9	127.1	111.1	110.7	107.2	107.3	115.3	115.3	113.6	113.6
C6’	152.5	153.3	169.8	169.8	171.1/57.0	170.7/57.1	152.7	153.4	152.9	153.6
Cc6	152.8	153.7	153.6	154.0	154.1	154.4	152.8	153.6	152.7	153.6
Cc5	128.0	128.6	127.8	128.2	127.5	128.2	128.0	128.5	128.0	128.5
Cc4	138.0	139.1	138.0	138.6	137.2	138.6	137.4	138.6	137.6	138.7
Cc3	124.4	124.8	123.8	124.0	123.6	123.9	124.1	124.6	124.1	124.6
Cc2	159.5	159.8	161.2	161.5	161.3	160.7	160.0	160.2	159.7	160.0
Ct2	158.7	159.3	160.1	160.6	160.8	160.3	159.7	160.2	159.3	159.9
Ct3	123.3	123.9	122.3	122.7	122.1	122.7	123.0	123.7	123.1	123.7
Ct4	135.1	136.7	135.0	135.7	133.5	136.1	133.6	135.6	134.2	135.9

[a] Chemical shifts in ppm, referenced from the resonance for the methyl carbons of d_6-acetone at 29.92 ppm. Unless otherwise specified, data are for samples dissolved in d_6-acetone / H_2O (85 : 15 v/v), observed at 150.752 MHz, 30 ^{o}C. In cases where a OCH_3 substituent is at the ring position indicated, data shown refer to the ring carbon, followed by chemical shift of the methoxy carbon. [b] Data on sample in d_6-acetone. Because of very low solubility (see text) the ^{13}C shifts were not obtainable from ^{13}C NMR spectra, rather by using gHSQC and gHMBC crosspeaks.[14]

when the 6 position (bipy position closest to ligand X) bears a hydrogen, conversion of X = Cl to X = H_2O leads to a pronounced upfield shift of about 0.5 ppm (**3.17**, **3.17b**, **3.19**, **3.19b**; the other compounds are substituted in this position and there is no proton). Other proton chemical shifts changed at most about 0.1 ppm on ionization. In ^{13}C NMR spectra, out of 90 pairwise comparisons between data for individual carbons of the chloride and triflate analogs, the largest change in ^{13}C chemical shift seen after ionization is 2.0 ppm; considering the increase in positive charge on the metal this seems like little change (Table 3.2).

The ^{15}N data show the largest changes, possibly because the nitrogen atoms

Table 3.3. ^{1}H NMR data.[a]

ligand	atom	**3.12**	**3.12b**	**3.16**	**3.16b**	**3.18**
bipy	H6	10.13 (ddd, 5.57, 1.61, 0.83)	9.64 (ddd, 5.54, 1.55, 0.87)	12.10 (OH) (d, 0.56)	nd (OH)	4.08 (OCH_3) (s)
ring cis	H5	8.00 (ddd, 7.68, 5.54, 1.30)	8.09 (ddd, 7.70, 5.47, 1.34)	7.21 (dd, 8.27, 1.15)	7.19 (dd, 7.4, 2.0)	7.55 (dd, 8.46, 1.07)
to X	H4	8.32 (ddd, 8.26, 7.58, 1.57)	8.38 (ddd, 8.23, 7.65, 1.46)	8.16 (ddd, 8.31, 7.75, 0.50)	8.10 (m)	8.36 (dd, 8.45, 7.78)
	H3	8.78 (ddd, 8.29, 1.34, 0.85)	8.82 (ddd, 8.28, 1.33, 0.86)	8.22 (dd, 7.82, 1.19)	8.10 (m)	8.48 (dd, 7.82, 1.05)
bipy	H3’	8.49 (ddd, 8.29, 1.44, 0.82)	8.49 (ddd, 8.23, 1.46, 0.81)	7.91 (dd, 7.87, 1.12)	7.87 (d, 7.8)	8.20 (dd, 7.87, 1.08)
ring	H4’	7.74 (ddd, 8.19, 7.47, 1.47)	7.75 (ddd, 8.14, 7.52, 1.49)	7.54 (dd, 8.17, 7.81)	7.51 (t, 8.0)	7.75 (dd, 8.30, 7.82)
trans to	H5’	7.03 (ddd, 7.47, 5.82, 1.38)	7.05 (ddd, 7.49, 5.88, 1.49)	6.35 (dd, 8.15, 1.08)	6.32 (dd, 8.2, 1.1)	6.61 (dd, 8.30, 1.14)
X	H6’	7.42 (ddd, 5.82, 1.48, 0.79)	7.43 (ddd, 5.84, 1.51, 0.73)	nd (OH)	nd (OH)	3.28 (OCH_3) (s)
terpy	Hc6	7.72 (ddd, 5.57, 1.55, 0.80)	7.83 (ddd, 5.53, 1.56, 0.78)	8.01 (ddd, 5.50, 1.55, 0.80)	8.04 (bd, 4.9)	8.05 (ddd, 5.55, 1.56, 0.85)
rings	Hc5	7.33 (ddd, 7.55, 5.53, 1.32)	7.40 (ddd, 7.62, 5.51, 1.36)	7.40 (ddd, 7.58, 5.50, 1.35)	7.45 (bd, 6.4)	7.39 (ddd, 7.55, 5.54, 1.36)
cis to	Hc4	7.93 (ddd, 8.14, 7.51, 1.52)	8.02 (ddd, 8.12, 7.63, 1.57)	7.96 (ddd, 8.07, 7.56, 1.53)	7.99 (bd, 7.3)	7.93 (ddd, 8.04, 7.56, 1.55)
bipy	Hc3	8.53 (ddd, 8.08, 1.39, 0.79)	8.58 (ddd, 8.10, 1.35, 0.87)	8.48 (ddd, 8.08, 1.38, 0.79)	8.50 (bd, 8.1)	8.54 (ddd, 8.00, 1.37, 0.90)
terpy	Ht3	8.66 (d, 8.12)	8.72 (d, 8.13)	8.52 (d, 8.08)	8.56 (d, 8.2)	8.63 (d, 8.03)
trans to bipy	Ht4	8.16 (t, 8.09)	8.28 (t, 8.12)	8.07 (t, 8.07)	8.13 (t, 8.1)	8.05 (t, 8.02)
aquo	H_2O	--	6.15 (br s)	--	nd	--

[a] Chemical shifts in ppm, referenced from the resonance for the C*H*D_2 of d_6-acetone = 2.05 ppm. Coupling constants *J* (Hz) are listed after multiplicity. Unless for **3.18**, where solvent was acetone-d_6, data are for samples dissolved in d_6-acetone / H_2O (85 : 15 v/v), observed at 600 MHz, 30 ^{o}C. “nd” means not detected. Spectra were acquired with sw = ca. 5000 Hz and np = 524288, resulting in a digital resolution of 0.02 Hz / pt. For exact values of sw, see full NMR data tables at the end of the chapter. The *J* values were determined by using a shifted sine bell weighting function. Instead of using the difference of the top of the peaks, the difference of the center of the peak at its widest point were used, followed by the averaging of like coupling constants for a given proton. In cases where a substituent (OH, OCH_3) is at the ring position indicated, data shown refer to the proton(s) on the substituent.

Table 3.3. continued ^{1}H NMR data.[a]

ligand	atom	**3.18b**	**3.17**	**3.17b**	**3.19**	**3.19b**
bipy ring cis to X	H6	4.13 (OCH_3) (s)	9.77 (d, 6.34)	9.27 (d, 6.30)	9.87 (d, 6.42)	9.39 (d, 6.39)
	H5	7.58 (dd, 7.86, 1.62)	7.45 (dd, 6.32, 2.61)	7.51 (dd, 6.29, 2.56)	7.62 (dd, 6.48, 2.71)	7.68 (dd, 6.41, 2.72)
	H4	8.36 (m)	nd (OH)	nd (OH)	4.18 (OCH_3) (s)	4.18 (OCH_3) (s)
	H3	8.36 (m)	8.05 (d, 2.59)	8.04 (d, 2.56)	8.32 (d, 2.72)	8.36 (d, 2.72)
bipy ring trans to X	H3’	8.06 (dd, *J* = 7.95, 1.00)	7.78 (d, 2.66)	7.73 (d, 2.64)	8.04 (d, 2.78)	8.04 (d, 2.81)
	H4’	7.71 (dd, 8.40, 7.87)	nd (OH)	nd (OH)	3.81 (OCH_3) (s)	3.80 (OCH_3) (s)
	H5’	6.54 (dd, 8.38, 1.07)	6.46 (dd, 6.57, 2.66)	6.46 (dd, 6.59, 2.67)	6.62 (dd, 6.69, 2.78)	6.62 (dd, 6.73, 2.81)
	H6’	3.19 (OCH_3) (s)	6.91 (d, 6.55)	6.91 (d, 6.59)	7.08 (d, 6.68)	7.08 (d, 6.70)
terpy rings cis to bipy	Hc6	7.99 (ddd, 5.56, 1.55, 0.83)	7.85 (ddd, 5.54, 1.57, 0.81)	7.94 (ddd, 5.54, 1.59, 0.79)	7.80 (ddd, 5.54, 1.57, 0.80)	7.90 (ddd, 5.52, 1.56, 0.81)
	Hc5	7.38 (ddd, 7.60, 5.52, 1.29)	7.38 (ddd, 7.52, 5.51, 1.32)	7.44 (ddd, 7.58, 5.53, 1.35)	7.35 (ddd, 7.55, 5.53, 1.31)	7.41 (ddd, 7.58, 5.47, 1.29)
	Hc4	7.96 (m)	7.91 (ddd, 8.12, 7.46, 1.51)	8.00 (ddd, 8.11, 7.52, 1.50)	7.92 (ddd, 8.11, 7.56, 1.52)	8.00 (ddd, 8.13, 7.53, 1.51)
	Hc3	8.48 (ddd, 7.98, 1.33, 0.90)	8.52 (ddd, 8.12, 1.37, 0.81)	8.57 (ddd, 8.11, 1.35, 0.77)	8.51 (ddd, 8.09, 1.38, 0.84)	8.55 (ddd, 8.12, 1.37, 0.79)
terpy trans to bipy	Ht3	8.60 (d, 8.11)	8.62 (d, 8.10)	8.69 (d, 8.11)	8.62 (d, 8.11)	8.68 (d, 8.14)
	Ht4	8.19 (t, 8.08)	8.07 (t, 8.09)	8.19 (t, 8.09)	8.10 (t, 8.06)	8.20 (t, 8.13)
aquo	H_2O	5.12 (br s)	--	5.80 (br s)	--	5.89 (br s)

[a] Chemical shifts in ppm, referenced from the resonance for the C*H*D$_2$ of d_6-acetone = 2.05 ppm. Coupling constants *J* (Hz) are listed after multiplicity. Unless for **3.18**, where solvent was d_6-acetone, data are for samples dissolved in d_6-acetone / H_2O (85 : 15 v/v), observed at 600 MHz, 30 ^{o}C. “nd” means not detected. Spectra were acquired with sw = ca. 5000 Hz and np = 524288, resulting in a digital resolution of 0.02 Hz / pt. For exact values of sw, see full NMR data tables at the end of the chapter. The *J* values were determined by using a shifted sine bell weighting function. Instead of using the difference of the top of the peaks, the difference of the center of the peak at its widest point were used, followed by the averaging of like coupling constants for a given proton. In cases where a substituent (OH, OCH_3) is at the ring position indicated, data shown refer to the proton(s) on the substituent.

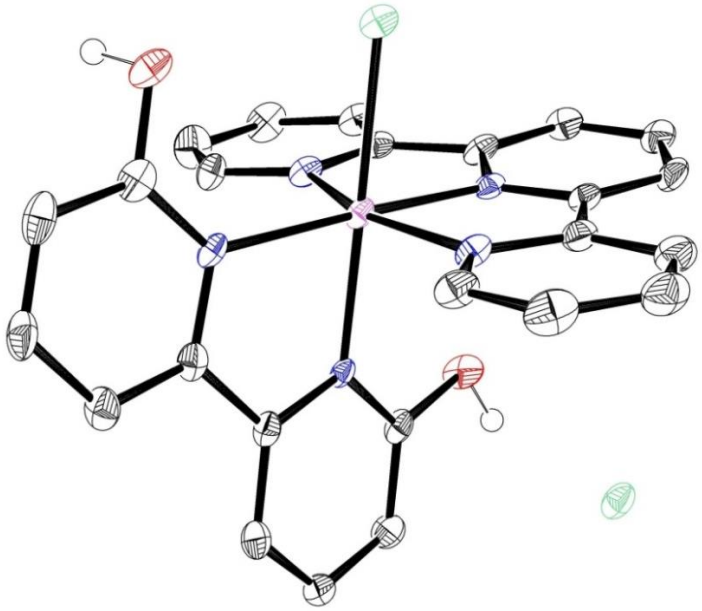

Figure 3.11. Molecular structure of **3.16.** The metal-containing cation is shown with the chloride counterion.

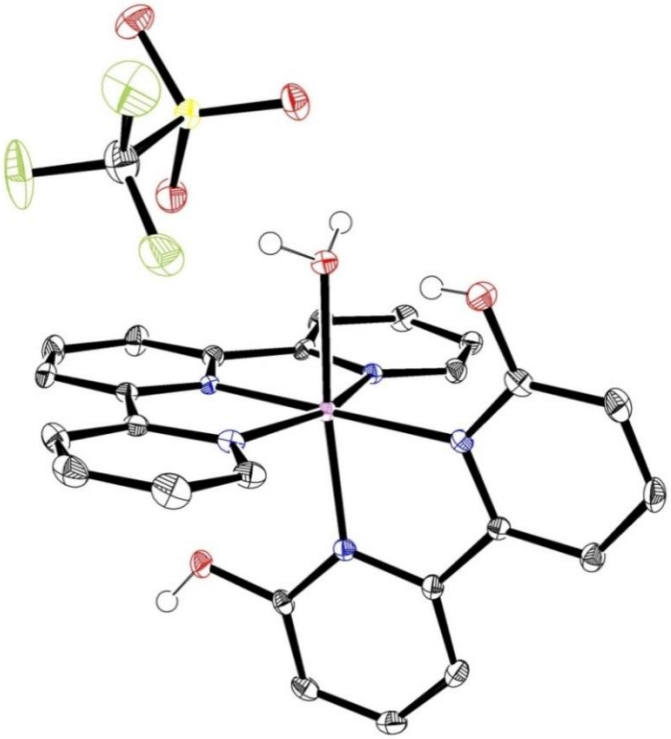

Figure 3.12. Molecular structure of **3.16b**. The metal-containing cation is shown with one of the two triflate counterions, which accepts a hydrogen bond from the bound aquo ligand.

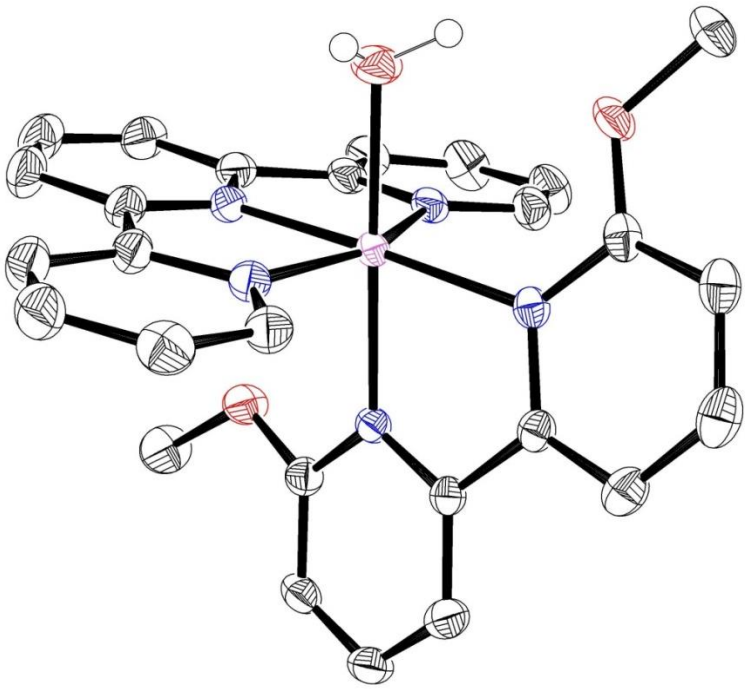

Figure 3.13. Molecular structure of **3.18b**. The metal-containing cation is shown without either one of the two triflate counterions, which are not involved in hydrogen bonding with the bound aquo ligand. The methoxy group accepts a hydrogen bond from the bound water.

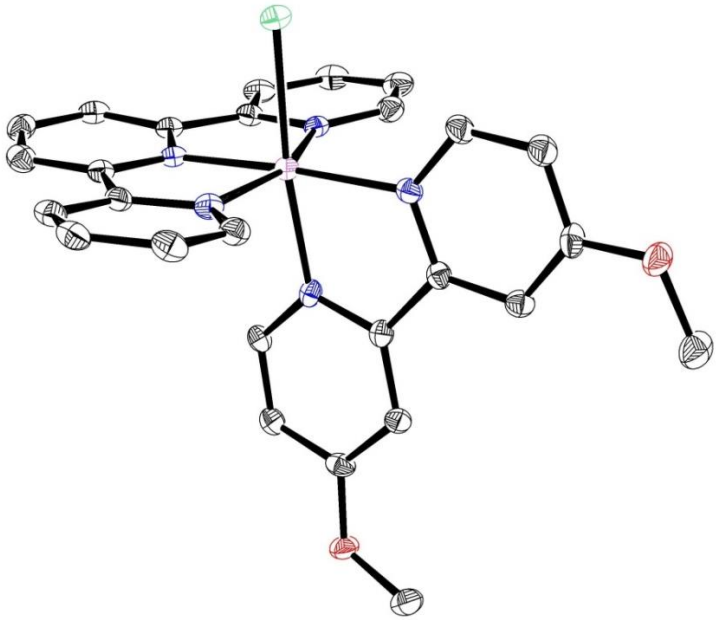

Figure 3.14. Molecular structure of **3.19**. The metal-containing cation is shown with the outer sphere chloride counter ion omitted.

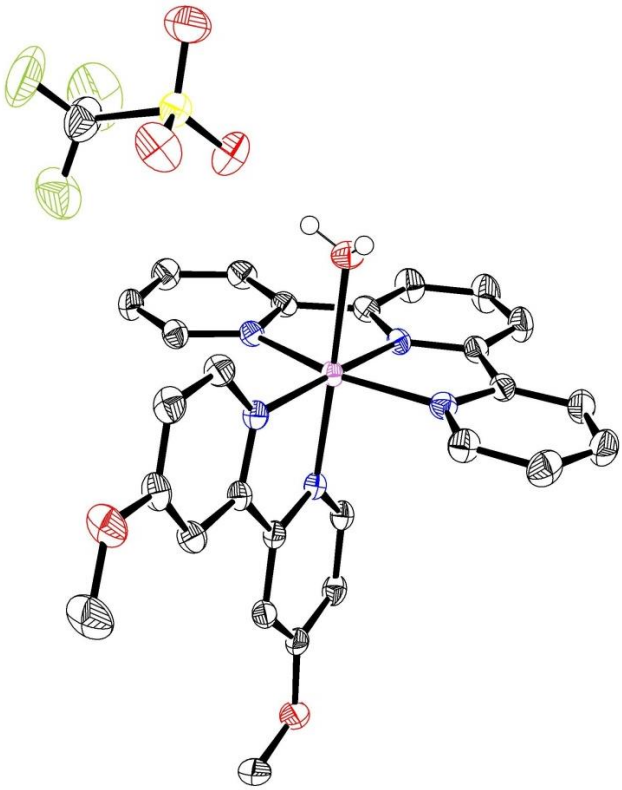

Figure 3.15. Molecular structure of **3.19b**. The metal-containing cation is shown with one of the two triflate counterions, which accepts a hydrogen bond from the bound aquo ligand.

experience the greatest change on increasing the charge on the complex, because they are directly bonded to the metal (Table 3.1). Looking at the 4,4'-dimethoxy series, ionization caused upfield shifts of all ^{15}N resonances, from -2.2 to -8.3 ppm (Δ values in Table 3.1). Both kinds of terpy nitrogens were shifted upfield similarly, whereas for the bipy nitrogens, the one trans to changing X was shifted upfield the most (-8.3 ppm) and the one cis the least (-2.2 ppm). The 4,4'-dihydroxy case and the parent species, with no substituents on the bipy, showed similar data.

The 6,6' dihydroxy case shows lesser upfield shifts and virtually no change for the N cis to X. The differences suggest a change in bonding between 4,4' and 6,6' series, which would be consistent with an intramolecular interaction in the 6,6' case.

It was found that when the 6,6'-dimethoxy complex **3.18** was dissolved in the typical NMR solvent mixture there was a mixture of two species, formulated as **3.18**, and the aquo complex **3.18b-2Cl**. In an attempt to characterize **3.18** without formation of

presumed component **3.18b-2Cl**, **3.18** was dissolved in 100% d_6-acetone and NMR spectra showed only one species. One major problem was that **3.18** is only partially soluble in d_6-acetone, enough to identify all the protons and most of the carbons. The carbons not observed by one-dimensional ^{13}C NMR spectroscopy were identified by HSQC and HMBC. Attempts at obtaining the ^{15}N chemical shift values were unsuccessful, so to make **3.18** more soluble the outer-sphere chloride was replaced with the more lipophilic PF_6^- ion using potassium hexafluorophosphate to give **3.18-PF$_6$**, which was then soluble enough to obtain ^{15}N chemical shift values. Significantly, the ^{15}N chemical shift data for bis triflate aquo complex **3.18b** and the species formed from **3.18** in acetone-water are virtually identical, affirming the assignment of the latter as **3.18b-2Cl**. Thus, the ^{15}N chemical shift data confirm that the proximal methoxy group helps aquation (and therefore can potentially aid in ligand release and turnover in water oxidation).

Key bond-length data for four new complexes are shown in Table 3.4, along with the X-ray diffraction data we obtained for known complex **3.19**[10,18]. The molecular structures of five of the complexes are shown in Figures 3.11 to 3.15. As in reported structures of parent complexes **3.12** (PF_6^- instead of Cl^- salt)[15] and **3.12b** (bis ClO_4^-[19] or PF_6^-salts[20]), the complexes shows slightly distorted octahedral geometries. Looking at the Ru–N bond lengths, in both literature structures of **3.12** and **3.12b** as well as the novel structures reported here, the bond to the central terpy nitrogen atom Nt1 (see definitions on structure in Figure 3.10) trans to bipy is significantly closer than the two slightly unequal bonds to the outer terpy nitrogen atoms Nc1 (each cis to bipy). Similarly, for the bipy ligand, Ru– N1 is longer than Ru–N1’ in all cases. Others have proposed the lengthening of the Ru–bipy bond cis to X as the effect of interligand steric repulsion[20]. Other repulsive effects unique to the new complexes reported here can be seen from the fact that in the 6,6’-disubstituted species **3.16**, **3.16b**, and **3.18b** both Ru–bipy bond lengths are longer than in their counterparts without 6,6-substituents.

Relevant to the proposed bifunctionality of the new complexes, in the structure of **3.16b** (Figure 3.12) the bipy OH group proximal to the aquo ligand is seen to donate a

Table 3.4. Key bond lengths [Å] and angles (deg)[a] for hydroxy and methoxy complexes as well as parent complexes **3.12** and **3.12b**.

	3.16	**3.16b**	**3.18b**	**3.19**	**3.19b**	**3.12**[15]	**3.12b**[16]
bipy subst.	6,6‘-$(OH)_2$	6,6‘-$(OH)_2$	6,6’-$(OMe)_2$	4,4‘-$(OMe)_2$	4,4‘-$(OMe)_2$	none	none
X	Cl	H_2O	H_2O	Cl	H_2O	Cl	H_2O
Ru-N1	2.125(3)	2.108(2)	2.107(2)	2.075(3)	2.0823(18)	2.069(2)	2.069(4)
Ru-N1‘	2.075(3)	2.063(2)	2.057(2)	2.041(3)	2.0257(18)	2.031(2)	2.009(4)
Ru-Nt1	1.951(3)	1.959(2)	1.961(2)	1.953(3)	1.9587(18)	1.951(2)	1.957(4)
Ru-Nc1	2.057(3), 2.072(3)	2.068(2), 2.075(2)	2.067(2), 2.070(2)	2.043(3), 2.064(3)	2.0610(18), 2.0824(18)	2.059(2), 2.070(2)	2.063(4), 2.083(4)
Ru-X	2.4353(11)	2.1594(18)	2.124(2)	2.3994(9)	2.1468(16)	2.2969(7)	2.146(3)
other	[b]	O-H---O[b] 2.668 (171.86°)	O-H---O[b] 2.736 (128.08°)				
X-Ru-N1	99.1(1)	95.17(8)	98.71(8)	94.75(9)	96.67(7)	94.26(7)	95.57(14)
X-Ru-Nt1	82.3(1)	85.18(8)	82.62(9)	88.17(9)	85.88(7)	87.73(7)	88.02(14)

[a] Data for **3.12** (PF_6 salt) and **3.12** (bis ClO_4 salt) are from references [15] and [16]; for a structure of the bis PF_6 salt of **3.12b**, see [17]. Ligand atoms are defined in the same way as for listing NMR data, as follows (see also Figure 3.10: N1 = bipy N cis to X; N1’ = bipy N trans to X; Nt1 and Nc1 are terpy nitrogens trans and cis to bipy N1, respectively. Two lengths are shown for Ru-Nc1. [b] For **3.16b**, the values listed are for the proximal ligand OH and aquo oxygen interaction. For **3.16**, the ligand OH proximal to Cl is pointing away from the Cl, presumably to a MeOH solvate molecule. The unit cell contained four MeOH per Ru which required SQUEEZE to render properly, and the O-H distances were constrained, hence no entry is given for the hydrogen bonding environment in the crystal of **3.16**.

hydrogen bond to the coordinated water molecule, with a near-linear O–H···O arrangement and an O–O distance of only 2.668 Å. Notable too in **3.16b** is the O–Ru–N1 angle of 95.17(8)°, which is fully 4° less than the Cl–Ru–N1 angle in to well-defined intramolecular hydrogen bonding that brings the OH group closer to the O of the bound water, thereby overcoming expected steric interactions. Whereas in **3.16b** the aquo ligand is the hydrogen-bond acceptor, in **3.18b**, the aquo ligand is the donor. The linearity of the hydrogen bond is reduced (O–H···OMe angle 128.08°) and the O···O distance is about 0.07 Å greater.

C. Catalyst Evaluation

In initial studies, catalyst activity with CAN was determined for all of the aquo complexes using fluorescence-based measurements in the reaction vessel headspace.

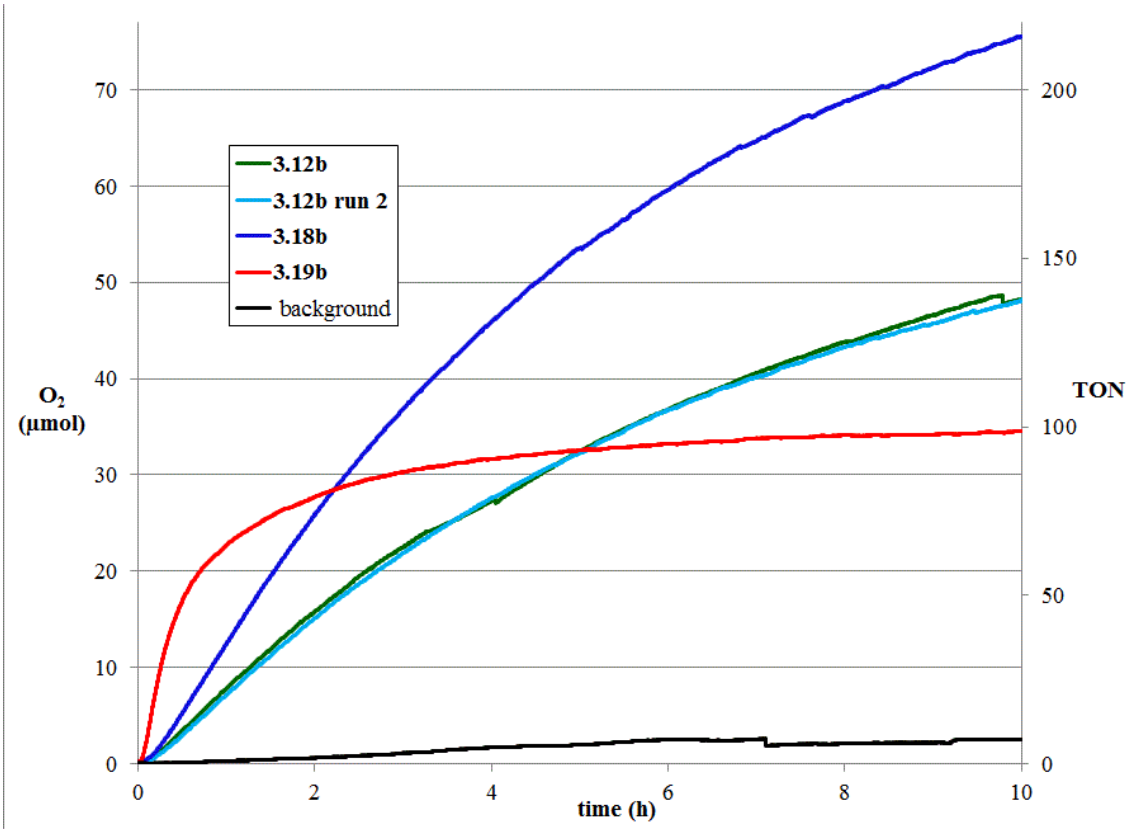

Figure 3.16. Molecular oxygen evolution (µmol) monitored by NeoFox optical sensor in a reaction vessel (15.0 mL) containing initial concentrations of $[CAN]_0$ = 78 mM, $[HNO_3]_0$ = 0.1 M, and $[catalyst]_0$ = 50 µM (total liquid volume 7.0 mL). After 10 h, TON for each catalyst were found to be **3.12b** = 138, **3.18b** = 215, and **3.19b** = 98. A repeat trial was done for **3.12b**.

3.16b and **3.17b**, the hydroxy analogs, gave essentially the same amount of oxygen as in a control experiment without added catalyst; in other words, these were not active catalysts, so the data are not shown on the graph. In distinct contrast, although the 4,4'-dimethoxy complex **3.19b** is initially faster than the 6,6'-isomer **3.18b**, the latter continues to be active and performs better than the parent complex without oxygenated substituents (Figure 3.16). Significantly, **3.18b** gives over 20 times more turnovers than the previously reported 6,6'-difluorobipyridine analog using CAN in 0.1 M TfOH.[21]

3.18b was surprisingly one of the more interesting compounds in this study, because under the typical NMR conditions, it was the only analog that showed ionization to **3.18b-Cl**, which shows the potential aid in ligand release and turnover in water oxidation. The effect of the 6,6' substituents was also seen in the crystal structure where both Ru-bipy bond lengths were longer in the cases of **3.18b**, as well at **3.16** and **3.16b** compared to the parent case or other cases (e.g. 4,4'-substituted ones) that feature unsubstituted 6,6' positions.

Although the results above clearly establish the significant effects of bipy substituents on activity of a closely related family of catalysts, we also want to compare the catalysts just described with others in this thesis, using more than one testing method. In the course of following up on the results shown in Fig. 3.16, we uncovered some systematic errors, as described here. One must consider various aspects of the methods of oxygen detection. In the second chapter we used a Clark electrode, which was the first technique used in the Grotjahn lab to quantitate oxygen production; Clark electrodes have been used by many others (examples: [22,23]). The sensitivity of the Clark electrode system is 0.1 % O_2, where the percentage reported is of the amount of oxygen by volume in the gas phase, or in the liquid phase, depending on which phase is being analyzed, relative to 100% = the maximum amount of O_2 at saturation. The general procedure for setting up a Clark electrode testing run is as follows: a drop of saturated KCl solution is added to the tip of the electrode, and a fresh membrane (permeable to gas but not liquid) is secured to encapsulate the KCl/water drop, using a rubber O-ring. The assembled electrode is then calibrated by bubbling nitrogen through the liquid, or flowing nitrogen through the gas phase, and setting the meter reading to 0 % O_2. Then the nitrogen is replaced by pure

oxygen, and the meter reading is set to 100 % O_2. Finally the oxygen is replaced by nitrogen to give 0 % O_2 again. The process of setting up a testing run was rather tedious and time consuming, but one of the advantages of the Clark electrode system is that readings in either the liquid or gas phase could be obtained. When testing a catalyst using CAN we were interested in both the concentration of oxygen in the solution as well as the headspace to be able to calculate the total amount of oxygen at any given time. We therefore designed a cell that had two Clark electrodes, one in the headspace and one in the solution to observe total O_2 generation. A problem with monitoring oxygen in a solution of CAN is that the acidity of the solution would eventually lead to degradation of the electrode which could be observed by oxygen values that wouldn't stabilize when trying to calibrate the system. Another issue is that the response time of detecting changes in O_2 concentration can be insufficient when testing very fast catalysts such as some catalysts from Sun et al., which are discussed in Chapter 4, that consume sacrificial oxidant CAN in less than 10 sec. However the response time is acceptable for the slower catalysts tested in this thesis.

The second method that was utilized was a product from Ocean Optics called NeoFox which detects the O_2 by measuring effects of fluorescence quenching[22,24,25]. The specific probe we initially used is called "FOXY", which was not designed for acidic solutions. To conserve the probe one can monitor reactions in only the headspace, which was thought to be an accurate analysis for slower catalysts, as long as a cell was designed such that at equilibrium, the majority of the oxygen would diffuse into the headspace. The general procedure for using the NeoFox system starts with a nitrogen-purged apparatus, and a factory-set calibration would be loaded into the software, a much faster and simpler set up than that when using the Clark electrode. Also the sensitivity of the NeoFox system was 0.01 % O_2, 10 times better than when using the Clark electrode. NeoFox was thought to be the ideal testing method, with a simple set up that gave very nice reproducible data (see Fig. 3.16). However, one disadvantage of NeoFox was that occasionally the O_2 value would suddenly decrease by anywhere from a fraction of a percent to a couple percent (for examples of this behavior see in Figure 3.16 the

background reading at around 7 h and **8.12b** run 1 at around 9.5 h; the sudden drops are examples of relatively small value changes).

A more serious problem noticed over a period of months of use was that when the oxygen sensor would be exposed to regular air in the lab, the reading would be typically around 15 % O_2, whereas for air the reading should have been 20.9 %. After talking with Ocean Optics engineers over a period of months they sent a new probe, "FOSPOR", that they were confident was more reliable. Preliminary experiments at SDSU confirmed the claim that the new probe was better, but it gave about 80-90 % of the actual value, which is still not good enough for our needs. The only solution that I figure would work would be to calibrate the probe before each use, but this would be a very time consuming task. To calibrate the probe a number of different oxygen gas mixtures (at least 10) between 0 % and 100 % oxygen must be used at a number of different temperatures around room temperature. Due to these issues we decided to look for another method.

A third method that has been used previously in literature to quantitate O_2 is measuring increases in pressure in a closed system[26]. Some of the advantages are that the response time is the fastest of the methods discussed; for example, with very fast catalysts, one can quantitate the formation of 400 µmol of oxygen over as little as 3 seconds, conditions under which the reactant aqueous phase becomes supersaturated and any attempts to analyze O_2 concentrations would be impossible because of bubbling and lack of homogeneity in the analyte solution. Moreover, the setup is not labor intensive and the data were more reproducible. The largest limitation is that we are monitoring the pressure, so we are assuming that the generated pressure is from oxygen and not other gases like CO_2 or CO from catalyst ligand degradation or possibly nitrogen-containing gases derived from nitrate ions of the CAN. However when using the pressure monitoring method, there was never an experiment that gave over 100 % yield of the theoretical oxygen pressure and when an experiment was designed to test the observed amount of generated O_2, by using a catalyst that would give a quantitative yield of O_2 we observed a 98 % yield, much better than readings obtained with the NeoFox system. As for the set-up we designed a cell (48 mL) with a 14/20 neck and a nipple that can be connected to a pressure transducer via tubing (see Figure 3.S4 at the end of the chapter). Because of the

effects of lab temperature on pressure we found that we needed to run the testing in a constant temperature water bath at 30 ^{o}C (Figure 3.S5). The pressure-measuring setup procedure is simpler than when using Clark electrodes or the NeoFox, in part because the initial reaction need not be air-free: one adds the appropriate amount of CAN solution, ultra-pure water, and nitric acid, followed by equipping a septum and tube to the pressure transducer and using copper wire to make sure the septum and tubing are leak free. To make sure the vessel and assembly was leak free it was pressurized to approximately three times the expected pressure generated in the reaction and monitored for leaks. After it was shown not to leak the vessel was vented and the catalyst was injected and the cell was placed in the water bath.

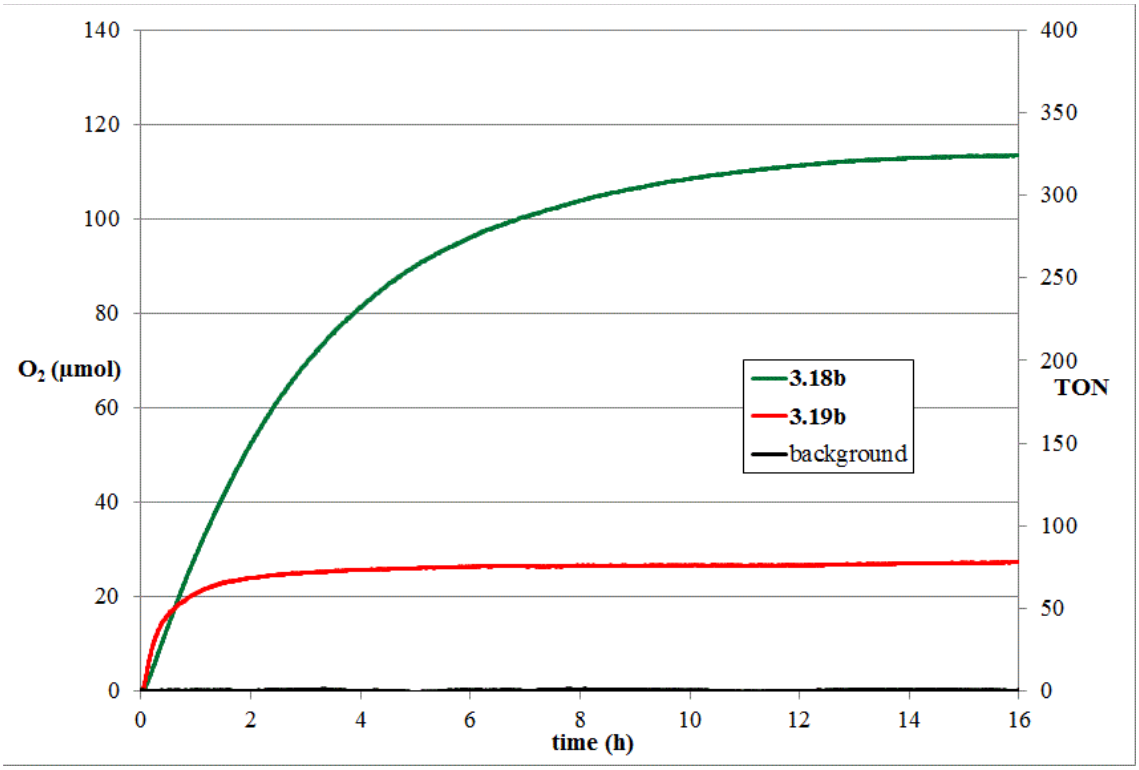

Figure 3.17. Molecular oxygen evolution (micromoles) monitored by pressure sensor in a reaction vessel (48 mL) containing initial concentrations of $[CAN]_0$ = 78 mM, $[HNO_3]_0$= 0.1 M, and $[catalyst]_0$ = 50 µM (total liquid volume 7.0 mL at 30 ^{o}C).

Testing **3.18b** and **3.19b** again under the same conditions but using pressure to detect the O_2 showed that **3.18b** showed a higher yield of O_2 after 10 h, about 108 µmol of O_2 or 310 turnovers (Figure 3.17), compared to 75 µmol and 210 turnovers when measured using the NeoFox system (Figure 3.16). However pressure tests for **3.18b** show

that it generated slightly less O_2 (about 80 turnovers), versus the 98 which was observed by NeoFox. The pressure method was impervious to the length of the testing runs, so we were able to observe **3.18b** oxygen generation stop after about 14 h, unlike the results obtained using NeoFox where we had issues with the length of a run due to random, sudden drops in the reading of O_2 concentration.

To conclude, we tried three testing methods over the years that have been used in literature and found that monitoring the reaction by pressure gave the best most reliable data. The remainder of the testing discussed was done using the pressure sensor method; the full experimental details can be found at the end of the chapter in "CAN Testing Conditions" (Figure S.4 and Figure S.5).

D. Catalysts Featuring Ligands with a Pendant Base Further from the Ring

After the success of complex **3.18b**, we were curious if we could enhance catalysis by adding a pendant base to the ligand, further from the bipy ring; this work was done with the assistance of undergraduate Jake Gooing. The base would be added to the methyl of the methoxy group, and could be flexible to deprotonate any incoming water molecules, such as structure **3.20** (Figure 3.18). It was thought that differently-substituted ethoxy analogs with a high degree of rotation could enable such chemistry. Three different analogs were targeted with the second pendant group being methoxy, **3.22**, N,N-dimethylamino, **3.23**, and N,N-diisopropylamino, **3.24**. The ligands were synthesized starting from 6,6'-dibromopyridine[27], **3.21**, by refluxing in toluene with the sodium salt of 2-methoxyethanol, 2-dimethylaminoethanol, or 2-diisopropylaminoethanol for 13 to 41 h (Figure 3.19).

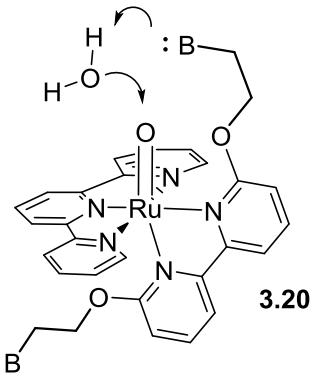

Figure 3.18. Proposed benefits of the addition of a pendant base further from the ring.

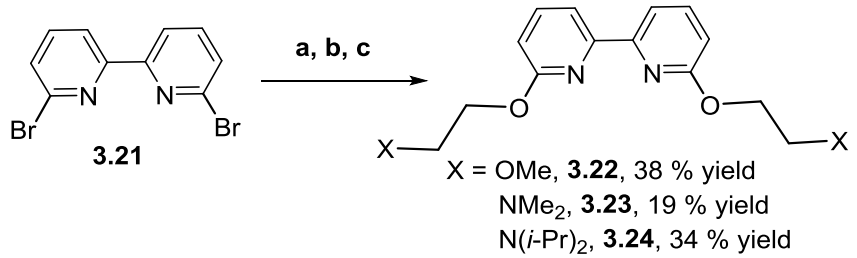

Figure 3.19. Ligand syntheses of **3.22**, **3.23**, **3.24**.
a) **3.21** (1.0 equiv), 2-methoxyethanol (3.5 equiv), NaH (2.9 equiv), toluene, reflux, 41 h, 38 % yield. (b) **3.21** (1.0 equiv). 2-dimethylaminoethanol (3.55 equiv), NaH (3.2 equiv), toluene, reflux, 13 h, 19 % yield. (c) **3.21** (1.0 equiv) 2-diisopropylaminoethanol (3.5 equiv), NaH (3.0 equiv), toluene, reflux, 13 h, 34 % yield.

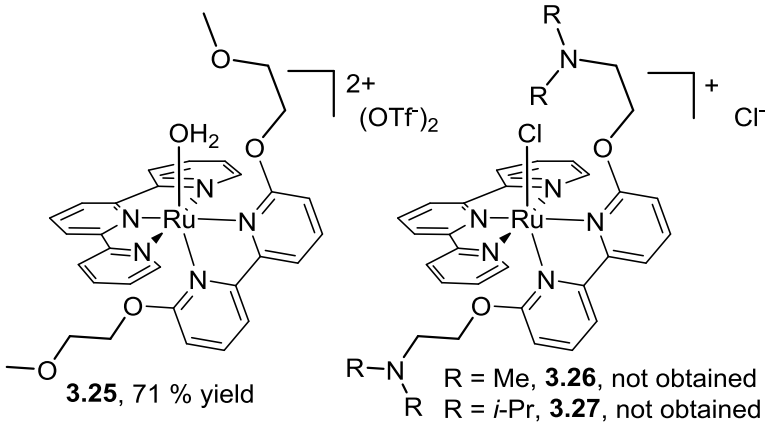

Figure 3.20. Metal complexes **3.25**, **3.26**, **3.27**.

Target complex **3.25** was formed by heating **3.22** with Ru(terpy)Cl_2 dimer, **3.13**, in methanol at 100 ^{o}C for 6 d. The chloride complex was not isolated, but instead the crude mixture was treated with silver trifluoromethanesulfonate; after filtration, the residue was then crystalized by vapor diffusion of diethyl ether into methanol yielding complex **3.25** in a 71 % yield (Figure 3.20). We were unsuccessful in isolating **3.26** with the pendant amines, because a number of unknown species were formed as observed in the ^{1}H NMR spectra. We hypothesized that reversible coordination of the amine lone pair to the metal may be responsible. The *N*,*N*-diisopropylamino analog **3.24** with more steric hindrance should inhibit coordination to the metal. After monitoring the metalation of **3.24** over 10 d by removing aliquots of the reaction and acquiring ^{1}H NMR spectrum in CD_3OD, it appeared a new complex had formed, as evidenced by the presence of 17 protons in the aromatic region, as expected for **3.27** (Figure 3.S1). After filtering the

mixture through a medium frit and crystallizing by vapor diffusion, another NMR spectrum showed that the desired product was no longer present: the isopropyl and methylene groups were no longer present and there was now possibly an OH as evidenced by a signal at around 12 ppm (Figure 3.S2). One possible explanation for apparent degradation of the presumed product is that the methylene group could be susceptible to nucleophilic attack (Figure 3.21), but it is puzzling why **3.25** appeared to be stable under metalation conditions at 100 ^{o}C for days. Regardless of the reason, we discontinued pursuit of the amino species because one could imagine that they might also degrade under harsher conditions like those needed for water oxidation.

Due to the questionable stability of the methylene groups, a more robust linker lacking sp^3 carbons was targeted, as in compounds **3.28** and **3.29** (Figure 3.22). Ligands **3.28** and **3.29** were synthesized according to a method developed by Buchwald et al. coupling aryl halides and phenols[28]. The yields of **3.28** and **3.29** were both poor, but for

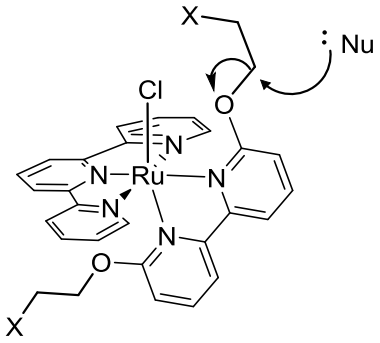

Figure 3.21. Possible decomposition pathway for **3.26** and **3.27**.

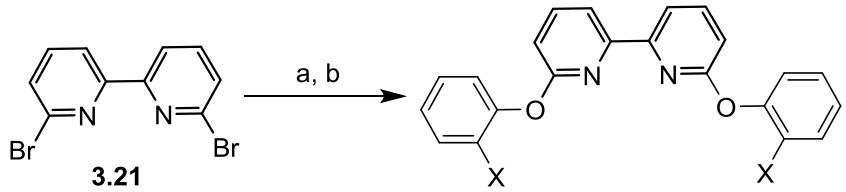

X = OMe, **3.28** 8.7 % yield
X = NMe_2, **3.29** 12 % yield

Figure 3.22. Synthesis of **3.28** and **3.29**.
(a) (for **3.28**) **3.21** (1.0 equiv), guaiacol (2.5 equiv), K_3PO_4 (4 equiv), CuI (20 mol %), picolinic acid (40 mol %), DMSO, 90 ^{o}C, 64 h, 8.7 % yield. (b) (for **3.29**) **3.21** (1.0 equiv), 2-*N*,*N*-dimethylaminophenol (2.5 equiv), K_3PO_4 (4 equiv), CuI (20 mol %), picolinic acid (40 mol %), DMSO, 90 ^{o}C, 3 d, 12 % yield.

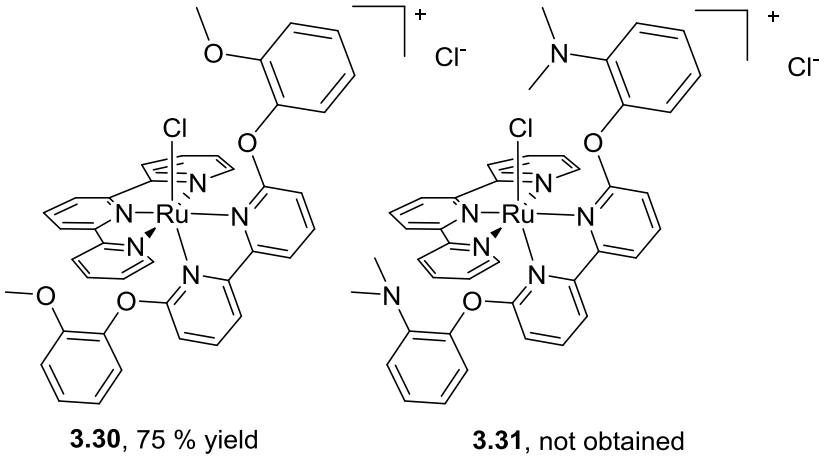

3.30, 75 % yield **3.31**, not obtained

Figure 3.23. Complexes **3.30** and **3.31**.

the sake of time were not optimized. Metalation of the ligands had a similar outcome as previously, where the methoxy analog **3.30** was isolated in 70 % yield after crystallization whereas attempted synthesis of the amino analog **3.31** gave a mixture of species which could not be separated (Figure 3.23). NMR spectra of complex **3.30** in d_6-acetone and water consisted mostly of sharp peaks, with the exception of those for the protons of outer pyridine ring of the terpy that were broader (Figure 3.S3). The broad peaks suggest that there is something unusual about the structure, such as hindered rotation of the large substituents, or the terpy being bent out of plane, or no longer being symmetrical due to the sterics of the bipy ligand that has two large aryloxy groups adjacent to the coordinating nitrogens.

3.25 and **3.30** were tested for their water oxidation capabilities using the same conditions as previously and using pressure to detect O_2 formation. **3.30** was only slightly active giving just over 20 turnovers over 4 h. **3.25** was still fairly active giving over 90 turnovers over about 4 h, however it is not as robust as **3.18b** (Figure 3.24). Unfortunately, the amino analogs of **3.25** and **3.30** were not isolable. **3.25** and **3.30** were still active catalysts but not as active as **3.18b**, with **3.25** having a similar initial rate as **3.18b** over approximately the first 30 min. A number of effects could be responsible, including that since the initial rates are similar for **3.25** and **3.18b** the catalyst was not improved or hindered but **3.25** decomposes at a faster rate possibly due to attack of the methylene, which was discussed earlier (Figure 3.21). As for **3.30**, the reason for the

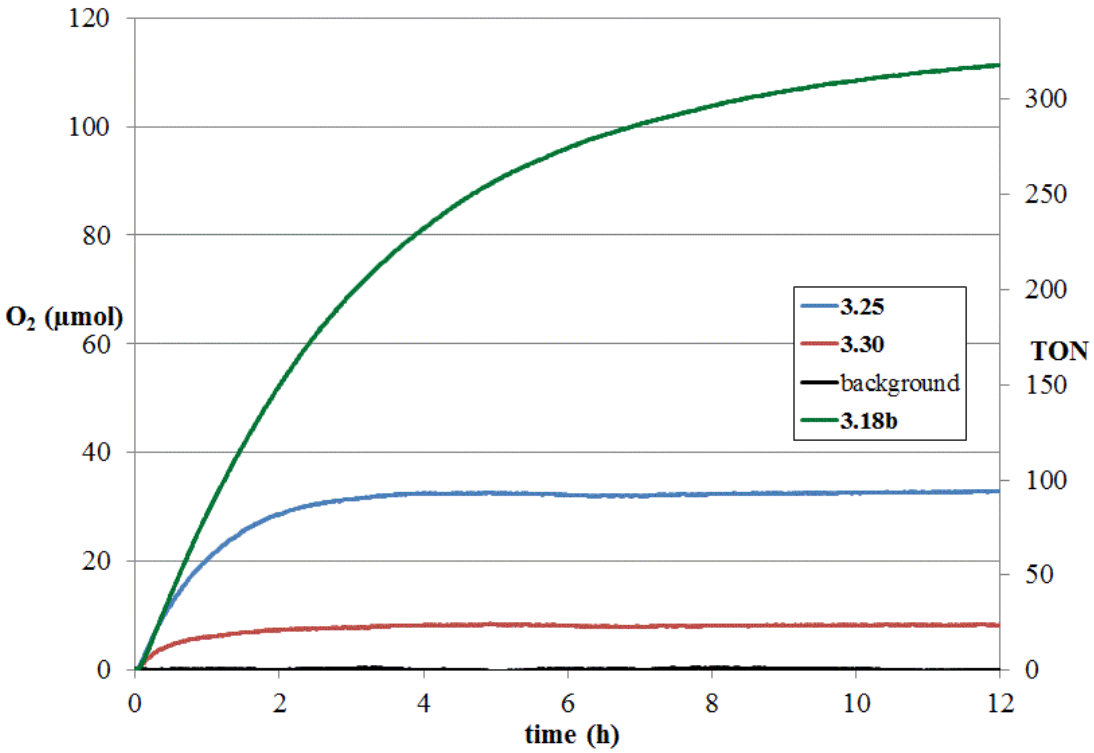

Figure 3.24. Molecular oxygen evolution (micromoles) monitored by pressure in a reaction vessel (48 mL) containing initial concentrations of $[CAN]_0$ = 78 mM, $[HNO_3]_0$ = 0.1 M, and $[catalyst]_0$ = 50 µM (total liquid volume 7.0 mL at 30 ^oC).

lower activity is less clear; the added aryl rings may change the electronics of the system which could be having an effect on ligand loss which would decrease the rates of reaction, slowing catalysis and accelerating decomposition. After our work was completed, papers from the Llobet group highlight the consequences of bipy ligand loss. Both catalyst systems discussed showed that the addition of a pendant group is not beneficial to this system.

E. Synthesis and Characterization of Complexes with Amino Substituents Directly Attached to Ligand Ring

So far we have looked at a number of complexes with hydroxy or methoxy as the pendant group, but we also wanted to explore the amino analogs, because the lone pair of the pendant amino groups would be more likely to accept a proton than the methoxy group in analog **3.18b**, which was a successful catalyst (above). One example of a 6,6'-diaminobipyridine ruthenium complex was published by Schlaf et al., who found that

3.32 (Figure 3.25) was a transfer hydrogenation catalyst that enables a possible bifunctional step involving the amino groups[29]. However the Schlaf paper is lacking solid evidence for the bifunctional interaction during catalysis by **3.32**, where the observed initial rate was only about 3.3 times greater than when using the bipyridine analog, and **3.32** gave only 50 % more turnovers than did the bipy analog, which these modest changes could easily be due to a combination of the sterics and / or electronics of the amino groups. Another simple analog that Schlaf should have explored was the 4,4'-diamino complex that would have been electronically similar but without the possible bifunctional activity. Even though the evidence is lacking for **3.32** being a bifunctional catalyst, the idea is plausible, hence we looked to study the amino analogs as was done in section 3.B above for hydroxy and methoxy analogs. Specifically, the target molecules were isomeric 6,6'- and 4,4'-diamino and –bis(dimethylamino) bipyridine complexes.

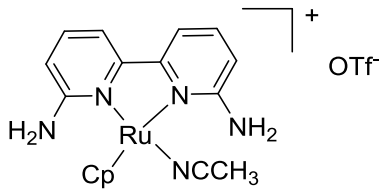

3.32

Figure 3.25. Known ruthenium 6,6'diamino-bipyridine complex.

As for the requisite bipyridine ligands, 4,4'-diaminobipyridine[30] (**3.33**) and 6,6'-diaminobipyridine[31] (**3.34**) were synthesized by known procedures; whereas the *N*,*N*-dimethylamino analogs were synthesized by exhaustive alkylation of the amino compounds in DMF with sodium hydride followed by the addition of methyl iodide. The yields for **3.35** and **3.36** were modest (29-40%), but enough ligand was obtained, so the reactions were not optimized (Figure 3.26). To form the metal complexes, the ligands were heated with the Ru(terpy)Cl_2 dimer **3.13** in methanol for 1 to 3 d at 100 ^{o}C. The complexes were then purified by vapor diffusion of diethyl ether into methanol to give good to moderate yields of **3.37**, **3.38**, and **3.40** (Figure 3.27). Attempts at synthesizing **3.39** by the same method but heating for 10 d gave mostly one product by ^{1}H NMR spectroscopy but showed the formation of an undesired but interesting product, **3.41**. The structure of **3.41** was assigned based on the ^{1}H NMR spectra by examining the methyl

peaks; one peak integrating to 6 protons at 1.60 ppm for the NMe_2 group under the terpy ring system, which is expected, but the other NMe_2 group was not observed, instead there were two other singlets at 1.95 ppm and 2.77 ppm that integrated to 2 and 3 protons respectively. The asymmetry observed, with the integration of one of the methyls being 2 suggested that one methyl had lost a hydrogen and that a new bond had been formed; with the methyls being in a close proximity to the metal, it seemed like a logical possibility that the new bond was between the methyl and ruthenium. The 0.82 ppm upfield shift of the protons on the methylene that is now bound to the ruthenium compared to protons of the methyl that is not, could be expected considering the electron-releasing inductive effect of the metal. More evidence observed in the ^{1}H NMR spectra requires going into more detail on general trends in the ^{1}H NMR data for (terpy)(bipy)RuL_n structures: the bipyridine is asymmetrical with one of the pyridines being opposite the terpy ring system and the other being under the terpy ring system. It is trivial to tell which bipy ring protons are under the terpy because of the shielding that is created by the terpy ring, an effect that is very predictable with only minor changes occurring due to the location of the amino group; see ^{1}H NMR data for **3.37-3.40** (H3-H6 for pyridine that is trans the terpy system and H3'-H6' for pyridine under the terpy system). However when examining the ^{1}H NMR data for **3.41**, it shows that for the pyridine ring under the terpy ring system of the bipyridine ligand, signals for protons H3'-H5' are shifted downfield by about 0.5 ppm compared to proton signals for the other amino analogs, evidence that in **3.41** the bipyridine ligand is not in the same location relative to the terpy ligand as in the other analogs, **3.37-3.40**. In **3.41** the bipyridine ligand is tridentate, which would not experience the same steric interactions as in the other bipyridine analogs that contain an aquo or chlorido ligand in the open site (illustrated in structure drawing in Figure 3.27). The target complex **3.39** likely formed but then transformed to **3.41**, where one of the pendant amino methyl groups is close enough to the metal which activates the C-H bond on the methyl forming the alkyl complex. Due to the synthetic problems in making complex **3.39**, its study was abandoned and the other analogs were further studied.

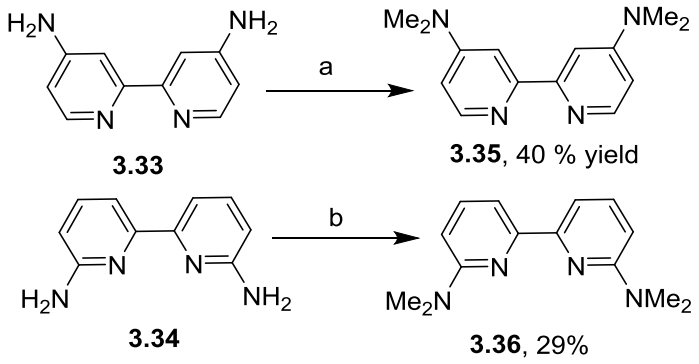

Figure 3.26. Synthesis of bis(N,N-dimethylamino)bipyridine ligands **3.35** and **3.36** (a) **3.33** (1.0 equiv), NaH (5.2 equiv), MeI (4.1 equiv), DMF, 0 ^{o}C, 45 min, RT, 4.5 h, 40 % yield. (b) **3.34** (1.0 equiv), NaH (5.3 equiv), MeI (4.3 equiv), DMF, 0 ^{o}C, 1 h, RT, 2 d, 29 % yield.

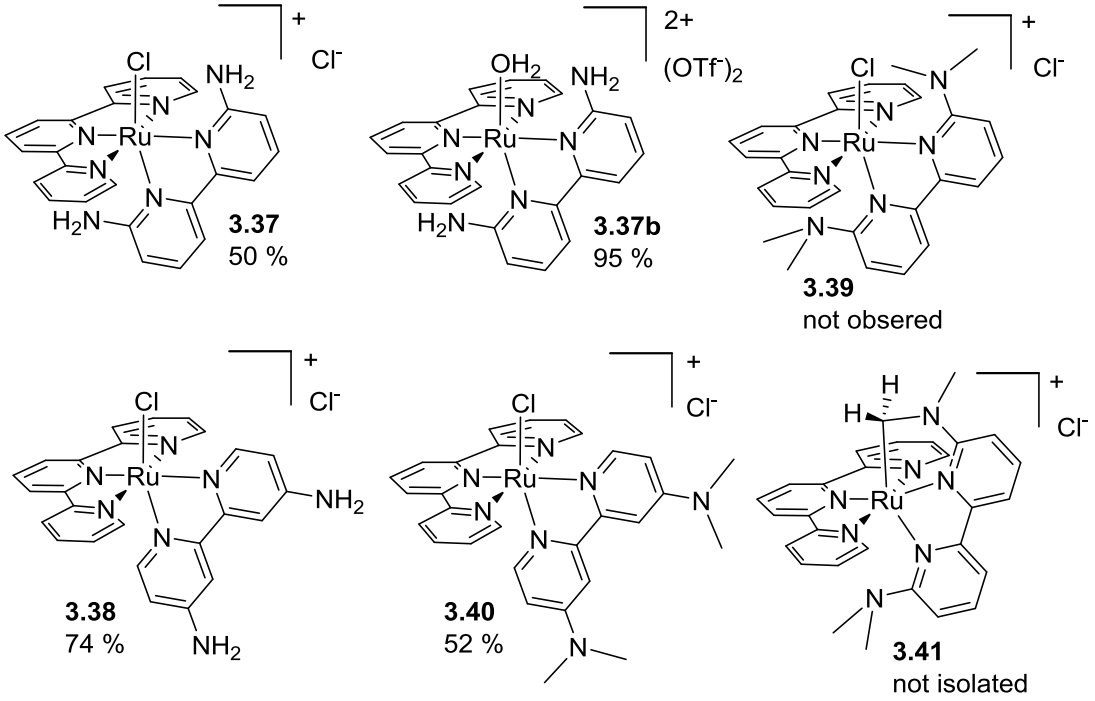

Figure 3.27. Amino complexes **3.37**, **3.37b**, **3.38**, and **3.40**. Expected complex **3.39** was not observed; instead **3.41** was formed but not isolated.

The triflate analog of **3.37** was synthesized by ionization using silver triflate in a acetone/water mixture and recrystallized by vapor diffusion to give **3.37b** in 83 % yield. However when the same method was used to ionize **3.38**, the triflate analog proved to be hard to isolate and even attempts at recrystallization under under nitrogen led to decomposition. To avoid any further decomposition of the amino analogs, we proceeded to study the stable chloride analogs.

Table 3.5. ^{1}H NMR data[a] for amino analogs.

ligand	atom	**3.12**[b]	**3.12b**[b]	**3.37**	**3.37b**	**3.38**	**3.40**	**3.41**
bipy ring cis to X	H6	10.13 (ddd, 5.57, 1.61, 0.83)	9.64 (ddd, 5.54, 1.55, 0.87)	7.77 (NH_2)	7.22 (NH_2)	9.41 (d, 6.2)	9.59 (d, 6.8)	1.95 (NCH_2M) (s), 2.77 (NMe) (s)
	H5	8.00 (ddd, 7.68, 5.54, 1.30)	8.09 (ddd, 7.70, 5.47, 1.34)	7.03 (dd, 8.4, 1.0)	7.09 (dd, 8.4, 1.1)	7.14 (dd, 6.3, 2.5)	7.23 (dd, 6.8, 2.7)	6.66 (d, 8.4)
	H4	8.32 (ddd, 8.26, 7.58, 1.57)	8.38 (ddd, 8.23, 7.65, 1.46)	7.84 (t, 8.0)	7.90 (dd, 8.4, 7.7)	6.51 (NH_2)	3.32 (NMe_2)	7.86-7.83 (m)
	H3	8.78 (ddd, 8.29, 1.34, 0.85)	8.82 (ddd, 8.28, 1.33, 0.86)	7.76 (dd, 7.7, 1.0)	7.81 (dd, 7.7, 1.0)	7.71 (d, 2.4)	7.86 (d, 2.7)	7.79 (d, 7.7)
bipy ring trans to X	H3'	8.49 (ddd, 8.29, 1.44, 0.82)	8.49 (ddd, 8.23, 1.46, 0.81)	7.58 (dd, 7.8, 1.0)	7.61 (dd, 7.7, 1.2)	7.43 (d, 2.4)	7.57 (d, 2.9)	8.08 (d, 7.3)
	H4'	7.74 (ddd, 8.19, 7.47, 1.47)	7.75 (ddd, 8.14, 7.52, 1.49)	7.29 (t, 7.9)	7.33 (dd, 8.1, 7.7)	6.15 (NH_2)	2.95 (NMe_2)	7.75 (t, 7.9)
	H5'	7.03 (ddd, 7.47, 5.82, 1.38)	7.05 (ddd, 7.49, 5.88, 1.49)	6.17 (dd, 8.2, 1.0)	6.21 (dd, 8.2, 1.2)	6.13 (dd, 6.6, 2.5)	6.19 (dd, 6.9, 2.8)	6.68 (d, 7.7)
	H6'	7.42 (ddd, 5.82, 1.48, 0.79)	7.43 (ddd, 5.84, 1.51, 0.73)	4.99 (NH_2)	5.06 (NH_2)	6.42 (d, 6.5)	6.56 (d, 6.9)	1.60 (NMe_2) (s)
terpy rings cis to bipy	Hc6	7.72 (ddd, 5.57, 1.55, 0.80)	7.83 (ddd, 5.53, 1.56, 0.78)	8.21 (ddd, 5.5, 1.4, 0.7)	8.24 (ddd, 5.4, 1.5, 0.8)	7.86-7.90 (m)	7.88 (d, 5.5)	7.59 (d, 5.5)
	Hc5	7.33 (ddd, 7.55, 5.53, 1.32)	7.40 (ddd, 7.62, 5.51, 1.36)	7.48 (ddd, 7.6, 5.6, 1.4)	7.57 (ddd, 7.6, 5.6, 1.3)	7.38 (ddd, 7.4, 5.6, 1.3)	7.41-7.38 (m)	7.28 (ddd, 7.3, 5.8, 1.2)
	Hc4	7.93 (ddd, 8.14, 7.51, 1.52)	8.02 (ddd, 8.12, 7.63, 1.57)	7.98 (dt, 7.8, 1.5)	8.07 (ddd, 8.1, 7.7, 1.5)	7.86-7.90 (m)	7.92-7.89 (m)	7.88 (td, 7.8, 1.3)
	Hc3	8.53 (ddd, 8.08, 1.39, 0.79)	8.58 (ddd, 8.10, 1.35, 0.87)	8.52 (bd, 7.8)	8.58 (ddd, 8.1, 1.3, 0.8)	8.47-8.45 (m)	8.51 (d, 8.0)	8.56 (d, 8.0)
terpy trans to aquo	Ht3	8.66 (d, 8.12)	8.72 (d, 8.13)	8.61 (d, 8.1)	8.71 (d, 8.2)	8.56 (d, 8.2)	8.61 (d, 8.0)	8.60 (d, 7.9)
	Ht4	8.16 (t, 8.09)	8.28 (t, 8.12)	8.07 (t, 8.1)	8.23 (t, 8.1)	7.99 (t, 8.1)	8.02 (t, 8.0)	7.86 (t, 8.0)
	H_2O	--	6.15 (br s)	--	6.32 (br s)	--	--	--

[a] Chemical shifts in ppm, referenced from the resonance for the C*H*D$_2$ of d_6-acetone = 2.05 ppm. Coupling constants *J* (Hz) are listed after multiplicity. Data are for samples dissolved in d_6-acetone / H_2O (85 : 15 v/v), observed at 600 MHz, 30 ^{o}C. In cases where a substituent (NH_2, $N(CH_3)_2$) is at the ring position indicated, data shown refer to the proton(s) on the substituent.

[b] Spectra were acquired with sw = ca. 5000 Hz and np = 524288, resulting in a digital resolution of 0.02 Hz / pt. For exact values of sw, see full NMR data tables at the end of the chapter. The *J* values were determined by using a shifted sine bell weighting function. Instead of using the difference of the top of the peaks, the difference of the center of the peak at its widest point were used, followed by the averaging of like coupling constants for a given proton.

Table 3.6. ^{13}C {^{1}H} NMR spectral data for amino complexes.[a]

	parent		6,6‘-disubstituted			4.4‘-disubstituted	
	3.12	**3.12b**	**3.37**	**3.37b**	**3.41**	**3.38**	**3.40**
C6	153.0	151.2	165.9	165.7	160.7/52.9/38.8	151.8	151.6
C5	127.7	128.2	112.6	112.9	105.1	112.3	110.0
C4	137.6	138.2	138.5	138.8	136.5	156.2	155.6/39.8
C3	124.3	124.7	112.8	113.1	109.8	108.0	105.8
C2	156.8	156.6	156.4	155.9	153.6	156.6	156.6
C2’	159.5	160.0	158.5	158.7	157.5	158.7	158.7
C3’	124.1	124.2	113.6	113.9	118.5	108.2	106.0
C4’	136.4	136.8	137.8	138.1	138.9	155.2	154.5/39.4
C5’	126.9	127.1	110.6	111.2	115.0	111.8	109.6
C6’	152.5	153.3	165.0	165.5	167.4/42.6	150.4	150.1
Cc6	152.8	153.7	153.9	154.7	149.9	152.5	152.6
Cc5	128.0	128.6	128.2	129.0	126.5	127.8	127.8
Cc4	138.0	139.1	137.9	139.2	134.6	136.9	136.9
Cc3	124.4	124.8	124.3	124.9	123.1	123.8	123.9
Cc2	159.5	159.8	160.6	160.7	159.0	160.0	160.2
Ct2	158.7	159.3	161.3	161.6	155.2	159.9	160.1
Ct3	123.3	123.9	123.6	124.7	121.2	122.7	122.8
Ct4	135.1	136.7	135.0	137.0	126.6	132.7	132.6

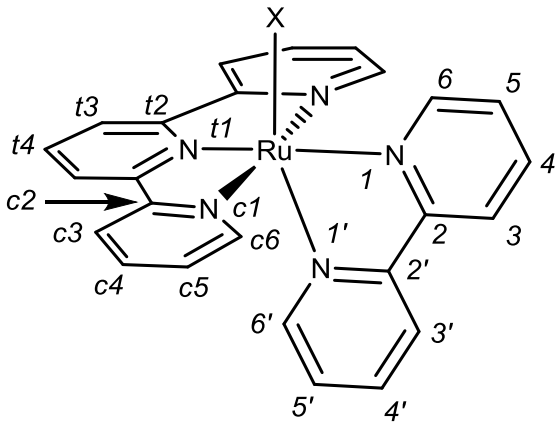

[a] Chemical shifts in ppm, referenced from the resonance for the methyl carbons of d_6-acetone at 29.92 ppm. Data are for samples dissolved d_6-acetone / H_2O (85 : 15 v/v), observed at 150.752 MHz, 30 ^{o}C. In cases where a $N(CH_3)_2$ substituent is at the ring position indicated, data shown refer to the ring carbon, followed by chemical shift of the dimethylamino carbons, or in the case of **3.41**, of the dimethylamino and metallated substituents.

Table 3.7. ^{15}N chemical-shift comparison for chloro and aquo complexes, in which Δ is the difference upon going from chloro to aquo.[a]

		parent			6,6‘-substituted amino			4,4‘-substituted amino		4,4‘-substituted oxygen					
ligand	atom	**3.12**	Δ	**3.12b**	**3.37**	Δ	**3.37b**	**3.38**	**3.40**	**3.17**	Δ	**3.17b**	**3.19**	Δ	**3.19b**
bipy	N1	-119.8	-1.9	-121.7	-178.8	-1.7	-180.5	-162.7	-165.0	-147.9	-2.2	-150.1	-143.6	-2.2	-145.8
bipy-N(H_2/Me_2)[b]	C6/C4	--	--	--	nd	--	-302.1	nd	-315.3	--	--	--	--	--	--
bipy	N1’	-130.7	-7.2	-137.9	-194.4	-8.6	-203.0	-182.5	-184.1	-163.8	-8.7	-172.5	-158.4	-8.3	-166.7
bipy-N(H_2/Me_2)[b]	C6‘/C4‘	--	--	--	-303.6	0.6	-303.0	nd	-314.3	--	--	--	--	--	--
terpy	Nc1	-132.5	-6.6	-139.1	-134.2	-7.9	-142.1	-128.6	-128.2	-129.7	-7.1	-136.8	-131.0	-6.6	-137.6
terpy	Nt1	-94.9	-6.2	-101.1	-89.4	-9.5	-98.9	-86.7	-86.0	-89.5	-7.1	-96.6	-91.8	-6.2	-98.0

[a] Data (ppm) obtained on natural abundance material using ^{1}H-^{15}N gHMBC experiments. In d_6-acetone / H_2O (85 : 15 v/v) unless otherwise specified. [b] Row refers to the NH_2 or NMe_2 substituted in the 4,4’ or 6,6’ positions on the bipy rings. nd = not detected.

Table 3.8. Key bond lengths [Å] and angles (deg).[a]

	3.40[a]	**3.19**	**3.12**[15]
bipy subst.	4,4‘-(NMe_2)$_2$	4,4‘-(OMe)$_2$	none
X	Cl	Cl	Cl
Ru-N1	2.086(2); 2.099(2)	2.075(3)	2.069(2)
Ru-N1‘	2.051(2); 2.051(2)	2.041(3)	2.031(2)
Ru-Nt1	1.947(2); 1.951(2)	1.953(3)	1.951(2)
Ru-Nc1	2.060(2), 2.069(2); 2.058(2), 2.071(2)	2.043(3), 2.064(3)	2.059(2), 2.070(2)
Ru-X	2.4157(7); 2.4271(7)	2.3994(9)	2.2969(7)
X-Ru-N1	94.04(6); 92.96(6)	94.75(9)	94.26(7)
X-Ru-Nt1	91.01(7); 91.52(7)	88.17(9)	87.73(7)

[a] N1 = bipy N cis to X; N1’ = bipy N trans to X; Nt1 and Nc1 are terpy N trans and cis to bipy N1, respectively. Two lengths are shown for Ru-Nc1. [a]Two independant molecules were in the unit cell, so bond lengths and angles are shown for both.

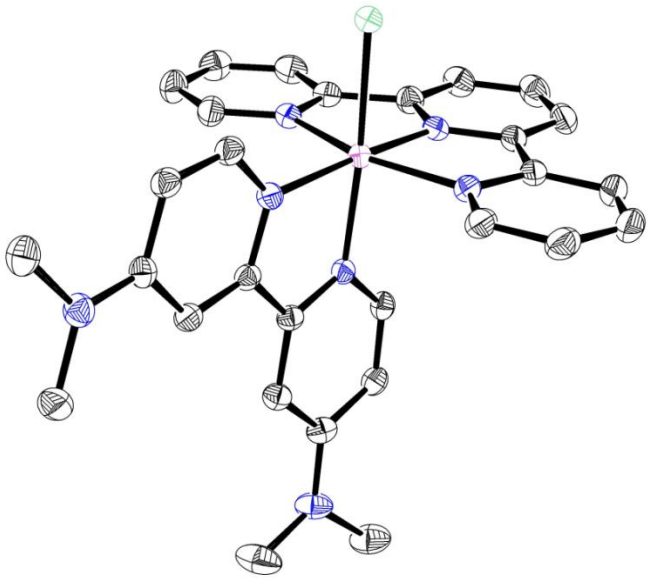

Figure 3.28. Molecular structure of **3.40**. There are two metal-containing cations with corresponding chloride counterions and methanol in the unit cell. For clarity one of the metal-containing cations, both chloride couterions, solvent, and hydrogen atoms are not shown.

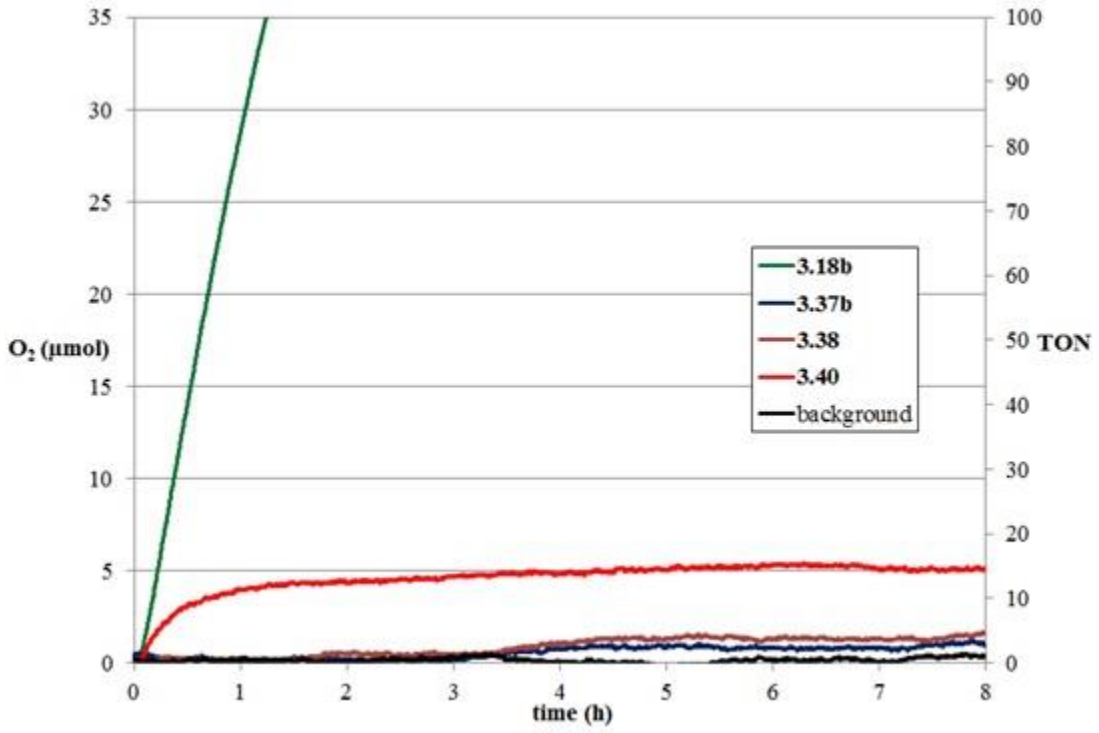

Figure 3.29. Molecular oxygen evolution (micromoles) monitored by pressure in a reaction vessel (48 mL) containing initial concentrations of $[CAN]_0$ = 78 mM, $[HNO_3]_0$ = 0.1 M, and $[catalyst]_0$ = 50 µM (total liquid volume 7.0 mL at 30 ^oC).

A combination of COSY, HSQC, and HMBC data were used to establish connectivity and assign most ^{1}H, ^{13}C, and ^{15}N signals for complexes **3.37**, **3.37b**, **3.38**, and **3.40** (for graphical representations of all complexes and their NMR data, see NMR section at the end of the chapter). Looking at ^{1}H NMR data (Table 3.5) of **3.37** compared to those of **3.37b**, there are only minor shifts of less than 0.1 ppm except for the signal for 6-NH_2 protons next to the metal is shifted 0.55 ppm upfield after ionization. The other ^{13}C NMR chemical shifts did not change enough to discern a pattern (Table 3.6).

The ^{15}N NMR data showed the same pattern as in Table 3.1 of upfield shifts when **3.37** was ionized to **3.37b**. Looking at bipy substituent effects, the 4,4'-diamino and 4,4'-bis(*N*,*N*-dimethylamino) complexes **3.38** and **3.40** showed similar data for the nitrogens that were observed, although in some cases the amino nitrogen crosspeaks were not detected (Table 3.7). Both nitrogens of the bipy ring in the 4,4'-amino complexes show large upfield shifts (about 40 and 50 ppm) compared to the parent complex; the effect is less for the hydroxy / methoxy analogs (shifted about 20 and 40 ppm), which can be explained by the stronger donor ability of amino and strong but lesser donor ability of hydroxy/methoxy substituents. For the 4,4'-amino complexes **3.38** and **3.40** the terpy nitrogens all experience downfield shifts, but the nitrogen trans to the bipy ligand being is shifted the most, 9 ppm whereas the cis nitrogens only about 4 ppm, which can be explained by the amino bipyridine ligand being a stronger donor and weakening the terpy donation. The same logic can be used for the 4,4' oxygenated compounds that have less of a downfield shift of about 5 ppm for the trans nitrogen and 3 ppm for the cis nitrogens.

Only one crystal structure of an amino-substituted complex was obtained, that of **3.40** (key bond lengths in Table 3.8 and structure shown in Figure 3.28). One thing worth noting is the ruthenium-chloride bond length is 0.12 Å longer for **3.40** compared to the parent compound **3.12** with the other metal bonds only slightly longer. Another observation that could explain the Ru-Cl bond length, is that the two methyls of the amino are planar with the pyridine ring, showing that the amino lone pair is conjugated with pyridine making it a stronger donor, so it would be expect to lengthen the Ru-Cl bond. Looking at the 4,4'-OMe analog **3.19** shows that the Ru-Cl bond is longer than the

parent compound **3.12** but not as long as the **3.40** showing that it most likely the electronics of the donating ligand that lengthens the Ru-Cl bond.

The catalysts were tested using CAN and HNO_3 (78 mM and 0.1 M, respectively, both initial concentrations) with 50 µM initial catalyst concentration, detecting the oxygen by pressure which showed that **3.37b** and **3.38** are not active catalysts. **3.40** was only slightly better with about 10 turnovers over the first hour and a total of 15 turnovers total. The amino complexes proved to be a disappointment, but going forward we decided to try one more simple analog.

F. Synthesis and Characterization of a Complex with Thioether Substituents Directly Attached to Ligand Ring

In an attempt to further look at analogs similar to the 6,6'-methoxy complex, we wanted to look at the sulfur analog which might have comparable reactivity. The thioether analog would not be as good of a hydrogen bond acceptor as the methoxy analog[32]. It is also possible that the thioether sulfur could be oxidized to sulfoxide of sulfone but that could be a positive side reaction since either of these could act as a hydrogen bond acceptor[33-36]. The ligand was synthesized by adding a solution of lithium thiomethoxide to 6,6'-dibromobipyridine in DMF giving the desired ligand **3.42** in 84 % yield. Metalation was done as before with Ru(terpy)Cl_2 dimer, **3.13**, in methanol for 2 d at 100 ^oC. The chloride species was not isolated, rather it was ionized with silver triflate and crystallized by vapor diffusion giving **3.43** in 83 % yield (Figure 3.30).

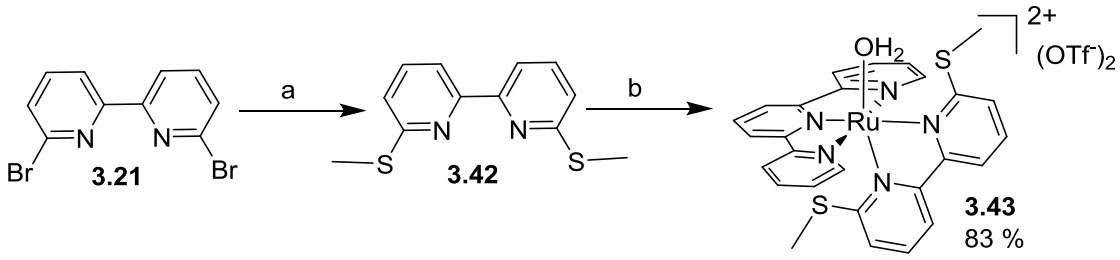

Figure 3.30. Synthesis of complex **3.43**.
(a) **3.21** (1.0 equiv), dimethyl disulfide (2.2 equiv), THF, -78 ^oC, n-BuLi (2.2 equiv), 30 min, 3.21 (1.0 equiv), DMF, RT, 1.5 h, 84 % yield. (b) **3.42** (1.0 equiv), [Ru(terpy)Cl_2]$_2$ (0.5 equiv), MeOH, 2 d, 100 ^oC, AgOTf (2.2 equiv), acetone, water, 4 d, 83 % yield.

Examining the NMR chemical shift values, as one would expect comparing **3.18b** (6,6'-OMe) to **3.43,** the XCH_3 protons of the 6,6' bipyridine are shifted more downfield

Table 3.9. ^{1}H NMR data[a] for **3.43** (left), and ^{13}C {^{1}H} NMR data[b] for **3.43** (right).

ligand	atom	**3.18b**[c]	**3.43**
bipy ring cis to X	H6	4.13 (OCH_3) (s)	2.71 (SMe)
	H5	7.58 (dd, 7.86, 1.62)	7.86 (d, 8.0)
	H4	8.36 (m)	8.29 (t, 8.0)
	H3	8.36 (m)	8.57 (d, 8.0)
bipy ring trans to X	H3'	8.06 (dd, *J* = 7.95, 1.00)	8.26 (d, 8.4)
	H4'	7.71 (dd, 8.40, 7.87)	7.67 (t, 8.0)
	H5'	6.54 (dd, 8.38, 1.07)	6.91 (d, 8.0)
	H6'	3.19 (OCH_3) (s)	2.11 (SMe)
terpy rings cis to bipy	Hc6	7.99 (ddd, 5.56, 1.55, 0.83)	8.21 (d, 5.5)
	Hc5	7.38 (ddd, 7.60, 5.52, 1.29)	7.50 (br t, 6.5)
	Hc4	7.96 (m)	8.06 (dd, 7.9, 1.3)
	Hc3	8.48 (ddd, 7.98, 1.33, 0.90)	8.54 (d, 8.0)
terpy trans to bipy	Ht3	8.60 (d, 8.11)	8.64 (d, 8.0)
	Ht4	8.19 (t, 8.08)	8.23 (t, 8.0)
aquo	H_2O	5.12 (br s)	5.46 (br s)

	3.18b	**3.43**
C6	170.4/58.0	171.2/16.9
C5	109.5	123.8
C4	141.6	138.6
C3	117.9	120.6
C2	156.3	158.4
C2'	159.1	161.1
C3'	117.6	120.5
C4'	140.4	137.3
C5'	107.3	122.2
C6'	170.7/57.1	173.0/16.7
Cc6	154.4	155.2
Cc5	128.2	128.1
Cc4	138.6	139.3
Cc3	123.9	124.3
Cc2	160.7	161.2
Ct2	160.3	161.3
Ct3	122.7	123.7
Ct4	136.1	137.6

[a] Chemical shifts in ppm, referenced from the resonance for the C*H*D$_2$ of d_6-acetone = 2.05 ppm. Coupling constants *J* (Hz) are listed after multiplicity. Data are for samples dissolved in d_6-acetone / H_2O (85 : 15 v/v), observed at 600 MHz, 30 ^{o}C. In cases where a substituent (SCH_3) is at the ring position indicated, data shown refer to the proton(s) on the substituent.

[b] Chemical shifts in ppm, referenced from the resonance for the methyl carbons of d_6-acetone at 29.92 ppm. Data are for samples dissolved in d_6-acetone / H_2O (85 : 15 v/v), observed at 150.752 MHz, 30 ^{o}C. In cases where a SCH_3 substituent is at the ring position indicated, data shown refer to the ring carbon, followed by chemical shift of the methylthio ether carbon.

[c] Spectra were acquired with sw = ca. 5000 Hz and np = 524288, resulting in a digital resolution of 0.02 Hz / pt. For exact values of sw, see full NMR data tables at the end of the chapter. The *J* values were determined by using a shifted sine bell weighting function. Instead of using the difference of the top of the peaks, the difference of the center of the peak at its widest point were used, followed by the averaging of like coupling constants for a given proton.

in the methoxy case (4.13/3.19 ppm for **3.18b** to 2.71/2.11 ppm for **3.43**), but the shielding effect of the terpy ring remains similar (Δ = 0.94 ppm for **3.18b** and Δ = 0.60 ppm for **3.43**). Other large chemical shift changes are seen for the C5/C5' and the H5/H5'

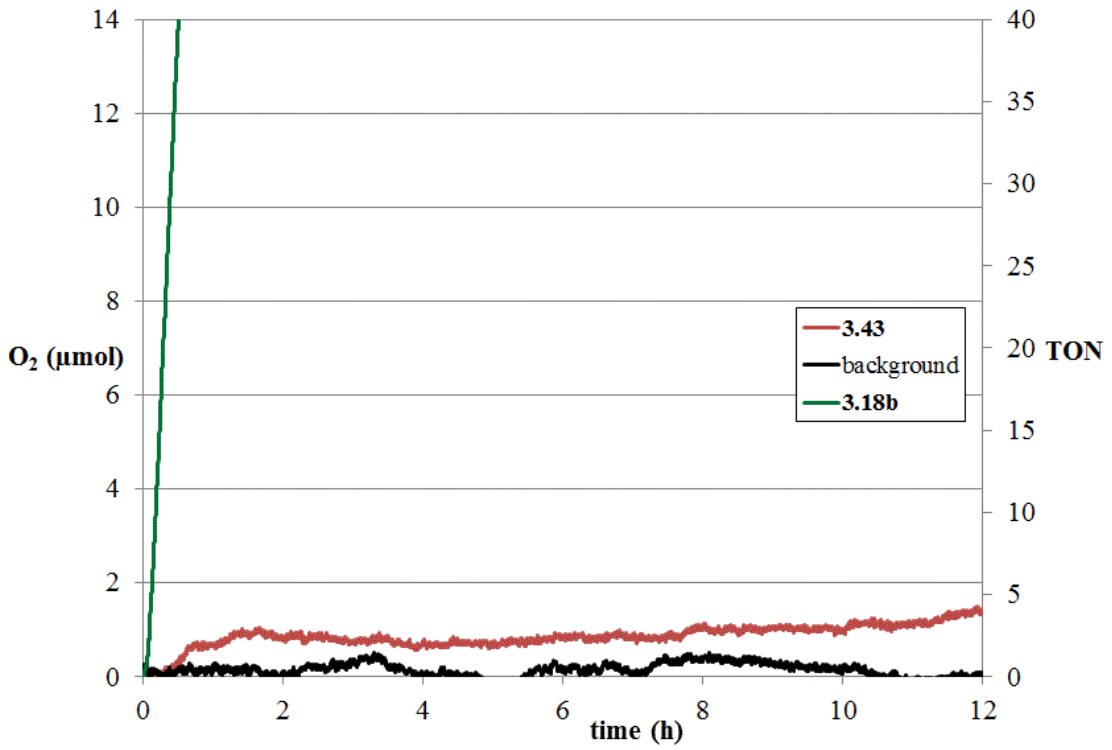

Figure 3.31. Molecular oxygen evolution (micromoles) monitored by a pressure sensor in a reaction vessel (48 mL) containing initial concentrations of $[CAN]_0$ = 78 mM, $[HNO_3]_0$ = 0.1 M, and $[catalyst]_0$ = 50 µM (total liquid volume 7.0 mL).

nuclei, with values changing from 109.5/107.3 for **3.18b** to 123.8/122.2 for **3.43**, and the H5/H5' changing from 7.58/6.54 ppm to 7.86/6.91ppm (See Table 3.9 left and right)

Testing of complex **3.43** was done using initial concentrations of CAN (78 mM) and HNO_3 (0.1 M) with 50 µM catalyst and using pressure to detect the amount of generated O_2. Unfortunately Figure 3.31 shows that the complex is not active while using CAN. To this point we have made a number of analogs with pendant heteroatoms that are sp3 hybridized and not part of a heterocycle, and few of the catalysts were active; we next wanted to have the pendant base be a nitrogen atom that is part of an aromatic system.

G. Synthesis and Characterization of Complexes with Annelated Heterocyclic Bases, Extended π Systems

Another analog of (terpy)(bipy)RuX complexes contains the pendant base as part of an aromatic ring, such as the extended π system bisnaphthyridine (Figure 3.32). Compounds **3.44** and **3.45** were reported by Thummel et al in 2004, and **3.44b** and **3.45b**

were also prepared but as the PF_6 salts. The Thummel paper discusses the preparation and characterization of the complexes but not their water oxidation activity[37].

Our synthesis of the metal complexes was performed by reacting Ru(terpy)Cl_2 dimer **3.13** in methanol with the corresponding bisnaphthyridine ligand at 100 ^oC for 1 d giving **3.44** and **3.45** in 79 and 87 % yield, respectively. The chlorides were replaced using silver triflate in acetone and water mixture to give **3.44b** and **3.45b** after recrystallization in 98 % and 81 % yields (Figure 3.33). An analog of naphthyridine with more basic nitrogens would be ligand **3.52**, with pendant imidazoles. The synthesis of **3.52** was done in 6 steps: (1) 2,6-dichloro-3-nitropyridine **3.46** is an electron poor

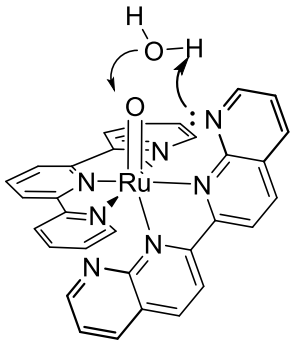

Figure 3.32. Illustration of a possible bifunctional interaction with a naphthyridine acting as the pendant base.

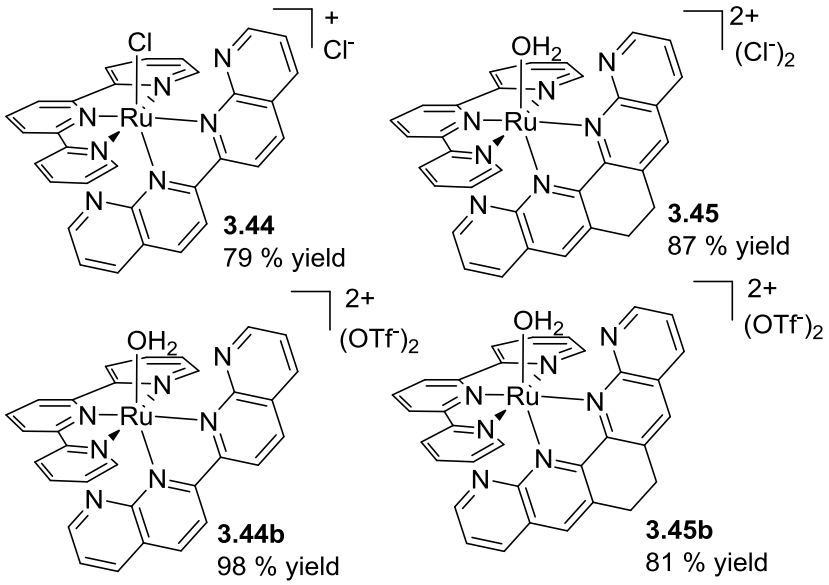

Figure 3.33. Compounds **3.44**, **3.44b**, **3.45**, and **3.45b**.

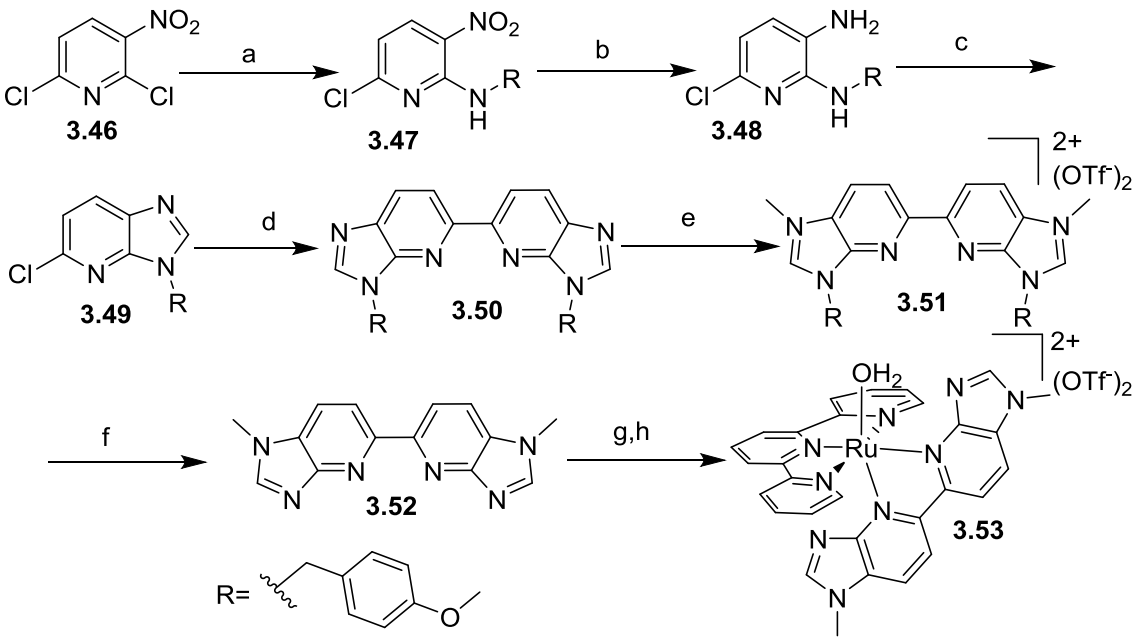

Figure 3.34. Synthesis of ligand **3.52** and complex **3.53**.
(a) **3.46** (1.0 equiv), 4-methoxybenzylamine (1.15 equiv), TEA (1.3 mL), THF, RT, 3 h. (b) **3.47** (1.0 equiv), 5 % sulfided Pt/C, H_2 (50 psi), THF, RT, 6 h. (c) **3.48** (1.0 equiv), triethylorthoformate (1.7 equiv), *p*-toluenesulfonic acid monohydrate (8 mol %), toluene, reflux, 16 h, 31 % yield over three steps. (d) **3.49** (1.0 equiv), $NiBr_2(PPh_3)_2$[8] (25 mol %), zinc powder (1.7 equiv), lithium chloride (1.7 equiv), tetraethylammonium iodide (1.0 equiv), THF, reflux, 10.5 h, 84 % yield. (e) **3.50** (1.0 equiv), methyl trifluoromethansulfonate (4.05 equiv), DMF, 100 ^oC, 2.6 h, 86 % yield. (f) **3.51** (1.0 equiv), formic acid, 130 ^oC, 3 d, 74 % yield. (g) **3.52** (1.0 equiv), **3.13** (1.0 equiv), methanol, 100 ^oC, 27 h. (h) AgOTf (2.5 equiv), acetone/H_2O, RT, 1 h, 48 % yield over two steps.

substrate that is known to directly add amines via aromatic nucleophilic substitution[38-40]. Here, use of 4-methoxybenzylamine gave **3.47**. (2) The nitro group was reduced to an amine using 5 % sulfided Pt/C, giving **3.48**[41]. (3) The imidazole ring was then formed by refluxing the diamino compound in the presence of triethylorthoformate to give **3.49**. (4) The chloro compound was subjected to known reductive coupling conditions using $NiBr_2(PPh_3)_2$ and zinc as the reducing agent[42], giving **3.50**. (5) Double methylation using methyl trifluoromethansulfonate in DMF gave **3.51**, where the purpose of having the R group on the C2 amine was so that at this step, one could selectively add a methyl group to the C3 nitrogen. Attempts at synthesis without the R group lead toa mixture of methylation products so the synthesis was redone with this directing group. (6) The

Table 3.10. ^{1}H NMR data for **3.44**, **3.44b**, and **3.45**.

ligand	atom	**3.44**[b]	**3.44b**	**3.45/3.45b**
bipy ring cis to X	H8	9.27 (dd, 4.37, 1.93)	9.22 (dd, 4.4, 1.9)	9.15 (dd, 4.4, 1.9)
	H7	8.15 (dd, 8.23, 4.36)	8.13 (dd, 8.3, 4.4)	8.07 (dd, 8.1, 4.4)
	H6	9.15 (dd, 8.28, 1.90)	9.10 (dd, 8.3, 1.9)	9.01 (dd, 8.2, 1.7)
	H4	9.18 (d, 8.83)	9.12 (d, 8.7)	8.87 (s)
	H3	9.39 (d, 8.84)	9.31 (d, 9.0)	3.69-3.66 (m)(CH_2)[c]
bipy ring trans to X	H3'	9.05 (d, 8.85)	8.97 (d, 8.9)	3.52-3.50 (m)(CH_2)[c]
	H4'	8.49 (d, 8.74)	8.45 (d, 8.7)	8.18 (s)
	H6'	8.37 (dd, 8.03, 2.00)	8.34 (dd, 8.1, 1.9)	8.26-8.24 (m)
	H7'	7.53 (dd, 8.02, 4.22)	7.52 (dd, 8.0, 4.3)	7.46 (dd, 8.0, 4.5)
	H8'	8.33 (dd, 4.23, 1.95)	8.31 (dd, 4.3, 1.9)	8.26-8.24 (m)
terpy rings cis to bipy	Hc6	7.74 (ddd, 5.59, 1.55, 0.76)	7.70 (ddd, 5.6, 1.5, 0.7)	7.70 (d, 5.3)
	Hc5	7.18 (ddd,7.55, 5.60, 1.34)	7.16 (ddd,7.6, 5.6, 1.3)	7.16 (ddd, 7.5, 5.6, 0.9)
	Hc4	7.92 (ddd, 8.01, 7.62, 1.53)	7.90 (ddd, 8.1, 7.6, 1.6)	7.90 (dt,7.8, 1.6)
	Hc3	8.55 (ddd, 8.10, 1.34, 0.81)	8.50 (ddd, 8.1, 1.4, 0.8)	8.49 (br d, 8.1)
terpy trans to aquo	Ht3	8.77 (d, 8.14)	8.72 (d, 8.3)	8.72 (d, 8.1)
	Ht4	8.43 (t, 8.14)	8.40 (t, 8.2)	8.40 (t, 8.1)
	H_2O	--	8.10 (br s)	--

[a] Chemical shifts in ppm, referenced from the resonance for the C*H*D_2 of d_6-acetone = 2.05 ppm. Coupling constants *J* (Hz) are listed after multiplicity. Data are for samples dissolved in d_6-acetone / H_2O (85 : 15 v/v), observed at 600 MHz, 30 ^{o}C. In cases where a substituent (CH_2) is at the ring position indicated, data shown refer to the proton(s) on the substituent.
[b] Spectra were acquired with sw = ca. 5000 Hz and np = 524288, resulting in a digital resolution of 0.02 Hz / pt. For exact values of sw, see full NMR data tables at the end of the chapter. The *J* values were determined by using a shifted sine bell weighting function. Instead of using the difference of the top of the peaks, the difference of the center of the peak at its widest point were used, followed by the averaging of like coupling constants for a given proton.

Table 3.11. ^{15}N chemical shift comparison for chloro and aquo complexes, in which Δ is the difference upon going from chloro to aquo.[a]

ligand	atom	**3.44**	Δ	**3.44b**	**3.45**
bipy	N1	-123.5	-0.1	-123.6	nd
bipy	N9	-102.4	-0.6	-103.0	-103.8
bipy	N1'	-126.9	-0.4	-127.3	nd
bipy	N9'	-74.1	-0.2	-74.3	-75.3
terpy	Nc1	-138.2	-0.2	-138.4	-138.3
terpy	Nt1	-97.6	-0.1	-97.5	-98.0

[a] Data (ppm) obtained on natural abundance material using ^{1}H-^{15}N gHMBC experiments. In d_6-acetone / H_2O (85:15 v/v) unless otherwise specified. nd = not detected.

Table 3.12. ^{13}C {^{1}H} NMR spectral data for amino complexes.[a]

	3.44	**3.44b**	**3.45**
C10	159.9	159.7	158.9
C8	154.8	154.6	153.8
C7	126.4	126.3	126.1
C6	142.1	141.9	141.9
C5	127.0	126.9	127.2
C4	139.5	139.4	136.9
C3	124.5	124.2	137.5/27.4
C2	162.5	162.3	159.8
C2’	164.4	134.2	161.6
C3’	123.4	123.3	136.5/27.3
C4’	138.1	138.1	135.9
C5’	124.6	124.4	124.7
C6’	139.5	139.4	138.8
C7’	125.7	125.6	125.4
C8’	153.9	153.9	153.2
C10’	159.4	159.3	158.5
Cc6	154.5	154.3	154.4
Cc5	128.0	127.9	127.9
Cc4	139.2	139.1	139.1
Cc3	124.4	124.2	124.2
Cc2	161.1	160.9	160.9
Ct2	159.3	159.1	159.2
Ct3	123.1	122.9	122.9
Ct4	137.7	137.6	137.5

[a] Chemical shifts in ppm, referenced from the resonance for the methyl carbons of d_6-acetone at 29.92 ppm. Unless otherwise specified, data are for samples dissolved in d_6-acetone / H_2O (85 : 15 v/v), observed at 150.752 MHz, 30 ^{o}C. In cases where a OCH_3 substituent is at the ring position indicated, data shown refer to the ring carbon, followed by chemical shift of the methoxy carbon.[14]

4-methoxybenzyl group was removed under acidic conditions using formic acid at 130 ^{o}C, giving target ligand **3.52**. The complex was formed by heating in methanol with Ru(terpy)Cl_2 dimer **3.13** for 27 h then the crude chloride complex was ionized with silver

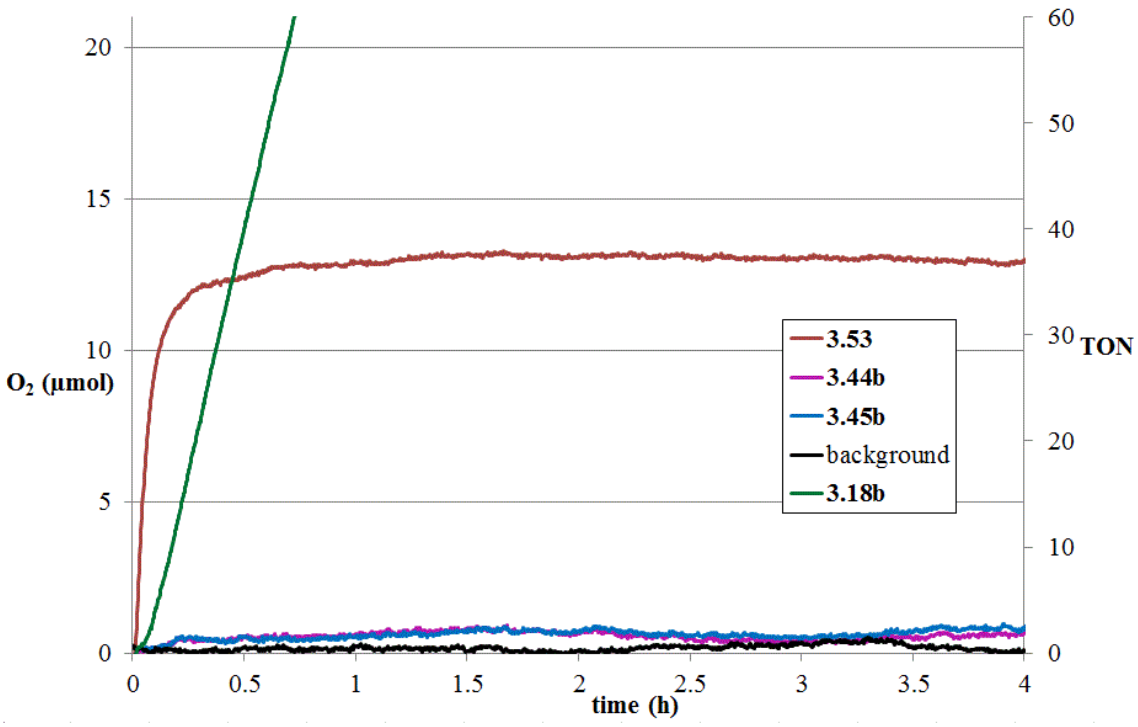

Figure 3.35. Molecular oxygen evolution (micromoles) monitored by a pressure sensor in a reaction vessel (48 mL) containing initial concentrations of $[CAN]_0$ = 78 mM, $[HNO_3]_0$ = 0.1 M, and $[catalyst]_0$ = 50 µM (total liquid volume 7.0 mL at 30 ^oC).

trifluoromethansulfonate in a acetone and water mixture which was then purified by vapor diffusion giving **3.53** (Figure 3.34).

Examining the ^1H, ^{13}C, and ^{15}N chemical shift values for complexes **3.44**, **3.44b**, **3.45** show very little changes between these complexes (See Table 3.10, 3.11, 3.12), for **3.53** see NMR section for values.

Testing of complexes **3.44b**, **3.45b**, and **3.53** was done using initial concentrations of CAN (78 mM), and 0.1 M HNO_3 with 50 µM of catalyst, with the oxygen being detected by the change in pressure (Figure 3.35). Complexes **3.44b** and **3.45b** were both not active catalysts, whereas **3.53** was initially quite fast giving 35 turnovers over approximately 20 min, but afterwards, minimal amounts of oxygen were formed. One possible explanation for the inactivity of **3.44b** and **3.45b** is the naphthyridine ligand is being attacked and degrading. For a different analog, a pyridylnaphthyridine complex, Yagi et al[43] computed the location of the LUMO of one of the isomers which contains large coefficients partially delocalized on the naphthyridine ring trans to the terpy ligand,

which could lead to attack and degradation of the ring (this will be discussed in more detail later).

Some questions arose: what about the naphthyridine system leads to catalyst deactivation? Are one or both of the uncoordinated basic nitrogens a site for oxidation? Or is it the extended π system that is a site for degradation? The simplest example of extended π system of a bipyridine analog would be bisisoquinoline, **3.54**, which replaces the second pyridine ring with a benzene ring. Another idea was removing the extended π system completely, but retaining the ring, such as **3.55**. Both of these ligands would have no bifunctional interaction, but we could make analogs that do. The main purpose of

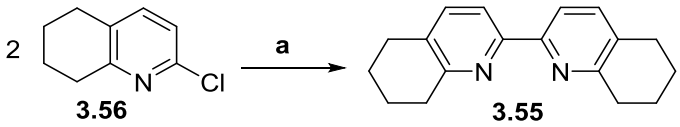

Figure 3.36. Synthesis of ligand **3.55**.
(a) **3.56** (1.0 equiv), $NiBr_2(PPh_3)_2$[8] (29 mol %), zinc powder (1.6 equiv), tetraethylammonium iodide (1.05 equiv), THF, reflux, 17 h, 46 % yield.

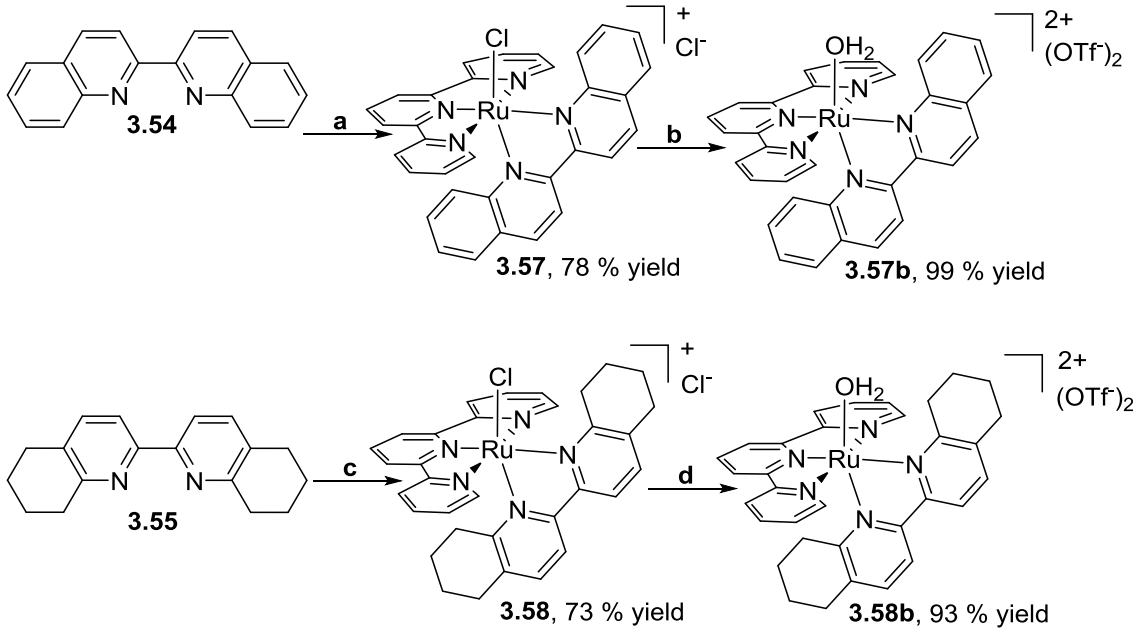

Figure 3.37. Synthesis of complexes **3.57**, **3.57b**, **3.58**, and **3.58b**.
(**3.57**); (a) **3.13** (1.04 equiv), **3.54** (1.0 equiv), methanol, 100 ^{o}C, 4 days, 78 % yield. (b) **3.57** (1.0 equiv), silver trifluoromethanesulfonate (2.1 equiv), acetone/water, RT, 16.5 h, 99 % yield. (c) **3.13** (1.04 equiv), **3.55** (1.0 equiv), methanol, 100 ^{o}C, 2 days, 73 % yield. (d) **3.58** (1.0 equiv), silver trifluoromethanesulfonate (2.1 equiv), acetone/water, RT, 30 h, 93 % yield.

Table 3.13. ^{1}H NMR data for **3.57**, **3.57b**, **3.58**, and **3.58b**.

ligand	atom	**3.58**	**3.58b**	**3.57**	**3.57b**
bipy ring cis to X	H9	3.80[b] (m)	3.35-3.33 (m)	9.69 (d, 8.8)	8.90-8.88 (m)
	H8	1.84-1.79 (m)	1.91-1.89 (m)	7.80-7.77 (m)	7.94-7.91 (m)
	H7	1.84-1.79 (m)	1.91-1.89 (m)	7.87-7.85 (m)	7.94-7.91 (m)
	H6	3.06-3.04 (m)	3.13-3.10 (m)	8.31-8.30 (m)	8.40-8.39 (m)
	H4	8.01 (d, 8.1)	8.09-8.06 (m)	8.94 (d, 8.8)	9.02 (d, 8.8)
	H3	8.53-8.51 (m)	8.54 (d, 8.4)	9.03 (d, 9.0)	9.10 (d, 8.8)
bipy ring trans to X	H3'	8.20 (d, 8.1)	8.21 (d, 8.4)	8.74 (d, 8.8)	8.79 (d, 8.8)
	H4'	7.39 (d, 8.3)	7.43 (d, 8.2)	8.31-8.30 (m)	8.35 (d, 8.8)
	H6'	2.48-2.46 (m)	2.50-2.48 (m)	7.82 (d, 8.1)	7.86 (d, 8.0)
	H7'	1.31-1.29 (m)	1.33-1.29 (m)	7.45 (t, 7.5)	7.49 (t, 7.1)
	H8'	1.17-1.15 (m)	1.22-1.18 (m)	7.24 (t, 7.9)	7.31 (ddd, 8.8, 6.9, 1.4)
	H9'	1.59-1.57 (m)	1.72-1.70 (m)	6.83 (d, 9.0)	6.96 (d, 9.0)
terpy rings cis to bipy	Hc6	8.09-8.05 (m)	8.15 (d, 5.5)	7.86-7.85 (m)	7.94 (d, 5.6)
	Hc5	7.45 (t, 6.2)	7.53 (t, 6.6)	7.34 (t, 6.6)	7.42 (ddd, 7.0, 5.6, 1.1)
	Hc4	7.97 (t, 7.7)	8.08-8.06 (m)	7.96 (t, 7.8)	8.04 (dt, 7.8, 1.4)
	Hc3	8.53-8.51 (m)	8.59 (d, 8.0)	8.53 (d, 8.5)	8.60 (d, 8.0)
terpy trans to	Ht3	8.60 (d, 8.1)	8.71 (d, 8.0)	8.69 (d, 8.1)	8.81 (d, 8.2)
	Ht4	8.07 (t, 8.1)	8.25 (t, 8.0)	8.23 (t, 8.1)	8.40 (t, 8.0)
aquo	H_2O	--	5.43	--	6.29

[a] Chemical shifts in ppm, referenced from the resonance for the C*H*D$_2$ of d_6-acetone = 2.05 ppm. Coupling constants *J* (Hz) are listed after multiplicity. Data are for samples dissolved in d_6-acetone / H_2O (85 : 15 v/v), observed at 600 MHz, 30 ^{o}C.

Table 3.14. ^{15}N chemical-shift comparison for chloro and aquo complexes, in which Δ is the difference upon going from chloro to aquo.[a]

ligand	atom	**3.57**	Δ	**3.57b**
bipy	N1	-121.2	-2.5	-123.7
bipy	N1'	-130.9-	-8.1	-139.0
terpy	Nc1	-134.1	-7.2	-141.3
terpy	Nt1	-93.5	-8.8	-102.3

[a] Data (ppm) obtained on natural abundance material using ^{1}H-^{15}N gHMBC experiments. In d_6-acetone / H_2O (85:15 v/v) unless otherwise specified. nd = not detected.

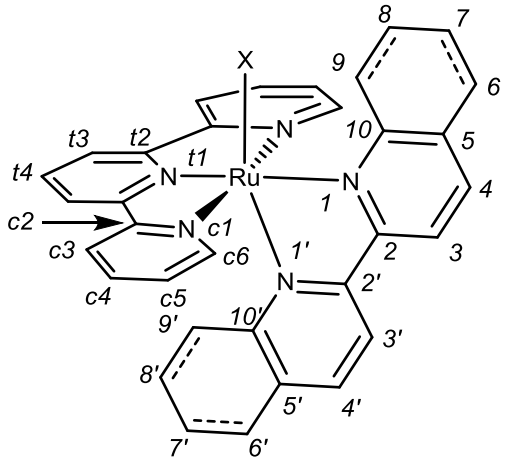

Table 3.15. ^{13}C {^{1}H} NMR spectral data for compounds **3.57**, **3.57b**, **3.58**, and **3.58b**.[a]

	3.58	**3.58b**	**3.57**	**3.57b**
C10	167.4	165.6	151.9	151.6
C9	35.8	33.8	131.8	128.3
C8	23.1	23.2	131.2	132.8
C7	22.2	22.2	130.0	130.2
C6	29.2	29.3	129.5	130.4
C5	136.8	137.2	130.1	130.2
C4	138.9	139.6	139.3	139.7
C3	124.2	121.9	121.6	121.8
C2	156.4	156.1	159.4	159.4
C2’	158.6	159.1	162.6	163.0
C3’	121.2	121.3	121.7	121.7
C4’	138.4	138.8	137.3	138.0
C5’	135.1	135.6	129.1	129.0
C6’	28.8	28.9	130.2	130.4
C7’	21.4	21.3	129.3	129.5
C8’	23.1	23.2	131.5	132.0
C9’	31.4	31.8	124.5	124.4
C10’	164.9	165.6	152.6	153.0
Cc6	153.9	154.7	153.3	154.3
Cc5	127.8	128.8	127.9	128.8
Cc4	138.0	139.3	138.5	139.7
Cc3	124.2	124.8	124.6	125.2
Cc2	160.7	160.8	160.0	160.2
Ct2	160.8	161.0	159.6	160.1
Ct3	123.1	124.1	123.6	124.6
Ct4	135.1	137.2	136.5	138.5

[a] Chemical shifts in ppm, referenced from the resonance for the methyl carbons of d_6-acetone at 29.92 ppm. Unless otherwise specified, data are for samples dissolved in d_6-acetone / H_2O (85 : 15 v/v), observed at 150.752 MHz, 30 ^{o}C[14].

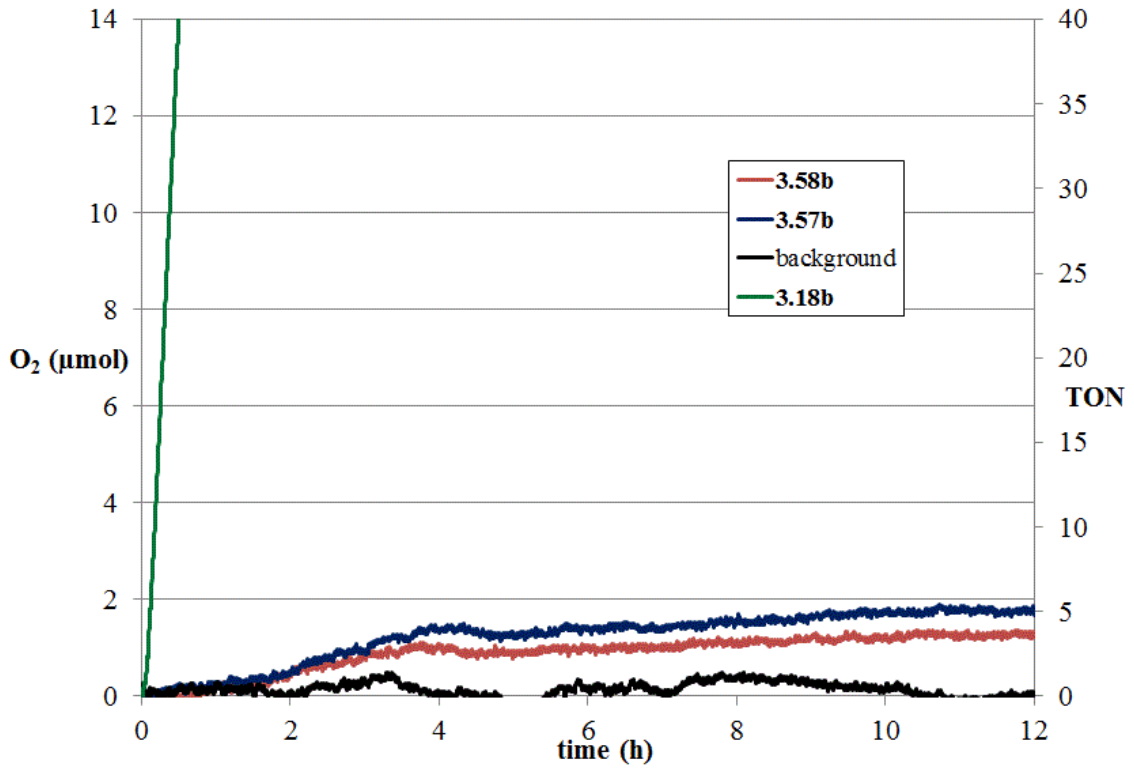

Figure 3.38. Molecular Oxygen evolution (micromoles) monitored by a pressure sensor in a reaction vessel (48 mL) containing initial concentrations of $[CAN]_0$ = 78 mM, $[HNO_3]_0$ = 0.1 M, and $[catalyst]_0$ = 50 µM (total liquid volume 7.0 mL).

making these analogs would be to see if they were about as effective as the parent bipyridine catalysts **3.12** and **3.12b**; if so, then other analogs could be explored, introducing a bifunctional aspect.

Synthesis of the known ligand 2,2'-biquinoline **3.54** was done by the published method of Oda et al.[8]. The synthesis of **3.55** started with **3.56** made by a procedure described by Pfaltz et al[44] which was then reductively coupled giving **3.55** (Figure 3.36). Both of the ligands were complexed using Ru(terpy)Cl_2 dimer **3.13** in methanol at 100 ^oC for 2 to 4 d, then purified by recrystallization giving **3.57** (78%) and **3.58** (73%). Both complexes were treated with silver trifluoromethanesulfonate in an acetone/water mixture giving **3.57b** in 99% yield or **3.58b** in 93% yield (Figure 3.37). The biggest change in the ^1H NMR chemical shifts in transforming **3.57** and **3.58** to **3.57b** and **3.58b**, respectively, is seen for the H9 proton, which shifted upfield by 0.46 ppm and 0.2 ppm respectively (Table 3.13).

^{13}C chemical shifts (Table 3.15) show only minor changes. ^{15}N chemical shift values move upfield for nitrogen N1', Nc1, and Nt1 about 8 ppm upon ionization of **3.57** to **3.57b** which has been typical for these (terpy)(bpy)Ru complexes (Table 3.14).

The aquo complexes **3.57b** and **3.58b** (50 μM initial concentration) were tested for their water oxidation capabilities using CAN (78 mM) as a sacrificial oxidant in the presence of HNO_3 (0.1 M; all initial concentrations) and monitoring oxygen production by pressure. Both catalysts were shown to be inactive for water oxidation using CAN (Figure 3.38), which dissuaded us from exploring any other extended saturated or unsaturated bipyridine analogs. We learned that the inactivity of the extended pi system complexes was not limited to the naphthyridine case but also was true for the quinoline analog, this make us wonder why these extended systems were not active catalysts.

H. Synthesis and Characterization of Complexes with Annelated Heterocyclic Bases, with Extended π Systems Sterically Protected

A very interesting paper was published by Thummel et al. in 2011 looking at compounds **3.59** and **3.60**, both of which are quite similar to **3.44** and **3.44b**, which were both inactive. Significantly, **3.44** has a symmetrical bisnaphthyridine ligand, which gives only one isomer once metalated, whereas **3.59** and **3.60** contain a pyridylnaphthyridine ligand, which is unsymmetrical and gives two isomeric complexes, one where the naphthyridine is proximal to the open site (**3.60**) and one distal to the open site (**3.59**). Now comparing the two isomers, we would expect that the proximal isomer **3.60** would be a much better catalyst because the adjacent naphthyridine could assist in any proton transfers, which is precisely the reactivity we have been trying to harness. However **3.60** was found to be inactive (<1 reported turnovers) whereas **3.59** gave 2700 turnovers after 2 d and **3.59-(OH_2)** gave over 3200 turnovers (Figure 3.39)[45]. As briefly discussed earlier, Yagi et al. then computed the location of the LUMO for both isomers at the Ru(IV) oxidation state, finding that the LUMO of the oxidized form of **3.59** contains a large coefficient that was localized on the ruthenium oxo, the ideal location for WNA reactivity, but the LUMO of the oxidized form of **3.60** has large coefficients partially delocalized on the naphthyridine ring[43], which could mean that nucleophilic attack and degradation of the ring is possible.

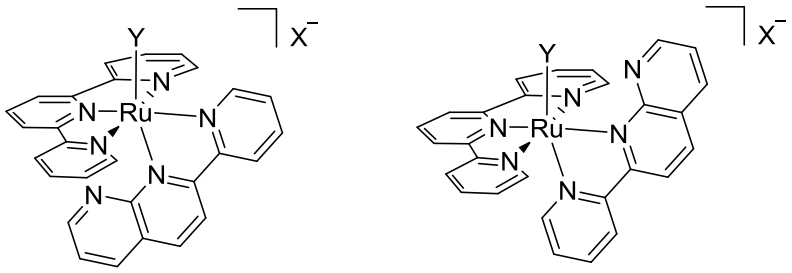

3.59 Y=X=Cl
3.59-H_2O Y=H_2O X = 2 PF_6^-

3.60 Y=X=Cl
3.60-H_2O Y=H_2O X = 2 PF_6^-

Figure 3.39. Known compounds **3.59** and **3.60**.

In the absence of any experimental confirmation of degradation of the extended pi system of the naphthyridine ring of **3.60** during water oxidation catalysis, we were curious if we could protect the extended π system from degradation by adding steric bulk around and on both sides of the naphthyridine ring. One means to do so could be to add a phenyl substituent that itself was substituted in the 2,6-positions with bulky groups that would be pointed on top and bottom of the ring would be an effective way to protect the naphthyridine (Figure 3.40). The first analog that came to mind was mesityl, where R would be methyl, but one concern was that the benzylic positions could be oxidized under water oxidation conditions. Thus we thought another good possibility would be R = trifluoromethyl, adding steric bulk and electron withdrawing groups to make the ligand harder to oxidize as White et al. reported for a CH oxidation catalyst of iron [46]. A control would feature R = trifluoromethyl but instead of in the 2,6-positions of the phenyl, at the 2,4 positions, giving similar electronic effects as the 2,6-isomer but reduced steric bulk. To really shield the naphthyridine ring, the last analog that would use extremely bulky (3,5-di-trifluoromethylphenyl)phenyl as the R groups, where now there would be a phenyl ring and two trifluoromethyl groups on the top and below the ring. Osichow et al.[47] recently reported (3,5-di-trifluoromethylphenyl)phenyl substituents in an electron poor nickel complex that was used to polymerize ethylene, and reported a crystal structure that gives an idea of the bulk of the substituent. Olaru et al.[48] studied the organic reactivity of similarly bulky electron poor aryl groups.

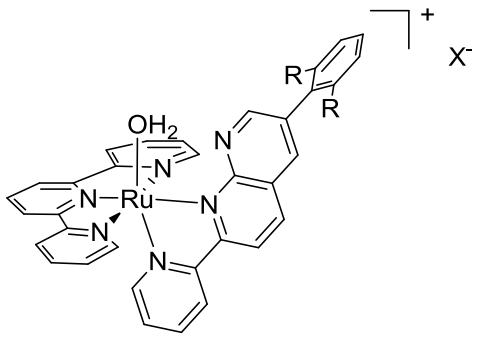

Figure 3.40. Target structure that could prevent degradation by the use of steric bulk of two R groups to slow down attack of the naphthyridine ring.

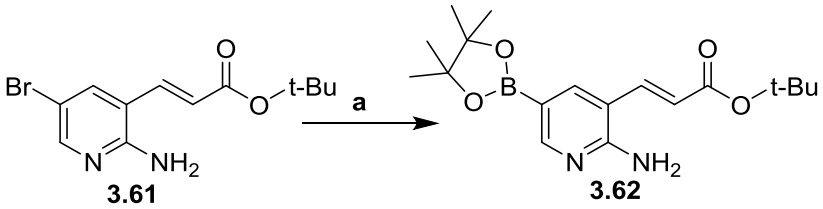

Figure 3.41. Synthesis of **3.62**.
(a) **3.61** (1.0 equiv), bis(pinacolate)diboron (2.0 equiv), KOAc (3.1 equiv), dppf (15 mol %), $Pd(OAc)_2$ (15 mol %), NMP, 21 h, 80^o C, 76 % yield.

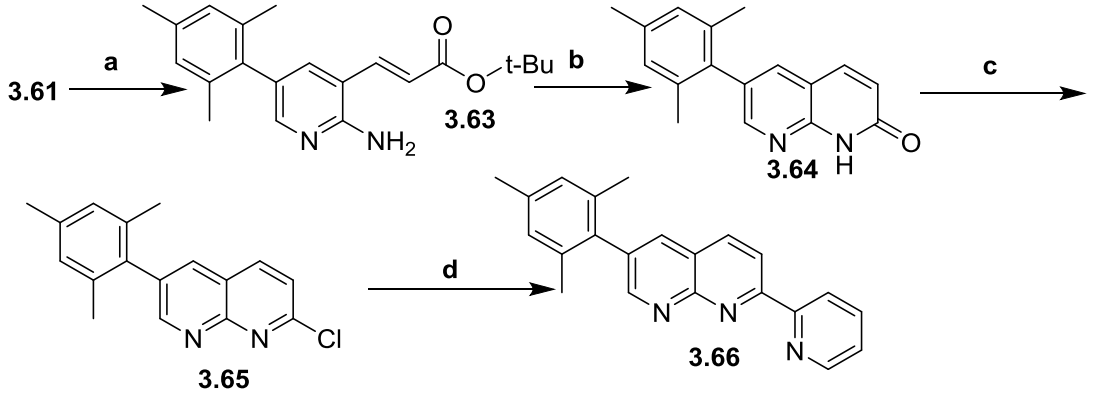

Figure 3.42. Synthesis of **3.66**.
(a) **3.61** (1.0 equiv), 2,4,6-trimethylphenylboronic acid (2.0 equiv), K_3PO_4 (2.07 equiv), $Pd(OAc)_2$ (10 mol %), X-Phos (10 mol %), toluene/water (10:1), 80 ^{o}C, 19 h. (b) **3.63** (1.0 equiv), NaOMe (5.0 equiv), MeOH, 80 ^{o}C, 4 h. (c) **3.64** (1.0 equiv), $POCl_3$, 100 ^{o}C, 45 min, 39 % over 3 steps. (d) **3.65** (1.0 equiv), 2-(tributylstannyl)pyridine (1.6 equiv), $Pd(PPh_3)_4$ (5 mol %), toluene, 100 ^{o}C, 3 d, 29 % yield.

This project was done with undergraduate Ryan Shirey and with some assistance by Farhana Barmare with the chemistry in Fig. 3.45. The synthesis of the ligands started with 2-amino-5-bromopyridine, by electrophilic iodination to obtain 2-amino-5-bromo-3-

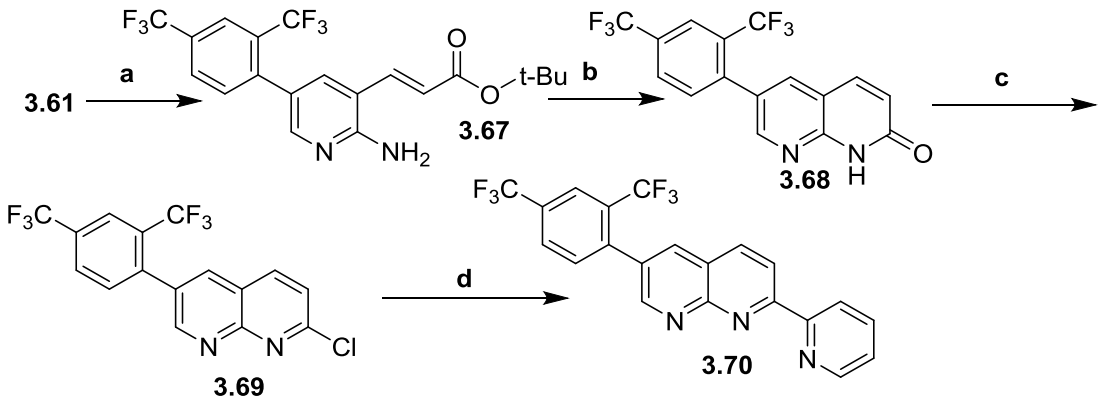

Figure 3.43. Synthesis of **3.70**.
(a) **3.61** (1.0 equiv), 2,4-bis(trifluoromethyl)phenylboronic acid (1.6 equiv), K_3PO_4 (2.0 equiv), $Pd(OAc)_2$ (10 mol %), X-Phos (10 mol %), toluene/water (10:1), 80 ^oC, 17 h. (b) **3.67** (1.0 equiv), NaOMe (5.0 equiv), MeOH, 80 ^oC, 4 h, 36 % yield over two steps. (c) **3.68** (1.0 equiv), $POCl_3$, 100 ^oC, 1 h, 41 % yield. (d) **3.69** (1.0 equiv), 2-(tributylstannyl)pyridine (1.6 equiv), $Pd(PPh_3)_4$ (5 mol %), toluene, 100 ^oC, 3 d, 82 % yield.

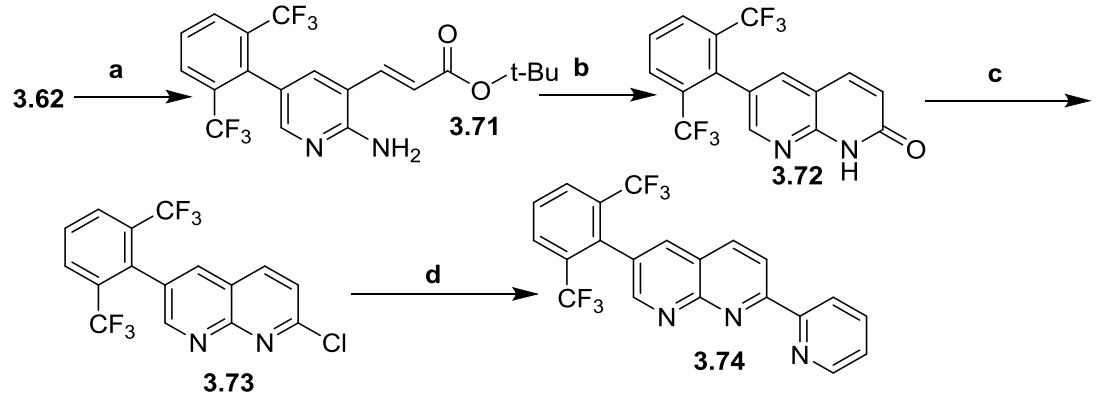

Figure 3.44. Synthesis of **3.74**.
(a) **3.62** (1.0 equiv), 2-bromo-1,3-bis(trifluoromethyl)benzene (2.2 equiv), K_2CO_3 (2.1 equiv), PEPPSI-*i*-Pr (5 mol %), ethanol/water (95:5), 80 ^oC 18 h, 41 % yield. (b) **3.71** (1.0 equiv), NaOMe (5.0 equiv), MeOH, 80 ^oC, 5 h. (c) **3.72** (1.0 equiv), $POCl_3$, 100 ^oC, 2 h, 69 % yield over two steps. (d) **3.73** (1.0 equiv), 2-(tributylstannyl)pyridine (1.5 equiv), $Pd(PPh_3)_4$ (5 mol %), toluene, 100 ^oC, 13 h, 81 % yield.

iodopyridine, which was then coupled with *tert*-butyl acrylate in a Heck coupling giving **3.61** (Fig. 3.41). **3.61** could then be coupled with mesityl boronic acid or 2,4-bis(trifluoromethyl)phenyl boronic acid using $Pd(OAc)_2$ and X-Phos giving **3.63** or **3.67**, respectively. Attempts at forming the 2,6-bis(trifluoromethyl)phenyl analog **3.71** were unsuccessful by this method, because the 2,6-bis(trifluoromethyl)phenyl boronic acid is believed to decompose to 1,3-bis(trifluoromethyl)benzene[49]. Therefore the Suzuki

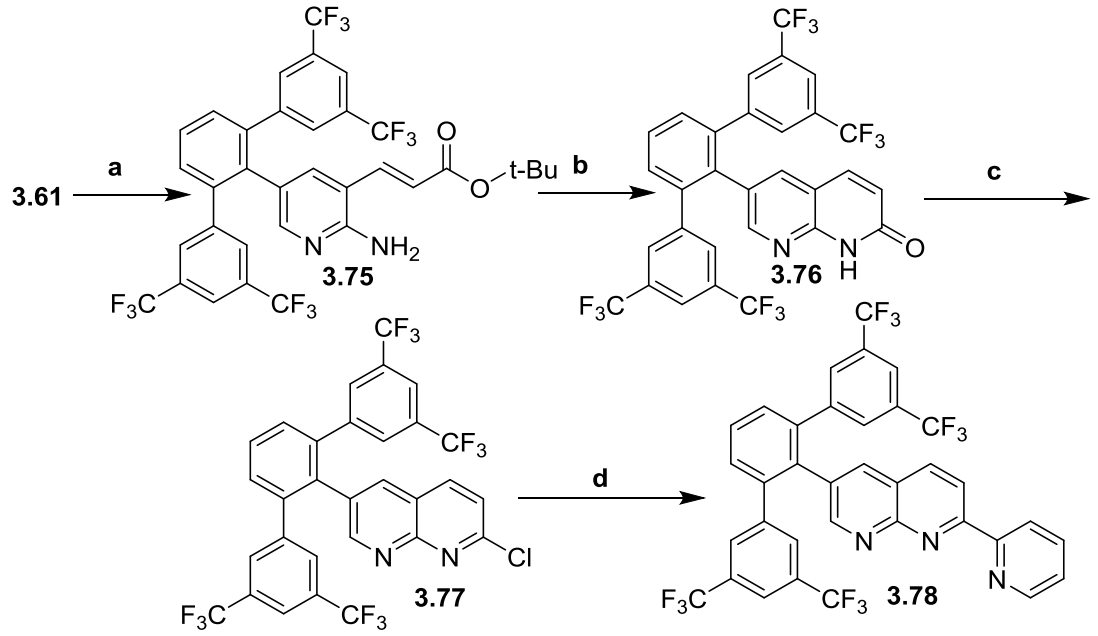

Figure 3.45. Synthesis of **3.78**.
(a) **3.61** (1.0 equiv), 2,6-bis(3,5-bis(trifluoromethylphenyl))bromobenzene (0.79 equiv), $Pd(PPh_3)_4$ (6 mol %), Na_2CO_3 (2 M), dioxane, 100 ^oC 20 h, 66 % yield. (b) **3.75** (1.0 equiv), NaOMe (5.1 equiv), MeOH, 80 ^oC, 4h, 97 % crude yield. (c) **3.76** (1.0 equiv), $POCl_3$, 100 ^oC, 1 h, 75 % yield. (d) **3.77** (1.0 equiv), 2-(tributylstannyl)pyridine (1.8 equiv), $Pd(PPh_3)_4$ (5 mol %), toluene, 100 ^oC, 20 h, 76 % yield.

coupling was attempted by first converting **3.61** to the corresponding boronic ester **3.62** (Figure 3.41) which was then coupled to 2,6-bis(trifluoromethyl)bromobenzene using PEPPSI-*i*-Pr catalyst[50,51] giving **3.71**. **3.75** was also formed using **3.62** but coupling with 2,6-bis(3,5-bis(trifluoromethylphenyl))bromobenzene (made by Farhana Barmare, not shown) using $Pd(PPh_3)_4$. After formation of **3.63**, **3.67**, **3.71**, and **3.75** the synthesis was similar for the remaining steps; under basic conditions with sodium methoxide cyclization to the naphthyridone yielded **3.64**, **3.68**, **3.72**, and the chlorinated products **3.76**. **3.65**, **3.69**, **3.73**, and **3.77** were formed using phosphorus oxychloride. Finally, Stille couplings with 2-tributylstannyl pyridine gave the target ligands **3.66**, **3.70**, **3.74**, and **3.78** (Figures 3.42-Figure 3.44). For detailed synthetic procedures and NMR characterization figures see corresponding sections later in the chapter.

Complexes **3.79**-**3.82** were formed by heating at 100 ^oC for 2 to 6 d, giving a mixture or the proximal (p) and distal (d) isomers. The isomers were then separated by

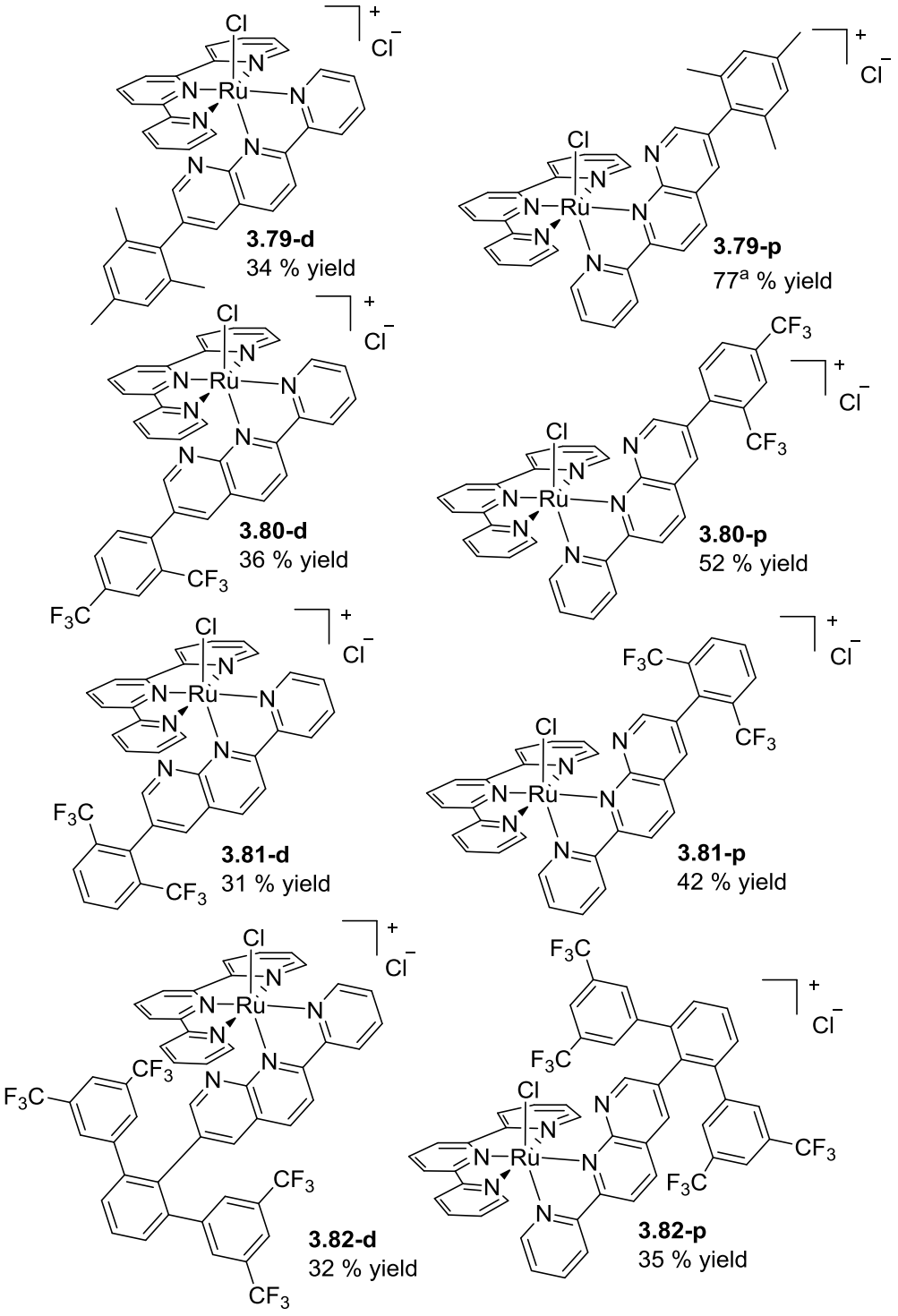

Figure 3.46. Structures and yields of **3.79**-**3.83p** and **3.79**-**3.83d**.

[a] Unable to use elemental analysis to find the molecular weight with solvation so yield appears higher than actual, see experimental procedure of **3.79**-**p** for more details.

Table 3.16. ^{1}H NMR data for **3.79-p**, **3.80-p**, **3.81-p**, and **3.82-p**.

ligand	atom	**3.79-p**	**3.80-p**	**3.81-p**	**3.82-p**
naphthy	H8	9.05 (d, 2.4)	9.28 (d, 2.6)	9.25 (s)	8.95 (s)
ring cis to X	H6	8.86 (d, 2.4)	9.14 (d, 2.6)	9.11 (d, 2.2)	8.76 (d, 2.3)
	H4	9.11 (d, 8.8)	9.18 (d, 8.7)	9.16 (d, 8.8)	8.77 (d, 8.9)
	H3	9.16 (d, 8.8)	9.20 (d, 8.8)	9.22 (d. 9.0)	9.05 (d, 8.9)
py ring	H3’	8.90 (d, 8.1)	8.93 (d, 8.8)	8.94 (d, 8.1)	8.84 (d, ~8)
trans to X	H4’	7.90 (ddd, 8.1, 7.6, 1.3)	7.91 (td, 7.9, 1.5)	7.92 (ddd, 8.1, 7.6, 1.4)	7.88 (td, 7.6, 1.2)
	H5’	7.25 (ddd, 7.5, 5.9, 1.4)	7.27 (ddd, 7.3, 6.0, 1.1)	7.28 (ddd, 7.5, 5.9, 1.4)	7.27-7.23 (m)
	H6’	7.82 (dd, 5.9, 0.7)	7.85 (d, 5.6)	7.87 (d, 5.6, 1.5, 0.7)	7.82 (d, 5.9)
terpy rings	Hc6	7.88 (ddd, 5.6, 1.5, 0.7)	7.89 (dd, 5.4, 1.4)	7.87 (ddd, 5.6, 1.5, 0.7)	7.50 (d, 5.1)
cis to bipy	Hc5	7.29 (ddd, 7.5, 5.6, 1.3)	7.31 (ddd, 7.0, 5.8, 1.1)	7.31 (ddd, 7.5, 5.6, 1.3)	7.27-7.23 (m)
	Hc4	8.04 (td, 7.8, 1.5)	8.05 (td, 7.8, 1.4)	8.06 (ddd, 8.1, 7.6, 1.5)	8.08 (td, 7.9, 1.4)
	Hc3	8.68 (br d, 7.8)	8.68 (d, 8.0)	8.70 (ddd, 8.1, 1.3, 0.8)	8.70 (d, 8.1)
terpy trans	Ht3	8.84 (d, 8.2)	8.84 (d, 8.2)	8.85 (d, 8.2)	8.84 (d, 8.2)
to bipy	Ht4	8.41 (t, 8.1)	8.41 (t, 8.1)	8.42 (t, 8.1)	8.42 (t, 8.2)
aquo	H_2O	7.73 (s)	--	7.54 (s)	

[a] Chemical shifts in ppm, referenced from the resonance for the C*H*D$_2$ of d_6-acetone = 2.05 ppm. Coupling constants *J* (Hz) are listed after multiplicity. Data are for samples dissolved in d_6-acetone / H_2O (85 : 15 v/v), observed at 600 MHz (500 MHz for **3.82-p**), 25 ^{o}C.

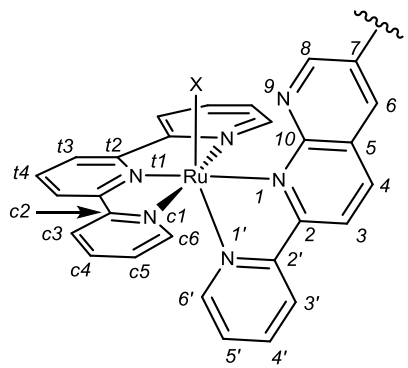

Table 3.17. ^{1}H NMR data for **3.79-d**, **3.80-d**, **3.81-d**, and **3.82-d**.

ligand	atom	**3.79-d**	**3.80-d**	**3.81-d**	**3.82-d**
py ring cis to X	H6	10.54 (ddd, 5.6, 1.5, 0.7)	10.42 (d, 4.8)	10.47 (ddd, 5.6, 1.5, 0.7)	10.43 (d, 5.7)
	H5	8.08 (ddd, 7.6, 5.7, 1.3)	8.09 (ddd, 7.5, 5.7, 1.3)	8.11 (ddd, 7.6, 5.7, 1.3)	8.06 (ddd, 7.5, 5.7, 1.2)
	H4	8.42 (ddd, 8.1, 7.6, 1.5)	8.44-8.40 (m)	8.44 (ddd, 8.2, 7.6, 1.6)	8.39 (td, 7.8, 1.5)
	H3	9.10 (d, 8.2)	9.11 (d, 8.2)	9.14 (d, 8.2)	9.05 (d, 8.3)
naphthy ring trans to X	H3’	8.75 (d, 8.8)	8.78 (d, 8.8)	8.81 (d, 8.8)	8.63 (d, 8.8)
	H4’	8.38 (d, 8.7)	8.44-8.40 (m)	8.43 (d, 8.7)	8.04 (d, 8.6)
	H6’	8.08 (d, 2.4)	8.33 (d, 2.5)	8.31 (d, 2.2)	7.92 (d, 2.3)
	H8’	7.91 (d, 2.5)	8.15 (s)	8.07 (s)	7.58 (d, 2.4)
terpy rings cis to bipy	Hc6	7.69 (ddd, 5.6, 1.5, 0.7)	7.66 (d, 5.0)	7.68 (ddd, 5.6, 1.5, 0.7)	7.56 (br d, 5.5)
	Hc5	7.25 (ddd, 7.5, 5.6, 1.3)	7.24 (ddd, 7.5, 5.6, 1.2)	7.26 (ddd, 7.5, 5.6, 1.3)	7.23 (ddd, 7.6, 5.6, 1.2)
	Hc4	7.85 (ddd, 8.0, 7.6, 1.5)	7.85 (td, 7.8, 1.5)	7.87 (ddd, 8.0, 7.5, 1.5)	7.89 (td, 7.8, 1.4)
	Hc3	8.45 (ddd, 8.1, 1.2, 0.7)	8.44-8.40 (m)	8.45 (ddd, 8.1, 1.3, 0.9)	8.33 (d, 8.0)
terpy trans to bipy	Ht3	8.62 (d, 8.1)	8.60 (d, 8.1)	8.61 (d, 8.1)	8.39 (d, 8.1)
	Ht4	8.13 (t, 8.1)	8.13 (t, 8.1)	8.11 (t, 8.2)	7.95 (t, 8.0)

[a] Chemical shifts in ppm, referenced from the resonance for the C*H*D$_2$ of d_6-acetone = 2.05 ppm. Coupling constants *J* (Hz) are listed after multiplicity. Data are for samples dissolved in d_6-acetone / H_2O (85 : 15 v/v), observed at 600 MHz (500 Hz for **3.82-d)**, 25 ^{o}C.

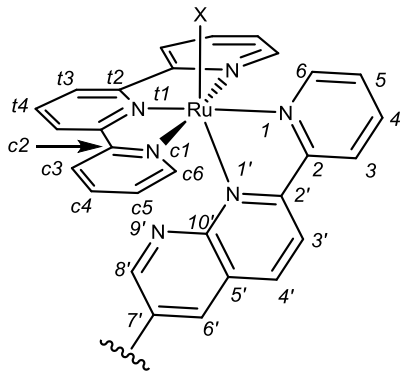

Table 3.18. ^{13}C {^{1}H} NMR spectral data for **3.79-p**, **3.80-p**, **3.81-p**, and **3.82-p** (left) and **3.79-d**, **3.80-d**, **3.81-d**, and **3.82-d** (right).[a]

	3.79-p	**3.80-p**	**3.81-p**	**3.82-p**
C10	158.4	159.1	159.0	157.6
C8	155.9	154.2	154.9	156.6
C7	138.6	135.7	132.2	136.6
C6	141.3	141.0	142.0	143.8
C5	126.7	126.0	125.3	125.4
C4	139.8	140.1	139.9	139.0
C3	122.6	123.2	123.3	123.1
C2	161.1	162.1	162.4	162.1
C2’	160.0	159.9	159.9	159.6
C3’	127.5	127.8	127.8	127.8
C4’	136.7	136.7	136.7	136.7
C5’	128.2	128.4	128.4	128.5
C6’	153.8	154.0	154.0	154.0
Cc6	154.5	154.6	154.4	153.8
Cc5	128.6	128.7	128.6	128.3
Cc4	139.4	139.5	139.6	139.7
Cc3	125.3	125.3	125.3	125.5
Cc2	159.8	159.8	159.8	160.0
Ct2	159.2	159.3	159.2	159.1
Ct3	124.4	124.5	124.5	124.6
Ct4	138.0	138.2	138.2	138.4

	3.79-d	**3.80-d**	**3.81-d**	**3.82-d**
C6	154.0	154.0	154.1	154.1
C5	127.8	128.1	128.1	128.0
C4	137.1	137.2	137.2	137.1
C3	126.7	127.0	127.0	126.8
C2	158.1	157.9	158.0	157.8
C2’	163.6	164.6	164.7	163.9
C3’	121.2	121.8	121.8	121.3
C4’	137.5	137.7	137.5	136.7
C5’	123.9	123.2	122.6	122.9
C6’	138.6	138.5	139.6	141.2
C7’	137.3	134.5	131.0	135.3
C8’	154.2	152.2	153.1	154.8
C10’	158.0	158.5	158.4	157.2
Cc6	152.9	152.9	152.9	152.6
Cc5	127.5	127.5	127.5	127.3
Cc4	137.7	137.8	137.7	137.6
Cc3	123.6	123.6	123.5	123.3
Cc2	160.9	160.8	160.8	160.6
Ct2	158.8	158.7	158.7	158.5
Ct3	122.0	122.0	122.0	121.4
Ct4	134.7	134.8	134.7	134.2

[a] Chemical shifts in ppm, referenced from the resonance for the methyl carbons of d_6-acetone at 29.92 ppm. Unless otherwise specified, data are for samples dissolved in d_6-acetone / H_2O (85 : 15 v/v), observed at 150.7 MHz (125.7 MHz for **3.82**), 25 ^{o}C.

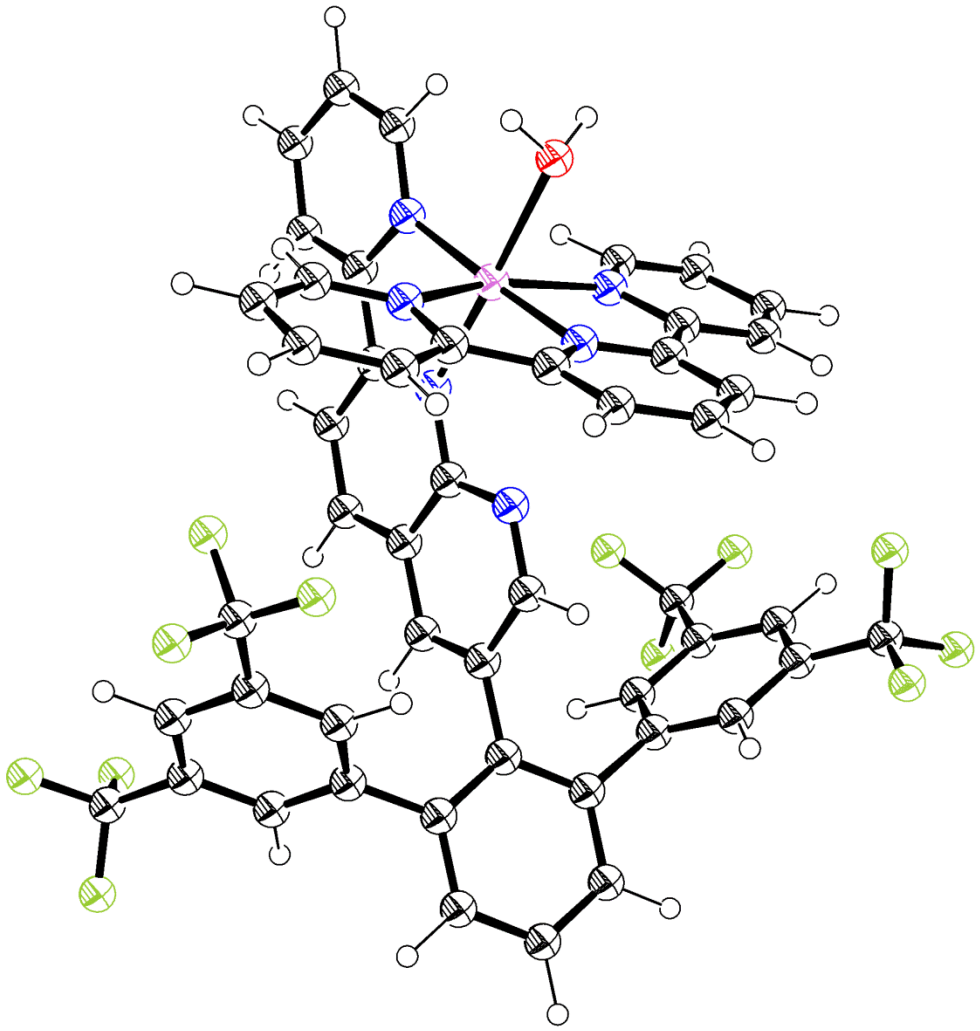

Figure 3.47. Computed structure of the dication of **3.82-d**, showing the shielding of the naphthyridine ligand and to a lesser extent the middle pyridine on the terpy. Braden Silva is thanked for these data.

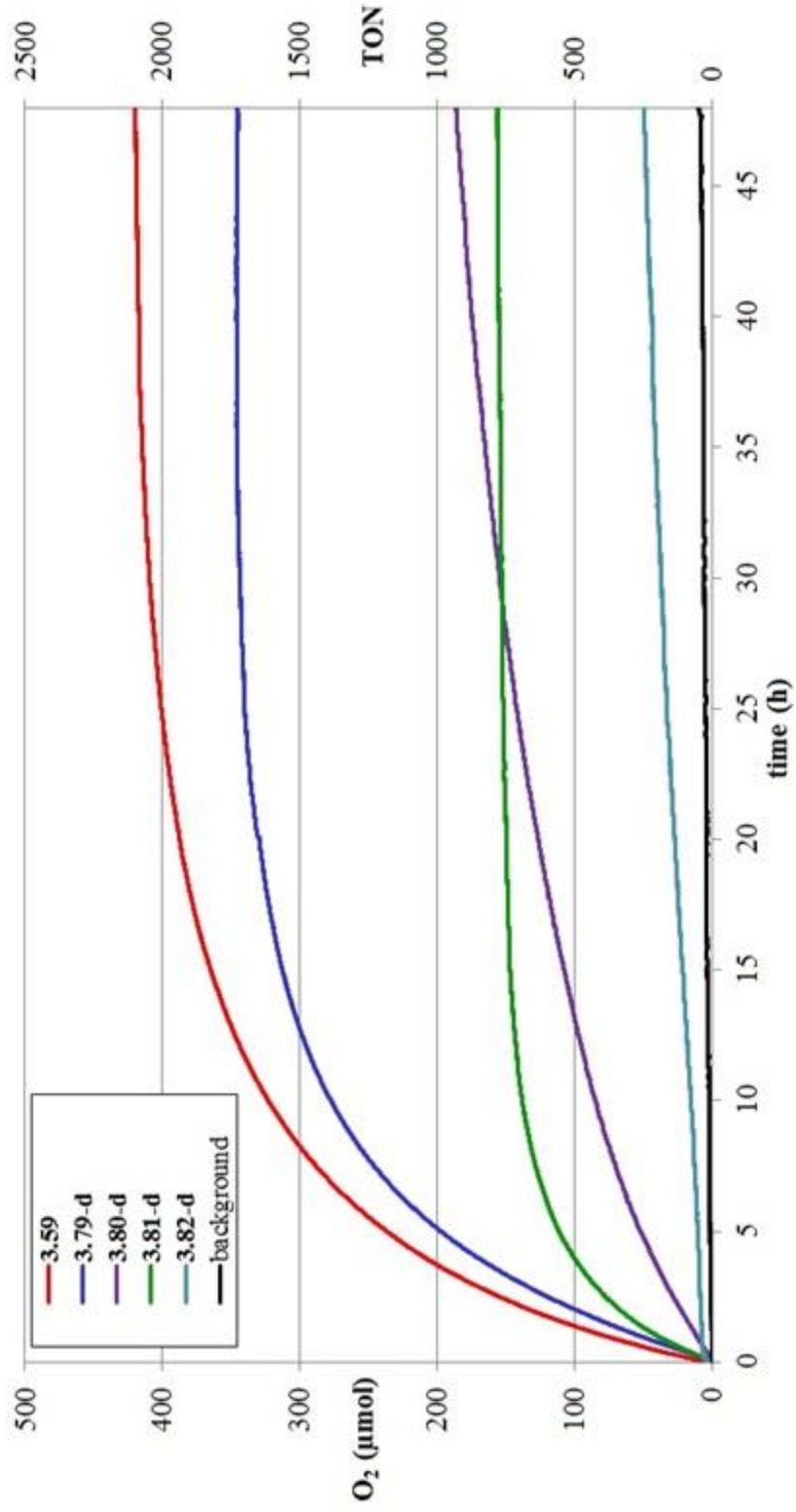

Figure 3.48. Molecular oxygen evolution (micromoles) monitored by a pressure sensor in a reaction vessel (48 mL) containing initial concentrations of $[CAN]_0$ = 500 mM, $[HNO_3]_0$ = 0.1 M, and $[catalyst]_0$ = 50 µM (total liquid volume 4.0 mL).

silica or neutral alumina column chromatography using acetone and water to elute.

Comparing the ^{1}H NMR spectra of **3.79-d**, **3.80-d**, and **3.81-d**, the largest changes in chemical shifts are for the H6' and H8' protons (Table 3.17) which are the protons on the naphthyridine ring adjacent to the ring that is varied in these structures (Mes, 2,4-bis(trifluoromethyl)phenyl), 2,6-bis(trifluoromethyl)phenyl, respectively). As would be expected based on the inductive effect, for the electron donating mesityl compound **3.79-d** the protons are shifted upfield by about 0.2 ppm compared to the proton signals of both of the electron withdrawing CF_3 compounds **3.80-d** and **3.81-d**. Looking at **3.82-d** compared to the other complexes there are a number of protons that are shifted upfield: H4', H6', H8', Ht3, and Ht4 by 0.2 to 0.5 ppm. H4', H6', and H8' are on the naphthyridine ring which is probably shielded due to the phenyl rings which are above and below the naphthyridine ring. Ht3 and Ht4 (the protons on the middle pyridine of terpy) are shifted by about 0.2 ppm downfield for complex **3.82-d** but not **3.82-p**. In the case of the distal isomer the benzene ring is shielding the terpy ring underneath, whereas in the proximal case the benzene rings are now by the open site, hence terpy signals are not being shifted. In the absence of X-ray diffraction data, Figure 3.47 shows a computed geometry of the distal isomer where you can see the location of the benzene rings under the central terpy ring. Similar trends for H4, H6, and H8 were seen for the proximal isomers (Table 3.16). A similar analysis confirms the different isomer geometry; for all of the distal isomers, naphthyridine ring proton signals are shifted upfield of the corresponding signals for the proximal isomers, due to the naphthyridine being shielded by the terpy ring. In contrast, for the proximal isomers the pyridine ring proton signals are shifted upfield compared to the corresponding signals for the distal isomers, now showing that the pyridine ring is under the terpy ring.

Comparing the proximal isomer ^{13}C NMR spectra shows that the carbon chemical shift that differs the most among the four analogs is that of C7 (Table 3.18 for numbering Table 3.16 for values), which is logical because that is the carbon that is attached to the group that changes among the analogs. Among the analogs the largest difference is between **3.79-p** and **3.81-p** (138.6 and 132.2 ppm); looking at just the inductive effect one would expect the ^{13}C NMR shift of **3.81** with the electron withdrawing CF_3 groups to

be downfield of **3.79** with the electron donating methyls, but that is not the case. The same trend is seen for the distal isomer ^{13}C NMR spectra, where for C7', in the cases of **3.79-d** and **3.81-d** the values are 137.3 and 131.0 ppm, respectively.

Testing these catalysts we used a higher initial CAN concentration (500 mM) than the 78 mM value used above, but retained the initial catalyst concentration of 50 μM and of HNO_3, 0.1 M (Figure 3.48). The distal isomers were still active but were not as active as the parent unsubstituted complex. The proximal isomers were inactive, which was surprising. Either the degradation pathway was not stopped by even the greatest amount of steric hindrance that we have added in these complexes, or they degrade by another pathway. Llobet recently looked in detail at the [Ru(X)(terpy)(bipy)]X system and suggested that it goes by WNA but that it also slowly transforms into **3.83**, which is a robust water oxidation catalyst[52]. For the distal isomers, possibly increasing steric bulk simply facilitates ligand loss through relief of steric strain. Possibly in future work, this hypothesis could be verified by examining mixtures derived from various catalysts and increasing amounts of CAN, to see at what point, if any, detectable or significant amounts of bidentate ligand appear in the reactions mixtures.

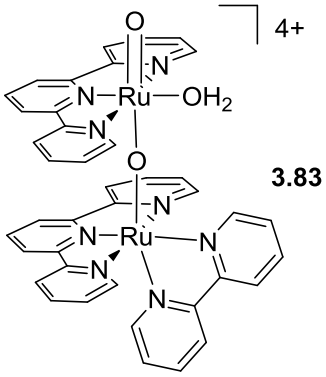

Figure 3.49. Transformation product of [Ru(X)(terpy)(bipy)]X shown by Llobet, where one metal center has lost its bidentate bipy ligand.

I. Conclusions

In conclusion, in an attempt to find improved, bifunctional water oxidation catalysts a number of [Ru(X)(terpy)(bipy)]X analogs have been synthesized, with the 6,6'-dimethoxy complex **3.18b** giving more turnovers than the parent compound; this fact and facile aquation of **3.18** by aqueous acetone at ambient temperature, without addition

of ionizing reagents, suggest favorable bifunctional interactions, certainly at the Ru(II) state. When a more remote pendant base is added to **3.18b**, as in structures **3.25** and **3.30** with flexible side arms, the catalysts are still active but slower and less robust. The 4,4'-dimethylamino complex **3.40** was only slightly active with the other amino analogs not yielding any O_2, and the same is true for the bis(methylthioether) species **3.43**. Next we explored extended π systems, finding the bisnaphthyridine analogs inactive whereas the bispyrimidazole complex **3.53** showed a faster initial rate than any of the other novel catalysts in this Chapter, comparable to the initial rate obtained with **3.59**, but **3.53** deactivated rapidly. Finally, looking at published computational studies that suggested extended pi systems may be susceptible to nucleophilic attack, we attempted to protect the naphthyridine ring from degradation by using bulky groups like mesityl (**3.79**), or bulky fluorinated groups around the ring, as in **3.80**-**3.82**, but were unsuccessful with no oxygen generated from the proximal isomers (the possibly bifunctional isomers) and no increase in catalysis rate or durability from the distal isomers. As our work was nearing completion, evidence for a proposed decomposition pathway involving bipy ligand loss was disclosed by the group of Llobet, who documented the generation of dinuclear complex **3.83**. Before 2008-2009 when T. J. Meyer published the [Ru(X)(terpy)(bipy)]X system and Bernhard published their Ir complex it was thought that two metal centers were needed to be an active water oxidation catalyst. Even some of the mononuclear catalysts are thought to operate by a dinuclear mechanism, hence one logical target system should contain two metal centers in close proximity, which leads to the next Chapter on dinuclear water oxidation catalysts.

Part of the material and discussion covered in chapter 3 is from published work "How Do Proximal Hydroxy or Methoxy Groups on the Bidentate Ligand Affect (terpy)Ru(N,N)X Water Oxidation Catalysts? Synthesis, Characterization, and Reactivity at Acidic and Near-neutral pH" which was published in *Eur. J. Inorg. Chem.* **2014**, *2014*, 676. This work was a result of collaboration between four different universities. I would like to thank Dr. Salome Bhagan, David Charboneau, Kristine Schroeder, Jayneil Kamdar, Amanda McGettigan, Benjamin Freeman, Dr. Curtis Moore, Dr. Arnold Rheingold, Dr. Andrew Cookey, Dr. Diane Smith, Dr. Jared Paul, Dr. Elizabeth Papish,

and Dr. Douglas Grotjahn for their contributions. I must also thank Ryan J. Shirey, Farhana Barmare, and Dr. Douglas B. Grotjahn for their work on another section covered in the chapter, which is part of a manuscript that is in preparation titled “Synthesis and Water Oxidation Activity of Sterically Hindered [Ru(Cl)(terpy)pyridylnaphthyridine] Cl Analogs; an Attempt at Fluorinated Oxidatively Resilient Ligands”

J. Experimental Procedure

Note: For those compounds not analyzed by 2D NMR, ^{1}H and ^{13}C NMR data are given immediately after preparative details below. But for many compounds, ^{1}H, ^{13}C NMR data and assignments from 2D NMR experiments are summarized on pages after the section of preparative details.

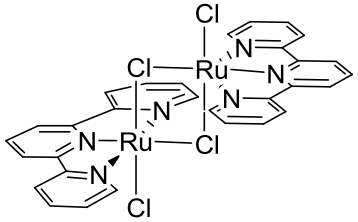

Synthesis of $[Ru(terpy)Cl_2]_2$ (3.13)

$[RuCl_2(cymene)]_2$[53] (1.0002 g,1.63 mmol, 1.0 equiv), which was dissolved in deoxygenated CH_2Cl_2 (20 mL) was added under nitrogen to a three-necked, round-bottomed flask (250 mL), equipped with a nitrogen adaptor, septum, and addition funnel. Terpyridine (terpy)[54] (0.7649 g, 3.28 mmol) dissolved in deoxygenated CH_2Cl_2 (80 mL), which was added dropwise over 1 h to form a dark purple solid, was added to the addition funnel. The reaction mixture was filtered through a medium frit and washed with CH_2Cl_2 (3 x 30 mL), acetone (30 mL), and diethyl ether (30 mL). The purple solid was transferred to a vial and dried under oil pump vacuum to afford $[(terpy)Ru(Cl)_2]_2$ (**9**, 1.1220 g, analyzed as a monohydrate, hence 1.35 mmol, 83.1%). Anal. calcd. for $C_{30}H_{22}Cl_4N_6Ru_2$ (810.49): C, 44.46; H, 2.74; N, 10.37. Found: C, 43.23; H, 2.88; N, 10.06. Calcd. for $C_{30}H_{22}C_{l4}N_6Ru_2 + H_2O$ (828.50): C, 43.49; H, 2.92; N, 10.14. ^{1}H NMR (d_6-DMSO, 599.492 MHz): δ 9.35 (d, J = 5.4 Hz, 4 H), 8.66 (d, J = 8.4 Hz, 4 H), 8.57 (d, J = 7.2 Hz, 4 H), 8.18 (t, J = 7.8 Hz, 2 H), 7.99 (td, J = 7.8, 1.2 Hz, 4 H), 7.53 (ddd, J = 7.2, 5.6, 1.6 Hz, 4 H) ppm. ^{13}C NMR (d_6-DMSO, 125.724 MHz): δ 158.7, 156.9, 155.7, 136.8, 136.1, 126.3, 123.0, 121.3 ppm. The compound is sparingly soluble even in DMSO, in which it might have converted to $[(terpy)Ru(Cl)_2(DMSO)]$.

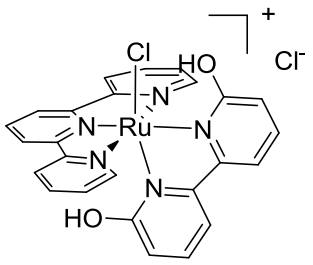

Synthesis of [Ru(Cl)(terpy)(6,6'-dihydroxy-2,2'-bipyridyl)]Cl (3.16)

$[Ru(terpy)Cl_2]_2$ (**3.13**, 90.4 mg, 0.109 mmol), 6,6'-dihydroxy-2,2'-bipyridine[7] (**3.6**, 42.2 mg, 0.224 mmol), a stir bar, and methanol (6 mL) were added to a vial in a glovebox. The reaction vial was placed in a 100 °C oil bath for 30 h, then cooled to room temperature and filtered through a fine frit. Solvent in the filtrate was reduced to a minimal amount, and diethyl ether was allowed to mix by vapor diffusion. After formation of crystals, the mixture was filtered through a fine frit, and the dark solid was washed with diethyl ether (3 x 2 mL). The solid was transferred to a vial and dried under oil pump vacuum to yield [Ru(Cl)(terpy)(6,6'-dihydroxy-2,2'-bipyridyl)]Cl (H_2O) (**3.16**, 54.3 mg, 0.0888 mmol, 41 % yield). Anal. calcd for $C_{25}H_{19}Cl_2N_5O_2Ru$ (H_2O) (mol. wt. 611.44): C, 49.11; H, 3.46; N, 11.45. Found: C, 49.57; H, 3.84; N, 11.52.

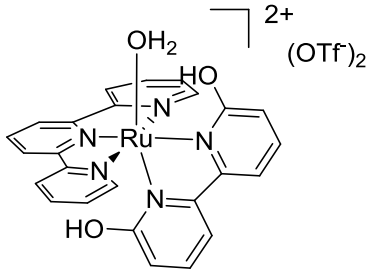

Synthesis of $[Ru(OH_2)(terpy)(6,6'-dihydroxy-2,2'-bipyridyl)](OTf)_2$ (3.16b)

[Ru(Cl)(terpy)(6,6'-dihydroxy-2,2'-bipyridyl)]Cl hydrate (**3.16**, 150.0 mg, 0.245 mmol), silver trifluoromethanesulfonate (149.6 mg, 0.582 mmol), acetone (6.0 mL), water (1.0 mL), trifluoromethanesulfonic acid (100 μL), and a stir bar were added to a vial in a glovebox. The reaction was stirred for 20 h at room temperature, and then filtered through a fine frit in the glovebox. Methanol (7 mL) was added to the solution, and diethyl ether was allowed to mix by vapor diffusion. After formation of crystals, the mixture was filtered through a medium frit, and the dark brown solid was washed with diethyl ether (3 x 5 mL). The solid was transferred to a vial and dried under oil pump

vacuum to yield [Ru(OH_2)(terpy)(6,6'-dihydroxy-2,2'-bipyridyl)] ($OTf)_2$ (**3.16b**, 154.6 mg, 0.184 mmol, 75% yield). Anal. calcd. for $C_{27}H_{21}F_6N_5O_9RuS_2$ (mol. wt. 838.67): C, 38.67; H, 2.52; N, 8.35. Found: C, 38.79; H, 2.32; N, 8.29. The addition of TfOH during the reaction was needed only in the case of making **3.16b**, which is more acidic than **8.17b**.

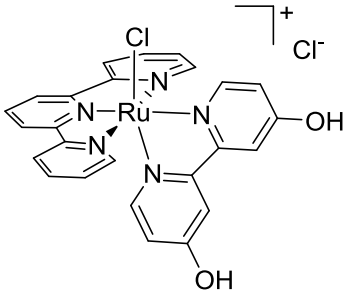

Synthesis of [Ru(Cl)(terpy)(4,4'-dihydroxy-2,2'-bipyridyl)]Cl (3.17)

To a three neck round bottom flask (100 mL) equipped with a magnetic stir bar was added a 1:1 mixture of water:ethanol (60 mL), which was deoxygenated for 30 min. $[Ru(terpy)Cl_2]_2$ (**3.13**, 0.3040 g, 0.3751 mmol) and 4,4'-dihydroxy-2,2'-bipyridine[55] (**3.8**, 0.1453 g, 0.7640 mmol) were added to the reaction flask that was heated at 80^{o}C under argon overnight. The solution was allowed to cool to room temperature before it was filtered through a Büchner funnel. The solvent of the filtrate was removed by rotary evaporation to obtain the product [Ru(Cl)(terpy)(4,4'-dihydroxy-2,2'-bipyridyl)]Cl $(H_2O)_3$ (**3.17**, 0.4007 g, 0.6021 mmol, 80 % yield). Anal. calcd. for $C_{25}H_{19}Cl_2N_5O_2Ru$ $(H_2O)_3$ (mol. wt. 665.49): C, 46.38; H, 3.89; N, 10.82. Found: C, 46.72; H, 3.41; N, 10.88.

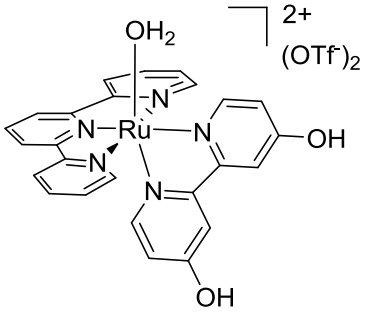

Synthesis of [Ru(OH$_2$)(terpy)(4,4'-dihydroxy-2,2'-bipyridyl)](OTf)$_2$ (3.17b)

To a vial in the glovebox added [Ru(Cl)(terpy)(4,4'-dihydroxy-2,2'-bipyridyl)]Cl (**3.17**, 150.0 mg, 0.253 mmol), silver trifluoromethanesulfonate (151.9 mg, 0.591 mmol), acetone (6 mL), water (1 mL), and stir bar. The reaction vial was placed in a 70 ^{o}C oil bath for 9.5 h, then allowed to cool to room temperature and filtered through a fine frit in the glovebox. Methanol (3 mL) was added to the solution and ether was allowed to mix by vapor diffusion. After formation of crystals, the mixture was filtered through a medium frit and the dark brown solid was washed with tetrahydrofuran (3 x 2 mL) and diethyl ether (3 x 5 mL). The solid was dissolved in a mixture of acetone and water, then solvent was removed by oil pump vacuum and dried with phosphorus pentoxide, yielding [Ru(OH$_2$)(terpy)(4,4'-dihydroxy-2,2'-bipyridyl)](OTf)$_2$ (**3.17b**, 148.0 mg, 0.176 mmol, 70% yield). Anal. calcd. for $C_{27}H_{21}F_6N_5O_9S_2Ru$ (mol. wt. 838.67): C, 38.67; H, 2.52; N, 8.35. Found: C, 38.65; H, 2.63; N, 8.40.

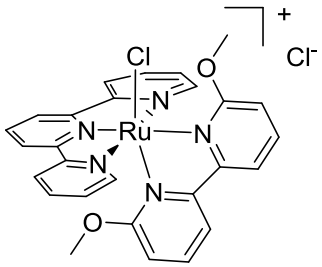

Synthesis of [Ru(Cl)(terpy)(6,6'-dimethoxy-2,2'-bipyridyl)]Cl (3.18)

To a vial in a glovebox added [Ru(terpy)Cl$_2$]$_2$ (**3.13**, 180.0 mg, 0.444 mmol) and 6,6'-dimethoxy-2,2'-bipyridyl[8] (**3.7**, 96.6 mg, 0.446 mmol), a stir bar, and methanol (12 mL). The reaction vial was placed in a 100 ^{o}C oil bath for 40 h, after which the mixture was allowed to cool to room temperature and filtered through a fine frit. Solvent in the filtrate was reduced to a minimal amount and a mixture of ethyl acetate (50 mL) and

diethyl ether (60 mL) was added. The mixture was then placed in a –20 ^{o}C freezer for 12 h, solvent was decanted and the brown solid was washed with diethyl ether (3 x 20 mL). The product was transferred to a vial and dried under oil pump vacuum with phosphorus pentoxide yielding [Ru(Cl)(terpy)(6,6'-dimethoxy-2,2'-bipyridyl)]Cl $(H_2O)_7$(**3.18**, 253.2 mg, 0.339, mmol, 76% yield). Anal. calcd. for $C_{27}H_{23}N_5O_2Cl_2Ru$ $(H_2O)_7$ (mol. wt. 747.59): C, 43.38; H, 4.99; N, 9.37. Found: C, 43.34; H, 5.24; N, 9.91.

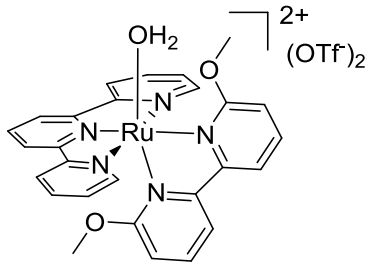

Synthesis of [Ru(OH_2)(terpy)(6,6'-dimethoxy-2,2'-bipyridyl)](OTf)$_2$ (3.18b)

To a vial in a glovebox was added [RuCl(terpy)(6,6'-dimethoxy-2,2'-bipyridyl)]Cl (**3.18**, 50.2 mg, 0.081 mmol), silver trifluoromethanesulfonate (51.3 mg, 0.200 mmol), acetone (4.5 mL), and water (0.5 mL). After 3 h the reaction was filtered through a fine frit. The brown solution was transferred to a 120 mL jar. Methanol (5 mL) was added to the solution followed by ether (100 mL), which was then cooled to -20 ^{o}C for 6.5 h. The solution was decanted leaving a brown powder. The remaining brown powder was washed with diethyl ether (3 x 10 mL), then dissolved in acetone and transferred to a vial. The decanted solution was filtered through a fine frit, the brown solid was washed with diethyl ether (3 x 10 mL) then dissolved in acetone and combined with the previous fraction. The solvent was removed by oil pump vacuum and dried with phosphorus pentoxide, yielding [Ru(OH_2)(terpy)(6,6'-dimethoxy-2,2'-bipyridyl)](OTf)$_2$ $(H_2O)_2$ (**3.18b**, 55.0 mg, 0.061 mmol, 75% yield). Anal. calcd. for $C_{29}H_{25}F_6N_5O_9S_2Ru$ $(H_2O)_2$ (mol. wt. 902.76): C, 38.58; H, 3.24; N, 7.76. Found: C, 38.79; H, 3.48; N, 7.92.

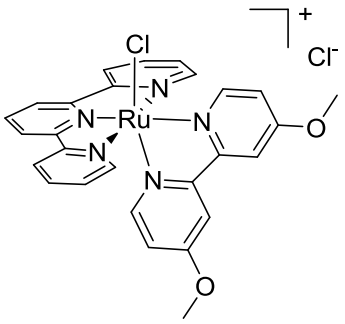

Synthesis of [Ru(Cl)(terpy)(4,4'-dimethoxy-2,2'-bipyridyl)]Cl (8.19)

To a three neck round bottom flask (100 mL) equipped with a magnetic stir bar was added a 1:1 mixture of water:ethanol (60 mL), which was deoxygenated for 30 min. $[Ru(terpy)Cl_2]_2$ (**3.13**, 0.2013 g, 0.2484 mmol) and 4,4'-dimethoxy-2,2'-bipyridine (**3.9**, 0.1078 g, 0.4985 mmol) were added to the reaction flask that was heated at 80^o C under argon overnight. The solution was allowed to cool to room temperature before it was filtered through a Büchner funnel. The solvent of the filtrate was removed by rotary evaporation to obtain the product [Ru(Cl)(terpy)(4,4'-dimethoxy-2,2'-bipyridyl)]Cl (**8.19**, 0.2654 g, 0.4693 mmol, 95% crude yield). The complex was recrystallized from methanol to obtain Ru(Cl)(terpy)(4,4'-dimethoxy-2,2'-bipyridyl)]Cl $(H_2O)_5$ (**3.19**, 0.1205 g, 0.1693 mmol, 34.1% yield). Anal. calcd. for $C_{27}H_{23}Cl_2N_5O_2Ru$ $(H_2O)_5$ (711.56): C, 45.57; H, 4.67; N, 9.84. Found: C, 45.29; H, 4.19; N, 9.83.

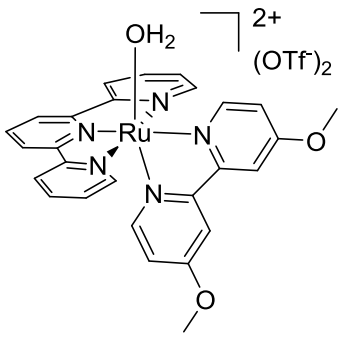

Synthesis of $[Ru(OH_2)(terpy)(4,4'-dimethoxy-2,2'-bipyridyl)](OTf)_2$ (3.19b)

To a 50 mL round bottom flask in a glovebox added [Ru(Cl)(terpy)(4,4'-dimethoxy-2,2'-bipyridyl)]Cl (**3.19**, 251.0 mg, 0.404 mmol), silver trifluoromethanesulfonate (256.2 mg, 0.997 mmol), acetone (23 mL), water (3 mL), and stir bar. The round bottom flask was equipped with a reflux condenser and refluxed for 3

h, then allowed to cool to room temperature and filtered through a fine frit in the glovebox. Methanol (5 mL) was added to the solution and diethyl ether was allowed to mix by vapor diffusion. After formation of crystals, the mixture was filtered through a medium frit. The solid was dissolved in a mixture of acetone and water, then solvent was removed by oil pump vacuum and dried with phosphorus pentoxide, yielding [Ru(OH_2)(terpy)(4,4'-dimethoxy-2,2'-bipyridyl)]($OTf)_2$ (**3.19b**, 231.4 mg, 0.267 mmol, 66% yield). Anal. calcd. for $C_{27}H_{21}F_6N_5O_9S_2Ru$ (mol. wt. 866.73): C, 40.19; H, 2.91; N, 8.08. Found: C, 39.99; H, 2.80; N, 8.01.

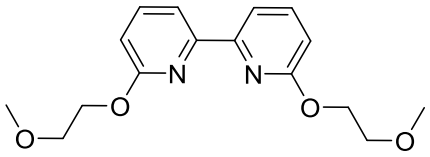

Synthesis of 6,6'-bis(2-methoxyethoxy)-2,2'-bipyridine (3.22)

To a 15 mL two neck round bottom flask in a glovebox was added toluene (4.0 mL), sodium hydride 95 % (110.6 mg, 4.38 mmol), and 2-methoxyethanol (408.0 mg, 5.36 mmol). After five minutes hydrogen gas stopped evolving and 6,6'-dibromo-2,2'-bipyridine[27] (**3.21**, 478.5 mg, 1.52 mmol) was added. Keeping the reaction under nitrogen a reflux condenser with a nitrogen inlet and a Teflon stopper were installed on the flask, and the mixture was refluxed for 41 h. After cooling to room temperature the reaction was diluted with ethyl acetate (8 mL) and washed with water (3 x 6 mL) and brine (4 mL). The organic layer was dried with Na_2SO_4, filtered through a pipet loaded with cotton and solvent was removed by rotary evaporation. The residual solid was purified by kugelrohr distillation, collecting product at 230 mtorr from 140 to 150 ^oC. The white solid was transferred to a vial using ether and dried under oil pump vacuum, yielding 6,6'-bis(2-methoxyethoxy)-2,2'-bipyridine (**3.22**, 174.9 mg, 0.575 mmol, 38 % yield). Anal. calcd. for $C_{16}H_{20}N_2O_4$ (mol. wt. 304.35): C, 63.14; H, 6.62; N, 9.20. Found: C, 62.83; H, 6.81; N, 9.43.

^1H NMR ($CDCl_3$, 499.94 MHz) δ 7.94 (d, *J* = 7.3 Hz, 2H), 7.66 (t, *J* = 7.8 Hz, 2H), 6.79 (d, *J* = 8.3 Hz, 2H), 4.60-4.58 (m, 4H), 3.80-3.78 (m, 4H), 3.45 ppm (s, 6H). ^{13}C NMR ($CDCl_3$, 125.723 MHz) 162.7, 153.1, 139.2, 113.7, 111.3, 71.0, 64.6, 59.0 ppm.

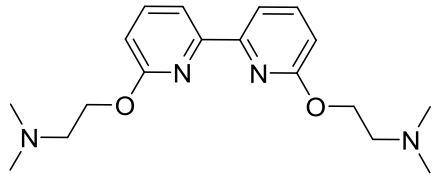

Synthesis of 6,6'-bis(2-(*N*,*N*-dimethylamino)ethoxy)-2,2'-bipyridine (3.23)

To a 25 mL two neck round bottom flask in a glovebox was added toluene (12.0 mL), stir bar, sodium hydride 95 % (227.8 mg, 9.49 mmol), and 2-*N*,*N*-dimethylaminoethanol (950.6 mg, 10.66 mmol). After 50 min hydrogen gas stopped evolving and 6,6'-dibromo-2,2'-bipyridine[27] (**3.21**, 942.9 mg, 3.00 mmol) was added. Keeping the reaction under nitrogen a reflux condenser with a nitrogen inlet was installed, and the mixture heated under reflux for 13 h. After cooling to room temperature the reaction was diluted with ethyl acetate (20 mL) and washed with water (3 x 20 mL). The aqueous layer was back extracted with ethyl acetate (3 x 30 mL), and the organic layers were combined and washed with brine (30 mL). The organic layer was dried with Na_2SO_4, filtered through a coarse frit and solvent was removed from the filtrate by rotary evaporation. The residual solid was purified on a silica (12.2 g) column, eluting the product by starting with 97.5 % EtOAc/ 2.5 % TEA and slowly changing to 95 % EtOAc/ 5 % TEA. Fractions containing product, which has an Rf ~0.5 in 95 % EtOAc/ 5 % TEA, were combined and solvent was removed by rotary evaporation. The off-white solid was transferred to a vial and dried under oil pump vacuum yielding 6,6'-bis(2-*N*,*N*-dimethylaminoethoxy)-2,2'-bipyridine (**3.23**, 191.6 mg, 0.580 mmol, 19 % yield). Anal. calcd. for $C_{18}H_{26}N_4O_2$ (mol. wt. 330.43): C, 65.43, H, 7.93, N, 16.96; Found: C, 64.96; H, 8.01; N, 17.01.

^{1}H NMR ($CDCl_3$, 499.94 MHz) δ 7.96 (d, J = 7.6 Hz, 2H), 7.67 (t, J = 7.7 Hz, 2H), 6.79 (d, J = 8.1 Hz, 2H), 4.56 (t, J = 5.9 Hz, 4H), 2.80 (t, J = 5.9 Hz, 4H), 2.38 ppm (s, 12H).
^{13}C NMR ($CDCl_3$, 125.723 MHz) 162.9, 153.3, 139.2, 113.6, 111.4, 63.2, 58.2, 45.8 ppm.

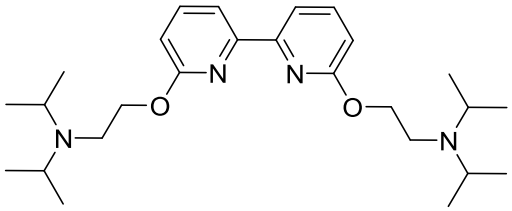

Synthesis of 6,6'-bis(2-(*N*,*N*-diisopropylamino)ethoxy)-2,2'-bipyridine (3.24)

To a 50 mL Schlenk flask in a glovebox was added toluene (7.0 mL), sodium hydride 95 % (140.0 mg, 5.83 mmol), and *N*,*N*-2-diisopropylaminoethanol (984.5 mg, 6.78 mmol). After 5 min hydrogen gas stopped evolving and 6,6'-dibromo-2,2'-bipyridine[27] (**3.21**, 604.0 mg, 1.92 mmol) was added. Keeping the reaction under nitrogen a reflux condenser with a nitrogen inlet was installed, and the mixture was heated under reflux for 13 h. After cooling to room temperature the reaction was diluted with ethyl acetate (30 mL) and washed with water (3 x 30 mL). The aqueous layer was back extracted with ethyl acetate (2 x 20 mL), and the organic layers were combined and washed with brine (30 mL). The organic layer was dried with Na_2SO_4, filtered through course frit and solvent was removed from the filtrate by rotary evaporation. The solid was purified on a silica (12.5 g) column, eluting the product by starting with 96 % hexanes/ 4 % TEA and slowly changing to 91 % hexanes/ 4 % TEA/ 5 % EtOAc. Fractions containing product were combined and solvent was removed by rotary evaporation. The product was further purified by kugelrohr distillation, collecting product at 160 mtorr and approximately 240 ^{o}C yielding a yellow oil, 6,6'-bis(*N*,*N*-2-diisopropylaminoethoxy)-2,2'-bipyridine (287.2 mg, 0.649 mmol, 34 % yield). Anal. calcd. for $C_{26}H_{42}N_4O_2$ (mol. wt. 442.65): C, 70.55; H, 9.56; N, 12.66; Found: C, 70.94; H, 9.17; N, 13.03.

^{1}H NMR ($CDCl_3$, 499.94 MHz) δ 7.99 (d, *J* = 7.3 Hz, 2H), 7.66 (d, *J* = 7.6 Hz, 2H), 6.72 (d, *J* = 8.1 Hz, 2H), 4.42-4.36 (m, 4H), 3.12-3.05 (m, 4H), 2.89-2.82 (m, 4H), 1.11-1.05 ppm (m, 24H). ^{13}C NMR ($CDCl_3$, 125.72 MHz) 163.0, 153.5, 139.1, 113.7, 111.0, 66.5, 49.7, 44.3, 20.8 ppm.

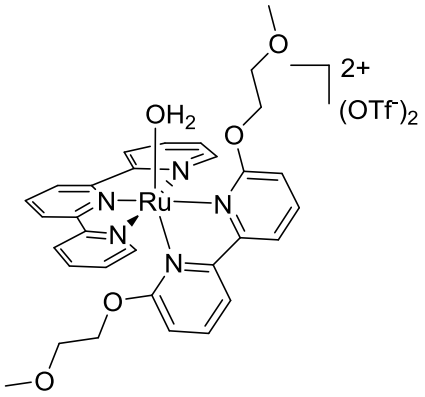

Synthesis of [Ru(OH$_2$)(terpy)(6,6'-bis(2-methoxyethoxy)-2,2'-bipyridine)](OTf)$_2$ (3.25)

[Ru(terpy)Cl$_2$]$_2$ (**3.13**, 102.9 mg, 0.124 mmol), 6,6'-bis(2-methoxyethoxy)-2,2'-bipyridine (76.1 mg, 0.250 mmol), a stir bar, and methanol (12.0 mL) were added to a vial in a glovebox. The reaction was placed in a 100 ^{o}C oil bath for 6 d, after which the cooled mixture was filtered through a medium frit and the filtrate transferred to a vial. Silver trifluoromethanesulfonate (133.0 mg, 0.518 mmol) and a stir bar were added. The reaction was further stirred at room temperature for 1 d then filtered through a fine frit, washing the frit with methanol. The product was then crystallized by vapor diffusion of diethyl ether into the methanol solution. After solid formed, the mixture was filtered through a fine frit and washed with diethyl ether (3 x 5 mL), and the dark brown solid was transferred to a vial and dried under oil pump vacuum yielding [Ru(OH$_2$)(terpy)(6,6'-bis(2-methoxyethoxy)-2,2'-bipyridine)](OTf)$_2$ (H$_2$O)$_2$ (**3.25**, 173.7 mg, 0.175 mmol, 71 % yield). Anal. calcd. for $C_{33}H_{33}F_6N_5O_{11}RuS_2$ (H$_2$O)$_2$ (mol. wt. 990.86): C, 40.00; H, 3.76; N, 7.07; Found: C, 40.00; H, 3.37; N,7.27.

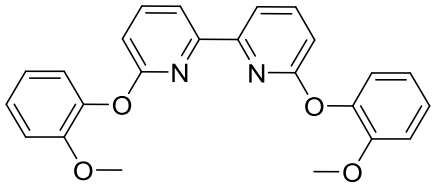

Synthesis of 6,6'-bis(2-methoxyphenoxy)-2,2'-bipyridine (3.28)

To a pressure vial (48 mL) with magnetic stir bar were added in a glovebox picolinic acid (0.3020 g, 2.45 mmol), K$_3$PO$_4$ (5.1025 g, 24.0 mmol), CuI (0.2288 g, 1.20 mmol), guaiacol (1.8822 g, 15.2 mmol), 6,6'-dibromo-2,2'-bipyridine[27] (**3.21**, 1.885 g, 6.00 mmol), and DMSO (24.0 mL). The reaction was placed in an oil bath at 90° C for 64

h. The reaction was diluted with DCM (100 mL) and transferred to a separatory funnel where it was washed with water (100 mL). The aqueous layer was extracted with DCM (70 mL), the organic layers were combined and washed with water (3 x 100 mL), brine (100 mL) and dried over sodium sulfate. The solution was filtered through a course frit and the filtrate concentrated by rotary evaporation. The residual solid was dissolved in hot ethyl acetate and was left to crystallize in the freezer. After formation of solid the mixture was filtered through a medium frit and the solid washed with pentanes. The white solid was again dissolved in hot ethyl acetate and crystals formed at room temperature. After formation of crystals the white solid was filtered through a medium frit and washed with pentanes, transferred to a vial and dried under oil pump vacuum, yielding 6,6'-bis(2-methoxyphenoxy)-2,2'-bipyridine $(C_4H_8O_2)_{0.2}$ (**3.28**, 0.2185 g, 0.523 mmol, 8.7% yield). Anal. calcd. for $C_{24}H_{20}N_2O_4$ $(C_4H_8O_2)_{0.2}$ (mol. wt. 418.06): C, 71.25; H. 5.21; N, 6.70; Found: C, 70.96; H, 5.48; N, 7.02. [$C_4H_8O_2$ = ethyl acetate]
^{1}H NMR ($CDCl_3$, 499.944 MHz) δ 7.78 (d, *J* = 7.6 Hz, 2H), 7.65 (t, *J* = 7.8 Hz, 2H), 7.25-7.19 (m, 4H), 7.04-6.99 (m, 4H), 6.79 (d, *J* = 8.1 Hz, 2H), 3.76 ppm (s, 6H). ^{13}C NMR ($CDCl_3$, 125.723 MHz) 162.9, 153.5, 152.0, 142.7, 139.9, 125.8, 123.1, 121.0, 115.2, 112.7, 110.1, 55.9 ppm.

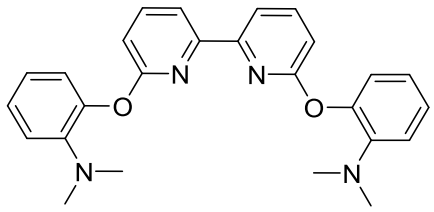

Synthesis of 6,6'-bis(2-(*N*,*N*-dimethylamino)phenoxy)-2,2'-bipyridine (3.29)

To a three neck round bottom flask (25 mL) with magnetic stir bar in the glovebox were added picolinic acid (0.1238 g, 1.01 mmol), K_3PO_4 (2.1180 g, 9.98 mmol), CuI (0.0950 g, 0.50 mmol), 2-(*N*,*N*-dimethylamino)phenol (0.9066 g, 6.61 mmol), 6,6'-bis(bromo)-2,2'-bipyridine[27] (**3.21**, 0.7860 g, 2.50 mmol), and DMSO (10.0 mL) were added in a glovebox. The reaction was placed in an oil bath at 90° C for 3 d. The reaction was diluted with DCM (100 mL) and transferred to a separatory funnel where it was washed with water (100 mL). The aqueous layer was extracted with DCM

(2 x 50 mL), and the organic layers were combined and washed with water (100 mL) which created an emulsion. The solution was concentrated by rotary evaporation. The obtained oil was purified on a silica (11.5 g) column, eluting the product by starting with 100% hexanes and slowly changing to 80 % hexanes/ 20 % diethyl ether. Fractions containing product, which has an Rf ~0.25 in 80 % hexanes/ 20 % diethyl ether, were combined and solvent was removed by rotary evaporation. The column was repeated and this time fractions containing only product were combined The white solid was transferred to a vial and dried under oil pump vacuum yielding (**3.29**, 0.1314 g, 0.308 mmol, 12 % yield). Anal. calcd. for $C_{26}H_{26}N_4O_2$ (mol. wt. 426.52): C, 73.22; H, 6.14; N, 13.14; Found: C, 72.67; H, 6.54; N, 13.22.

^{1}H NMR ($CDCl_3$, 499.94 MHz) δ 7.89 (d, *J* = 7.5 Hz, 2H), 7.66 (t, *J* = 7.8 Hz, 2H), 7.18 (ddd, *J* = 8.0, 7.3, 1.4 Hz, 2H), 7.12 (dd, *J* = 8.0, 1.3 Hz, 2H), 7.05 (br d, *J* = 7.0 Hz, 2H), 6.98 (br t, *J* = 7.4 Hz, 2H), 2.79 ppm (s, 12H). ^{13}C NMR ($CDCl_3$, 125.723 MHz) 162.8, 153.8, 146.1, 145.5, 139.9, 125.4, 123.2, 121.5, 118.6, 115.5, 110.5, 43.0 ppm.

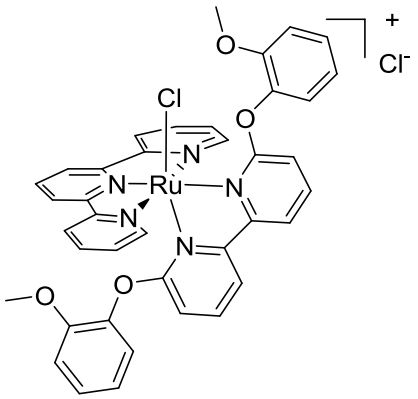

Synthesis of [Ru(Cl)(terpy)(6,6'-bis(2-methoxyphenoxy)-2,2'-bipyridine)]Cl (3.30)

[Ru(terpy)Cl_2]$_2$ (**3.13**, 105.0 mg, 0.127 mmol), 6,6'-bis(2-methoxyphenoxy)-2,2'-bipyridine (**3.28**, 121.1 mg, 0.290 mmol), a stir bar, and methanol (9.0 mL) were added to a vial in a glovebox. The reaction was placed in a 100 ^{o}C oil bath for 144 h. After cooling to room temperature the reaction was filtered through a medium frit which was washed with methanol. The filtrate was reduced under vacuum to a minimal volume and ether was mixed by vapor diffusion. The dark solid was filtered through a medium frit and washed with ether and dried under oil pump vacuum, yielding [Ru(OH_2)(terpy)(6,6'-bis(2-methoxyphenoxy)-2,2'-bipyridine)](OTf)$_2$. (H_2O)$_4$ (**3.30**, 166.6 mg, 0.190 mmol, 75

% yield). Anal. calcd. for $C_{39}H_{31}Cl_2N_5O_4Ru$ $(H_2O)_4$ (mol. wt. 877.74): C, 53.37; H, 4.48; N, 7.98; Found: C, 53.26; H, 4.78; N, 8.13.

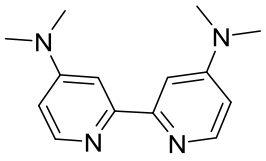

Synthesis of 4,4'-bis(*N*,*N*-dimethylamino)-2,2'-bipyridyl (3.35)

To a two neck round bottom flask (25 mL) in a glovebox was added 4,4'-diamino-2,2'-bipyridine[30] (**3.33**, 250.8 mg, 1.347 mmol) and a stir bar. To a vial in a glovebox added 95% sodium hydride (178.0 mg, 7.046 mmol) and DMF (10.0 mL), and the mixture was transferred to a syringe as a slurry. The round bottom flask was transferred to a hood, and while keeping under nitrogen a N_2 inlet and septum were placed on the flask. The DMF/sodium hydride mixture was added to the round bottom flask, giving a brown heterogeneous solution. The reaction was then placed in an ice bath, and once the solution was cold methyl iodide (790.6 mg, 5.570 mmol) was added dropwise over 5 min, giving a white heterogeneous solution. The mixture was allowed to stir at 0 ^oC for 1 h, followed by warming to room temperature. The reaction was monitored by ^1H NMR spectroscopic analysis of aliquots. After 2 d more MeI (15 μL, 7.5 μL, 5 μL) was added which resulted in no substantial change to the reaction mixture. DCM (25 mL) was added to the reaction followed by H_2O (15 mL). In a separatory funnel, the organic layer was washed with water (3 x 20 mL) and brine (10 mL). The organic layer was then dried with sodium sulfate and filtered through a course frit. Solvent was removed by rotary evaporation, and the obtained brown solid was transferred to a fine frit and washed with acetone (3 x 1 mL). The off-white solid was transferred to a vial and dried under oil pump vacuum to yield 4,4'-bis(*N*,*N*-dimethylamino)-2,2'-bipyridyl (**3.35**, 140.6 mg, 0.540 mmol, 40 % yield) Anal. calcd. for $C_{14}H_{18}N_4$ (H_2O) (mol. wt. 260.34): C, 64.59; H, 7.74; N, 21.52; found: C, 64.78; H, 7.45; N, 21.77.

^1H NMR ($CDCl_3$, 499.944 MHz) δ 8.30 (d, J = 6.1 Hz, 2H), 7.68 (d, J = 2.7 Hz, 2H), 6.50 (dd, J = 5.9, 2.7 Hz, 2H), 3.08 ppm (s, 12H). ^{13}C NMR ($CDCl_3$, 125.723 MHz) δ 156.9, 155.2, 149.0, 106.4, 104.0, 39.3 ppm.

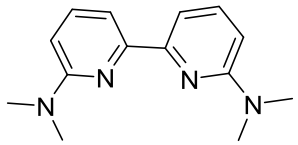

Synthesis of 6,6'-bis(*N*,*N*-dimethylamino)-2,2'-bipyridyl (3.36)

To a two neck round bottom flask (15 mL) in a glovebox was added 6,6'-diamino-2,2'-bipyridyl[31] (**3.34**, 189.1 mg, 1.02 mmol), 95 % sodium hydride (129.4 mg, 5.39 mmol), and a stir bar. Keeping the reaction under nitrogen the round bottom flask was equipped with a nitrogen inlet and a rubber septa. The reaction was cooled in an ice bath and DMF (6.0 mL) was added followed by MeI (617.3 mg, 4.35 mmol). After stirring for 45 min the reaction was warmed to room temperature and allowed to stir for 4.5 h. Solvent was removed under oil pump vacuum, and the residue dissolved in DCM (10 mL). The organic layer was washed with water (4 x 5 mL) and brine (3 mL), then dried with Na_2SO_4, which was filtered through a pipet loaded with cotton. Solvent was removed by a flow of air. The crude product was dissolved in DCM followed by the addition of silica (0.45 g), and solvent was removed under oil pump vacuum. The crude product on silica was loaded on top of a silica (5.0 g) column with hexanes (100 %). Ethyl acetate (10%) was slowly introduced to the eluding solvent mixture. The fractions with material R_f = 0.2 (Hexanes:EtOAc 90:10), which are green under longwave UV, were combined and solvent was removed by rotary evaporation followed by oil pump vacuum to obtain a white solid, 6,6'-bis(*N*,*N*-dimethylamino)-2,2'-bipyridyl (**3.36**, 70.9 mg, 0.293 mmol, 29 % yield). Anal. calcd. for $C_{14}H_{18}N_4$ (mol. wt. 242.33): C, 69.39; H, 7.49; N, 23.12. Found: C, 69.36; H, 7.80; N, 23.39.

^{1}H NMR ($CDCl_3$, 599.394 MHz) δ 7.72 (dd, *J* = 7.5 Hz, 0.6 Hz, 2H), 7.57 (dd, *J* = 8.4 Hz, 7.5 Hz, 2H), 6.54 (dd, *J* = 8.4 Hz, 0.6 Hz, 2H), 3.17 ppm (s, 12H). ^{13}C NMR ($CDCl_3$, 150.72 MHz) δ 158.8, 154.8, 137.7, 108.7, 105.6, 38.0 ppm.

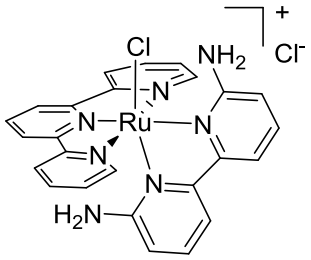

Synthesis of [Ru(terpy)(6,6'-diamino-2,2'-bipyridyl)(Cl)]Cl (3.37)

[2,2'-bipyridyl-6,6'-diaminium] dichloride (**3.34-2HCl**, 54.0 mg, 0.21 mmol), Amberjet 4400 OH strongly basic resin (348.6 mg) and methanol (3 mL), were added in a glovebox to a vial and allowed to stand for 20 min. To another vial in a glovebox was added $[Ru(terpy)Cl_2]_2$ (**3.13**, 90.5 mg, 0.11 mmol) and a stir bar, into which was filtered through a pipet loaded with cotton the transferred 6,6'-diamino-2,2'-bipyridyl mixture. The vial from neutralization of the 6,6'-diamino-2,2'-bipyridyl HCl salt was rinsed with methanol (2 x 1.5 mL), at which point a total of 6 mL of methanol was in the reaction. The sealed reaction vial was placed in a 100 ^{o}C oil bath for 30 h, then allowed to cool to room temperature and filtered through a fine frit. Solvent in the filtrate was reduced to a minimal amount and ether was allowed to mix by vapor diffusion. After formation of crystals, the mixture was filtered through a medium frit and the dark solid was washed with diethyl ether (3 x 2 mL). The solid was transferred to a vial and placed under oil pump vacuum, yielding [RuCl(terpy)(6,6'-diamino-2,2'-bipyridyl)]Cl $(H_2O)_2$ (**3.37**, 65.7 mg, 0.105 mmol, 50 % yield). Anal. calcd. for $C_{25}H_{21}Cl_2N_7Ru$ $(H_2O)_2$ (mol. wt. 627.49): C, 47.85; H, 4.02; N, 15.63. Found: C, 48.38; H, 4.44; N, 15.57.

This reaction was also done with the neutral 6,6'-diamino-2,2'-bipyridyl ligand which was synthesized from 6,6'-dibromo-bipyiridine by the same method as Ihara[31] et al.

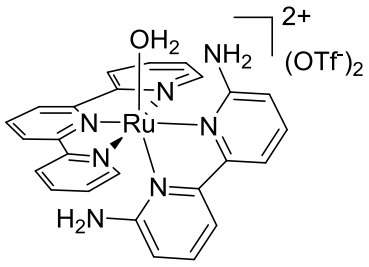

Synthesis of [Ru(OH$_2$)(terpy)(6,6'-diamino-2,2'-bipyridyl)](OTf)$_2$ (3.37b)

To a vial in the glovebox [RuCl(terpy)(6,6'-diamino-2,2'-bipyridyl)]Cl (**3.37**, 40.0 mg, 67.6 µmol), silver trifluoromethanesulfonate (36.3 mg, 141.3 µmol), a stir bar, acetone (3 mL), and water (1 mL) were added. The reaction was stirred for 2.75 h then filtered through a fine frit. The frit was rinsed with acetone (3 x 1 mL) and solvent removed under oil pump vacuum to obtain [Ru(OH$_2$)(terpy)(6,6'-diamino-2,2'-bipyridyl)](OTf)$_2$ (H$_2$O)$_2$ (**3.37b**, 56.1 mg, 64.3 µmol, 95 % yield). Anal. calcd. for $C_{27}H_{23}F_6N_7O_7RuS_2$ (H$_2$O)$_2$ (mol. wt. 872.73): C, 37.16; H, 3.12; N, 11.23. Found: C, 36.79; H, 2.73; N, 11.11.

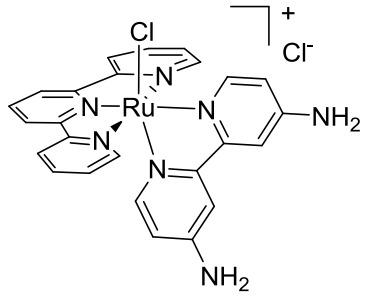

Synthesis of [Ru(Cl)(terpy)(4,4'-diamino-2,2'-bipyridyl)]Cl (3.38)

[Ru(terpy)Cl$_2$]$_2$ (**3.13**, 135.0 mg, 0.163 mmol), 4,4'-diamino-2,2'-bipyridine[30] (**3.33**, 62.2 mg, 0.334 mmol), a stir bar, and methanol (12 mL) were added to a vial in a glovebox. The reaction vial was placed in a 100 °C oil bath for 3 d, then cooled to room temperature and filtered through a medium frit. Solvent in the filtrate was reduced to approximately 5 mL, and diethyl ether was allowed to mix by vapor diffusion. After formation of crystals, the mixture was filtered through a medium frit, and the dark solid was washed with diethyl ether (3 x 5 mL). The solid was transferred to a vial and dried under oil pump vacuum to yield [Ru(Cl)(terpy)(4,4'-diamino-2,2'-bipyridyl)]Cl (H$_2$O)$_2$

(**3.38**, 151.6 mg, 0.242 mmol, 74% yield). Anal. calcd. for $C_{25}H_{21}Cl_2N_7Ru$ $(H_2O)_2$ (mol. wt. 627.49): C, 47.85; H, 4.02; N, 15.63. Found C 47.58, H 4.27, N 15.51.

It should be noted that attempts at ionization using AgOTf in the case of $[Ru(OH_2)(terpy)(4,4'\text{-diamino-}2,2'\text{-bipyridyl})](OTf)_2$ gave reaction mixtures that proved to be sensitive and the product was not isolable.

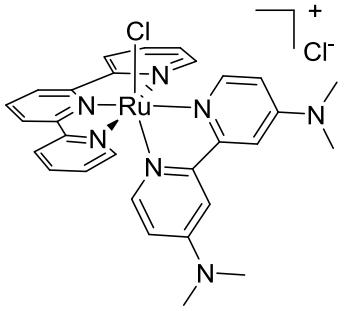

Synthesis of [Ru(terpy)(4,4'-bis(*N*,*N*-dimethylamino)-2,2'-bipyridyl)(Cl)]Cl (3.40)

$[Ru(terpy)Cl_2]_2$ (**3.13**, 150.0 mg, 0.181 mmol), 4,4'-bis(*N*,*N*-dimethylamino)-2,2'-bipyridine (**3.35**, 89.4 mg, 0.369 mmol), a stir bar, and methanol (13 mL) were added to a vial in a glovebox. The reaction vial was placed in a 100 °C oil bath for 3 d, then cooled to room temperature and filtered through a fine frit, rinsing the frit with methanol (5 mL). Diethyl ether was allowed to mix by vapor diffusion. After formation of crystals, the mixture was filtered through a fine frit, and the dark solid was washed with diethyl ether (3 x 4 mL). The solid was transferred to a vial and dried under oil pump vacuum to yield [Ru(terpy)(4,4'-bis(*N*,*N*-dimethylamino)-2,2'-bipyridyl)(Cl)]Cl $(H_2O)_{2.5}$ (**3.40**, 130.4 mg, 0.188 mmol, 52 % yield). $C_{29}H_{29}Cl_2N_7Ru$ $(H_2O)_{2.5}$ (mol. wt. 692.61): Anal. calcd. for C, 50.29; H, 4.95; N, 14.16; Found C, 50.49; H, 5.63; N, 14.26.

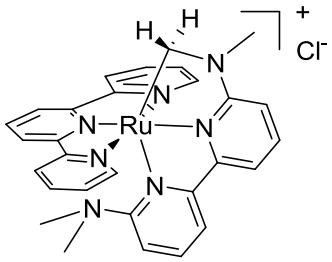

Synthesis of [Ru(terpy)(6,6'-bis(*N*,*N*-dimethylamino)-2,2'-bipyridyl)(Cl)]Cl (3.41)

$[Ru(terpy)Cl_2]_2$ (**3.13**, 101.0 mg, 0.125 mmol), 6,6'-bis(N,N-dimethylamino)-2,2'-bipyridine (**3.36**, 59.8 mg, 0.247 mmol), a stir bar, and methanol (40 mL) were added to a

pressure vessel (150 mL) in a glovebox. The reaction mixture was heated in a 100 ^{o}C oil bath for 8 d. The product was purified on a neutral alumina (8.0 g) column by eluting with a mixture of acetone and methanol, starting at 100 % acetone and continuing until starting ligand **3.36** eluted, and then increasing polarity to 4 % methanol, which eluted a purple material. The purple fractions were combined and solvent was removed by rotary evaporation and the residue dried under oil pump vacuum. The solid was dissolved in d_6-acetone and water and then characterized by NMR spectrometry, showing evidence for structure **3.41** (see text).

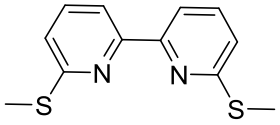

Synthesis of 6,6'-bis(methylthio)-2,2'-bipyridine (3.42)

To a 25 mL two neck round bottom flask was added a stir bar, and an N_2 adapter and rubber septum were installed. The reaction vessel was purged with nitrogen, and dimethyl disulfide (950 µL, 10.7 mmol) and dry THF (10.0 mL) were added. The reaction was cooled in a Dry Ice/acetone bath and n-BuLi in hexanes (4.2 mL, 2.5 M, 10.5 mmol) was added dropwise via syringe over 30 min. The reaction was allowed to warm to room temperature and solvent was removed under oil pump vacuum. A slurry of 6,6'-dibromo-2,2'-bipyridine[27] (**3.21**, 1.4993 g, 4.78 mmol) in DMF (10.0 mL) was added to the lithium thiomethoxide via syringe. The reaction stirred for 1.5 h, then transferred to a separatory funnel with ethyl acetate (100 mL) where it was washed with water (4 x 100 mL) and brine (50 mL). The organic layer was dried with Na_2SO_4 and filtered through a course frit. From the filtrate, solvent was reduced by rotary evaporation, and residual solid was transferred to a vial and dried under oil pump vacuum yielding 6,6'-bis(methylthio)-2,2'-bipyridine (**3.42**, 1.0005 g, 4.03 mmol, 84 % yield). Anal. calcd. for $C_{12}H_{12}N_2S_2$ (mol. wt. 248.36): C, 58.03; H, 4.87; N, 11.28; Found: C, 57.88; H, 4.97; N, 11.36.

^{1}H NMR ($CDCl_3$, 599.394 MHz) δ 8.17 (d, J = 7.6 Hz, 2H), 7.61 (t, J = 7.8 Hz, 2H), 7.20 (d, J = 7.9 Hz, 2H), 2.68 ppm (s, 6H). ^{13}C NMR ($CDCl_3$, 150.72 MHz) δ 158.9, 155.4, 136.5, 121.7, 116.3, 13.2 ppm.

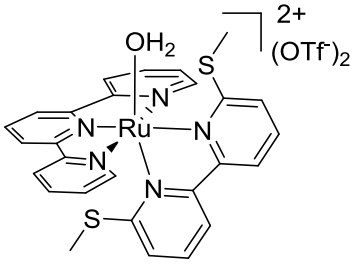

Synthesis of [Ru(OH$_2$)(terpy)(6,6'-bis(methylthio)-2,2'-bipyridine)] (OTf)$_2$ (3.43)

[Ru(terpy)Cl$_2$]$_2$ (**3.13**, 151.1 mg, 0.182 mmol), 6,6'-bis(methylthio)-2,2'-bipyridine (**3.42**, 92.0 mg, 0.370 mmol), a stir bar, and methanol (10 mL) were added to a vial in a glovebox. The reaction was placed in a 100 ^{o}C oil bath for 2 d then let cool to room temperature and filtered through a fine frit. Solvent of the filtrate was removed and in a glovebox silver trifluoromethanesulfonate (204.8 mg, 0.797 mmol), acetone (9.0 mL), and water (1.0 mL) were added to the vial. After 4 d of stirring the mixture was filtered through a fine frit and diethyl ether was allowed to mix by vapor diffusion. After formation of crystals, the mixture was filtered through a medium frit and the dark solid was washed with diethyl ether (3 x 5 mL). The solid was transferred to a vial and dried under high vacuum with phosphorus pentoxide, yielding [Ru(OH$_2$)(terpy)(6,6'-bis(methylthio)-2,2'-bipyridine](OTf)$_2$ (H$_2$O) (**3.43**, 276.8 mg, 0.302 mmol, 83 % yield). Anal. calcd. for $C_{29}H_{25}F_6N_5O_7RuS_4$ (H$_2$O) (mol. wt. 916.86): C, 37.99; H, 2.97; N, 7.64; Found: C, 37.78; H, 3.04; N, 7.65.

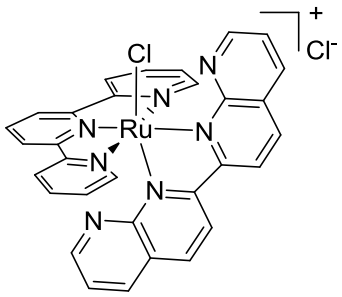

Synthesis of [Ru(terpy)(2,2'-bisnaphthyridineCl)]Cl (3.44)

[Ru(terpy)Cl$_2$]$_2$ (**3.13**, 90.9 mg, 0.110 mmol), 2,2'-bisnaphthyridine[56] (59.1 mg, 0.229 mmol), a stir bar, and methanol (6 mL) were added to a vial in a glovebox. The reaction vial was placed in a 100 ^{o}C oil bath for 24 h then cooled to room temperature and filtered through a fine frit. Solvent of the filtrate was reduced to a minimal amount; diethyl ether was allowed to mix by vapor diffusion. After formation of crystals, the

mixture was filtered through a fine frit and the dark solid was washed with diethyl ether (3 x 2 mL). The solid was transferred to a vial and dried under oil pump vacuum to yield [Ru(terpy)(2,2'-bisnaphthyridine)Cl]Cl $(H_2O)_{5.5}$ (**3.44**, 131.8 mg, 0.173 mmol, 79 % yield). Anal. calcd. for $C_{25}H_{21}Cl_2N_7Ru$ $(H_2O)_{5.5}$ (mol. wt. 762.61): C, 48.82; H, 4.23; N, 12.86; Found: C, 48.89; H, 4.09; N, 13.09.

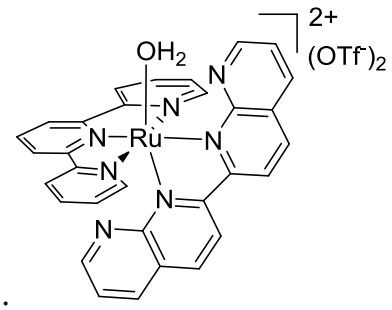

.

Synthesis of [Ru(OH$_2$)(terpy)(2,2'-bisnaphthyridine)](OTf)$_2$ (3.44b)

[Ru(terpy)(2,2'-bisnaphthyridine)Cl]Cl (**3.44**, 60.2 mg, 0.079 mmol), silver trifluoromethanesulfonate (47.6 mg, 0.185 mmol), acetone (0.3 mL), water (0.2 mL), and a stir bar were added to a vial in a glovebox. The reaction stirred at room temperature for 25 h, then filtered through a fine frit in the glovebox, and acetone (5 mL) was used to rinse the frit. Solvent of the filtrate was removed under oil pump vacuum, and the residual solid was dissolved in methanol (2 mL). Ether was allowed to mix by vapor diffusion; after formation of crystals, the mixture was filtered through a medium frit and the dark solid was washed with diethyl ether (3 x 4 mL). The solid was dissolved in a mixture of acetone (2 mL) and water (1 mL), which was removed by oil pump vacuum and the residual solids were dried under oil pump vacuum with phosphorus pentoxide, yielding [Ru(OH$_2$)(terpy)(2,2'-bisnaphthyridine)](OTf)$_2$ (**3.44b**, 70.7 mg, 0.078 mmol, 98% yield). Anal. calcd. for $C_{33}H_{23}F_6N_7O_7RuS_2$ (mol. wt. 908.77): C, 43.62; H, 2.55; N, 10.79. Found: C, 43.12; H, 2.07; N, 10.60.

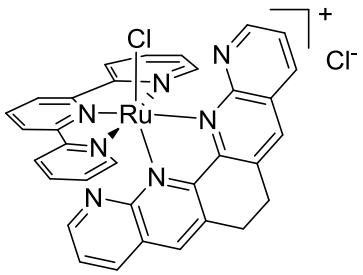

Synthesis of [Ru(Cl)(terpy)(3,3'-Dimethylene-2,2'-bisnaphthyridine)]Cl (3.45)

$[Ru(terpy)Cl_2]_2$ (**3.13**, 90.6 mg, 0.109 mmol), 3,3'-dimethylene-2,2'-bisnaphthyridine[56] (64.0 mg, 0.225 mmol), a stir bar, and methanol (6 mL) were added to a vial in a glovebox. The reaction was placed in a 100 ^{o}C oil bath for 24 h then let cool to room temperature and filtered through a medium frit. Solvent of the filtrate was reduced to a minimal amount and diethyl ether was allowed to mix by vapor diffusion. After formation of crystals, the mixture was filtered through a medium frit and the dark green solid was washed with acetone (3 x 1mL) and diethyl ether (3 x 2 mL). The solid was transferred to a vial and dried under high vacuum yielding [RuCl(terpy)(3,3'-dimethylene-2,2'-bisnaphthyridine)Cl]Cl $(H_2O)_{3.5}$ (**3.45**, 142.8 mg, 0.190 mmol, 87 % yield). Anal calcd. for $C_{33}H_{23}Cl_2N_7Ru$ $(H_2O)_{3.5}$ (mol. wt. 752.62): C, 52.66; H, 4.02; N, 13.03. Found: C, 52.47; H, 3.76; N, 13.36.

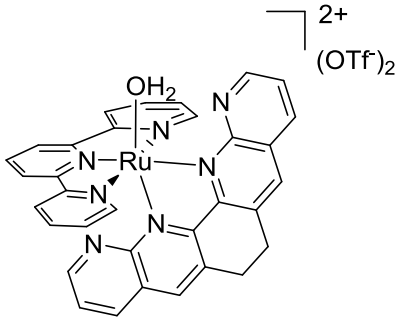

Synthesis of [Ru(OH_2)(terpy)(3,3'-dimethylene-2,2'-bisnaphthyridine)]$(OTf)_2$ (3.45b)

To a vial in the glovebox were added to a vial [Ru(terpy)(3,3'-dimethylene-2,2'-bisnaphthyridine)Cl]Cl (**3.45**, 60.6 mg, 0.081 mmol), silver trifluoromethanesulfonate (41.0 mg, 0.160 mmol), acetone (0.3 mL), water (0.2 mL), and stir bar. The reaction was stirred at room temperature for 25 h, then filtered through a fine frit in the glovebox, rinsing the frit with acetone (5 mL). Solvent was removed under oil pump vacuum, and

the residue was dissolved in methanol (2.5 mL) and ether was allowed to mix by vapor diffusion. After formation of crystals, the mixture was filtered through a medium frit and the dark solid was washed with diethyl ether (3 x 4 mL). The solid was dissolved in a mixture of acetone (2 mL) and water (1 mL), then solvent was removed by oil pump vacuum and dried with phosphorus pentoxide, yielding [$Ru(OH_2)$(terpy)(3,3'-dimethylene-2,2'-bisnaphthyridine)]$(OTf)_2$ (**3.45b**, 60.6 mg, 0.065 mmol, 81% yield). Anal calcd. for $C_{35}H_{25}F_6N_7O_7RuS_2$ (mol. wt. 934.81): C, 44.97; H, 2.70; N, 10.49. Found: C, 43.12; H, 2.07; N, 10.60.

The PF_6 analog of this complex has been synthesized by Thummel et al.[37]

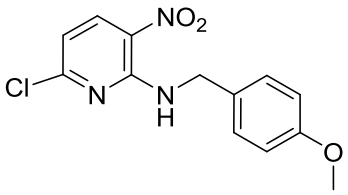

Synthesis of 6-chloro-2-(4-methoxybenzylamine)-3-nitropyridine (3.47)

In the glovebox to a 250 mL three neck round bottom flask was added 2,6-dichloro-3-nitropyridine (**3.46**, 15.04 g, 77.9 mmol, 1 equiv), dry triethylamine (10.2570 g, 101.4 mmol, 1.3 equiv), a stir bar, and dry THF (120 mL). The flask was equipped with a thermometer, addition funnel, and nitrogen inlet. Outside the glovebox, the reaction was cooled in an acetone/ice bath and the addition funnel was charged with 4-methoxybenzylamine (12.2765 g, 89.5 mmol, 1.15 equiv), which was added dropwise over 20 min, whereupon a bright yellow precipitate formed. The reaction was allowed to warm to room temperature and stirred for 3 h. At room temperature was added more 4-methoxybenzylamine (0.502 g, 3.7 mmol, 0.05 equiv) and stirring continued for 45 min. The reaction mixture was transferred to a 500 mL round bottom flask to remove solvent by rotary evaporation. The residual yellow oil was transferred to a 2 L separatory funnel with diethyl ether (1.0 L) and the resulting solution shaken with aq. NaH_2PO_4 (300 mL, 5%). The aqueous phase was extracted with diethyl ether (2 x 200 mL). Combined organic layers were washed with aq. NaH_2PO_4 (200 mL), saturated aq. sodium carbonate (350 mL), brine (100 mL) then dried with magnesium sulfate. The mixture was filtered through a course frit into a round bottom flask and solvent was removed by rotary

evaporation followed by storage under oil pump vacuum to obtain the crude yellow solid, 6-chloro-2-(4-methoxybenzylamine)-3-nitropyridine (**3.47**, crude 23.7 g) used without purification.

^{1}H NMR ($CDCl_3$, 500 MHz) δ 8.54 (broad s, 1H), 8.36 (d, *J* = 8.5 Hz, 1H), 7.34-7.31 (m, 2H), 6.92-6.89 (m, 2H), 6.65 (d, *J* = 8.5 Hz, 1H), 4.75 (d, *J*= 5.5 Hz, 2H), 3.82 ppm (s, 3H).

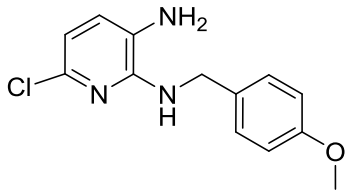

Synthesis of 6-chloro-2-(4-methoxybenzylamine)-3-aminopyridine (3.48)

To a 500 mL Parr hydrogenation bottle were added 5% sulfided Pt/C (0.738 g) and THF (35 mL). To an Erlenmeyer flask was added crude 6-chloro-2-(4-methoxybenzylamine)-3-nitropyridine (**3.47**, 11.60 g, 46.6 mmol) followed by THF (75 mL), making a solution which was then transferred to the Parr bottle containing the Pt/C. The Erlenmeyer flask was rinsed with THF (75 mL) and the solution transferred to the Parr bottle. The Parr bottle was flushed with 50 psi hydrogen gas three times using a hydrogenator then kept at 50 psi hydrogen while being shaken for 6 h. The reaction was filtered through Celite, blowing nitrogen over the filtration mixture. The Celite was rinsed with THF (100 mL) and the combined filtrates dried with sodium sulfate. After filtration through a course frit into a round bottom flask, solvent was removed by rotary evaporation. The same reaction was repeated using more crude 6-chloro-2-(4-methoxybenzylamine)-3-aminopyridine (**3.47**, 11.55 g, 46.4 mmol) and 5% sulfided Pt/C (0.738 g) then the two crude product fractions were combined and used without further purification.

^{1}H NMR ($CDCl_3$, 500 MHz) δ 7.33 (d, *J* = 8.5 Hz, 2H), 6.90-6.88 (m, 2H), 6.82 (d, *J* = 8.0 Hz, 1H), 6.53 (d, *J* = 8.0 Hz, 1H), 4.54 (d, *J* = 8.0 Hz, 2H), 4.43 (broad s, 1H), 3.82 (s, 3H), 3.11 ppm (broad s, 2H).

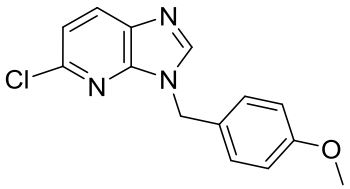

Synthesis of 5-chloro-3-(4-methoxybenzyl)-imidazo[4,5]pyridine (3.49)

Under nitrogen both fractions of 6-chloro-2-(4-methoxybenzylamine)-3-aminopyridine **3.48** from the above procedurewere dissolved in toluene (250 mL) and transferred to a 1 L round bottomed flask. Triethyl orthoformate (23.70 g, 159.9 mmol) and *p*-toluenesulfonic acid monohydrate (1.48 g, 7.8 mmol) were added, then the reaction was refluxed for 15 h. After cooling to room temperature, the mixture was shaken with saturated sodium carbonate (100 mL). The aqueous layer was extracted with toluene (2 x 50 mL), and combined organic layers were washed with water (2 x 200 mL). The combined aqueous washes were back-extracted with toluene (2 x 100 mL), and all combined organic layers were dried with magnesium sulfate. After filtration through a coarse frit, solvent was removed by rotary evaporation and heat. The crude product was purified by a silica column (600g SiO_2, diam = 8 cm, length = 35 cm) using a gradient solvent system, starting with DCM/TEA (99:1) and over time going to DCM/EtOAc/TEA (79:20:1). The fractions containing a TLC spot with an R_f of ~0.25 were combined and solvent removed by rotary evaporation and high vacuum. The dark brown solid was dissolved in DCM, then air was blown over the mixture until there was a minimal amount of black solution and a white solid. The mixture was filtered through a medium frit and washed with cold DCM (3 x 2 mL), and the solid transferred to a vial. The process was repeated the process one more time, and the two fractions of solid were combined. Storage of the off white solid under oil pump vacuum yielded 5-chloro-3-(4-methoxybenzyl)-imidazo[4,5]pyridine (**3.49**, 6.6612 g, 24.3 mmol, 31.3% yield over three steps). Anal. calcd. for $C_{14}H_{12}ClN_3O$ (mol. wt. 273.72): C, 61.43; H, 4.42; N, 15.35. Found: C, 61.33; H. 4.90; N, 15.65.

^{1}H NMR ($CDCl_3$, 600 MHz) δ 7.95 (d, *J* = 8.4 Hz, 1H), 7.94 (s, 1H), 7.25-7.22 (m, 2H), 7.21 (d, *J* = 8.2 Hz, 1H), 6.86-6.82 (m, 2H), 5.31 (s, 2H), 3.74 ppm (s, 3H). ^{13}C NMR

($CDCl_3$, 150.7 MHz) δ 159.6, 146.2, 145.7, 143.9, 134.1, 130.1, 129.4, 127.2, 118.5, 114.3, 55.1, 46.6 ppm.

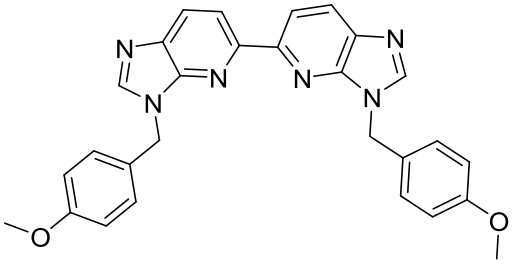

Synthesis of 3,3'-bis((4-methoxybenzyl)-imidazo[4,5]pyridine) (3.50)

In the glovebox to a three neck-round bottom flask (250 mL) was added 5-chloro-3-(4-methoxybenzyl)-3H-imidazo[4,5]pyridine (**3.49**, 5.0032 g, 18.3 mmol), $NiBr_2(PPh_3)_2$[8] (3.3939 g, 4.57 mmol, 25 mol %), zinc powder (2.0317 g, 31.1 mmol), lithium chloride (1.3355 g, 31.5 mmol), tetraethylammonium iodide (4.6998 mg, 18.3 mmol), dry THF (120 mL), and a stir bar. Under nitrogen the reaction was refluxed for 10.5 h then was cooled to room temperature and transferred to a 2 L separatory funnel. DCM (350 mL) and ammonium hydroxide (10%, 300 mL) were added and the mixture shaken. The aqueous layer was extracted with DCM (2 x 350 mL). All organic layers were combined and washed with water (2 x 250 mL), brine (300 mL), and then the aqueous layers were back extracted with DCM (3 x 150 mL). Organic layers were dried with magnesium sulfate and filtered through a coarse frit. From the filtrate, solvent was removed by rotary evaporation, and DCM (50 mL) was added to the residue to make a slurry which was filtered through a medium frit. The off white solid was washed with DCM (2 x 10 mL, 15 mL) then transferred to a vial and dried under oil pump vacuum to obtain 3,3'-bis(4-methoxybenzyl)-5,5'-biimidazo[4,5]pyridine (**3.50**, 3.6620 g, 7.68 mmol, 84% yield). Anal. calcd. for $C_{28}H_{24}N_6O_2$ (mol. wt. 476.54): C, 70.57; H, 5.08; N, 17.64. Found: C, 69.79; H, 5.61; N, 17.75.

^{1}H NMR ($CDCl_3$, 600 MHz) δ 8.61 (d, *J* = 8.4 Hz, 2H), 8.19 (d, *J* = 8.4 Hz, 2H), 8.05 (s, 2H), 7.41 – 7.36 (m, 4H), 6.93 – 6.88 (m, 4H), 5.51 (s, 4H), 3.80 ppm (s, 6H). ^{13}C NMR ($CDCl_3$, 150.7 MHz) δ 159.7, 151.7, 146.8, 144.4, 135.6, 129.6, 128.3, 128.1, 116.4, 114.4, 55.3, 46.7 ppm.

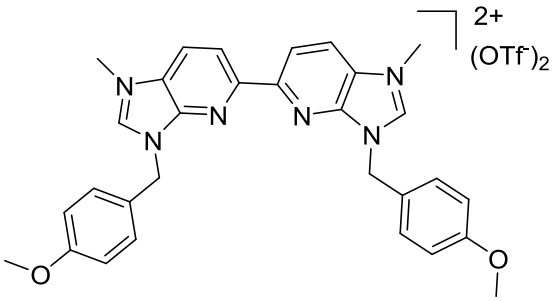

Synthesis of 3,3'-bis(4-methoxybenzyl)-1,1'-dimethyl-[5,5'-biimidazo[4,4,5]pyridine]-1,1'-diium (OTf)$_2$ (3.51)

To a vial in the glovebox added 3,3'-bis(4-methoxybenzyl)-5,5'-biimidazo[4,5]pyridine (**3.50**, 569.3 mg, 1.19 mmol, 1.0 equiv), dry DMF (10 mL), a stir bar, and methyl trifluoromethansulfonate (791.2 mg, 4.82 mmol, 4.05 equiv). The reaction vial was transferred to a 100 ^{o}C oil bath for 2.6 h and then let cool to room temperature. The reaction mixture was transferred to an Erlenmeyer flask a mixture of DCM (30 mL) and pentane (50 mL) was added; a light yellow precipitate formed which was filtered through a medium frit and washed with DCM (2 x 3 mL) and pentanes (2 x 3 mL). The solid was transferred to a vial and stored under oil pump vacuum obtaining 3,3'-bis(4-methoxybenzyl)-1,1'-dimethyl-[5,5'-biimidazo[4,5]pyridine]-1,1'-diium ditriflate (**3.51**, 827.9 mg, 1.03 mmol, 86.1% yield). Anal. calcd. $C_{32}H_{30}F_6N_6O_8S_2$ (mol. wt. 804.74): C, 47.76; H, 3.76; N, 10.44. Found: C, 47.86; H, 3.81; N, 10.63. ^{1}H NMR (DMSO-d_6, 600 MHz) δ 10.02 (s, 2H), 8.93 (d, J = 8.4 Hz, 2H), 8.77 (d, J = 9.0 Hz, 2H), 7.62 (AA'BB' d, J = ca. 9.0 Hz, 4H), 6.98 (AA'BB' d, J = ca. 9.0 Hz, 4H), 5.78 (s, 4H), 4.16 (s, 6H), 3.74 ppm (s, 6H). ^{13}C NMR ($CDCl_3$, 150.7 MHz) δ 159.6, 152.4, 145.2, 142.5, 130.7, 126.1, 125.8, 125.0, 119.7, 114.3, 55.2, 48.1, 34.2 ppm.

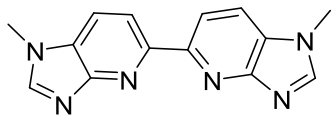

Synthesis of 1,1'-dimethyl-5,5'-biimidazo[4,5]pyridine (3.52)

To a two-neck round bottom flask (25 mL) was added 3,3'-bis(4-methoxybenzyl)-1,1'-dimethyl-[5,5'-biimidazo[4,5]pyridine]-1,1'-diium ditriflate (**3.51**, 3.0378 g, 3.77 mmol), a stir bar, and formic acid (15 mL). The reaction was heated in a 130 ^{o}C oil bath for 3 d, and then solvent was removed under oil pump vacuum. The protonated product

was dissolved in DMSO (25 mL), then a solution of sodium hydroxide (0.6190 g, 15.48 mmol) dissolved in water (17 mL) and DMSO (17 mL) was added. After the formation of an off white solid, the mixture was filtered through a medium frit and washed with water (3 x 10 mL), acetone (2 x 5 mL), and pentane (3 x 5 mL). Solid was transferred to a vial and stored under oil pump vacuum to obtain 1,1'-dimethyl-5,5'-biimidazo[4,5-b]pyridine (**3.52**, 737.8 mg, 2.79 mmol, 74.0% yield). Anal. calcd. for $C_{14}H_{12}N_6$ (mol. wt. 264.29): C, 63.62; H, 4.58; N, 31.80. Found: C, 63.13; H, 5.08; N, 31.44. ^{1}H NMR (DMSO-d_6, 600 MHz) δ 8.49 (d, J = 8.4 Hz, 2H), 8.47 (s, 2H), 8.17 (d, J = 8.4 Hz, 2H), 3.92 ppm (s, 6H). ^{13}C NMR (DMSO-d_6, 150.7 MHz) δ 155.5, 151.0, 147.4, 126.9, 119.3, 114.9, 31.2 ppm.

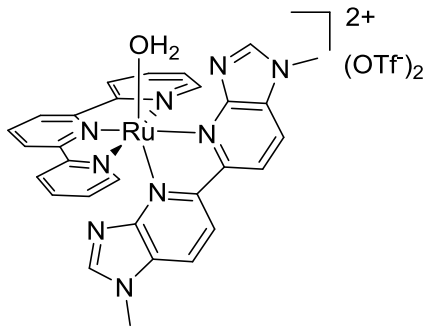

Synthesis of [Ru(OH$_2$)(terpy)(1,1'-dimethyl-5,5'-biimidazo[4,5]pyridine)](OTf)$_2$ (3.53)

[Ru(terpy)Cl$_2$]$_2$ (**3.13**, 135.9 mg, 0.164 mmol), 1,1'-dimethyl-5,5'-biimidazo[4,5]pyridine (**3.52**, 88.0 mg, 0.333 mmol), a stir bar, and methanol (12.0 mL) were added to a vial in a glovebox. The reaction was placed in a 100 ^{o}C oil bath for 27 h then allowed to cool to room temperature; solvent was removed by a flow of nitrogen and transferred to a glovebox. Silver trifluoromethanesulfonate (215.6 mg, 0.839 mmol), acetone (10.0 mL), and water (2.0 mL) were added to the vial, which was stirred for 1 h. The dark brown mixture was then filtered through a fine frit and solvent was removed. The sample was dissolved in acetone (6 mL) and water (0.4 mL), and diethyl ether was allowed to mix by vapor diffusion. After formation of crystals, the mixture was filtered through a fine frit and the dark solid was washed with THF (3 x 1mL) and diethyl ether (3 x 4 mL). The solid was transferred to a vial and dried under high vacuum with phosphorus pentoxide, yielding [Ru(H$_2$O)(1,1'-dimethyl-5,5'-

biimidazo[4,5]pyridine)(terpy)] $(OTf)_2$ (**3.53**, 142.7 mg, 0.156 mmol, 48 % yield). Anal. calcd. $C_{31}H_{25}F_6N_9O_7RuS_2$ (mol. wt. 866.73): C, 40.70; H, 2.75; N, 13.78. Found: C, 40.34; H, 2.59; N, 13.66.

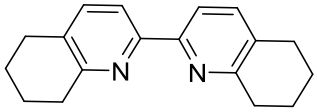

Synthesis of 2,2'-bis(tetrahydroquinoline) (3.55)

2-Chloro-5,6,7,8-tetrahydroquinoline[44] (**3.56**, 0.9393g, 5.60 mmol), $NiBr_2(PPh_3)_2$[8] (1.2470 g, 1.68 mmol), tetraethylammonium iodide (1.5138 g, 5.89 mmol), zinc dust (0.5787 g, 8.84 mmol), a stir bar, and dry THF (13.0 mL) were added to a vial in a glovebox. The mixture was heated in a 70 ^oC oil bath for 17 h, then cooled to room temperature and transferred to an Erlenmeyer flask with 10 % NH_4OH (50 mL) and let stir for 10 min. The solution was the transferred to a separatory funnel and extracted with ether (3 x 75 mL). The organic layer was then washed with water (3 x 75 mL) and brine (30 mL), and dried with Mg_2SO_4. The solution was filtered through a course frit followed by removing the solvent under rotary evaporation. A column of silica (19.5 g) using hexanes, ethyl acetate, triethyl amine (9:1:1%) was loaded. The crude product was dissolved in DCM, silica (2.0 g) was added, solvent was removed by rotary evaporation and the silica/crude product mixture was loaded on the column and eluted with the same solvent mixture hexanes, ethyl acetate, and triethylamine (90:10:1). Fractions containing product with an R_f ~0.1 were combined and dissolved in hot acetone, and left to crystalize at 3 ^oC. After crystallization the mixture was filtered through a medium frit and the white solid was transferred to a vial and dried under oil pump vacuum yielding 2,2'-bis(tetrahydroquinoline) (**3.55**, 337.3 mg, 46 % yield). Anal. calcd. for $C_{18}H_{20}N_2$ (mol. wt. 264.37): C, 81.78; H, 7.63; N, 10.60. Found: C, 81.53; H, 8.00; N, 10.73. ^1H NMR ($CDCl_3$, 499.944 MHz) δ 8.06 (d, *J* = 8.1 Hz, 2H), 7.44 (d, *J* = 8.1 Hz, 2H), 3.01-2.98 (m, 4H), 2.82-2.79 (m, 4H), 1.96-1.90 (m, 4H), 1.87-1.82 ppm (m, 4H). ^{13}C NMR ($CDCl_3$, 125.723 MHz) δ 156.6, 153.8, 137.4, 131.9, 118.2, 32.8, 28.7, 23.2, 22.8 ppm.

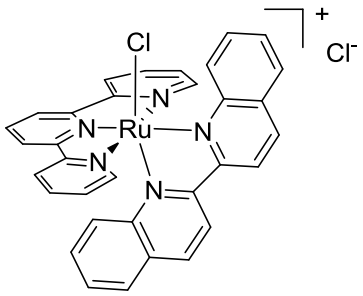

Synthesis of [Ru(Cl)(terpy)(2,2'-bisquinoline)]Cl (3.57)

[Ru(terpy)Cl_2]$_2$ (**3.13**, 150.5 mg, 0.182 mmol), 2,2'-bisquinoline[8] (**3.54**, 96.8 mg, 0.378 mmol), a stir bar, and methanol (10 mL) were added to a vial in a glovebox. The reaction was placed in a 100 ^{o}C oil bath for 4 d then cooled to room temperature and filtered through a fine frit, washed with methanol (3 x 2 mL). The volume of the filtrate was reduced to approximately 3 mL and diethyl ether was allowed to mix by vapor diffusion. After formation of crystals, the mixture was filtered through a medium frit and the dark solid was washed with diethyl ether (3 x 3 mL). The solid was transferred to a vial and dried under high vacuum over phosphorus pentoxide, yielding [Ru(Cl)(terpy)(2,2'-bisquinoline)]Cl $(H_2O)_4$ (**3.57**, 204.2 mg, 78 % yield). Anal. calcd. for $C_{33}H_{23}Cl_2N_5Ru$ $(H_2O)_3$ (mol. wt. 715.60): C, 55.39; H, 4.08; N, 9.79. Found: C, 55.66; H, 4.73; N, 9.99.

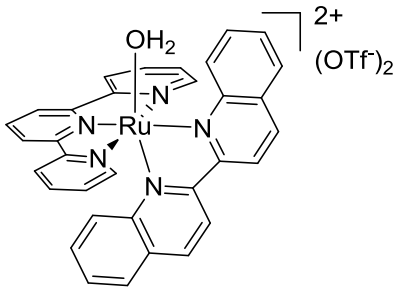

Synthesis of [Ru(OH_2)(terpy)(2,2'-bisquinoline)](OTf)$_2$ (3.57b)

[Ru(terpy)(2,2'-bisquinoline)Cl]Cl (**3.58**, 155.0 mg, 0.217 mmol), silver trifluoromethanesulfonate (122.9 mg, 0.478 mmol), acetone (13.5 mL), water (3.0 mL), and a stir bar were added to a vial in a glovebox. The reaction stirred at room temperature for 16.5 hours, then filtered through a fine frit. Solvent was removed under oil pump vacuum, and dried with phosphorus pentoxide, yielding [Ru(OH_2)(terpy)(2,2'-bisquinoline)](OTf)$_2$ (H2O)$_2$ (**3.57b**, 204.1 mg, 0.216 mmol, 99 % yield). Anal. calcd. for

$C_{35}H_{25}F_6N_5O_7RuS_2$ $(H_2O)_2$ (mol. wt. 942.82): C, 44.59; H, 3.10; N, 7.43. Found: C, 44.34; H, 2.71; N, 7.71.

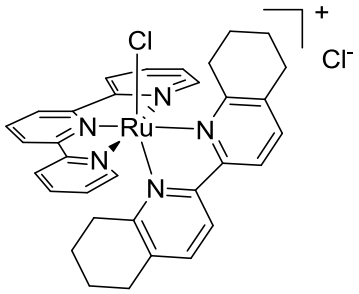

Synthesis of [Ru(Cl)(terpy)(2,2'-bis(tetrahydroquinoline)](Cl) (3.58)

$[Ru(terpy)Cl_2]_2$ (**3.13**, 150.9 mg, 0.182 mmol), 2,2'-bis(tetrahydroquinoline (**3.55**, 99.3 mg, 0.377 mmol), a stir bar, and methanol (10 mL) were added to a vial in a glovebox. The reaction was placed in a 100 ^oC oil bath for 2 d then cooled to room temperature and filtered through a fine frit. The volume of the filtrate was reduced to approximately 5 mL and diethyl ether was allowed to mix by vapor diffusion. After formation of crystals, the mixture was filtered through a medium frit and the dark solid was washed with diethyl ether (3 x 5 mL). The solid was transferred to a vial and dried under high vacuum over phosphorus pentoxide, yielding [RuCl(terpy)(2,2'-bis(tetrahydroquinoline)Cl]Cl $(H_2O)_3$ (**3.58**, 191.5 mg, 0.264 mmol, 73 % yield). Anal. calcd. for $C_{33}H_{31}Cl_2N_5Ru$ $(H_2O)_3$ (mol. wt. 723.66): C, 54.77; H, 5.15; N, 9.68. Found: C, 54.73; H, 5.99; N, 9.81.

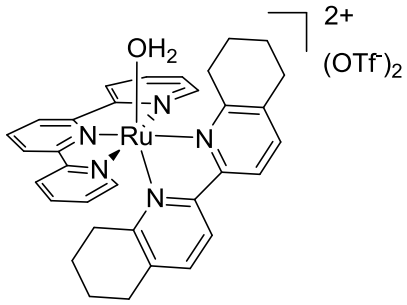

Synthesis of [Ru(OH_2)(terpy)(2,2'-bis(tetrahydroquinoline)](OTf)$_2$ (3.58b)

[Ru(terpy)(2,2'-bis(tetrahydroquinoline))Cl]Cl (**3.58**, 148.8 mg, 0.222 mmol), silver trifluoromethanesulfonate (121.5 mg, 0.473 mmol), acetone (9.0 mL), water (1.0 mL), and a stir bar were added to a vial in a glovebox. The reaction stirred at room temperature for 30 h, then filtered through a fine frit. Solvent was removed under oil

pump vacuum, and the residue dried under oil pump vacuum over phosphorus pentoxide, yielding [Ru(OH_2)(terpy)(2,2'-bis(tetrahydroquinoline))]($OTf)_2$ $(H_2O)_{3.5}$ (**3.58b**, 202.9 mg, 0.207 mmol, 93 % yield). Anal. calcd. for $C_{35}H_{33}F_6N_5O_7RuS_2$ $(H_2O)_{3.5}$ (mol. wt. 977.91): C, 42.99; H, 4.12; N, 7.16. Found: C, 42.84; H, 3.61; N, 7.28

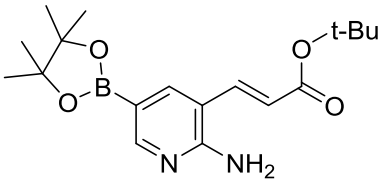

Synthesis of 3.62 (experiments to make 3.62-3.74 were done by undergraduate Ryan Shirey under my supervision)

Tert-butyl (*E*)-3-(2-amino-5-(bromo)pyridin-3-yl)acrylate (**3.61**, 659.6 mg, 2.205 mmol), bis(pinacolate)diboron (1.1182 g, 4.403 mmol), potassium acetate (668.6 mg, 6.813 mmol), 1,1'-bis(diphenylphosphino)ferrocene (184.0 mg, 0.332 mmol), $Pd(OAc)_2$ (74.1 mg, 0.330 mmol), a stir bar, and NMP (15 mL) were added to a vial in a glovebox. The reaction was stirred for 21 h at 80 ^oC in an oil bath, and after cooling to room temperature the reaction was diluted with EtOAc (80 mL) and washed with brine (3 x 50 mL). The organic layer was dried with Na_2SO_4, filtered through a course frit and solvent was removed by rotary evaporation and under oil pump vacuum. The sample was redissolved in EtOAc (20 mL) and washed with HCl (1 M, 19.5 mL) and brine (2 x 19 mL), the aqueous layers were combined and neutralized with solid sodium bicarbonate until giving a pH of 7. The aqueous layer was extracted with EtOAc (3 x 30 mL), this organic layer was then dried with Na_2SO_4, filtered through a course frit and solvent was removed by rotary evaporation. The original organic layer was washed again with HCl (1 M, 19.5 mL) and same workup was repeated. After removal of solvent by rotary evaporation the samples were dried under oil pump vacuum yielding *tert*-butyl (*E*)-3-(2-amino-5-(4,4,5,5-tetramethyl-1,3,2-dioxaborolan-2-yl)pyridin-3-yl)acrylate as an off-white solid; fraction 1 (from first HCl wash) (**3.62**, 407.7 mg, 1.178 mmol, 53%), and fraction 2 (from second HCl wash) (**3.62**, 173.7 mg, 0.502 mmol, 23%). Anal. calcd. for $C_{18}H_{27}BN_2O_4$ (mol. wt. 346.23): C, 62.44; H, 7.86; N, 8.09. Found: C, 61.84; H, 7.73; N, 7.93.

^{1}H NMR ($CDCl_3$, 499.944 MHz) δ 8.42 (s, 1H), 7.97 (s, 1H), 7.55 (d, *J* = 15.9 Hz, 1H), 6.35 ppm (d, *J* = 15.9 Hz, 1H). ^{13}C NMR ($CDCl_3$, 125.723 MHz) δ 166.0, 158.2, 156.3, 142.4, 137.6, 122.0, 113.9, 83.8, 80.7, 28.1, 24.8 ppm.

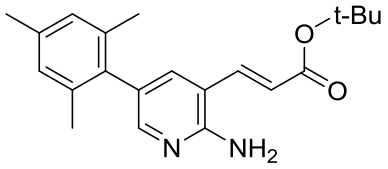

Synthesis of *tert*-butyl (*E*)-3-(2-amino-5-mesitylpyridin-3-yl) acrylate (3.63)

Tert-butyl (*E*)-3-(2-amino-5-bromopyridin-3-yl) acrylate (**3.61**, 501.4 mg, 1.676 mmol), 2,4,6-trimethylphenylboronic acid (550.8 mg, 3.358 mmol), K_3PO_4 (735.2 mg, 3.464 mmol), $Pd(OAc)_2$ (37.9 mg, 0.165 mmol), 2-dicyclohexylphosphino-2′,4′,6′-triisopropylbiphenyl (X-phos, 80.0 mg, 0.168 mmol), a stir bar, toluene (10.0 mL), and water (1.0 mL) were added to a vial in a glovebox. The reaction was placed in a 80 ^{o}C oil bath for 19 h, then cooled to room temperature and transferred to a separatory funnel and diluted with DCM (40 mL). The organic layer was washed with water (100 mL), then the aqueous layer was back extracted with DCM (3 x 40 mL). After combining the organic layers, they were washed with water (100 mL) which was then back extracted with DCM (3 x 40 mL). The organic layers were combined and dried with sodium sulfate, filtered through a course frit and solvent was removed by rotary evaporation. The crude product was purified on a silica (17.0 g) column, by dissolving the crude solid with hexanes (2 mL) and loading on the column. Pure product was eluted with a mixture of hexanes and ethyl acetate, starting at 100 % hexanes and going to a 30 % ethyl acetate mixture. Fractions containing only a TLC spot of R_f ~ 0.2, using hexanes:ethyl acetate (3:1) to elute were combined. Solvent was removed by rotary evaporation and the residue dried under high vacuum pump to yield *tert*-butyl (*E*)-3-(2-amino-5-mesitylpyridin-3-yl) acrylate (**3.63**, 441.7 mg crude, 1.305 mmol crude, 78 % crude yield) as a yellow solid.

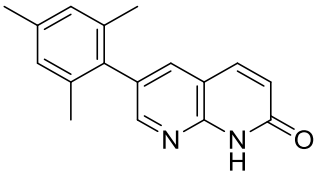

Synthesis of 6-mesityl-1,8-naphthyridin-2-one (3.64)

Tert-butyl (*E*)-3-(2-amino-5-mesitylpyridin-3-yl)acrylate (**3.63**, 425.3 mg, 1.26 mmol), sodium methoxide (340.5 mg, 6.31 mmol), anhydrous methanol (10.0 mL), and a stir bar were added to a vial in a glovebox. The reaction was stirred for 4 h at 80 ^{o}C, after cooling to room temperature solvent was removed by rotary evaporation. 1 M HCl (6 mL) was added to the solid which was sonicated until mostly dissolved, at which time the solution was neutralized with saturated sodium bicarbonate. The mixture was then filtered through a medium frit and washed with water (3 x 1 mL) and diethyl ether (3 x 1 mL). The solid was transferred to a vial and dried under oil pump vacuum to yield 6-mesityl-1,8-naphthyridin-2-one (**3.64**, 281.1 mg, 1.06 mmol, 84 % yield) as an off-white solid. Product was used without further purification.

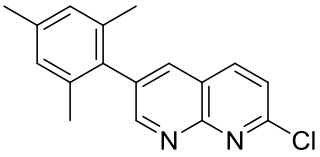

Synthesis of 2-chloro-6-mesityl-1,8-naphthyridine (3.65)

6-mesityl-1,8-naphthyridin-2-one (**3.64**, 274.4 mg, 1.04 mmol), a stir bar, and phosphorus oxychloride (1.0 mL) were added to a vial in the glovebox. The reaction was stirred for 45 min at 100 ^{o}C, then cooled to room temperature and the mixture was transferred to a sepratory funnel and diluted with water (75 mL). The mixture was neutralized with saturated sodium bicarbonate, and extracted with EtOAc (75 mL). The organic layer was washed with water (75 mL) amd brine (25 mL). The combined aqueous layers were extracted with EtOAc (2 x 75 mL) and DCM (75 mL). The organic layers were combined and dried with sodium sulfate, solvent was removed by rotary evaporation and oil pump vacuum. Crude product was dry loaded on silica by dissolving in DCM and adding silica (0.5 g), solvent was removed by oil pump vacuum. The crude product/silica mixture was loaded on a silica (15.0 g) column, eluding with a mixture of hexanes and ethyl acetate, starting at 100 % hexanes and going to a 20 % ethyl acetate

mixture. Fractions containing only a TLC spot of R_f ~ 0.25, using hexanes:ethyl acetate (4:1) to elute were combined. Solvent was removed by rotary evaporation and the residue dried under high vacuum pump to yield 2-chloro-6-mesityl-1,8-naphthyridine as a white solid (**3.65**, 184.7 mg, 0.65 mmol, 63 % yield, or 39 % yield over three steps). Anal. calcd. for $C_{17}H_{15}N_2Cl$ (mol. wt. 282.77): C, 72.21; H, 5.35; N, 9.91. Found: C, 71.85; H, 5.74; N, 9.80.

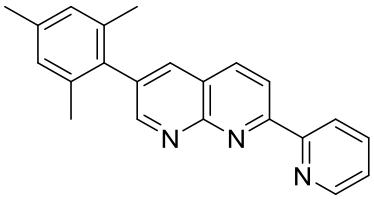

Synthesis of 2-pyridyl-6-mesityl-1,8-naphthyridine (3.66)

2-chloro-6-mesityl-1,8-naphthyridine (**3.65**, 169.3 mg, 0.60 mmol), 2-(tributylstannyl)pyridine (362.5 mg, 0.98 mmol), $Pd(PPh_3)_4$ (35.9 mg, 0.031 mmol), a stir bar, and dry toluene (3.0 mL) were added to a vial in a glovebox. The reaction was stirred for 3 d at 100 ^oC in an oil bath, and after cooling to room temperature the reaction was loaded onto a silica (15.5 g) column. The product was eluted with a mixture of hexanes and ethyl acetate, starting at 100 % hexanes and going to a 30 % ethyl acetate in hexanes. Fractions containing only a TLC spot of R_f ~ 0.25, using hexanes:ethyl acetate (7:3) to elute were combined. Solvent was removed by rotary evaporation and the residue stored under oil pump vacuum to yield 2-pyridyl-6-mesityl-1,8-naphthyridine as a white solid (**3.66**, 56.6 mg, 0.174 mmol, 29 % yield). Anal. calcd. for $C_{22}H_{19}N_3$ (mol. wt. 325.41): C, 81.20; H, 5.89; N, 12.91. Found: C, 80.82; H, 6.26; N, 12.89.

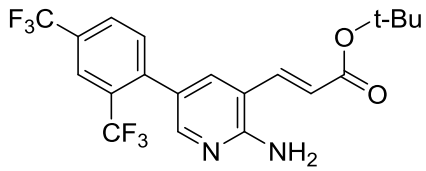

Synthesis of 3.67

Tert-butyl (*E*)-3-(2-amino-5-(bromo)pyridin-3-yl)acrylate (**3.61**, 500.9 mg, 1.674 mmol), 2,4-bis(trifluoromethyl)phenylboronic acid (686.0 mg, 2.660 mmol), K_3PO_4 (718.0 mg, 3.382 mmol), $Pd(OAc)_2$ (37.5 mg, 0.167 mmol), 2-dicyclohexylphosphino-2′,4′,6′-triisopropylbiphenyl (X-phos, 80.0 mg, 0.168 mmol), a stir bar, toluene (10.0

mL), and water (1.0 mL) were added to a vial in a glovebox. The reaction was placed in a 80 ^{o}C oil bath for 17 h and stirred, allowed to cool to room temperature and transferred to a speratory funnel. Water (30 mL) was added and the reaction was extracted with DCM (3 x 30 mL), and organic layers were combined and washed with water (40 mL). The aqueous layer was back-extracted with DCM (20 mL) and combined with the other organic layer. Solvent was removed by rotary evaporation and product was purified on a silica column. The product was eluted with a mixture of hexanes and ethyl acetate, starting at 100 % hexanes and going slowly to a 60 % ethyl acetate – hexanes mixture. Solvent was removed by rotary evaporation and the residue stored under oil pump vacuum pump to yield *tert*-butyl (*E*)-3-(2-amino-5-(2,4-bis(trifluoromethyl)phenyl)pyridin-3-yl)acrylate (**3.67**, 441.0 mg, 1.020 mmol crude, 61 % crude yield) as an off-white solid, which was used without further purification.

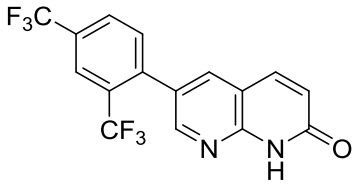

Synthesis of 6-(2,4-bis(trifluoromethyl)phenyl)-1,8-naphthyridin-2-one (3.68)

Tert-butyl (*E*)-3-(2-amino-5-(2,4-bis(trifluoromethyl)phenyl)pyridin-3-yl)acrylate (**3.67**, 437.0 mg, 1.011 mmol), sodium methoxide (278.8 mg, 5.164 mmol), a stir bar, and anhydrous methanol (6.0 mL) were added to a vial in a glovebox. The vial was then stirred in an 80 ^{o}C oil bath for 4 h, and after cooling to room temperature, solvent was removed by rotary evaporation. HCl (0.5 M, 6 mL) was added to the vial with the crude solid, which was then neutralized with solid sodium bicarbonate. The heterogeneous mixture was transferred to a medium frit and washed with water (3 x 2 mL) and diethyl ether (3 x 6 mL). The solid was allowed to dry, then using water (6 mL), and ethyl acetate (2 x 6 mL) was transferred to a vial and the mixture concentrated under oil pump vacuum yielding 6-(2,4-bis(trifluoromethyl)phenyl)-1,8-naphthyridin-2-one $(H_2O)_{0.5}$ (**3.68**, 223.5 mg, 0.609 mmol, 36 % yield over two steps) as an off-white solid. Anal. calcd. for $C_{16}H_8F_6N_2O$ $(H_2O)_{0.5}$ (mol. wt. 367.25): C, 52.33; H, 2.47; N, 7.63. Found: C, 52.36; H, 2.93; N, 7.54.

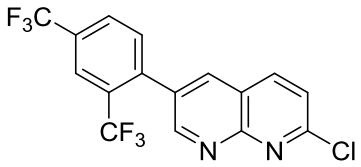

Synthesis of 6-(2,4-bis(trifluoromethyl)phenyl)-2-chloro-1,8-naphthyridine (3.69)

6-(2,4-bis(trifluoromethyl)phenyl)-1,8-naphthyridin-2-one $(H_2O)_{0.5}$ (**3.68**, 223.3 mg, 0.608 mmol), phosphorus oxychloride (1.0 mL), and a stir bar were added to a vial in a glovebox. The vial was stirred in a 100 ^{o}C oil bath for 1 h, and after cooling to room temperature the solution was transferred to an Erlenmeyer flask (250 mL) and diluted with water (75 mL). The solution was neutralized with solid sodium bicarbonate and extracted with EtOAc (3 x 75 mL). Solvent was removed from the organic layer by rotary evaporation and the crude product was purified on a silica (10 g) column, by dissolving the crude solid with DCM and loading on the column. Pure product was eluted with a mixture of hexanes and ethyl acetate, starting at 100 % hexanes and going to a 30 % ethyl acetate – hexanes mixture. Fractions containing only a TLC spot of R_f ~ 0.35, using hexanes:ethyl acetate (7:3) to elute were combined. Solvent was removed by rotary evaporation and the residue stored under oil pump vacuum to yield 6-(2,4-bis(trifluoromethyl)phenyl)-2-chloro-1,8-naphthyridine (**3.69**, 94.8 mg, 0.252 mmol, 41% yield) as a white solid. Anal. calcd. for $C_{16}H_7ClF_6N_2$ (mol. wt. 376.69): C, 51.02; H, 1.87; N, 7.44. Found: C, 50.79; H, 2.48; N, 7.44.

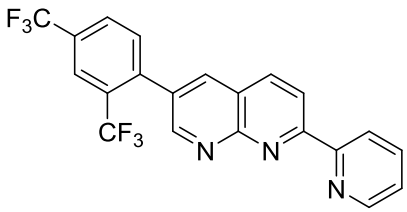

Synthesis of 6-(2,4-bis(trifluoromethyl)phenyl)-2-(pyridin-2-yl)-1,8-naphthyridine (3.70)

6-(2,4-bis(trifluoromethyl)phenyl)-2-chloro-1,8-naphthyridine (**3.69**, 79.6 mg, 0.211 mmol), 2-(tributylstannyl)pyridine (123.0 mg, 0.334 mmol), $Pd(PPh_3)_4$ (14.4 mg, 0.012 mmol), toluene (2.0 mL), and a stir bar were added to a vial in a glovebox. The vial was stirred in a 100 ^{o}C oil bath for 20 h, after which time the reaction was cooled to room temperature and solvent was removed by a flow of air. The crude product was

purified on a silica (12 g) Biotage column, by dissolving the crude solid with DCM and loading on the column. Pure product was eluted with a mixture of hexanes and ethyl acetate, starting at 100 % hexanes and going to a 40 % ethyl acetate mixture over 10 min, then maintaining at 40% EtOAc for 5 min, by the end of which product had finished eluting. Solvent of fractions containing product were combined and solvent was removed by rotary evaporation, and the material transferred to a vial and stored under oil pump vacuum, yielding 6-(2,4-bis(trifluoromethyl)phenyl)-2-(pyridin-2-yl)-1,8-naphthyridine $(H_2O)_{0.4}$ (**3.70**, 73.6 mg, 0.173 mmol, 82 % yield) as a white solid. Anal. calcd. for $C_{21}H_{11}F_6N_3$ $(H_2O)_{0.4}$ (mol. wt. 426.54): C, 59.13; H, 2.79; N, 9.85. Found: C, 59.40; H, 3.31; N, 9.90.

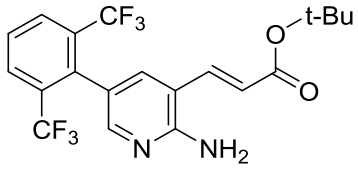

Synthesis of *tert*-butyl (*E*)-3-(2-amino-5-(2,6-bis(trifluoromethyl)phenyl)pyridin-3-yl)acrylate (3.71)

Tert-butyl (*E*)-3-(2-amino-5-(4,4,5,5-tetramethyl-1,3,2-dioxaborolan-2-yl)pyridin-3-yl)acrylate (**3.62**, 578.4 mg, 1.671 mmol), 2-bromo-1,3-bis(trifluoromethyl)benzene (1.0820 g, 3.693 mmol), potassium carbonate (492.0 mg, 3.560 mmol), [1,3-bis(2,6-diisopropylphenyl)imidazol-2-ylidene](3-chloropyridyl)palladium(II) dichloride (PEPPSI-*i*-Pr, 61.1 mg, 0.090 mmol), ethanol (17 mL), water (0.88 mL), and a stir bar were added to a vial in a glovebox. The reaction vial was heated in an 80 ^oC oil bath for 18 h, and after cooling to room temperature the reaction mixture was transferred to a separatory funnel and diluted with EtOAc (30 mL). The organic layer was washed with water (3 x 30 mL) and brine (30 mL), the aqueous layers were combined and extracted with EtOAc (2 x 30 mL). The organic layers were combined and dried with Na_2SO_4, filtered through a course frit, and solvent was removed by rotary evaporation and stored under oil pump vacuum. The crude product was purified on a silica (40 g) column, by dissolving the crude solid with DCM (5 mL), forming a heterogeneous mixture, and loading on the column. Product was eluted with a mixture of hexanes and ethyl acetate, starting at 100 % hexanes and going to a 30 % ethyl acetate–hexanes mixture. Fractions

containing a TLC spot of R_f ~ 0.5, using hexanes:ethyl acetate (7:3) to elute were combined; there was a small impurity R_f ~ 0.4. Solvent was removed by rotary evaporation, material was transferred to a vial, and the solid was washed with pentane (3 x 2 mL), and stored under oil pump vacuum to yield *tert*-butyl (*E*)-3-(2-amino-5-(2,6-bis(trifluoromethyl)phenyl)pyridin-3-yl)acrylate (**3.71**, 294.7 mg, 0.682 mmol, 41 % yield) as a white solid. Anal. calcd. for $C_{20}H_{18}F_6N_2O_2$ (mol. wt. 432.37): C, 55.56; H, 4.20; N, 6.48. Found: C, 55.18; H, 4.60; N, 6.55.

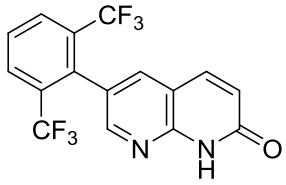

Synthesis of 6-(2,6-bis(trifluoromethyl)phenyl)-1,8-naphthyridin-2(1H)-one (3.72)

Tert-butyl (*E*)-3-(2-amino-5-(2,6-bis(trifluoromethyl)phenyl)pyridin-3-yl)acrylate (**3.71**, 288.6 mg, 0.667 mmol), sodium methoxide (181.3 mg, 3.356 mmol), anhydrous methanol (5.0 mL), and a stir bar were added to a vial in a glovebox. The vial was heated in an 80 ^{o}C oil bath for 5 h, then cooled to room temperature and solvent was removed by rotary evaporation. HCl (1 M, 4 mL) was added which gave a homogeneous solution, and solid sodium bicarbonate was added until pH was ~7. The now heterogeneous white mixture was filtered through a medium frit, washing the solid with water (3 mL) and Et_2O (3 mL), then the solid was transferred to a vial. From the mother liquor, water was removed by rotary evaporation, and the obtained solid was dissolved in HCl (1 M, 1 mL), then neutralized with solid sodium bicarbonate until pH 7. The mixture was filtered through a medium frit and washed with water (3 mL) and Et_2O (3 mL). Both fractions of solids were combined and stored under oil pump vacuum yielding 6-(2,6-bis(trifluoromethyl)phenyl)-1,8-naphthyridin-2(1H)-one (**3.72**, 199.0 mg, 0.555 mmol, 83 % crude yield) as an off-white solid, which was used without further purification.

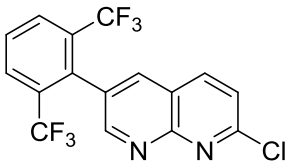

Synthesis of 6-(2,6-bis(trifluoromethyl)phenyl)-2-chloro-1,8-naphthyridine (3.73)

6-(2,6-bis(trifluoromethyl)phenyl)-1,8-naphthyridin-2(1H)-one (**3.72**, 192.3 mg, 0.537 mmol), phosphorus oxychloride (1.0 mL), a stir bar were added to a vial. The vial was heated in a 100 ^{o}C oil bath for 2 h. After cooling to room temperature the reaction was transferred to a separatory funnel and diluted with cold water (50 mL) and neutralized with solid sodium carbonate. The product was extracted with EtOAc (3 x 30 mL), which was then dried with Na_2SO_4, filtered through a course frit and solvent was removed by rotary evaporation. The residual solid was transferred to a vial and solids stored under oil pump vacuum to yield 6-(2,6-bis(trifluoromethyl)phenyl)-2-chloro-1,8-naphthyridine (**3.73**, 172.8 mg, 0.459 mmol, 85% yield, 69% yield over two steps). Anal. calcd. for $C_{16}H_7ClF_6N_2$ (mol. wt. 376.69): C, 51.02; H, 1.87; N, 7.44. Found: C, 51.23; H, 2.25; N, 7.60.

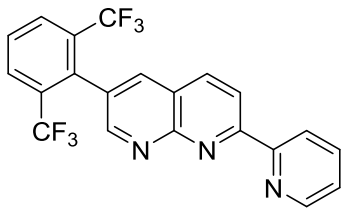

Synthesis of 6-(2,6-bis(trifluoromethyl)phenyl)-2-(pyridin-2-yl)-1,8-naphthyridine (3.74)

6-(2,6-bis(trifluoromethyl)phenyl)-2-chloro-1,8-naphthyridine (**3.73**, 162.1 mg, 0.430 mmol), 2-(tributylstanyl)pyridine (239.6 mg, 0.651 mmol), $Pd(PPh_3)_4$ (24.1 mg, 0.021 mmol), toluene (4.0 mL), and a stir bar were added to a vial in a glovebox. The vial was heated in a 100 ^{o}C oil bath for 13 h. After cooling to room temperature the mixture was purified on a silica (12.5 g) column, by loading the toluene reaction mixture on the column. Pure product was eluted with a mixture of hexanes and ethyl acetate, starting at 100 % hexanes and going to a 30 % ethyl acetate-hexanes mixture. Fractions containing only a TLC spot of R_f ~ 0.3, using hexanes:ethyl acetate (7:3) to elute were combined. Solvent was removed by rotary evaporation and residual solids stored under oil pump vacuum to yield 6-(2,6-bis(trifluoromethyl)phenyl)-2-(pyridin-2-yl)-1,8-naphthyridine (**3.74**, 145.9 mg, 0.348 mmol, 81 % yield) as a white solid. Anal. calcd. for $C_{21}H_{11}F_6N_3$ (mol. wt. 419.33): C, 60.15; H, 2.64; N, 10.02. Found: C, 59.76; H, 3.00; N, 9.98.

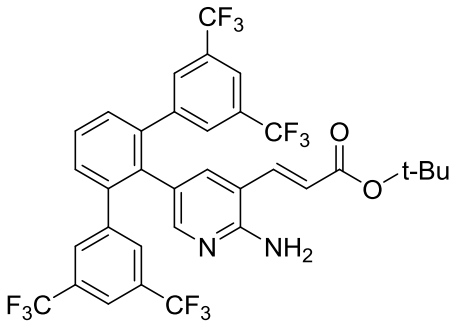

Synthesis of 3.75 (experiments to make 3.75-3.78 were done by Farhana Barmare)

2,6-bis(3,5-di-trifluoromethylphenyl)bromobenzene (0.8354 g, 1.437 mmol), *tert*-butyl (*E*)-3-(2-amino-5-bromopyridin-3-yl) acrylate (**3.61**, 0.5941 g, 1.828 mmol), $Pd(PPh_3)_4$ (103.8 mg, 0.090 mmol), Na_2CO_3 (2 M, 1.8 mL in water), dioxane (15.0 mL) were added to a Schlenk flask (50 mL) in a glovebox. The reaction mixture was stirred at 100 °C for 20 h. The reaction mixture was concentrated by rotary evaporation and then DCM (100 mL) was added to the residue which was filtered through Celite. The organic filtrate was washed with water (3 x mL), brine, dried over $MgSO_4$, filtered through a course frit, and concentrated by rotary evaporation. The crude product was purified by silica column chromatography using a gradient of 100 % hexanes to 80 % hexanes : 20 % ethyl acetate. The fractions containing a TLC spot of R_f~ 0.4 using 80 % hexanes and 20 % ethyl acetate were combined and solvent was removed by rotary evaporation. The obtained solid was stored under oil pump vacuum yielding a yellow fluffy solid, **3.75** (688.6 mg, 0.950 mmol, 66.1%). Anal. calcd for $C_{34}H_{24}N_2O_2F_{12}$ (mol. wt. 724.55): C, 56.67; H, 3.36; N, 3.89. Found: C, 56.60; H, 3.32; N, 3.92.

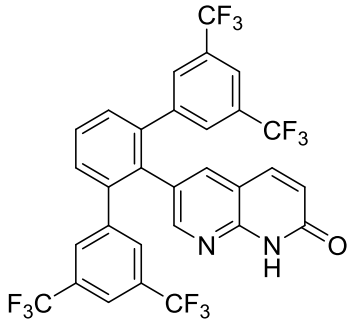

Synthesis of 3.76

3.75 (306.1 mg, 0.422 mmol), sodium methoxide (116.9 mg, 2.165 mmol), methanol (5.0 mL), and a stir bar were added to a scintillation vial (20 mL) which was

heated in a 80 °C oil bath for 4 h. To the reaction mixture concentrated by rotary evaporation, then saturated NaH_2PO_4 solution was added to the residue dropwise while stirring until pH was approximately 7. The aqueous mixture was then extracted with DCM (2 x 100 mL), and organic extracts were combined and washed with water (3 times), brine, dried over Na_2SO_4, and filtered through a course frit. The filtrate was concentrated by rotary evaporation and residual solids stored under oil pump vacuum yielding a light yellow solid, **3.76** (265.6 mg, 0.410 mmol, 97.3 %), that was used without further purification.

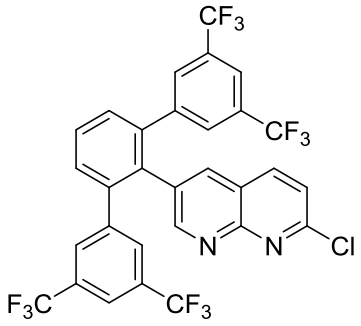

Synthesis of 3.77

3.76 (198.1 mg, 0.306 mmol), $POCl_3$ (2.0 mL), and a stir bar were added to a scintillation vial (20 mL) in a glovebox, which was then heated in a 100 °C oil bath for 1 h. The reaction mixture was added dropwise to ice cold water (exothermic step), then saturated sodium carbonate solution was added until the pH was neutral. The aqueous mixture was extracted with DCM (2 x 100 mL), the combined DCM layers were washed with water (3 times), brine, dried over Na_2SO_4, filtered through a course frit, and the filtrate concentrated by rotary evaporation. The crude product was purified by silica column chromatography using a gradient of 100 % hexanes to 80 % hexanes : 20 % ethyl acetate. The fraction containing a TLC spot of R_f~ 0.4 using 80 % hexanes and 20 % ethyl acetate were combined and solvent was removed by rotary evaporation. The obtained solid was stored under oil pump vacuum yielding a white fluffy solid, **3.77** (154.8 mg, 0.232 mmol, 75.3%). Anal. calcd for $C_{30}H_{13}N_2ClF_{12}$ (mol. wt. 664.87): C, 54.19; H, 1.97; N, 4.21. Found: C, 53.98; H, 2.32; N, 4.33.

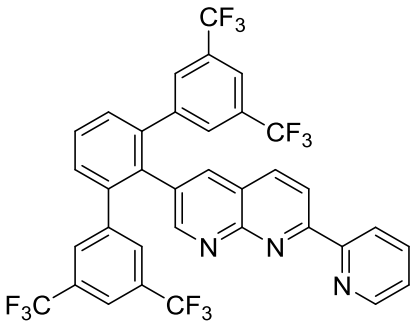

Synthesis of 3.78

3.77 (130.1mg, 0.195 mmol), $Pd(PPh_3)_4$ (12.0 mg, 0.090 mmol), 2-(tributylstannyl)pyridine (127.9 mg, 0.347 mmol), toluene (5.0 mL), and a stir bar were added to a scintillation vial (20 mL) in a glovebox. The reaction mixture was then heated in a 100 °C oil bath for 20 h. The mixture was concentrated and then ethyl acetate (100 mL) was added to the residue and filtered through celite. The organic filtrate was washed with water (3 times), brine, dried over $MgSO_4$, filtered through a course frit, and the filtrate concentrated by rotary evaporation. The crude product was purified by silica column chromatography using a gradient of 100 % petroleum ether to 80 % petroleum ether: 20 % ethyl acetate. The fraction containing a TLC spot of R_f~ 0.3 using 80 % petroleum ether and 20 % ethyl acetate were combined and solvent was removed by rotary evaporation. The obtained solid was stored under oil pump vacuum yielding a white solid, **3.78** (105.0 mg, 0.148 mmol, 76.0%). Anal. calcd for $C_{35}H_{17}N_3F_{12}$ (mol. wt. 707.51): C, 59.43; H, 2.42; N, 5.94. Found: C, 59.35; H, 2.82; N, 6.00.

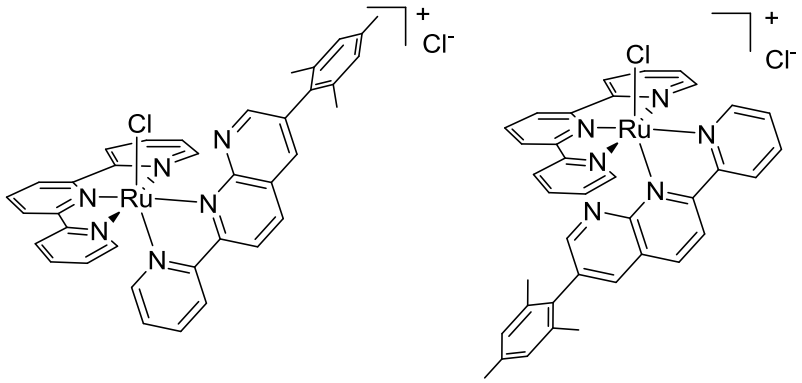

Synthesis of [Ru(Cl)(terpy)(distal-6-(mesityl)-2-(pyridin-2-yl)-1,8-naphthyridine)]Cl (3.79-d) and [Ru(Cl)(terpy)(proximal-6-(2,4-bis(mesityl)-2-(pyridin-2-yl)-1,8-naphthyridine)]Cl (3.79-p)

6-(mesityl)-2-(pyridin-2-yl)-1,8-naphthyridine (**3.66**, 48.1 mg, 0.148 mmol), $[(terpy)Ru(Cl)_2]_2$ (**3.13**, 30.9 mg, 0.038 mmol), a stir bar, and methanol (4.0 mL) were added to a vial in a glovebox. The vial was stirred in a 100 ^oC oil bath for 6 d, then more $[(terpy)Ru(Cl)_2]_2$ (35.0 mg, 0.043 mmol) was added and heated for another 8 d, after which the solvent was then removed by rotary evaporation. The distal and proximal isomers were separated on a neutral alumina (7.3 g) column by eluting with a mixture of acetone and water, starting at 100 % acetone and going to a 10 % water-acetone mixture then 20% water-acetone. The distal isomer was the first to elute as a purple solution, followed by the proximal isomer as a red solution. The different isomers were transferred to vials and solvent was removed by a flow of nitrogen then crystallized under nitrogen by vapor diffusion of diethyl ether into EtOH:acetone (1:1). Once crystalline solid had formed, the solids were filtered through a medium frit and washed with diethyl. The separate solids were transferred to vials and dried under oil pump vacuum, yielding **3.79-d** $(H_2O)_4$ (40.6 mg, 0.0506 mmol, 34 % yield). Anal. calcd. for $C_{37}H_{30}Cl_2N_6Ru$ $(H_2O)_4$ (mol. wt. 802.72): C, 55.36; H, 4.77; N, 10.47. Found: C, 55.70; H, 5.01; N, 10.47. For **3.79-p** (83.0 mg, 0.114 mmol if pure, 77 % yield if pure), anal. calcd. $C_{37}H_{30}Cl_2N_6Ru$ (mol. wt. 730.66): C, 60.82; H, 4.14; N, 11.50. Found: C, 43.51; H, 3.68; N, 8.50. Note: the combined yield of isomers is over 100 %. Several samples of **3.79-p** were subjected to elemental analyses, but the sample appears to not be a typical hydrate or solvate: the carbon the value is 71.5 % of what was expected, for nitrogen, 73.9 % of

expected, and for hydrogen, 88.9 % of expected. Possibly there is an inorganic impurity from the alumina or it is a polyhydrate. The number of mmol and therefore the % yield must be lower.

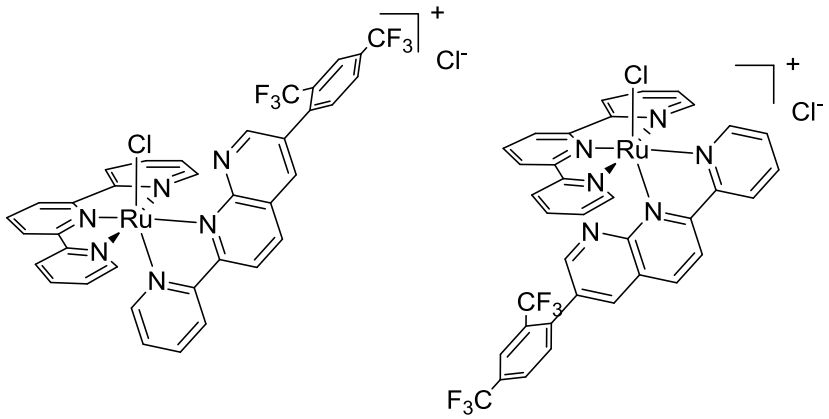

Synthesis of [Ru(Cl)(terpy)(distal-6-(2,4-bis(trifluoromethyl)phenyl)-2-(pyridin-2-yl)-1,8-naphthyridine)]Cl (3.80-d) and [Ru(Cl)(terpy)(proximal-6-(2,4-bis(trifluoromethyl)phenyl)-2-(pyridin-2-yl)-1,8-naphthyridine)]Cl (3.80-p)

6-(2,4-bis(trifluoromethyl)phenyl)-2-(pyridin-2-yl)-1,8-naphthyridine $(H_2O)_{0.4}$ (**3.70**, 31.9 mg, 0.075 mmol), $[(terpy)Ru(Cl)_2]_2$ (**3.13**, 32.6 mg, 0.080 mmol), a stir bar, and methanol (4.1 mL) were added to a vial in a glovebox. The vial was stirred in a 100 ^oC oil bath for 2 d, and after cooling, the solvent was then removed by rotary evaporation. The distal and proximal isomers were separated on a neutral alumina (8 g) column by eluting with a mixture of acetone and water, starting at 100 % acetone and going to a 10 % water-acetone mixture then 20% water-acetone. The distal isomer was the first to elute as a purple solution, followed by the proximal isomer as a red solution. The different isomers were transferred to vials and solvent was removed by a flow of nitrogen and dried under oil pump vacuum, yielding distal $(acetone)_1$ $(H_2O)_3$ (**3.80-d**, 25.5 mg, 0.027 mmol, 36 % yield). Anal. calcd. for $C_{36}H_{22}Cl_2F_6N_6Ru$ $(C_3H_6O)(H_2O)_3$ (mol. wt. 936.70): C, 50.01; H, 3.66; N, 8.97. Found: C, 50.32; H, 3.81; N, 9.23. The proximal isomer was obtained a a nonahydrate (**3.80-p**$(H_2O)_9$, 38.2 mg, 0.039 mmol, 52 % yield). Anal. calcd. for $C_{36}H_{22}Cl_2F_6N_6Ru$ $(H_2O)_9$ (mol. wt. 986.71): C, 43.82; H, 4.09; N, 8.52. Found: C, 43.56; H, 3.75; N 8.67.

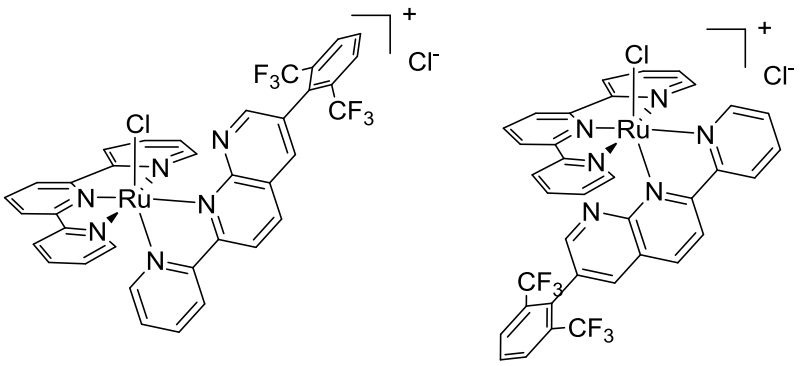

Synthesis of [Ru(Cl)(terpy)(distal-6-(2,6-bis(trifluoromethyl)phenyl)-2-(pyridin-2-yl)-1,8-naphthyridine)]Cl (3.81-d) and [Ru(Cl)(terpy)(proximal-6-(2,6-bis(trifluoromethyl)phenyl)-2-(pyridin-2-yl)-1,8-naphthyridine)]Cl (3.81-p)

6-(2,6-bis(trifluoromethyl)phenyl)-2-(pyridin-2-yl)-1,8-naphthyridine (**3.74**, 124.8 mg, 0.298 mmol), $[(terpy)Ru(Cl)_2]_2$ (**3.13**, 128.6 mg, 0.317 mmol), a stir bar, and methanol (6.0 mL) were added to a vial in a glovebox. The vial was stirred in a 100 ^oC oil bath for 61 h, and after cooling the solvent was removed by rotary evaporation. The distal and proximal isomers were separated on a neutral alumina (12.5 g) column by eluting with a mixture of acetone and water, starting at 100 % acetone and going to 90:10 acetone:water. The distal isomer was the first to elute as a purple solution, followed by the proximal isomer as a red solution. The distal isomer contained a small amount of proximal impurity so another column using the same method was used to purify completely. The different isomers were transferred to vials and solvent was removed by a flow of nitrogen and dried under oil pump vacuum, yielding **3.81-d** $(acetone)_4$ $(H_2O)_1$ (99.6 mg, 0.0927 mmol, 31 % yield). Anal. calcd. for $C_{36}H_{22}Cl_2F_6N_6Ru$ $(C_3H_6O)_4(H_2O)_1$ (mol. wt. 1074.91): C, 53.64; H, 4.50; N 7.82. Found: C, 53.77; H, 4.71; N, 7.76. The proximal isomer was obtained as a pentahydrate, **3.81-p** $(H_2O)_5$ (115.0 mg, 0.126 mmol, 42 % yield). Anal. calcd. for $C_{36}H_{22}Cl_2F_6N_6Ru$ $(H_2O)_5$ (mol. wt. 914.65): C, 47.27; H, 3.53; N, 9.19. Found: C, 47.07; H, 4.23; N, 9.25.

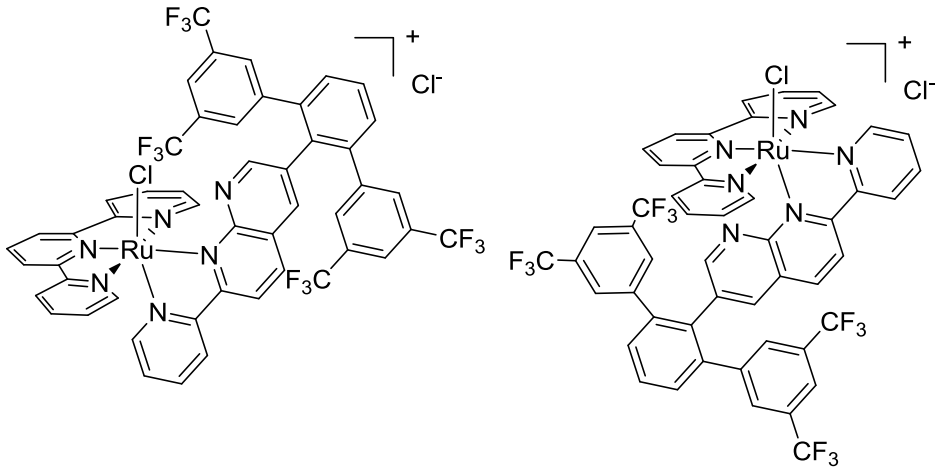

Synthesis of [Ru(Cl)(terpy)(distal-6-(2,6-bis(trifluoromethyl)phenyl)-2-(pyridin-2-yl)-1,8-naphthyridine)]Cl (3.82-d) and [Ru(Cl)(terpy)(proximal-6-(2,6-bis(trifluoromethyl)phenyl)-2-(pyridin-2-yl)-1,8-naphthyridine)]Cl (3.82-p)

6-(2,6-bis(trifluoromethyl)phenyl)-2-(pyridin-2-yl)-1,8-naphthyridine (**3.78**, 67.9 mg, 0.096 mmol), $[(terpy)Ru(Cl)_2]_2$ (**3.13**, 42.8 mg, 0.053 mmol), a stir bar, and methanol (5.0 mL) were added to a pressure vessel (48 mL) in a glovebox. The reaction was stirred in a 100 ^oC oil bath for 3 d, and after cooling the solvent was then removed by a flow of nitrogen. The distal and proximal isomers were separated on a silica (18.5 g) column by eluding with a mixture of acetone and water, starting at 90:10 acetone:water and changing to 80:20 acetone:water. The distal isomer was the first to elute as a purple solution. The distal isomer was transferred to a vial and solvent was removed by a flow of nitrogen and stored under oil pump vacuum, yielding **3.82-d** $(H_2O)_{10}$ (39.8 mg, 0.031 mmol, 32 % yield). Anal. calcd. for $C_{50}H_{28}Cl_2F_{12}N_6Ru$ $(H_2O)_{10}$ (mol. wt. 1292.92): C, 46.67; H, 3.61; N, 6.40. Found: C, 46.45; H, 3.74; N, 6.50. The proximal isomer was eluted by adding lithium chloride (5 mg for 1 mL of water) to the solvent system that was maintained at 80:20 acetone:water. Fractions of the second compound were combined and solvent was removed by rotary evaporation. DCM (5 mL) was added to the residue which was filtered through a fine frit, rinsing the frit with DCM (3 x 5 mL). The organic was then diluted with more DCM (30 mL) and washed with water (15 mL), the aqueous was a dark color so it was back extracted with DCM (2 x 50 mL). The combined organic layers were dried wited Na_2SO_4, filtered through a course frit and solvent was removed

by rotary evaporation. The residue was then dissolved in acetone and transferred to a vial where the solvent was removed by a flow of nitrogen and the residue stored under oil pump vacuum, yielding **3.82-p** $(H_2O)_3$ (39.6 mg, 0.034 mmol, 35 % yield). Anal. calcd. for $C_{50}H_{28}Cl_2F_{12}N_6Ru$ $(H_2O)_3$ (mol. wt. 1166.81): C, 49.56; H, 3.24; N, 6.94. Found: C, 49.45; H, 2.93; N, 7.32.

K. NMR Figures

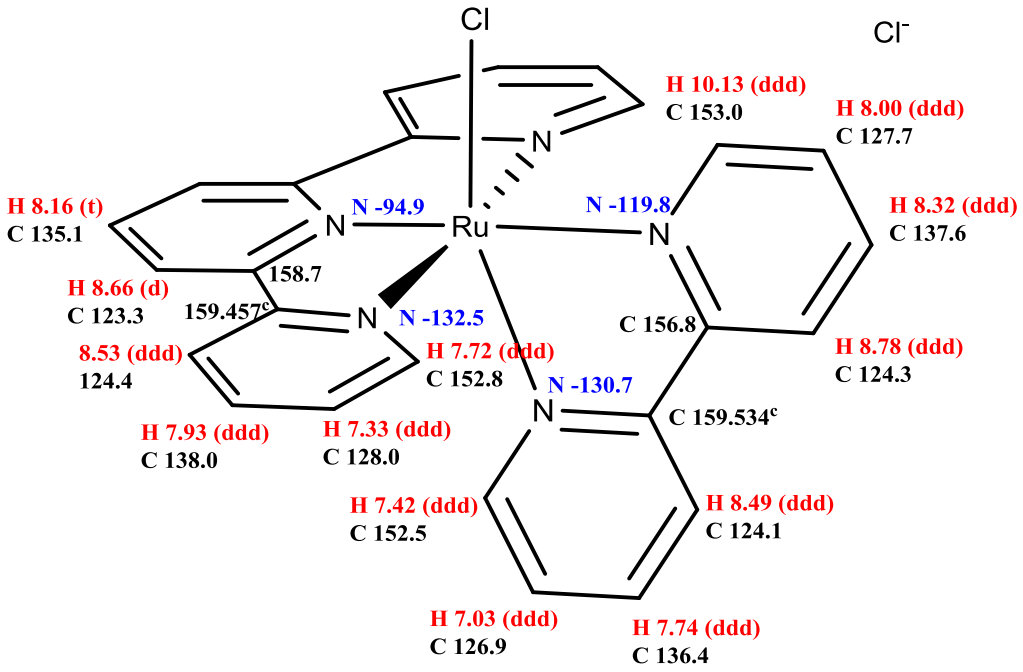

^{1}H -^{15}N gHMBCAD[a]		
^{1}H	bonds	^{15}N
8.66	3	-94.9
10.13	2	-119.8
8.78	3	-119.8
8.00	3	-119.8
8.49	3	-130.7
7.42	2	-130.7
7.03	3	-130.7
8.53	3	-132.5
7.72	2	-132.5
7.33	3	-132.5
[a] J_{nxh} = 5.0 Hz J_{1xh} = 90.0 Hz		

^{1}H-^{13}C HSQCAD	
^{1}H	^{13}C
10.13	153.0
8.78	124.3
8.66	123.3
8.53	124.4
8.49	124.1
8.32	137.6
8.16	135.1
8.00	127.7
7.93	138.0
7.74	136.4
7.72	152.8
7.42	152.5
7.33	128.0
7.03	126.9

gCOSY
10.13↔8.00
8.78↔8.32
8.66↔8.16
8.53↔7.93
8.49↔7.74
8.00↔8.32
7.93↔7.33
7.74↔7.03
7.72↔7.33
7.42↔7.03

Figure 3.50. NMR data for **3.12**.

[c] Two separate carbon shifts were observed in the 1-D carbon NMR spectrum, 159.534 and 159.457 (both would have been rounded to 159.5), peaks were able to be differentiated in the 2D HSQCAD and HMBCAD experiments.

^{1}H -^{13}C gHMBCAD[b]		
^{1}H	bonds	^{13}C
10.13	4	124.3(w)
10.13	2	127.7
10.13	3	137.6
10.13	3	156.8
8.78	3	127.7
8.78	2	137.6(w)
8.78	4	153.0(w)
8.78	2	156.8
8.78	3	159.534[c]
8.66	1,3	123.3
8.66	2	158.7
8.66	3	159.457[c]
8.53	3	128.0
8.53	2	138.0(w)
8.53	4	152.8(w)
8.53	3	158.7
8.53	2	159.457[c]
8.49	3	126.9
8.49	2	136.4(w)
8.49	4	152.5(w)
8.49	3	156.8
8.49	2	159.534[c]
8.32	2	124.3(w)
8.32	3	153.0
8.32	3	156.8
8.16	2	123.3
8.16	3	158.7
8.16	4	159.457[c]
8.00	3	124.3
8.00	2	153.0

^{1}H -^{13}C gHMBCAD cont.[b]		
^{1}H	bonds	^{13}C
7.93	2	124.4(w)
7.93	2	128.0
7.93	3	152.8
7.93	3	159.457[c]
7.74	2	124.1(w)
7.74	3	152.5
7.74	3	159.534[c]
7.72	4	124.4
7.72	2	128.0
7.72	3	138.0
7.72	2	159.457[c]
7.42	4	124.1(w)
7.42	2	126.9
7.42	3	136.4
7.42	3	159.534[c]
7.33	3	124.4
7.33	2	152.8
7.33	4	159.457(w)[c]
7.03	3	124.1
7.03	2	152.5(w)
[b] J_{nxh} = 8.0 Hz J_{1xh} = 146.0 Hz		

^{1}H (599.48 MHz) sw = 5165.3 Hz np = 524288	
^{1}H	$^{X}J_{HH}$
10.13 (ddd)	5.57 Hz (3), 1.61 Hz (4), 0.83 Hz (5)
8.78 (ddd)	8.29 Hz (3), 1.34 Hz(4), 0.85 Hz (5)
8.66 (d)	8.12 Hz (3)
8.53 (ddd)	8.08 Hz (3), 1.39 Hz (4), 0.79 Hz (5)
8.49 (ddd)	8.29 Hz (3), 1.44 Hz (4), 0.82 Hz (5)
8.32 (ddd)	8.26 Hz (3), 7.58 Hz (3), 1.57 Hz (4)
8.16 (t)	8.09 Hz (3)
8.00 (ddd)	7.68 Hz (3), 5.54 Hz (3), 1.30 Hz (4)
7.93 (ddd)	8.14 Hz (3), 7.51 Hz (3), 1.52 Hz (4)
7.74 (ddd)	8.19 Hz (3), 7.47 Hz (3), 1.47 Hz (4)
7.72 (ddd)	5.57 Hz (3), 1.55 Hz (4), 0.80 Hz (5)
7.42 (ddd)	5.82 Hz (3), 1.48 Hz (4), 0.79 Hz (5)
7.33 (ddd)	7.55 Hz (3), 5.53 Hz (3), 1.32 Hz (4)
7.03 (ddd)	7.47 Hz (3), 5.82 Hz (3), 1.38 Hz (4)
Bonds between hydrogen atoms being coupled in parentheses.	

Figure 3.50 cont. NMR data for **3.12**.

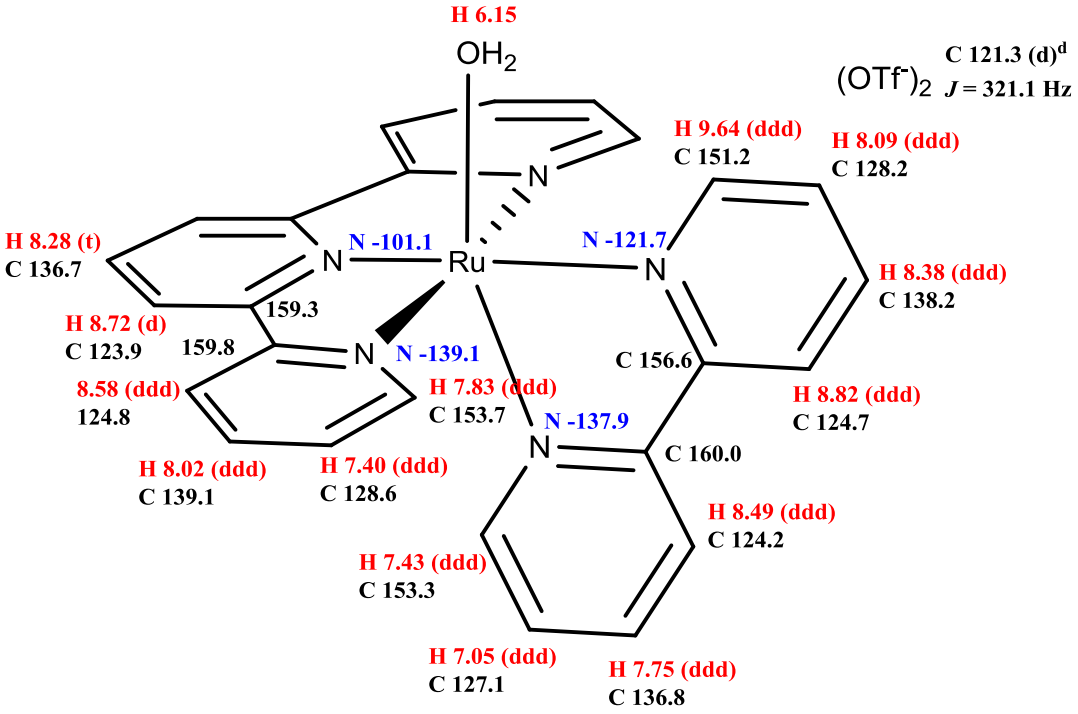

^{1}H - ^{15}N gHMBCAD[a]		
^{1}H	bonds	^{15}N
8.72	3	-101.1
9.64	2	-121.7
8.82	3	-121.7
8.09	3	-121.7
8.49	3	-137.9
7.43	2	-137.9
7.05	3	-137.9
8.58	3	-139.1
7.83	2	-139.1
7.40	3	-139.1
[a] J_{nxh} = 5.0 Hz J_{1xh} = 90.0 Hz		

^{1}H-^{13}C HSQCAD	
^{1}H	^{13}C
9.64	151.2
8.82	124.7
8.72	123.9
8.58	124.8
8.49	124.2
8.38	138.2
8.28	136.7
8.09	128.2
8.02	139.1
7.83	153.7
7.75	136.8
7.43	153.3
7.40	128.6
7.05	127.1

gCOSY
9.64↔8.09
8.82↔8.38
8.72↔8.28
8.58↔8.02
8.49↔7.75
8.38↔8.09
8.02↔7.40
7.83↔7.40
7.75↔7.05
7.43↔7.05

Figure 3.51. NMR data for **3.12b**.

[d] Only the two most intense peaks of the trifluoromethanesulfonate carbon quartet were observed.

^{1}H -^{13}C gHMBCAD[b]		
^{1}H	bonds	^{13}C
9.64	4	124.7(w)
9.64	2	128.2
9.64	3	138.2
9.64	3	156.6
8.82	3	128.2
8.82	2	156.6
8.82	3	160.0
8.72	1,3	123.9
8.72	2	159.3
8.72	3	159.8
8.58	3	128.6
8.58	3	159.3
8.58	2	159.8
8.49	3	127.1
8.49	3	156.6
8.49	2	160.0
8.38	3	151.2
8.38	3	156.6
8.28	2	123.9
8.28	3	159.3
8.28	4	159.8(w)
8.09	3	124.7
8.09	2	151.2
8.02	2	124.8(w)
8.02	3	153.7
8.02	3	159.8

^{1}H -^{13}C gHMBCAD cont.[b]		
^{1}H	bonds	^{13}C
7.83	4	124.8(w)
7.83	2	128.6
7.83	3	139.1
7.83	3	159.8
7.75	3	153.3
7.75	3	160.0
7.43	2	127.1
7.43	3	136.8
7.43	3	160.0
7.40	3	124.8
7.40	2	153.7
7.05	3	124.2
7.05	2	153.3
[b]J_{nxh} = 8.0 Hz J_{1xh} = 146.0 Hz		

^{1}H (599.48 MHz) sw = 5387.9Hz np = 524288	
^{1}H	$^{x}J_{HH}$
9.64 (ddd)	5.54 Hz (3), 1.55 Hz (4), 0.87 Hz (5)
8.82 (ddd)	8.28 Hz (3), 1.33 Hz(4), 0.86 Hz (5)
8.72 (d)	8.13 Hz (3)
8.58 (ddd)	8.10 Hz (3), 1.35 Hz (4), 0.87 Hz (5)
8.49 (ddd)	8.23 Hz (3), 1.46 Hz (4), 0.81 Hz (5)
8.38 (ddd)	8.23 Hz (3), 7.65 Hz (3), 1.46 Hz (4)
8.28 (t)	8.12 Hz (3)
8.09 (ddd)	7.70 Hz (3), 5.47 Hz (3), 1.34 Hz (4)
8.02 (ddd)	8.12 Hz (3), 7.63 Hz (3), 1.57 Hz (4)
7.83 (ddd)	5.53 Hz (3), 1.56 Hz (4), 0.78 Hz (5)
7.75 (ddd)	8.14 Hz (3), 7.52 Hz (3), 1.49 Hz (4)
7.43 (ddd)	5.84 Hz (3), 1.51 Hz (4), 0.73 Hz (5)
7.40 (ddd)	7.62 Hz (3), 5.51 Hz (3), 1.36 Hz (4)
7.05 (ddd)	7.49 Hz (3), 5.88 Hz (3), 1.49 Hz (4)
Bonds between Hydrogen atoms being coupled in parentheses.	

Figure 3.51 cont. NMR data for **3.12b**.

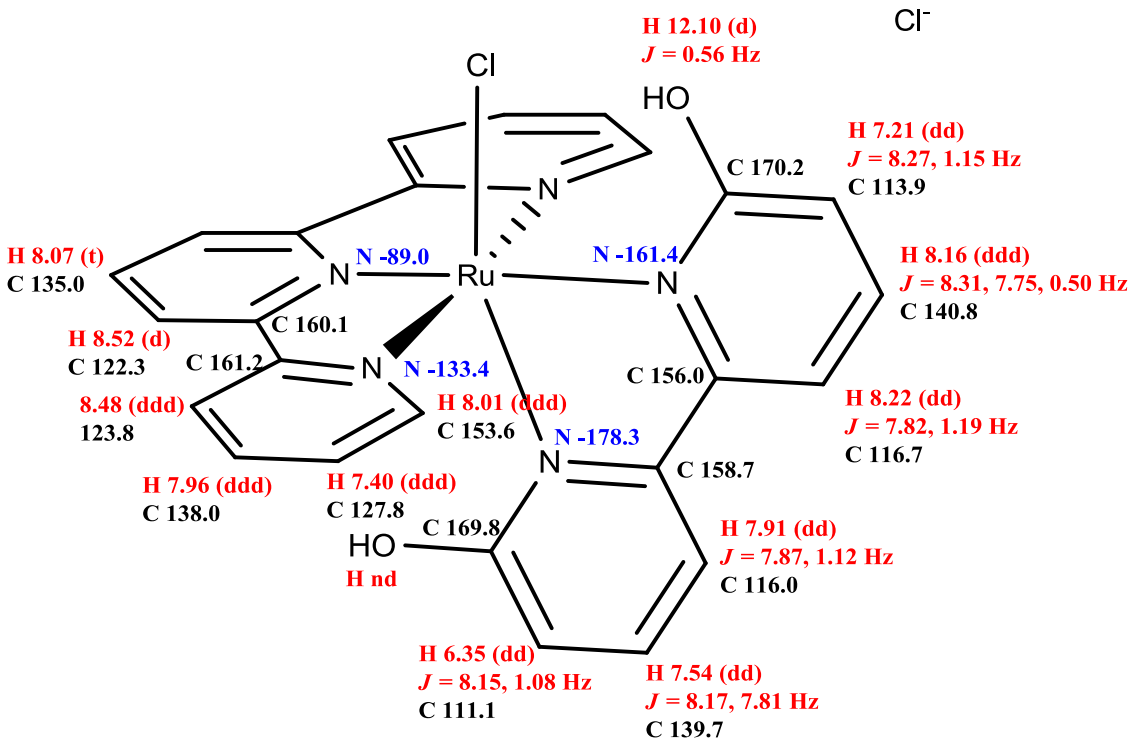

^{1}H -^{15}N **gHMBCAD**[a]		
^{1}H	bonds	^{15}N
8.52	3	-89.0
8.48	3	-133.4
8.01	2	-133.4
7.40	3	-133.4
8.22	3	-161.4
7.91	3	-178.3
[a]J_{nxh} = 5.0 Hz J_{1xh} = 90.0 Hz		

^{1}H-^{13}C **HSQCAD**	
^{1}H	^{13}C
8.52	122.3
8.48	123.8
8.22	116.7
8.16	140.8
8.07	135.0
8.01	153.6
7.96	138.0
7.91	116.0
7.54	139.7
7.40	127.8
7.21	113.9
6.35	111.1

gCOSY
8.52↔8.07
8.48↔7.96
8.22↔8.16
8.16↔7.21
8.01↔7.40
7.96↔7.40
7.91↔7.54
7.54↔6.35

Figure 3.52. NMR data for **3.16**.

^{1}H -^{13}C gHMBCAD[b]		
^{1}H	bonds	^{13}C
12.10	3	113.9
12.10	4	140.8(w)
12.10	2	170.2
8.52	1,3	122.3
8.52	2	160.1
8.52	3	161.2
8.48	3	127.8
8.48	3	160.1
8.48	2	161.2
8.22	3	113.9
8.22	2	156.0
8.22	3	158.7
8.16	3	156.0
8.16	3	170.2
8.07	3	160.1
8.01	4	123.8(w)
8.01	2	127.8
8.01	3	138.0
8.01	3	161.2
7.96	3	153.6
7.96	3	161.2
7.91	3	111.1
7.91	3	156.0
7.91	2	158.7
7.54	3	158.7
7.54	3	169.8
7.40	3	123.8
7.40	2	153.6
7.40	4	161.2(w)
7.21	3	116.7
6.35	3	116.0
[b]J_{nxh} = 8.0 Hz J_{1xh} = 146.0 Hz		

^{1}H (599.48 MHz) sw = 8389.3 Hz np = 524288	
^{1}H	$^{x}J_{HH}$
12.10 (d)	0.56 Hz (5)
8.52 (d)	8.08 Hz (3)
8.48 (ddd)	8.08 Hz (3), 1.38 Hz (4), 0.79 Hz (5)
8.22 (dd)	7.82 Hz (3), 1.19 Hz (4)
8.16 (ddd)	8.31 Hz (3), 7.75 Hz (3), 0.50 Hz (5)
8.07 (t)	8.07 Hz (3)
8.01 (ddd)	5.50 Hz (3), 1.55 Hz (4), 0.80 Hz (5)
7.96 (ddd)	8.07 Hz (3), 7.56 Hz (3), 1.53 Hz (4)
7.91 (dd)	7.87 Hz (3), 1.12 Hz (4)
7.54 (dd)	8.17 Hz (3), 7.81 Hz (3)
7.40 (ddd)	7.58 Hz (3), 5.50 Hz (3), 1.35 Hz (4)
7.21 (dd)	8.27 Hz (3), 1.15 Hz (4)
6.35 (dd)	8.15 Hz (3), 1.08 Hz (4)
Bonds between Hydrogen atoms being coupled in parentheses.	

Figure 3.52 cont. NMR data for **3.16**.

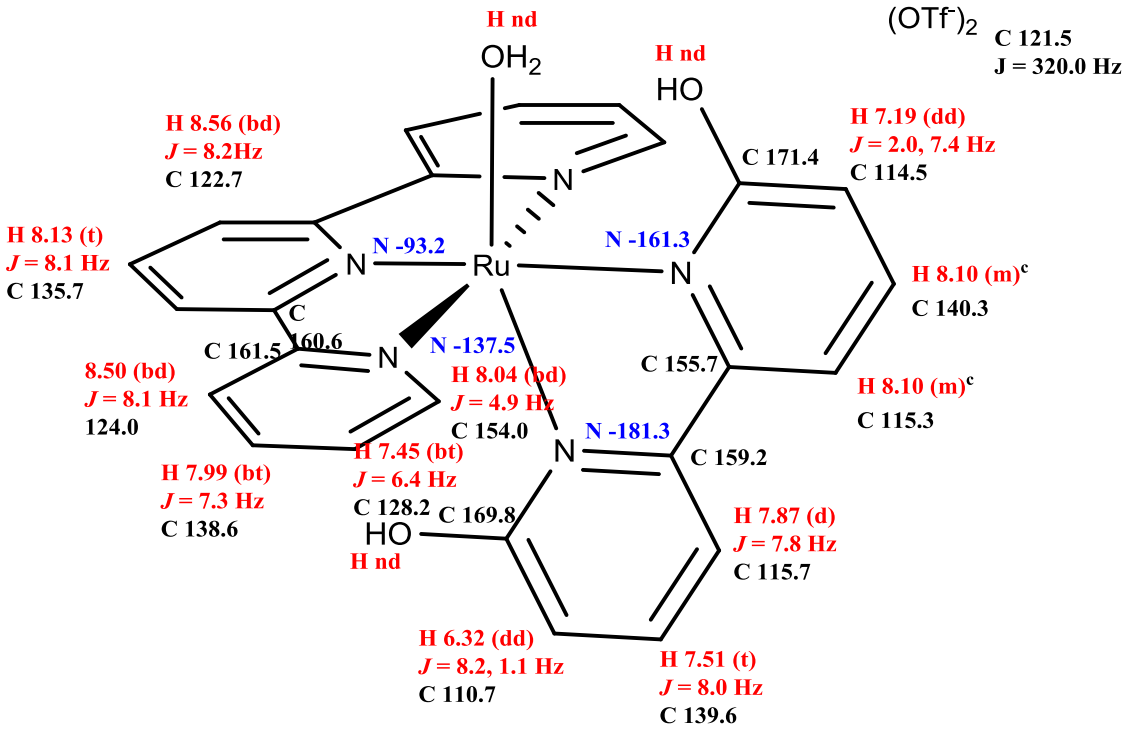

^{1}H -^{15}N gHMBCAD[a]		
^{1}H	bonds	^{15}N
8.56	3	-93.2
8.50	3	-137.5
8.04	2	-137.5
7.45	3	-137.5
8.10	3	-161.3
7.19	3	-161.3
7.87	3	-181.3
6.32	3	-181.3
[a]J_{nxh} = 5.0 Hz J_{1xh} = 90.0 Hz		

^{1}H-^{13}C HSQCAD	
^{1}H	^{13}C
8.56	122.7
8.50	124.0
8.13	135.7
8.10	115.3
8.10	140.3
8.04	154.0
7.99	138.6
7.87	115.7
7.51	139.6
7.45	128.2
7.19	114.5
6.32	110.7

gCOSY
8.56↔8.13
8.50↔7.99
8.10↔7.19
8.04↔7.45
7.99↔7.45
7.87↔7.51
7.51↔6.32

Figure 3.53. NMR data for **3.16b**.

[c] Proton resonances exhibit non-first order splitting and are indistinguishable from each other. The carbon of 140.3 is assigned based on the trend of the downfield carbon shift being para to the nitrogen on the bipy ligand.

*Note-The proton NMR peaks are very broad in comparison to those of the other complexes, which leads to the averaged coupling constant values of the two highest values.

^{1}H -^{13}C gHMBCAD[b]		
^{1}H	bonds	^{13}C
8.56	1,3	122.7
8.56	2	160.6
8.56	3	161.5
8.50	3	128.2
8.50	4	154.0(w)
8.50	3	160.6
8.50	2	161.5
8.13	2	122.7
8.13	3	160.6
8.13	4	161.5
8.10[c]	2,3	114.5
8.10[c]	2,3	155.7
8.10[c]	3,4	159.2
8.10[c]	3,4	171.4
8.04	4	124.0(w)
8.04	2	128.2
8.04	3	138.6
8.04	3	161.5

^{1}H -^{13}C gHMBCAD[b] cont.		
^{1}H	bonds	^{13}C
7.99	3	154.0
7.99	3	161.5
7.87	3	110.7
7.87	3	155.7
7.87	2	159.2
7.87	4	169.8
7.51	2	110.7(w)
7.51	2	115.7(w)
7.51	4	155.7(w)
7.51	3	159.2
7.51	3	169.8
7.45	3	124.0
7.45	2	154.0
7.45	4	161.5(w)
7.19	3	115.3
7.19	4	155.7(w)
7.19	2	171.4(w)
6.32	3	115.7
6.32	2	169.8(w)
[b] J_{nxh} = 8.0 Hz J_{1xh} = 146.0 Hz		

Figure 3.53 cont. NMR data for **3.16b**.

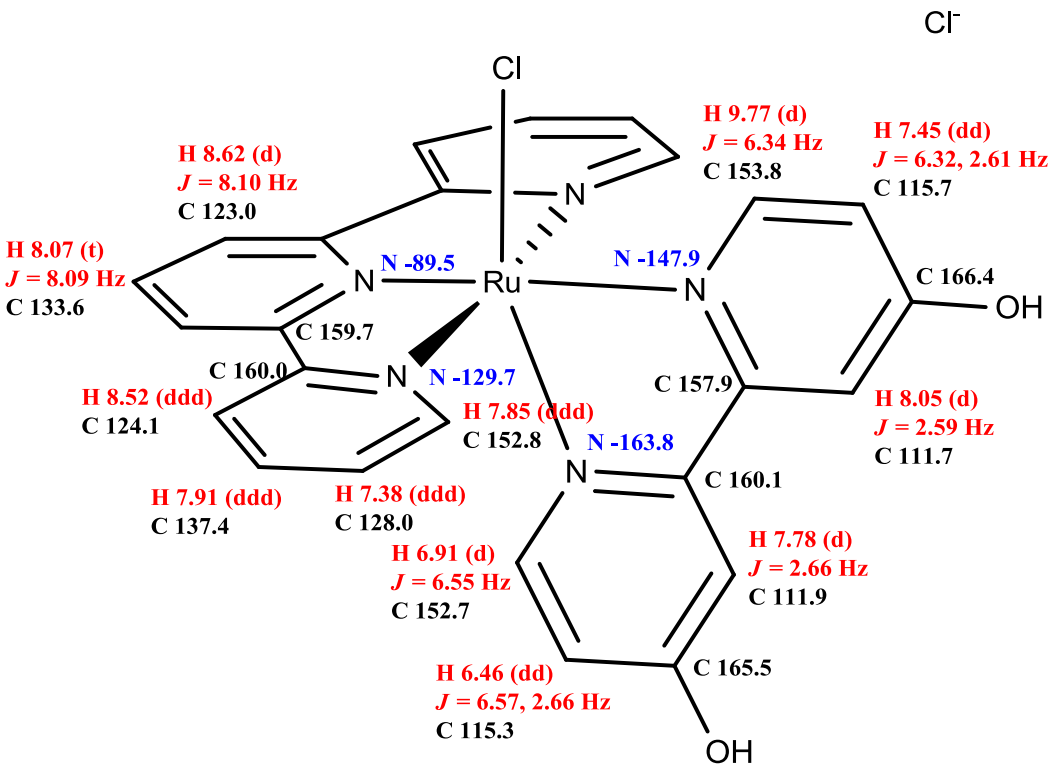

^{1}H - ^{15}N **gHMBCAD**[a]		
^{1}H	bonds	^{15}N
8.62	3	-89.5
8.52	3	-129.7
7.85	2	-129.7
7.38	3	-129.7
9.77	2	-147.9
6.91	2	-163.8
[a] J_{nxh} = 5.0 Hz J_{1xh} = 90.0 Hz		

^{1}H-^{13}C **HSQCAD**	
^{1}H	^{13}C
9.77	153.8
8.62	123.0
8.52	124.1
8.07	133.6
8.05	111.7
7.91	137.4
7.85	152.8
7.78	111.9
7.45	115.7
7.38	128.0
6.91	152.7
6.46	115.3

gCOSY
9.77↔7.45
8.62↔8.07
8.52↔7.91
8.05↔7.45
7.91↔7.38
7.85↔7.38
7.78↔6.46
6.91↔6.46

Figure 3.54. NMR data for **3.17**.

^{1}H -^{13}C gHMBCAD[b]		
^{1}H	bonds	^{13}C
9.77	2	115.7
9.77	3	157.9
9.77	3	166.4
8.62	1,3	123.0
8.62	2	159.7
8.52	3	128.0
8.52	3	159.7
8.52	2	160.0
8.07	3	159.7
8.05	3	115.7
8.05	3	160.1
8.05	2	166.4
7.91	3	152.8
7.91	3	160.0
7.85	4	124.1(w)
7.85	2	128.0
7.85	3	137.4
7.85	3	160.0
7.78	3	115.3
7.78	3	157.9
7.78	2	165.5
7.45	3	111.7
7.45	2	153.8(w)
7.38	3	124.1
7.38	2	152.8
6.91	4	111.9(w)
6.91	2	115.3
6.91	3	160.1
6.91	3	165.5
6.46	3	111.9
6.46	2	152.7(w)
6.46	2	165.5(w)
$^{b}J_{nxh}$ = 8.0 Hz J_{1xh} = 146.0 Hz		

^{1}H (599.48 MHz) sw = 5387.9 Hz np = 524288	
^{1}H	$^{x}J_{HH}$
9.77 (d)	6.34 Hz (3)
8.62 (d)	8.10 Hz (3)
8.52 (ddd)	8.12 Hz (3), 1.37 Hz (4), 0.81 Hz (5)
8.07 (t)	8.09 Hz (3)
8.05 (d)	2.59 Hz (4)
7.91 (ddd)	8.12 Hz (3), 7.46 Hz (3), 1.51 Hz (4)
7.85 (ddd)	5.54 Hz (3), 1.57 Hz (4), 0.81 Hz (5)
7.78 (d)	2.66 Hz (4)
7.45 (dd)	6.32 Hz (3), 2.61 Hz (4)
7.38 (ddd)	7.52 Hz (3), 5.51 Hz (3), 1.32 Hz (4)
6.91 (d)	6.55 Hz (3)
6.46 (dd)	6.57 Hz (3), 2.66 Hz (4)
Bonds between Hydrogen atoms being coupled in parentheses.	

Figure 3.54 cont. NMR data for **3.17**.

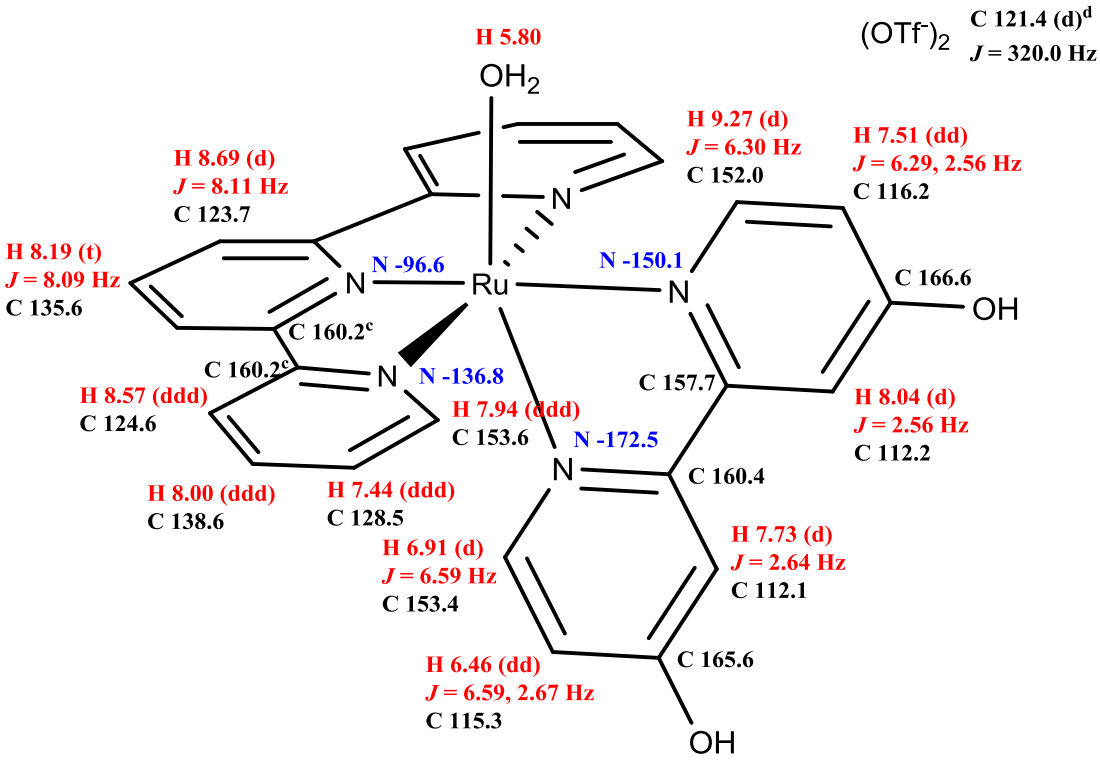

^{1}H - ^{15}N gHMBCAD[a]		
^{1}H	bonds	^{15}N
8.69	3	-96.6
8.57	3	-136.8
7.94	2	-136.8
7.44	3	-136.8
9.27	2	-150.1
6.91	2	-172.5
[a]J_{nxh} = 5.0 Hz J_{1xh} = 90.0 Hz		

^{1}H-^{13}C HSQCAD	
^{1}H	^{13}C
9.27	152.0
8.69	123.7
8.57	124.6
8.19	135.6
8.04	112.2
8.00	138.6
7.94	153.6
7.73	112.1
7.51	116.2
7.44	128.5
6.91	153.4
6.46	115.3

gCOSY
9.27↔7.51
8.69↔8.19
8.57↔8.00
8.04↔7.51
8.00↔7.44
7.94↔7.44
7.73↔6.46
6.91↔6.46

Figure 3.55. NMR data for **3.17b**.

[c] Two separate carbon shifts were observed in the carbon NMR spectrum, 160.182 and 160.161, however the peaks were not able to be differentiated in the 2D HSQCAD and HMBCAD experiments.
[d] Only the two most intense peaks of the trifluoromethanesulfonate carbon quartet were observed.

^{1}H -^{13}C gHMBCAD[b]		
^{1}H	bonds	^{13}C
9.27	4	112.2(w)
9.27	2	116.2
9.27	3	157.7
9.27	3	166.6
8.69	1,3	123.7
8.69	2 or 3[c]	160.2
8.57	3	128.5
8.57	4	153.6(w)
8.57	2 or 3[c]	160.2
8.19	2	123.7
8.19	3	160.2
8.04	3	116.2
8.04	2	157.7
8.04	3	160.4
8.04	2	166.6
8.00	2	124.6(w)
8.00	3	153.6
8.00	3	160.2
7.94	4	124.6(w)
7.94	2	128.5
7.94	3	138.6
7.94	3	160.2
7.73	3	115.3
7.73	3	157.7
7.73	2	160.4
7.73	2	165.6
7.51	3	112.2
7.51	2	152.0(w)
7.51	2	166.6
7.44	3	124.6
7.44	2	153.6
7.44	4	160.2(w)
6.91	4	112.1(w)
6.91	2	115.3
6.91	3	160.4
6.91	3	165.6
6.46	3	112.1
6.46	2	153.4
6.46	2	165.6
[b] J_{nxh} = 8.0 Hz J_{1xh} = 146.0 Hz		

^{1}H (599.48 MHz) sw = 4921.3 Hz np = 524288	
^{1}H	$^{x}J_{HH}$
9.27 (d)	6.30 Hz (3)
8.69 (d)	8.11 Hz (3)
8.57 (ddd)	8.11 Hz (3), 1.35 Hz (4), 0.77 Hz (5)
8.19 (t)	8.09 Hz (3)
8.04 (d)	2.56 Hz (4)
8.00 (ddd)	8.11 Hz (3), 7.52 Hz (3), 1.50 Hz (4)
7.94 (ddd)	5.54 Hz (3), 1.59 Hz (4), 0.79 Hz (5)
7.73 (d)	2.64 Hz (4)
7.51 (dd)	6.29 Hz (3), 2.56 Hz (4)
7.44 (ddd)	7.58 Hz (3), 5.53 Hz (3), 1.35 Hz (4)
6.91 (d)	6.59 Hz (3)
6.46 (dd)	6.59 Hz (3), 2.67 Hz (4)
Bonds between Hydrogen atoms being coupled in parentheses.	

Figure 3.55 cont. NMR data for **3.17b**.

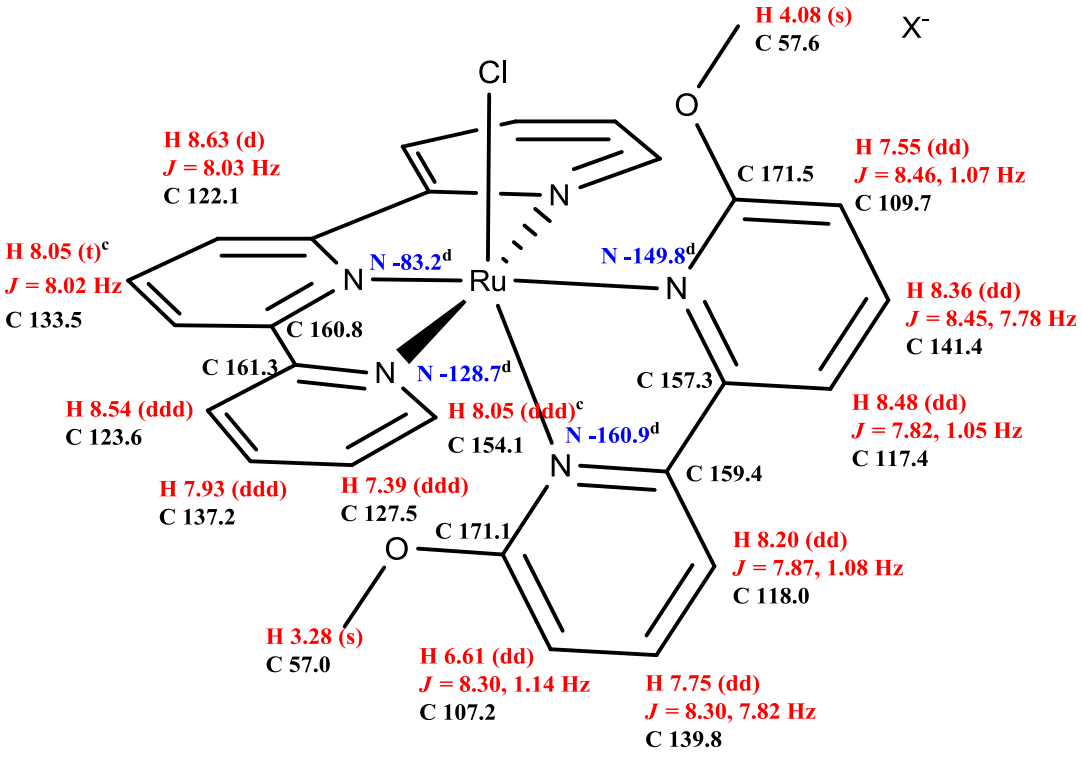

^{1}H -^{15}N gHMBCAD[a,d]		
^{1}H	bonds	^{15}N
8.59	3	-83.2
8.50	3	-128.7
8.05	2	-128.7
7.39	3	-128.7
8.42	3	-149.8
8.13	3	-160.9
$^{a}J_{nxh}$ = 5.0 Hz J_{1xh} = 90.0 Hz		

^{1}H-^{13}C HSQCAD	
^{1}H	^{13}C
8.63	122.1
8.54	123.6
8.48	117.4
8.36	141.4
8.20	118.0
8.05	133.5
8.05	154.1
7.93	137.2
7.75	139.8
7.55	109.7
7.39	127.5
6.61	107.2
4.08	57.6
3.28	57.0

gCOSY
8.63↔8.05
8.54↔7.93
8.48↔8.36
8.36↔7.55
8.20↔7.75
8.05↔7.39
7.93↔7.39
7.75↔6.61

Figure 3.56. NMR data for **3.18**.

[d] ^{15}N data was obtained on the PF_6 analog in d_6-acetone, because of insolubility of the chloride analog.

^{1}H -^{13}C gHMBCAD[b]		
^{1}H	bonds	^{13}C
8.63	1,3	122.1
8.63	2	160.8
8.54	3	127.5
8.54	3	160.8
8.54	2	161.3
8.48	3	109.7
8.48	2	157.3
8.48	3	159.4
8.36	3	157.3
8.36	3	171.5
8.20	3	107.2
8.20	3	157.3
8.20	2	159.4
8.05(ddd)	2	127.5
8.05(ddd)	3	137.2
8.05(t)	3	160.8
8.05(ddd)	3	161.3
7.93	3	154.1
7.93	3	161.3
7.75	3	159.4
7.75	3	171.1
7.55	3	117.4
7.39	3	123.6
7.39	2	154.1
6.61	3	118.0
4.08	3	171.5
3.28	3	171.1
$^{b}J_{nxh}$ = 8.0 Hz J_{1xh} = 146.0 Hz		

^{1}H comparison for Cl or PF_6 counter ion	
^{1}H of 7d-Cl	^{1}H of 7d-PF6
8.63	8.59
8.54	8.50
8.48	8.42
8.36	8.36
8.20	8.13
8.05	8.05
8.05	8.05
7.93	7.93
7.75	7.74
7.55	7.55
7.39	7.39
6.61	6.59
4.08	4.08
3.28	3.28

^{1}H (599.48 MHz) sw = 4807.7 Hz np = 524288	
^{1}H	$^{x}J_{HH}$
8.63 (d)	8.03 Hz (3)
8.54 (ddd)	8.00 Hz (3), 1.37 Hz (4), 0.90 Hz (5)
8.48 (dd)	7.82 Hz (3), 1.05 Hz (4)
8.36 (dd)	8.45 Hz (3), 7.78 Hz (3)
8.20 (dd)	7.87 Hz (3), 1.08 Hz (4)
8.05 (t)	8.02 Hz (3)
8.05 (ddd)	5.55 Hz (3), 1.56 Hz (4), 0.85 Hz (5)
7.93 (ddd)	8.04 Hz (3), 7.56 Hz (3), 1.55 Hz (4)
7.75 (dd)	8.30 Hz (3), 7.82 Hz (3)
7.55 (dd)	8.46 Hz (3), 1.07 Hz (4)
7.39 (ddd)	7.55 Hz (3), 5.54 Hz (3), 1.36 Hz (4)
6.61 (dd)	8.30 Hz (3), 1.14 Hz (4)
Bonds between Hydrogen atoms being coupled in parentheses.	

Figure 3.56 cont. NMR data for **3.18**.

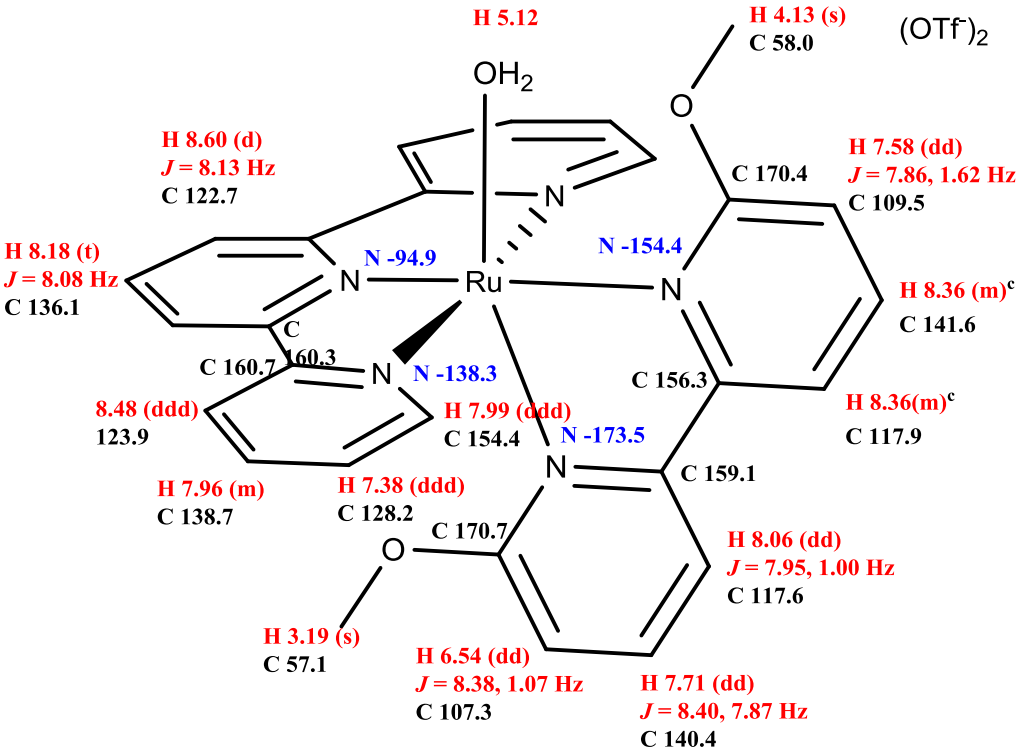

^{1}H -^{15}N **gHMBCAD**[a]		
^{1}H	bonds	^{15}N
8.60	3	-94.9
8.48	3	-138.3
7.99	2	-138.3
7.38	3	-138.3
8.36	3	-154.4
7.58	3	-154.4
8.06	3	-173.5
6.54	3	-173.5
[a] J_{nxh} = 5.0 Hz J_{1xh} = 90.0 Hz		

gCOSY
8.60↔8.18
8.48↔7.96
8.36↔7.58
8.06↔7.71
7.99↔7.38
7.96↔7.38
7.71↔6.54

^{1}H-^{13}C **HSQCAD**	
^{1}H	^{13}C
8.60	122.7
8.48	123.9
8.36	117.9
8.36	141.6
8.18	136.1
8.06	117.6
7.99	154.4
7.96	138.6
7.71	140.4
7.58	109.5
7.38	128.2
6.54	107.3
4.13	58.0
3.19	57.1

Figure 3.57. NMR data for **3.18b**.

[c] Protons resonances exhibit non-first-order splitting and are indistinguishable from each other. The carbon resonance at 141.6 is assigned based on the trend of the downfield carbon shift being para to the nitrogen on the bipy ligand.

^{1}H -^{13}C gHMBCAD[b]		
^{1}H	bonds	^{13}C
8.60	1,3	122.7
8.60	2	160.3
8.48	3	128.2
8.48	4	154.4(w)
8.48	3	160.3
8.48	2	160.7
8.36[c]	2,3	109.5
8.36[c]	2,3	156.3
8.36[c]	3,4	159.1
8.36[c]	3,4	170.4
8.18	2	122.7
8.18	3	160.3
8.18	4	160.7
8.06	3	107.3
8.06	3	156.3
8.06	2	159.1
8.06	4	170.7(w)
7.99	2	128.2
7.99	3	138.6
7.99	3	160.7
7.96	2	123.9(w)
7.96	3	154.4
7.96	3	160.7
7.71	2	107.3(w)
7.71	2	117.6(w)
7.71	3	159.1
7.71	3	170.7
7.58	3	117.9
7.58	2	141.6(w)
7.58	2	170.4
7.38	3	123.9
7.38	2	154.4
7.38	4	160.7(w)
6.54	3	117.6
6.54	2	140.4(w)
4.13	3	170.4
3.19	3	170.7
[b] J_{nxh} = 8.0 Hz J_{1xh} = 146.0 Hz		

^{1}H (599.48 MHz) sw = 4496.4 Hz np = 524288	
^{1}H	$^{x}J_{HH}$
8.60 (d)	8.13 Hz (3)
8.48 (ddd)	7.98 Hz (3), 1.33 Hz (4), 0.90 Hz (5)
8.36 (m)	-
8.36 (m)	-
8.18 (t)	8.08 Hz (3)
8.06 (dd)	7.95 Hz (3), 1.00 Hz (4)
7.99 (ddd)	5.56 Hz (3), 1.55 Hz (4), 0.83 Hz (5)
7.96 (m)	-
7.71 (dd)	8.40 Hz (3), 7.87 Hz (3)
7.58 (dd)	7.86 Hz (3), 1.62 Hz (4)
7.38 (ddd)	7.60 Hz (3), 5.52 Hz (3), 1.29 Hz (4)
6.54 (dd)	8.38 Hz (3), 1.07 Hz (4)
Bonds between Hydrogen atoms being coupled in parentheses.	

Figure 3.57 cont. NMR data for **3.18b**.

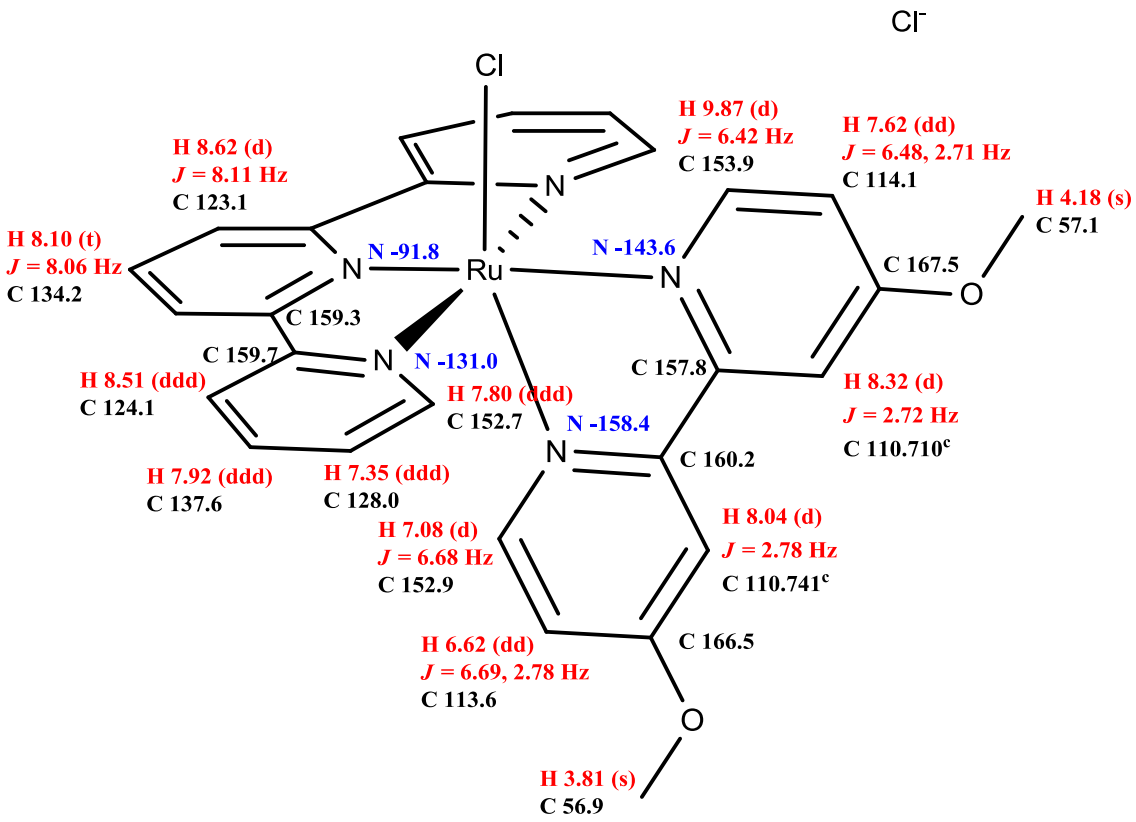

^{1}H - ^{15}N gHMBCAD[a]		
^{1}H	bonds	^{15}N
8.62	3	-91.8
8.51	3	-131.0
7.80	2	-131.0
7.35	3	-131.0
9.87	2	-143.6
8.32	3	-143.6(w)
8.04	3	-158.4(w)
7.08	2	-158.4
[a] J_{nxh} = 5.0 Hz J_{1xh} = 90.0 Hz		

gCOSY
9.87↔7.62
8.62↔8.10
8.51↔7.92
8.32↔7.62
8.04↔6.62
7.92↔7.35
7.80↔7.35
7.08↔6.62

^{1}H-^{13}C HSQCAD	
^{1}H	^{13}C
9.87	153.9
8.62	123.1
8.51	124.1
8.32	110.710
8.10	134.2
8.04	110.741
7.92	137.6
7.80	152.7
7.62	114.1
7.35	128.0
7.08	152.9
6.62	113.6
4.18	57.1
3.81	56.9

Figure 3.58. NMR data for **3.19**.

[c] Two separate carbon shifts were observed in the 1-D carbon NMR spectrum, 110.710 and 110.741, and although different by only 0.031ppm, the peaks were able to be differentiated in the 2D HSQCAD and HMBCAD experiments.

^{1}H -^{13}C gHMBCAD[b]		
^{1}H	bonds	^{13}C
9.87	4	110.710
9.87	2	114.1
9.87	3	157.8
9.87	3	167.5
8.62	1,3	123.1
8.62	2	159.3
8.51	3	128.0
8.51	3	159.3
8.51	2	159.7
8.32	3	114.1
8.32	2	157.8(w)
8.32	3	160.2
8.32	2	167.5
8.10	2	123.1
8.10	3	159.3
8.04	3	113.6
8.04	3	157.8
8.04	2	160.2
8.04	2	166.5
7.92	2	124.1(w)
7.92	2	128.0(w)
7.92	3	152.7
7.92	3	159.7
7.80	4	124.1
7.80	2	128.0
7.80	3	137.6
7.80	3	159.7
7.62	3	110.7
7.62	2	153.9
7.62	2	167.5
7.35	3	124.1
7.35	2	152.7
7.35	4	159.7
7.08	4	110.7(w)
7.08	2	113.6
7.08	3	160.2
7.08	3	166.5
6.62	3	110.741
6.62	2	152.9(w)
6.62	2	166.5
4.18	3	167.5
3.81	3	166.5
$^{b}J_{nxh}$ = 8.0 Hz J_{1xh} = 146.0 Hz		

^{1}H (599.48 MHz) sw = 5387.9 Hz np = 524288	
^{1}H	$^{x}J_{HH}$
9.87 (d)	6.42 Hz (3)
8.62 (d)	8.11 Hz (3)
8.51 (ddd)	8.09 Hz (3), 1.38 Hz (4), 0.84 Hz (5)
8.32 (d)	2.72 Hz (4)
8.10 (t)	8.06 Hz (3)
8.04 (d)	2.78 Hz (4)
7.92 (ddd)	8.11 Hz (3), 7.56 Hz (3), 1.52 Hz (4)
7.80 (ddd)	5.54 Hz (3), 1.57 Hz (4), 0.80 Hz (5)
7.62 (dd)	6.48 Hz (3), 2.71 Hz (4)
7.35 (ddd)	7.55 Hz (3), 5.53 Hz (3), 1.31 Hz (4)
7.08 (d)	6.68 Hz (3)
6.62 (dd)	6.69 Hz (3), 2.78 Hz (4)
Bonds between Hydrogen atoms being coupled in parentheses.	

Figure 3.58 cont. NMR data for **3.19**.

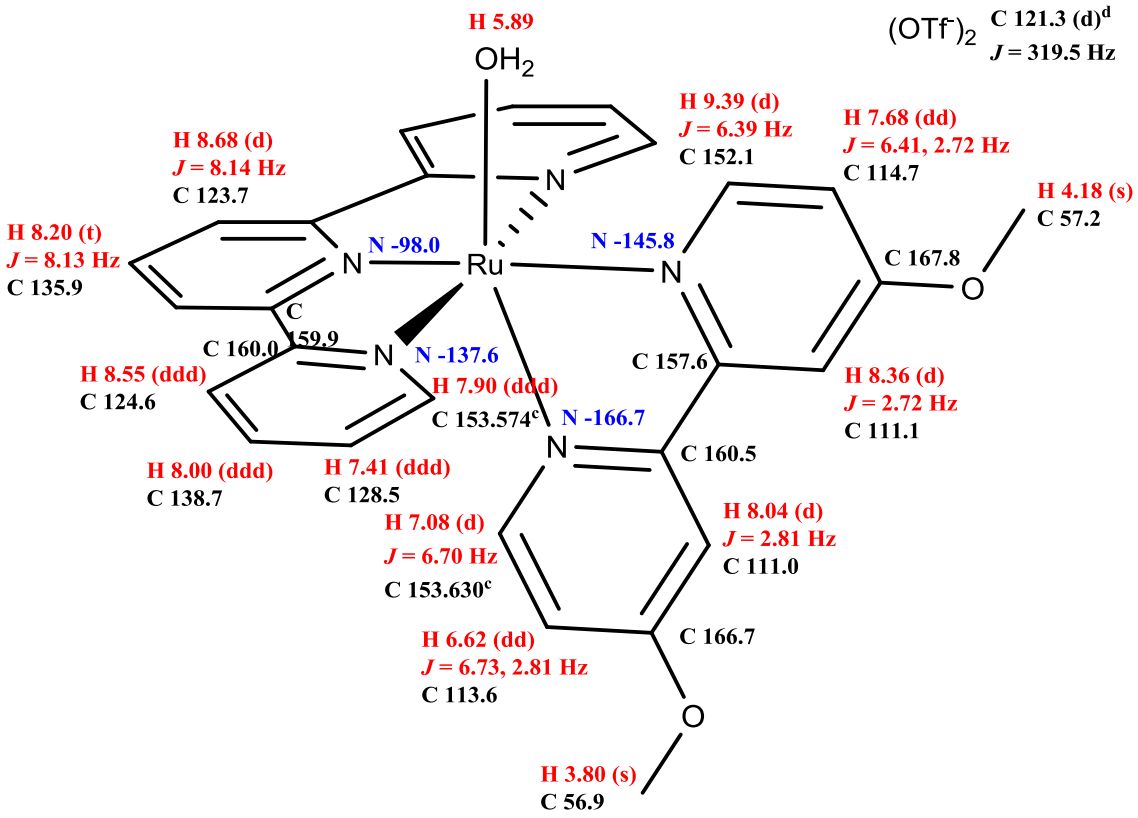

^{1}H - ^{15}N **gHMBCAD**[a]		
^{1}H	bonds	^{15}N
8.68	3	-98.0
8.55	3	-137.6
7.90	2	-137.6
7.41	3	-137.6
9.39	2	-145.8
7.08	2	-166.7
[a] J_{nxh} = 5.0 Hz J_{1xh} = 90.0 Hz		

gCOSY
9.39↔7.68
8.68↔8.20
8.55↔8.00
8.36↔7.68
8.04↔6.62
8.00↔7.41
7.90↔7.41
7.08↔6.62

Figure 3.59. NMR data for **3.19b**.

[c] Two separate carbon shifts were observed in the 1-D carbon NMR and although different by only 0.056 ppm, the peaks were able to be differentiated in the 2-D HSQCAD and HMBCAD experiments.
[d] Only the two most intense peaks of the trifluoromethanesulfonate carbon quartet were observed.

^{1}H -^{13}C gHMBCAD[b]		
^{1}H	bonds	^{13}C
9.39	4	111.1
9.39	2	114.7
9.39	3	157.6
9.39	3	167.8
8.68	1,3	123.7
8.68	3	160.0
8.55	3	128.5
8.55	4	153.6(w)
8.55	3	159.9
8.36	3	114.7
8.36	2	157.6(w)
8.36	3	160.5
8.36	2	167.8
8.20	2	123.7
8.20	3	159.9
8.04	3	113.6
8.04	4	153.6(w)
8.04	3	157.6
8.04	2	160.5
8.04	2	166.7
8.00	2	124.6(w)
8.00	2	128.5(w)
8.00	3	153.6
8.00	3	160.0
7.90	4	124.6
7.90	2	128.5
7.90	3	138.7
7.90	3	160.0
7.68	3	111.1
7.68	2	152.1
7.68	2	167.8
7.41	3	124.6
7.41	2	153.6
7.41	4	160.0
7.08	4	111.0
7.08	2	113.6
7.08	3	160.5
7.08	3	166.7
6.62	3	111.0
6.62	2	153.6
6.62	2	166.7
4.18	3	167.8
3.81	3	166.7
$^{b}J_{nxh}$ = 8.0 Hz J_{1xh} = 146.0 Hz		

^{1}H (599.48 MHz) sw = 5102.0 Hz np = 524288	
^{1}H	$^{x}J_{HH}$
9.39 (d)	6.39 Hz (3)
8.68 (d)	8.14 Hz (3)
8.55 (ddd)	8.12 Hz (3), 1.37 Hz (4), 0.79 Hz (5)
8.36 (d)	2.72 Hz (4)
8.20 (t)	8.13 Hz (3)
8.04 (d)	2.81 Hz (4)
8.00 (ddd)	8.13 Hz (3), 7.53 Hz (3), 1.51 Hz (4)
7.90 (ddd)	5.52 Hz (3), 1.56 Hz (4), 0.81 Hz (5)
7.68 (dd)	6.41 Hz (3), 2.72 Hz (4)
7.41 (ddd)	7.58 Hz (3), 5.47 Hz (3), 1.29 Hz (4)
7.08 (d)	6.70 Hz (3)
6.62 (dd)	6.73 Hz (3), 2.81 Hz (4)
Bonds between Hydrogen atoms being coupled in parentheses.	

^{1}H-^{13}C **HSQCAD**	
^{1}H	^{13}C
9.39	152.1
8.68	123.7
8.55	124.6
8.36	111.1
8.20	135.9
8.04	111.0
8.00	138.7
7.90	153.574
7.68	114.7
7.41	128.5
7.08	153.630
6.62	113.6
4.18	57.2
3.81	56.9

Figure 3.59 cont. NMR data for **3.19b.**

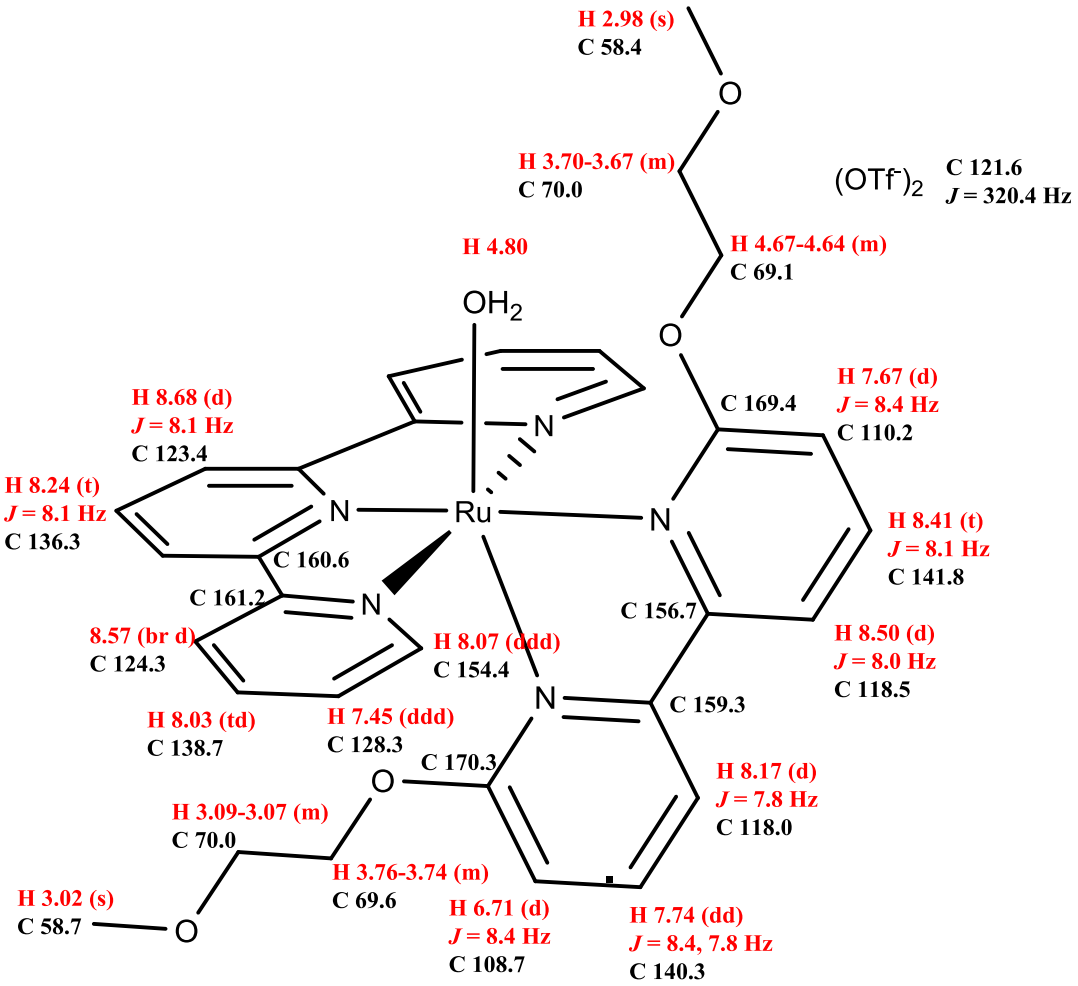

^{1}H-^{13}C HSQCAD	
^{1}H	^{13}C
8.68	123.4
8.57	124.3
8.50	118.5
8.41	141.8
8.24	136.3
8.17	118.0
8.07	154.4
8.03	138.7
7.74	140.3
7.67	110.2

^{1}H-^{13}C HSQCAD	
^{1}H	^{13}C
7.45	128.3
6.71	108.7
4.67-4.64	69.1
3.76-3.74	69.6
3.70-3.67	70.0
3.09-3.07	70.0
3.02	58.7
2.98	58.4

gCOSY
8.68↔8.24
8.57↔8.03
8.50↔8.41
8.41↔7.67
8.17↔7.74
8.07↔7.45
8.03↔7.45
7.74↔6.71
4.65↔3.68
3.75↔3.08

Figure 3.60. NMR data for **3.25**.

^{1}H -^{13}C gHMBC[a]		
^{1}H	bonds	^{13}C
8.68	1,3	123.4
8.68	3	160.6
8.57	3	128.3
8.57	3	160.6
8.57	2	161.2
8.50	3	110.2
8.50	2	156.7
8.41	3	156.7
8.41	3	169.4
8.24	3	160.6
8.17	3	108.7
8.17	3	156.7(w)
8.17	2	159.2
8.07	2	128.3
8.07	3	138.7
8.07	3	161.2
8.03	3	154.4
8.03	3	161.2
7.74	3	159.3
7.74	3	170.3
7.67	3	118.5
7.45	3	124.3
7.45	2	154.4
6.70	3	118.0
3.02	3	70.0
2.97	3	70.0
$^{a}J_{nxh}$ = 8.0 Hz J_{1xh} = 140.0 Hz		

^{1}H (399.75 MHz) sw = 4006.4 Hz np = 524288	
^{1}H	$^{x}J_{HH}$
8.57 (br d)	8.1 Hz (3)
8.07 (ddd)	5.5 Hz (3). 1.5 Hz (4), 0.7 Hz (5)
8.03 (td)	7.9 Hz (3), 1.6 Hz (4)
7.45 (ddd)	7.6 Hz (3), 5.5 Hz (3), 1.3 Hz (4)
Bonds between Hydrogen atoms being coupled in parentheses.	

Figure 3.60 cont. NMR data for **3.25**.

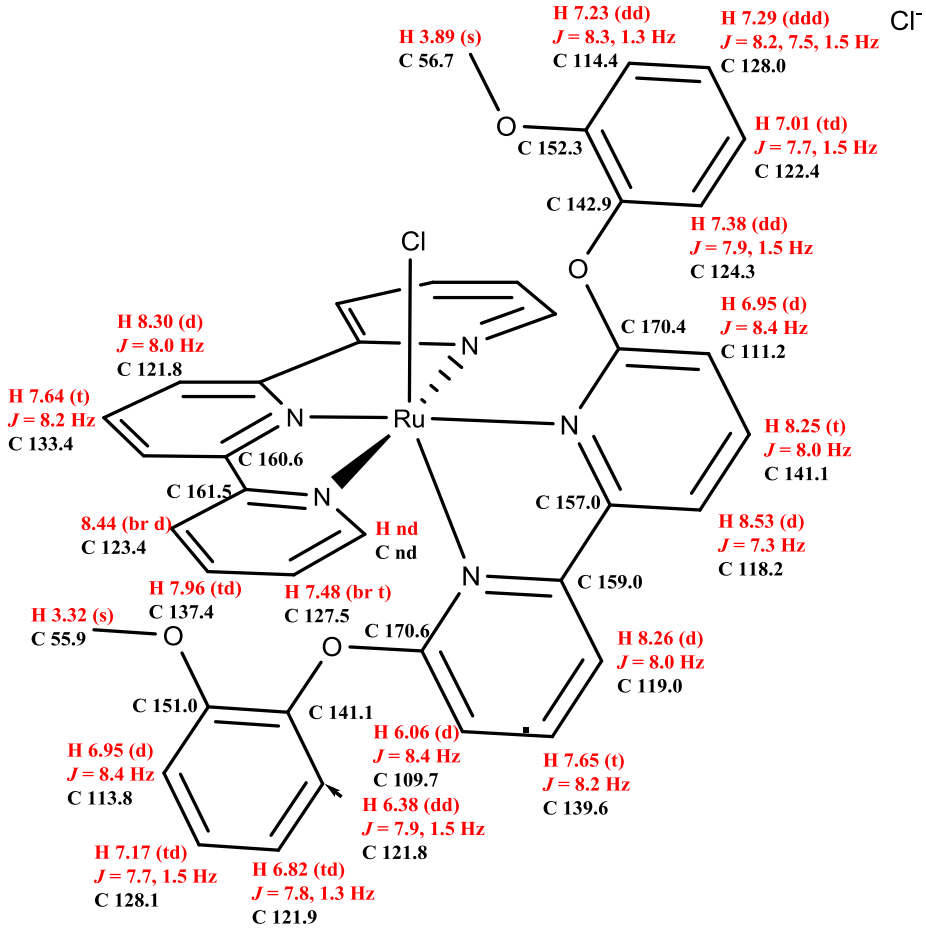

^{1}H-^{13}C HSQCAD	
^{1}H	^{13}C
8.53	118.2
8.44	123.4
8.30	121.8
8.26	119.0
8.25	141.1
7.96	137.4
7.65	139.6
7.64	133.4
7.48	127.5
7.38	124.3
7.29	128.0

^{1}H-^{13}C HSQCAD continued	
^{1}H	^{13}C
7.23	114.4
7.17	128.1
7.01	122.4
6.95	113.8
6.95	111.2
6.82	121.9
6.38	121.8
6.06	109.7
3.89	56.7
3.32	55.9

^{1}H (599.37 MHz) sw = 5980.9 Hz np = 524288	
^{1}H	$^{x}J_{HH}$
8.44 (br d)	7.1 Hz (3)
7.96 (td)	7.8 Hz (3). 1.3 Hz (4)
7.48 (br t)	6.2 Hz (3)
Bonds between Hydrogen atoms being coupled in parentheses.	

Figure 3.61. NMR data for **3.28**.

^{1}H -^{13}C gHMBC[a]		
^{1}H	bonds	^{13}C
8.53	3	111.2
8.53	2	157.0
8.53	3	159.0
8.44	3	127.5 (w)
8.44	2	161.5 (w)
8.30	1,3	121.8
8.30	2	160.6
8.30	3	161.5
8.26	3	109.7
8.26	2	157.0
8.26	3	159.0
8.25	3	157.0
8.25	3	170.4
7.96	**3**	**153.9**
7.96	**3**	**154.7**
7.96	3	161.5
7.65	3	159.0
7.65	3	170.6
7.64	3	160.6
7.48	3	123.4
7.48	**3**	**153.9**
7.48	**3**	**154.7**
7.38	3	128.0
7.38	2	142.9
7.38	3	152.3
7.29	3	124.3
7.29	3	152.3

^{1}H -^{13}C gHMBC[a]		
^{1}H	bonds	^{13}C
7.23	3	122.4
7.23	3	142.9
7.17	3	121.8
7.17	3	151.0
7.01	3	114.4
7.01	3	142.9
6.95(pyr)	3	118.2
6.95(ben)	3	121.9
6.95(ben)	3	141.1
6.95(ben)	2	151.0(w)
6.82	3	113.8
6.82	3	141.1
6.38	3	128.1
6.38	2	141.1
6.38	3	151.0
6.06	3	119.0
3.89	3	152.3
3.32	3	151.0
[a] J_{nxh} = 8.0 Hz J_{1xh} = 140.0 Hz		

gCOSY
8.53↔8.25
8.44↔7.96
8.30↔7.64
8.26↔7.65
8.25↔6.95
7.96↔7.48
7.65↔6.06
7.38↔7.01
7.29↔7.23
7.29↔7.01
7.17↔6.95
7.17↔6.82
6.82↔6.39

Figure 3.61 cont. NMR data for **3.28**.

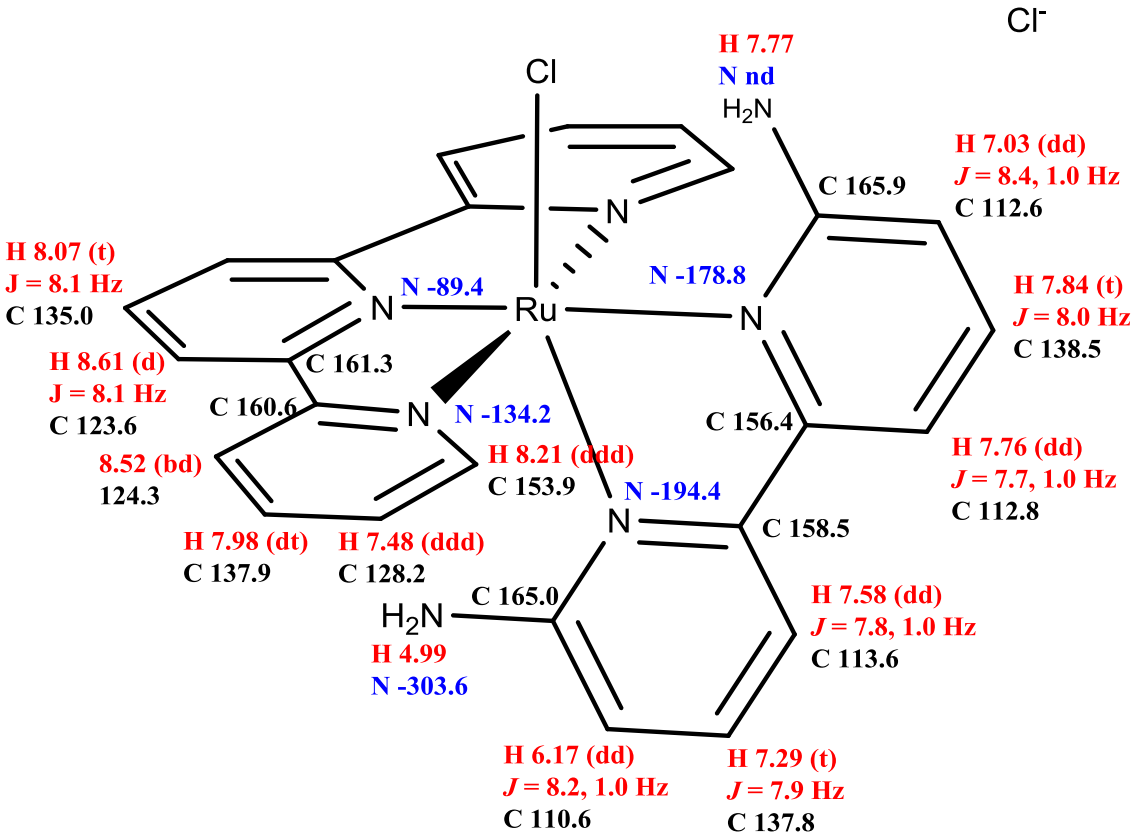

^{1}H - ^{15}N gHMBCAD[a]		
^{1}H	bonds	^{15}N
8.61	3	-89.4
8.52	3	-134.2
8.21	2	-134.2
7.76	3	-178.8
7.58	3	-194.4
7.48	3	-134.2
7.03	3	-178.8
6.17	3	-194.4
6.17	3	-303.6
4.99	3	-303.6
[a] J_{nxh} = 8.0 Hz J_{1xh} = 90.0 Hz		

^{1}H-^{13}C HSQCAD	
^{1}H	^{13}C
8.61	123.6
8.52	124.3
8.21	153.9
8.07	135.0
7.98	137.9
7.84	138.5
7.76	112.8
7.58	113.6
7.48	128.2
7.29	137.8
7.03	112.6
6.17	110.6

gCOSY
8.61↔8.07
8.52↔7.98
8.21↔7.48
7.98↔7.48
7.84↔7.76
7.84↔7.03
7.58↔7.29
7.29↔6.17

Figure 3.62. NMR data for **3.37**.

The digital resolution of the ^{1}H NMR spectrum was not great enough to see the individual coupling constants of the terpy ligand. Instead an average of the coupling constants was observed.

^{1}H -^{13}C gHMBCAD[b]		
^{1}H	bonds	^{13}C
8.61	1,3	123.6
8.61	3	160.6
8.61	2	161.3
8.52	3	128.2
8.52	4	153.9(w)
8.52	2	160.6
8.52	3	161.3
8.21	4	124.3(w)
8.21	2	128.2
8.21	3	137.9
8.21	3	160.6
8.07	2	123.6(w)
8.07	4	160.6(w)
8.07	3	161.3
7.98	2	124.3(w)
7.98	2	128.2(w)
7.98	3	153.9
7.98	3	160.6
7.84	2	112.8(w)
7.84	3	156.4
7.84	3	165.9
7.76	3	112.6
7.76	2	156.4
7.76	3	158.5
7.58	3	110.6
7.58	3	156.4
7.58	2	158.5
7.48	3	124.3
7.48	2	153.9
7.48	4	160.6(w)
7.29	3	158.5
7.29	3	165.0
7.03	3	112.8
7.03	2	165.9
6.17	3	113.6
6.17	2	165.0
4.99	3	110.6
$^{b}J_{nxh}$ = 8.0 Hz J_{1xh} = 146.0 Hz		

^{1}H (599.48 MHz) sw = 5707.8 Hz np = 524288	
^{1}H	$^{x}J_{HH}$
8.61 (d)	8.0 Hz (3)
8.52 (bd)	7.8 Hz (3)
8.21 (ddd)	5.5 Hz (3), 1.4 Hz (4), 0.7 Hz (5)
8.07 (t)	8.0 Hz (3)
7.98 (dt)	7.8 Hz (3), 1.5 Hz (4)
7.84 (t)	8.0 Hz (3)
7.76 (dd)	7.7 Hz (3), 1.0 Hz (4),
7.58 (dd)	7.8 Hz (3), 1.0 Hz (4)
7.48 (ddd)	7.6 Hz (3), 5.6 Hz (3). 1.4 Hz (4)
7.29 (t)	7.9 Hz (3)
7.03 (dd)	8.4 Hz (3), 1.0 Hz (3)
6.17 (dd)	8.2 Hz (3), 1.0 Hz (3)
Bonds between Hydrogen atoms being coupled in parentheses.	

Figure 3.62 cont. NMR data for **3.37**.

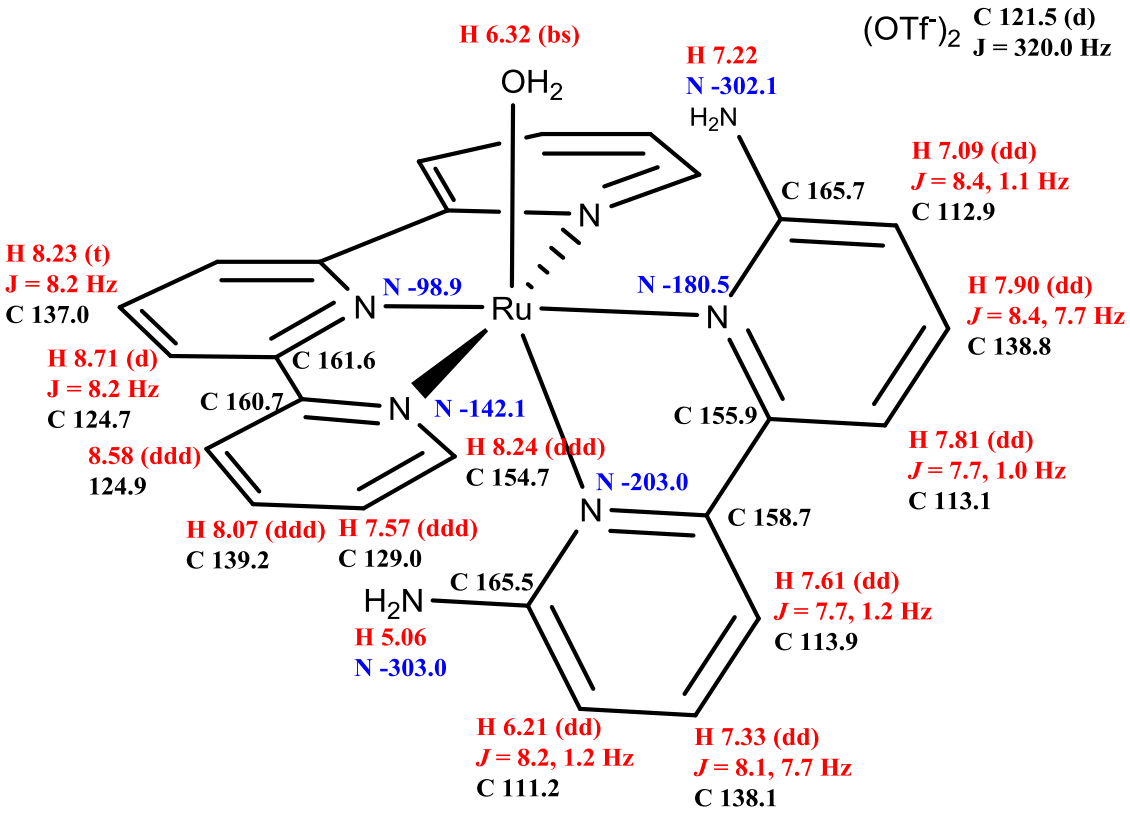

^{1}H - ^{15}N **gHMBCAD**[a]		
^{1}H	bonds	^{15}N
8.71	3	-98.9
8.58	3	-142.1
8.24	2	-142.1
7.81	3	-180.5
7.61	3	-203.0
7.57	3	-142.1
7.09	2	-180.5
6.21	3	-203.0
5.06	3	-203.0
[a] J_{nxh} = 5.0 Hz J_{1xh} = 90.0 Hz		

^{1}H - ^{15}N **HSQCAD**	
^{1}H	^{15}N
7.22	-302.1
5.06	-303.0

gCOSY
8.71↔8.23
8.58↔8.07
8.24↔7.57
8.07↔7.57
7.90↔7.81
7.90↔7.09
7.61↔7.33
7.33↔6.21

^{1}H-^{13}C **HSQCAD**	
^{1}H	^{13}C
8.71	124.7
8.58	124.9
8.24	154.7
8.23	137.0
8.07	139.2
7.90	138.8
7.81	113.1
7.61	113.9
7.57	129.0
7.33	138.1
7.09	112.9
6.21	111.2

Figure 3.63. NMR data for **3.37b**.

^{1}H -^{13}C gHMBCAD[b]		
^{1}H	bonds	^{13}C
8.71	1,3	124.9
8.71	3	160.7
8.71	2	161.6
8.58	3	129.0
8.58	4	154.7(w)
8.58	2	160.7
8.58	3	161.6
8.24	2	129.0
8.24	3	139.2
8.24	3	160.7
8.23	3	161.6
8.07	2	124.9(w)
8.07	3	154.7
8.07	3	160.7
7.90	3	155.9
7.90	3	165.7
7.81	3	112.9
7.81	2	155.9
7.81	3	158.7
7.61	3	111.2
7.61	3	155.9
7.61	2	158.7
7.57	3	124.9
7.57	2	154.7
7.57	4	160.7(w)
7.33	3	158.7
7.33	3	165.5
7.22	3	112.9(w)
7.09	3	113.1
7.09	2	165.7
6.21	3	113.9
6.21	2	165.5(w)
5.05	3	111.2
$^{b}J_{nxh}$ = 8.0 Hz J_{1xh} = 146.0 Hz		

^{1}H (599.48 MHz) sw = 5387.9 Hz np = 524288	
^{1}H	$^{x}J_{HH}$
8.71 (d)	8.2 Hz (3)
8.58 (ddd)	8.1 Hz (3), 1.3 Hz (4), 0.8 Hz (5)
8.24 (ddd)	5.4 Hz (3), 1.5 Hz (4), 0.8 Hz (5)
8.23 (t)	8.1 Hz (3),
8.07 (ddd)	8.1 Hz (3), 7.7 Hz (3), 1.5 Hz (4)
7.90 (dd)	8.4 Hz (3), 7.7 Hz (3)
7.81 (dd)	7.7 Hz (3), 1.0 Hz (4),
7.61 (dd)	7.7 Hz (3), 1.2 Hz (4)
7.57 (ddd)	7.6 Hz (3), 5.6 Hz (3). 1.3 Hz (4)
7.33 (dd)	8.1 Hz (3), 7.7 Hz (3)
7.09 (dd)	8.4 Hz (3), 1.1 Hz (4)
6.21 (dd)	8.2 Hz (3), 1.2 Hz (3)
Bonds between Hydrogen atoms being coupled in parentheses.	

Figure 3.63 cont. NMR data for **3.37b**.

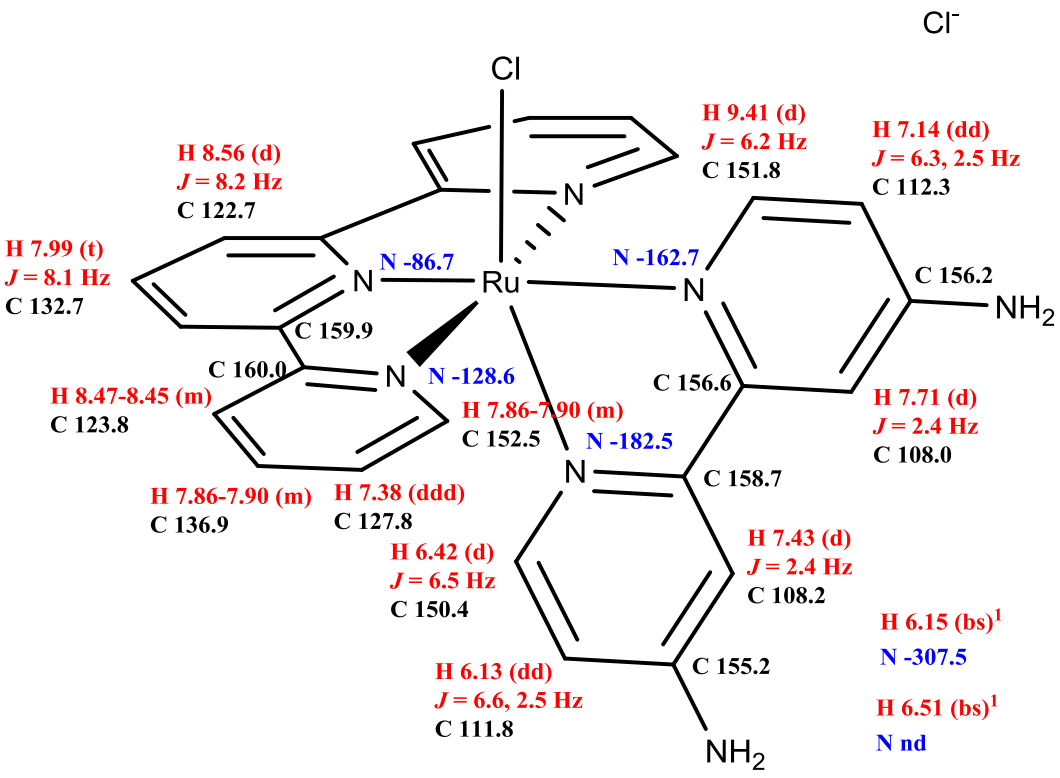

^{1}H -^{15}N **HSQCAD**[a]	
^{1}H	^{15}N
6.15	-307.5
[a]J_{1xh} = 90.0 Hz	

^{1}H -^{15}N **gHMBCAD**[a]		
^{1}H	bonds	^{15}N
9.41	2	-162.7
8.56	3	-86.7
8.47-8.45	3	-128.6
7.87	2	-128.6
7.38	3	-128.6
6.42	2	-182.5
[a]J_{nxh} = 5.0 Hz J_{1xh} = 90.0 Hz		

Figure 3.64. NMR data for **3.38**.

The digital resolution of the ^{1}H NMR spectrum was not great enough to see the individual coupling constants of the terpy ligand. Instead an average of the coupling constants was observed.

^{1}H -^{13}C gHMBCAD[b]		
^{1}H	bonds	^{13}C
9.41	2	112.3
9.41	3	156.2
9.41	3	156.6
8.56	1,3	122.7
8.56	3	160.0
8.47-8.45	3	127.8
8.47-8.45	2	136.9(w)
8.47-8.45	2	152.5(w)
8.47-8.45	4	160.0
7.99	2	122.7(w)
7.99	3	159.9
7.90-7.86	2,2	123.8(w)
7.90-7.86	2,4	127.8
7.90-7.86	1,3	136.9
7.90-7.86	1,3	152.5
7.90-7.86	3,3	160.0
7.71	3	112.3
7.71	2	156.2(w)
7.71	2	156.6(w)
7.71	3	158.7(w)
7.43	3	111.8
7.43	2	155.2(w)
7.43	3	156.6(w)
7.43	2	158.7(w)
7.38	3	123.8
7.38	4	152.5
7.38	2	160.0(w)
7.14	3	108.0
7.14	2	151.8(w)
6.42	4	108.2(w)
6.42	2	111.8
6.42	3	155.2
6.42	3	158.7
6.13	3	108.2
6.13	2	150.4
[b]J_{nxh} = 8.0 Hz J_{1xh} = 146.0 Hz		

^{1}H-^{13}C HSQCAD	
^{1}H	^{13}C
9.41	151.8
8.56	122.7
8.46	123.8
7.99	132.7
7.90-7.86	136.9
7.90-7.86	152.5
7.71	108.0
7.43	108.2
7.38	127.8
7.14	112.3
6.42	150.4
6.13	111.8

Figure 3.64 cont. NMR data for **3.38**.

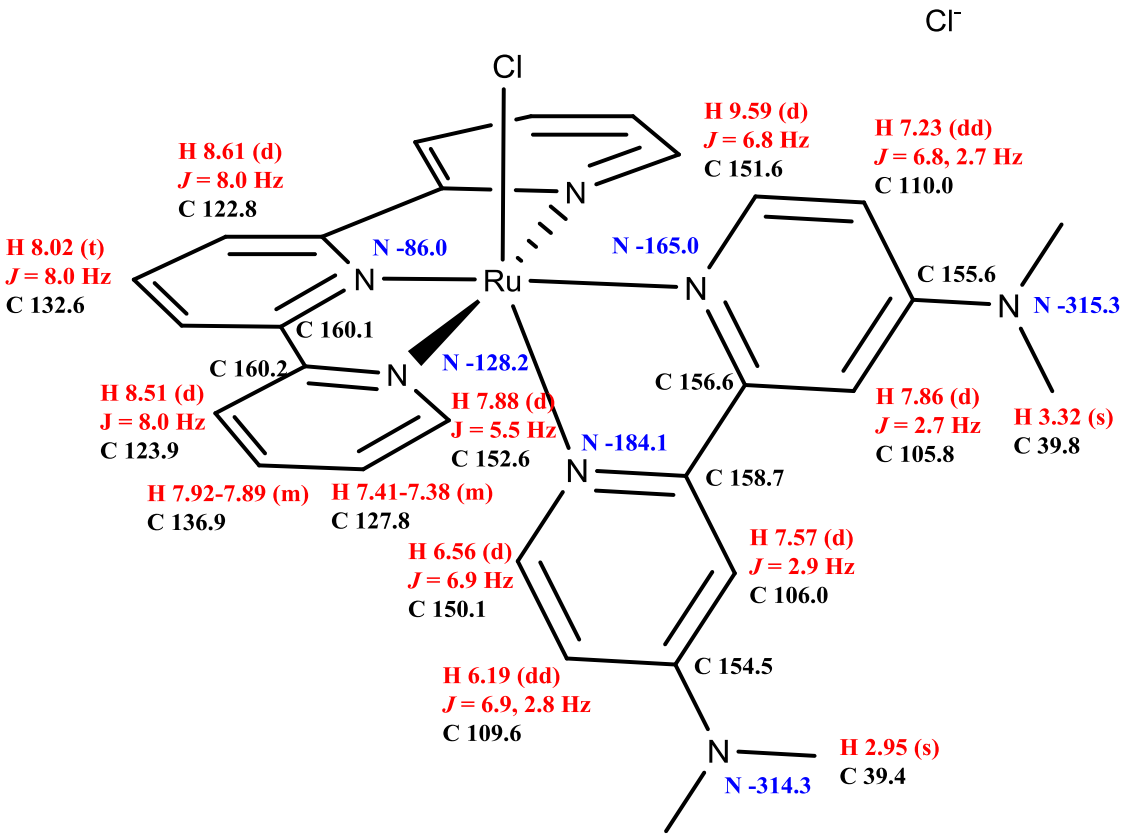

gCOSY
9.59↔7.23
8.61↔8.02
8.51↔7.92-7.89
7.92-7.89↔7.41-7.38
7.88↔7.39
7.86↔7.23
7.57↔6.19
6.56↔6.19

^{1}H -^{15}N gHMBCAD[a]		
^{1}H	bonds	^{15}N
9.59	2	-165.0
8.61	3	-86.0
8.51	3	-128.2
7.88	2	-128.2
7.57	3	-184.1
7.41-7.38	3	-128.2
6.56	2	-184.1
3.32	2	-315.3
2.95	2	-314.3
[a] J_{nxh} = 5.0 Hz J_{1xh} = 90.0 Hz		

^{1}H-^{13}C HSQCAD	
^{1}H	^{13}C
9.59	151.6
8.61	122.8
8.51	123.9
8.02	132.6
7.92-7.89	136.9
7.88	152.6
7.86	105.8
7.57	106.0
7.41-7.38	127.8
7.23	110.0
6.56	150.1
6.19	109.6
3.32	39.8
2.95	39.4

Figure 3.65. NMR data for **3.40**.

The digital resolution of the ^{1}H NMR spectrum was not great enough to see the individual coupling constants of the terpy ligand. Instead an average of the coupling constants was observed.

^{1}H -^{13}C gHMBCAD[b]		
^{1}H	bonds	^{13}C
9.59	2	110.0
9.59	3	155.6
9.59	3	156.6
8.61	1,3	122.8
8.61	2	160.1
8.61	3	160.2
8.51	3	127.8
8.51	3	160.1
8.51	2	160.2
8.02	3	160.1
7.92-7.89	3	152.6
7.92-7.89	3	160.2
7.88	2	127.8
7.88	3	136.9
7.88	3	160.2
7.86	3	110.0(w)
7.86	3	158.7(w)
7.57	3	109.6(w)
7.57	3	156.6(w)
7.41-7.38	3	123.9
7.41-7.38	2	152.6(w)
7.23	3	105.8(w)
6.56	2	109.6
6.56	3	154.5
6.56	3	158.7
6.19	3	106.0
3.32	1,3	39.8
3.32	3	155.6
2.95	1,3	39.4
2.95	3	154.5
[b]J_{nxh} = 8.0 Hz J_{1xh} = 146.0 Hz		

Figure 3.65 cont. NMR data for **3.40**.

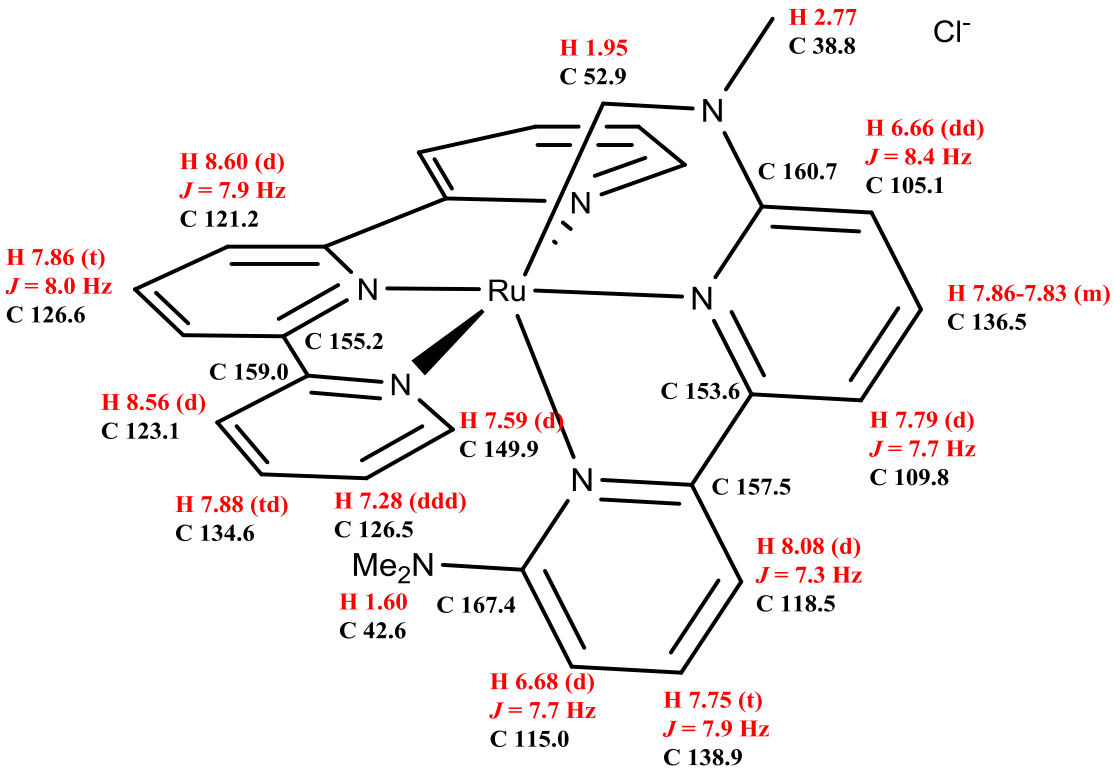

gCOSY
8.60↔7.86
8.56↔7.88
8.08↔7.75
7.88↔7.28
7.86-7.83↔7.79
7.86-7.83↔6.66
7.75↔6.68
7.59↔7.28
2.77↔1.95

^{1}H-^{13}C HSQCAD	
^{1}H	^{13}C
8.60	121.2
8.56	123.1
8.08	118.5
7.88	134.6
7.86	126.6
7.86-7.83	136.5
7.79	109.8
7.75	138.9
7.59	149.9
7.28	126.5
6.68	115.0
6.66	105.1
2.77	38.8
1.95	52.9
1.60	42.6

^{1}H - ^{1}H NOSEY1D	
Irradiated ^{1}H	Effected ^{1}H
2.77	1.95
2.77	6.66
1.95	2.77
1.95	7.59(w)

Figure 3.66. NMR data for **3.41**.

The digital resolution of the ^{1}H NMR spectrum was not great enough to see the individual coupling constants of the terpy ligand. Instead an average of the coupling constants was observed.

^{1}H -^{13}C gHMBCAD[b]		
^{1}H	bonds	^{13}C
8.60	1,3	121.2
8.60	2	155.2
8.60	3	159.0(w)
8.56	3	126.5
8.56	3	155.2(w)
8.56	2	159.0
8.08	3	115.0
8.08	3	153.6
8.08	2	157.5
7.88	3	149.9
7.88	3	159.0
7.86	2	121.2(w)
7.86	3	155.2
7.86-7.83	2	105.1(w)
7.86-7.83	3	153.6
7.86-7.83	3	160.7
7.79	3	105.1
7.79	2	153.6
7.79	3	157.5(w)
7.75	3	157.5

^{1}H -^{13}C gHMBCAD[b] cont.		
7.75	3	167.4
7.59	4	123.1(w)
7.59	2	126.5
7.59	3	134.5
7.58	3	159.0(w)
7.28	3	123.1
7.28	2	149.9
7.28	4	159.0(w)
6.68	3	118.5
6.68	2	167.4(w)
6.66	3	109.8
6.66	2	160.7
2.77	3	52.9
2.77	3	160.7
1.95	3	38.8
1.95	3	160.7
1.60	1,3	42.6
1.60	3	167.4
[b] J_{nxh} = 8.0 Hz J_{1xh} = 146.0 Hz		

^{1}H (599.37 MHz) sw = 5980.9 Hz np = 524288	
^{1}H	$^{x}J_{HH}$
8.56 (d)	8.0 Hz (3)
7.88 (td)	7.8 Hz (3), 1.3 Hz (4)
7.59 (d)	5.5 Hz (3)
7.28 (ddd)	7.3 Hz (3), 5.8 Hz (3), 1.2 Hz (4)
Bonds between Hydrogen atoms being coupled in parentheses.	

Figure 3.66 cont. NMR data for **3.41**.

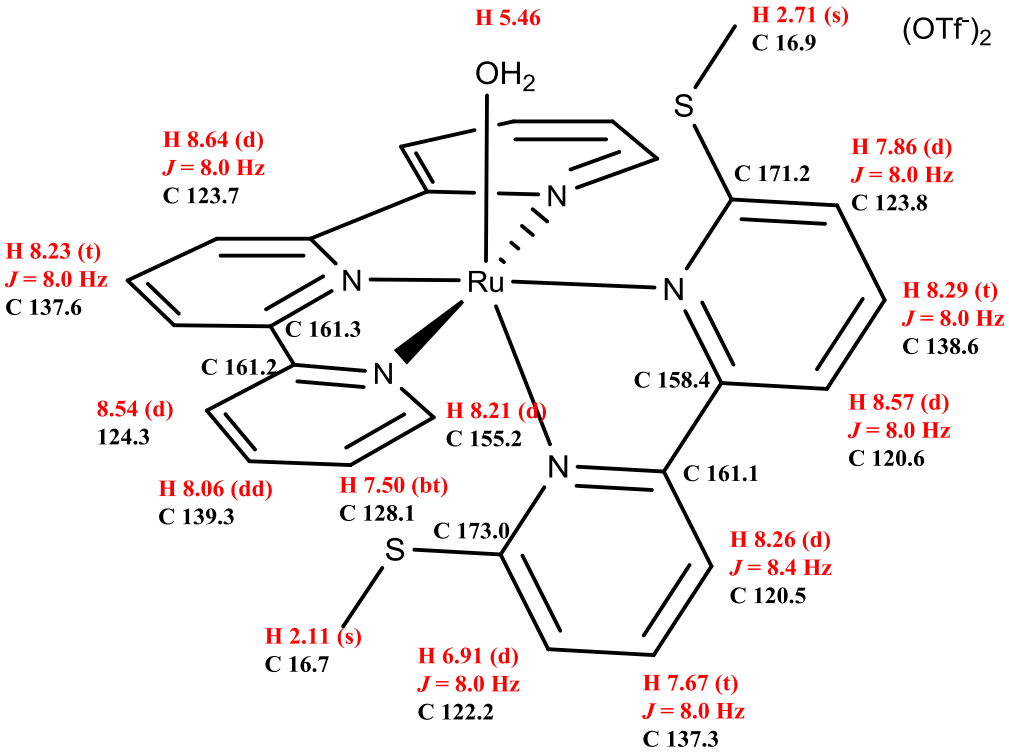

^{1}H-^{13}C HSQCAD	
^{1}H	^{13}C
8.64	123.7
8.57	120.6
8.54	124.3
8.29	138.6
8.26	120.5
8.23	137.6
8.21	155.2
8.06	139.3
7.86	123.8
7.67	137.3
7.50	128.1
6.91	122.2
2.71	16.9
2.11	16.7

gCOSY
8.64↔8.23
8.57↔8.29
8.54↔8.06
8.29↔7.86
8.26↔7.67
8.21↔7.50
8.06↔7.50
7.67↔6.91

^{1}H -^{13}C gHMBCAD continued		
^{1}H	bonds	^{13}C
7.50	3	124.3
7.50	2	155.2
7.50	4	161.2(w)
6.92	3	120.5
6.92	2	137.3(w)
6.92	4	161.1(w)
6.92	2	173.0
$^{b}J_{nxh}$ = 8.0 Hz J_{1xh} = 146.0 Hz		

Figure 3.67. NMR data for **3.43**.

The digital resolution of the ^{1}H NMR spectrum was not great enough to see the individual coupling constants of the terpy ligand. Instead an average of the coupling constants was observed.

^{1}H -^{13}C gHMBCAD[b]		
^{1}H	bonds	^{13}C
8.64	1,3	123.7
8.64	3	161.2
8.57	3	123.8
8.57	2	138.6(w)
8.57	2	158.4
8.57	3	161.1
8.57	4	171.2(w)
8.54	3	128.1
8.54	2	139.3(w)
8.54	4	155.2(w)
8.54	3	161.3
8.29	2	120.6(w)
8.29	2	123.8(w)
8.29	3	158.4
8.29	3	171.2
8.26	3	122.2
8.26	2	137.3(w)
8.26	3	158.4
8.26	2	161.1
8.26	4	173.0(w)
8.23	2	123.7(w)
8.23	3	161.3
8.21	4	124.3(w)
8.21	2	128.1
8.21	3	139.3
8.21	3	161.2
8.06	2	124.3(w)
8.06	2	128.1(w)
8.06	3	155.2
8.06	3	161.2
7.86	3	120.6
7.86	4	158.4(w)
7.86	2	171.2
7.67	2	120.5(w)
7.67	2	122.2(w)
7.67	4	158.4(w)
7.67	3	161.1
7.67	3	173.0
7.50	3	124.3
7.50	2	155.2
7.50	4	161.2(w)
6.92	3	120.5
6.92	2	137.3(w)
6.92	4	161.1(w)
6.92	2	173.0
[b] J_{nxh} = 8.0 Hz J_{1xh} = 146.0 Hz		

^{1}H (599.48 MHz) sw = 5980.9 Hz np = 524288	
^{1}H	$^{x}J_{HH}$
8.64 (d)	8.0 Hz (3)
8.57 (d)	8.0 Hz (3)
8.54 (d)	8.0 Hz (3)
8.29 (t)	8.0 Hz (3)
8.26 (d)	8.4 Hz (3)
8.23 (t)	8.0 Hz (3)
8.21 (d)	5.5 Hz (3)
8.06 (dd)	7.9 Hz (3), 1.3 Hz (4)
7.86 (d)	8.0 Hz (3)
7.67 (t)	8.0 Hz (3)
7.50 (bt)	6.5 Hz (3)
6.91 (d)	8.0 Hz (3)
Bonds between Hydrogen atoms being coupled in parentheses.	

Figure 3.67 cont. NMR data for **3.43**.

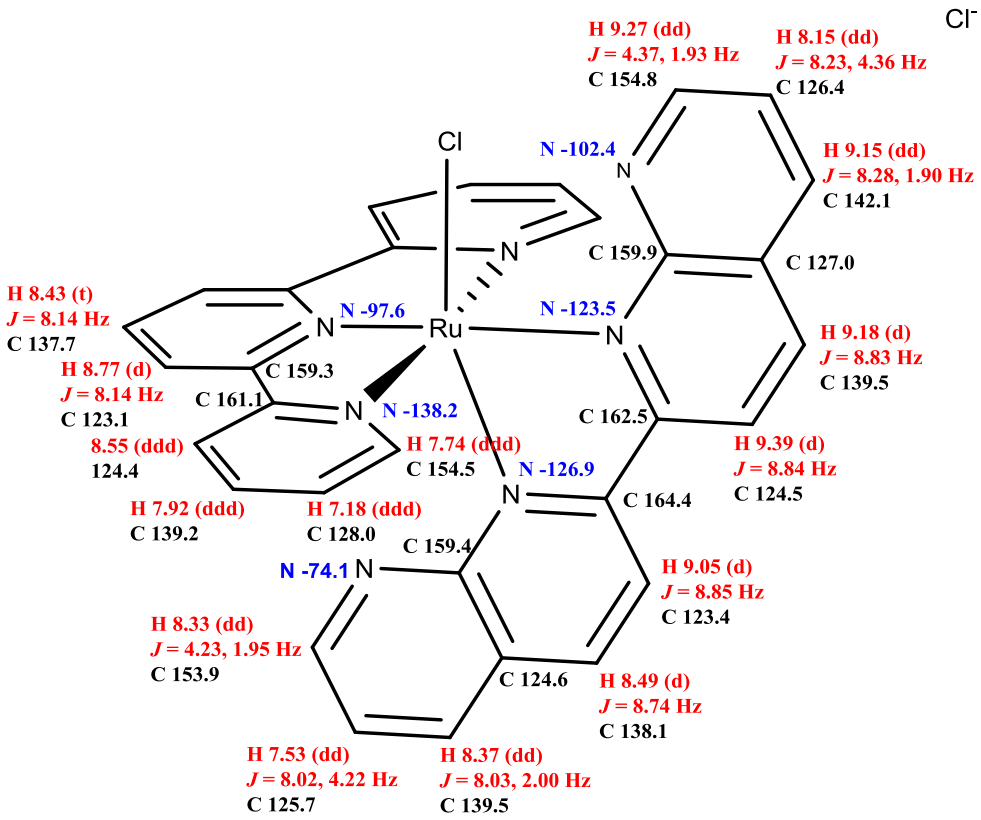

^{1}H - ^{15}N **gHMBCAD**[a]		
^{1}H	bonds	^{15}N
9.39	3	-123.5
9.05	3	-126.9
8.77	3	-97.6
8.55	3	-138.2
8.33	2	-74.1
8.15	3	-102.4
7.74	2	-138.2
7.18	3	-138.2
[a] J_{nxh} = 5.0 Hz J_{1xh} = 90.0 Hz		

gCOSY
9.39↔9.18
9.27↔8.15
9.15↔8.15
9.05↔8.49
8.77↔8.43
8.55↔7.92
8.33↔7.53
8.37↔7.53
7.92↔7.18
7.74↔7.18

^{1}H-^{13}C **HSQCAD**	
^{1}H	^{13}C
7.18	128.0
7.53	125.7
7.74	154.5
7.92	139.2
8.15	126.4
8.33	153.9
8.37	139.5
8.43	137.7
8.49	138.1
8.55	124.4
8.77	123.1
9.05	123.4
9.15	142.1
9.18	139.5
9.27	154.8
9.39	124.5

Figure 3.68. NMR data for **3.44**.

^{1}H -^{13}C gHMBCAD[b]		
^{1}H	bonds	^{13}C
9.39	3	127.0
9.39	2	162.5
9.39	3	164.4
9.27	2	126.4
9.27	3	142.1
9.27	3	159.9
9.18	2	124.5
9.18	2	127.0
9.18	3	142.1
9.18	3	159.9
9.18	3	162.5
9.15	2	127.0
9.15	3	139.5
9.15	3	154.8
9.15	3	159.9
9.05	3	124.6
9.05	2	138.1
9.05	3	162.5
9.05	2	164.4
8.77	1,3	123.1
8.77	2	159.3
8.77	3	161.1
8.55	3	128.0
8.55	2	139.2
8.55	4	154.5
8.55	3	159.3
8.55	2	161.1
8.49	2	124.6
8.49	3	139.5

^{1}H -^{13}C gHMBCAD continued[b]		
^{1}H	bonds	^{13}C
8.49	3	159.4
8.49	3	164.4
8.43	2	123.1
8.43	3	159.3
8.43	4	161.1
8.37	2	124.6
8.37	3	138.1
8.37	3	153.9
8.37	3	159.4
8.33	2	125.7
8.33	3	139.5
8.33	4	124.6
8.15	3	127.0
8.15	2	154.8
7.92	2	124.4
7.92	2	128.0
7.92	3	154.5
7.92	3	161.1
7.74	4	124.4
7.74	2	128.0
7.74	3	139.2
7.74	3	161.1
7.53	3	124.6
7.53	2	153.9
7.18	3	124.4
7.18	2	154.5
7.18	4	161.1
[b] J_{nxh} = 8.0 Hz J_{1xh} = 146.0 Hz		

^{1}H (599.48 MHz) sw = 5980.9 Hz np = 524288	
^{1}H	$^{x}J_{HH}$
9.39 (d)	8.84 Hz (3)
9.27 (dd)	4.34 Hz (3), 1.92 Hz (4)
9.18 (d)	8.82 Hz (3)
9.15 (dd)	8.28 Hz (3), 1.90 Hz (4)
9.05 (d)	8.81 Hz (3)
8.77 (d)	8.15 Hz (3)
8.55 (ddd)	8.10 Hz (3), 1.34 Hz (4), 0.81 Hz (5)
8.49 (d)	8.74 Hz (3)
8.43 (t)	8.14 Hz (3)
8.37 (dd)	8.03 Hz (3), 2.00 Hz (4)
8.33 (dd)	4.23 Hz (3), 1.95 Hz (4)
8.15 (dd)	8.23 Hz (3), 4.36 Hz (3)
7.92 (ddd)	8.01 Hz (3), 7.62 Hz (3), 1.53 Hz (4)
7.74 (ddd)	5.59 Hz (3), 1.55 Hz (4), 0.76 Hz (5)
7.53 (dd)	8.02 Hz (3), 4.22 Hz (3)
7.18 (ddd)	7.55 Hz (3), 5.60 Hz (3), 1.34 Hz (4)
Bonds between Hydrogen atoms being coupled in parentheses.	

Figure 3.68 cont. NMR data for **3.44**.

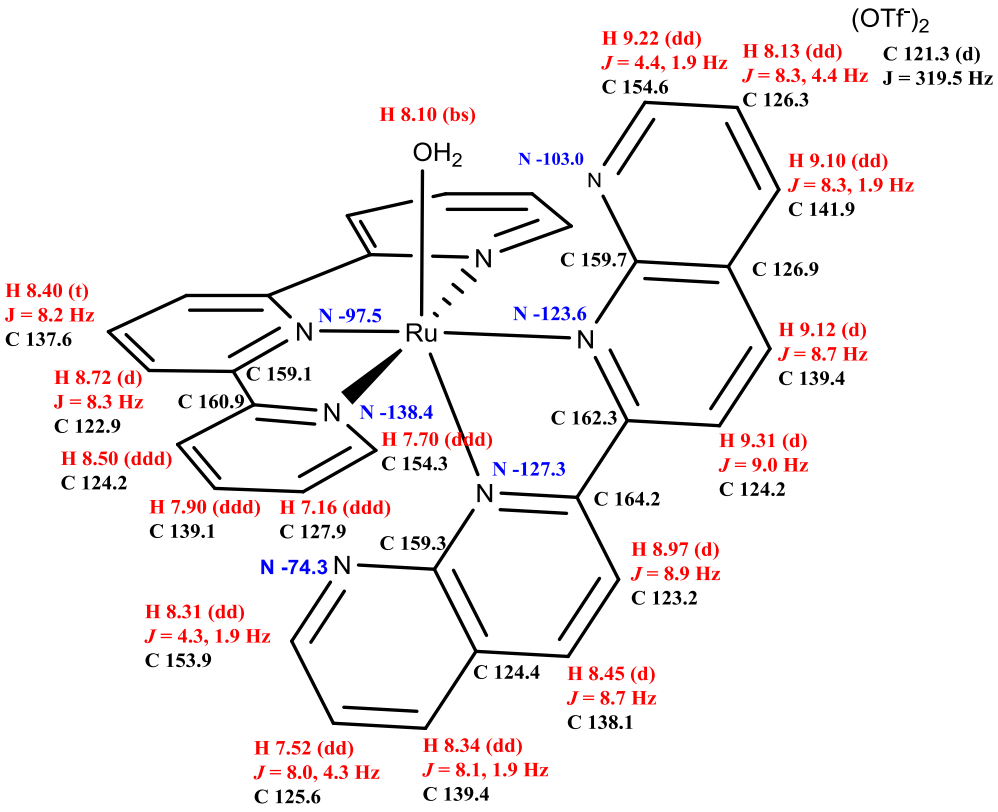

^{1}H - ^{15}N gHMBCAD[a]		
^{1}H	bonds	^{15}N
9.31	3	-123.6
8.97	3	-127.3
8.72	3	-97.5
8.50	3	-138.4
8.31	2	-74.3
8.13	3	-103.0
7.70	2	-138.4
7.16	3	-138.4
[a] J_{nxh} = 5.0 Hz J_{1xh} = 90.0 Hz		

^{1}H-^{13}C HSQCAD	
^{1}H	^{13}C
9.31	124.2
9.22	154.6
9.12	139.4
9.10	141.9
8.97	123.2
8.72	122.9
8.50	124.2
8.45	138.1
8.40	137.6
8.34	139.4
8.31	153.9
8.13	126.3
7.90	139.1
7.70	154.3
7.52	125.6
7.16	127.9

gCOSY
9.31↔9.12
9.22↔9.10
9.22↔8.13
9.10↔8.13
8.97↔8.45
8.72↔8.40
8.50↔7.90
8.50↔7.16
8.34↔7.52
8.31↔7.52
7.90↔7.70
7.90↔7.16
7.70↔7.16

Figure 3.69. NMR data for **3.44b**.

^{1}H -^{13}C gHMBCAD[b]		
^{1}H	bonds	^{13}C
9.31	3	126.9
9.31	2	139.4
9.31	4	159.7
9.31	2	162.3
9.31	3	164.2
9.22	2	126.3
9.22	3	141.9
9.22	3	159.8
9.12	2	124.2
9.12	2	126.9
9.12	3	141.9
9.12	3	159.7
9.12	3	162.3
9.12	4	164.2
9.10	2	126.9
9.10	3	139.4
9.10	3	154.6
9.10	3	159.7
8.97	3	124.4
8.97	2	138.1
8.97	4	159.3
8.97	3	162.3
8.97	2	164.2
8.72	1,3	122.9
8.72	2	159.1
8.72	3	160.9
8.50	3	127.9
8.50	2	139.1
8.50	4	154.3
8.50	3	159.1
8.50	2	160.9
8.45	2	123.2
8.45	3	124.4

^{1}H -^{13}C gHMBCAD continued[b]		
^{1}H	bonds	^{13}C
8.45	3	139.4
8.45	3	159.3
8.45	4	162.3
8.45	3	164.2
8.40	2	122.9
8.40	3	159.1
8.40	4	160.9
8.34	2	124.4
8.34	3	138.1
8.34	3	153.9
8.34	3	159.3
8.31	2	125.6
8.31	3	139.4
8.31	3	159.3
8.13	3	126.9
8.13	2	141.9
8.13	2	154.6
8.13	4	159.7
7.90	2	124.2
7.90	2	127.9
7.90	3	154.3
7.90	4	159.1
7.90	3	160.9
7.70	4	124.2
7.70	2	127.9
7.70	3	139.1
7.70	3	160.9
7.52	3	124.4
7.52	2	139.4
7.52	2	153.9
7.52	4	159.3
7.16	3	124.2
7.16	2	154.3
7.16	4	160.9
[b] J_{nxh} = 8.0 Hz J_{1xh} = 146.0 Hz		

^{1}H (599.48 MHz) sw = 5102.0 Hz np = 524288	
^{1}H	$^{x}J_{HH}$
9.31 (d)	9.0 Hz (3)
9.22 (dd)	4.4 Hz (3), 1.9 Hz (4)
9.12 (d)	8.7 Hz (3)
9.10 (dd)	8.3 Hz (3), 1.9 Hz (4)
8.97 (d)	8.9 Hz (3)
8.72 (d)	8.3 Hz (3)
8.50 (ddd)	8.1 Hz (3), 1.4 Hz (4), 0.8 Hz (5)
8.45 (d)	8.7 Hz (3)
8.40 (t)	8.2 Hz (3)
8.34 (dd)	8.1 Hz (3), 1.9 Hz (4)
8.31 (dd)	4.3 Hz (3), 1.9 Hz (4)
8.13 (dd)	8.3 Hz (3), 4.4 Hz (3)
7.90 (ddd)	8.1 Hz (3), 7.6 Hz (3), 1.6 Hz (4)
7.70 (ddd)	5.6 Hz (3), 1.5 Hz (4), 0.7 Hz (5)
7.52 (dd)	8.0 Hz (3), 4.3 Hz (3)
7.16 (ddd)	7.6 Hz (3), 5.6 Hz (3), 1.3 Hz (4)
Bonds between Hydrogen atoms being coupled in parentheses.	

Figure 3.69 cont. NMR data for **3.44b**.

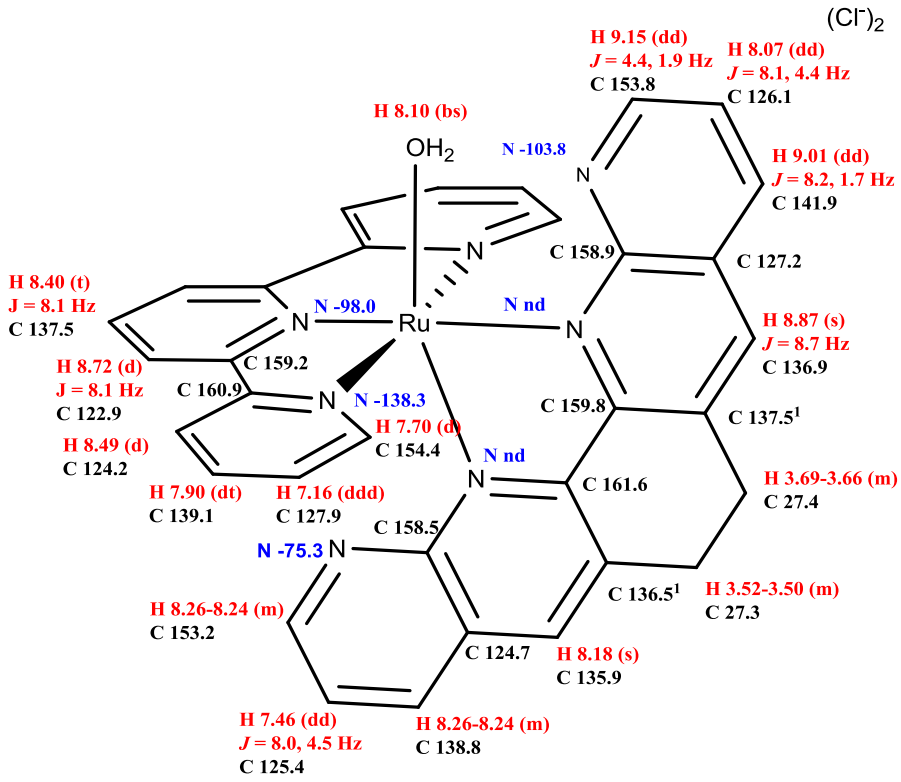

^{1}H - ^{15}N **gHMBCAD**[a]		
^{1}H	bonds	^{15}N
8.72	3	-98.0
8.49	3	-138.3
8.24	2	-75.3
8.07	3	-103.8
7.70	2	-138.3
7.16	3	-138.3
[a] J_{nxh} = 5.0 Hz J_{1xh} = 90.0 Hz		

gCOSY
9.15↔8.07
9.01↔8.07
8.72↔8.40
8.49↔7.90
8.26-8.24↔7.46
7.90↔7.16
7.70↔7.16
8.87↔3.69-3.66
8.18↔3.52-3.50
3.69-3.66↔3.52-3.50

^{1}H-^{13}C **HSQCAD**	
^{1}H	^{13}C
9.15	153.8
9.01	141.4
8.87	136.9
8.72	122.9
8.49	124.2
8.40	137.5
8.26-8.24	153.2
8.26-8.24	138.8
8.18	135.9
8.07	126.1
7.90	139.1
7.70	154.4
7.46	125.4
7.16	127.9
3.69-3.66	27.4
3.52-3.50	27.3

Figure 3.70. NMR data for **3.45**.

^{1}H -^{13}C gHMBCAD[b]		
^{1}H	bonds	^{13}C
9.15	2	126.1
9.15	3	141.4
9.15	3	158.9(w)
9.01	2	127.1(w)
9.01	3	136.9
9.01	3	153.8
9.01	3	158.9
8.87	2	127.2(w)
8.87	3	141.4
8.87	3	158.9
8.87	3	159.8
8.87	4	161.6(w)
8.87	3	27.4
8.72	1,3	122.9
8.72	2,4	159.2
8.72	3	160.9
8.49	3	127.9
8.49	2	139.1(w)
8.49	4	154.4(w)
8.49	3	159.2
8.49	2	160.9
8.40	2	122.9(w)
8.40	3	159.2
8.40	4	160.9(w)
8.26-8.24	2,4	124.7
8.26-8.24	2,2	125.4
8.26-8.24	5,3	135.9
8.26-8.24	3,1	138.8
8.26-8.24	1,3	153.2
8.26-8.24	3,3	158.5
8.18	2	124.7
8.18	3	138.8
8.18	3	158.5
8.18	4	159.8(w)
8.18	3	161.6
8.18	3	27.3

^{1}H -^{13}C gHMBCAD continued[b]		
^{1}H	bonds	^{13}C
8.07	3	127.2
8.07	2	153.7
7.90	2	124.2(w)
7.90	3	154.4
7.90	4	159.2(w)
7.90	3	160.9
7.70	4	124.2(w)
7.70	2	127.9
7.70	3	139.1
7.70	3	160.9
7.46	3	124.7
7.46	2	153.2(w)
7.16	3	124.2
7.16	2	154.4
7.16	4	160.9(w)
3.69-3.66	-[1]	136.5
3.69-3.66	-[1]	137.5
3.69-3.66	3	159.8
3.52-3.50	-[1]	136.5
3.52-3.50	-[1]	137.5
3.52-3.50	3	161.6
[b]J_{nxh} = 8.0 Hz J_{1xh} = 146.0 Hz		

^{1}H (599.48 MHz) sw = 5102.0 Hz np = 2884	
^{1}H	$^{x}J_{HH}$
9.15 (dd)	4.4 Hz (3), 1.9 Hz (4)
9.01 (dd)	8.2 Hz (3), 1.7 Hz (4)
8.72 (d)	8.1 Hz (3)
8.49 (bd)[2]	8.1 Hz (3)
8.40 (t)	8.1 Hz (3)
8.07 (dd)	8.1 Hz (3), 4.4 Hz (3)
7.90 (dt)[2]	7.8 Hz (3), 1.6 Hz (4),
7.70 (d)[2]	5.3 Hz (3)
7.46 (dd)	8.0 Hz (3), 4.5 Hz (3)
7.16 (ddd)[2]	7.5 Hz (3), 5.6 Hz (3), 0.9 Hz (4)
Bonds between Hydrogen atoms being coupled in parentheses.	

Figure 3.70 cont. NMR data for **3.45**.

nd= not detected
[1]Carbons could not be assigned.
[2] The digital resolution of the ^{1}H NMR spectrum was not great enough to see the individual coupling constants of the terpy ligand. Instead an average of the coupling constants was observed.

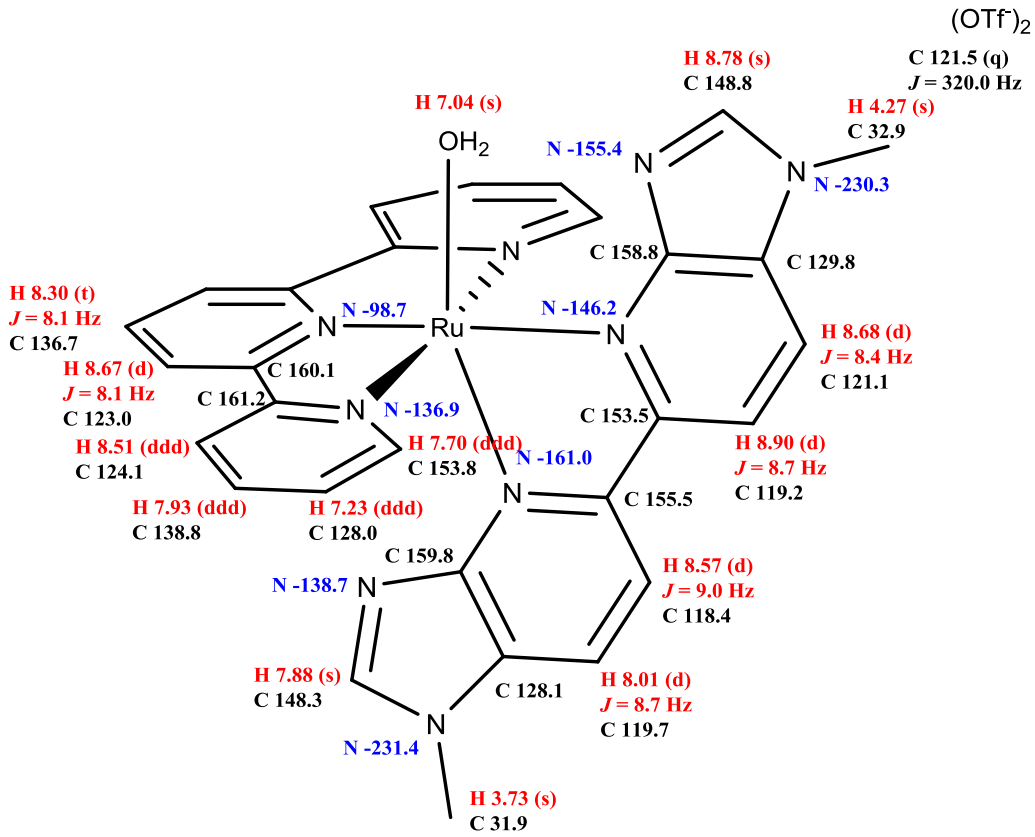

^{1}H -^{15}N **gHMBCAD**[a]		
^{1}H	bonds	^{15}N
8.90	3	-146.2
8.78	3	-230.3
8.78	3	-155.4(w)
8.67	3	-98.7
8.57	3	-161.0
8.51	3	-136.9
7.88	3	-231.4
7.88	3	-138.7
7.70	2	-136.9
7.23	3	-136.9
4.27	2	-231.4
3.73	2	-230.3
[a]J_{nxh} = 5.0 Hz J_{1xh} = 90.0 Hz		

gCOSY
8.90↔8.68
8.67↔8.30
8.57↔8.01
8.51↔7.93
7.93↔7.23
7.70↔7.23
3.80↔1.84
3.05↔1.84
2.47↔1.30
1.58↔1.16
1.30↔1.16

^{1}H-^{13}C **HSQCAD**	
^{1}H	^{13}C
8.90	119.2
8.78	148.8
8.68	121.1
8.67	123.0
8.57	118.4
8.51	124.1
8.30	136.7
8.01	119.7
7.93	138.8
7.88	148.3
7.70	153.8
7.23	128.0
4.27	32.8
3.73	31.9

Figure 3.71. NMR data for **3.53**.

^{1}H -^{13}C gHMBCAD[b]		
^{1}H	bonds	^{13}C
8.90	3	129.8
8.90	2	153.5
8.90	3	155.5
8.90	4	158.8(w)
8.78	3	129.8
8.78	3	158.8
8.78	3	32.9
8.68	3	153.5
8.68	4	155.5(w)
8.68	3	158.8
8.67	1,3	123.0
8.67	2	160.1
8.67	3	161.2
8.57	3	128.1
8.57	3	153.5
8.57	2	155.5
8.57	4	159.8(w)
8.51	3	128.0
8.51	4	153.8 (w)
8.51	3	160.1
8.51	2	161.2
8.30	2	123.0
8.30	3	160.1
8.30	4	161.2
8.01	3	155.5
8.01	3	159.8
7.93	3	153.8
7.93	3	161.2
7.88	3	128.1
7.88	3	159.8
7.88	3	31.9
7.70	4	124.1(w)
7.70	2	128.0
7.70	3	138.8
7.70	3	161.2
7.23	3	124.1
7.23	2	153.8
7.23	4	161.2(w)
4.27	3	129.8
4.27	3	148.8
3.73	3	128.1
3.73	3	148.3
$^{b}J_{nxh}$ = 8.0 Hz J_{1xh} = 146.0 Hz		

^{1}H (599.48 MHz) sw = 5102.0 Hz np = 524288	
^{1}H	$^{x}J_{HH}$
8.90 (d)	8.7 Hz (3)
8.78 (s)	-
8.68 (d)	8.4 Hz (3)
8.67 (d)	8.1 Hz (3)
8.57 (d)	9.0 Hz (3)
8.51 (ddd)	8.1 Hz (3), 1.2 Hz (4), 0.6 Hz (5)
8.30 (t)	8.1 Hz (3)
8.01 (d)	8.7 Hz (3)
7.93 (ddd)	8.1 Hz (3), 7.5 Hz (3), 1.6 Hz (4)
7.88 (s)	-
7.70 (ddd)	5.6 Hz (3), 1.6 Hz (4), 0.6 Hz (5)
7.23 (ddd)	7.5 Hz (3), 5.6 Hz (3), 1.2 Hz (4)
7.04 (s)	-
4.27 (s)	-
3.73 (s)	-
Bonds between Hydrogen atoms being coupled in parentheses.	

Figure 3.71 cont. NMR data for **3.53**.

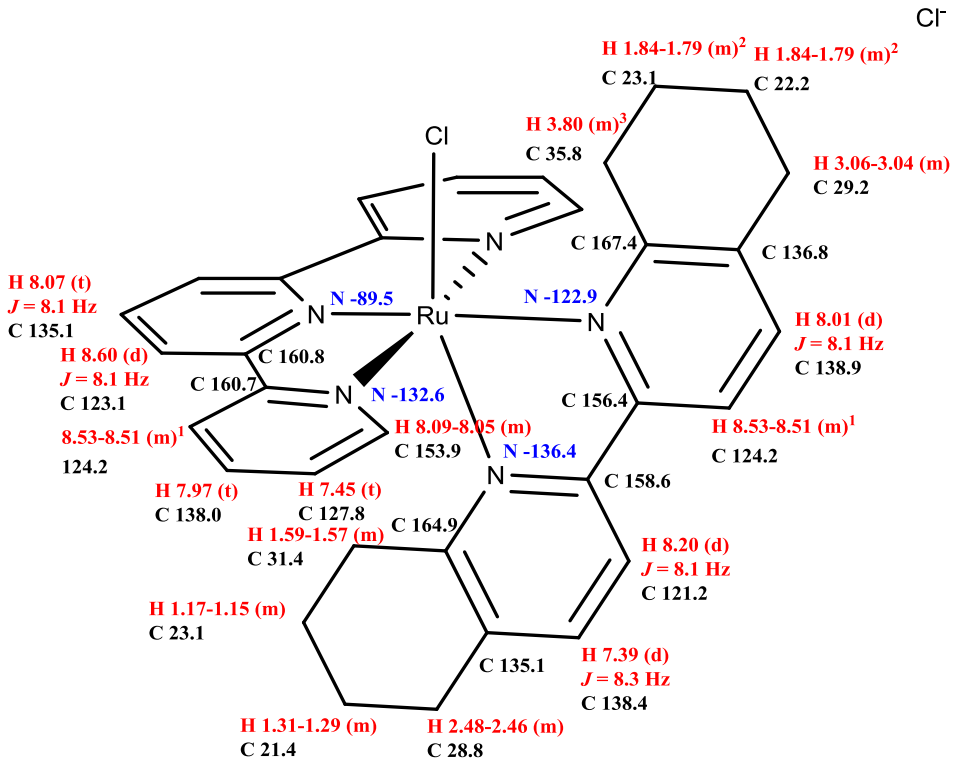

^{1}H - ^{15}N **gHMBCAD**[a]		
^{1}H	bonds	^{15}N
8.60	3	-89.5
8.53-8.51	3	-122.9
8.53-8.51	3	-132.6
8.20	3	-136.4
8.09-8.05	2	-132.6
7.45	3	-132.6
3.80	3	-122.9
1.59-1.57	3	-136.4
[a] $^{a}J_{nxh}$ = 5.0 Hz J_{1xh} = 90.0 Hz		

gCOSY
8.60↔8.07
8.53-8.51↔8.01
8.53-8.51↔7.97
8.20↔7.39
8.09↔7.45
7.97↔7.45
3.80↔1.84-1.79
3.06-3.04↔1.84-1.79
2.48-2.46↔1.31-1.29
1.59-1.57↔1.17-1.15
1.31-1.29↔1.17-1.15

^{1}H-^{13}C **HSQCAD**	
^{1}H	^{13}C
8.60	123.1
8.53-8.51	124.2
8.53-8.51	121.3
8.20	121.2
8.09-8.05	153.9
8.07	135.1
8.01	138.9
7.97	138.0
7.45	127.8
7.39	138.4
3.80	35.8
3.06-3.04	29.2
2.48-2.46	28.8
1.84-1.79	23.1
1.84-1.79	22.2
1.59-1.57	31.4
1.31-1.29	21.4
1.17-1.15	23.1

Figure 3.72. NMR data for **3.58**.

^{1}H (599.48 MHz) sw = 7183.9 Hz np = 524288	
^{1}H	$^xJ_{HH}$
8.60 (d)	8.1 Hz (3)
8.53-8.51 (m)	-
8.53-8.51 (m)	-
8.20 (d)	8.1 Hz (3)
8.09-8.05 (m)	-
8.07 (t)	8.1 Hz (3)
8.01 (d)	8.1 Hz (3)
7.97 (t)	7.7 Hz (3)
7.45 (t)	6.2 Hz (3)
7.39 (d)	8.3 Hz (3)
3.80 (m)	-
3.06-3.04 (m)	-
2.48-2.46 (m)	-
1.84-1.79 (m)	-
1.84-1.79 (m)	-
1.59-1.57 (m)	-
1.31-1.29 (m)	-
1.17-1.15 (m)	-
Bonds between Hydrogen atoms being coupled in parentheses.	

^{1}H -^{13}C gHMBCAD[b]		
^{1}H	bonds	^{13}C
8.60	1,3	123.1
8.60	3	160.7
8.53-8.51	3(tpy)	127.8
8.53-8.51	3(bpy)	136.8
8.53-8.51	4(tpy)	153.9(w)
8.53-8.51	2(bpy)	156.4
8.53-8.51	3(bpy)	158.6
8.53-8.51	2(tpy)	160.7
8.20	3	135.1
8.20	3	156.4
8.20	2	158.6
8.09-8.05	4	124.2(w)
8.09-8.05	2	127.8
8.09-8.05	3	138.0
8.09-8.05	3	160.7
8.07	2	123.1(w)
8.07	3	160.8
8.01	3	156.4
8.01	3	167.4
8.01	3	29.2
7.97	2	124.2(w)
7.97	2	127.8(w)
7.97	3	153.9
7.97	3	160.7
7.45	3	124.2
7.45	2	153.9
7.45	4	160.7
7.39	3	158.6
7.39	3	164.9
7.39	3	28.8

^{1}H -^{13}C gHMBCAD continued[b]		
^{1}H	bonds	^{13}C
3.80	3	22.2
3.80	2	23.1
3.80	3	136.8
3.80	2	167.4
3.06-3.04	2	22.2
3.06-3.04	3	23.1
3.06-3.04	2	136.8
3.06-3.04	3	138.9
3.06-3.04	3	167.4
2.48-2.46	2	21.4
2.48-2.46	3	23.1
2.48-2.46	2	135.1
2.48-2.46	3	138.4
2.48-2.46	3	164.9
1.84-1.79	1,2	22.2
1.84-1.79	1,2	23.1
1.84-1.79	3,4	136.8(w)
1.84-1.79	3,4	167.4(w)
1.59-1.57	3	21.4
1.59-1.57	2	23.1
1.59-1.57	3	135.1
1.59-1.57	2	164.9
1.31-1.29	2	28.8
1.31-1.29	3	31.4
1.31-1.29	3	135.1
1.17-1.15	3	28.8
1.17-1.15	2	31.4
1.17-1.15	3	164.9
[b] J_{nxh} = 8.0 Hz J_{1xh} = 146.0 Hz		

Figure 3.72 cont. NMR data for **3.58**.

[1] ^{1}H peaks are on top of each other making the coupling constants unreliable.
[2] ^{1}H peaks are on top of each other, making it hard to assign corresponding carbon peak.
[3] Peak was not observed in the ^{1}H NMR spectrum; it was under the H_2O. ^{1}H shift was assigned by HMBC and HSQC.
[4] The digital resolution of the ^{1}H NMR spectrum was not great enough to see the individual coupling constants of the terpy ligand. Instead an average of the coupling constants was observed.

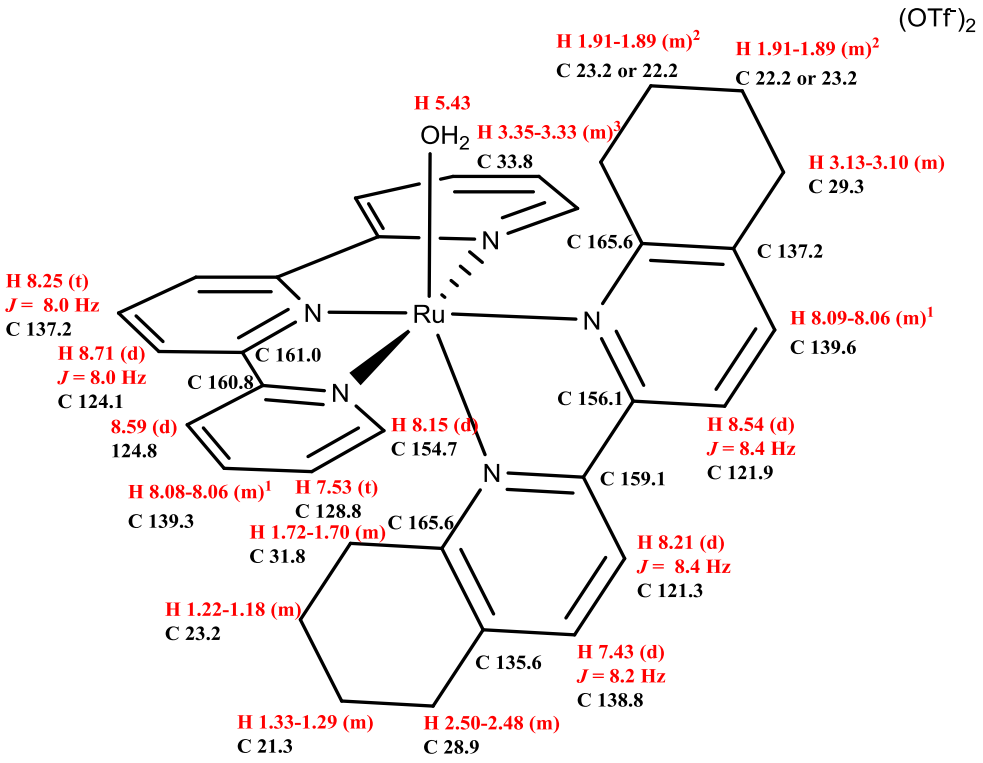

^{1}H-^{13}C HSQCAD	
^{1}H	^{13}C
8.71	124.1
8.59	124.8
8.54	121.9
8.25	137.2
8.21	121.3
8.15	154.7
8.09-8.06	139.6
8.08-8.06	139.3
7.53	128.8
7.43	138.8

^{1}H-^{13}C HSQCAD	
^{1}H	^{13}C
3.35-3.33	33.8
3.12-3.10	29.3
2.50-2.48	28.9
1.91-1.89	23.2
1.91-1.89	22.2
1.72-1.70	31.8
1.33-1.29	21.3
1.22-1.18	23.2

gCOSY
8.60↔8.07
8.52↔8.01
8.52↔7.97
8.20↔7.39
8.09↔7.45
7.97↔7.45
3.80↔1.84
3.05↔1.84
2.47↔1.30
1.58↔1.16
1.30↔1.16

Figure 3.73. NMR data for **3.58b**.

[1] ^{1}H peaks are on top of each other making the coupling constants unreliable.
[2] ^{1}H peaks are on top of each other, making it hard to assign which carbon peak.
[3] Peak was not observed in the ^{1}H spectrum, it was under the H_2O. ^{1}H shift was assigned by HMBC and HSQC.
[4] The digital resolution of the ^{1}H NMR spectrum was not great enough to see the individual coupling constants of the terpy ligand. Instead an average of the large coupling constants was observed.

^{1}H (599.36 MHz) sw = 5980.9 Hz np = 524288	
^{1}H	$^{x}J_{HH}$
8.71 (d)	8.0 Hz (3)
8.59 (d)	8.0 Hz (3)
8.54 (d)	8.4 Hz (4)
8.25 (t)	8.0 Hz (3)
8.21 (d)	8.4 Hz (3)
8.15 (d)	5.5 Hz (3)
8.09-8.06 (m)	-
8.08-8.06 (m)	-
7.53 (t)	6.6 Hz (3)
7.43 (d)	8.2 Hz (3)
3.35-3.33 (m)	-
3.12-3.10 (m)	-
2.50-2.48 (m)	-
1.91-1.89 (m)	-
1.91-1.89 (m)	-
1.72-1.70 (m)	-
1.33-1.29 (m)	-
1.22-1.18 (m)	-
Bonds between Hydrogen atoms being coupled in parentheses.	

^{1}H -^{13}C gHMBCAD[b]		
^{1}H	bonds	^{13}C
8.71	1,3	124.1
8.71	3	161.0
8.59	3	128.8
8.59	2	160.8
8.54	3	137.2
8.54	2	156.1
8.54	3	159.1
8.25	3	161.0
8.21	3	135.6
8.21	3	156.1
8.21	2	159.1
8.15	2	128.8
8.15	3	139.3
8.15	3	160.8
8.09-8.06	3	29.3
8.09-8.06	3	156.1
8.09-8.06	3	165.6
8.08-8.06	3	154.7
8.08-8.06	3	160.8
7.53	3	124.8
7.53	2	154.7
7.43	3	28.9
7.43	3	159.1
7.43	3	165.6
3.35-3.33	2 or 3	22.2
3.35-3.33	2 or 3	23.2
3.35-3.33	3	137.2
3.35-3.33	2	165.6
3.12-3.10	2 or 3	22.2
3.12-3.10	2 or 3	23.2
3.12-3.10	2	137.2
3.12-3.10	3	139.6
3.12-3.10	3	165.6

^{1}H -^{13}C gHMBCAD continued[b]		
^{1}H	bonds	^{13}C
2.50-2.48	2	21.3
2.50-2.48	3	23.2
2.50-2.48	2	135.6
2.50-2.48	3	138.8
2.50-2.48	3	165.6
1.91-1.89	1 or 2	22.3
1.91-1.89	1 or 2	23.3
1.72-1.70	3	21.3
1.72-1.70	2	23.2
1.72-1.70	3	135.6
1.72-1.70	2	165.6
1.33-1.29	2	28.9
1.33-1.29	3	31.8
1.33-1.29	3	135.6
1.22-1.18	3	28.9
1.22-1.18	2	31.8
1.22-1.18	3	165.6
$^{b}J_{nxh}$ = 8.0 Hz J_{1xh} = 146.0 Hz		

Figure 3.73 cont. NMR data for **3.58b**.

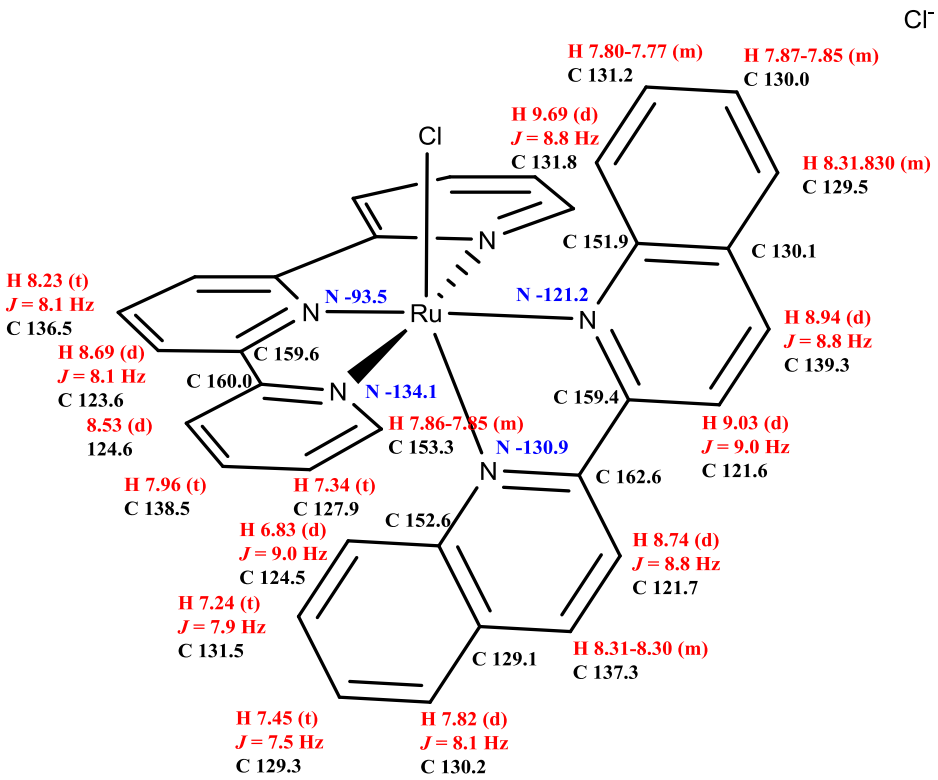

^{1}H - ^{15}N gHMBCAD[a]		
^{1}H	bonds	^{15}N
9.69	3	-121.2
9.03	3	-121.2
8.74	3	-130.9
8.69	3	-93.5
8.53	3	-134.1
7.86-7.85	2	-134.1
7.34	3	-134.1
6.83	3	-130.9
[a] J_{nxh} = 5.0 Hz J_{1xh} = 90.0 Hz		

gCOSY
9.69↔7.80-7.77
9.03↔8.94
8.74↔8.31-8.30
8.69↔8.23
8.53↔7.96
8.31-8.30↔7.87-7.85
7.96↔7.34
7.87-7.85↔7.80-7.77
7.86-7.85↔7.34
7.82↔7.45
7.45↔7.24
7.24↔6.83

^{1}H-^{13}C HSQCAD	
^{1}H	^{13}C
9.69	131.8
9.03	121.6
8.94	139.3
8.74	121.7
8.69	123.6
8.53	124.6
8.31-8.30	129.5
8.31-8.30	137.3
8.23	136.5
7.96	138.5
7.87-7.85	130.0
7.86-7.85	153.3
7.82	130.2
7.80-7.77	131.2
7.45	129.3
7.34	127.9
7.24	131.5
6.83	124.5

Figure 3.74. NMR data for **3.57**.

The digital resolution of the ^{1}H NMR spectrum was not great enough to see the individual coupling constants of the terpy ligand. Instead an average of the coupling constants was observed.

^{1}H (599.48 MHz) sw = 7183.9 Hz np = 524288	
9.69 (d)	8.8 Hz (3)
9.03 (d)	9.0 Hz (3)
8.94 (d)	8.8 Hz (3)
8.74 (d)	8.8 Hz (3)
8.69 (d)	8.1 Hz (3)
8.53 (d)	8.1 Hz (3)
8.31-8.30 (m)	-
8.31-8.30 (m)	-
8.23 (t)	8.1 Hz (3)
7.96 (t)	7.8 Hz (3)
7.87-7.85 (m)	-
7.86-7.85 (m)	-
7.82 (d)	8.1 Hz (3)
7.80-7.77 (m)	-
7.45 (t)	7.5 Hz (3)
7.34 (t)	6.6 Hz (3)
7.24 (t)	7.9 Hz (3)
6.83 (d)	9.0 Hz (3)
Bonds between hydrogen atoms being coupled in parentheses.	

^{1}H -^{13}C gHMBCAD[b]		
^{1}H	bonds	^{13}C
9.69	3	130.0
9.69	3	130.1
9.03	3	130.1
9.03	2	139.3
9.03	2	159.4
9.03	3	162.6
8.94	3	129.5
8.94	2	130.1(w)
8.94	3	151.9
8.94	3	159.4
8.74	3	129.1
8.74	2	137.3(w)
8.74	3	159.4
8.74	2	162.6
8.69	1,3	123.6
8.69	2	159.6
8.53	3	127.9
8.53	2	138.5(w)
8.53	4	153.3(w)
8.53	2	160.0
8.31-8.30	2(py)	129.1(w)
8.31-8.30	3(py)	130.2
8.31-8.30	3(ph)	131.2
8.31-8.30	3(ph)	139.3
8.31-8.30	3(ph)	151.9
8.31-8.30	3(py)	152.6
8.31-8.30	3(py)	162.6
8.23	2	123.6(w)
8.23	3	159.6

^{1}H -^{13}C gHMBCAD continued[b]		
^{1}H	bonds	^{13}C
7.96	2	124.6
7.96	3	153.3
7.96	3	160.0
7.87-7.85	3	130.1
7.87-7.85	3	131.8
7.87-7.85	4	151.9(w)
7.86-7.85	4	124.6(w)
7.86-7.85	2	127.9
7.86-7.85	3	138.5
7.86-7.85	3	160.0
7.82	2	129.1(w)
7.82	3	131.5
7.82	3	137.3
7.82	3	152.6
7.80-7.77	3	129.5
7.80-7.77	3	151.9
7.45	3	124.5
7.45	3	129.1
7.45	2	131.5(w)
7.34	3	124.6
7.34	2	153.3
7.34	4	160.0
7.24	2	129.3(w)
7.24	3	130.2
7.24	3	152.6
6.83	3	129.3
[b] J_{nxh} = 8.0 Hz J_{1xh} = 146.0 Hz		

Figure 3.74 cont. NMR data for **3.57**.

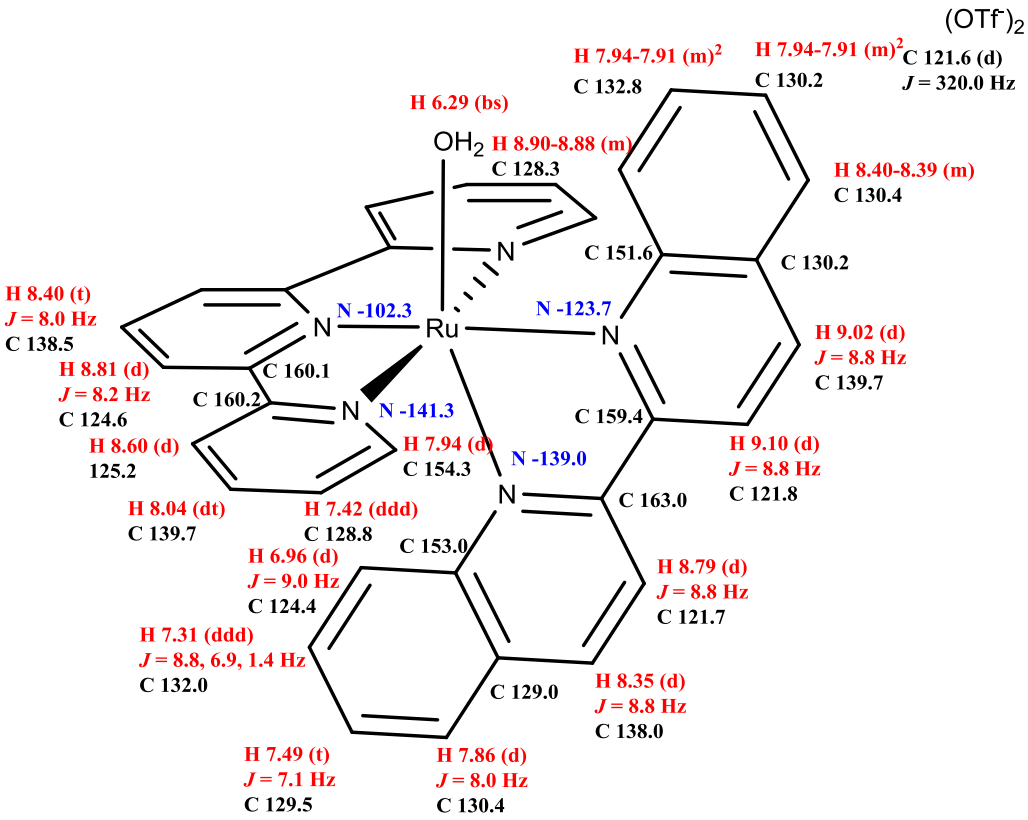

gCOSY
9.10↔9.02
8.90-8.88↔8.40-8.39
8.90-8.88↔7.94-7.91
8.81↔8.40
8.79↔8.35
8.60↔8.04
8.40-8.39↔7.94-7.91
8.04↔7.42
7.94↔7.42
7.86↔7.49
7.49↔7.31
7.31↔6.96

^{1}H -^{15}N **gHMBCAD**[a]		
^{1}H	bonds	^{15}N
9.10	3	-123.7
8.90-	3	-123.7
8.81	3	-102.3
8.79	3	-139.0
8.60	3	-141.3
7.94	2	-141.3
7.42	3	-141.3
6.96	3	-139.0
[a] J_{nxh} = 5.0 Hz J_{1xh} = 90.0 Hz		

^{1}H-^{13}C **HSQCAD**	
^{1}H	^{13}C
9.10	121.8
9.02	139.7
8.90-	128.3
8.81	124.6
8.79	121.7
8.60	125.2
8.40	138.5
8.40-	130.4
8.35	138.0

^{1}H-^{13}C **HSQCAD Cont.**	
^{1}H	^{13}C
8.04	139.7
7.94	154.3
7.94-7.91	132.8
7.94-7.91	130.2
7.86	130.4
7.49	129.5
7.42	128.8
7.31	132.0
6.96	124.4

Figure 3.75. NMR data **3.57b**.

The digital resolution of the ^{1}H NMR spectrum was not great enough to see the individual coupling constants of the terpy ligand. Instead an average of the coupling constants was observed.
[2] Protons are at the same chemical shift, the attached carbons were assigned based on HMBC

^{1}H (599.48 MHz) sw = 6578.9 Hz np = 524288	
^{1}H	$^{X}J_{HH}$
9.10 (d)	8.8 Hz (3)
9.02 (d)	8.8 Hz (3)
8.90-8.88 (m)	-
8.81 (d)	8.2 Hz (3)
8.79 (d)	8.8 Hz (3)
8.60 (d)	8.0 Hz (3)
8.40-8.39 (m)	-
8.40 (t)	8.0 Hz
8.35 (d)	8.8 Hz (3)
8.04 (dt)	7.8 Hz (3), 1.4 Hz (4)
7.94 (d)	5.6 Hz (3)
7.94-7.91 (m)	-
7.94-7.91 (m)	-
7.86 (d)	8.0 Hz (3)
7.49 (t)	7.1 Hz (3)
7.42 (ddd)	7.0 Hz (3), 5.6 Hz (3), 1.1 Hz (3)
7.31 (ddd)	8.8 Hz (3), 6.9 Hz (3), 1.4 Hz (4)
6.96 (d)	9.0 Hz (3)
Bonds between hydrogen atoms being coupled in parentheses.	

^{1}H -^{13}C gHMBCAD[b]		
^{1}H	bonds	^{13}C
9.10	3	130.2
9.10	2	139.7(w)
9.10	2	159.4
9.10	3	163.0(w)
9.02	3	130.4
9.02	3	151.6
9.02	3	159.4
8.90-8.88	3	130.2
8.90-8.88	4	139.7(w)
8.90-8.88	2	151.6
8.81	1,3	124.6
8.81	2	160.1
8.79	3	129.0
8.79	2	138.0(w)
8.79	3	159.4(w)
8.79	2	163.0
8.60	3	128.8
8.60	2	160.2
8.40	2	124.6(w)
8.40	3	160.1
8.40-8.39	2(bpy)	130.2(w)
8.40-8.39	3(bpy)	132.8
8.40-8.39	3(bpy)	139.7(w)
8.40-8.39	3(bpy)	151.6
8.35	2	129.0(w)
8.35	3	130.4
8.35	3	153.0
8.35	3	163.0
8.04	2	128.8(w)
8.04	3	154.3
8.04	3	160.2

^{1}H -^{13}C gHMBCAD continued[b]		
^{1}H	bonds	^{13}C
7.94	4	125.2(w)
7.94	2	128.8
7.94	3	139.7
7.94	3	160.2
7.94-7.91	2,3	128.3
7.94-7.91	2,3	130.4
7.94-7.91	3,4	151.6
7.86	2	129.0
7.86	3	132.0
7.86	3	138.0
7.86	3	153.0
7.49	3	124.4
7.49	3	129.0
7.49	2	132.0(w)
7.42	3	125.2
7.42	2	154.3
7.42	4	160.2(w)
7.31	3	130.4
7.31	3	153.0
6.96	3	129.0
6.96	3	129.5
[b] J_{nxh} = 8.0 Hz J_{1xh} = 146.0 Hz		

Figure 3.75 cont. NMR data **3.57b**.

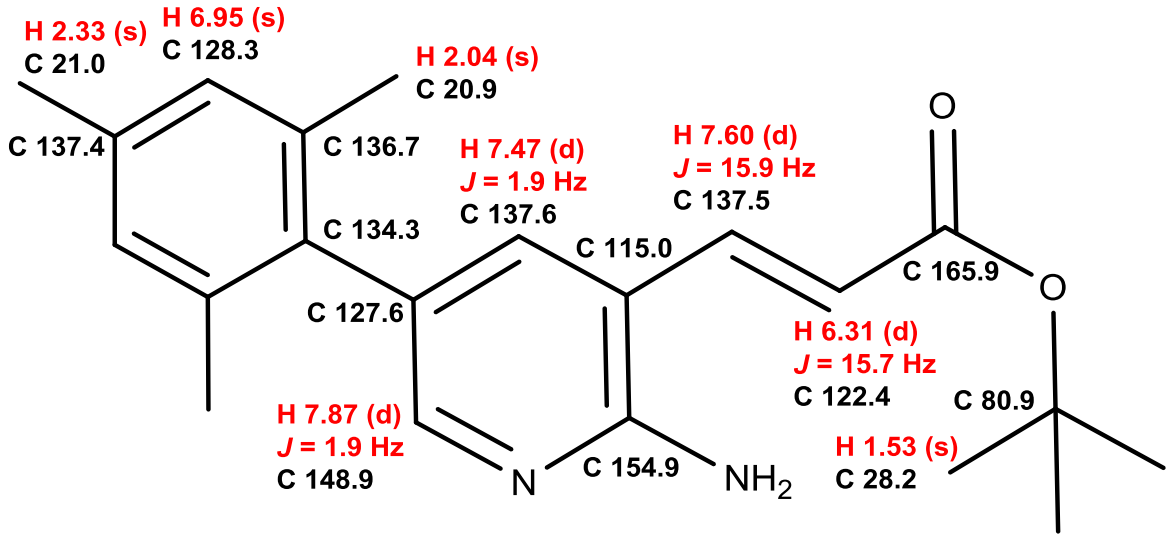

^{1}H -^{13}C gHMBCAD[a]		
^{1}H	bonds	^{13}C
7.87	2	127.6
7.87	3	134.4(w)
7.87	3	137.6
7.87	3	154.9
7.60	2	115.0
7.60	2	122.4
7.60	3	137.6
7.60	3	154.9
7.60	3	165.9
7.47	3	134.3
7.47	3	137.5
7.47	3	148.9
7.47	3	154.9
6.95	1,3	128.3
6.95	3	134.3
6.95	2	136.7(w)
6.95	2	137.4(w)

^{1}H -^{13}C gHMBCAD[a] cont.		
^{1}H	bonds	^{13}C
6.95	3	21.0
6.95	3	20.9
6.31	3	115.0
6.31	2	165.9
2.33	3	128.3
2.33	2	137.4
2.04	3	128.3
2.04	3	134.3
2.04	2	136.7
1.53	2	80.9
1.53	1,3	28.2
[a] J_{nxh} = 8.0 Hz J_{1xh} = 146.0 Hz		

gCOSY
7.87↔7.47
7.60↔6.31
6.95↔2.33
6.95↔2.04

^{1}H-^{13}C HSQCAD	
^{1}H	^{13}C
7.87	148.9
7.60	137.5
7.47	137.6
6.95	128.3
6.31	122.4
2.33	21.0
2.04	20.9
1.53	28.2

Figure 3.76. NMR data for **3.63**.

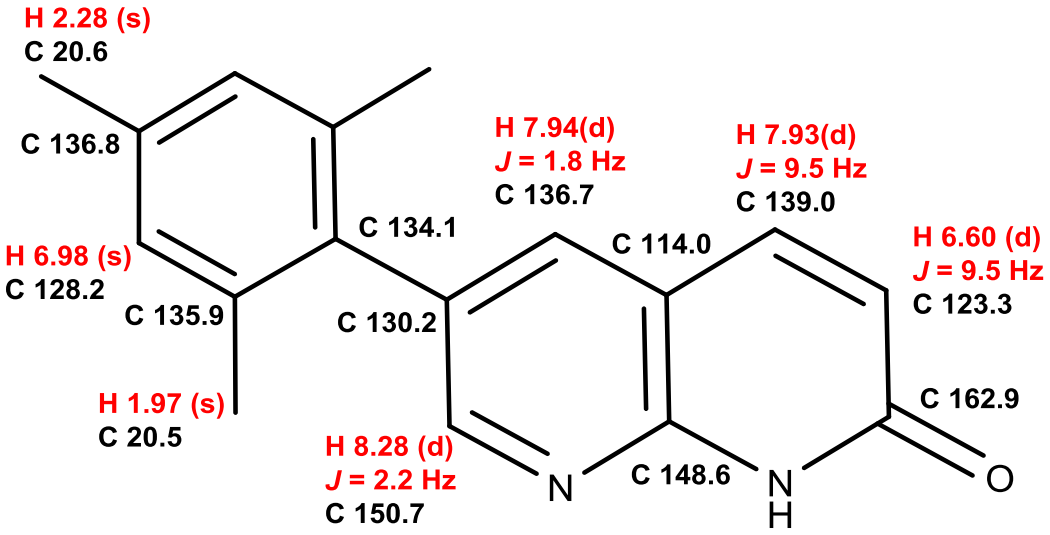

^{1}H -^{13}C gHMBCAD[a]		
^{1}H	bonds	^{13}C
8.28	2	130.2
8.28	3	134.1(w)
8.28	3	136.7
8.28	3	148.6
7.94	3	134.1
7.94	3	139.0
7.94	3	148.6
7.94	3	150.7
7.93	2	114.0
7.93	3	136.7
7.93	3	148.6
7.93	3	162.9
6.98	3	20.5
6.98	3	20.6
6.98	1,3	128.2

^{1}H -^{13}C gHMBCAD continued[a]		
^{1}H	bonds	^{13}C
6.98	3	134.1
6.60	3	114.0
6.60	2	162.9(w)
2.28	3	128.2
2.28	2	136.8
1.97	3	128.2
1.97	3	134.1
1.97	2	135.9
[a]J_{nxh} = 8.0 Hz J_{1xh} = 146.0 Hz		

gCOSY
8.28↔7.94
7.93↔6.60
6.98↔2.28
6.98↔1.97

^{1}H-^{13}C HSQCAD	
^{1}H	^{13}C
8.28	150.7
7.94	136.7
7.93	139.0
6.98	128.2
6.60	123.3
2.28	20.6
1.97	20.5

Figure 3.77. NMR data for **3.64**.

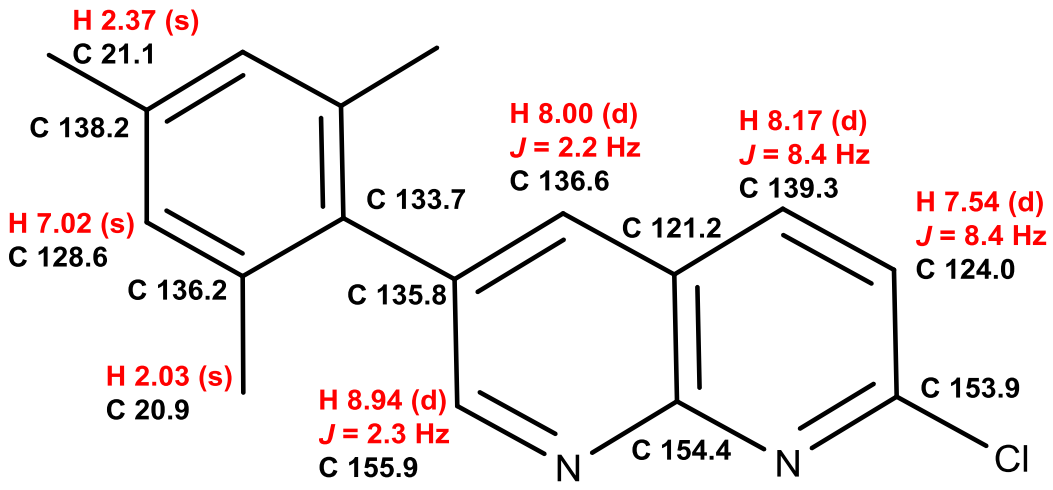

^{1}H -^{13}C gHMBCAD[a]		
^{1}H	bonds	^{13}C
8.94	4	121.2(w)
8.94	3	133.7(w)
8.94	2	135.8
8.94	3	136.6
8.94	3	154.4
8.17	2	121.2(w)
8.17	2	124.0(w)
8.17	3	136.6
8.17	3	154.4
8.00	2	121.2(w)
8.00	3	133.7
8.00	3	139.3
8.00	3	154.4
8.00	3	155.9
7.54	3	121.2
7.02	1,3	128.6
7.02	3	133.7
7.02	2,4	136.2
7.02	2	138.2(w)
7.02	3	21.1
2.37	3	128.6
2.37	2	138.2
2.03	3	128.6
2.03	3	133.7
2.03	2,4	136.2
[a]J_{nxh} = 8.0 Hz J_{1xh} = 146.0 Hz		

gCOSY
8.94↔8.00
8.17↔7.54
7.02↔2.37
7.02↔2.03

^{1}H-^{13}C HSQCAD	
^{1}H	^{13}C
8.94	155.9
8.17	139.3
8.00	136.6
7.54	124.0
7.02	128.6
2.37	21.1
2.03	20.9

Figure 3.78. NMR data for **3.65**.

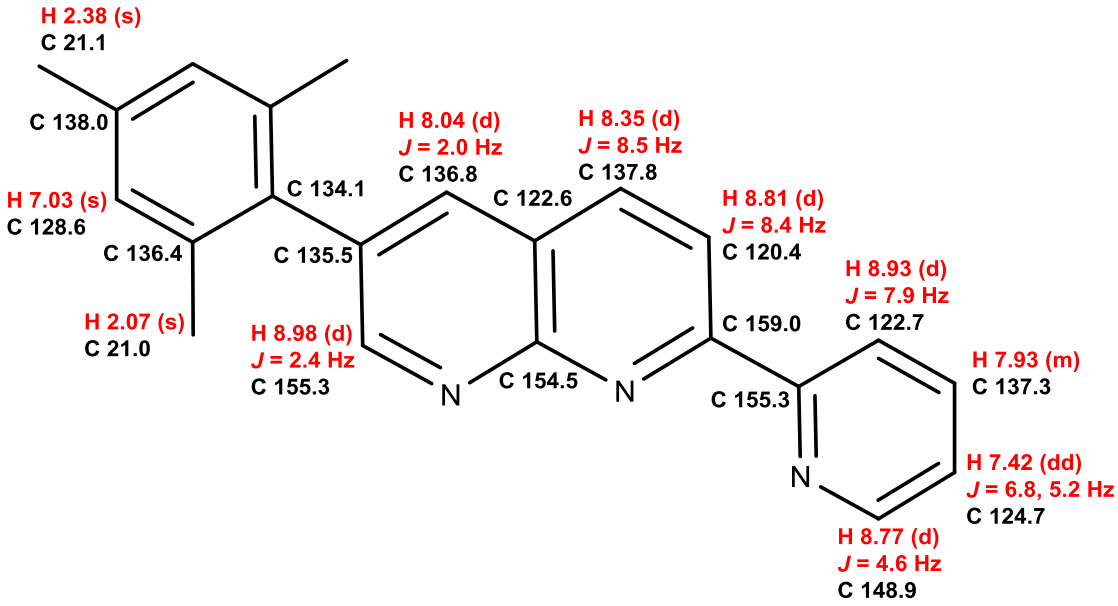

^{1}H -^{13}C gHMBCAD[a]		
^{1}H	bonds	^{13}C
8.98	3	134.1(w)
8.98	2	135.5
8.98	3	136.8
8.98	3	154.5(w)
8.93	3	124.7
8.93	3	159.0
8.81	3	122.6
8.81	2	159.0(w)
8.77	2	124.7
8.77	3	137.3
8.77	3	155.3
8.35	2	122.6
8.35	3	136.8
8.35	3	154.5
8.35	3	159.0
8.04	2	122.7(w)
8.04	3	134.1
8.04	3	137.8

^{1}H -^{13}C gHMBCAD continued[a]		
^{1}H	bonds	^{13}C
8.04	3	154.5
8.04	3	155.3
7.93	3	148.9
7.93	3	155.3
7.42	3	122.7
7.42	2	148.9
7.03	1,3	128.6
7.03	3	134.1
7.03	4	135.5(w)
7.03	2	136.4
7.03	2	138.0
2.38	3	128.6
2.38	2	138.0
2.07	3	128.6
2.07	3	134.1
2.07	2,4	136.4
[a]J_{nxh} = 8.0 Hz		
J_{1xh} = 146.0 Hz		

^{1}H-^{13}C HSQCAD	
^{1}H	^{13}C
8.98	155.3
8.93	122.7
8.81	120.4
8.77	148.9
8.35	137.8
8.04	136.8
7.93	137.3
7.42	124.7
7.03	128.6
2.38	21.1
2.07	21.0

gCOSY
8.98↔8.04
8.93↔7.93
8.81↔8.35
8.77↔7.42
7.93↔7.42
7.03↔2.38
7.03↔2.07

Figure 3.79. NMR data for **3.66**.

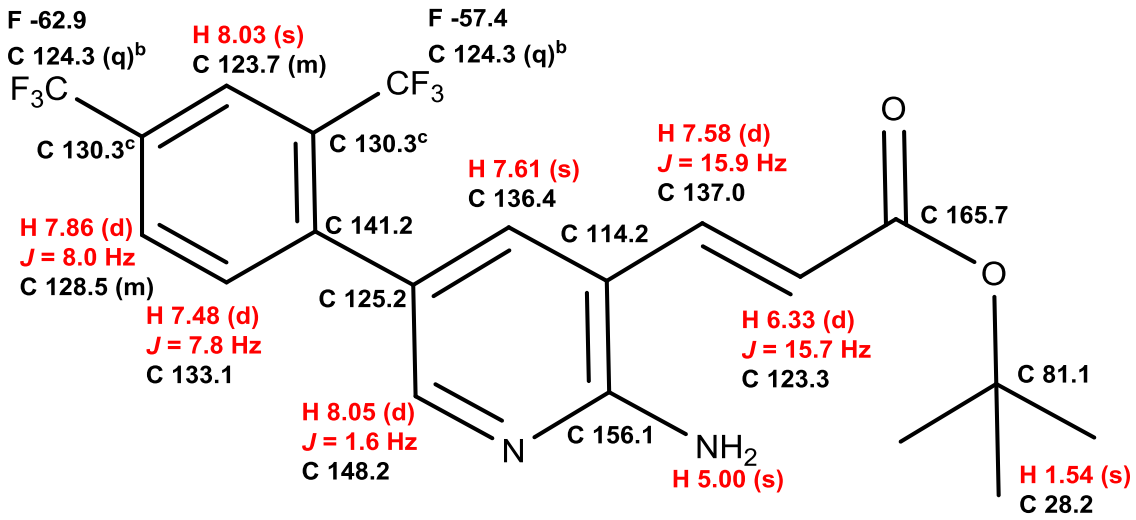

^{1}H-^{13}C HSQCAD	
^{1}H	^{13}C
8.05	148.2
8.03	123.7
7.86	128.5
7.61	136.4
7.58	137.0
7.48	133.1
6.33	123.3
1.54	28.2

^{1}H -^{13}C gHMBCAD[a]		
^{1}H	bonds	^{13}C
8.05	2	125.2
8.05	3	136.4
8.05	3	156.1
8.03	**3**	**124.3 (q)**[b]
8.03	3	128.5
8.03	3	141.2
7.86	3	123.7
7.86	3	141.2
7.61	3	137.0
7.61	3	141.2
7.61	3	148.2
7.61	3	156.1
7.58	2	114.2

^{1}H -^{13}C gHMBCAD continued[a]		
^{1}H	bonds	^{13}C
7.58	2	123.3
7.58	3	136.4
7.58	3	156.0
7.58	3	165.7
7.48	3	125.2
7.48	**3**	**130.3**[c]
6.33	3	114.2
6.33	2	165.7
[a] J_{nxh} = 8.0 Hz J_{1xh} = 146.0 Hz		

gCOSY
7.86↔7.48
7.58↔6.33

Figure 3.80. NMR data for **3.67**.

[b] Peaks were not observed in the ^{13}C spectra, they were assigned based on a correlation in the HMBC between the proton at 8.03 ppm and carbon at 124.3 ppm. The two carbons should have separate values but due to the insensitivity of HMBC an average value of the two carbons is reported.
[c] Peaks were not observed in the ^{13}C spectra, peaks were assigned based on a correlation in the HMBC between the proton at 7.48 ppm and carbon at 130.3 ppm. The two carbons should have separate values but due to the insensitivity of HMBC an average value of the two carbons is reported.

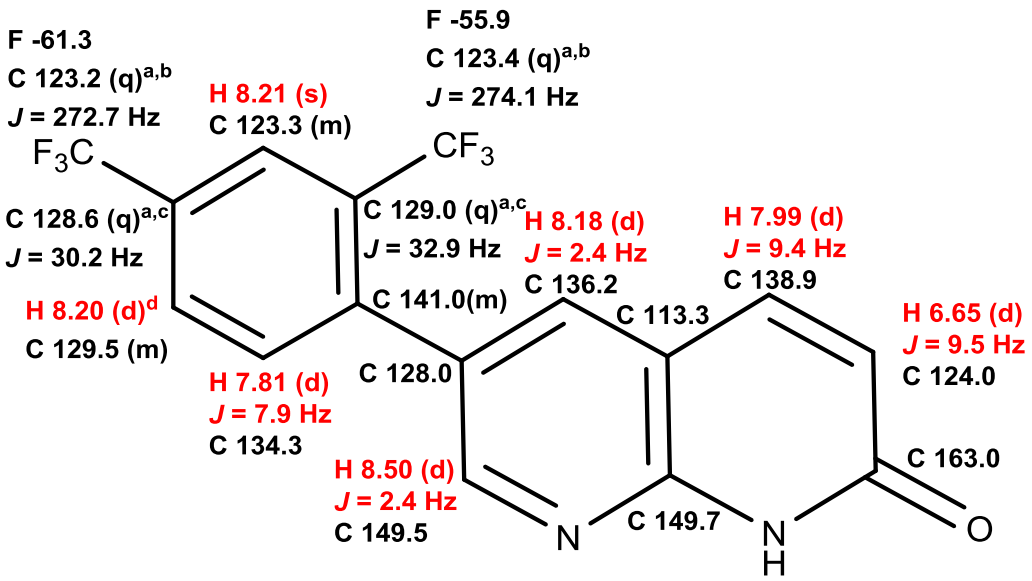

gCOSY
8.50↔8.18
8.20↔7.81
7.99↔6.65

^{1}H-^{13}C HSQCAD	
^{1}H	^{13}C
8.50	149.5
8.21	123.3
8.20	129.5
8.18	136.2
7.99	138.9
7.81	134.3
6.65	124.0

^{1}H -^{13}C gHMBCAD[a]		
^{1}H	bonds	^{13}C
8.50	2	128.0
8.50	3	136.2
8.50	3	149.7
8.21	3	123.2[b]
8.21	3	123.4[b]
8.21	3	129.5
8.21	3	141.0
8.20	3 or 5	123.2[b]
8.20	3 or 5	123.4[b]
8.20	3	123.3
8.20	3	141.0
8.18	3	138.9
8.18	3	141.0

^{1}H -^{13}C gHMBCAD continued[a]		
^{1}H	bonds	^{13}C
8.18	3	149.5
8.18	3	149.7
7.99	2	113.3(w)
7.99	3	136.2
7.99	3	149.7
7.99	3	163.0
7.81	3	128.6[c]
7.81	3	129.0[c]
6.65	3	113.3
6.65	2	163.0
[a] J_{nxh} = 8.0 Hz J_{1xh} = 146.0 Hz		

Figure 3.81. NMR data for **3.68**.

[a] Only the two inner peaks of the quartet are observed
[b] These two carbons did not have enough data to assign with certainty and assignment could be reversed.
[c] These two carbons did not have enough data to assign with certainty and assignment could be reversed.
[d] Half of the doublet was under the singlet at 8.21, which gives an unreliable coupling.

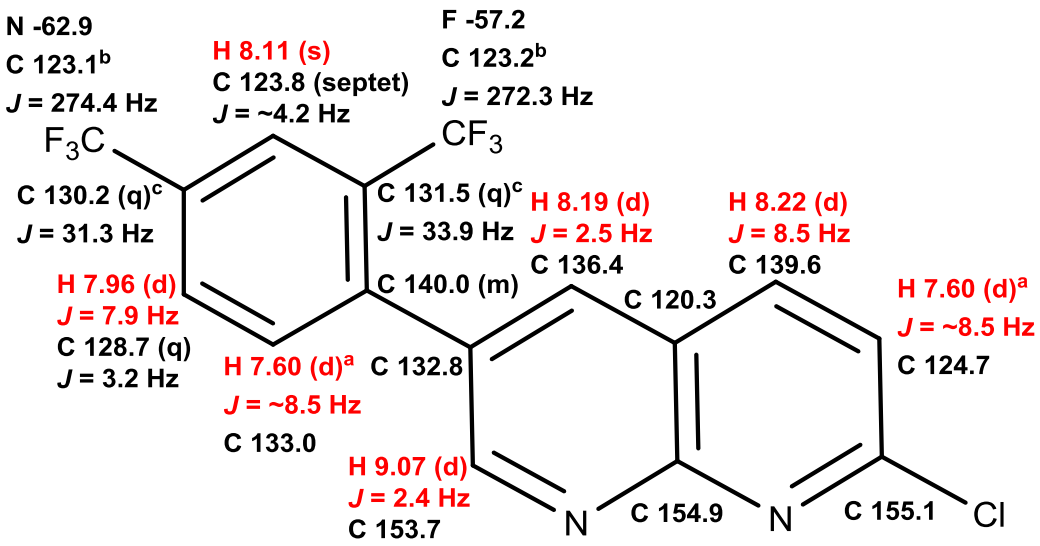

gCOSY
9.07↔8.19
8.22↔7.60
7.96↔7.60

^{1}H-^{13}C HSQCAD	
^{1}H	^{13}C
9.07	153.7
8.22	139.6
8.19	136.4
8.11	123.8
7.96	128.7
7.60	133.0
7.60	124.7

^{1}H -^{13}C gHMBCAD[a]		
^{1}H	bonds	^{13}C
9.07	2	132.8
9.07	3	136.4
9.07	3	140.0
9.07	3	154.9
8.22	2	120.3
8.22	2	124.7(w)
8.22	3	136.4
8.22	3	154.9
8.22	3	155.1
8.19	3	139.6
8.19	3	153.7
8.19	3	154.9
8.11	3	123.1[b]
8.11	3	123.2[b]
8.11	3	128.7
8.11	2	130.2(w)[c]
8.11	2	131.5(w)[c]

^{1}H -^{13}C gHMBCAD continued[a]		
^{1}H	bonds	^{13}C
8.11	4	133.0(w)
8.11	3	140.0
7.96	2 or 4	123.1[b]
7.96	2 or 4	123.2[b]
7.96	2 or 4	130.2[c]
7.96	3	140.0
7.60(pyr)	3	120.3
7.60(ben)	4	123.1
7.60(ben)	4	123.2
7.60(ben)	2	128.7
7.60(ben)	3	130.2[c]
7.60(ben)	3	131.5[c]
7.60(ben)	3	132.8
7.60(ben)	2	140.0
[a]J_{nxh} = 8.0 Hz J_{1xh} = 146.0 Hz		

Figure 3.82. NMR data for **3.69**.

[a] Two proton peaks were on top of each other, the observed doublet had a coupling of 8.5 Hz.
[b] These two carbons did not have enough data to assign with certainty and assignment could be reversed.
[c] These two carbons did not have enough data to assign with certainty and assignment could be reversed.

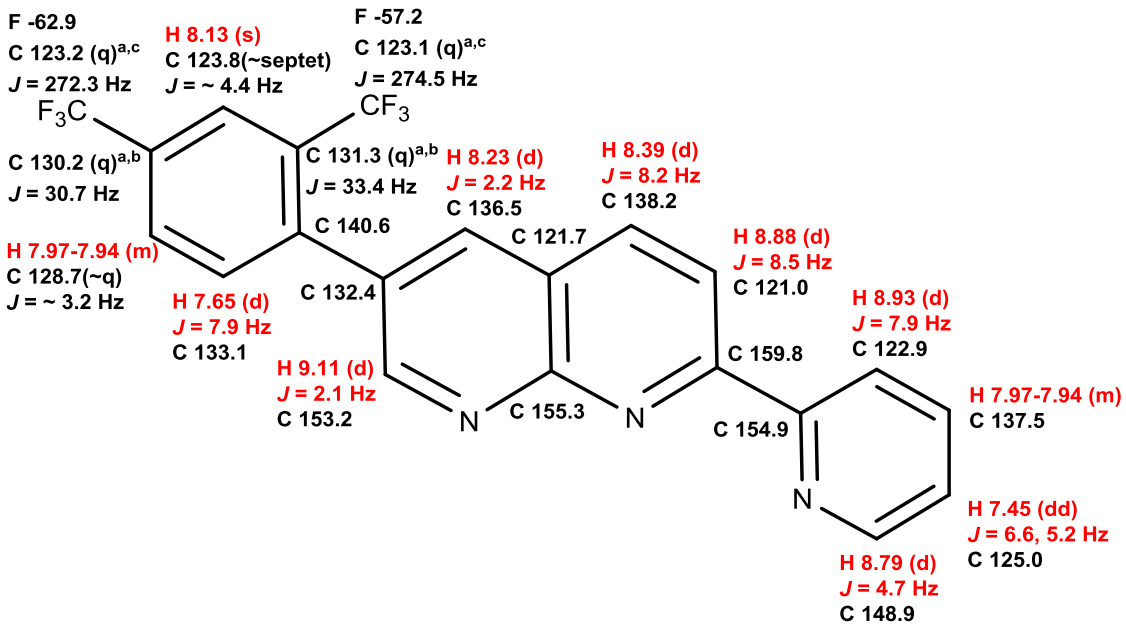

^{1}H -^{13}C gHMBCAD[a]		
^{1}H	bonds	^{13}C
8.13	3	140.6
8.23	3	138.2
8.23	3	140.5
8.23	3	153.2
8.23	3	155.3
8.39	2	121.7(w)
8.39	3	136.5
8.39	3	155.3
8.39	3	159.8
8.79	2	125.0
8.79	3	137.5
8.79	3	154.9
8.88	3	121.7
8.93	3	125.0
8.93	3	159.8
9.11	2	132.4
9.11	3	136.5
9.11	3	140.6(w)

^{1}H -^{13}C gHMBCAD[a] cont.		
^{1}H	bonds	^{13}C
7.45	3	122.9
7.45	2	148.9
7.65	4	123.8(w)
7.65	2	128.7(w)
7.65	3	130.2
7.65	3	131.3
7.65	3	132.4
7.65	2	140.6(w)
7.97-7.94	3	148.9
7.97-7.94	3	154.9
7.97-7.94	3	123.8
7.97-7.94	3	140.6
8.13	3	123.1
8.13	3	123.2
8.13	3	128.7
[a] J_{nxh} = 8.0 Hz J_{1xh} = 146.0 Hz		

^{1}H-^{13}C HSQCAD	
^{1}H	^{13}C
9.11	153.2
8.93	122.9
8.88	121.0
8.79	148.9
8.39	138.2
8.23	136.5
8.13	123.8
7.97-7.94	137.5
7.97-7.94	128.7
7.65	133.1
7.45	125.0

gCOSY
9.11↔8.23
8.93↔7.97-7.94
8.88↔8.39
8.79↔7.45
8.13↔7.97-7.94
7.97-7.94↔7.65
7.97-7.94↔7.45

Figure 3.83. NMR data for **3.70**.

[a] Only the two inner peaks of the quartet are observed
[b] These two carbons did not have enough data to assign with certainty and assignment could be reversed.
[c] These two carbons did not have enough data to assign with certainty and assignment could be reversed.

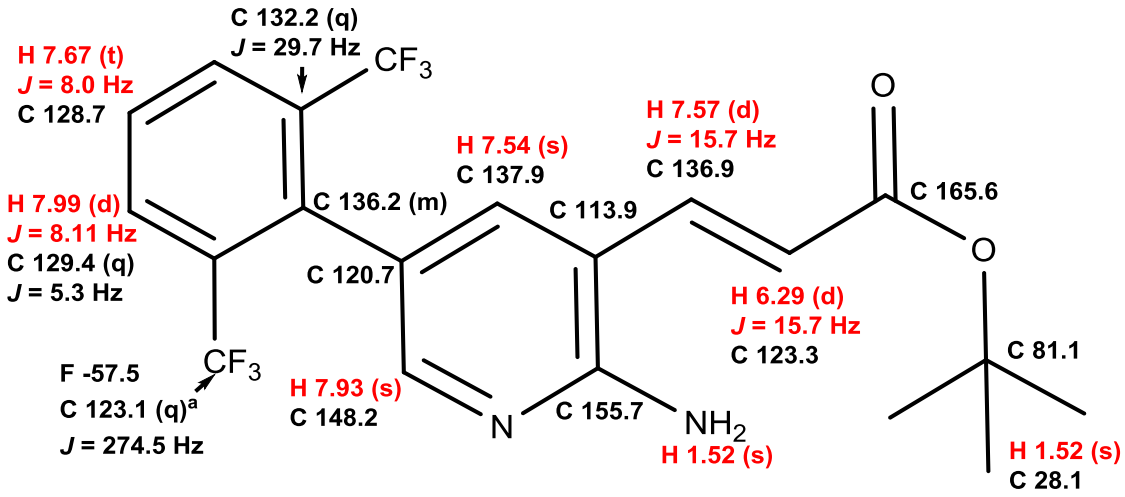

^{1}H - ^{13}C gHMBCAD[a]		
^{1}H	bonds	^{13}C
7.99	3	123.1
7.99	1,3	129.4
7.99	3	136.2
7.93	2	120.7
7.93	3	137.9
7.93	3	155.7
7.67	2	129.4
7.67	3	132.2
7.57	2	113.9
7.57	2	123.3
7.57	3	137.9
7.57	3	155.7
7.57	3	165.6
7.54	3	136.2
7.54	3	136.9
7.54	3	148.2
7.54	3	155.7
6.29	3	113.9
6.29	2	165.6
1.52	2	28.1
1.52	1,3	81.1
[a] J_{nxh} = 8.0 Hz J_{1xh} = 146.0 Hz		

gCOSY
7.99↔7.67
7.93↔7.54
7.57↔6.29

^{1}H-^{13}C HSQCAD	
^{1}H	^{13}C
7.99	129.4
7.93	148.2
7.67	128.7
7.57	136.9
7.54	137.9
6.29	123.3
1.52	28.1

Figure 3.84. NMR data for **3.71**.

[a] Only the two inner peaks of the quartet are observed.

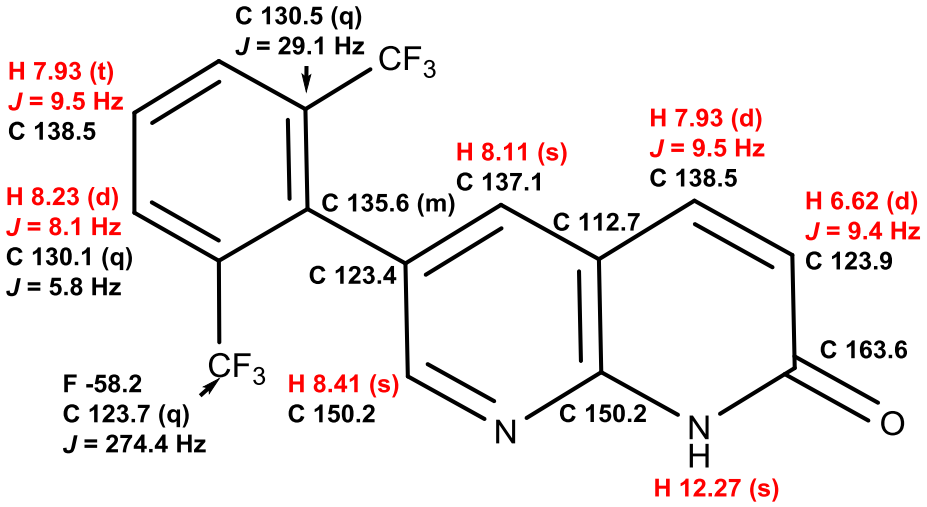

^{1}H -^{13}C gHMBCAD[a]		
^{1}H	bonds	^{13}C
8.41	2	123.4
8.41	3	137.1
8.41	3	150.2
8.23	3	123.7
8.23	1,3	130.1
8.23	3	135.6
8.11	3	135.6
8.11	3	138.5
8.11	3	150.2
7.93(pyr)	2	112.7
7.93(ben)	3	130.5
7.93(pyr)	3	137.1
7.93(pyr)	3	150.2
7.93(pyr)	3	163.6
6.62	3	112.7
6.62	2	163.6
[a] J_{nxh} = 8.0 Hz J_{1xh} = 146.0 Hz		

gCOSY
8.41↔8.11
8.23↔7.93
7.93↔6.62

^{1}H-^{13}C HSQCAD	
^{1}H	^{13}C
6.62	123.9
7.93	130.1
7.93	138.5
8.11	137.1
8.23	130.1
8.41	150.2

Figure 3.85. NMR data for **3.72**.

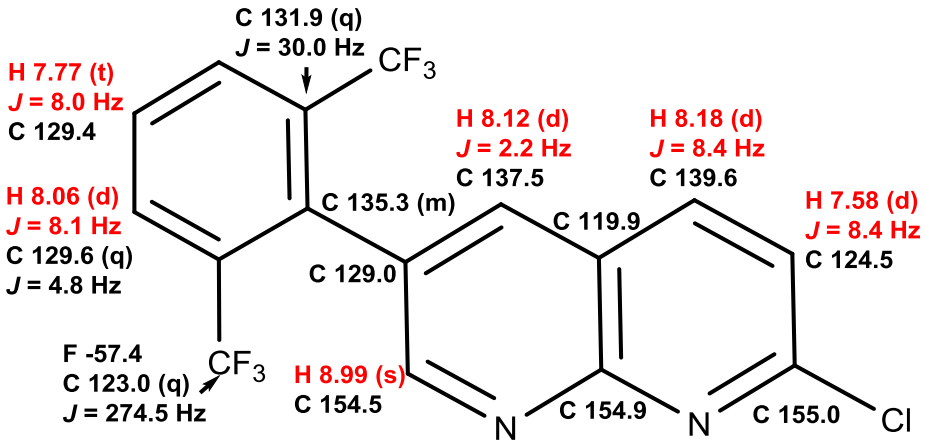

^{1}H-^{13}C HSQCAD	
^{1}H	^{13}C
8.99	154.5
8.18	139.6
8.12	137.5
8.06	129.6
7.77	129.4
7.58	124.5

gCOSY
8.99↔8.12
8.18↔7.58
8.06↔7.77

^{1}H -^{13}C gHMBCAD[a]		
^{1}H	bonds	^{13}C
8.99	2	129.0
8.99	3	137.5
8.99	3	154.9
8.18	2	119.9(w)
8.18	3	137.5
8.18	3	154.9
8.18	3	155.0
8.12	3	135.3
8.12	3	139.6
8.12	3	154.4
8.12	3	154.9
8.06	3	123.0
8.06	1,3	129.6
8.06	3	135.3
7.77	3	131.9
7.58	3	119.9
[a] J_{nxh} = 8.0 Hz J_{1xh} = 146.0 Hz		

Figure 3.86. NMR data for **3.73**.

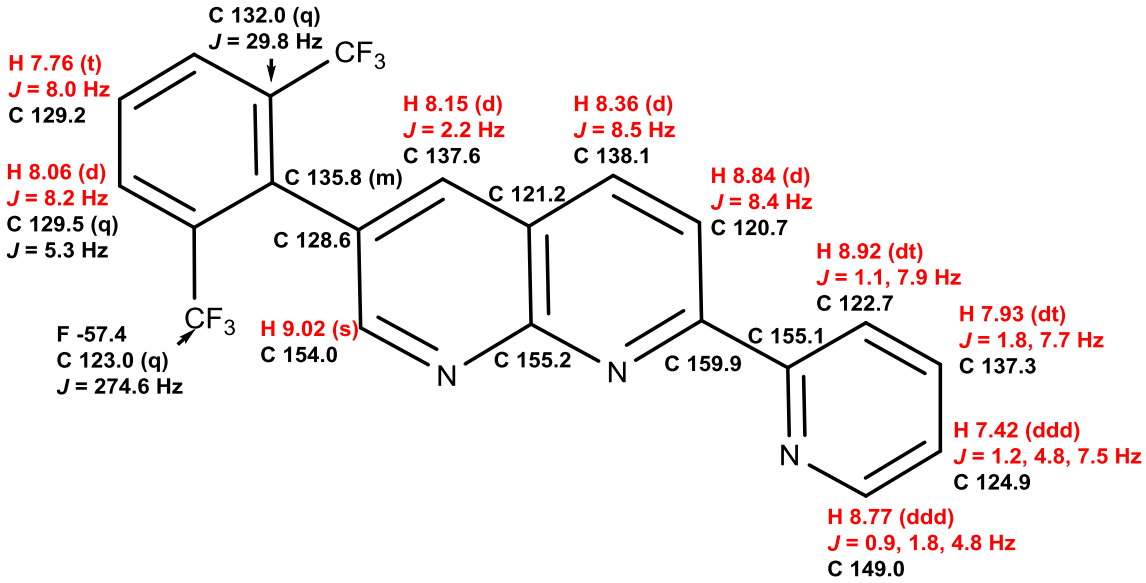

gCOSY
9.02↔8.15
8.92↔7.93
8.84↔8.36
8.77↔7.42
8.06↔7.76
7.93↔7.42

^{1}H-^{13}C HSQCAD	
^{1}H	^{13}C
9.02	154.0
8.92	122.7
8.84	120.7
8.77	149.0
8.36	138.1
8.15	137.6
8.06	129.5
7.93	137.3
7.76	129.2
7.42	124.9

^{1}H -^{13}C gHMBCAD[a]		
^{1}H	bonds	^{13}C
9.02	2	128.6
9.02	3	137.6
9.02	3	155.2(w)
8.92	3	124.9
8.92	3	159.9(w)
8.84	3	121.2
8.77	2	124.9
8.77	3	137.3
8.77	3	155.1
8.36	2	121.2
8.36	3	137.6
8.36	3	155.2
8.36	3	159.9

^{1}H -^{13}C gHMBCAD continued[a]		
^{1}H	bonds	^{13}C
8.15	3	135.8
8.15	3	138.1
8.15	3	154.0
8.15	3	155.2
8.06	3	123.0
8.06	1,3	129.5
8.06	3	135.8
7.93	3	149.0
7.93	3	155.1
7.76	2	129.5
7.76	3	132.0
7.42	3	122.7
7.42	2	149.0
[a] J_{nxh} = 8.0 Hz		
J_{1xh} = 146.0 Hz		

Figure 3.87. NMR data for **3.74**.

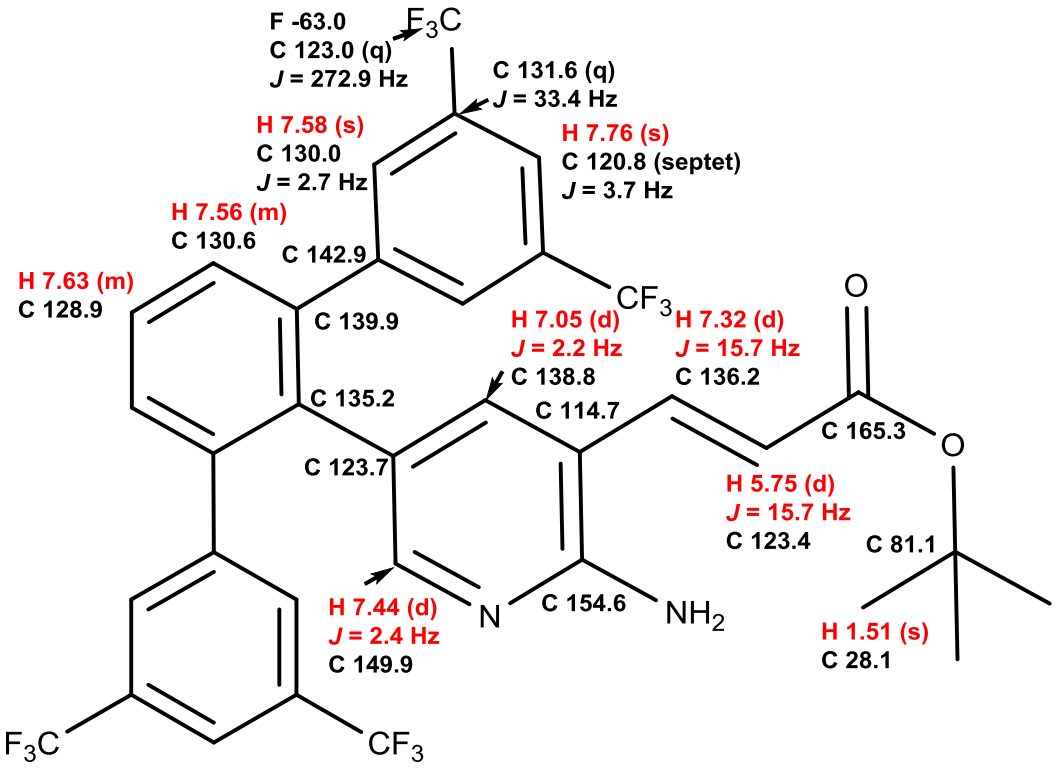

^{1}H-^{13}C HSQCAD	
^{1}H	^{13}C
7.76	120.8
7.63	128.9
7.58	130.0
7.56	130.6
7.44	nd[a]
7.32	136.2
7.05	138.8
5.75	123.4
1.51	28.1

gCOSY
7.76↔7.58
7.44↔7.05
7.32↔5.75

^{1}H -^{13}C gHMBCAD[i]		
^{1}H	bonds	^{13}C
7.76	3	123.0
7.76	3	130.0
7.63	3	139.9
7.58	3	120.8
7.58	3	123.0
7.58	1,3	130.0
7.58	2	131.6(w)
7.58	3	139.9
7.56	1,3	130.6
7.56	3	135.2
7.56	3	142.9
7.44	2	123.7
7.44	3	138.8
7.44	3	154.6

^{1}H -^{13}C gHMBCAD continued[a]		
^{1}H	bonds	^{13}C
7.32	2	114.7
7.32	2	123.4
7.32	3	138.8
7.32	3	154.6
7.32	3	165.3
7.05	3	135.2
7.05	3	136.2
7.05	3	149.9[a]
7.05	3	154.6
5.75	3	114.7
5.75	2	165.3
1.51	1,3	28.1
1.51	2	81.1
[i]J_{nxh} = 8.0 Hz		
J_{1xh} = 146.0 Hz		

Figure 3.88. NMR data for **3.75**.

[a] ^{1}H ^{13}C HSQCAD correlation not detected, the carbon peak is also broad in the ^{13}C NMR but was assigned by ^{1}H ^{13}C HMBCAD correlation with the proton at 7.05 ppm.

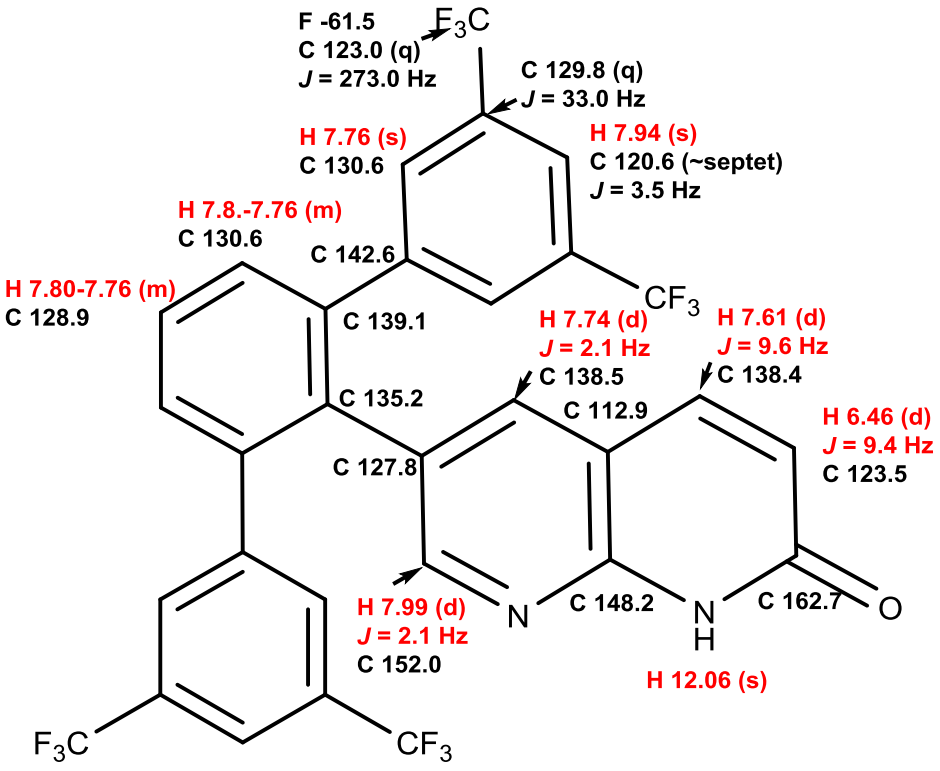

^{1}H-^{13}C HSQCAD	
^{1}H	^{13}C
7.99	152.0
7.94	120.6
7.80-7.76	130.6
7.80-7.76	129.1
7.76	130.6
7.74	138.5
7.61	138.4
6.46	123.5

gCOSY
7.99↔7.74
7.94↔7.76
7.61↔6.46

^{1}H -^{13}C gHMBCAD[i]		
^{1}H	bonds	^{13}C
7.99	2	127.8
7.99	3	135.2(w)
7.99	3	138.5
7.99	3	148.2
7.94	3	123.0(q)
7.94	3	130.6
7.80	1,3	130.6
7.80	3	135.2
7.80	3	139.1
7.80	3	142.6
7.76	3	120.6
7.76	3	123.0(q)
7.76	1,3	130.6
7.76	3	139.1
7.74	3	135.2

^{1}H -^{13}C gHMBCAD continued[a]		
^{1}H	bonds	^{13}C
7.74	3	138.4
7.74	3	148.2
7.74	3	152.0
7.61	2	112.8 (w)
7.61	3	138.5
7.61	3	148.2
7.61	3	162.7
6.46	3	112.9
6.46	2	162.6(w)
$^{1}J_{nxh}$ = 8.0 Hz J_{1xh} = 140.0 Hz		

Figure 3.89. NMR data for **3.76**.

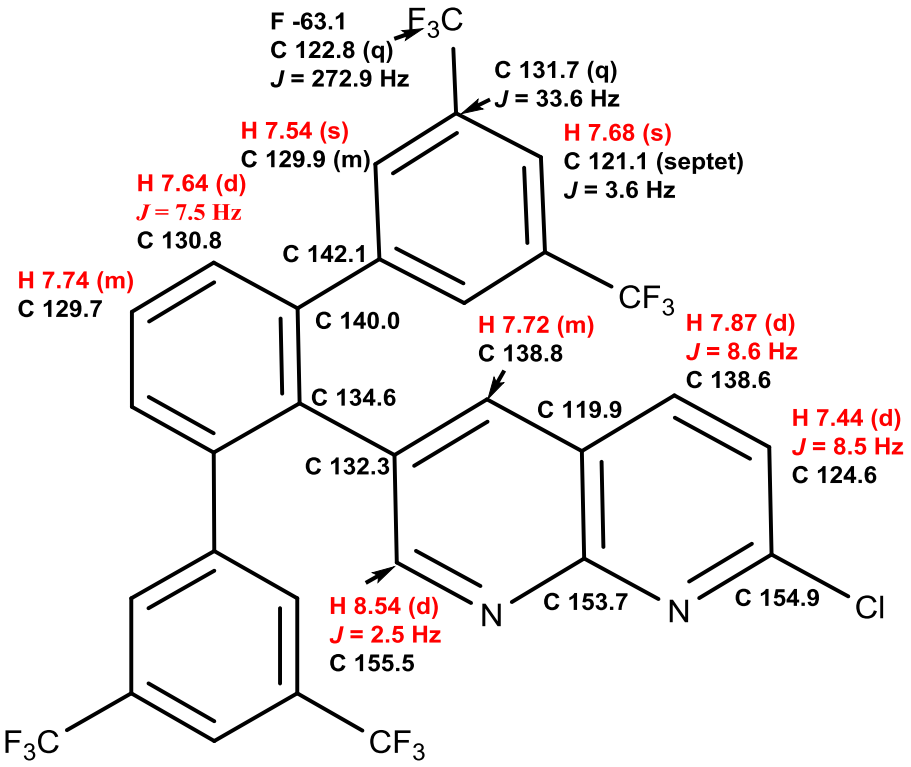

^{1}H-^{13}C HSQCAD	
^{1}H	^{13}C
8.54	155.5
7.87	138.6
7.74	129.7
7.72	138.4
7.68	121.1
7.64	130.8
7.54	129.9
7.44	124.6

gCOSY
8.54↔7.72
7.87↔7.44
7.74↔7.64
7.68↔7.54

^{1}H -^{13}C gHMBCAD[i]		
^{1}H	bonds	^{13}C
8.54	2	132.3
8.54	3	138.8
7.87		138
7.87	3	153.7
7.87	3	154.9
7.74	3	140.0
7.72	3	134.6(w)
7.72	3	138.6
7.72	3	153.7
7.72	3	155.5
7.68	3	122.8(q)
7.68	3	129.9
7.64	1,3	130.8
7.64	3	134.6
7.64	3	142.1
7.54	3	121.1
7.54	3	122.8(q)
7.54	1,3	129.9
7.54	3	140.0
7.45	3	119.9
$^{i}J_{nxh}$ = 8.0 Hz J_{1xh} = 140.0 Hz		

Figure 3.90. NMR data for **3.77**.

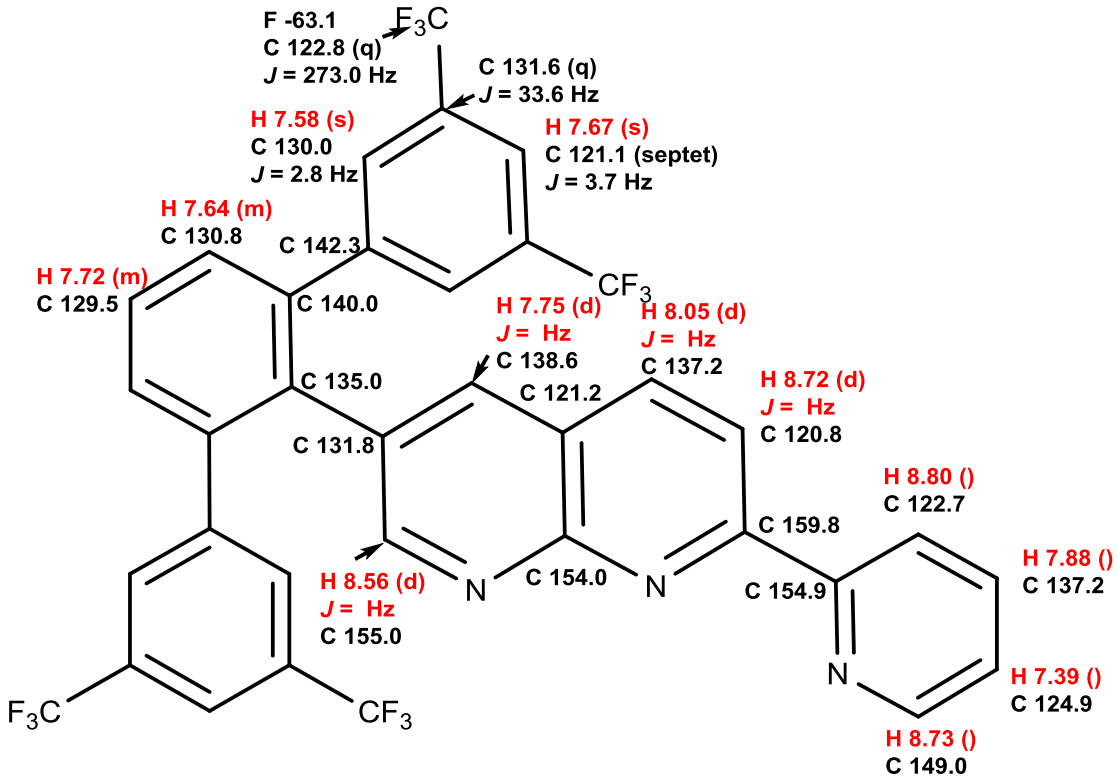

^{1}H-^{13}C gHSQC	
^{1}H	^{13}C
8.80	122.7
8.73	149.0
8.72	120.8
8.56	155.0
8.05	137.2
7.88	137.2
7.75	138.6
7.72	129.5
7.67	121.1
7.64	130.8
7.58	130.0
7.39	124.9

gCOSY
8.80↔7.88
8.73↔7.39
8.72↔8.05
8.56↔7.75
7.88↔7.39
7.72↔7.64
7.67↔7.58

^{1}H -^{13}C gHMBC[i]		
^{1}H	bonds	^{13}C
8.80	3	124.9
8.73	2	124.9
8.73	3	137.2
8.73	3	154.9
8.72	3	121.2
8.72	2	159.8
8.56	2	131.8
8.56	3	138.6
8.56	3	154.0
8.05	2	121.2(w)
8.05	3	138.6
8.05	3	154.0
8.05	3	159.8
7.88	3	149.0
7.88	3	154.9
7.75	3	135.0
7.75	3	137.2

^{1}H -^{13}C gHMBCAD continued[a]		
^{1}H	bonds	^{13}C
7.75	3	154.0
7.75	3	155.0
7.72	3	140.0
7.67	3	122.8
7.67	3	130.0
7.64	1,3	130.8
7.64	3	135.0
7.64	2	140.0(w)
7.64	3	142.3
7.58	3	121.1
7.58	3	122.8
7.58	1,3	130.0
7.58	3	140.0
7.39	3	122.7
7.39	2	149.0(w)
$^{1}J_{nxh}$ = 8.0 Hz J_{1xh} = 146.0 Hz		

Figure 3.91. NMR data for **3.78**.

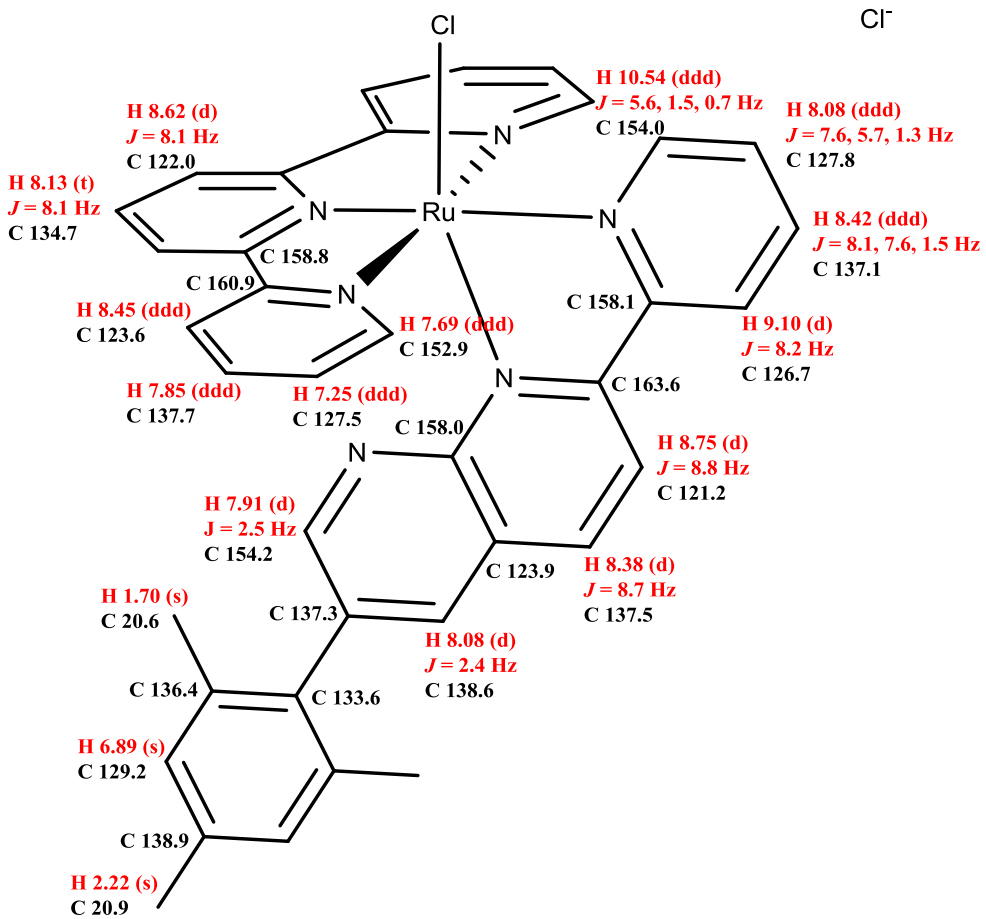

gCOSY
10.45↔8.08
9.10↔8.42
8.75↔8.38
8.62↔8.13
8.45↔7.85
8.42↔8.08
8.08↔7.91
7.85↔7.25
7.69↔7.25
6.89↔2.22
6.89↔1.70

^{1}H-^{13}C HSQCAD	
^{1}H	^{13}C
10.54	154.0
9.10	126.7
8.75	121.2
8.62	122.0
8.45	123.6
8.42	137.1
8.38	137.5
8.13	134.7
8.08	138.6
8.08	127.8

^{1}H-^{13}C HSQCAD Cont.	
^{1}H	^{13}C
7.91	154.2
7.85	137.7
7.69	152.9
7.25	127.5
6.89	129.2
2.22	20.9
1.70	20.6

Figure 3.92. NMR data for **3.79-d**.

^{1}H -^{13}C gHMBCAD[a]		
^{1}H	bonds	^{13}C
10.54	2	127.8
10.54	3	137.1
10.54	2	158.1
9.10	3	127.8
9.10	2	158.1
9.10	3	163.6
8.75	3	123.9
8.75	3	158.1
8.75	2	163.6
8.62	1,3	122.0
8.62	2	158.8
8.62	3	160.9
8.45	3	127.5
8.45	3	158.8
8.45	2	160.9
8.42	3	154.0
8.42	3	158.1
8.38	2	123.9(w)
8.38	3	138.6
8.38	3	158.0
8.38	3	163.6

^{1}H -^{13}C gHMBCAD[a] continued		
^{1}H	bonds	^{13}C
8.13	2	122.0(w)
8.13	3	158.8
8.08(pyr)	3	126.7
8.08(pyr)	2	154.0(w)
8.08(nap)	2	123.9(w)
8.08(nap)	3	133.6
8.08(nap)	2	137.3
8.08(nap)	3	154.2
8.08(nap)	3	158.0
7.91	2	137.3
7.91	3	138.6
7.91	2	158.0(w)
7.85	3	152.9
7.85	3	160.9
7.69	2	127.5
7.69	3	137.7
7.69	2	160.9
7.25	3	123.6
7.25	2	152.9
6.89	3	20.6
6.89	1,3	129.2
6.89	3	133.6
2.22	3	129.2
2.22	2	138.9
1.70	3	129.2
1.70	3	133.6
1.70	3	136.4
$^{1}J_{nxh}$ = 8.0 Hz J_{1xh} = 146.0 Hz		

^{1}H (599.345 MHz) sw = 9615.4 Hz np = 524288	
^{1}H	$^{x}J_{HH}$
8.45 (ddd)	8.1 Hz (3), 1.2 Hz (4), 0.7 Hz (5)
7.85 (ddd)	8.0 Hz (3), 7.6 Hz (3), 1.5 Hz (4)
7.69 (ddd)	5.6 Hz (3), 1.5 Hz (4), 0.7 Hz (5)
7.25 (ddd)	7.5 Hz (3), 5.6 Hz (3), 1.3 Hz (4)
Bonds between Hydrogen atoms being coupled in parentheses.	

Figure 3.92 cont. NMR data for **3.79-d**.

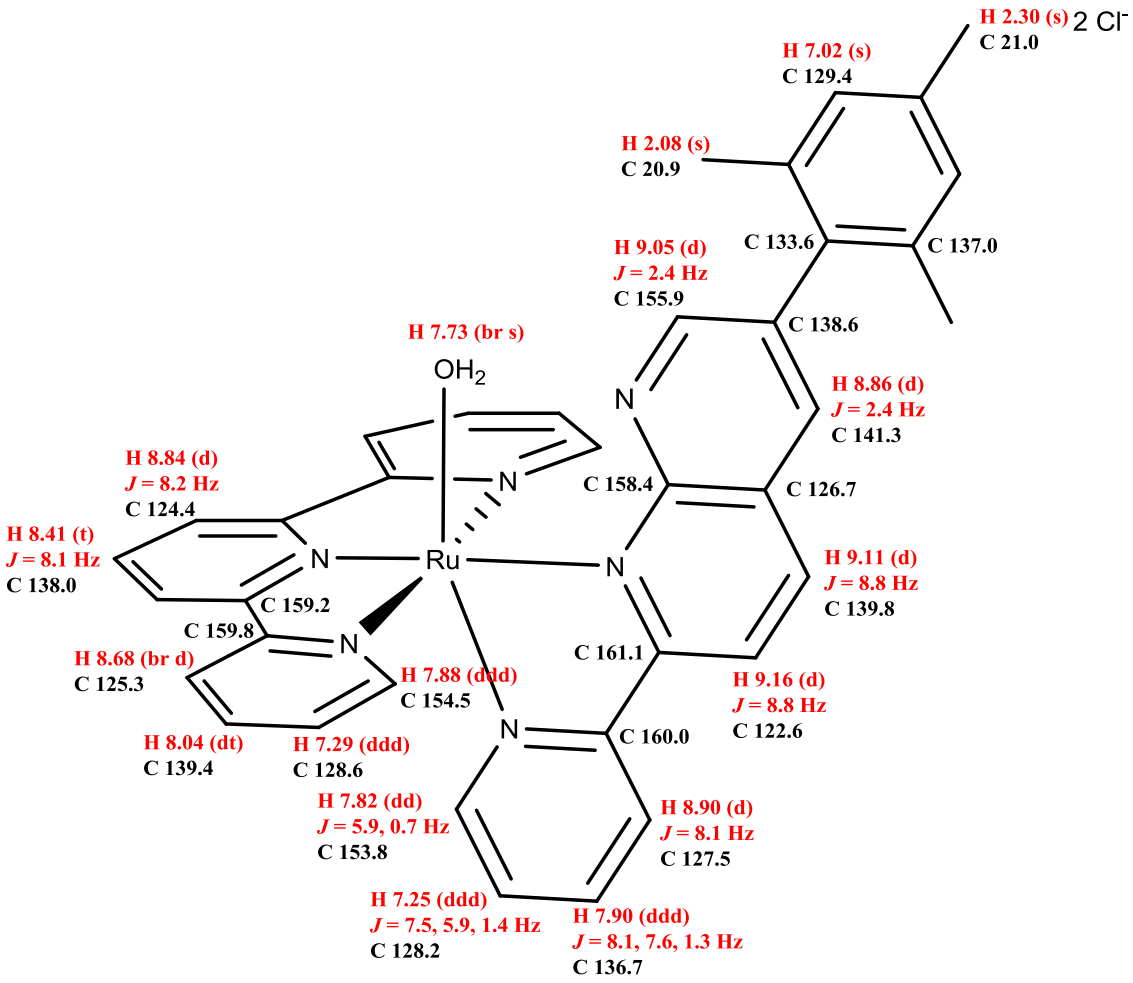

gCOSY
9.16↔9.11
9.05↔8.86
8.90↔7.90
8.84↔8.41
8.68↔8.04
8.04↔7.29
7.90↔7.25
7.88↔7.29
7.82↔7.25
7.02↔2.30
7.02↔2.08

^{1}H-^{13}C HSQCAD	
^{1}H	^{13}C
9.16	122.6
9.11	139.8
9.05	155.9
8.90	127.5
8.86	141.3
8.84	124.4
8.68	125.3
8.41	138.0
8.04	139.4
7.90	136.7

^{1}H-^{13}C HSQCAD cont.	
^{1}H	^{13}C
7.88	154.5
7.82	153.8
7.29	128.6
7.25	128.2
7.02	129.4
2.30	21.0
2.08	20.9

Figure 3.93. NMR data for **3.79-p**.

^{1}H -^{13}C gHMBCAD[a]		
^{1}H	bonds	^{13}C
9.16	3	126.7
9.11	3	141.3
9.11	3	158.4
9.11	3	161.1
9.05	2	138.6
9.05	3	141.3
9.05	2	158.4
8.90	3	128.2
8.90	2	160.0
8.90	3	161.1
8.86	3	133.6
8.86	3	139.8
8.86	3	155.9
8.86	3	158.4
8.84	1,3	124.4
8.84	2	159.2
8.84	3	159.8
8.68	3	128.6
8.68	3	159.2
8.68	2	159.8
8.41	3	159.2
8.04	3	154.5
8.04	3	159.8
7.90	3	153.8
7.90	3	160.0

^{1}H -^{13}C gHMBCAD[a] continued		
^{1}H	bonds	^{13}C
7.88	4	125.3(w)
7.88	2	128.6
7.88	3	139.4
7.88	2	159.8
7.82	2	128.2
7.82	3	136.7
7.82	2	160.0
7.29	3	125.3
7.29	3	154.5
7.25	3	127.5
7.25	2	153.8
7.02	1,3	129.4
7.02	3	133.6
7.02	3	21.0
2.30	3	129.4
2.30	2	139.2
2.08	3	129.4
2.08	3	133.6
2.08	2	137.0
$^{1}J_{nxh}$ = 8.0 Hz J_{1xh} = 146.0 Hz		

^{1}H (599.345 MHz) sw = 9615.4 Hz np = 524288	
^{1}H	$^{x}J_{HH}$
8.68 (br d)	7.8 Hz (3)
8.04 (td)	7.8 Hz (3), 1.5 Hz (4)
7.88 (ddd)	5.6 Hz (3), 1.5 Hz (4), 0.7 Hz (5)
7.29 (ddd)	7.5 Hz (3), 5.6 Hz (3), 1.3 Hz (4)
Bonds between Hydrogen atoms being coupled in parentheses.	

Figure 3.93 cont. NMR data for **3.79-p**.

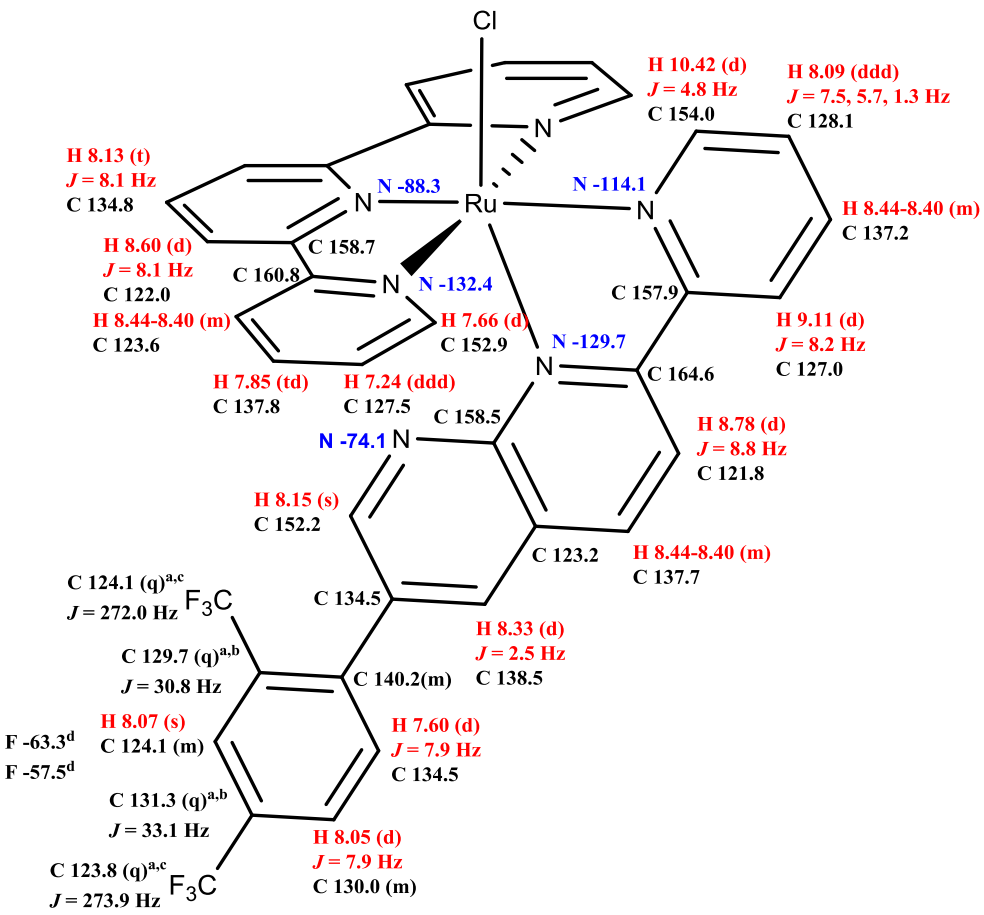

^{1}H-^{13}C **HSQCAD**	
^{1}H	^{13}C
10.24	154.0
9.11	127.0
8.78	121.8
8.60	122.0
8.44-8.40	123.6
8.44-8.40	137.2
8.44-8.40	137.7
8.33	138.5
8.15	152.2
8.13	134.8
8.09	128.1

^{1}H-^{13}C **HSQCAD continued**	
^{1}H	^{13}C
8.07	124.1
8.05	130.0
7.85	137.8
7.66	152.9
7.60	134.5
7.24	127.5

^{1}H -^{15}N **gHMBCAD**[d]		
^{1}H	bonds	^{15}N
10.42	2	-114.1
9.11	3	-114.1(w)
8.78	3	-129.7
8.60	3	-88.3
8.44-8.40	3	-132.4
8.09	3	-114.1(w)
8.15	2	-74.1
7.66	2	-132.4
7.24	3	-132.4
[d]J_{nxh} = 5.0 Hz J_{1xh} = 90.0 Hz		

Figure 3.94. NMR data for **3.80-d**.

^{1}H -^{13}C gHMBCAD[i]		
^{1}H	bonds	^{13}C
10.42	2	128.1
10.42	3	137.2
10.42	3	157.9
9.11	3	128.1
9.11	2	157.9
9.11	3	164.6(w)
8.78	3	123.2
8.78	3	157.9(w)
8.78	2	164.6
8.60	1,3	122.0
8.60	2	158.7
8.60	3	160.8
8.44-8.40(nap)	2	123.2(w)
8.44-8.40(tpy)	3	127.5
8.44-8.40(nap)	3	138.5
8.44-8.40(pyr)	3	154.0
8.44-8.40(pyr)	3	157.9
8.44-8.40(tpy)	3	158.7
8.44-8.40(tpy)	2	160.8
8.44-8.40(nap)	3	164.6

^{1}H -^{13}C gHMBCAD continued[i]		
^{1}H	bonds	^{13}C
8.33	3	137.7
8.33	3	140.2
8.33	3	152.2
8.33	3	158.5
8.15	2	134.5
8.15	3	138.5
8.13	3	158.7
8.09	3	127.0
8.09	2	154.0
8.07	3	123.8
8.07	3	124.1
8.07	3	130.0
8.07	3	140.2
8.05	3	124.1
8.05	3	140.2
7.85	3	152.9
7.85	3	160.8
7.66	4	123.6(w)
7.66	2	127.5
7.66	3	137.8
7.66	3	160.8
7.60	3	129.7
7.60	3	131.3
7.60	3	134.5
7.24	3	123.6
7.24	2	152.9
$^{i}J_{nxh}$ = 8.0 Hz J_{1xh} = 146.0 Hz		

gCOSY
10.42↔8.09
9.11↔8.44-8.40
8.78↔8.44-8.40
8.60↔8.13
8.44-8.40↔7.85
8.44-8.40↔8.09
8.33↔8.15
8.05↔7.60
7.85↔7.24
7.66↔7.24

^{1}H (599.345 MHz) sw = 9615.4 Hz np = 96154	
^{1}H	$^{x}J_{HH}$
7.85 (td)	7.8 Hz (3), 1.5 Hz (4)
7.66 (d)	5.0 Hz (3)
7.24 (ddd)	7.5 Hz (3), 5.6 Hz (3), 1.2 Hz (4)
Bonds between hydrogen atoms being coupled in parentheses.	

Figure 3.94 cont. NMR data for **3.80-d**.

[a] Only the two inner peaks of the quartet are observed.
[b] These two carbons did not have enough data to assign with certainty and assignment could be reversed.
[c] These two carbons did not have enough data to assign with certainty and assignment could be reversed.
[d] Fluorine NMR acquired at ^{19}F 376.095 MHz, peaks are not assigned.

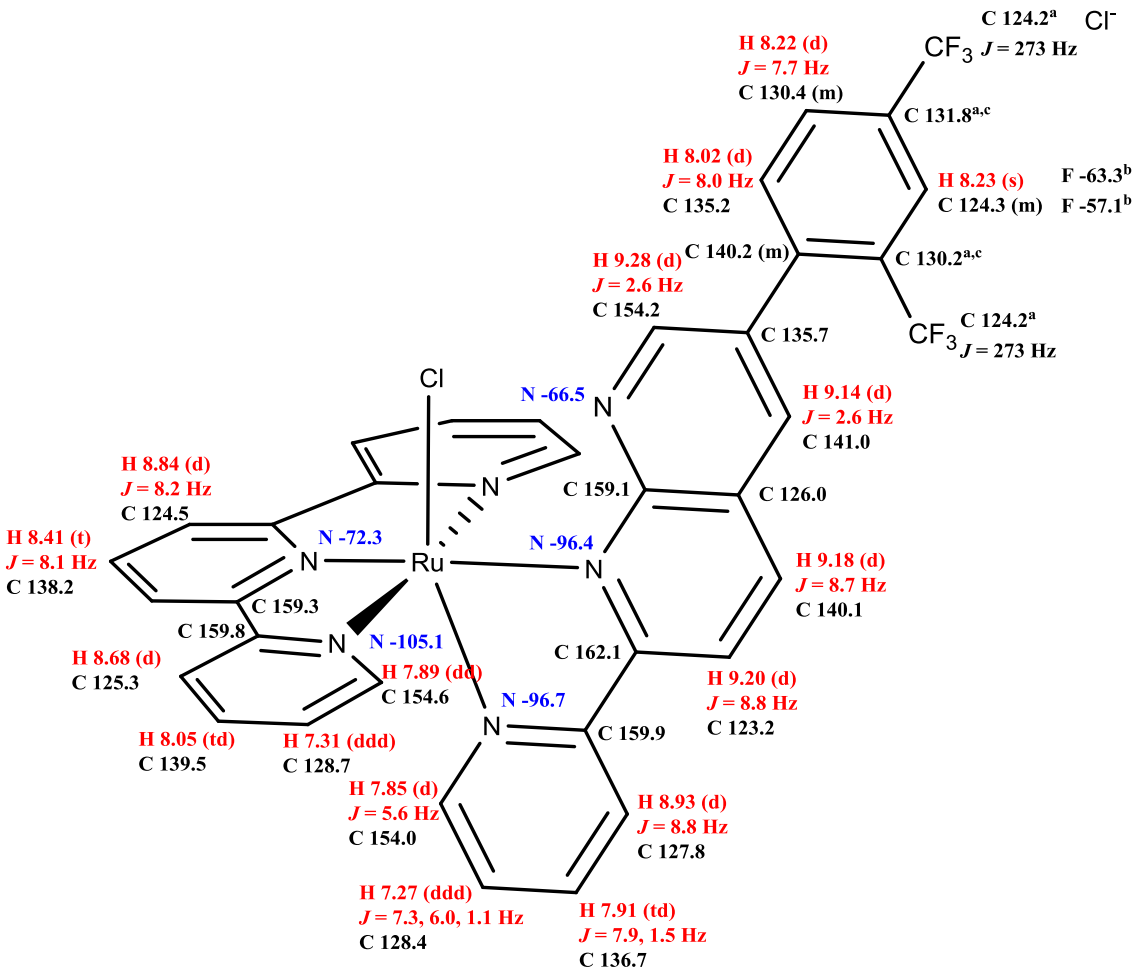

gCOSY
9.28↔9.14
9.20↔9.18
8.93↔7.91
8.84↔8.41
8.68↔8.05
8.22↔8.02
8.05↔7.31
7.89↔7.31
7.91↔7.27
7.85↔7.27

^{1}H-^{13}C HSQCAD	
^{1}H	^{13}C
9.28	154.2
9.20	123.2
9.18	140.1
9.14	141.0
8.93	127.8
8.84	124.5
8.68	125.3
8.41	138.2
8.23	124.3

^{1}H-^{13}C HSQCAD continued	
^{1}H	^{13}C
8.22	130.4
8.05	139.5
8.02	135.2
7.91	136.7
7.89	154.6
7.85	154.0
7.31	128.7
7.27	128.4

Figure 3.95. NMR data for **3.80-p**.

^{1}H -^{13}C gHMBCAD[i]		
^{1}H	bonds	^{13}C
9.28	3	135.7
9.28	3	141.0
9.28	3	159.1
9.20	3	126.0
9.20	2	162.1
9.18	2	126.0
9.18	3	141.0
9.18	3	159.1
9.18	3	162.1
9.14	3	140.2
9.14	3	154.2
9.14	3	159.1
8.93	3	128.4
8.93	2	159.9
8.93	3	162.1
8.84	1,3	124.5
8.84	2	159.3
8.84	3	159.8
8.68	3	128.7
8.68	3	159.3
8.68	2	159.8
8.41	3	159.3
8.23	3	124.2

^{1}H -^{13}C gHMBCAD[i] continued		
^{1}H	bonds	^{13}C
8.23	3	130.4
8.23	3	140.2
8.22	3	124.2
8.22	3	124.3
8.22	3	140.2
8.05	3	154.6
8.05	3	159.8
8.02	3	130.2
8.02	3	131.8
8.02	3	135.7
7.91	3	154.0
7.91	3	159.9
7.89	2	128.7
7.89	3	139.5
7.89	2	159.8
7.85	2	128.4
7.85	3	136.7
7.85	2	159.9
7.31	3	125.3
7.31	2	154.6
7.27	3	127.8
7.27	2	154.0
[i]J_{nxh} = 8.0 Hz J_{1xh} = 146.0 Hz		

^{1}H -^{15}N gHMBCAD[d]		
^{1}H	bonds	^{15}N
9.28	2	-66.5
9.20	3	-96.4(w)
8.93	3	-96.7
8.84	3	-72.3
8.68	3	-105.1
7.89	2	-105.1
7.85	2	-96.7
7.31	3	-105.1
7.27	3	-96.7
[d]J_{nxh} = 8.0 Hz J_{1xh} = 90.0 Hz		

^{1}H (499.94 MHz) sw = 7999.2 Hz np = 79992	
^{1}H	$^{x}J_{HH}$
8.68 (d)	8.0 Hz (3)
8.05 (td)	7.8 Hz (3), 1.4 Hz (4)
7.89 (dd)	5.4 Hz (3), 1.4 Hz (4)
7.31 (ddd)	7.0 Hz (3), 5.8 Hz (3), 1.1 Hz (4)
Bonds between hydrogen atoms being coupled in parentheses.	

Figure 3.95 cont. NMR data for **3.80-p**.

[a] peaks not observed in ^{13}C spectra but in HMBC.
[b] Fluorine spectrum acquired at ^{19}F 376.095 MHz, peaks are not assigned
[c] These two carbons did not have enough data to assign with certainty and assignment could be reversed.

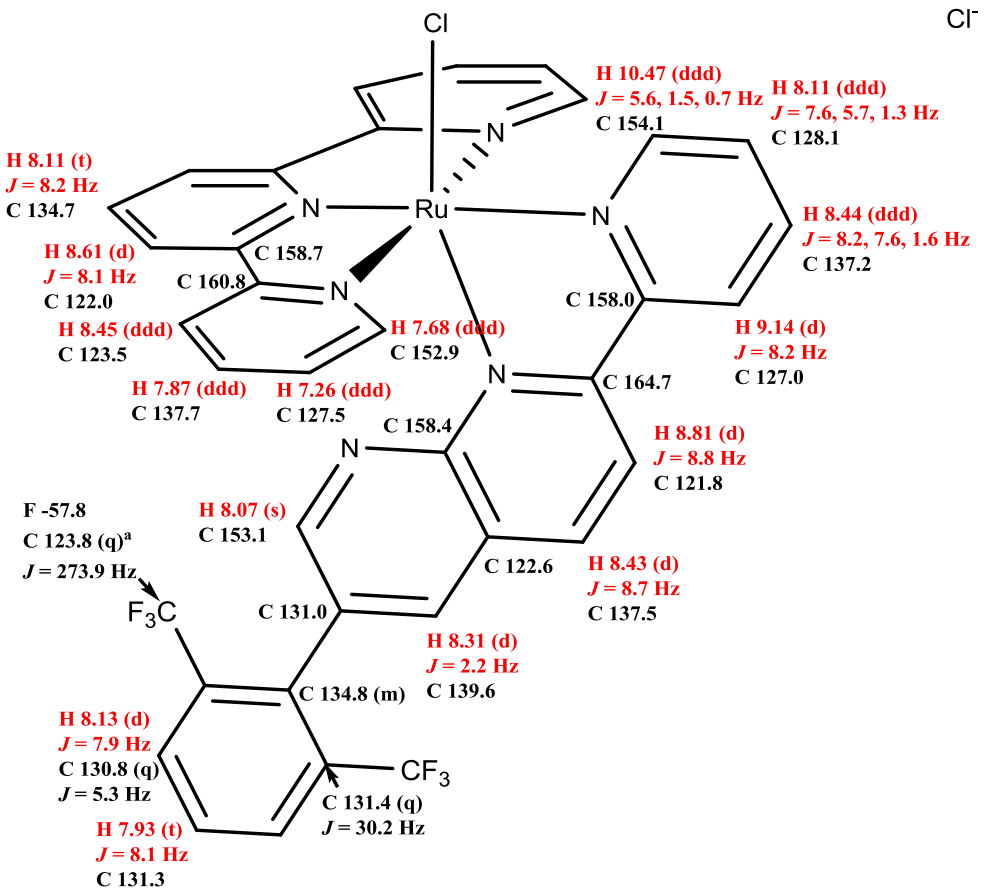

gCOSY
10.42↔8.09
9.11↔8.44-8.40
8.78↔8.44-8.40
8.60↔8.13
8.44-8.40↔7.85
8.44-8.40↔8.09
8.33↔8.15
8.05↔7.60
7.85↔7.24
7.66↔7.24

^{1}H-^{13}C HSQCAD	
^{1}H	^{13}C
10.47	154.1
9.14	127.0
8.81	121.8
8.61	122.0
8.45	123.5
8.44	137.2
8.43	137.5
8.31	139.6

^{1}H-^{13}C HSQCAD continued	
^{1}H	^{13}C
8.13	130.8
8.11	134.7
8.11	128.1
8.07	153.1
7.93	131.3
7.87	137.7
7.68	152.9
7.26	127.5

Figure 3.96. NMR data for **3.81-d**.

^{1}H -^{13}C gHMBCAD[a]		
^{1}H	bonds	^{13}C
10.47	2	128.1
10.47	3	137.2
10.47	3	158.0
9.14	3	128.1
9.14	2	158.0
9.14	3	164.7(w)
8.81	3	122.6
8.81	3	158.0(w)
8.81	2	164.7
8.61	1,3	122.0
8.61	2	158.7
8.61	3	160.8
8.45	3	127.5
8.45	3	158.7
8.45	2	160.8
8.44	3	154.1
8.44	3	158.0
8.43	3	139.6
8.43	3	158.4
8.43	3	164.7
8.31	3	134.8
8.31	3	137.5
8.31	3	153.1
8.31	3	158.4

^{1}H -^{13}C gHMBCAD[a] **continued**		
^{1}H	bonds	^{13}C
8.13	3	123.8
8.13	1,3	130.8
8.13	3	134.8
8.11	3	127.0
8.11	2	154.1
8.07	2	131.0
8.07	3	139.6
7.93	3	131.4
7.87	3	152.9
7.87	3	160.8
7.68	2	127.5
7.68	3	137.7
7.68	3	160.8
7.26	3	123.5
7.26	2	152.9
$^{1}J_{nxh}$ = 8.0 Hz J_{1xh} = 146.0 Hz		

^{1}H (599.345 MHz) sw = 9615.4 Hz np = 524288	
^{1}H	$^{x}J_{HH}$
8.45 (ddd)	8.1 Hz (3), 1.3 Hz (4), 0.9 Hz (5)
7.87 (ddd)	8.0 Hz (3), 7.5 Hz (3), 1.5 Hz (4)
7.68 (ddd)	5.6 Hz (3), 1.5 Hz (4), 0.7 Hz (5)
7.26 (ddd)	7.5 Hz (3), 5.6 Hz (3), 1.3 Hz (4)
Bonds between hydrogen atoms being coupled in parentheses.	

Figure 3.96 cont. NMR data for **3.81-d**.

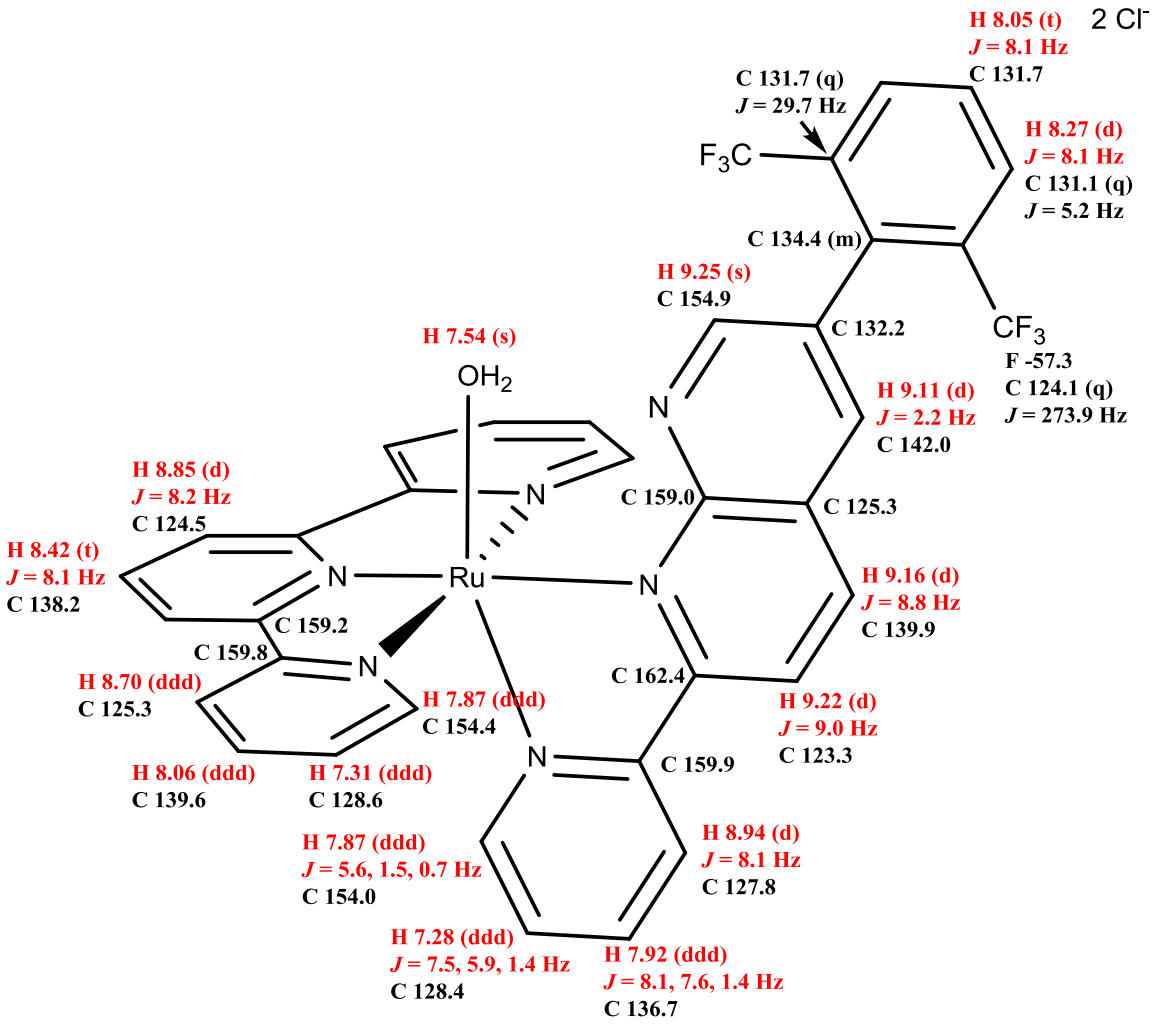

gCOSY
9.22↔9.16
9.25↔9.11
8.94↔7.92
8.85↔8.42
8.70↔8.06
8.27↔8.05
8.06↔7.31
7.92↔7.28
7.87↔7.31
7.87↔7.28

^{1}H-^{13}C HSQCAD	
^{1}H	^{13}C
9.25	154.9
9.22	123.3
9.16	139.9
9.11	142.0
8.94	127.8
8.85	124.5
8.70	125.3
8.42	138.2

^{1}H-^{13}C HSQCAD continued	
^{1}H	^{13}C
8.27	131.1
8.06	139.6
8.05	131.7
7.92	136.7
7.87	154.4
7.87	154.0
7.31	128.6
7.28	128.4

Figure 3.97. NMR data for **3.81-p**.

^{1}H -^{13}C gHMBCAD[a]		
^{1}H	bonds	^{13}C
9.25	2	132.2
9.25	3	142.0
9.25	3	159.0
9.22	3	125.3
9.22	2	162.4
9.16	2	125.3(w)
9.16	3	142.0
9.16	3	159.0
9.16	3	162.4
9.11	3	134.4
9.11	3	139.9
9.11	3	154.9
9.11	3	159.0
8.94	3	128.4
8.94	2	159.8
8.94	3	162.4(w)
8.85	1,3	124.5
8.85	2	159.2
8.85	3	159.8(w)
8.70	3	128.6
8.70	3	159.2
8.70	2	159.9
8.42	3	159.2
8.27	3	124.1
8.27	1,3	131.1
8.27	3	134.4

^{1}H -^{13}C gHMBCAD[a] continued		
^{1}H	bonds	^{13}C
8.06	3	154.4
8.06	3	159.9
8.05	3	131.7
7.92	3	154.0
7.92	3	159.8
7.87	2	128.4(pyr)
7.87	2	128.6(tpy)
7.87	3	136.7(pyr/pyr)
7.87	3	139.6(tpy)
7.87	3	159.8(tpy/pyr)
7.31	3	125.3
7.31	2	154.4
7.28	3	127.8
7.28	2	154.0
$^{i}J_{nxh}$ = 8.0 Hz J_{1xh} = 146.0 Hz		

^{1}H (599.345 MHz) sw = 9615.4 Hz np = 524288	
^{1}H	$^{X}J_{HH}$
8.70 (ddd)	8.1 Hz (3), 1.3 Hz (4), 0.8 Hz (5)
8.06 (ddd)	8.1 Hz (3), 7.6 Hz (3), 1.5 Hz (4)
7.87 (ddd)	5.6 Hz (3), 1.5 Hz (4), 0.7 Hz (5)
7.31 (ddd)	7.5 Hz (3), 5.6 Hz (3), 1.3 Hz (4)
Bonds between hydrogen atoms being coupled in parentheses.	

Figure 3.97 cont. NMR data for **3.81-p**.

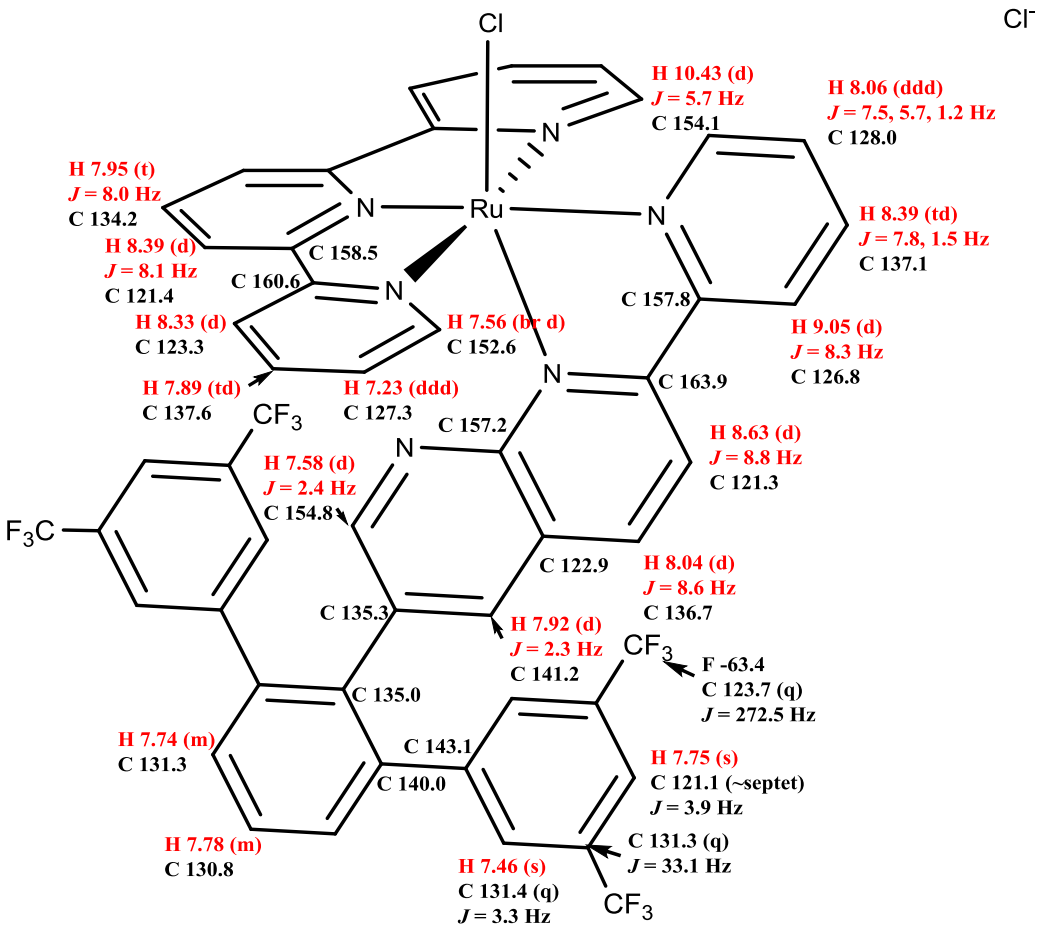

gCOSY
10.43↔8.06
9.05↔8.39
8.63↔8.04
8.39↔8.06
8.39↔7.95
8.33↔7.89
7.92↔7.58
7.89↔7.23
7.75↔7.46
7.56↔7.23

^{1}H-^{13}C HSQCAD	
^{1}H	^{13}C
10.43	154.1
9.05	126.8
8.63	121.3
8.39	121.4
8.39	137.1
8.33	123.3
8.06	128.0
8.04	136.7
7.95	134.2

^{1}H-^{13}C HSQCAD continued	
^{1}H	^{13}C
7.92	141.2
7.89	137.6
7.78	130.8
7.75	121.1
7.74	131.3
7.58	154.8
7.56	152.6
7.46	131.4
7.23	127.3

Figure 3.98. NMR data for **3.82-d**.

^{1}H -^{13}C gHMBCAD[a]		
^{1}H	bonds	^{13}C
10.43	2	128.0
10.43	3	137.1
10.43	3	157.8
9.05	3	128.0
9.05	2	157.8
8.63	3	122.9
8.63	2	163.9
8.39(t)	1,3	121.4
8.39(b)	3	154.1
8.39(b)	3	157.8
8.39(t)	2	158.5
8.39(t)	3	160.6
8.33	3	127.3
8.33	3	158.5
8.33	2	160.6
8.06	3	126.8
8.06	2	154.1
8.04	3	141.2
8.04	3	157.2
8.04	3	163.9
7.95	3	158.5
7.92	3	135.0
7.92	3	136.7
7.92	3	154.8
7.92	3	157.2

^{1}H -^{13}C gHMBCAD[a] cont.		
^{1}H	bonds	^{13}C
7.89	3	152.6
7.89	3	160.6
7.78	3	140.0
7.75	3	123.7
7.75	3	131.4
7.74	3	131.3
7.74	3	135.0
7.74	3	143.1
7.58	2	135.3
7.58	3	141.2(w)
7.58	3	157.2
7.56	2	127.3
7.56	3	137.6
7.56	3	160.6
7.46	3	121.1
7.46	3	123.7
7.46	1,3	131.4
7.46	3	140.0
7.23	3	123.3
7.23	2	152.6
$^{i}J_{nxh}$ = 8.0 Hz J_{1xh} = 140.0 Hz		

^{1}H (499.946 MHz) sw = 5316.3 Hz np = 53164	
^{1}H	$^{x}J_{HH}$
8.33 (d)	8.0 Hz (3)
7.89 (td)	7.8 Hz (3), 1.4 Hz (4)
7.56 (br d)	5.5 Hz (3)
7.23 (ddd)	7.6 Hz (3), 5.6 Hz (3), 1.2 Hz (4)
Bonds between hydrogen atoms being coupled in parentheses.	

Figure 3.98 cont. NMR data for **3.82-d**.

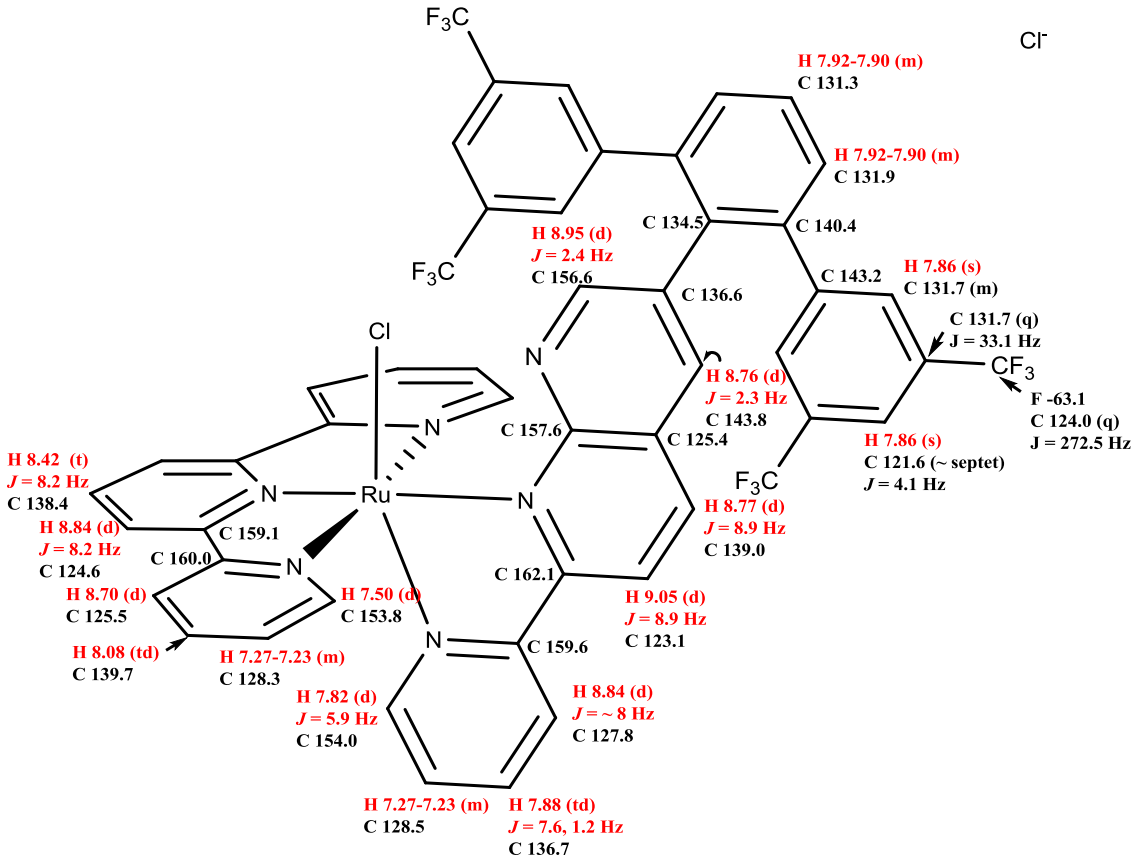

gCOSY
9.05↔8.77
8.84↔8.42
8.84↔7.88
8.70↔8.08
8.08↔7.27-7.23
7.88↔7.27-7.23
7.82↔7.27-7.23
7.50↔7.27-7.23

^{1}H-^{13}C HSQCAD	
^{1}H	^{13}C
9.05	123.1
8.95	156.6
8.84	127.8
8.84	124.6
8.77	139.0
8.76	143.8
8.70	125.5
8.42	138.4
8.08	139.7

^{1}H-^{13}C HSQCAD continued	
^{1}H	^{13}C
7.92-7.90	131.9
7.92-7.90	131.3
7.88	136.7
7.86	131.7
7.86	121.6
7.82	154.0
7.50	153.8
7.27-7.23	128.5
7.27-7.23	128.3

Figure 3.99. NMR data for **3.82-p**.

^{1}H -^{13}C gHMBCAD[a]		
^{1}H	bonds	^{13}C
9.05	3	125.4
9.05	2	162.1
8.95	2	136.6
8.95	3	143.8
8.95	3	157.6
8.84(terp)[d]	1,3	124.6
8.84(pyr)[d]	3	128.5
8.84(terp)[d]	2	159.1
8.84(pyr)[d]	2	159.6
8.84(pyr)[d]	3	162.1
8.77	3	143.8
8.77	3	157.6
8.77	3	162.1
8.76	3	134.5
8.76	3	139.0
8.76	3	156.6
8.76	3	157.6
8.70	3	128.3
8.70	3	159.1
8.70	2	160.0
8.42	3	159.1
8.08	3	153.8
8.08	3	160.0
7.92-7.90[b]	3 or 4	134.5
7.92-7.90[b]	2 or 3	140.4
7.92-7.90[b]	3 or 4	143.2
7.88	3	154.0
7.88	3	159.6

^{1}H -^{13}C gHMBCAD[a] cont.		
^{1}H	bonds	^{13}C
7.86[c]	3 or 1	121.6
7.86[c]	3 or 3	124.0
7.86[c]	2 or 2	131.7
7.86[c]	3 or 5	140.4
7.82	2	128.5
7.82	3	136.7
7.82	3	159.6
7.50	2	128.3
7.50	3	139.7
7.50	3	160.0
7.27-7.23(trpy)[d]	3	125.5
7.27-7.23(pyr)[d]	3	127.8
7.27-7.23(trpy)[d]	2	153.8
7.27-7.23(pyr)[d]	2	154.0
$^{i}J_{nxh}$ = 8.0 Hz J_{1xh} = 140.0 Hz		

^{1}H (499.946 MHz) sw = 7999.2 Hz np = 79992	
^{1}H	$^{x}J_{HH}$
8.70 (d)	8.1 Hz (3)
8.08 (td)	7.9 Hz (3), 1.4 Hz (4)
7.50 (d)	5.1 Hz (3)
7.27-7.23 (m)	-
Bonds between Hydrogen atoms being coupled in parentheses.	

Figure 3.99 cont. NMR data for **3.82-p**.

[b] Two peaks are overlapping making it impossible to tell if one of both of the protons are actually showing a correlation with the carbon, number of bonds between the possible correlations are shown.
[c] Two peaks are overlapping making it impossible to tell if one of both of the protons are actually showing a correlation with the carbon, number of bonds between the possible correlations are shown
[d] Even though the protons are overlapping the correlation was assigned with certainty because the protons are on separate ligands of the complex.

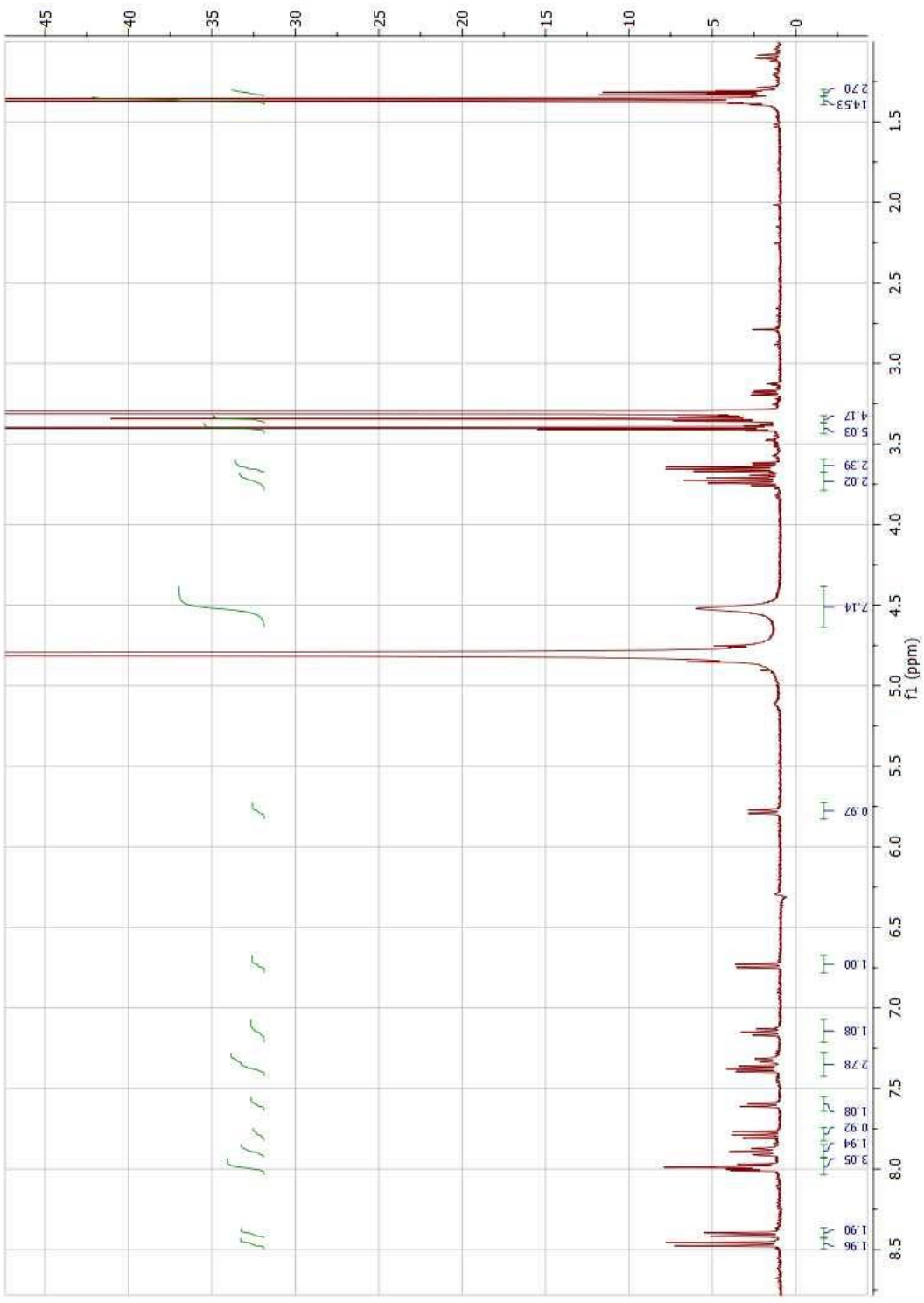

Figure 3.S1. ^{1}H NMR spectrum of an aliquot of **3.27** in CD_3OD before crystallization.

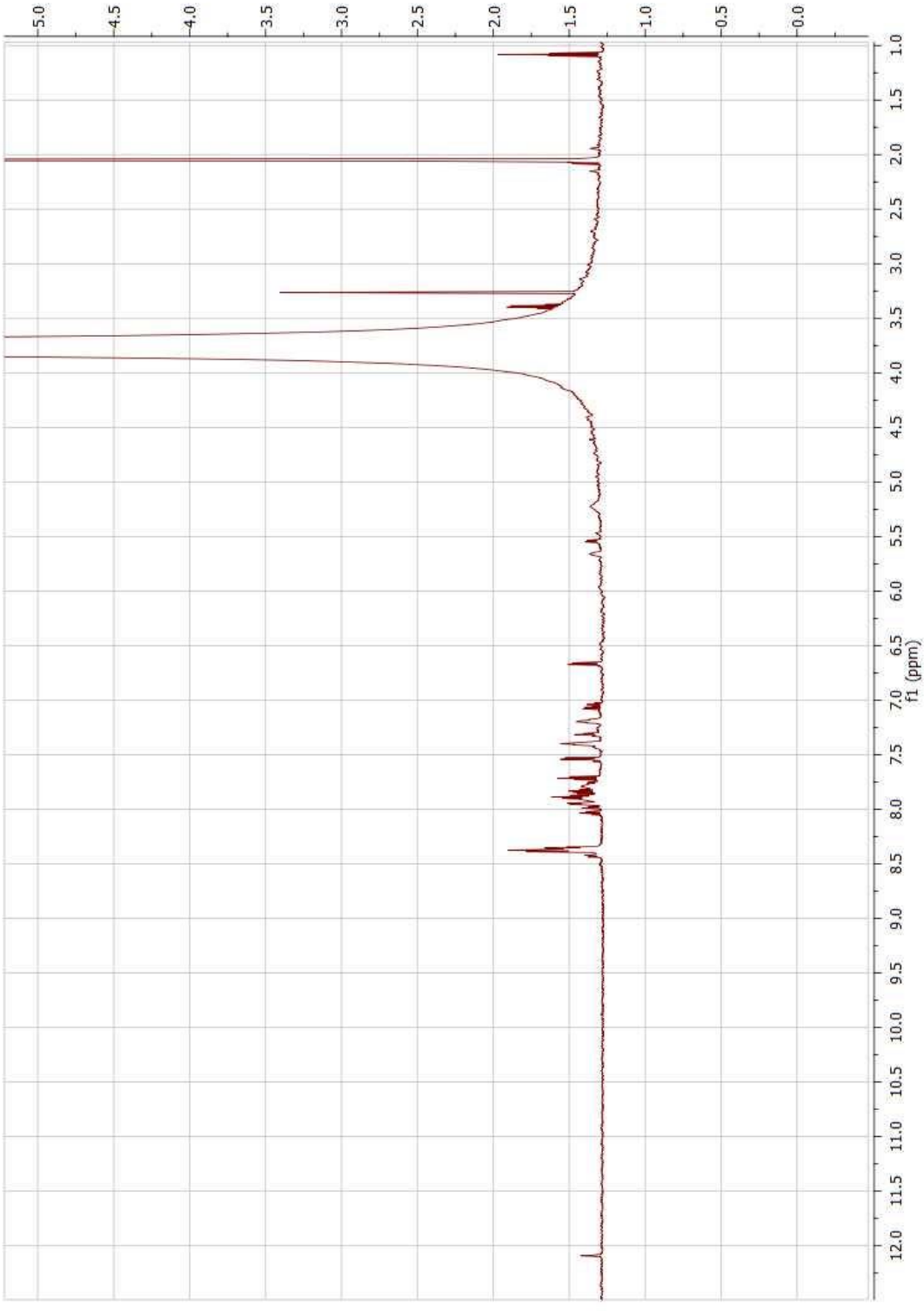

Figure 3.S2. ^{1}H NMR spectrum of **3.27** after crystallization in d_6-acetone : H_2O (85:15), showing the lack of isopropyl groups.

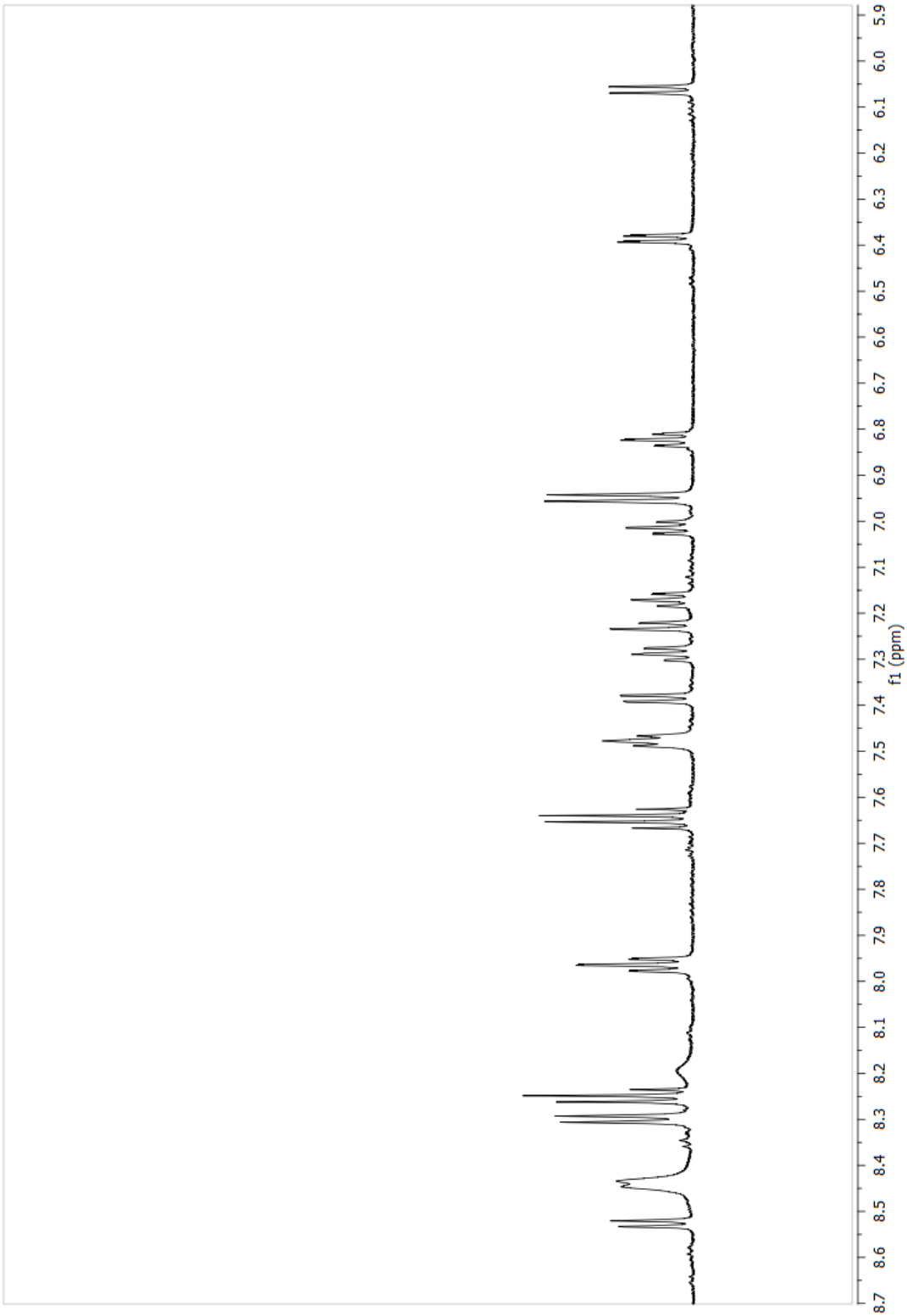

Figure 3.S3. ^{1}H NMR spectrum of **3.30** in a mixture of d_6-acetone and water (85:15), showing that some peaks are broad.

L. CAN Testing Conditions

The oxygen evolution was recorded with a pressure transducer (Omega PX138- 015D5V) driven at 12.00 V using a power supply (SSA-0601S-1) plus a data acquisition module (Omega OMB-DAQ-56; running at 0.1 Hz). The pressure transducer was connected with Watts SVEB20 1/4-Inch Diameter by 0.170-Inch Clear Vinyl Tubing to a reaction vessel with a 14/20 neck and a 0.2 inch diameter 0.7 inch long barb (volume = 48 mL, see picture). To the reaction flask was added a freshly made solution of $Ce(NH_4)_2(NO_3)_6$ (concentration of stock solution varied but final molar amounts and reaction volumes were either 2 mmol in 4 mL reaction, meaning $[CAN]_0$ = 500 mM (for pyridylnapthyridine/terpy complexes) or 0.546 mmol in 7 mL reaction, meaning $[CAN]_0$ = 78 mM (for all other terpy complexes in this Chapter)), ultrapure water (varied depending on the volume of CAN stock solution added and catalyst solution), and HNO_3 (25 μL of 15.8 M was added to give 100 mM in 4 mL (for pyridylnapthyridine/terpy complexes) or 44 μL in 7 mL (for all other terpy complexes in this Chapter)). Tubing was attached to the long barb, and copper wire was wrapped around and tightened, and a rubber septum was placed in the 14/20 neck and tightened on the glass using copper wire or a hose clamp (Figure 3.S4). The vessel was pressurized and placed in a 30 ^{o}C constant temperature water bath for 30 min to make sure pressure stayed constant, indicating the system was leak-free; the pressure was vented and a solution of catalyst (depending on the run) was immediately injected to the above solution, then the vessel was submerged again in the water bath for the duration of the testing (Figure 3.S5). During the testing the water bath and reactions were kept in the dark. For pyridylnapthyridine/terpy complexes, initial concentrations of catalyst = 50.0 μM, CAN = 500 mM, and HNO_3 = 0.1 M, with a total volume of 4 mL. For all other testing in this Chapter the initial concentrations of catalyst = 50.0 μM, CAN = 78 mM, and HNO_3 = 0.1 M, with a total volume of 7 mL.

Example of pyridylnapthyridine/terpy complex testing conditions:

Preparation of **3.77-d** stock solution:

To a vial was added **3.77-d** (10.1 mg, 12.6 μmol) then dissolved in ultrapure water (10.0 mL), giving a solution of 1.26 mM.

Example procedure for preparation of CAN solution:

CAN (4.1339 g, 7.5406 mmol) was added to a volumetric flask (10 mL), then filling the flask with ultrapure water to give a total volume of 10 mL.(754 mM).

Example procedure for reaction solution:

CAN solution (754 mM, 2.653 mL) was added to the pressure vessel followed by ultrapure water (1.163 mL), HNO_3 (25 μL), and a stir bar. After checking for leaks, a solution of **3.77-d** (1.26 mM, 159 μL) was injected.

Example of testing conditions for all other terpy complexes in this Chapter:

Preparation of **3.18b** stock solution:

To a vial was added **3.18b** (11.3 mg, 12.5 μmol) then dissolved in ultrapure water (10.0 mL), giving a solution of 1.25 mM.

Example procedure for preparation of CAN solution:

CAN (1.1221 g, 2.047 mmol) was added to a volumetric flask (10 mL), then filling the flask with ultrapure water to give a total volume of 10 mL.(204.7 mM).

Example procedure for reaction solution:

CAN solution (204.7 mM, 2.667 mL) was added to the pressure vessel followed by ultrapure water (4.009 mL), HNO_3 (44 μL), and a stir bar. After checking for leaks, a solution of **4.46** (1.25 mM, 280 μL) was injected.

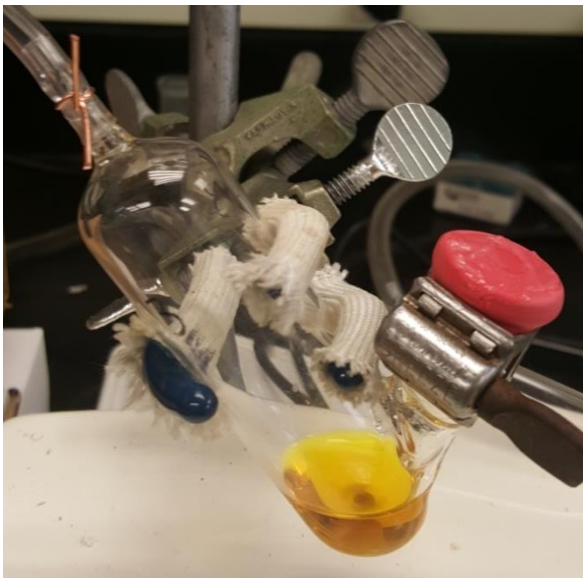

Figure 3.S4. Pressure testing vessel (total volume ~48 mL).

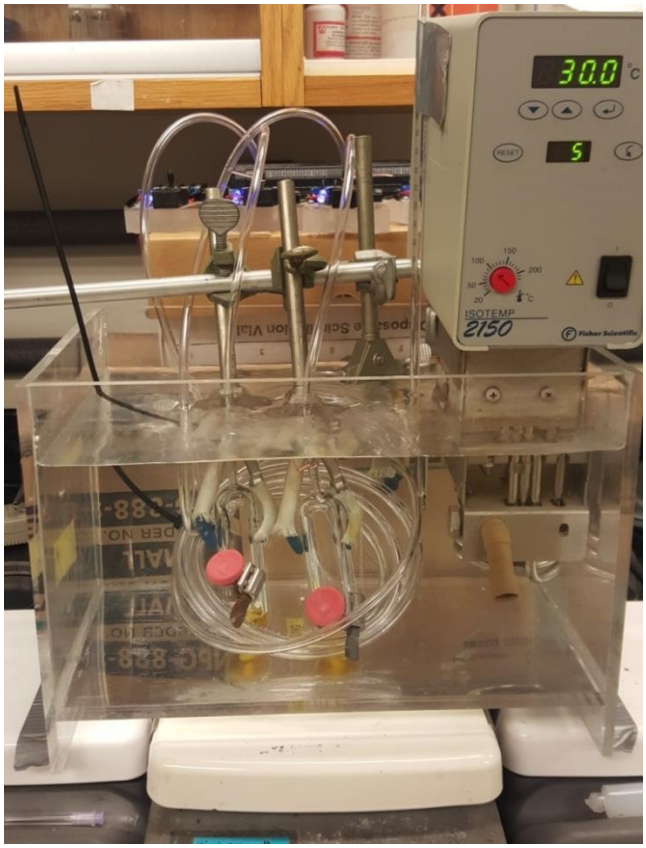

Figure 3.S5. Pressure testing vessels in the 30 ^{o}C constant temperature water bath.

M. Computations for Structure of 3.82-d

The structure was optimized at the PM6 level of theory with the Gaussian 09, Revision D.01 program. Braden Silva is thanked for these data.

Ru	-2.007828	-2.738244	0.134076
O	-3.480260	-3.884947	1.459475
H	-3.184929	-4.768357	1.728504
H	-4.368194	-3.996743	1.087209
N	-0.438956	-3.565933	1.312310
N	-2.092169	-1.568294	1.788062
N	-3.617375	-1.434815	-0.358483
N	-0.670144	-1.744569	-1.124653
N	-2.001383	-3.995230	-1.511063
C	-0.277928	-2.929290	2.539021
C	0.737979	-3.312507	3.427055
H	0.859326	-2.803908	4.388432
C	1.608104	-4.351570	3.072420
C	1.449513	-4.989502	1.839237
C	0.418424	-4.572666	0.983635
H	0.256337	-5.038953	0.000373
C	-1.239055	-1.830183	2.831382
C	-3.072991	-0.611111	1.874881
C	-3.206816	0.147370	3.049872
H	-3.981366	0.914690	3.140298
C	-2.330985	-0.100432	4.115601
H	-2.425404	0.484146	5.039542
C	-1.343798	-1.090496	4.021457
C	-3.906207	-0.514696	0.644631
C	-4.333729	-1.381957	-1.516465
H	-4.061882	-2.122651	-2.283460
C	-5.353013	-0.440646	-1.726232

H	-5.905317	-0.427218	-2.672255
C	-5.649131	0.475747	-0.713787
H	-6.445016	1.218058	-0.852091
C	-4.920811	0.440369	0.482043
C	-0.460845	-2.345997	-2.333286
C	-1.200372	-3.602059	-2.567927
C	-2.720422	-5.156700	-1.639362
C	-2.669362	-5.943621	-2.791832
C	-1.855819	-5.537769	-3.862601
C	-1.116587	-4.362018	-3.753164
H	-0.477335	-4.031529	-4.578614
C	0.423475	-1.805541	-3.318237
H	0.542977	-2.331334	-4.271886
C	1.110255	-0.645188	-3.067392
C	0.929522	0.012940	-1.813954
C	0.028310	-0.553633	-0.862326
H	-1.805064	-6.143713	-4.775477
H	1.793731	-0.215142	-3.809465
H	-5.146025	1.154764	1.280526
H	-0.674488	-1.283736	4.864125
H	2.409863	-4.656249	3.756998
H	2.122038	-5.800307	1.538975
H	-3.256089	-6.866477	-2.861567
H	-3.339423	-5.427785	-0.774707
N	-0.204430	0.041567	0.374854
C	0.447206	1.165477	0.663761
C	1.386970	1.797919	-0.230630
C	1.612500	1.216636	-1.458756
H	0.244489	1.622567	1.646134
C	2.082011	3.033062	0.188875

H	2.314902	1.660626	-2.173491
C	1.376256	4.248493	0.300004
C	2.047170	5.418396	0.683999
C	3.416390	5.385637	0.958543
C	4.123348	4.185633	0.853507
C	3.463808	3.009038	0.470017
C	-0.074318	4.318221	0.008629
H	1.499668	6.362300	0.759407
H	3.936606	6.302353	1.254691
H	5.194661	4.163672	1.074335
C	4.241176	1.751649	0.372896
C	5.224862	1.609850	-0.616505
C	5.950175	0.413902	-0.711344
C	5.709263	-0.636238	0.181969
C	4.723272	-0.485323	1.169557
C	3.998353	0.706707	1.276773
H	5.421520	2.437702	-1.307794
C	6.978547	0.283394	-1.809580
H	6.283054	-1.568735	0.117598
C	4.448426	-1.639539	2.093916
H	3.249647	0.846701	2.059770
C	-0.541079	4.112501	-1.296621
C	-1.917488	4.161618	-1.560515
C	-2.826768	4.446417	-0.536109
C	-2.351023	4.652180	0.768322
C	-0.980620	4.599353	1.043650
H	0.175372	3.922634	-2.102168
C	-2.387200	3.876321	-2.963836
H	-3.900416	4.516048	-0.743470
C	-3.351977	4.898786	1.868034

H	-0.597635	4.779981	2.053470
F	3.540874	-1.417800	3.063247
F	3.942786	-2.716908	1.456734
F	5.508972	-2.119214	2.751975
F	7.692622	-0.849387	-1.815936
F	6.428311	0.328372	-3.036531
F	7.897333	1.257775	-1.818680
F	-2.849419	5.218789	3.067596
F	-4.251232	5.855903	1.615927
F	-4.100854	3.803371	2.124013
F	-3.710740	3.925780	-3.169029
F	-1.872114	4.676047	-3.904247
F	-2.055396	2.632408	-3.371249

N. References

(1) Concepcion, J. J.; Jurss, J. W.; Templeton, J. L.; Meyer, T. J. *J. Am. Chem. Soc.* **2008**, *130*, 16462.

(2) Nieto, I.; Livings, M. S.; Sacci, J. B.; Reuther, L. E.; Zeller, M.; Papish, E. T. *Organometallics* **2011**, *30*, 6339.

(3) Kawahara, R.; Fujita, K.-i.; Yamaguchi, R. *J. Am. Chem. Soc.* **2012**, *134*, 3643.

(4) Wang, W.-H.; Hull, J. F.; Muckerman, J. T.; Fujita, E.; Himeda, Y. *Energ Environ. Sci.* **2012**, *5*, 7923.

(5) DePasquale, J.; Nieto, I.; Reuther, L. E.; Herbst-Gervasoni, C. J.; Paul, J. J.; Mochalin, V.; Zeller, M.; Thomas, C. M.; Addison, A. W.; Papish, E. T. *Inorg. Chem.* **2013**, *52*, 9175.

(6) Hong, D.; Murakami, M.; Yamada, Y.; Fukuzumi, S. *Energy Environ. Sci.* **2012**, *5*, 5708.

(7) Geissler, H.; Gross, P.; Axiva GmbH, Germany: 2002.

(8) Iyoda, M.; Otsuka, H.; Sato, K.; Nisato, N.; Oda, M. *Bull. Chem. Soc. Jpn.* **1990**, *63*, 80.

(9) Takeuchi, K. J.; Thompson, M. S.; Pipes, D. W.; Meyer, T. J. *Inorg. Chem.* **1984**, *23*, 1845.

(10) Wasylenko, D. J.; Ganesamoorthy, C.; Koivisto, B. D.; Henderson, M. A.; Berlinguette, C. P. *Inorg. Chem.* **2010**, *49*, 2202.

(11) Suen, H. F.; Wilson, S. W.; Pomerantz, M.; Walsh, J. L. *Inorg. Chem.* **1989**, *28*, 786.

(12) Norrby, T.; Boerje, A.; Aakermark, B.; Hammarstroem, L.; Alsins, J.; Lashgari, K.; Norrestam, R.; Maartensson, J.; Stenhagen, G. *Inorg. Chem.* **1997**, *36*, 5850.

(13) Concepcion, J. J.; Jurss, J. W.; Norris, M. R.; Chen, Z.; Templeton, J. L.; Meyer, T. J. *Inorg. Chem.* **2010**, *49*, 1277.

(14) Jacobsen, N. E. *NMR Spectroscopy Explained*; John Wiley & Sons: Hoboken, New Jersy, 2007.

(15) Taketoshi, A.; Koizumi, T.-a.; Kanbara, T. *Tetrahedron Lett.* **2010**, *51*, 6457.

(16) Qvortrup, K.; McKenzie, C. J.; Bond, A. D. *Acta. Crystallogr.Sect. E* **2007**, *63*, m1400.

(17) Yang, X.-J. D., Friedrich; Wu, Biao; Sun, Wen-Hua; Haehnel, Wolfgang; Janiak, Christoph *Dalton Trans.* **2005**, 256.

(18) Takeuchi, K. J.; Thompson, M. S.; Pipes, D. W.; Meyer, T. J. *Inorg. Chem.* **1984**, *23*, 1845.

(19) Qvortrup, K.; McKenzie, C. J.; Bond, A. D. *Acta. Crystallogr. Sect. E* **2007**, *63*, m1400.

(20) Yang, X.-J.; Drepper, F.; Wu, B.; Sun, W.-H.; Haehnel, W.; Janiak, C. *Dalton Trans.* **2005**, 256.

(21) Maji, S.; Lopez, I.; Bozoglian, F.; Benet-Buchholz, J.; Llobet, A. *Inorg. Chem.* **2013**, *52*, 3591.

(22) Xu, Y.; Fischer, A.; Duan, L.; Tong, L.; Gabrielsson, E.; Åkermark, B.; Sun, L. *Angew. Chem. Int. Ed.* **2010**, *49*, 8934.

(23) Neudeck, S.; Maji, S.; López, I.; Meyer, S.; Meyer, F.; Llobet, A. *J. Am. Chem. Soc.* **2013**, *136*, 24.

(24) Deng, Z.; Tseng, H.-W.; Zong, R.; Wang, D.; Thummel, R. *Inorg. Chem.* **2008**, *47*, 1835.

(25) Xu, Y.; Duan, L.; Åkermark, T.; Tong, L.; Lee, B.-L.; Zhang, R.; Åkermark, B.; Sun, L. *Chem. – Eur. J.* **2011**, *17*, 9520.

(26) McDaniel, N. D.; Coughlin, F. J.; Tinker, L. L.; Bernhard, S. *J. Am. Chem. Soc.* **2008**, *130*, 210.

(27) Bai, X.-L.; Liu, X.-D.; Wang, M.; Kang, C.-Q.; Gao, L.-X. *Synthesis* **2005**, *2005*, 458.

(28) Maiti, D.; Buchwald, S. L. *J. Org. Chem.* **2010**, *75*, 1791.

(29) DiMondo, D.; Thibault, M. E.; Britten, J.; Schlaf, M. *Organometallics* **2013**, *32*, 6541.

(30) Kavanagh, P.; Leech, D. *Tetrahedron Lett.* **2004**, *45*, 121.

(31) Shimada, H.; Sakurai, T.; Kitamura, Y.; Matsuura, H.; Ihara, T. *Dalton Trans.* **2013**, *42*, 16006.

(32) Allen, F. H.; Bird, C. M.; Rowland, R. S.; Raithby, P. R. *Acta. Crystallogr. Sect. B* **1997**, *53*, 696.

(33) Eccles, K. S.; Elcoate, C. J.; Stokes, S. P.; Maguire, A. R.; Lawrence, S. E. *Cryst. Growth. Des.* **2010**, *10*, 4243.

(34) Steiner, T. *J. Chem. Soc., Chem. Commun.* **1994**, 2341.

(35) Posner, G. H.; Wang, Q.; Han, G.; Lee, J. K.; Crawford, K.; Zand, S.; Brem, H.; Peleg, S.; Dolan, P.; Kensler, T. W. *J. Med. Chem.* **1999**, *42*, 3425.

(36) Solà, J.; Riera, A.; Verdaguer, X.; Maestro, M. A. *Organometallics* **2006**, *25*, 5795.

(37) Zong, R. F.; Naud, F.; Segal, C.; Burke, J.; Wu, F. Y.; Thummel, R. *Inorg. Chem.* **2004**, *43*, 6195.

(38) Oguchi, M.; Wada, K.; Honma, H.; Tanaka, A.; Kaneko, T.; Sakakibara, S.; Ohsumi, J.; Serizawa, N.; Fujiwara, T.; Horikoshi, H.; Fujita, T. *J. Med. Chem.* **2000**, *43*, 3052.

(39) Deasy, R. E.; Slattery, C. N.; Maguire, A. R.; Kjell, D. P.; Hawk, M. K. N.; Joo, J. M.; Gu, R. L.; Moynihan, H. *J. Org. Chem.* **2014**, *79*, 3688.

(40) Wang, X.-F.; Tian, X.-T.; Ohkoshi, E.; Qin, B.; Liu, Y.-N.; Wu, P.-C.; Hour, M.-J.; Hung, H.-Y.; Qian, K.; Huang, R.; Bastow, K. F.; Janzen, W. P.; Jin, J.; Morris-Natschke, S. L.; Lee, K.-H.; Xie, L. *Bioorg. Med. Chem. Lett.* **2012**, *22*, 6224.

(41) Kasparian, A. J.; Savarin, C.; Allgeier, A. M.; Walker, S. D. *J. Org. Chem.* **2011**, *76*, 9841.

(42) Barenys, M.; Boix, N.; Farran-Codina, A.; Palma-Linares, I.; Montserrat, R.; Curto, A.; Gomez-Catalan, J.; Ortiz, P.; Deza, N.; Llobet, J. M. *Food Chem. Toxicol.* **2014**, *71*, 254.

(43) Hirahara, M.; Ertem, M. Z.; Komi, M.; Yamazaki, H.; Cramer, C. J.; Yagi, M. *Inorg. Chem.* **2013**, *52*, 6354.

(44) Woodmansee, D. H.; Muller, M.-A.; Neuburger, M.; Pfaltz, A. *Chem. Sci.* **2010**, *1*, 72.

(45) Boyer, J. L.; Polyansky, D. E.; Szalda, D. J.; Zong, R. F.; Thummel, R. P.; Fujita, E. *Angew. Chem. Int. Ed.* **2011**, *50*, 12600.

(46) Gormisky, P. E.; White, M. C. *J. Am. Chem. Soc.* **2013**, *135*, 14052.

(47) Osichow, A.; Göttker-Schnetmann, I.; Mecking, S. *Organometallics* **2013**, *32*, 5239.

(48) Olaru, M.; Beckmann, J.; Raţ, C. I. *Organometallics* **2014**, *33*, 3012.

(49) Qinli Cao, private communication.

(50) Kantchev, E. A. B.; O'Brien, C. J.; Organ, M. G. *Angew. Chem. Int. Ed.* **2007**, *46*, 2768.

(51) Chartoire, A.; Frogneux, X.; Boreux, A.; Slawin, A. M. Z.; Nolan, S. P. *Organometallics* **2012**, *31*, 6947.

(52) López, I.; Ertem, M. Z.; Maji, S.; Benet-Buchholz, J.; Keidel, A.; Kuhlmann, U.; Hildebrandt, P.; Cramer, C. J.; Batista, V. S.; Llobet, A. *Angew. Chem. Int. Ed.* **2014**, *53*, 205.

(53) Hodson, E.; Simpson, S. J. *Polyhedron* **2004**, *23*, 2695.

(54) Jameson, D. L.; Guise, L. E. *Tetrahedron Lett.* **1991**, *32*, 1999.

(55) Hong, Y. R.; Gorman, C. B. *J. Org. Chem.* **2003**, *68*, 9019.

(56) Thummel, R. P.; Lefoulon, F.; Cantu, D.; Mahadevan, R. *J. Org. Chem.* **1984**, *49*, 2208.

CHAPTER 4

Synthesis and Activity of Binuclear Water Oxidation Catalysts

A. Introduction

One of the most fruitful homogeneous water oxidation catalysts has been a family of catalysts studied by Duan et al., of which **4.1-4.3** (Figure 4.1) are just three examples[1-4]. What led the Sun group to the use of bipyridinedicarboxylic acid (bda) was that they previously showed anionic ligands lower the potential to go from Ru(II) to Ru(III), and also could help stabilize the higher oxidation states needed for water oxidation[5]. In the first paper on these catalysts, kinetic studies using CAN showed that the reaction was second order with respect to catalyst, leading them to believe that the mechanism for **4.1** was binuclear, presumably I2M. Surprisingly the Sun group was able to get a crystal structure of an oxidized form of the catalyst where two Ru(IV)-OH units are bridged by a proton (Figure 4.2). The structure suggests how two of these now seven coordinate metal complexes could come together in a binuclear fashion[1]. In a following paper exploring complex **4.1**, rather than using CAN as a sacrificial oxidant, light and $Ru(bpy)_3$ as a photosensitizer and sodium persulfate as the sacrificial oxidant were employed. One interesting detail found in this paper[1] is that when complex **4.1** was dissolved in acetonitrile, and left for one day at room temperature, the solution color changed from red to green; mass spectrometry showed that one picoline methyl had been oxidized to the carboxylic acid or both methyls to the aldehyde. This led to the proposal that one catalyst transformation pathway could be oxidation of the organic ligands by the Ru(IV) species generated during the water oxidation reaction[2].

Complex **4.2** was first published in 2011 showed a similar turnover frequency (TOF) as photosystem II, the process in nature to oxidize water. Using a relatively high concentration of catalyst, 216 mM, complex **4.2** achieved a TOF of 303.0 s^{-1} whereas **4.1** operated with a TOF of 32.8 s^{-1}. As for turnover numbers (TON) at the lower initial catalyst concentrations, at 15 mM, **4.2** gave ~ 8360 turnovers and **4.1** at 58.8 mM gave 2010 turnovers. As to the possible decomposition pathways of **4.2**, using CAN (8000

equiv) as the sacrificial oxidant, extracting the mixture with DCM, and analyzing the organic-soluble residue by MS, the presence of some isoquinoline was seen, but no effort was made to quantify the yield, nor was effort made to analyze the reaction mixture directly[4]. Thus, some axial ligand appears to be lost, but we don't know to what extent this occurs. The proposed rate limiting step for these bipyridinedicarboxylic acid catalysts

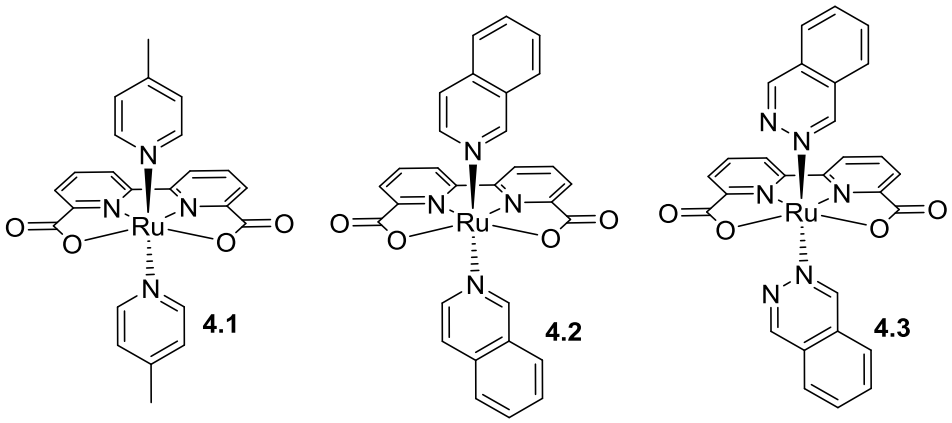

Figure 4.1. Selected water oxidation catalysts published by Sun et al.

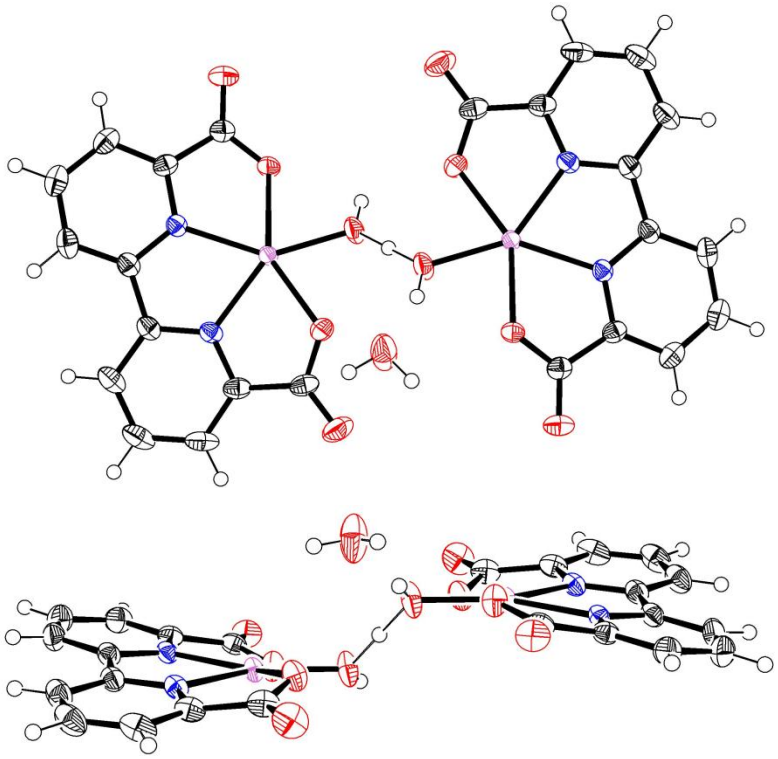

Figure 4.2. Crystal structure of Ru(IV) dinuclear complex formed from **4.1** after oxidation with CAN. Axial picoline ligands not shown for clarity.

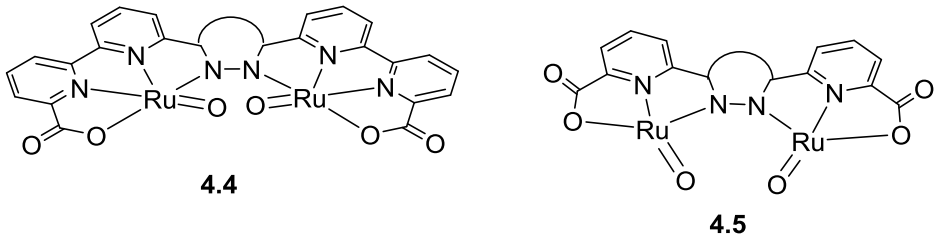

Figure 4.3. Proposed generic structures of oxidized intermediates for binuclear water oxidation catalysts. Two axial ligands on each Ru omitted for clarity.

involves two metal-oxo intermediates coming in contact with each other so that the oxos can form the O-O bond. The increase in catalytic rate using **4.2** rather than **4.1** lead to the postulate that the isoquinoline axial ligands have a larger π system which creates a stronger π stacking interaction between two intermediate molecules, helping bring the intermediates together in the correct orientation. In 2012 Sun et al looked at a number of different axial ligands and found that using phthalazine-containing catalyst **4.3** was not as fast as **4.2** but was the most robust analog, giving 55,419 ±959 turnovers[3].

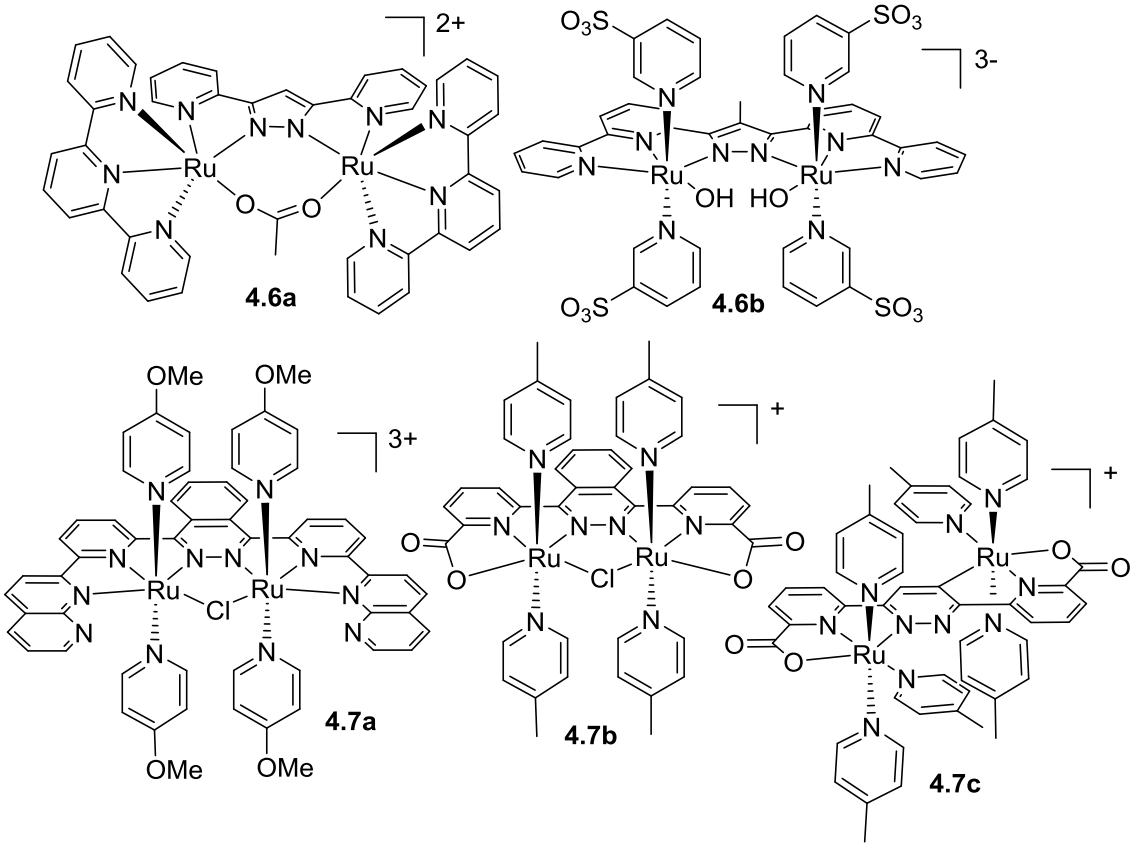

Figure 4.4. Known binuclear ruthenium water oxidation catalysts.

Of the proposed deactivation mechanisms, one constant theme is the loss or oxidation of the axial ligands. If the mechanism is dependent on the axial ligands staying coordinated to assist in bring two molecules together, the next logical step would be to form a catalyst with two metal centers next to each other so there is no dependence on π stacking of the axial ligands to bring the catalysts together.

Ideal structures that would make use of the success of the bipyridinedicarboxylic acid ligand and maintain the pyridine- or bipyridinecarboxylate ligand but make binuclear systems could be **4.4** and **4.5** (Figure 4.3). **4.4** would maintain the bipyridine but to bridge two molecules one of the carboxylates is replaced with a heterocycle. Would **4.4** still operate by way of a seven-coordinate intermediate as suggested for **4.1-4.3**? Structure **4.5** is similar to **4.4** but instead of a bipyridine for each metal only one pyridine is present, so this analog could operate by a more traditional 6-coordinate intermediate.

The binuclear idea is not a new one; binuclear species have a long history in WOC, starting with the blue dimer in 1982[6]. More recently, binucleating ligands have been used to guarantee connecting two metal centers as in examples **4.6a-b**, which used a -1 charged pyrazolato bridge, and **4.7a-c** which used a neutral phthalazine or pyridazine bridge.

Complex **4.6a** was published in 2004 by Llobet et al.; after treating the bridging acetate complex with acid the diaquo complex was formed and shown to be a capable water oxidation catalyst using CAN. Using CAN as sacrificial oxidant, rate of product formation was pseudo-first-order in catalyst but only 18.6 turnovers (73.2 % efficiency) was achieved.[7] The authors further studied the complex using electrochemistry, completing a Pourbaix diagram that showed oxygen was generated at Ru(IV) + Ru(IV) oxidation states. They concluded that this complex operates by the binuclear radical coupling mechanism, I2M. Complex **4.6b** was reported by Llobet et al. in 2013; using CAN they observed 22.6 turnovers and 90.6 % efficiency. The authors also did a number of oxygen labeling experiments where they determined that **4.6b** operates by a water nucleophilic attack mechanism.[8]

The phthalazine- or pyridazine-bridged complexes were first studied by Thummel et al. in 2004 where they synthesized a number of analogs with complex **4.7a** giving the most turnovers (689). Testing the picoline analog of **4.7a** they found first-order kinetics with respect to catalyst but concluded that the reaction could proceed by either WNA or I2M mechanism.[9] Structures **4.7b** and **4.7c** were published in the same paper in 2010 by Sun et al. where using CAN as a sacrificial oxidant, **4.7b** gave about 10400 turnovers and **4.7c** gave 4700 turnovers. Using a different sacrificial oxidant (sodium persulfate) and Ru(bipy)(4,4'-$(CO_2Et)_2$-bipy)$_2$) Cl_2 as a photosensitizer Sun et al. showed that **4.7b** gave 580 turnovers and **4.7c** gave no oxygen.[10] Structure **4.7 c** illustrates when synthesizing complexes containing a pyridazine unit, the back carbons should be blocked like in phthalazine or undesired metalation can occur at a ring carbon. Another paper looked at different pyridazine analogs with groups in the back of the pyridazine ring[11]. The catalyst with the highest TON was **4.7b** out of the binuclear systems discussed; this is encouraging since it is similar to the envisioned catalyst design of **4.4** and **4.5**.

B. Synthesis of Ligands and Complexes

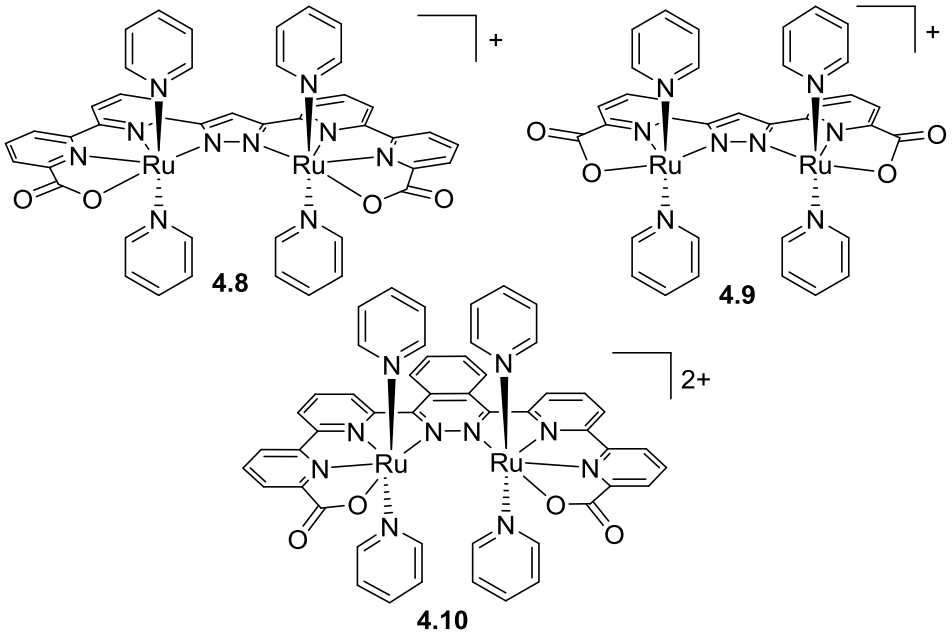

Figure 4.5. Targeted binuclear complexes unknown before this thesis work.

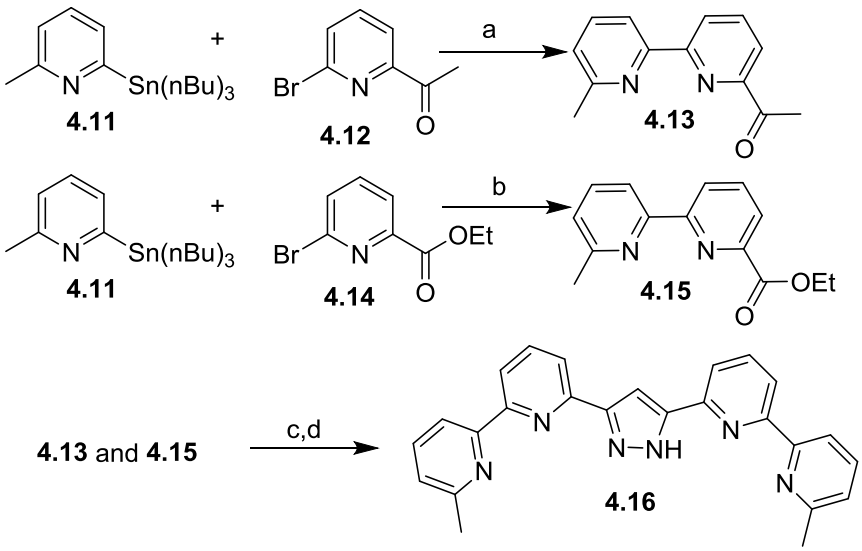

Figure 4.6. Synthesis of **4.16**.
(a) 6-bromo-2-acetyl-pyridine (**4.12**, 1.0 equiv), 2-methyl-6-(tri(n-butyl)stannyl)pyridine (**4.11**, 1.1 equiv), $Pd(PPh_3)_4$ (2.0 mol %), PPh_3 (7 mol %), toluene, reflux, 21 h, 79 % yield. (b) 6-bromo-2-ethylester-pyridine (**4.14**, 1.0 equiv), 2-methyl-6-(tri(n-butyl)stannyl)pyridine (**4.11**, 1.05 equiv), $Pd(PPh_3)_4$ (5.0 mol %), PPh_3 (7 mol %), toluene, reflux, 44 h, 52 % yield. (c) **4.13** (1.0 equiv), **4.15** (1.0 equiv), NaOEt (1.1 equiv), toluene, RT, 42 h. (d) hydrazine hydrate , benzene, reflux, 2 d, 60 % yield over the last two steps.

The known complexes used pyrazole or phthalazine as the linker part of the ligand, with either pyridine or bipyridine arms. The goal is to use the same linkers with either pyridine or bipyridine *carboxylates* on either side arm giving structures **4.8-4.10,** which had not been published at the start of the project.

The known synthesis of 3,5-bispyridyl(pyrazole) analogs typically starts with Claisen condensation of 2-acetyl-pyridine and 2-ester-pyridine analogs, giving the corresponding dipyridyl-1,3-diketone which can then be converted to the pyrazole by addition of hydrazine[12-17]. Synthesis of the target ligand **4.17** was achieved by the same method, by crossed Claisen reaction between 2-acetyl-bipyridine **4.13** and 2-ester-bipyridine **4.15**. **4.13** was synthesized by a Stille coupling between known compounds 2-methyl-6-(tri(n-butyl)stannyl)pyridine[18] **4.11** and 6-bromo-2-acetyl-pyridine[19] **4.12** in 79 % yield. The ester **4.15** was synthesized also by a Stille coupling between 2-methyl-6-(tri(n-butyl)stannyl)pyridine[18] **4.11** and 6-bromo-2-ethylester-pyridine **4.14** giving **4.15** in 52 % yield. **4.15** and **4.13** were condensed under basic conditions in toluene to give the

intermediate enol, which was then refluxed in benzene with hydrazine to obtain **4.16** in 60 % yield (Figure 4.6). Attempts at oxidation to **4.17** using CrO_3 in H_2SO_4 ended up giving a mixture of **4.17** and **4.18** (Figure 4.7), which are insoluble, except in DMSO or strong acid, and were found to be inseparable. The ratio of **4.17** to **4.18** would vary even when using the same reaction conditions and workup. It should be noted that the structure of **4.17** was not fully characterized except for ^{1}H NMR data and is assumed to be the desired product based on those data. **4.18** was found to be the impurity by adding a portion of authentic **4.18** to a NMR tube that contained an aliquot of the oxidation reaction that had previously been shown to contain the impurity (Figure 4.8). The doublet at 8.75 ppm, triplet at 8.18 ppm, and doublet at 8.14 ppm increase after the addition of **4.18**.

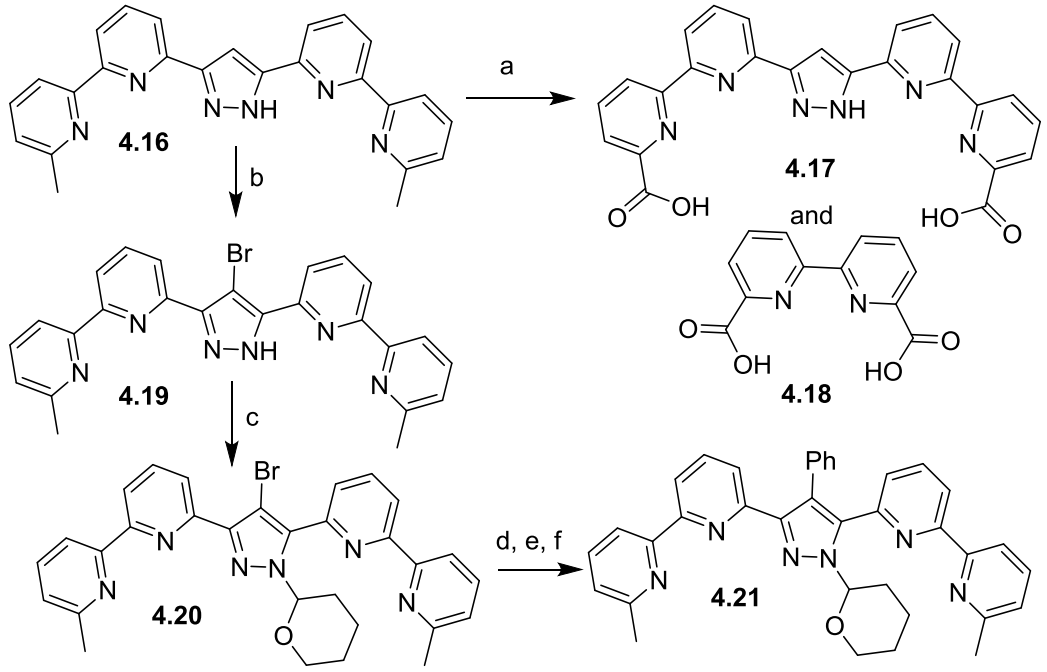

Figure 4.7. Synthesis of new target compound, **4.21**, after synthesis of **4.17** led to a mixture of **4.17** and **4.18**.
(a) **4.16** (1.0 equiv), CrO_3 (6.6 equiv), H_2SO_4. (b) **4.16** (1.0 equiv), N-bromosuccinimide (1.04 equiv), $CHCl_3$. (c) **4.19** (1.0 equiv), trifluoroacetic acid (13 mol %), 3,4-dihydro-2H-pyran, 80 ^{o}C, 4 h, 45 % yield over b and c. (d) **4.20** (1 equiv), phenylboronic acid (1.5 equiv), K_2CO_3 (2.5 equiv), PPh_3 (20 mol %), $Pd(PPh_3)_4$ (10 mol %), toluene, ethanol, water, 80 ^{o}C, 19 h, 100 ^{o}C, 24 h. (e) N-bromosuccinimide (0.94 equiv), $CHCl_3$. (f) phenylboronic acid (1.5 equiv), K_2CO_3 (2.5 equiv), PPh_3 (20 mol %), $Pd(PPh_3)_4$ (10 mol %), toluene, ethanol, water, 100 ^{o}C, 21 h, 39 % yield. Steps e and f were needed to increase the yield of **4.21**, for more details see experimental procedure for **4.21**.

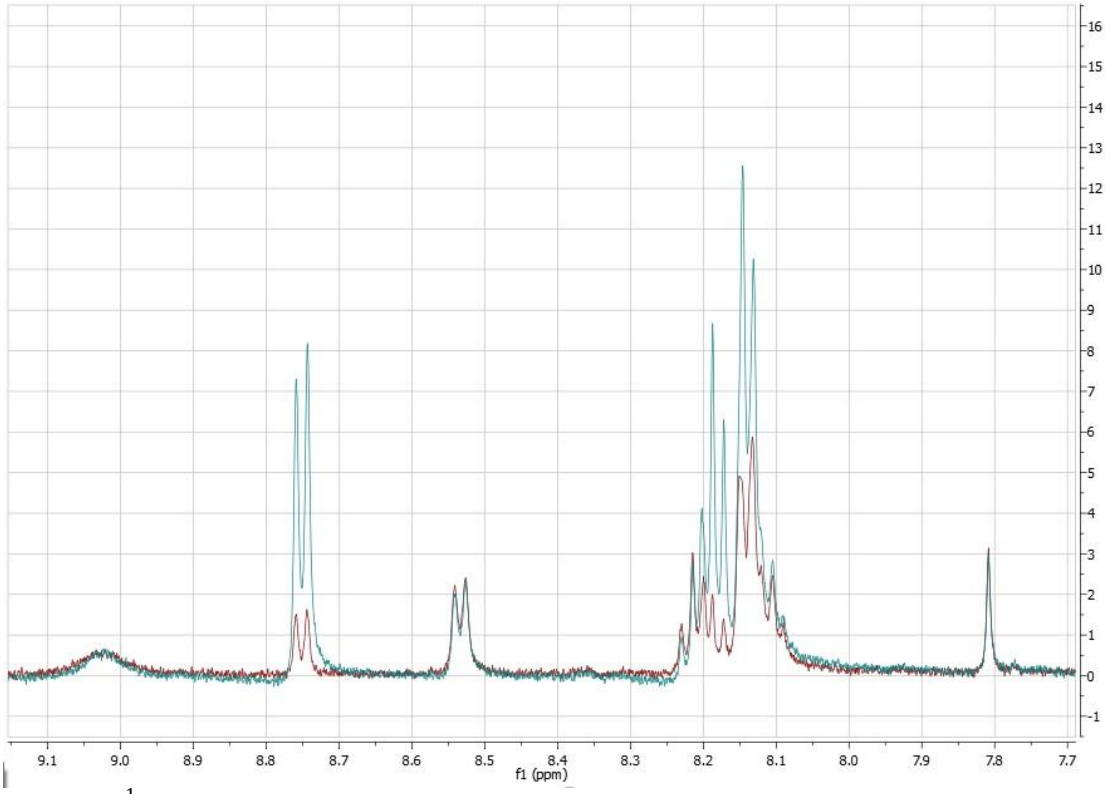

Figure 4.8. ^{1}H NMR spectrum of the oxidation of **4.16** to **4.17** after precipitation workup in d_6-DMSO (red) and after addition of authentic **4.18** to the same sample (green) showing that **4.17** is a byproduct in the reaction.

Decomposition of **4.17** to **4.18** illustrates a possible design flaw in the ligand, where under these oxidative conditions the pyrazole backbone is degrading. Considering that during water oxidation the ligand will have to withstand harsh oxidative conditions, we decided on a new ligand design that blocks the aromatic CH of the pyrazole from being oxidized.

To protect the CH position on the pyrazole, the hydrogen needs to be replaced with a group such as an alkyl or aryl group, with the easiest change at this stage in the synthesis being a phenyl group. **4.16** was brominated with N-bromosuccinimide giving **4.19** which was then protected with THP, giving **4.20**. With no NH group in **4.20**, it made it easier to purify by column chromatography, giving 45 % yield over the two steps. Phenylboronic acid was then coupled in a Suzuki reaction giving **4.21**. Unfortunately there was a substantial amount of a byproduct, the protiodebromination product, which was hard to separate from **4.21**. To increase the ratio of **4.21** to the side product, the

Suzuki reaction was done once then the mixture was reacted with NBS which reacted with the protiodebrominated byproduct, regenerating **4.20,** and not reacting with **4.21**. This mixture was then subjected to the Suzuki coupling conditions, which gave a high enough ratio of **4.21** to be separated. After a couple of attempts at oxidizing **4.21** using CrO_3, there was so little material that isolation of the product was quite a challenge. It was thought that with the number of steps involved that this was not a practical way of synthesizing this molecule. The next idea was to introduce the phenyl at an earlier stage in the synthesis.

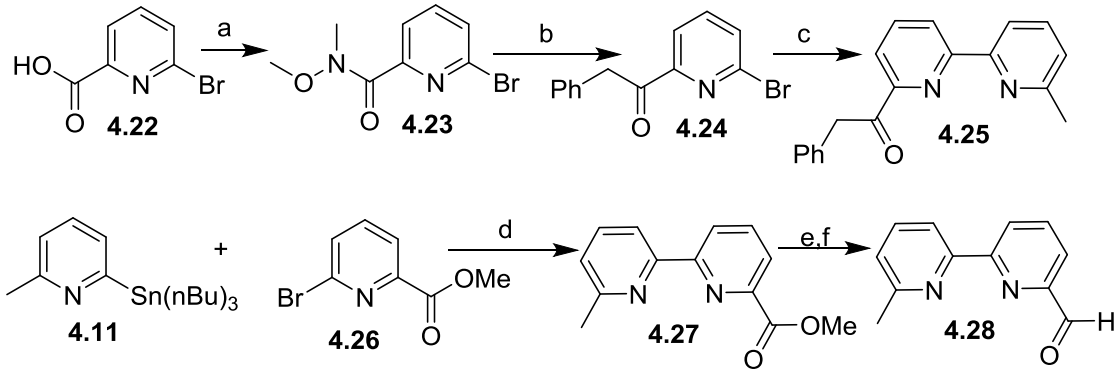

Figure 4.9. Synthesis of **4.25** and **4.28** with the goal of installing a phenyl group on the pyrazole ring.
(a) 6-bromopicolinic acid (**4.22**, 1 equiv), 1,1'-carbonyl-diimidazole (1.5 equiv), DMF, RT, 2 h, N,O-dimethylhydroxylamine HCl (1.04 equiv), RT, 2 h, 86 % yield. (b) **4.23** (1.0 equiv), freshly prepared benzyl grignard (1.3 equiv), Et_2O, -5 ^oC, 45 min, RT, 19 h, 61 % yield. (c) **4.24** (1 equiv), **4.11** (1 equiv), $Pd(PPh_3)_4$ (2 mol %), PPh_3 (7 mol %), toluene, reflux, 16 h, 71 % yield. (d) 6-bromo-2-methylester-pyridine (**4.26**, 1.0 equiv), 2-methyl-6-(tri(n-butyl)stannyl)pyridine (**4.11**, 1.1 equiv), $Pd(PPh_3)_4$ (5.0 mol %), PPh_3 (7 mol %), toluene, reflux, 13 h, 58 % yield. (e) **4.27** (1.0 equiv), $NaBH_4$ (10.3 equiv), 7 h, RT (f) SeO_2 (1.04 equiv), dioxane, 120 ^oC, 15 min, 64 % yield over two steps.

To install a phenyl on the pyrazole ring earlier, the acetyl group in **4.13** needs to be replaced with a benzyl ketone group, **4.25**. 6-bromopicolinic acid **4.22** was converted into the Weinreb amide **4.23** by adding CDI followed by N,O-dimethylhydroxylamine HCl which gave the desired product in 86 % yield. The Weinreb amide was then reacted with benzylmagnesium chloride Grignard reagent to give the ketone **4.24**, in 61 % yield. **4.24** was then coupled to **4.11** using $Ph(PPh_3)_4$ giving 71 % yield (Figure 4.9). When attempting to form the dione intermediate **4.29** (Figure 4.10) under the same conditions as before, no reaction was observed. Increasing the strength of the base by using sodium

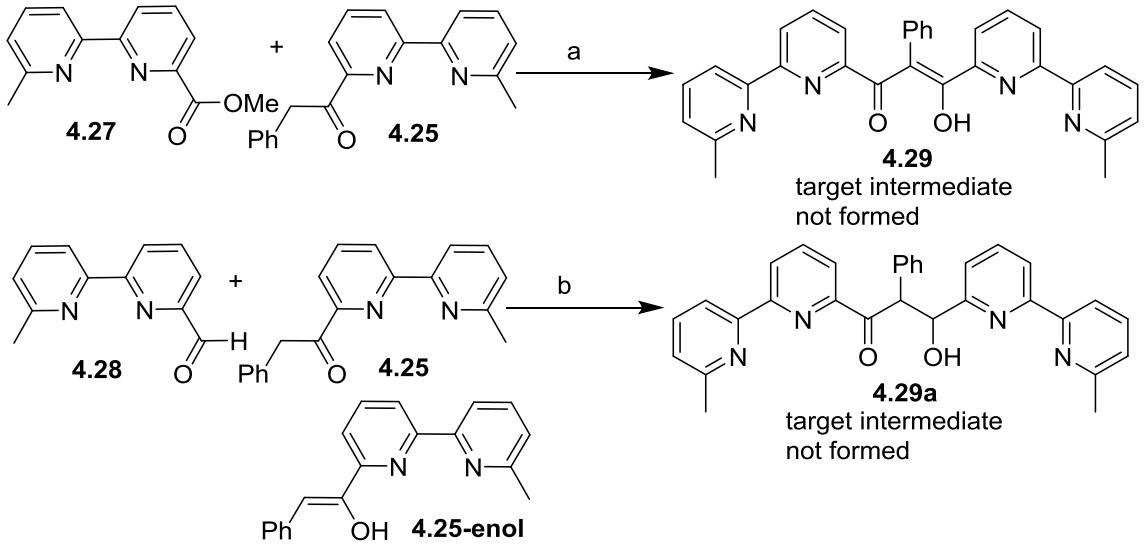

Figure 4.10. Attempted synthesis of **4.29** and **4.29a** with **4.25-enol** being an observed unreactive intermediate.
(a) **4.27** (1.0 equiv), **4.25** (1.0 equiv), NaH (2.05 equiv), toluene, 70 ^{o}C, 21 h, no **4.29** detected, **4.25-enol** is the only new product.

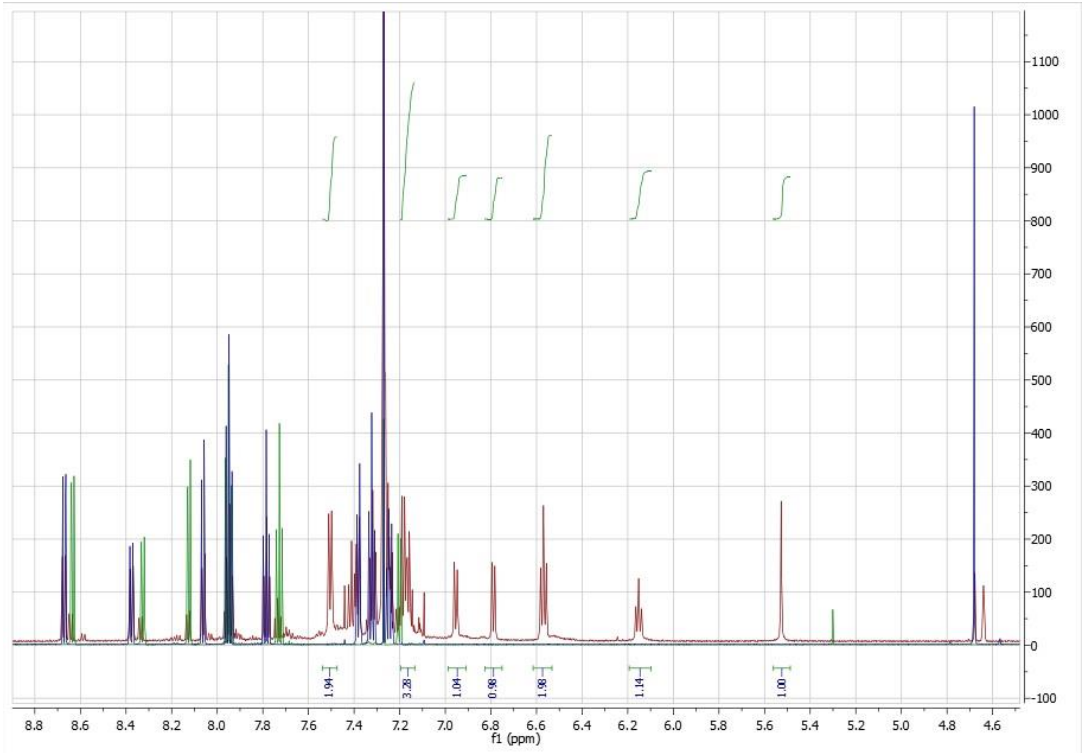

Figure 4.11. ^{1}H NMR spectra in $CDCl_3$ of **4.25** (blue), **4.27** (green), and the reaction between **4.25** and **4.27** described in Figure 4.10 after an aqueous workup (red).

hydride also gave no detectable product, but it became clear that the desired enol **4.25-enol** was forming, but not reacting. The ^{1}H NMR spectra of both starting materials, **4.25** (Figure 4.11, blue) and **4.27** (Figure 4.11, green) are shown on top of each other along with the NMR spectrum of the reaction mixture after addition of base (Figure 4.11, red). The mixture shows that of the two starting materials there is less **4.27**, which has been converted to **4.25-enol**. The structure of **4.25-enol** is assigned from the ^{1}H NMR spectral data with the new peak at 5.5 ppm being the new alkene proton.

The problem must be that this enol is less reactive because the charge is delocalized into the phenyl ring. To try to counteract this, a more reactive electrophile was synthesized with an aldehyde instead of an ester, **4.28**. The obtained intermediate **4.29a** would then need to be oxidized to form the aromatic pyrazole ring. Unfortunately there was no reaction between **4.28** and **4.25-enol**.

Reflecting on the synthesis resulted in the conclusion that there must be a more efficient way to synthesize the target ligands; after all, they are symmetrical about the bridging heterocycle at the head of the molecule. Retrosynthetic analysis shows that the simplest way to make **4.A** and **4.B** would be via a coupling of the bridging pyrazole, **4.C**, or phthalazine, **4.D** with the bipyridine analog, **4.E** (Figure 4.12). For improving **4.E**, it was also thought that instead of having a methyl on the bipyridine a more easily oxidizable group should be present, such as an aldehyde or its protected form, an acetal.

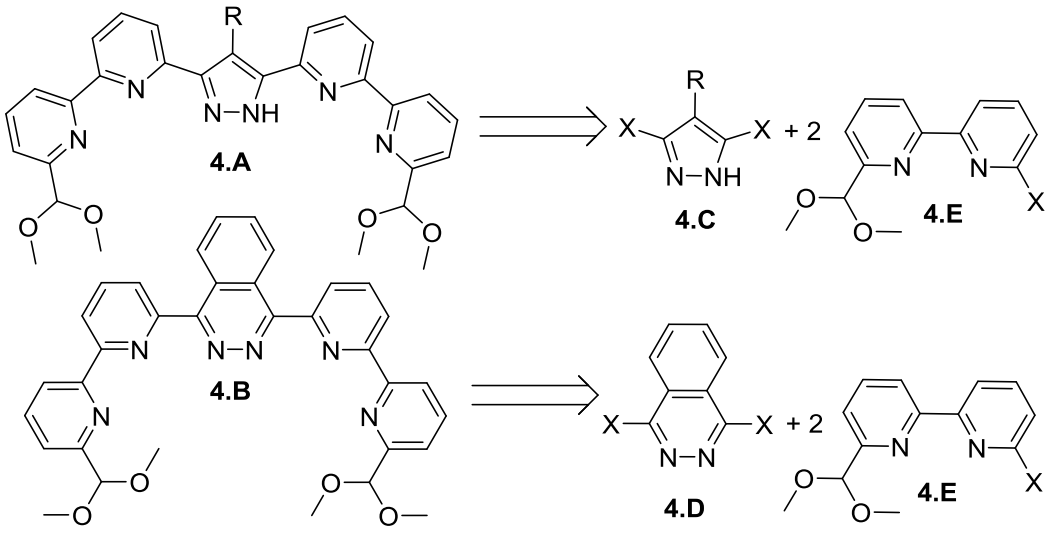

Figure 4.12. Retrosynthesis of **4.A** and **4.B**, shows the need for **4.E** where X = $Sn(nBu)_3$ and **4.C** and **4.D** where X = halogen.

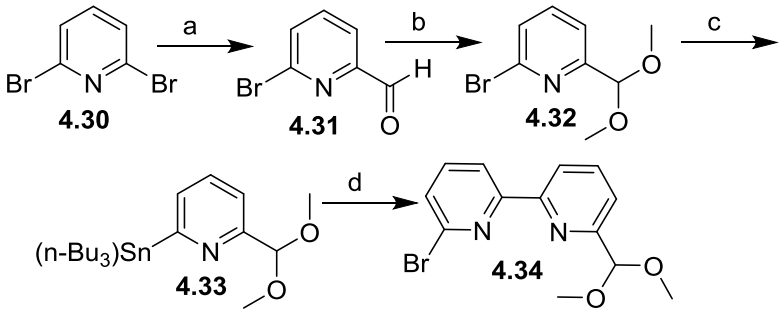

Figure 4.13. Synthesis of **4.34**.
(a) 2,6-dibromopyridine (**4.30**, 1 equiv), n-BuLi (1 equiv), DCM, -78 ^{o}C, 1 h, DMF (1.5 equiv), -78 ^{o}C, 1 h then warm to RT, 62.9 % yield. (b) **4.31** (1.0 equiv), p-toluenesulfonic acid hydrate (2 mol %), trimethylorthoformate (4.0 equiv), MeOH, reflux, 11 h, 92 % yield. (c) **4.32** (1.0 equiv), n-BuLi (1.0 equiv), Et_2O, -95 ^{o}C, 30 min, -78 ^{o}C , 1 h, tributyltin chloride (1.1 equiv), -95 ^{o}C for addition over 15 min, -78 ^{o}C, 1 h then warm to RT, 94 % yield with 10 % tributyltin chloride impurity. (d) **4.33** (1.15 equiv), 2,6-dibromopyridine (4.30, 1.0 equiv), lithium chloride (1.15 equiv), $Pd(PPh_3)_4$ (16 mol %),toluene, 120 ^{o}C, 21 h, 55 % yield.

As for what kind of coupling to do to form **4.A** and **4.B**, a Stille coupling was thought to be ideal because of the success of the previous couplings described earlier in the chapter. For **4.E**, X was figured to be $Sn(nBu)_3$, meaning compound **4.35** would be the actual precursor needed, and for **4.C** and **4.D**, X would be a halogen, but if need be the roles could be reversed.

The synthesis of the **4.35**, starting from 2,6-dibromopyridine **4.30** began with halogen lithium exchange at -78 ^{o}C followed by addition of DMF making **4.31** in 63 % yield. Synthesis of **4.31** is a well-known reaction, just done under slightly different conditions[20-25]. **4.31** could then be protected as the dimethyl acetal by heating in methanol with trimethylorthoformate and catalytic p-toluenesufonic acid, giving **4.32** in 92 % yield[20,21]. **4.33** was formed by a halogen lithium exchange of **4.32**, followed by addition of tributyltin chloride; the synthesis was similar to that of the dioxolane analog[26]. **4.33** was purified by a kugelrhor distillation which was not able to separate the excess starting tributyltin chloride. The purity of the compound was approximately 90 % **4.33** and 10 % tributyltin chloride, which was consistent with ^{1}H NMR spectroscopic and elemental analysis. If less tributyltin chloride was used the yield would decrease with the same amount of tributyltin chloride impurity. Attempts at purification on a silica column led to protiodestannylation, so **4.33** was used as a mixture, which did not affect the reactivity.

4.33 was then coupled to 2,6-dibromopyridine to obtain the unsymmetrical bipyridine analog **4.34** with a small amount of the dicoupled diacetal-terpyridine as an impurity which could be removed by silica column chromatography (Figure 4.13). Attempts at halogen lithium exchange on **4.34** were unsuccessful which was surprising since it worked well on the pyridine case, going from **4.32** to **4.33** (Figure 4.14).

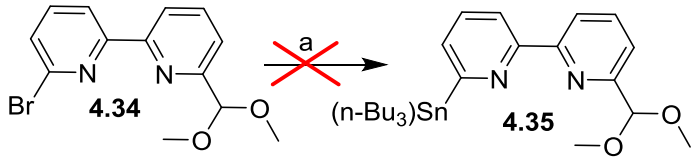

Figure 4.14. Unsuccessful synthesis of **4.35**.
(a) **4.34** (1.0 equiv), n-BuLi (1.0 equiv), Et_2O, -78 ^oC, 30 min, tributyltin chloride (1.1 equiv), 1 h.

To avoid doing lithium halogen exchange in the presence of the acetal group, the tin group should be installed previously. To do so 2,6-bis(trimethylstannyl)pyridine[27] was synthesized by a known procedure, which was then coupled with **4.32** giving **4.36** in a 47% yield after a kugelrhor distillation (Figure 4.15). The product was approximately 80 % pure, with unknown impurities but was used without further purification due to the sensitivity of the molecule. Now that the more challenging part of the molecule had been synthesized, the goal was to figure out to what pyrazole compound to couple it and how.

Attempts at synthesizing **4.C**, where R was phenyl, led to bromination of the phenyl ring. **4.37**, a known compound[28], that is easily synthesized from 4-ethyl pyrazolecarboxylate, was used instead of the phenyl analog. The pyrazole NH was then protected by tetrahydropyran giving **4.38**. Protecting the NH made purification easier (as described for **4.20** as well), which was then coupled to **4.36**. The coupling was slower than the pyridine Stille couplings done previously; instead of less than a day it was heated for 12 d and the obtained yield was only 30 %, which could be due to pyrazole being more electron rich than pyridine. **4.39** was then deprotected by dissolving in HCl (6 M) and stirring until both the THP was removed and the acetals were converted to aldehydes. The HCl was then removed by vacuum and the crude solid was dissolved in formic acid and hydrogen peroxide was used to oxidize the aldehydes to carboxylic acids giving **4.40** in 97 % yield (Figure 4.16).

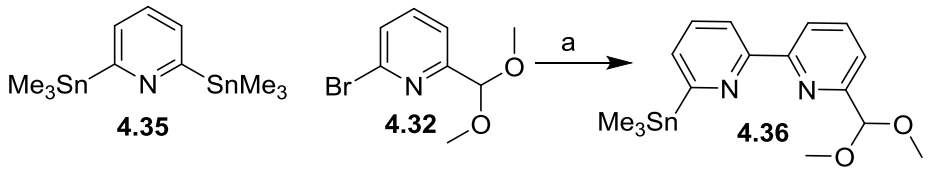

Figure 4.15. Synthesis of key intermediate **4.36**.
(a) **4.35** (1.0 equiv), **4.32** (1.0 equiv), $Pd(PPh_3)_4$ (1.5 mol %), toluene, reflux, 6.5 h, 47 % yield; product estimated to be ~ 80 % pure.

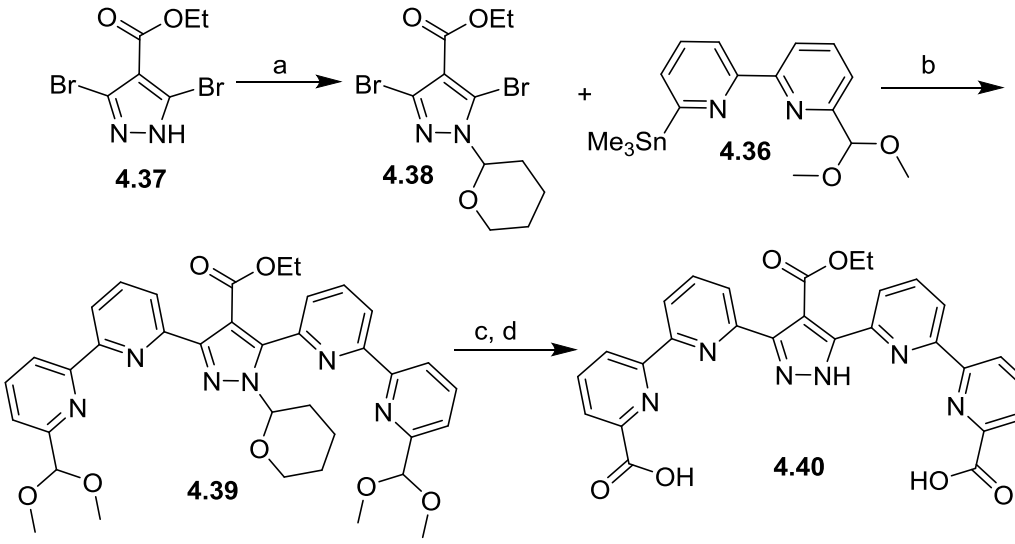

Figure 4.16. The successful synthesis of ligand **4.40**.
(a) **4.37** (1 equiv), p-toluenesulfonic acid (0.7 mol %), 3,4-dihydro-2H-pyran, RT, 40 min., 85 % yield. (b) **4.38** (1 equiv), **4.36** (3.0 equiv), $Pd(PPh_3)_4$ (15 mol %), toluene, 120 ^oC, 12 d, 30 % yield. (c) **4.39** (1.0 equiv), HCl (6 M), 2 h. (d) H_2O_2, formic acid, 97 % yield.

To make the phthalazine analog, 1,4-dichlorophthalazine[29] was synthesized by a known three step procedure and then coupled to **4.36.** The coupling reaction time was much shorter than when using the pyrazole analog, only 21.5 h at 120 ^oC and in a better yield of 60 %, likely because of the more electron-poor phthalazine ring. **4.42** was then deprotected by dissolving in HCl (6 M) and then oxidized by adding sodium chlorite giving **4.43** in 80 % yield (Figure 4.17).

The pyridine analog **4.45** was synthesized by coupling **4.38** with **4.33**, which needed the same long reaction time, 14 d, and gave a low yield, 37 %, as did the other pyrazole analog. Nonetheless, the **4.44** obtained was deprotected by dissolving in

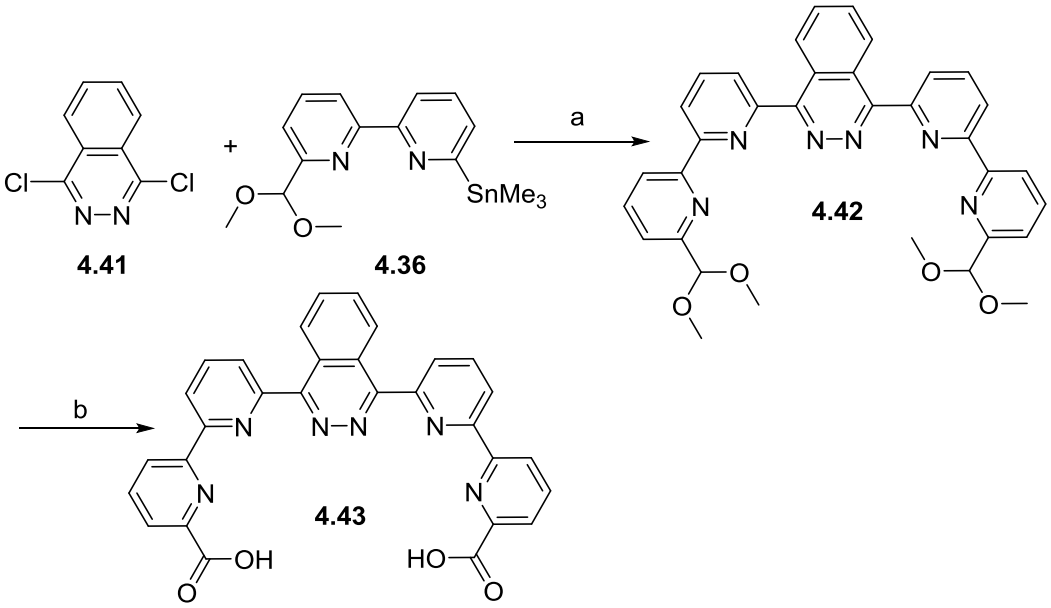

Figure 4.17. Synthesis of ligand **4.43**.
(a) 1,4-dichlorophthalazine (**4.41**, 1.0 equiv), **4.36** (2.5 equiv), $Pd(PPh_3)_4$ (8 mol %), toluene, 120 ^oC, 21.5 h, 60 % yield. (b) **4.42** (1.0 equiv), HCl (6 M), RT, 3.5 h, sodium chlorite 80 % (15.0 equiv), RT, 1 d, 80 % yield.

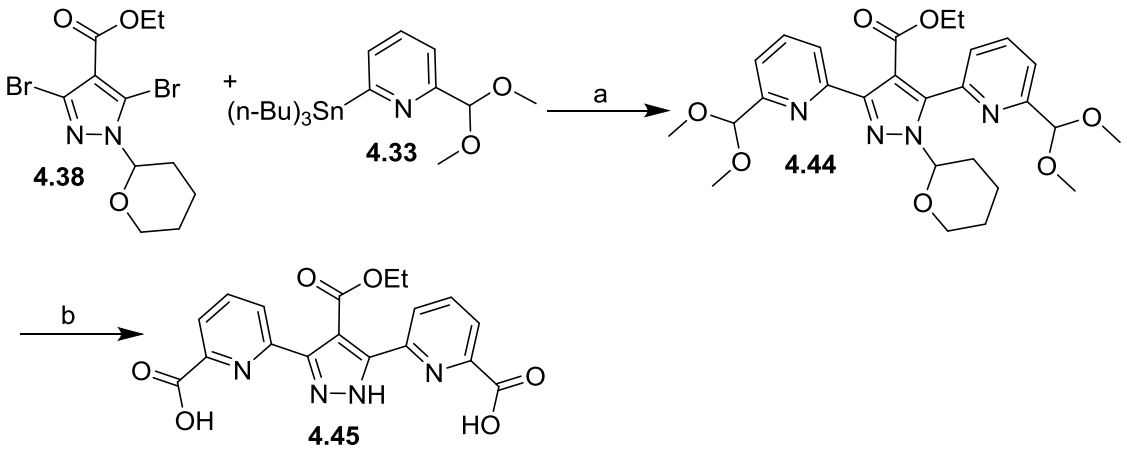

Figure 4.18. Synthesis of ligand **4.45**.
(a) **4.38** (1.0 equiv), **4.33** (2.5 equiv), $Pd(PPh_3)_4$ (15 mol %), toluene, 120 ^oC, 14 d, 37 % yield. (b) HCl (6 M), RT, 2 h, sodium chlorite 80% (13.5 equiv), RT, 45 min, 90 % yield.

HCl (6M) and then adding sodium chlorite to oxidize to the diacid, yielding **4.45** in 90 % yield (Figure 4.18).

Metalations of **4.45** and **4.40** were similar, as a solution of triethylamine and ethanol were added to the ligand. After about 5 min the ligand completely dissolved and

the metal precursor, $[Ru(cymene)Cl_2]_2$, was added followed by 4-picoline or phthalazine. The reaction was then heated in an oil bath at 100 ^oC for several days, and the crude products were purified by silica column chromatography (Figure 4.19). Metalation attempts using the same or similar procedures for **4.43** as a ligand gave a mixture of

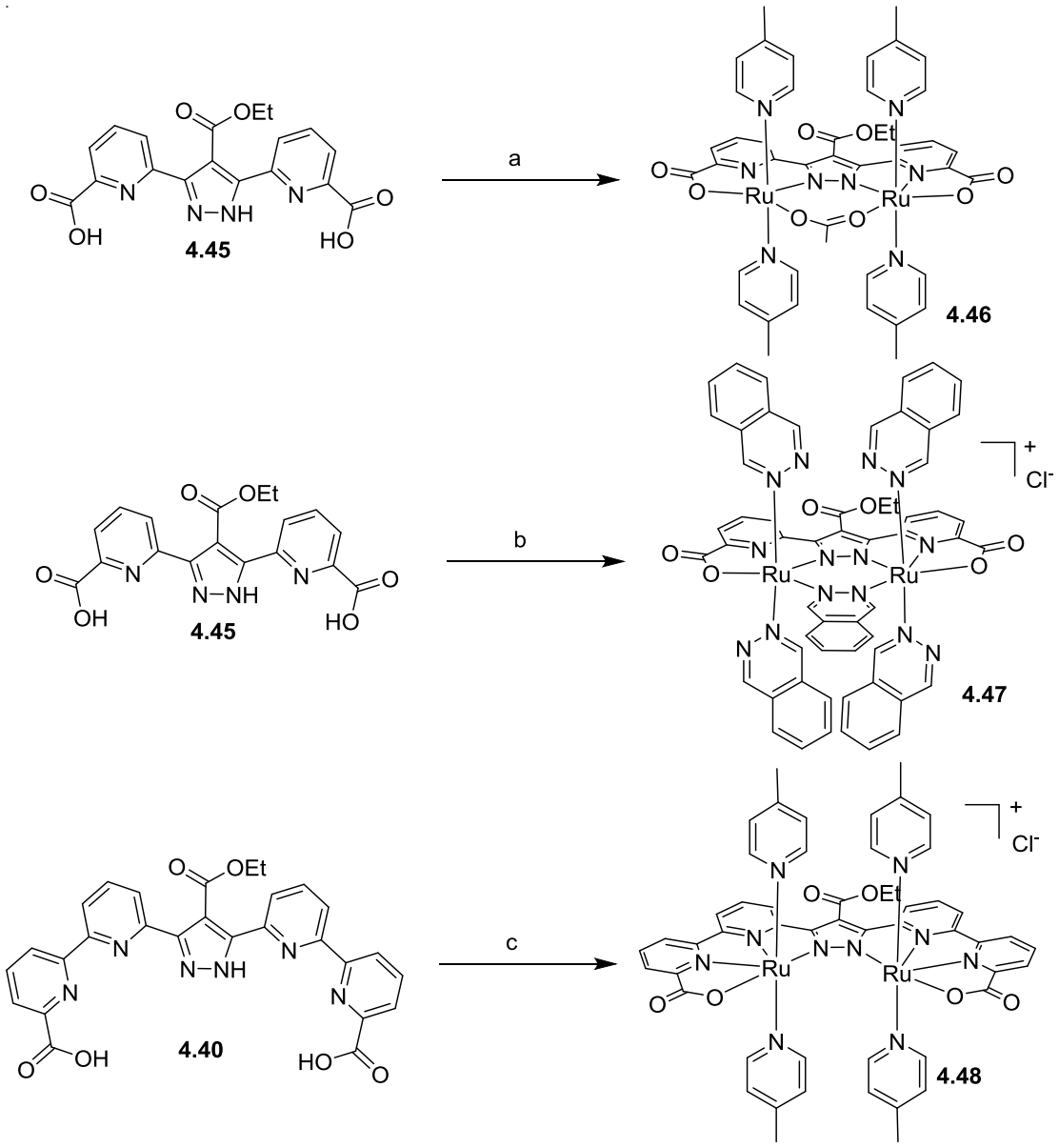

Figure 4.19. Synthesis of metal complexes **4.46**, **4.47**, and **4.48**.
(a) **4.45** (1.0 equiv), triethylamine (5.3 equiv), EtOH, 5 min, RT, $[Ru(cym)Cl_2]_2$ (1.05 equiv), 4-picoline (8.8 equiv), 100 ^oC, 2 d, 50 % yield. (b) **4.45** (1.0 equiv), triethylamine (5.2 equiv), EtOH, 5 min, RT, $[Ru(cym)Cl_2]_2$ (1.0 equiv), phthalazine (8.1 equiv), 100 ^oC, 1.5 d, 62 % yield. (c) **4.40** (1.0 equiv), triethylamine (11.0 equiv), EtOH, 5 min, RT, $[Ru(cym)Cl_2]_2$ (1.2 equiv), 4-picoline (9.3 equiv), 100 ^oC, 2 d, 59 % yield.

unknown products so this chemistry was not pursued further.

4.46, **4.47**, and **4.48** were characterized by ^{1}H and ^{13}C NMR spectroscopies and elemental analysis. Complex **4.48** gave ^{1}H and ^{13}C NMR spectra as expected. **4.46** interestingly formed a metal complex with a bridging acetate, where the acetate must have been formed from the oxidation of ethanol by a trace oxidant, such as oxygen or methyl isobutyl ketone found in denatured ethanol. **4.47** differs from **4.46** in that the axial ligands are phthalazine instead of 4-picoline which was thought to be desirable because of the success of the metal precursor, $[Ru(cymene)Cl_2]_2$, was added followed by 4-picoline or phthalazine. The reaction was then heated in an oil bath at 100 ^{o}C for several days, and the crude products were purified by silica column chromatography (Figure 4.19). Metalation attempts using the same or similar procedures for **4.43** as a ligand gave a mixture of unknown products so this chemistry was not pursued further.

4.46, **4.47**, and **4.48** were characterized by ^{1}H and ^{13}C NMR spectroscopies and elemental analysis. Complex **4.48** gave ^{1}H and ^{13}C NMR spectra as expected. **4.46** interestingly formed a metal complex with a bridging acetate, where the acetate must have been formed from the oxidation of ethanol by a trace oxidant, such as oxygen or methyl isobutyl ketone found in denatured ethanol. **4.47** differs from **4.46** in that the axial ligands are phthalazine instead of 4-picoline which was thought to be desirable because of the success of **4.3**; they also differ in that the phthalazine bridges the two metals instead of acetate, making **4.47** a cationic complex. The presence of the equatorial bidentate bridging phthalazine ligand was not planned but makes sense in hindsight; the lability of the bridging phthalazine is unknown. An attempt at synthesizing **4.47** without the bridging phthalazine was attempted by the addition of sodium acetate but unsuccessful.

C. Results and Conclusions

The catalysts were tested using CAN, with initial catalyst concentration of 100 μM and CAN concentration of 250 mM with a total volume of 4.0 mL in a 48 mL pressure vessel (Figure 4.21). The oxygen was detected by the change in pressure; for more details see CAN studies procedure at the end of the Chapter. **4.48** was only slightly active using CAN, giving about 60 TON over 48 h. The lack of activity shows the

possible need of an open site in these binuclear complexes, which was not needed for **4.1**, **4.2**, and **4.3**. Another possibility is the rigidity of the **4.48** system does not allow ideal bonding distances between the oxos, or perhaps there is only room for one oxo and not two to form.

4.46 was a capable catalyst with 100 turnovers in the first 25 min but slowed to give a total of 370 turnovers over 2 d. The much different initial rate (0 to 25 min gave 100 TON, 240 h^{-1}) compared to long term rate (15 h to 35 h gave about 60 TON, 3 h^{-1}) suggests a transformation of the initial active catalyst to a moderately active catalyst which finally becomes inactive after about 45 h. The phthalazine analog, **4.47**, was targeted because **4.3** was more robust than analogs with other axial ligands, however **4.47** was found to be inactive, but this makes sense given the fact that one phthalazine bridges the two catalytic metals.

At this point in the project I became aware of a publication by Llobet et al which studied a very similar complex without the ester on the back of the pyrazole (**4.49)**[30]. The Llobet group looked at **4.49** in detail using cyclic voltammetry, along with using sacrificial oxidant CAN. Comparing how **4.46** and **4.49** were tested using CAN, the same initial catalyst concentrations were used, 100 μM, but **4.49** was tested with limited amounts of CAN (10 mM, 100 equiv), while here in this work, **4.46** was tested with 25 times more CAN (250 mM, 2500 equiv). Compound **4.46** produced 25 turnovers after 400 sec (initial TOF_{25TON} ~0.28 sec^{-1}) whereas **4.49** produced 25 turnovers after about 125 sec (initial TOF_{25TON} 1.4 sec^{-1}), which makes it appear that **4.49** was faster, but note how low the CAN concentration was used to test **4.49**. Llobet found when more CAN was added the catalyst was slowed after 25 turnovers. To figure out why catalysis slowed, they ran an experiment to probe the effect of NO_3^- on catalysis, adding KNO_3 (600 equiv) in HOTf to a solution of catalyst, in order to simulate the effects of the addition of an additional 100 equiv of CAN, and then they injected CAN (100 equiv) and observed 17 turnovers after 300 sec (initial TOF ~0.18-0.2 sec^{-1}), a significant decrease from 1.4 sec^{-1}. Llobet et al. postulated that nitrate inhibits the binuclear system by reversibly binding to both open sites (see **4.49a** Figure 4.20) and reducing the amount of water binding. The coordination of nitrate could explain the difference in initial rate vs long term rate that

was discussed earlier; thus, it could be that catalyst **4.46** has not decomposed, instead the open sites are blocked by nitrate.

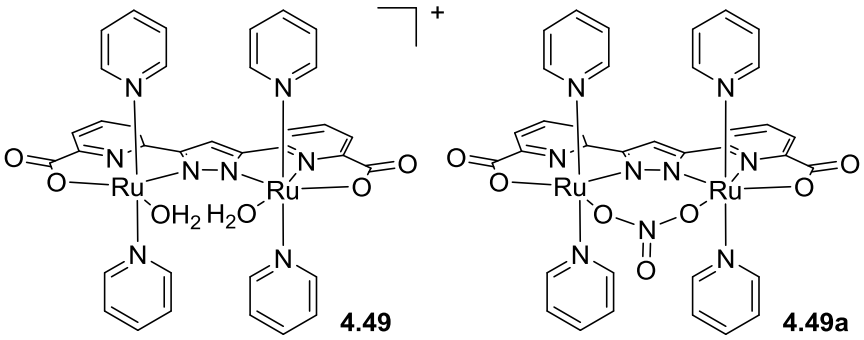

Figure 4.20. Water oxidation catalyst recently published by Llobet, **4.49**, and a proposed intermediate that inhibits the rate of catalysis, **4.49a**.

For future work, to get a better idea of the capability of **4.46** and the ability to compare to **4.49** and other analogs it would be logical to try a sacrificial oxidant such as periodate which might not coordinate or have a weaker binding to the complex. Periodate is not as strong an oxidant as cerium(IV) but it is worth an attempt, but questions have been rasied as to wether the oxygen forming dioxygen comes from water or periodate[31]. Or, instead of using a chemical oxidant one can use electrochemistry and do bulk electrolysis to quantify the amount of oxygen produced. Another interesting idea is to hydrolyze the ester substituent on the pyrazole and attach the catalyst to an electrode via an amide. When a nitrate free testing method is found then it would be interesting to modify the axial ligands, such as **4.47** with phthalazine, but find a way to avoid phthalazine metalation in the equatorial open sites. One way of doing this is adding sterics to one of the nitrogens to disfavor metalation of that nitrogen but not the other. The unhindered nitrogen could still coordinate to the axial open sites but the hindrance would disfavor the hindered nitrogen from coordinating to the equatorial open site, nullifying the chelate. Other studies have shown that axial ligands that contain electron withdrawing groups in the 4 positions have been found to increase water oxidation catalysis rates[32]. Analogs containing 4-ethyl pyridinecarboxylate, 4-(trifluoromethyl)pyridine, or 4-nitropyridine would be of interest. Another possible direction would be to add different metals to both **4.40** and **4.45** such as iridium or a first row metal such as cobalt[33].

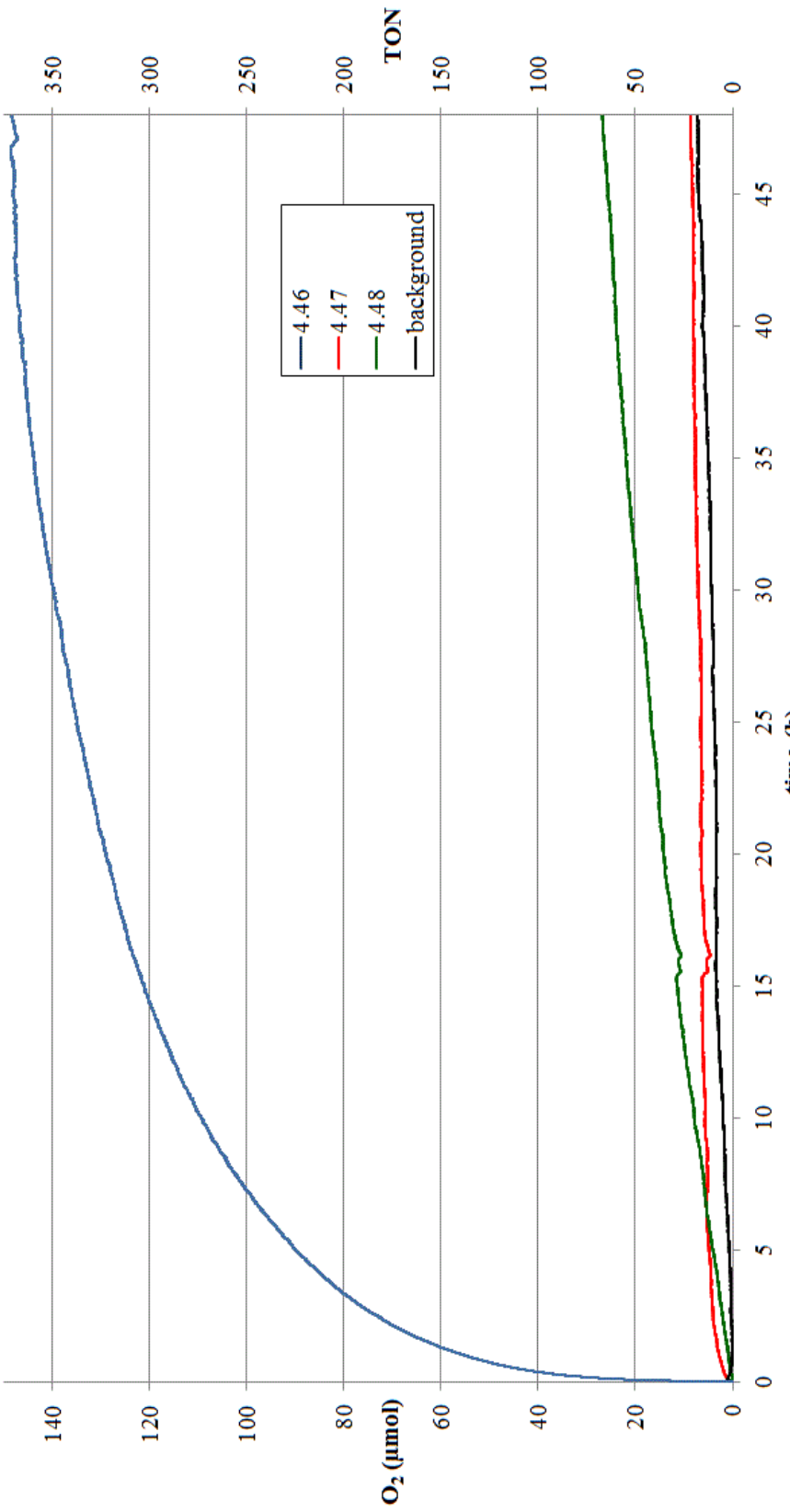

Figure 4.21. Oxygen evolution using CAN (250 mM) and catalysts **4.46-4.48** (100 µM, initial concentrations) over 2 d was monitored by the generation of pressure in a 48 mL pressure vessel with a total solution volume of 4.0 mL. For details see section of CAN studies at the end of the Chapter.

D. Synthesis

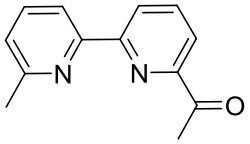

Synthesis of 6'-methyl-6-acetyl-(2,2'-bipyridine) (4.13)

To a three neck round bottom flask (100 mL) in a glovebox added 6-bromo-2-acetyl-pyridine[19] (**4.12**, 3.7763 g, 18.88 mmol), 2-methyl-6-(tri(n-butyl)stannyl)pyridine[18] (**4.11**, 7.9456 g, 20.79 mmol), $Pd(PPh_3)_4$ (0.4376 g, 0.38 mmol), PPh_3 (0.3466 g, 1.32 mmol), a stir bar, and dry toluene (51 mL). Keeping the contents under nitrogen, the flask was equipped with a reflux condenser with a nitrogen inlet and two teflon stoppers. The reaction was refluxed for 21 h. After cooling to room temperature the solution was filtered through a course frit loaded with Celite. The Celite was rinsed with toluene (3 x 10 mL). The filtrate was transferred to a separatory funnel and washed with saturated sodium bicarbonate (3 x 75 mL) and water (3 x 75 mL). The aqueous layer was back extracted with toluene (60 mL). The organic layers were combined and washed with brine (60 mL), dried with Na_2SO_4, then filtered through a course frit and from the filtrate solvent was removed by rotary evaporation. Crude product was dry loaded on silica by dissolving in DCM and adding silica (4.3 g), and solvent was removed by oil pump vacuum. The crude product/silica mixture was loaded on a silica (105 g) column, eluting with a mixture of hexanes and ethyl acetate, starting at 100 % hexanes and going to a 5 % ethyl acetate mixture. Fractions containing only a TLC spot of $R_f \sim 0.25$, using hexanes:ethyl acetate (8:2) to elute were combined. Solvent was removed by rotary evaporation and dried under high vacuum pump to yield 6'-methyl-6-acetyl-(2,2'-bipyridine) as white solid (**4.13**, 3.1584 g, 14.88 mmol, 79 % yield). Anal. calcd. for $C_{13}H_{12}N_2O$ (mol. wt. 212.25): C, 73.56; H, 5.70; N, 13.20. Found C, 74.06; H, 5.88; N, 13.48.

^{1}H NMR ($CDCl_3$, 499.944 MHz) δ 8.65 (d, *J* = 7.3 Hz, 1H), 8.32 (d, *J* = 7.6 Hz, 1H), 8.03 (d, *J* = 7.1 Hz, 1H), 7.93 (t, *J* = 7.6 Hz, 1H), 7.74 (t, *J* = 7.6 Hz, 1H), 7.21 (d, *J* = 7.1 Hz, 1H), 2.83 (s, 3H), 2.65 ppm (s, 3H). ^{13}C NMR ($CDCl_3$, 125.723 MHz) δ 200.4, 158.0, 155.7, 154.7, 152.9, 137.7, 137.1, 124.3, 123.6, 121.2, 118.1, 25.7, 24.6 ppm.

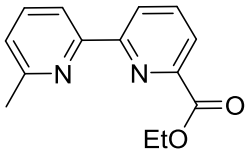

Synthesis of ethyl 6'-methyl-2,2'-bipyridine-6-carboxylate (4.15)

To a three neck round bottom flask (250 mL) in a glovebox added ethyl 6-bromopyridine-2-carboxylate (**4.14**, 2.0018 g, 8.70 mmol), 2-methyl-6-(tri(n-butyl)stannyl)pyridine[18] (**4.11**, 3.5020 g, 9.16 mmol), $Pd(PPh_3)_4$ (0.5303 g, 0.46 mmol), PPh_3 (0.1601 g, 0.61 mmol), a stir bar, and dry toluene (100 mL). Keeping the contents under nitrogen, the flask was equipped with a reflux condenser with a nitrogen inlet and two teflon stoppers. The reaction was refluxed for 44 h. After cooling to room temperature the solution was filtered through a course frit loaded with Celite. The Celite was rinsed with ethyl acetate (100 mL). The filtrate was transferred to a separatory funnel and washed with saturated sodium bicarbonate (3 x 50 mL), water (3 x 50 mL), and brine (2 x 50 mL). The organic layer was dried with Na_2SO_4, then filtered through a course frit and solvent was removed from the filtrate by rotary evaporation. Crude product was dry loaded on silica by dissolving in DCM and adding silica (5 g), and solvent was removed by oil pump vacuum. The crude product/silica mixture was loaded on a silica (75 g) column, eluting with a mixture of hexanes and ethyl acetate, starting at 100 % hexanes and going to a 10 % ethyl acetate mixture. Fractions containing only a TLC spot of $R_f \sim 0.2$, using hexanes:ethyl acetate (9:1) to elute, were combined. Solvent was removed by rotary evaporation and dried under high vacuum pump to yield ethyl 6'-methyl-2,2'-bipyridine-6-carboxylate as white solid (**4.15**, 1.0910 g, 4.50 mmol, 52 % yield). Anal. calcd. for $C_{14}H_{14}N_2O_2$ (mol. wt. 242.28): C, 69.41; H, 5.82; N, 11.56. Found C, 70.30; H, 6.11; N, 12.07.

^{1}H NMR ($CDCl_3$, 499.944 MHz) δ 8.62 (d, *J* = 7.8 Hz, 1H), 8.34 (d, *J* = 7.8 Hz, 1H), 8.09 (d, *J* = 7.8 Hz, 1H), 7.92 (t, *J* = 7.8 Hz, 1H), 7.71 (t, *J* = 7.8 Hz, 1H), 7.18 (d, *J* = 7.8 Hz, 1H), 4.48 (q, *J* = 7.1 Hz, 2H), 2.62 (s, 3H), 1.46 ppm (t, *J* = 7.1 Hz, 3H). ^{13}C NMR ($CDCl_3$, 125.723 MHz) δ 165.3, 157.8, 156.6, 154.6, 147.7, 137.6, 137.1, 124.7, 124.1, 123.7, 118.6, 61.7, 24.6, 14.3 ppm.

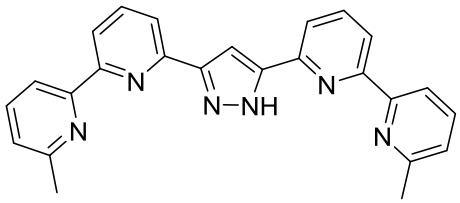

Synthesis of 4.16

To a vial in a glovebox added ethyl 6'-methyl-2,2'-bipyridine-6-carboxylate (**4.15**, 800.4 mg, 3.30 mmol), 6'-methyl-6-acetyl-(2,2'-bipyridine) (**4.13**, 703.7 mg, 3.32 mmol), sodium ethoxide (247.8 mg, 3.64 mmol), dry toluene (4.0 mL). The reaction was stirred at room temperature for 42 h, after which time it was transferred to a separatory funnel and acetic acid (5 M, 35 mL) was added. Product was extracted with DCM (3 x 40 mL), then washed with water (3 x 40 mL) and brine (40 mL). The organic layer was dried with Na_2SO_4, filtered through a course frit and solvent was removed from the filtrate by rotary evaporation. The obtained solid was transferred to a medium frit with DCM (10 mL) and washed with DCM (2 x 3 mL), then transferred to a vial (Fraction 1). Solvent of the filtrate was removed by rotary evaporation and the residual solid was transferred to a medium frit and washed with DCM (2 x 2 mL and 1 mL) (Fraction 2). Fractions 1 and 2 were combined into a three neck round bottom flask (100 mL) and dried under oil pump vacuum, yielding the crude enol (900.7 mg). Benzene (35 mL) was added to the flask and a Dean-Stark trap with a nitrogen inlet and two Teflon septa was added. The reaction vessel was purged with nitrogen for 5 min, then hydrazine hydrate (480 µL) was added. The reaction was refluxed for 2 d. After cooling to room temperature the mixture was transferred to a separatory funnel with benzene (50 mL) and the organic layer was washed with water (3 x 25 mL) and brine (25 mL). The organic layer was dried with Na_2SO_4, filtered through a course frit, and solvent was removed from the filtrate by rotary evaporation and the residue stored under oil pump vacuum, yielding **4.16** (795.1 mg, 1.96 mmol, 60 % yield) as off-white solid. Anal. calcd. for $C_{25}H_{20}N_6$ (mol. wt. 404.48): C, 74.24; H, 4.98; N, 20.78. Found C, 74.14; H, 5.68; N, 20.88.

^{1}H NMR ($CDCl_3$, 599.417 MHz) δ 12.1 (br s, 1H), 8.34 (d, *J* = 8.6 Hz, 2H), 8.31 (br d, *J* = 6.6 Hz, 2H), 7.90 (br s, 2H), 7.78 (t, *J* = 7.7 Hz, 2H), 7.64 (br t, *J* = 7.1 Hz, 2H), 7.53

(s, 1H), 7.14 (d, J = 7.6 Hz, 2H), 2.63 ppm (s, 6H). ^{13}C NMR ($CDCl_3$, 150.724 MHz) δ 157.8, 155.8, 155.3, 149 (br), 137.5, 136.9, 123.3, 120.1, 119.8, 118.3, 101.8, 24.6 ppm. Several ^{1}H NMR peaks are broad, and one of the ^{13}C NMR peaks is not observed, most likely that of the 3/5 position on the pyrazole due to the tautomerization of the pyrazole.

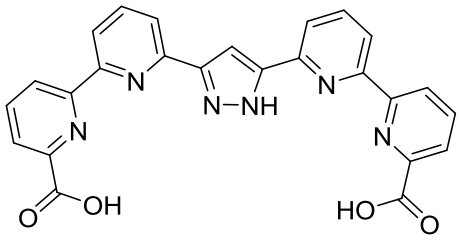

Attemped Synthesis of 4.17

CrO_3 (360.6 mg, 3.61 mmol) and a stir bar were added to a two neck round bottom flask (15 mL). **4.16** (220.4 mg, 0.545 mmol) and H_2SO_4 (2.0 mL) were added to a vial and sonicated until **4.16** completely dissolved. The solution of **4.16** was added to the round bottom flask with CrO_3 and allowed to stir for 4 d. The reaction was then added dropwise to water (100 mL), and the mixture was then filtered through a fine frit and the solids washed with water (3 x 5 mL) and Et_2O (3 x 15 mL). A small amount of retained solid was transferred to an NMR tube with d_6-DMSO for an initial ^{1}H NMR spectrum, which showed an impurity. Authentic **4.18** was then added, followed by acquiring another ^{1}H NMR spectrum showing the increase of the minor peaks. Further purification was not successful.

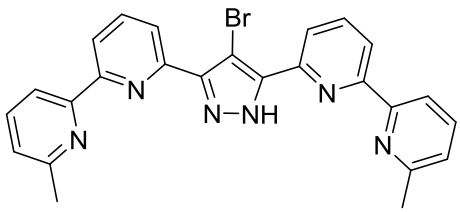

Synthesis of 4.19

To a three neck round bottom flask (100 mL) added **4.16** (914.3 mg, 2.26 mmol), N-bromosuccinimide (418.2 mg, 2.35 mmol), chloroform (60 mL), and stir bar. The reaction stirred at room temperature for 1.5 h, then filtered through a fine frit. The solution was transferred to a separatory funnel and washed with saturated sodium bicarbonate (3 x 30 mL), water (3 x 30 mL), and brine (30 mL). The organic layer was dried with Na_2SO_4, filtered through a course frit, and solvent was removed from the

filtrate by rotary evaporation and the residue stored under oil pump vacuum, yielding **4.19** (1.0251 g, 2.12 mmol, 94 % yield) as off-white solid. Product was used without further purification.

^{1}H NMR ($CDCl_3$, 499.944 MHz) δ 8.42 (d, *J* = 8.1 Hz, 2H), 8.32 (d, *J* = 7.6 Hz, 2H), 8.24 (d, *J* = 7.6 Hz, 2H), 7.89 (t, *J* = 7.8 Hz, 2H), 7.69 (t, *J* = 7.7 Hz, 2H), 7.19 (d, *J* = 7.6 Hz, 2H), 2.67 ppm (s, 6H). ^{13}C NMR ($CDCl_3$, 125.723 MHz) δ 157.9, 155.8, 155.2, 148.5 (br), 137.6, 137.2, 123.5, 121.3, 120.5, 118.5, 91.4, 24.6 ppm.

Several ^{1}H NMR peaks were broad, and one of the ^{13}C peaks is not observed, most likely the 3/5 position on the pyrazole.due to the tautamerization of the pyrazole hydrogen.

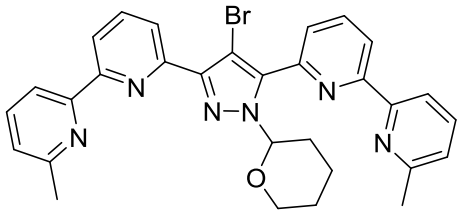

Synthesis of 4.20

To a vial was added **4.19** (1.0008 g, 2.07 mmol), trifluoroacetic acid (20 µL, 0.26 mmol), 3,4-dihydro-2H-pyran (15 mL), and a stir bar. The reaction vial was heated in an 80 ^{o}C oil bath for 4 h. After cooling to room temperature excess 3,4-dihydro-2H-pyran was removed by rotary evaporation. The residual mixture was dissolved in DCM (25 mL) and washed with water (3 x 20 mL). The organic layer was dried with Na_2SO_4, filtered through a course frit, and solvent was removed from the filtrate by rotary evaporation. The crude product was purified on a Combiflash, eluting with a mixture of hexanes and ethyl acetate, starting at 100 % hexanes and going to a 30 % ethyl acetate mixture over 20 min. Fractions containing product were combined and solvent was removed by rotary evaporation and the residue stored under oil pump vacuum, yielding **4.20** (0.6218 g, 1.10 mmol, 53 % yield or 45 % yield over two steps) as white solid. Anal. calcd. for $C_{30}H_{27}BrN_6O$ (mol. wt. 567.49): C, 63.50; H, 4.80; N, 14.81. Found C, 63.75; H, 5.25; N, 14.59.

^{1}H NMR ($CDCl_3$, 599.386 MHz) δ 8.57 (dd, *J* = 7.9, 1.1 Hz, 1H), 8.55 (d, *J* = 7.8 Hz, 1H), 8.47 (dd, *J* = 7.9, 1.1 Hz, 1H), 8.29 (d, *J* = 7.9 Hz, 1H), 8.09 (dd, *J* = 7.7, 1.1 Hz, 1H), 8.01 (t, *J* = 7.9 Hz, 1H), 7.89 (t, *J* = 7.7 Hz, 1H), 7.87 (dd, *J* = 7.7, 0.9 Hz, 6H), 7.73

(d, *J* = 7.7 Hz, 1H), 7.72 (d, *J* = 7.7 Hz, 1H), 7.22 (d, *J* = 7.5 Hz, 1H), 7.17 (d, *J* = 7.3 Hz, 1H), 5.89 (dd, *J* = 9.9, 2.4 Hz, 1H), 4.07-4.04 (m, 1H), 3.48-3.44 (m, 1H), 2.68 (s, 3H), 2.65 (s, 3H), 2.67-2.61 (m, 1H), 2.14-2.08 (m, 2H), 1.77-1.72 (m, 1H), 1.63-1.55 (m, 1H), 1.52-1.48 ppm (m, 1H). ^{13}C NMR ($CDCl_3$, 150.731 MHz) δ 158.0, 157.6, 156.4, 155.8, 155.5, 155.0, 151.0, 147.8, 147.2, 141.8, 137.5, 137.2, 137.1, 137.1, 125.8, 123.6, 123.2, 122.3, 120.6, 119.9, 118.7, 118.1, 94.3, 85.6, 68.0, 29.7, 24.8, 24.7, 22.7 ppm (one peak for an sp^3 carbon appears to be missing, but it is most likely that two peaks are on top of one another, because the 24.7 ppm signal is twice as tall as the others) .

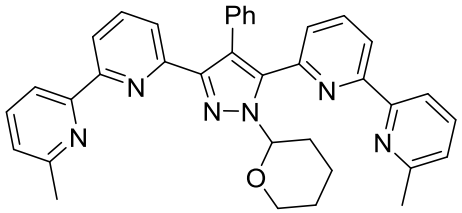

Synthesis of 4.21

4.20 (500.2 mg, 0.881 mmol), phenylboronic acid (161.5 mg, 1.32 mmol), K_2CO_3 (234.1 mg, 2.21 mmol), PPh_3 (47.0 mg, 0.179 mmol), $Pd(PPh_3)_4$ (102.2 mg, 0.09 mmol), a stir bar, toluene (14.0 mL), ethanol (3.5 mL), and water (0.7 mL) were added to a pressure vessel (48 mL) in a glovebox. The reaction was heated in a 80 ^oC for 19 h (but reaction was slow so heated at a higher temperature) followed by 100 ^oC for 24 h. After cooling to room temperature the reaction mixture was washed with water (3 x 15 mL), the washes were combined and back extracted with toluene (2 x 20 mL). The organic layers were then combined and dried with Na_2SO_4, then filtered through a course frit. Solvent was removed from the filtrate by rotary evaporation and under oil pump vacuum, to yield a mixture of product and protiodebrominated side product (~1 to 0.45). NBS (64.0 mg, 0.360 mmol) was added to a round bottom flask with $CHCl_3$ (30 mL) followed by the mixture of products. There was no change in the ^1H NMR spectrum so more NBS (62.8 mg, 0.353 mmol) was added followed by more NBS (20.0 mg, 0.112 mmol) which fully regenerated the **4.20** starting material from the protiodebrominated side product. The reaction was then filtered through medium frit, washing the solid with $CHCl_3$ (10 mL). The combined organic layers were then washed with saturated sodium bicarbonate (3 x 30 mL) and water (3 x 30 mL), dried with Na_2SO_4, and filtered through a course frit.

Solvent was removed by rotary evaporation from the filtrate and the residue stored under oil pump vacuum. This mixture was then transferred to a pressure vessel (48 mL) with phenylboronic acid (162.9 mg, 1.34 mmol), K_2CO_3 (265.4 mg, 2.50 mol), PPh_3 (47.3 mg, 0.18 mmol), $Pd(PPh_3)_4$ (102.0 mg, 0.09 mmol), a stir bar, toluene (14.0 mL), ethanol (3.5 mL), and water (0.7 mL). The reaction was then heated in a 100 ^oC oil bath for 21 h to give still a mixture of **4.21** and protiodebrominated species, but in a much better ratio (1 : 0.12) than before. The reaction mixture was then washed with water (3 x 15 mL). The aqueous washes were combined and back-extracted with toluene (2 x 20 mL). The organic layers were combined and dried with Na_2SO_4, then filtering through a course frit. Solvent was removed from the filtrate by rotary evaporation and under oil pump vacuum. Crude product was dry loaded on silica by dissolving in DCM and adding silica (5 g), solvent was removed by oil pump vacuum. The crude product/silica mixture was loaded on a silica (50 g) column, eluting with a mixture of hexanes and triethylamine, starting at 100 % hexanes and going to a 30 % triethylamine mixture. Care is needed in the separation, because the protiodebrominated side product spot is very close to the product spot with an $R_f \sim 0.35$. Fractions containing only a TLC spot of 0.4, using hexanes:triethylamine (7:3) to elute, were combined. Solvent was removed by rotary evaporation and the residue stored under high vacuum pump to yield **4.21** (192.7 mg, 0.341 mmol, 39 % yield) as white solid. Anal. calcd. for $C_{36}H_{32}N_6O$ (mol. wt. 564.69): C, 76.57; H, 5.71; N, 14.88. Found C, 77.52; H, 6.21; N, 15.39.

^1H NMR (599 MHz, $CDCl_3$) δ 8.39 (dd, *J* = 7.9, 1.0 Hz, 1H), 8.29 (dd, *J* = 7.8, 1.0 Hz, 1H), 8.17 (d, *J* = 7.8 Hz, 1H), 8.04 (dd, *J* = 7.8, 1.0 Hz, 1H), 7.79 (t, *J* = 7.8 Hz, 1H), 7.70 (t, *J* = 7.7 Hz, 1H), 7.66 (t, *J* = 7.8 Hz, 1H), 7.34 (d, *J* = 7.8 Hz, 1H), 7.30 – 7.27 (m, 2H), 7.27 – 7.23 (m, 3H), 7.19 (d, *J* = 7.6 Hz, 1H), 7.12 (dd, *J* = 7.7, 1.0 Hz, 1H), 7.08 (d, *J* = 7.9 Hz, 1H), 7.02 (d, *J* = 7.6 Hz, 1H), 5.99 (dd, *J* = 10.0, 2.4 Hz, 1H), 4.17 – 4.07 (m, 1H), 3.52 (td, *J* = 11.6, 2.4 Hz, 1H), 2.80 – 2.70 (m, 1H), 2.64 (s, 3H), 2.55 (s, 3H), 2.22 – 2.10 (m, 2H), 1.86 – 1.75 (m, 1H), 1.67-1.59 (m, 1H), 1.55-1.50 ppm (m, 1H). ^{13}C NMR ($CDCl_3$, 150.731 MHz) δ 158.0, 157.2, 156.1, 155.6, 155.3, 155.0, 152.0, 148.5, 148.5, 141.2, 137.1, 136.9, 136.5, 134.6, 131.0, 128.5, 128.0, 127.0, 126.1, 125.6, 123.4,

122.8, 122.0, 119.9, 119.0, 118.5, 118.1, 85.3, 68.1, 30.1, 25.0, 24.6, 24.6, 23.0. The C*H*Cl_3 peak was under other ^{1}H NMR peaks so could not be used as reference.

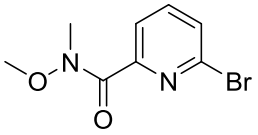

Synthesis of 6-bromo-*N*-methoxy-*N*-methylpicolinamide (4.23)

To a three neck round bottom flask (100 mL) in a glovebox added 6-bromopicolinic acid (**4.22**, 6.0011 g, 29.70 mmol), 1,1'-carbonyldiimidazole (7.2330 g, 44.60 mmol), and a stir bar. The reaction vessel was transferred to the hood, keeping the contents under nitrogen, and the flask was equipped with a nitrogen inlet and two septa. DMF (36 mL) was added to the reaction vessel, gas evolved and the reaction was stirred for 2 h giving a homogeneous orange solution. After the 2 h *N*,*O*-dimethylhydroxylamine HCl (4.5288 g, 46.43 mmol) was added and allowed to stir for another 2 h. Water (120 mL) was added. The reaction mixture was transferred to a separatory funnel where product was extracted with ethyl acetate (3 x 120 mL), and the phases were combined then washed with water (3 x 120 mL) and brine (30 mL). The organic layer was dried with Na_2SO_4, filtered through a course frit and solvent was removed from the filtrate by rotary evaporation. Crude product was purified on a silica (84 g) column, eluting with a mixture of hexanes and ethyl acetate, starting at 3:1 ratio and going to a 1:1 mixture. Fractions containing a TLC spot of $R_f \sim 0.5$, using hexanes:ethyl acetate (1:1) to elute, were combined and solvent was removed by rotary evaporation. Product was further purified by kugelrohr distillation (150 mtorr, 115 ^oC) yielding 6-bromo-*N*-methoxy-*N*-methylpicolinamide (**4.23**, 6.2389 g, 25.46 mmol, 86 % yield) as colorless oil. Product was used without further purification.

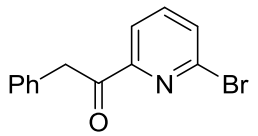

Synthesis of 4.24

To a three neck round bottom flask (100 mL) equipped with a reflux condenser with a nitrogen inlet, septa, and teflon stopper was added a stir bar and magnesium shavings (1.3580 g, 55.86 mmol). The reaction vessel was dried under oil pump vacuum

and then filled with nitrogen. Dry diethyl ether (50 mL) was added to the flask followed by benzyl chloride (3.3816 g, 26.71 mmol) over 30 sec. The reaction stirred for 45 min, as it refluxed for about 20 min. To a three neck round bottom flask (250 mL) equipped with an addition funnel with septum, nitrogen inlet, and thermometer added 6-bromo-*N*-methoxy-*N*-methylpicolinamide (**4.23**, 5.0005 g, 20.40 mmol) and a stir bar. Dry diethyl ether (40 mL) was transferred to the reaction vessel, which was cooled into an acetone/ ice bath. The benzyl Grignard solution was transferred by cannula to the addition funnel, and the solution was added dropwise over 45 min keeping the temperature below -5 ^{o}C. The reaction was then warmed to room temperature and stirred for 19 h, after which time EtOH:HCl (9:1, 15 mL) was added on ice. The mixture was transferred to a separatory funnel with DCM (120 mL) and washed with saturated sodium bicarbonate (120 mL), water (3 x 120 mL), and brine (40 mL). The organic layer was dried with Na_2SO_4, filtered through a course frit and solvent removed from the filtrate by rotary evaporation. The crude product was loaded on a silica (50 g) column, eluting with a mixture of hexanes and ethyl acetate, starting at 100 % hexanes and going to a 10 % ethyl acetate mixture. All fractions containing a TLC spot of $R_f \sim 0.3$, using hexanes:ethyl acetate (9:1) to elute were combined. Solvent was removed by rotary evaporation and the residue was further purified by kugelrohr distillation (220 mtorr, 135 ^{o}C) yielding **4.24** as white solid (3.4211 g, 12.39 mmol, 61 % yield). Anal. calcd. for $C_{13}H_{10}BrNO$ (mol. wt. 276.13): C, 56.55; H, 3.65; N, 5.07. Found C, 56.23; H, 4.00; N, 5.16.
^{1}H NMR ($CDCl_3$, 499.944 MHz) δ 8.01 (dd, *J* = 6.7, 1.8 Hz, 1H), 7.71-7.66 (m, 2H), 7.38-7.33 (m, 4H), 7.29-7.24 (m, 1H), 4.52 ppm (s, 2H). ^{13}C NMR ($CDCl_3$, 125.723 MHz) δ 197.5, 153.6, 141.2, 139.2, 134.2, 131.8, 130.0, 128.5, 126.8, 121.2, 44.1 ppm. In the ^{1}H NMR spectrum, the C*H*Cl_3 peak was under other peaks so could not be used as reference.

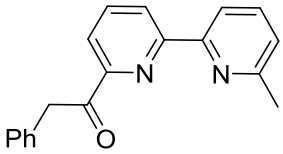

Synthesis of 4.25

To a three neck round bottom flask (100 mL) in a glovebox added **4.24** (3.0037 g, 10.88 mmol), 2-methyl-6-(tri(n-butyl)stannyl)pyridine[18] (**4.11**, 4.1554 g, 10.87 mmol), $Pd(PPh_3)_4$ (0.2518 g, 0.22 mmol), PPh_3 (0.2006 g, 0.76 mmol), dry toluene (35.0 mL), and a stir bar. Keeping the contents under nitrogen, the flask was equipped with a reflux condenser with a nitrogen inlet, septum, and teflon stopper. The reaction was refluxed for 16 h, after which time was cooled to room temperature and transferred to a separatory funnel and washed with saturated sodium bicarbonate (3 x 50 mL), water (3 x 50 mL), and brine (50 mL). The organic layer was dried with Na_2SO_4, filtered through a course frit and solvent removed from the filtrate by rotary evaporation. The crude oil was loaded on a silica (120 g) column, eluting with a mixture of hexanes and ethyl acetate, starting at 100 % hexanes and going to a 10 % ethyl acetate mixture. Fractions containing a TLC spot of $R_f \sim 0.25$, using hexanes:ethyl acetate (9:1) to elute were combined. Solvent was removed by rotary evaporation and the white solid was stored under oil pump vacuum yielding **4.25** (2.2129 g, 7.67 mmol, 71 % yield). Anal. calcd. for $C_{19}H_{16}N_2O$ (mol. wt. 288.35): C, 79.14; H, 5.59; N, 9.72. Found C, 78.88; H, 5.94; N, 9.87.
^{1}H NMR (599.3 MHz, $CDCl_3$) δ 8.67 (dd, *J* = 7.9, 1.1 Hz, 1H), 8.38 (dd, *J* = 7.8, 0.9 Hz, 1H), 8.06 (dd, *J* = 7.7, 1.1 Hz, 1H), 7.95 (t, *J* = 7.8 Hz, 1H), 7.79 (t, *J* = 7.7 Hz, 1H), 7.40 – 7.36 (m, 2H), 7.34 – 7.30 (m, 2H), 7.27 – 7.22 (m, 2H), 4.68 (s, 2H), 2.67 ppm (s, 3H).

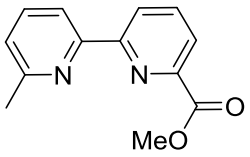

Synthesis of methyl 6'-methyl-2,2'-bipyridine-6-carboxylate (**4.27**)

To a three neck round bottom flask (250 mL) in a glovebox added methyl 6-bromopyridine-2-carboxylate (**4.26**, 3.0080 g, 13.92 mmol), 2-methyl-6-(tri(n-butyl)stannyl)pyridine[18] (**4.11**, 5.8578 g, 15.33 mmol), $Pd(PPh_3)_4$ (0.8050 g, 0.70 mmol), PPh_3 (0.2579 g, 0.98 mmol), a stir bar, and dry toluene (150 mL). Keeping the contents

under nitrogen, the flask was equipped with a reflux condenser with a nitrogen inlet and two teflon stoppers. The reaction was refluxed for 13 h. After cooling to room temperature the solution was filtered through a course frit loaded with Celite. The Celite was rinsed with toluene (3 x 10 mL). The filtrate was transferred to a separatory funnel and washed with saturated sodium bicarbonate (3 x 75 mL), water (3 x 75 mL), and brine (60 mL). The organic layer was dried with Na_2SO_4, then filtered through a course frit and solvent was removed from the filtrate by rotary evaporation. Crude product was dry loaded on silica by dissolving in DCM and adding silica (4.0 g), solvent was removed by oil pump vacuum. The crude product/silica mixture was loaded on a silica (60 g) column, eluting with a mixture of hexanes and ethyl acetate, starting at 100 % hexanes and going to a 30 % ethyl acetate mixture. Fractions containing only a TLC spot of R_f ~ 0.4, using hexanes:ethyl acetate (7:3) to elute were combined. Solvent was removed by rotary evaporation and the residue stored under high vacuum pump to yield methyl 6'-methyl-2,2'-bipyridine-6-carboxylate as white solid (**4.27**, 1.8467 g, 8.09 mmol, 58 % yield). Anal. calcd. for $C_{13}H_{12}N_2O_2$ (mol. wt. 228.25): C, 68.41; H, 5.30; N, 12.27. Found C, 68.12; H, 5.79; N, 12.38.

^{1}H NMR ($CDCl_3$, 499.944 MHz) δ 8.62 (d, *J* = 7.8 Hz, 1H), 8.31 (d, *J* = 7.8 Hz, 1H), 8.10 (d, *J* = 7.6 Hz, 1H), 7.93 (t, *J* = 7.8 Hz, 1H), 7.71 (t, *J* = 7.7 Hz, 1H), 7.18 (d, *J* = 7.8 Hz, 1H), 4.02 (s, 3H), 2.62 ppm (s, 3H). ^{13}C NMR ($CDCl_3$, 125.723 MHz) δ 165.9, 157.9, 156.7, 154.5, 147.4, 137.7, 137.1, 124.7, 124.3, 123.7, 118.6, 52.7, 24.5 ppm.

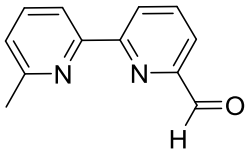

Synthesis of 6'-methyl-6-formyl-2,2'-bipyridine) (4.28)

Methyl 6'-methyl-2,2'-bipyridine-6-carboxylate (**4.27**, 117.3 mg, 0.51 mmol), MeOH (4.0 mL), and a stir bar were added to a vial. The vial was cooled in a water/ice bath and $NaBH_4$ (75.9 mg, 2.00 mmol) was added portionwise, and thenthe mixture was allowed to warm to room temperature. The mixture stirred for 21 h and after no change was observed in NMR spectra of aliquots, more $NaBH_4$ (122.2 mg, 3.23 mmol) was added at room temperature and the mixture stirred for 7 h. Solvent was removed by a

flow of air, then the residue dissolved in DCM (6 mL) and washed with water (3 x 3 mL) and brine (3 mL). The organic layer was dried with Na_2SO_4, and solid was removed by filtration through a pipet loaded with cotton. Solvent was removed by flow of air to yield the crude alcohol. ^{1}H NMR (599.3 MHz, $CDCl_3$) δ 8.36 (ddd, *J* = 7.8, 1.6, 0.7 Hz, 1H), 8.21 (ddd, *J* = 7.8, 0.9, 0.5 Hz, 1H), 7.81 (t, *J* = 7.7 Hz, 1H), 7.72 (t, *J* = 7.7 Hz, 1H), 7.23 (ddd, *J* = 7.7, 1.6, 0.7 Hz, 1H), 7.19 (ddd, *J* = 7.6, 0.9, 0.5 Hz, 1H), 4.83 (s, 2H), 4.03 (s, 1H), 2.65 ppm (s, 3H). In a glovebox the alcohol was transferred to a two neck round bottom flask (15 mL) with SeO_2 (58.8 mg, 0.53 mmol) and 1,4-dioxane (4 mL). The flask was equipped with a reflux condenser and a septum, then placed in a 120 ^{o}C oil bath for 15 min. The rust colored heterogeneous mixture was then filtered through a pipet loaded with cotton and solvent was removed by a flow of air. The red mixture was dissolved in DCM (3 mL) and filtered through a pad of Celite. Solvent was removed under oil pump vacuum yielding 6'methyl-6-formyl-2,2'-bipyridine as yellow solid (**4.28**, 64.8 mg, 0.327 mmol, 64 % yield). Product was used without further purification.
^{1}H NMR (599.3 MHz, $CDCl_3$) δ 10.18 (d, *J* = 0.7 Hz, 1H), 8.69 (dd, *J* = 7.2, 1.8 Hz, 1H), 8.34 (ddd, *J* = 7.8, 0.9, 0.5 Hz, 1H), 8.02 – 7.95 (m, 2H), 7.76 (t, *J* = 7.7 Hz, 1H), 7.23 (ddd, *J* = 7.6, 1.0, 0.5 Hz, 1H), 2.66 ppm (s, 3H).

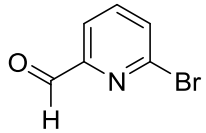

Synthesis of 6-bromopicolinaldehyde (4.31)

To a 1 L three neck round bottom flask was added 2,6-dibromopyridine (**4.30**, 40.00 g, 168.9 mmol) and a stir bar, and an addition funnel with septum, a thermometer, and a nitrogen inlet were installed on the flask. The reaction flask was left on high vacuum pump overnight and back filled with nitrogen (3x). Dry DCM (800 mL) was transferred by cannula to the reaction, which is then placed in an ethyl acetate and liquid nitrogen bath. N-butyllithium solution (2.5 M in hexanes, 67.5 mL, 168.8 mmol) was transferred by cannula to the addition funnel, and added drop wise over 60 min keeping the temperature below -78 ^{o}C. The addition funnel was rinsed with dry DCM (20 mL), and the green solution was allowed to stir for 50 min. DMF (20.0 mL, 260 mmol) was

added quickly over 2 min; after 60 min the flask was removed from the cold bath and let warm to 10 ^{o}C, at which time methanol (120 mL) was added. The reaction mixture was transferred to a separatory funnel and the organic layer was washed with saturated sodium bicarbonate (3 x 200 mL). The aqueous layer was back extracted with DCM (2 x 100 mL), the combined organic layers were washed with brine (50 mL) and dried with Na_2SO_4. The organic layer was filtered through a course frit, and solvent was removed from the filtrate by rotary evaporation to give a red oil. The crude product was partially purified by kugelrohr distillation (300 mtorr, room temperature to 110 ^{o}C), and the oily solid distillate was dissolved in acetone and transferred to a round bottom flask. Solvent was removed by rotary evaporation; solid was transferred to a medium frit and washed with hexanes (3 x 25 mL). The solid was transferred to a vial and dried under high vacuum pump yielding 6-bromopicolinaldehyde as light yellow solid (**4.31**, 19.7478 g, 106.2 mmol, 62.9 % yield). Anal. calcd. for C_6H_4BrNO (mol. wt. 186.01): C, 38.74; H, 2.17; N, 7.53. Found C, 38.54; H, 2.20; N, 7.58

^{1}H NMR (599.3 MHz, $CDCl_3$) δ 10.01 (d, *J* = 0.7 Hz, 1H), 7.93 (dd, *J* = 7.1, 1.3 Hz, 1H), 7.76 (td, *J* = 7.5, 0.7 Hz, 1H), 7.73 ppm (dd, *J* = 7.9, 1.3 Hz, 1H). ^{13}C NMR (150.7 MHz, $CDCl_3$) δ 191.6, 153.4, 142.5, 139.3, 132.6, 120.3 ppm.

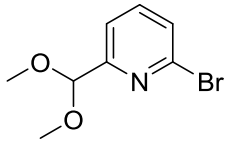

Synthesis of 6-bromo-2-(dimethoxymethyl)pyridine (4.32)

To a 500 mL three neck round bottom flask added 6-bromopicolinaldehyde (**4.31**, 19.9135 g, 107.1 mmol), p-toluenesulfonic acid hydrate (0.4238 g, 2.23 mmol) and a stir bar, and a reflux condenser with nitrogen inlet, and two septa were installed. Anhydrous methanol (200 mL) and trimethyl orthoformate (47.0 mL, 430 mmol) were added to the reaction flask, which was refluxed for 11 h under nitrogen. Once the reaction cooled to room temperature, the solution was transferred to a round bottom flask and solvent was removed by rotary evaporation. The crude product was purified by kugelrohr distillation (550 mtorr, 100 ^{o}C to 110 ^{o}C), yielding 6-bromo-2-(dimethoxymethyl)pyridine (**4.32**,

22.9005 g, 98.68 mmol, 92 % yield) as colorless oil. Anal. calcd. for $C_8H_{10}BrNO_2$ (mol. wt. 232.08): C, 41.40; H, 4.34; N, 6.04. Found C, 40.78; H, 4.36; N, 6.19.
^{1}H NMR ($CDCl_3$, 599.354 MHz) δ 7.59 (dd, *J* = 7.9, 7.5 Hz, 1H), 7.52 (d, *J* = 7.5 Hz, 1H), 7.45 (d, *J* = 7.9 Hz, 1H), 5.30 (s, 1H), 3.41 ppm (s, 6H). ^{13}C NMR ($CDCl_3$, 150.722 MHz) δ 158.8, 141.4, 138.9, 128.0, 120.0, 103.6, 54.0 ppm.

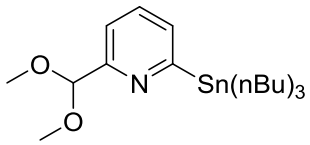

Synthesis of 2-(dimethoxymethyl)-6-(tributylstannyl)pyridine (4.33)

To a 500 mL three neck round bottom flask added 6-bromo-2-(dimethoxymethyl)pyridine (**4.32**, 20.0046 g, 86.20 mmol) and a stir bar, and an addition funnel with septum, a thermometer, and a nitrogen inlet were installed. The reaction flask was purged with nitrogen and dry diethyl ether (200 mL) was transferred by cannula to the reaction, which was placed in a toluene and liquid nitrogen bath. N-butyllithium (2.5 M in hexanes, 35.0 mL, 87.5 mmol) was transferred by cannula to the addition funnel, and the solution added drop wise over 30 min keeping the temperature below -95 ^{o}C. The reaction was allowed to warm up to -78 ^{o}C and maintained there for 1 h, after which time was cooled back to -95 ^{o}C. Tributyltin chloride (26.0 mL, 95.85 mmol) was added over 15 min, then the mixture was allowed to warm to -78 ^{o}C and kept for 1 hour. The reaction was then removed from the cold bath and allowed to warm to room temperature. The reaction mixture was filtered through a course frit loaded with Celite, washing the Celite with DCM. Solvent was removed by rotary evaporation and the residue purified by kugelrohr distillation (300 mtorr, 120 ^{o}C to 150 ^{o}C), transferring the yellow oily distillate to a vial yielding 2-(dimethoxymethyl)-6-(tributylstannyl)pyridine + 0.1 Bu_3SnCl (**4.33**, 35.8365 g, 75.48 mmol, 88 % yield)[a]. Anal. calcd. for $C_{20}H_{37}NO_2Sn$ $(SnC_{12}H_{27}Cl)_{0.1}$ (mol. wt. 474.78): C, 53.63; H, 8.43; N, 2.95. Found C, 53.76; H, 8.55; N, 3.27.
^{1}H NMR (400 MHz, $CDCl_3$) δ 7.58 – 7.47 (m, 1H), 7.41 – 7.30 (m, 2H), 5.33 (s, 1H), 3.44 (s, 6H), 1.70 – 1.46 (m, 6H), 1.43 – 1.25 (m, 6H), 1.22 – 1.00 (m, 6H), 0.88 ppm (t,

J = 7.3 Hz, 9H). ^{13}C NMR (126 MHz, $CDCl_3$) δ 173.0 , 157.6 , 133.7 (d, J = 31.1 Hz)[b], 132.1 (dd, J = 76.9, 1.7 Hz)[b], 119.0 (d, J = 10.6 Hz)[b], 105.6 , 54.1 , 29.1 (d, J = 20.7 Hz)[b], 27.3 (dd, J = 54.4. 1.2 Hz)[b], 13.7, 10.0 ppm (dd, J = 330.2, 7.5 Hz)[b].

[a]Attempts at purification on silica lead to protiodestannylation, so the 90% pure sample was used.

[b]Tin satellite.

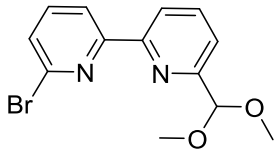

Synthesis of 6-bromo-6'-(dimethoxymethyl)-2,2'-bipyridine (4.34)

In a glovebox to a screw cap pressure vessel (48 mL) were added 2-(dimethoxymethyl)-6-(tributylstannyl)pyridine 90-85% pure (**4.33**, 2.5405 g, 5.35 mmol), 2,6-dibromopyridine (**4.30**, 1.1859 g, 5.01 mmol), lithium chloride (0.3927g, 9.26 mmol), $Pd(PPh_3)_4$ (0.0874 g, 0.08 mmol), toluene (17 mL), and a stir bar. The reaction was heated in a 120 ^{o}C oil bath for 21 h then cooled to room temperature and transferred to a separatory funnel. The reaction mixture was washed with water (3 x 20 mL) and brine (20 mL) then dried with Na_2SO_4, which was removed by filtering through a course frit and solvent removed from the filtrate by rotary evaporation. The crude oil was loaded on a silica (25 g) column, eluting with a mixture of hexanes and ethyl acetate, starting at 100 % hexanes and going to a 10 % ethyl acetate mixture. Fractions containing only a TLC spot of R_f ~ 0.25, using hexanes:ethyl acetate (9:1) to elute were combined. Solvent was removed by rotary evaporation and dried under high vacuum pump to yield 6-bromo-6'-(dimethoxymethyl)-2,2'-bipyridine (**4.34**, 0.8507 g, 2.75 mmol, 55 % yield) as white fluffy solid. Anal. calcd. for $C_{13}H_{13}BrN_2O_2$ (mol. wt. 309.16): C, 50.51; H, 4.24; N, 9.06. Found C, 51.61; H, 4.47; N, 9.48.

^{1}H NMR ($CDCl_3$, 499.944 MHz) δ 8.46 (d, J = 7.8 Hz, 1H), 8.39 (d, J = 7.8 Hz, 1H), 7.87 (t, J = 7.8 Hz, 1H), 7.66(t, J = 7.8 Hz, 1H), 7.59 (d, J = 7.8 Hz, 1H), 7.49 (d, J = 7.8 Hz, 1H), 5.43 (s, 1H), 3.46 ppm (s, 6H). ^{13}C NMR ($CDCl_3$, 125.723 MHz) δ 157.2, 156.9, 153.8, 141.5, 139.2, 137.6, 128.0, 121.7, 121.2, 120.1, 104.4, 53.9 ppm.

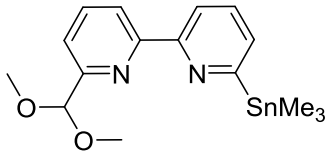

Synthesis of 6-(dimethoxymethyl)-6'-(trimethylstannyl)-2,2'-bipyridine (4.36)

2,6-bis(trimethylstannyl)pyridine[27] (**4.35**, 10.0360 g, 24.80 mmol), 6-bromo-2-(dimethoxymethyl)pyridine (**4.32**, 5.7306 g, 24.69 mmol), $Pd(PPh_3)_4$ (0.4314 g, 0.37 mmol), dry toluene (90 mL), and a stir bar were added to a three neck round bottom flask (250 mL) in a glovebox. Keeping the contents under nitrogen a reflux condenser with a nitrogen inlet and two teflon stoppers were installed. The reaction was refluxed for 6.5 h, after which time the mixture was cooled to room temperature and filtered through a course frit loaded with Celite. The Celite was washed with diethyl ether, then solvent was removed from the filtrate by oil pump vacuum (to neutralize any toxic volatile tin compounds the waste was treated with HCl). The crude orange oil was purified by kugelrohr distillation (200 mtorr, 120 ^{o}C to 140 ^{o}C) yielding 6-(dimethoxymethyl)-6'-(trimethylstannyl)-2,2'-bipyridine (**4.36**, 4.5725 g, 11.6 mmol, 47 % yield) as colorless oil; there are still minor amounts of PPh_3 and an unknown side product, but due to the sensitivity of the product it was used without further purification; purity is estimated at roughly 80 %.

^{1}H NMR ($CDCl_3$, 599.364 MHz) δ 8.52 (dd, *J* = 7.8, 0.9 Hz, 1H), 8.36[a] (dd, *J* = 8.0, 1.2 Hz, 1H), 7.86 (t, *J* = 7.8 Hz, 1H), 7.65 [a] (dd, *J* = 7.9, 7.3 Hz, 1H), 7.56 (dd, *J* = 7.7, 0.7 Hz, 1H), 7.45 [a] (dd, *J* = 7.3, 1.2 Hz, 1H), 5.45 (s, 1H), 3.47 (s, 6H), 0.39 ppm (s, with dd, *J* = 54.6, 1.2 Hz Sn satellites, 9H).^{13}C NMR ($CDCl_3$, 150.725 MHz) δ 172.6, 156.6, 156.1, 155.9, 137.2, 134.3, 131.5, 120.8, 120.8, 119.9, 104.7, 53.8, -9.4 ppm.

[a] Sn satellites are observed but the couplings appear to be multiplets.

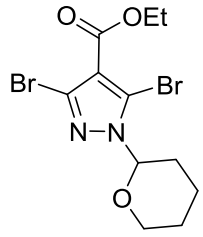

Synthesis of 3,5-dibromo-1-(tetrahydropyran)-4-ethylcarboxylate-pyrazole (4.38)

To a vial were added ethyl 3,5-dibromopyrazole-4-carboxylate[28] (**4.37**, 1.0029 g, 3.37 mmol), p-toluenesulfonic acid (4.7 mg, 0.025 mmol), 3,4-dihydro-2*H*-pyran (4.0 mL), and a stir bar. The starting material slowly dissolved, and after 40 min solvent was removed under oil pump vacuum. The white solid was transferred to a medium frit and washed with hexanes (3 x 4 mL), and the white solid was transferred to a vial and dried under oil vacuum pump, yielding **4.38** (1.0971 g, 2.87 mmol, 85 % yield). Anal. calcd. for $C_{11}H_{14}Br_2N_2O_3$ (mol. wt. 382.05): C, 34.58; H, 3.69; N, 7.33. Found C, 34.80; H, 3.51; N, 7.43.

^{1}H NMR ($CDCl_3$, 599.354 MHz) δ 5.55 (dd, *J*= 9.5, 2.4 Hz, 1H), 4.36 (q, *J*= 7.1 Hz, 2H), 4.07-4.02 (m, 1H), 3.70-3.64 (m, 1H), 2.46-2.38 (m, 1H), 2.16-2.10 (m, 1H), 1.94-1.88 (m, 1H), 1.77-1.64 (m, 2H), 1.63-1.57 (m, 1H), 1.39 ppm (t, *J*= 7.1 Hz, 3H). ^{13}C NMR ($CDCl_3$, 150.722 MHz) δ 160.6, 129.2, 119.6, 113.8, 85.4, 67.8, 60.9, 28.9, 24.6, 22.1, 14.1 ppm.

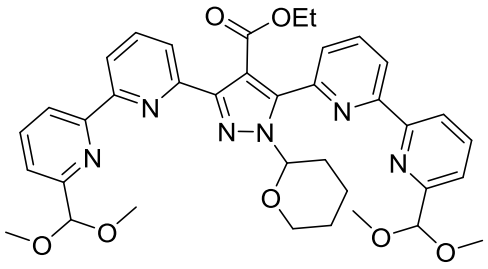

Synthesis of 4.39

6-(dimethoxymethyl)-6'-(trimethylstannyl)-2,2'-bipyridine ~ 80 % pure (**4.36**, 1.5688 g, 3.99 mmol), **4.38** (0.5094 g, 1.33 mmol), $Pd(PPh_3)_4$ (0.2307 g, 0.20 mmol), dry toluene (7.0 mL), and a stir bar were added to a vial in a glovebox. The reaction was heated in a 120 ^{o}C oil bath for 12 d, after which was filtered through a course frit loaded with Celite and washed with diethyl ether. Solvent was removed by a flow of air. Crude product was dissolved in DCM (3 mL) and purified on a silica (20.5 g) column (0.5 in. x 20 in.), eluting with a mixture of hexanes and diethyl ether, starting at a (1:1) mixture and going to a (1:2) ratio. Fractions containing a TLC spot of Rf ~ 0.25, using hexanes:diethyl ether (1:2) were combined, and removing solvent by rotary evaporation. The obtained white solid was transferred to a medium frit and washed with diethyl ether (3 x 2 mL) to yield **4.39** $(CDCl_3)_{0.25}$ (280.6 mg, 0.395 mmol, 30 % yield). Anal. calcd. for

$C_{37}H_{40}N_6O_7$ $(CDCl_3)_{0.25}$ (mol. wt. 710.86): C, 62.94 ; H, 5.74 ; N, 11.82. Found C, 62.93; H, 5.59; N, 11.99.

^{1}H NMR ($CDCl_3$, 599.361 MHz) δ 8.62 (d, *J* = 7.9 Hz, 1H), 8.48 (d, *J* = 7.9 Hz, 1H), 8.45 (d, *J* = 7.3 Hz, 1H), 8.44 (d, *J* = 6.2 Hz, 1H), 8.02(d, *J* = 7.7 Hz, 1H), 7.97 (t, *J* = 7.9 Hz, 1H), 7.89 (t, *J* = 7.8 Hz, 1H), 7.88 (t, *J* = 7.9 Hz, 1H), 7.84 (t, *J* = 7.7 Hz, 1H), 7.81 (d, *J* = 7.7 Hz, 1H), 7.61 (d, *J* = 7.5 Hz, 1H), 7.56 (d, *J* = 7.7 Hz, 1H), 5.74 (dd, *J* = 9.5, 1.6 Hz, 1H), 5.47 (s, 1H), 5.45 (s, 1H), 4.16-4.06 (m, 3H), 3.50 (s, 6H), 3.49 (br, 1H)[a], 3.48 (s, 3H), 3.47 (s, 3H), 2.67-2.60 (m, 1H), 2.14-2.12 (m, 1H), 2.08-2.05 (m, 1H), 1.80-1.74 (m, 1H), 1.62-1.51 (m, 2H), 0.95 ppm (t, *J* = 7.1 Hz, 3H). ^{13}C NMR ($CDCl_3$, 150.710 MHz) δ 165.2, 156.9, 156.6, 155.8, 155.6, 155.0, 154.9, 150.8, 150.2, 147.3, 143.6, 137.5, 137.5, 137.3, 137.2, 125.5, 122.2, 121.4, 121.2, 121.1, 120.9, 120.8, 120.4, 114.2, 104.8, 104.6, 85.1, 67.8, 60.8, 54.0, 54.0, 53.9, 53.9, 30.0, 24.8, 22.6, 13.9 ppm.

[a] Peak is hard to see in the ^{1}H NMR spectrum since it is under the methyl peaks. HSQC and COSY cross peaks confirm the location of this proton.

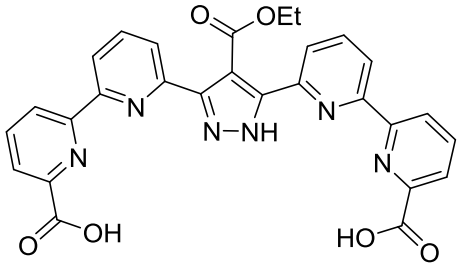

Synthesis of 4.40

To a vial was added **4.39** (167.5 mg, 0.2356 mmol), stir bar, and HCl (6 M, 4.0 mL). The mixture was sonicated until all dissolved. After stirring for 2 h, solvent was removed by rotary evaporation. The solid was dissolved in formic acid (5.0 mL) and then hydrogen peroxide (30 %, 185.7 mg) was added. After 2 h, solvent was removed by rotary evaporation and the residue stored under oil pump vacuum over phosphorus pentoxide yielding **4.40** $(H_2O)_3$ (134.7 mg, 0.2316 mmol, 98 % yield) as white solid. Anal. calcd. for $C_{28}H_{20}N_6O_6$ $(H_2O)_{2.5}$ (mol. wt. 581.54): C, 57.83 ; H, 4.33 ; N, 14.45. Found C, 58.27; H, 4.15; N, 14.05.

^{1}H NMR (500 MHz, d_6-DMSO) δ 8.68 (d, *J* = 7.8 Hz, 2H), 8.56 (d, *J* = 7.8 Hz, 2H), 8.22 (t, *J* = 7.8 Hz, 2H), 8.18 – 8.10 (m, 4H), 8.05 (d, *J* = 7.6 Hz, 2H), 4.31 (q, *J* = 7.1 Hz,

2H), 0.99 ppm (t, J = 7.1 Hz, 3H). ^{13}C NMR (125.7 MHz, d_6-DMSO)[a] δ 165.9, 165.9, 155.0, 154.2, 148.0, 138.6, 125.0, 123.8, 121.3, 120.5, 111.9, 60.7, 13.8 ppm.
[a] Three ^{13}C peaks were not observed, two of which could be very broad peaks at 148.5 and 145.0, See Figure 4.25.

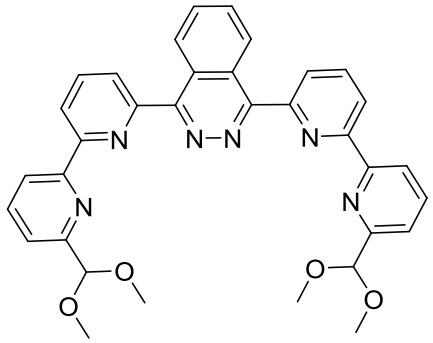

Synthesis of 4.42

To a vial in a glovebox added 6-(dimethoxymethyl)-6'-(trimethylstannyl)-2,2'-bipyridine ~ 80 % pure (**4.36**, 0.7407 g, 1.88 mmol), 1,4-dichlorophthalazine[29] (**4.41**, 0.1488 g, 0.748 mmol), $Pd(PPh_3)_4$ (0.0670 g, 0.058 mmol), dry toluene (8.0 mL). The reaction was heated in a 120 ^{o}C oil bath for 21.5 h, after which it was cooled in room temperature and filtered through a pipet loaded with Celite. The Celite was flushed with diethyl ether and solvent was removed by a flow of air. Crude product was purified on a silica (11.2 g) column (0.5 x 8 in), using a gradient of hexanes, ethyl acetate, and triethylamine, starting in a 2:1 and 5 % changed slowly to 1:2: and 5 %. Fractions containing a TLC spot of R_f~ 0.45 using 1:2 and 5 % solvent ratio were combined and solvent was removed by rotary evaporation. The obtained solid was transferred to a fine frit and washed with diethyl ether (3 x 4 mL), transferred to a vial and dried under oil pump vacuum yielding 1,4-bis(6'-(dimethoxymethyl)-[2,2'-bipyridin]-6-yl)phthalazine (**4.42**, 0.2617 g, 0.446 mmol, 60 % yield) as white solid. Anal. calcd. for $C_{34}H_{30}N_6O_4$ (mol. wt. 586.65): C, 69.61; H, 5.15; N, 14.33. Found C, 69.42; H, 5.55; N, 14.37. ^{1}H NMR ($CDCl_3$, 599.364 MHz) δ 9.00-8.98 (m, 2H), 8.73 (dd, J = 7.9, 0.8 Hz), 8.45 (dd, J = 7.9, 0.7 Hz), 8.35 (dd, J = 7.7, 0.9 Hz), 8.12 (t, J = 7.9 Hz), 7.97-7.96 (m, 2H), 7.88 (t, J = 7.9 Hz), 7.63 (dd, J = 7.7, 0.7 Hz), 5.51 (s, 2H), 3.52 ppm (s, 12H). ^{13}C NMR ($CDCl_3$, 150.725 MHz) δ 157.0, 156.9, 155.3, 155.2, 155.0, 138.1, 137.5, 132.0, 127.2, 126.3, 125.7, 121.4, 121.2, 120.8, 104.7, 54.0 ppm.

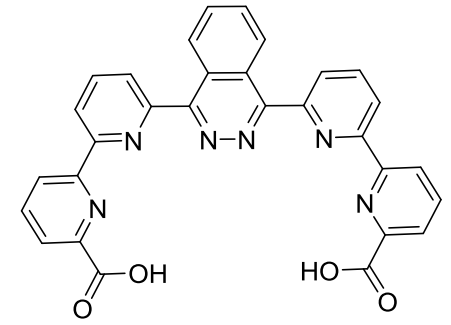

Synthesis of 4.43

1,4-bis(6'-(dimethoxymethyl)-[2,2'-bipyridin]-6-yl)phthalazine (**4.42**, 0.1353 g, 0.2306 mmol), a stir bar, and HCl (6 M, 13.0 mL) were added to a vial. After the solution was stirred for 3.5 h, sodium chlorite 80% was added (0.3136 g, 3.467 mmol) portionwise over 10 min, giving a yellow solution. After stirring for 1 d the solution was diluted with water (20.0 mL) and filtered through a fine frit. The solid was washed with water (4 x 20 mL) until the pH ~7, then washed with acetone (3 x 10 mL) and diethyl ether (3 x 10 mL). The solid was transferred to a vial and dried under oil pump vacuum, yielding 6',6''-(phthalazine-1,4-diyl)bis(([2,2'-bipyridine]-6-carboxylic acid)) $(H_2O)_3$ (**4.43**, 0.1068 g, 0.1840 mmol, 80 % yield) as off-white solid. Anal. calcd. for $C_{30}H_{18}N_6O_4$ $(H_2O)_3$ (mol. wt. 580.56): C, 62.07; H, 4.17; N, 14.48. Found C, 62.58; H, 4.82; N, 14.78.

^{1}H NMR ($CDCl_3$, 599.364 MHz) δ 8.81 (dd, *J* = 7.9, 1.0 Hz, 2H), 8.77-8.75 (m, 2H), 8.58-8.61 (m, 2H), 8.36 (t, *J* = 7.8 Hz), 8.30 (dd, *J* = 7.5, 1.0 Hz), 8.19-8.13 ppm (m, 6H).

^{13}C NMR ($CDCl_3$, 150.726 MHz) δ 165.9, 156.7, 154.8, 154.5, 153.9, 148.2, 139.0, 139.0, 133.3, 126.7, 126.0, 125.4, 125.0, 123.7, 121.6 ppm.

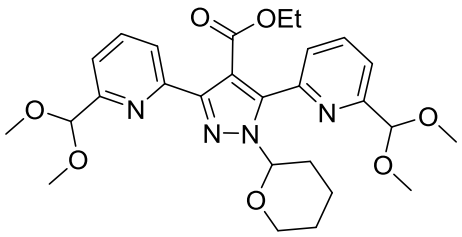

Synthesis of 4.44

Ethyl 3,5-dibromo-1-(tetrahydropyranyl)pyrazole-4-carboxylate (**4.38**, 1.9344 g, 5.06 mmol), 2-(dimethoxymethyl)-6-(tributylstannyl)pyridine (**4.33**, 5.5998g, 11.79

mmol), $Pd(PPh_3)_4$ (0.8794g, 0.76 mmol), stir bar, and dry toluene (20.0 mL) were added to a pressure vessel (48 mL) in a glovebox. The reaction vessel was heated in a 120 ^oC oil bath for 14 d, after which time the reaction was cooled to room temperature and filtered through a course frit loaded with Celite, washing the Celite with diethyl ether. Solvent was removed by rotary evaporation, giving an orange oil which was purified on a silica (115 g) column, eluting by a gradient of hexanes and diethyl ether, starting with 1:1 and finishing at 1:3 mixture. Fractions containing R_f of 0.15 were combined; it should be noted that a very close spot appears toward the end of the column. Solvent was removed by rotary evaporation, the residue was transferred to a vial by dissolving in DCM. Solvent was removed by a flow of air and the residue stored under oil pump vacuum, yielding **4.44** (0.9885 g, 1.88 mmol, 37.1 % yield) as colorless oil. Anal. calcd. for $C_{27}H_{34}N_4O_7$ (mol. wt. 526.59): C, 61.58; H, 6.51; N, 10.64. Found C, 61.32; H, 6.34; N, 10.76.

^1H NMR ($CDCl_3$, 599.361 MHz) δ 7.87 (t, *J* = 7.7 Hz, 1H), 7.82-7.78 (m, 2H), 7.72 (dd, *J* = 7.7, 0.9 Hz, 1H), 7.64 (dd, *J* = 7.7, 0.6 Hz, 1H), 7.55 (dd, *J* = 6.9, 1.6 Hz, 1H), 5.64 (dd, *J* = 9.7, 2.6 Hz, 1H), 5.40 (s, 1H), 5.36 (s, 1H), 4.10 (q, *J* = 7.1 Hz, 2H), 4.01-3.97 (m, 1H), 3.47 (s, 3H), 3.46 (s, 3H), 3.43 (s, 3H), 3.42 (s, 3H), 2.55-2.49 (m, 1H), 2.10-2.03 (m, 2H), 1.74-1.67 (m, 2H), 1.62-1.55 (m, 1H), 1.65-1.40 (m, 1H), 1.02 ppm (t, *J* = 7.1 Hz, 3H). ^{13}C NMR ($CDCl_3$, 150.726 MHz) δ 164.0, 157.1, 156.5, 151.1, 150.4, 147.4, 143.5, 136.8, 136.5, 125.7, 122.7, 120.9, 120.1, 113.6, 104.5, 104.1, 85.1, 67.5, 60.3, 53.8, 53.8, 53.7, 53.7, 29.5, 24.7, 22.4, 13.6 ppm.

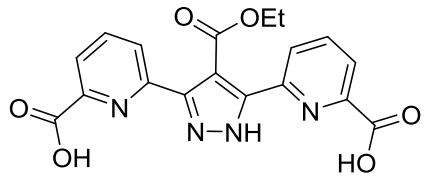

Synthesis of 4.45

To a vial was added **4.44** (0.9529 g, 1.81 mmol), stir bar, and HCl (6 M, 13.5 mL). The mixture was sonicated until all dissolved. After stirring for 1.5 h, sodium chlorite 80% (2.2205 g, 24.55 mmol) was added portion wise over 20 min. After stirring for 2 h with the cap loose, the heterogeneous solution was filtered through a medium frit and washed with water (8 x 15 mL) (last wash of water pH ~7). The white solid was

transferred to a vial and dried under oil pump vacuum over phosphorus pentoxide yielding **4.45** $(H_2O)_{0.5}$ (483.6 mg, 1.236 mmol, 68 % yield) as white solid. Anal. calcd. for $C_{18}H_{14}N_4O_6$ $(H_2O)_{0.5}$ (mol. wt. 391.34): C, 55.25 ; H, 3.86 ; N, 14.32. Found C, 55.12; H, 4.14; N, 14.65.

^{1}H NMR (500 MHz, d_6-DMSO) δ 13.05 (bs, 1H), 8.20-8.02 (m, 6H)[a], 4.28 (q, J = 7.1 Hz, 2H), 1.08 (t, J = 7.1 Hz, 3H). ^{13}C NMR (125.7 MHz, d_6-DMSO)[b] δ 165.6, 164.8, 150.5 (vb), 147.8, 138.8 (b), 124.4, 123.9, 111.8, 60.7, 13.6 ppm; b=broad vb= very broad.

[a] ^{1}H NMR aromatic peaks are broad and overlapping [b] There is one missing peak in the ^{13}C NMR, the ^{1}H NMR and ^{13}C NMR can be seen in Figure 4.26 and Figure 4.27.

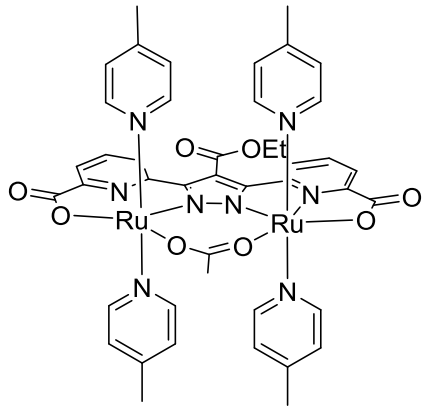

Synthesis of 4.46

4.45 (100.1 mg, 0.256 mmol), triethylamine (137.0 mg, 1.35 mmol), ethanol (12.5 mL), and a stir bar were added to a vial (20 mL) in a glovebox. After **4.45** dissolved, $[Ru(cym)Cl_2]_2$ (163.5 mg, 0.267 mmol) and 4-picoline (208.5 mg, 2.24 mmol) were added. The reaction was heated in a 100 ^{o}C oil bath for 2 d; after cooling to room temperature solvent was removed by rotary evaporation. The crude product was dissolved in DCM which was loaded on a silica (19.0 g) column, eluting by a gradient of DCM and MeOH, starting with 100 % DCM then moving to 10 % MeOH. The dark brown fractions were combined and solvent was removed by rotary evaporation and the residue stored under oil pump vacuum yielding **4.46** $(H_2O)_6$ as dark brown solid (142.6 mg, 0.127 mmol, 50 % yield). Anal. calcd. for $C_{44}H_{42}N_8O_8Ru_2$ $(H_20)_6$ (mol. wt. 1121.10): C, 47.14 ; H, 4.86 ; N, 10.00. Found C, 47.25; H, 5.17; N, 10.01.

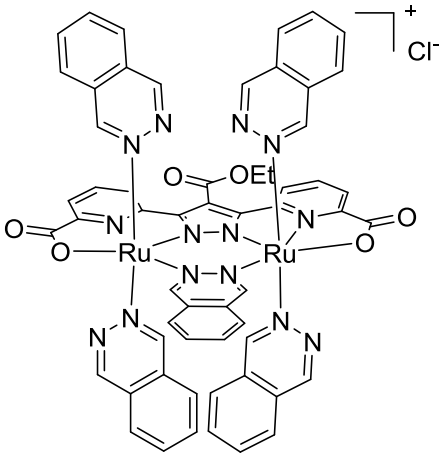

Synthesis of 4.47

4.45 (50.9 mg, 0.130 mmol), triethylamine (68.1 mg, 0.673 mmol), ethanol (6.0 mL), and a stir bar were added to a vial (20 mL) in a glovebox. After **4.45** dissolved, $[Ru(cym)Cl_2]_2$ (81.5 mg, 0.133 mmol) and phthalazine (137.3 mg, 1.05 mmol) were then added. The reaction was heated in a 100 ^{o}C oil bath for 1.5 d; after cooling to room temperature solvent was removed by rotary evaporation. The crude product was dissolved in DCM which was loaded on a silica (17.5 g) column, eluting by a gradient of DCM and MeOH, starting with 100 % DCM then slowly moving to 10 % MeOH. The dark red fractions were combined and solvent was removed by rotary evaporation and the residue stored under oil pump vacuum yielding **4.47** $(H_2O)_6$ $(C_6H_{16}N_1Cl_1)_1$ (121.0 mg, 0.080 mmol, 62 % yield) as dark red solid. Anal. calcd. for $C_{58}H_{41}Cl_1N_{14}O_6Ru_2$ $(H_2O)_6$ $(C_6H_{16}N_1Cl_1)_1$ (mol wt. 1513.39): C, 50.79; H, 4.60; N, 13.88. Found C, 50.70; H, 4.94; N, 13.95. ^{1}H and ^{13}C NMR spectra show the presence of the triethylamine.

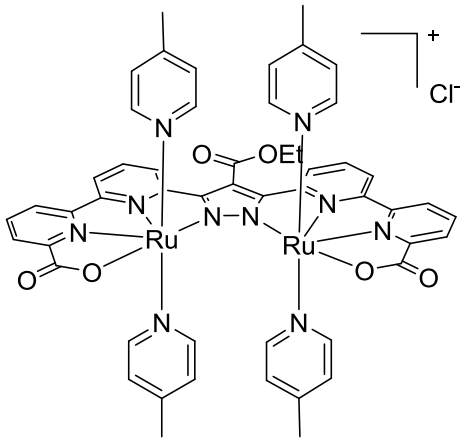

Synthesis of 4.48

4.40 $(H_2O)_3$ (30.8 mg, 0.0530 mmol), triethylamine (58.8 mg, 0.581 mmol), ethanol (4.0 mL), and a stir bar were added to a vial in a glovebox. **4.40** dissolved after 5 min, and $[Ru(cym)Cl_2]_2$ (38.4 mg, 0.063 mmol) and 4-picoline (45.7 mg, 0.491 mmol) were added. The reaction was heated in a 100 ^oC oil bath for 2 d; after cooling to room temperature solvent was removed by a flow of nitrogen. The crude solid was dissolved in DCM (10 mL) and washed with water (3 x 3 mL), the aqueous layers were combined and back extracted with DCM (5 mL). The combined organic layers were dried with sodium sulfate and filtered through a pipet loaded with cotton. Solvent was reduced to a minimal amount which was loaded on a silica (15.0 g) column, eluting by a gradient of DCM and MeOH, starting with 100 % DCM then moving to 10 % MeOH then 15% MeOH, which started to elute the main product fraction (second fraction, dark brown band), and then to 20% MeOH to finish eluting the main dark fraction. All fractions that contained the second main fraction were combined and solvent was removed by rotary evaporation and the residue stored under oil pump vacuum yielding **4.48** (39.9 mg, 0.0314 mmol, 59 % yield) as dark brown solid. Anal. calcd. for $C_{52}H_{45}N_{10}O_6ClRu_2$ $(H_2O)_7$ (mol. wt. 1269.69): C, 49.19 ; H, 4.68 ; N, 11.03. Found C, 48.91; H, 4.63; N, 10.64.

E. CAN studies procedure

The oxygen evolution was recorded with a pressure transducer (Omega PX138-015D5V) driven at 12.00 V using a power supply (SSA-0601S-1) plus a data acquisition module (Omega OMB-DAQ-56; running at 0.1 Hz). The pressure transducer was

connected with Watts SVEB20 1/4-Inch Diameter by 0.170-Inch Clear Vinyl Tubing to a reaction vessel with a 14/20 neck and a 0.2 inch diameter 0.7 inch long barb (space = 48 mL, see picture). To the reaction flask was added a freshly made solution of $Ce(NH_4)_2(NO_3)_6$ (concentration of stock solution varied but final molarity was 1 mmol in 4 mL; 250 mM), ultrapure water (varied depending on the volume of CAN solution added and catalyst), and HNO_3 (25 µL of 15.8 M was added to give 100 mM in 4 mL). Tubing was equipped to the long barb with copper wire and a septum with copper wire or a hose clamp. The vessel was pressurized and placed in a 30 ^oC constant temperature water bath to make sure there were no leaks. After 30 min of data showing no loss in pressure and no leaks, the pressure was vented and a solution of catalyst (depends on the run) was immediately injected to the above solution under vigorous stirring, and the cell was submerged again in the water bath for the duration of the testing. During the testing the water bath and reactions were kept in the dark. Initial concentrations of catalyst = 100.0 µM, CAN = 250 mM, and HNO_3 = 0.1 M.

Preparation of **4.46** stock solution:
To a vial in a glovebox was added **4.46** (9.1 mg, 8.12 µmol) then dissolved in 2,2,2-trifluoroethanol (1.0 mL), giving a solution of 8.12 mM.
Preparation of **4.47** stock solution:
To a vial in a glovebox was added **4.47** (11.4 mg, 7.53 µmol) then dissolved in a mixture of water (10.0 mL) and 2,2,2-trifluoroethanol (1.5 mL), giving a solution of 0.655 mM.
Preparation of **4.48** stock solution:
To a vial in a glovebox was added **4.48** (4.8 mg, 3.78 µmol) then dissolved in a water (5.0 mL), giving a solution of 0.756 mM.
Example procedure for preparation of CAN solution:
CAN (4.0119 g, 7.32 mmol) was added to a volumetric flask (10 mL), then filling the flask with ultrapure water to give a total volume of 10 mL.(732 mM)
Example procedure for reaction solution:

CAN solution (732 mM, 1.366 mL) was added to the pressure vessel followed by ultrapure water (2.560 mL), HNO_3 (25 μL), and a stir bar. After checking for leaks, a solution of **4.46** (8.12 mM, 49 μL) was injected.

F. NMR Figures

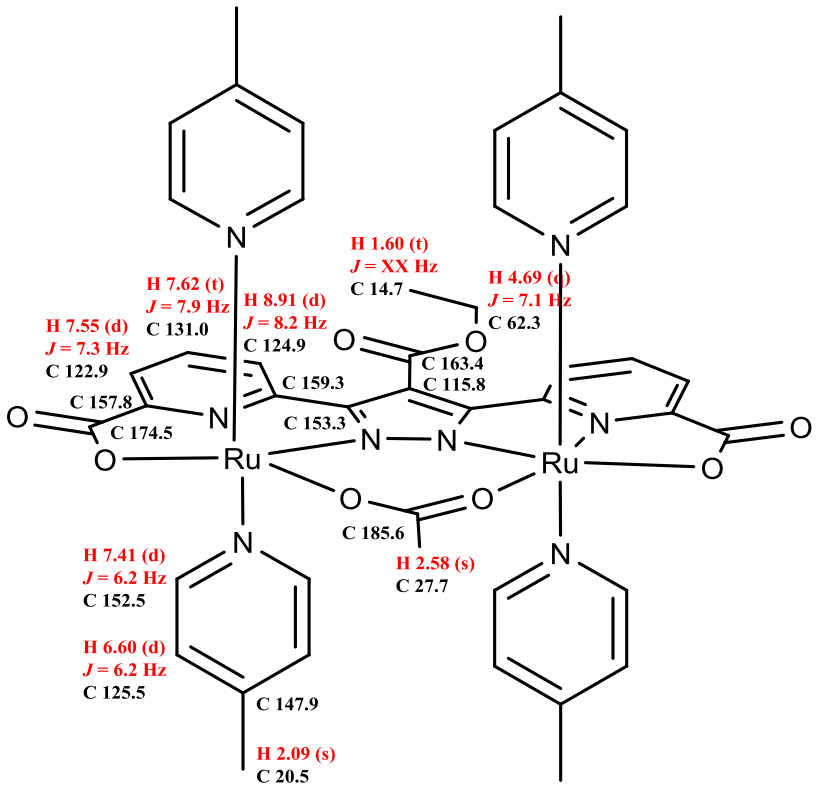

^{1}H -^{13}C gHMBCAD[a]		
^{1}H	bonds	^{13}C
8.91	3	122.9
8.91	3	153.3(w)
8.91	2	159.3
7.62	3	157.8
7.62	3	159.3
7.55	3	124.9
7.55	2	157.8
7.55	3	174.5
7.41	2	125.5
7.41	3	147.9
7.41	1,3	152.5
6.60	3	20.5
6.60	1,3	125.5
6.60	2	152.5
4.69	2	14.7
4.69	3	163.4
1.60	2	62.3
[a]J_{nxh} = 8.0 Hz J_{1xh} = 146.0 Hz		

^{1}H-^{13}C HSQCAD	
^{1}H	^{13}C
8.91	124.9
7.62	131.0
7.55	122.9
7.41	152.5
6.60	125.5
4.69	62.3
2.58	27.7
2.09	20.5
1.60	14.7

gCOSY
8.91↔7.62
7.62↔7.55
7.41↔6.60
4.69↔1.60

Figure 4.22 NMR data of **4.46** in d_6-acetone (0.6 mL) and water (0.1 mL).

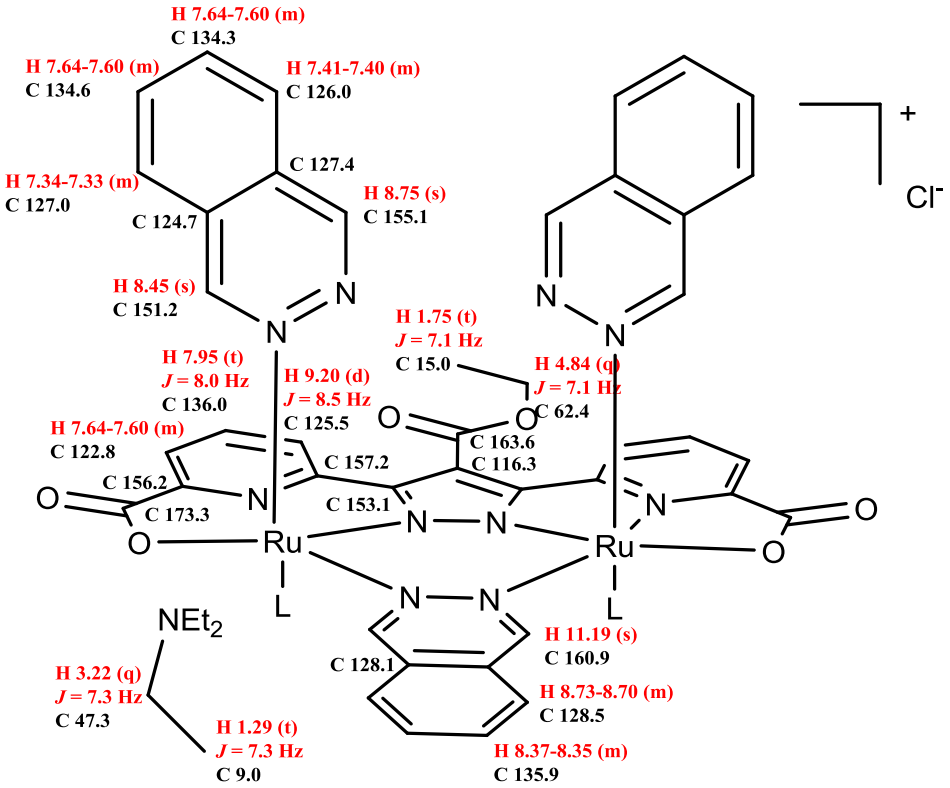

^{1}H -^{13}C gHMBCAD[a]		
^{1}H	bonds	^{13}C
11.19	2	128.1
11.19	3	128.5
9.20	2	157.2
9.20	3	153.1
9.20	3	122.8
8.75	3	124.7
8.75	3	126.0
8.75	2	127.4
8.73-8.70	2, 3	135.9
8.45	3	127.4
8.45	3	127.0
8.45	2	124.7

gCOSY
9.20↔7.95
8.37-8.35↔8.73-8.70
7.95↔7.64-7.60
7.64-7.60↔7.41-7.40
7.64-7.60↔7.34-7.33
3.22↔1.29

^{1}H-^{13}C HSQCAD	
^{1}H	^{13}C
11.19	160.9
9.20	125.5
8.75	155.1
8.73-8.70	128.5
8.45	151.2
8.37-8.35	135.9
7.95	136.0
7.64-7.60	134.6
7.64-7.60	134.3
7.64-7.60	122.8
7.41-7.40	126.0
7.34-7.33	127.0
4.84	62.4
1.75	15.0
3.22	47.3
1.29	9.0

^{1}H -^{13}C gHMBCAD[a] Cont		
^{1}H	bonds	^{13}C
7.95	3	157.2
7.95	3	156.2
7.64-7.60	3	173.3 (w)
7.64-7.60	2	156.2
7.64-7.60	[b]	124-127[b]
7.41-7.40	3	155.1
7.41-7.40	3	134.6
7.41-7.40	3	124.7
7.34-7.33	3	151.2
7.34-7.33	3	134.3
7.34-7.33	3	127.4
4.84	3	163.6
4.84	2	15.0
1.75	2	62.4
3.22	1,3	47.3
3.22	2	9.0
1.29	2	47.3
[a] J_{nxh} = 8.0 Hz J_{1xh} = 146.0 Hz		

Figure 4.23 NMR data of **4.47** in d_6-acetone (0.6 mL) and water (0.1 mL).

[b] There are too many peaks in this area to known what is actually correlated. The expected correlations would be to 125.5 (pyr), 124.7 (pht), 126.0 (pht), 127.0(pht), and 127.4(pht). pyr = pyridine and pht = phthalazine

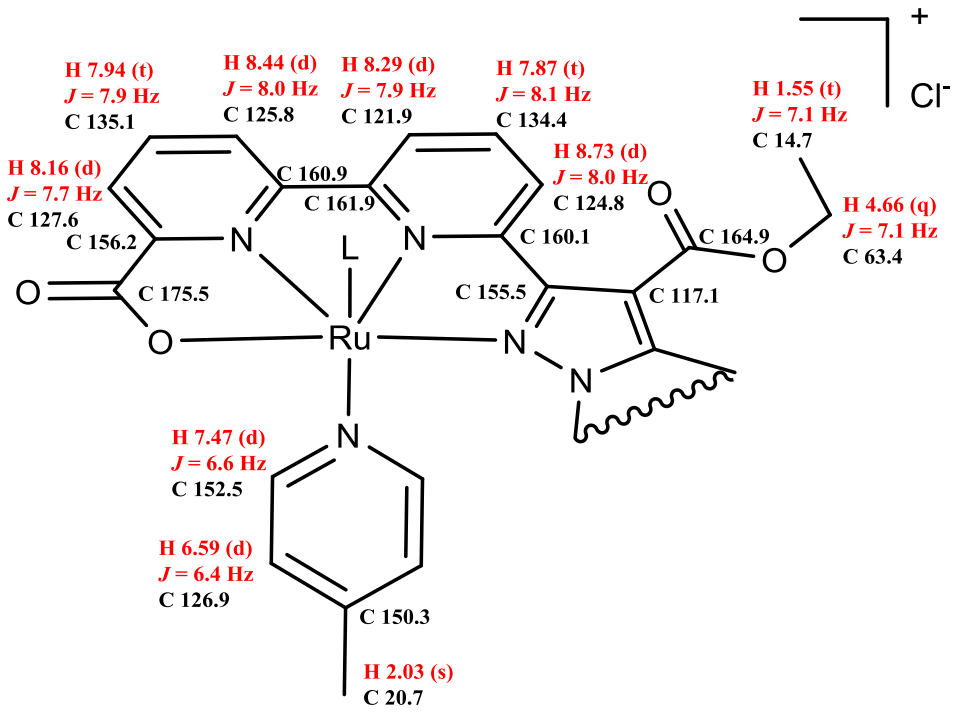

gCOSY
8.73↔7.87
8.44↔7.94
8.29↔7.87
8.16↔7.94
7.47↔6.59
6.59↔2.03
4.66↔1.55

^{1}H-^{13}C HSQCAD	
^{1}H	^{13}C
8.73	124.8
8.44	125.8
8.29	121.9
8.16	127.6
7.94	135.1
7.87	134.4
7.47	152.5
6.59	126.9
4.66	63.4
2.03	20.7
1.55	14.7

^{1}H - ^{13}C gHMBCAD[a]		
^{1}H	bonds	^{13}C
8.73	3	121.9
8.73	3	155.5
8.73	2	160.1
8.44	3	127.6
8.44	4	156.2(w)
8.44	2	160.9
8.44	3	161.9
8.29	3	124.8
8.29	4	160.1(w)
8.29	3	160.9
8.29	2	161.9
8.16	3	125.8
8.16	2	156.2
8.16	4	160.9(w)
8.16	3	175.5

^{1}H - ^{13}C gHMBCAD[a] Continued		
^{1}H	bonds	^{13}C
7.94	3	156.2
7.94	3	160.9
7.87	3	160.1
7.87	3	161.9
7.47	2	126.9
7.47	3	150.3
7.47	1,3	152.5
6.59	1,3	126.9
6.59	2	152.5
6.59	3	20.7
4.66	2	14.7
4.66	3	164.9
2.03	3	126.9
2.03	2	150.3
1.55	2	63.4
[a]J_{nxh} = 8.0 Hz J_{1xh} = 146.0 Hz		

Figure 4.24 NMR data of **4.48** in d_6-acetone (0.6 mL) and water (0.1 mL).

G. NMR Spectra

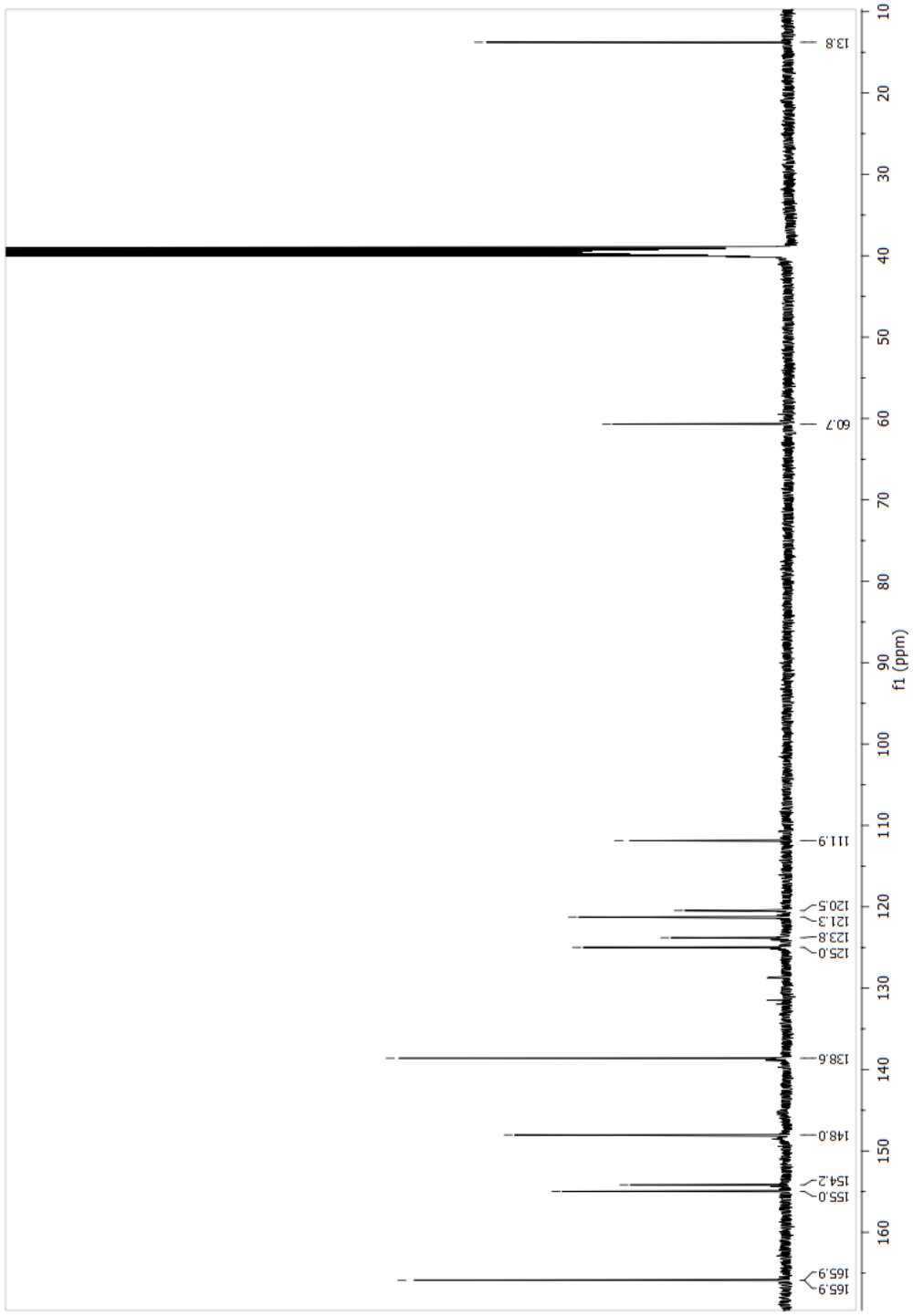

Figure 4.25. ^{13}C NMR spectrum of **4.40** in d_6-DMSO.

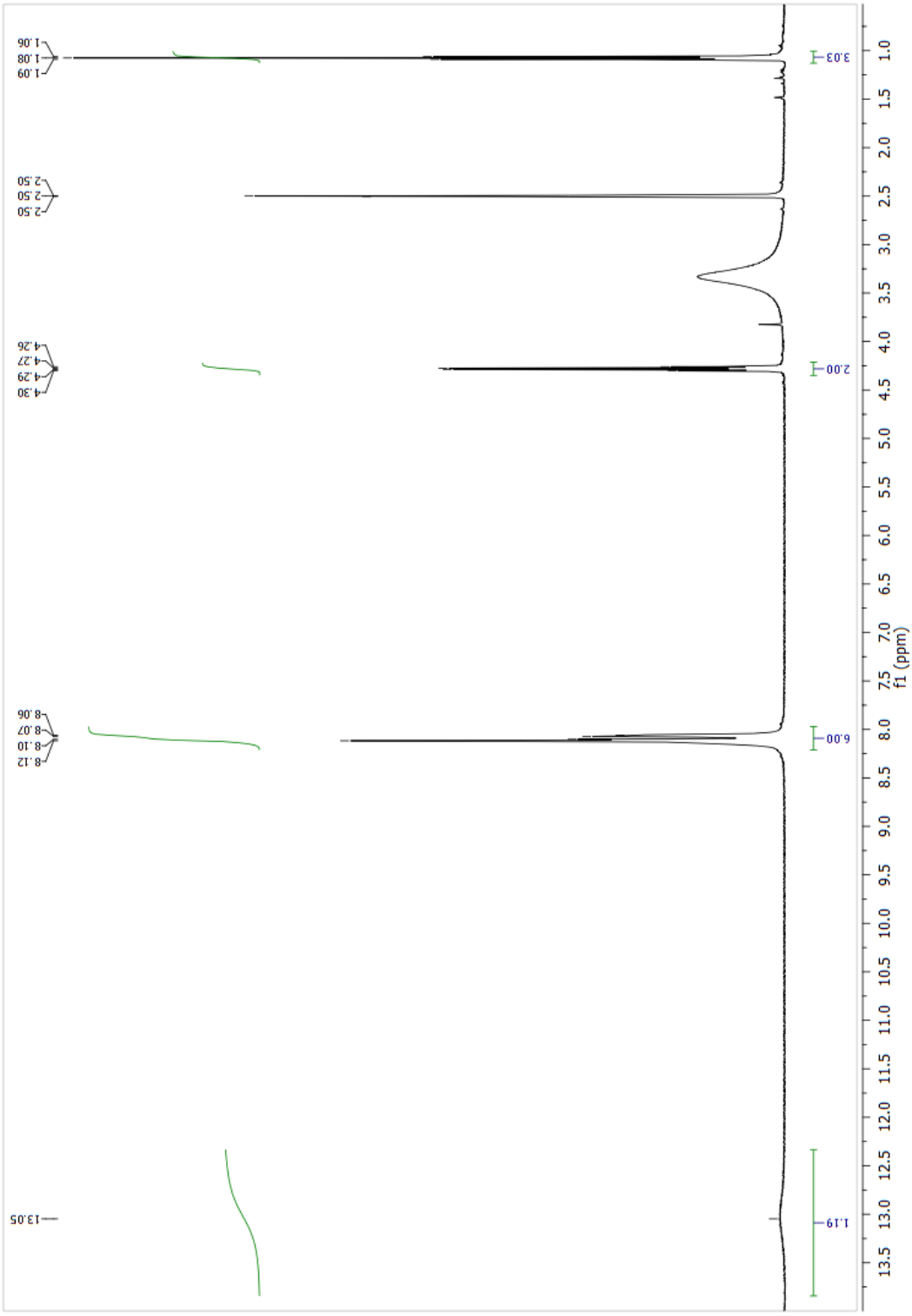

Figure 4.26. ^{1}H NMR spectrum of **4.45** in d_6-DMSO.

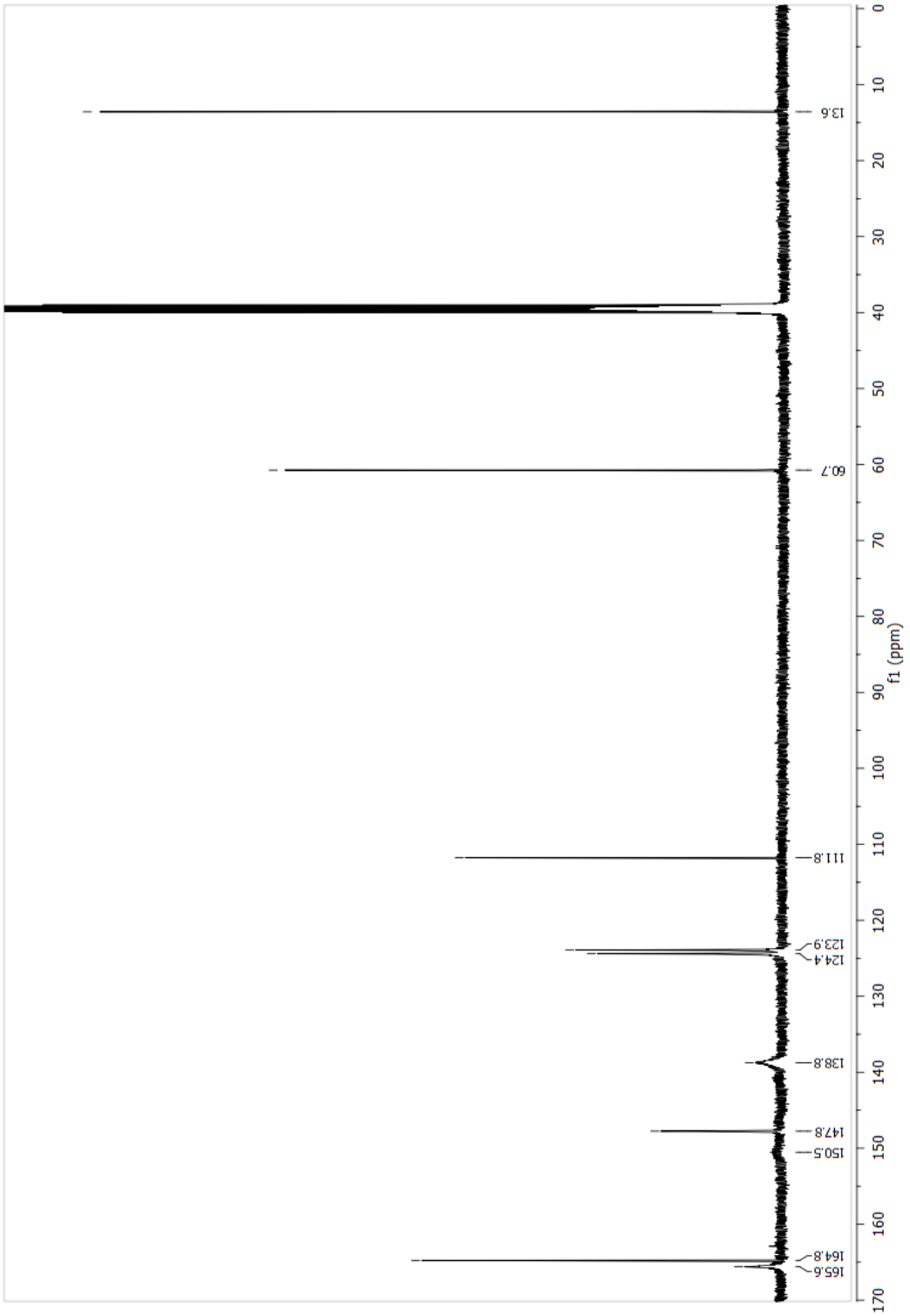

Figure 4.27. ^{13}C NMR spectrum of **4.45** in d_6-DMSO.

H. Refrences

(1) Duan, L. L.; Fischer, A.; Xu, Y. H.; Sun, L. C. *J. Am. Chem. Soc.* **2009**, *131*, 10397.

(2) Duan, L. L.; Xu, Y. H.; Zhang, P.; Wang, M.; Sun, L. C. *Inorg. Chem.* **2010**, *49*, 209.

(3) Duan, L. L.; Araujo, C. M.; Ahlquist, M. S. G.; Sun, L. C. *Proc. Natl. Acad. Sci. U.S.A.* **2012**, *109*, 15584.

(4) Duan, L. L.; Bozoglian, F.; Mandal, S.; Stewart, B.; Privalov, T.; Llobet, A.; Sun, L. C. *Nat. Chem.* **2012**, *4*, 418.

(5) Tong, L. P.; Wang, Y.; Duan, L. L.; Xu, Y. H.; Cheng, X.; Fischer, A.; Ahlquist, M. S. G.; Sun, L. C. *Inorg. Chem.* **2012**, *51*, 3388.

(6) Gersten, S. W.; Samuels, G. J.; Meyer, T. J. *J. Am. Chem. Soc.* **1982**, *104*, 4029.

(7) Sens, C.; Romero, I.; Rodriguez, M.; Llobet, A.; Parella, T.; Benet-Buchholz, J. *J. Am. Chem. Soc.* **2004**, *126*, 7798.

(8) Neudeck, S.; Maji, S.; López, I.; Meyer, S.; Meyer, F.; Llobet, A. *J. Am. Chem. Soc.* **2013**, *136*, 24.

(9) Deng, Z.; Tseng, H.-W.; Zong, R.; Wang, D.; Thummel, R. *Inorg. Chem.* **2008**, *47*, 1835.

(10) Xu, Y.; Fischer, A.; Duan, L.; Tong, L.; Gabrielsson, E.; Åkermark, B.; Sun, L. *Angew. Chem. Int. Ed.* **2010**, *49*, 8934.

(11) Xu, Y.; Duan, L.; Åkermark, T.; Tong, L.; Lee, B.-L.; Zhang, R.; Åkermark, B.; Sun, L. *Chem. – Eur. J.* **2011**, *17*, 9520.

(12) Samanta, S.; Demesko, S.; Dechert, S.; Meyer, F. *Angew. Chem. Int. Ed.* **2015**, *54*, 583.

(13) Zhang, W.; Liu, J.; Zhu, H.; Gao, W.; Sun, L. *Synth. Commun.* **2007**, *37*, 3393.

(14) Chen, J.-L.; Song, P.; Liao, J.; Wen, H.-R.; Hong, R.; Chen, Z.-N.; Chi, Y. *Inorg. Chem. Commun.* **2010**, *13*, 1057.

(15) van der Vlugt, J. I.; Demeshko, S.; Dechert, S.; Meyer, F. *Inorg. Chem.* **2008**, *47*, 1576.

(16) Pons, J.; Chadghan, A.; Garcia-Anton, J.; Ros, J. *Lett. Org. Chem.* **2010**, *7*, 178.

(17) Schneider, B.; Demeshko, S.; Neudeck, S.; Dechert, S.; Meyer, F. *Inorg. Chem.* **2013**, *52*, 13230.

(18) Schubert, U. S.; Eschbaumer, C.; Heller, M. *Org. Lett.* **2000**, *2*, 3373.

(19) Bianchini, C.; Giambastiani, G.; Rios, I. G.; Meli, A.; Oberhauser, W.; Sorace, L.; Toti, A. *Organometallics* **2007**, *26*, 5066.

(20) Hicks, R. G.; Koivisto, B. D.; Lemaire, M. T. *Org. Lett.* **2004**, *6*, 1887.

(21) Dry, E. F. V.; Clegg, J. K.; Breiner, B.; Whitaker, D. E.; Stefak, R.; Nitschke, J. R. *Chem. Commun.* **2011**, *47*, 6021.

(22) Mase, T.; Houpis, I. N.; Akao, A.; Dorziotis, I.; Emerson, K.; Hoang, T.; Iida, T.; Itoh, T.; Kamei, K.; Kato, S.; Kato, Y.; Kawasaki, M.; Lang, F.; Lee, J.; Lynch, J.; Maligres, P.; Molina, A.; Nemoto, T.; Okada, S.; Reamer, R.; Song, J. Z.; Tschaen, D.; Wada, T.; Zewge, D.; Volante, R. P.; Reider, P. J.; Tomimoto, K. *J. Org. Chem.* **2001**, *66*, 6775.

(23) Jovic, F.; Louise, L.; Mioskowski, C.; Renard, P.-Y. *Tetrahedron Lett.* **2005**, *46*, 6809.

(24) Orita, A.; Taniguchi, H.; Otera, J. *Chem. – Asian J.* **2006**, *1*, 430.

(25) Romero, F. M.; Ziessel, R.; DeCian, A.; Fischer, J.; Turek, P. *New J. Chem.* **1996**, *20*, 919.

(26) Champouret, Y. D. M.; Chaggar, R. K.; Dadhiwala, I.; Fawcett, J.; Solan, G. A. *Tetrahedron* **2006**, *62*, 79.

(27) Schubert, U. S.; Eschbaumer, C. *Org. Lett.* **1999**, *1*, 1027.

(28) Toto, P.; Chenault, J.; El Hakmaoui, A.; Akssira, M.; Guillaumet, G. *Synth. Commun.* **2008**, *38*, 674.

(29) Xue, D. Q.; Zhang, X. Y.; Wang, C. J.; Ma, L. Y.; Zhu, N.; He, P.; Shao, K. P.; Chen, P. J.; Gu, Y. F.; Zhang, X. S.; Wang, C. F.; Ji, C. H.; Zhang, Q. R.; Liu, H. M. *Eur. J. Med. Chem.* **2014**, *85*, 235.

(30) Sander, A. C.; Maji, S.; Francàs, L.; Böhnisch, T.; Dechert, S.; Llobet, A.; Meyer, F. *ChemSusChem* **2015**, *8*, 1697.

(31) Hetterscheid, D. G. H.; Reek, J. N. H. *Eur. J. Inorg. Chem.* **2014**, *2014*, 742.

(32) Sato, Y.; Takizawa, S.-y.; Murata, S. *Eur. J. Inorg. Chem.* **2015**, *2015*, 5495.

(33) Rigsby, M. L.; Mandal, S.; Nam, W.; Spencer, L. C.; Llobet, A.; Stahl, S. S. *Chem. Sci.* **2012**, *3*, 3058.